Acta Chimica Hungarica

VOLUME 119, NUMBER 1, MAY 1985

EDITOR-IN-CHIEF
F. MÁRTA

MANAGING EDITOR
GY. DEÁK

ASSISTANT EDITOR
L. HAZAI

EDITORIAL BOARD
M. T. BECK, R. BOGNÁR, GY. HARDY, K. LEMPERT, B. LENGYEL, K. POLINSZKY, E. PUNGOR, G. SCHAY, Z. G. SZABÓ, P. TÉTÉNYI

Akadémiai Kiadó, Budapest
ACTA CHIM. HUNG. ACHUDC 119 (1) 3—79 (1985) HU ISSN 0231—3146

ACTA CHIMICA HUNGARICA

A JOURNAL OF THE HUNGARIAN ACADEMY OF SCIENCES

Acta Chimica publishes original reports on all aspects of chemistry in English.

Acta Chimica is published in three volumes per year, each volume consisting of four issues, by

AKADÉMIAI KIADÓ

Publishing House of the Hungarian Academy of Sciences
H-1054 Budapest, Alkotmány u. 21.

Manuscripts and editorial correspondence should be addressed to

Acta Chimica
H-1450 Budapest P.O. Box 67

Subscription information

Orders should be addressed to

KULTURA Foreign Trading Company
H-1389 Budapest P.O. Box 149

or to its representatives abroad

Acta Chimica is indexed in Current Contents

NOTICE TO AUTHORS

Acta Chimica publishes original papers on all aspects of chemistry in English. Before preparing a manuscript for submission to this journal authors are advised to consult recent issues.

Form of manuscript

Manuscripts, tables and illustrations should be submitted in triplicate. Manuscripts should be typewritten double spaced (25 lines, 50 characters per line including spaces). The *title page* should include (1) the title of the paper, (2) the full names of the author(s) in the sequence to be published; apply an asterisk to designate the name of the author to whom correspondence should be addressed, (3) name and address of the institution where the work was done. If the paper is part of a series, reference to the previous communication must be given as a footnote.

Abstract

A summary is printed at the head of each paper. This should not exceed 200 words and should state briefly the principal results and major conclusions of the work. It should be suitable for use by abstracting services.

ACTA CHIMICA HUNGARICA

EDITORIAL BOARD

M. T. BECK, R. BOGNÁR, GY. HARDY,
K. LEMPERT, B. LENGYEL, K. POLINSZKY,
E. PUNGOR, G. SCHAY,
Z. G. SZABÓ, P. TÉTÉNYI

EDITOR-IN-CHIEF

F. MÁRTA

MANAGING EDITOR

GY. DEÁK

ASSISTANT EDITOR

L. HAZAI

VOLUME 119

AKADÉMIAI KIADÓ, BUDAPEST

1985

Abd-Allah, S. O. s. **Hammouda, H. A.**
Abd El Kader, A. E. K. K., Abd El Wahed, M. G., El Sayed, G.: Polarographic studies of some azo-triazol dyes (Short communication) 285
Abd El Wahed, M. G. s. **Abd El Kader. A. E. G. K.**
Ahmad, S., Jamaluddin, Shukla, I. C.: Determination of some amino compounds with ammonium metavanadate 339
Aly, A. s. **Mousa, M.**
Ancion, C., Poncelet, G.: Hydrogenation of ethylene by $Pt/H_xVMoO_{5.5}$ bronzes obtained by hydrogen spillover 185

Bankós, I., Papp, J., Kalló, D.: Intra- and imtermolecular methyl-transfer of *m*-xylene on H-zeolites 179
Barta-Szalai, G. s. **Simig, Gy.**
Bekheit, M. M. s. **Ibrahim, K. M.**
Bodart, P. s. **Dewaele, N.**
Bodart, P. s. **Nagy, J. B.**
Bogyai, I. s. **Schay, Z.**
Breining, T. s. **Horváth, G.**

Collette, H. s. **Maroie, S.**
Costa, J.-L., Demonceau, A., Drapier, J., Hubert, A., Noels, A., Teyssiè, P.: Reduction of carbon monoxide on cobalt(I) complexes 147

Dallons, J. L., Jannes, G., Delmon, B.: Competitive hydrogenation of a nitrile function and of an olefinic unsaturation on Raney nickel 223
Debras, G. s. **Gabelica, Z.**
Debras, G. s. **Nagy, J. B.**
De Gryse, R. s. **Landuyt, J. P.**
Delmon, B. s. **Dallons, J. L.**
Demonceau, A. s. **Costa, J.-L.**
Derouane, E. G. s. **Gabelica, Z.**
Derouane, E. G. s. **Nagy, J. B.**
Dewaele, N., Bodart, P., Gabelica, Z., Nagy, J. B.: Synthesis and characterization of Faujasite-type zeolites, I. Multinuclear NMR characterization of liquid and solid intermediate phases formed during synthesis of zeolite Y 233
Dobrovolszky, M. A., Paál, Z., Tétényi, P.: Homologation of hexane isomers catalyzed by platinum 95
Doleschall, G. s. **Simig, Gy.**
Drapier, J. s. **Costa, J.-L.**
Dudás, J. s. **Szalontai, G.**

El-Asmy, A. A. s. **Ibrahim, K. M.**
El Sayed, G. s. **Abd El Kader, A. E. G. K.**
Engelhardt, J..Kalló, D.: Methathesis and oligomerization of propene over molybdena-alumina catalysts 249
Eusebius, L. C. T. s. **Srivastava, U.**

Fetter, J. s. **Simig, Gy.**

Gabelica, Z., Nagy, J. B., Debras, G., Derouane, E. G.: Characterization of X-ray amorphous ZSM-5 zeolites by thermal analysis and high resolution solid state multinuclear NMR spectroscopy 275

Gabelica, Z. s. **Dewaele, N.**
Gabelica, Z. s. **Maroie, S.**
Gabelica, Z. s. **Nagy, J. B.**
Ghose, A. K. s. **Srivastava, U.**
Gizur, T. s. **Simig, Gy.**
Gombos, Zs. s. **Simig, Gy.**
Gourgue, A. s. **Ravet, I.**
Guczi, L. s. **Schay, Z.**
Gupta, K., Sharma, K. K.: Polarographic study of mixed ligand (*m*-butylthioglycolate--oxalate) complexes of cadmium(II), lead(II) and thallium(I) 65

Hammouda, H. A., Abd-Allah, S. O., Zoorob, H. H.: Reactions with 4,5-diphenylimidazolidine-2-thione, II 49
Harfoush, A. s. **Mousa, M.**
Hegedűs, M. s. **Margitfalvi, J.**
Heil, B. s. **Tőrös, Sz.**
Hermecz, I. s. **Horváth, G.**
Hermecz, I. s. **Martin, A.**
H-Kovács, Zs.: ^{1}H—NMR study of restricted rotation in dithiophosphoromethyl acetanilides 371
Hornyák, Gy. s. **Simig, Gy.**
Horváth, Á. s. **Horváth, G.**
Horváth, G., Breining, T., Hermecz, I., Horváth, Á., Pongor-Csákvári, M., Podányi, B., Kiss, Á. I., Martin, A.: Ultraviolet and infrared study of 9-arylhydrazono- and 9--arylaminomethylene-6,7,8,9-tetrahydropyridopyrimidine derivatives 305
Horváth, G. s. **Martin, A.**
Hubert, A. s. **Costa, J.-L.**

Ibrahim, K. M., El-Asmy, A. A., Bekheit, M. M., Mostafa, M. M.: New metal complexes of 4-phenyl-1-diacetylmonoxime-3-thiosemicarbazone (BMPTS) 355

Jacobs, P. A. s. **Martens, J. A.**
Jacobs, P. A. s. **Nagy, J. B.**
Jamaluddin s. **Ahmad, S.**
Jannes, G. s. **Dallons, J. L.**

Kajtár-Peredy, M. s. **Kalaus, Gy.**
Kajtár-Peredy, M. s. **Simig, Gy.**
Kalaus, Gy., Katona, I., Kajtár-Peredy, M., Szabó, L., Szántay, Cs.: Synthesis of Vinca alkaloids and related compounds, XX. Oxidative cleavage of C—C bonds of an indoloquinolizidine derivative (Short communication) 3
Kalló, D. s. **Bankós, I.**
Kalló, D. s. **Engelhardt, J.**
Katona, I. s. **Kalaus, Gy.**
Kirsch-De Mesmaeker, A., Maetens, D., Nasielski-Hinkens, R.: The ruthenium(II)-tris--(1,4,5,8-tetraazaphenanthrene) dication: a new photocatalyst in redox cycles for hydrogen production 245
Kiss, Á. I. s. **Horváth, G.**
Kiss, Á. I. s. **Martin, A.**
Kolb, I. s. **Vít, Z.**
Kollár, L. s. **Tőrös, Sz.**
Körtvélyessy, Gy.: Preparation of derivatives of citronellal 347

Landuyt, J. P., De Gryse, R., Vennik, J.: The $V_6O_{13}(001)$ surface studied by LEIS 193
Lempert, K. s. **Simig, Gy.**
Lufimpadio, N. s. **Ravet, I.**

Maetens, D. s. **Kirsch-De Mesmaeker, A.**
Mák, M., Tamás, J., Tuba, Z.: The mass spectra of nitrogen-containing steroids, III. Bisquaternary salts of piperazinoandrostanes 39
Mallát, T., Szabó, S., Petró, J.: Palladium catalysts poisoned by metal ions 127
Margitfalvi, J., Hegedűs, M., Szedlacsek, P., Nagy, F.: Kinetic study of *n*-hexane conversion over Pt/Al_2O_3 catalyst 213

Markó, L. s. **Sisak, A.**
Markó, L. s. **Tőrös, Sz.**
Maroie, S., Collette, H., Gabelica, Z., Verbist, J., Nagy, J. B.: Physicochemical characterization of uranium-antimony mixed oxide catalysts 167
Martens, J. A., Tielen, M., Jacobs, P. A.: Hydroisomerization and hydrocracking of methylnonanes over Pt/HZSM-5 203
Martin, A., Kiss, Á. I., Horváth, G., Hermecz, I.: Ionization properties of 6,7,8,9-tetrahydro-4*H*-pyrido[1,2-*a*]pyrimidin-4-one derivatives having a conjugated side chain in position 9 321
Martin, A. s. **Horváth, G.**
Mostafa, M. M. s. **Ibrahim, K. M.**
Mousa, M., Aly, A., Harfoush, A.: Kinetic study on the hydrolysis of benzenesulfonyl chloride in water-dioxane solutions 363

Nagy, Á. G.: Substituent effects in ketoferrocenes 33
Nagy, F. s. **Margitfalvi, J.**
Nagy, J. B., Gabelica, Z., Debras, G., Bodart, P., Derouane, E. G., Jacobs, P. A.: High resolution magic angle spinning ^{29}Si—NMR characterization of zoolites 265
Nagy, J. B. s. **Dewaele, N.**
Nagy, J. B. s. **Gabelica, Z.**
Nagy, J. B. s. **Maroie, S.**
Nagy, J. B. s. **Ravet, I.**
Nasielski-Hinkens, R. s. **Kirsch-De Mesmaeker, A.**
Noels, A. s. **Costa, J.-L.**
Nyitrai, J. s. **Simig, Gy.**

Paál, Z. s. **Dobrovolszky, M. A.**
Paál, Z. s. **Tétényi, P.**
Papp, J. s. **Bankós, I.**
Peev, T. M., Vértes, A.: A possibility of estimation of the changes in the size of particles containing Mössbauer atoms 57
Petró, J. s. **Mallát, T.**
Podányi, B. s. **Horváth, G.**
Poncelet, G. s. **Ancion, C.**
Pongor-Csákvári, M. s. **Horváth, G.**

Ravet, I., Lufimpadio, N., Gourgue, A., Nagy, J. B.: Physico-chemical characterization of reversed micelles CTAB—1-Hexanol—Water containing Co(II) ions 155

Schay, Z., Bogyay, I., Guczi, L.: Support effect in cluster derived catalysts 105
Sengupta, S. K. s. **Yadav, H. S.**
Sharma, K. K. s. **Gupta, K.**
Shukla, I. C. s. **Ahmad, S.**
Simig, Gy., Fetter, J., Hornyák, Gy., Zauer, K., Doleschall, G., Lempert, K., Nyitrai, J., Gombos, Zs., Gizur, T., Barta-Szalai, G., Kajtár-Peredy, M.: Simple and condensed β-lactams, II. The synthesis of new diethyl 4-oxoazetidino-2,2-dicarboxylates and some manipulations of their functional groups and *N*-substituents 17
Sisak, A., Ungváry, F., Markó, L.: Base catalyzed reactions of cobalt carbonyls related to hydroformylation 115

Srivastava, U., Ghose, A. K., Eusebius, L. C. T.: Separation of Hg(II), La(III) and Ce(III) on Dowex 50W—X8 columns in mixed NH_4NO_3—CH_3COOH media 295
Szabó, L. s. **Kalaus, Gy.**
Szabó, S. s. **Mallát, T.**
Szalontai, G., Dudás, J.: ^{13}C- and ^1H—NMR study of tetrahydro-3,5-dialkyl-1,3,5-thiadiazin-2-thiones. A large thione anisotropy effect 7
Szántay, Cs. s. **Kalaus, Gy.**
Szedlacsek, P. s. **Margitfalvi, J.**

Tamás, J. s. **Mák, M.**
Tétényi, P., Paál, Z.: Reaction centre shift in metal catalyzed reactions 83
Tétényi, P. s. **Dobrovolszky, M. A.**
Teyssié, P. s. **Costa, J.-L.**

Tielen, M. s. **Martens, J. A.**
Tőrös, Sz., Heil, B., Kollár, L., Markó, L.: Enantio- and stereo-selective hydrogenation of ketones with phosphinerhodium catalytic systems 135
Tripathi, S. C. s. **Yadav, H. S.**
Tuba, Z. s. **Mák, M.**

Ungváry, F. s. **Sisak, A.**

Vennik, J. s. **Landuyt, J. P.**
Verbist, J. s. **Maroie, S.**
Vértes, A. s. **Peev, T. M.**
Vít, Z., Kolb, I.: By-products in the preparation of 1,1,1,5-tetrachloropent-3-ene from 1,3-butadiene and tetrachloromethane (Short comúunication) 345

Yadav, H. S., Sengupta, S. K., Tripathi, S. C.: Dioxouranium(VI) complexes of terdentate 16-membered macrocyclic ligands 333

Zauer, K. s. **Simig, Gy.**
Zoorob, H. H. s. **Hammouda, H. A.**

CONTENTS

PHYSICAL AND INORGANIC CHEMISTRY

A possibility of estimation of the changes in the size of particles containing Mössbauer atoms, **T. M. Peev, A. Vértes** 57

Polarographic study of mixed ligand (*n*-butylthioglycolate-oxalate) complexes of cadmium(II), lead(II) and thallium(I), **K. Gupta, K. K. Sharma** 65

ORGANIC CHEMISTRY

Synthesis of vinca alkaloids and related compounds, XX. Oxidative cleavage of C—C bonds of an indoloquinolizidine derivative (Short communication), **Gy. Kalaus, I. Katona, M. Kajtár-Peredy, L. Szabó, Cs. Szántay** 3

^{13}C- and ^{1}H-NMR study of tetrahydro-3,5-dialkyl-1,3,5-thiadiazin-2-thiones. A large thione anisotropy effect, **G. Szalontai, J. Dudás** 7

Simple and condensed β-lactams, II. The synthesis of new diethyl 4-oxoazetidine-2,2-dicarboxylates and some manipulations of their functional groups and *N*-substituents, **Gy. Simig, J. Fetter, Gy. Hornyák, K. Zauer, G. Doleschall, K. Lempert, J. Nyitrai, Zs. Gombos, T. Gizur, G. Barta-Szalai, M. Kajtár-Peredy** 17

Substituent effects in ketoferrocenes, **Á. G. Nagy** 33

The mass spectra of nitrogen-containing steroids, III. Bisquaternary salts of piperazinoandrostanes, **M. Mák, J. Tamás, Z. Tuba** 39

Reactions with 4,5-diphenylimidazolidine-2-thione, II, **H. A. Hammouda, S. O. Abd-Allah, H. H. Zoorob** 49

BOOK REVIEWS 71

Acta Chimica Hungarica 119 (1), pp. 3—6 (1985)

SYNTHESIS OF VINCA ALKALOIDS AND RELATED COMPOUNDS, XX*

OXIDATIVE CLEAVAGE OF C—C BONDS OF AN INDOLOQUINOLIZIDINE DERIVATIVE

(SHORT COMMUNICATION)

György KALAUS[1], Ildikó KATONA[1], Mária KAJTÁR-PEREDY[2], Lajos SZABÓ[1] and Csaba SZÁNTAY[1,2]**

([1]Institute of Oragnic Chemistry, Technical University, H-1521 Budapest, Gellért tér 4. and [2]Central Research Institute for Chemistry of the Hungarian Academy of Sciences, H-1025 Budapest, Pusztaszeri út 59—67)

Received March 5, 1984
Accepted for publication July 24, 1984

Earlier [2] the indoloquinolizidine derivative with structure **1a** was described. The oxidation of this compound under mild conditions yields an intermediate (**1b**) of the synthesis of vinca alkaloids [3, 4].

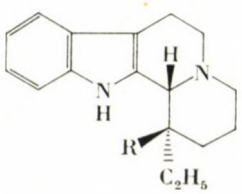

1 a R = CH_2OH
b R = CHO

The reactions of **1a** were investigated in the presence of manganese(IV) oxide and chromium(VI) oxide.

Compound **1a** reacted with activated manganese(IV) oxide in hot acetone slowly; the starting material disappeared from the reaction mixture only after five days. On processing the solution, two well-defined substances were isolated, **2** and **3**, in 1.8 : 1 ratio.

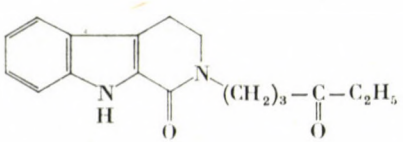

2

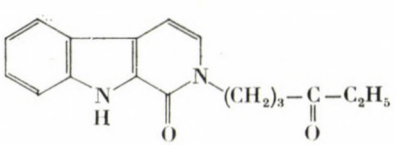

3

* Part XIX: Ref. [1]
** To whom correspondence should be addressed

In the course of the reaction thus an oxidative cleavage of the $C_1—C_{12b}$ linkage occured, and compound **2**, formed during the prolonged boiling, was oxidized partly further into the more stable isocarbostyryl derivative **3**.

Similar results were also obtained when the oxidation was effected with chromium(VI) oxide in pyridine with mild heating, or in a mixture of pyridine and glacial acetic acid at room temperature.

The unusual reaction causing the cleavage of carbon-carbon bonds takes place thus in the presence of both oxidizing agents.

Both derivatives can be reduced to the corresponding alcohols **4** and **5** with sodium tetrahydridoborate(III).

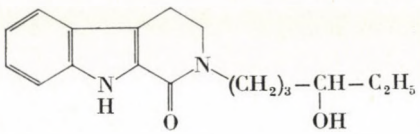

4

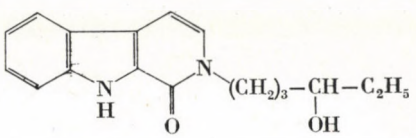

5

Experimental

M.p.'s are uncorrected. The IR spectra were recorded with a Spectromom 2000 instrument, the UV spectra were obtained with a Unicam SP 700 spectrophotometer; the NMR spectra were recorded with a Varian XL-100-15 instrument and a JEOL-LMS-01-SG-2 mass spectrometer was used.

1-(1,2,3,4-Tetrahydro-2-carbolin-1-one-2-yl)-4-hexanone (2) and 1-(1,2-dihydro-2-carbolin-1-one-2-yl)-4-hexanone (3)

(a) Compound **1a** [2] (0.56 g; 2.00 mmol) was dissolved in acetone (40 mL). Activated manganese(IV) oxide (9.00 g; 103.8 mmol) was added to the solution and the mixture was refluxed, with continuous stirring, for five days. At the end of the reaction time, the mixture was filtered while hot and the solvent was evaporated. The residual brown oil was crystallized from methanol to obtain a mixture of **2** and **3** (0.16 g). The mixture was separated by preparative thin-layer chromatography on Kieselgel 60 $PF_{254+366}$ adsorbent of 1.5 mm layer thickness (20 × 20 cm) in two runs, using benzene-methanol (10 : 1) as the developing mixture. After elution and evaporation to dryness, both products were crystallized from methanol. Compound **2** (0.07 g; 12.5%) was a white crystalline substance having the higher R_f value; m.p. 142—143 °C.

$C_{17}H_{20}N_2O_2$ (284.35). Calcd. C 71.80; H 7.09; N 9.85. Found C 72.01; H 6.98; N 10.10%.

IR(KBr): ν_{max} 3240 (ind-NH), 1735 (ketone C=O), 1640 (amide C=O) cm^{-1}.

UV (methanol): λ_{max} (log ε): 224 (4.1116), 239 (3.9858), 300 nm (3.000).

^{1}H-NMR ($CDCl_3$ + DMSO-d_6, 3 : 1): δ 1.00 (3H, t, J = 7.3 Hz, —CO—CH_2—CH_3), 1.94 (2H, m, N2—CH_2—CH_2—CH_2—), 2.40 (2H, q, —CO—CH_2—CH_3), 2.51 (2H, t, N2—CH_2—CH_2—CH_2), 3.04 (2H, t, J = 7.0 Hz, C4—H_2), 3.59 (2H, t, N2—CH_2—), 3.70 (2H, t, C3—H_2), 10.66 (1H, br. s, NH) ppm.

^{13}C-NMR ($CDCl_3$ + DMSO-d_6, 2 : 1): δ 7.73 (—CO—CH_2—CH_3), 20.65 (C4), 21.98 (N2—CH_2—CH_2—CH_2—), 35.72 (—CO—CH_2—CH_3), 39.12 (N2—CH_2—CH_2—CH_2), 45.53 (N2—CH_2—), 47.83 (C3), 112.81 (C8), 117.80) C4a), 161.57 (N—CO—), 210.66 (—CO—) ppm.

MS (m/z): 284 (87), 283 (19), 267 (0.7), 255 (0.9), 237 (0.8), 227 (13), 213 (33), 212 (74), 199 (100), 157 (31), 144 (15), 143 (14), 129 (38), 99 (16), 57 (8.5).

Compound **3** (0.04 g; 7.15%) was a yellow, powder-like substance with the lower R_f value; m.p. 190—192 °C.

$C_{17}H_{18}N_2O_2$ (282.34). Calcd. C 72.31; H 6.42; N 9.92. Found C 72.23; H 6.35; N 10.12%.

IR (KBr): ν_{max} 3160 (ind-NH), 1735 (ketone C=O), 1665 (amide C=O), 1600 cm^{-1} (—CH=CH—).

UV (methanol): λ_{max} (log ε): 236 (4.4048), 256 (4.0086), 264 (3.7824), 282 (3.7134), 294 (3.7323), 318 (3.55.14), 328 (3.6263), 344 nm (3.5465).

^{1}H-NMR ($CDCl_3$): δ 1.01 (3H, t, J = 7.2, Hz, $-CO-CH_2-CH_3$), 2.19 (2H, m, $N2-CH_2-CH_2-CH_2$), 2.40 (2H, q, $-CO-CH_2-CH_3$), 2.54 (2H, t, $N2-(CH_2)_2-CH_2-$), 4.27 (2H, t, $N2-CH_2-$), 6.96 + 7.09 (2H, d, J = 7 Hz, C3—H + C4—H), 7.24 (1H, ddd, J = 8.0 + 7.0 + 1.3 Hz, C7—H), 7.47 (1H, ddd, J = 8.1 + 7.0 + 1.2 Hz, C6—H), 7.68 (1H, ddd, J = 8.1 + 1.3 + 0.7 Hz, C5—H), 7.93 (1H, dm, C8—H), 11.14 (1H, br. s, NH) ppm.

MS: (*m/z*): 282 (73), 265 (5.4), 253 (1.4), 225 (43), 212 (8.2), 211 (11), 199 (11), 198 (19), 185 (50), *184* (100), 129 (10), 99 (18), 57 (21).

(b) Chromium(IV) oxide (1.00 g; 10.0 mmole) was added to anhydrous pyridine (10 mL), with continuous stirring, at 15—20 °C temperature. Then a solution of **1a** (1.00 g; 3.53 mmole) in anhydrous pyridine (10 mL) was added to the yellow suspension. The reaction mixture was stirred for five days at room tepmerature then at 50 °C in a both for 30 h. At the end of the reaction time, water (200 mL) was added to the mixture, it was made alkaline (pH 10—11), with conc. ammonium hydroxide, then extracted with dichloromethane. The organic solution was dried over magnesium sulfate, and evaporated to dryness. The residual oil was crystallized from methanol to obtain a crystalline mixture of **2** and **3** (0.20 g).

Chromatographic separation of the two products gave compounds **2** (0.10 g; 10.0%) and **3** (0.05 g; 5.0%).

(c) Chromium(VI) oxide (2.00 g; 20.0 mmole) was dissolved in a mixture of anhydrous pyridine (12 mL) and glacial acetic acid (8 mL). A solution of **1a** (2.00 g; 7.06 mmol) in anhydrous pyridine (12 mL) and glacial acetic acid (8 mL) was then added. The reaction mixture was allowed to stand at room temperature for 24 h, then diluted with water (250 mL) and made alkaline (pH 10—11) with *conc.* ammonium hydroxide. The mixture was extracted with dichloromethane, the extract was dried over magnesium sulfate then evaporated to dryness. The residual dark brown oil was crystallized from methanol to yield **2**+**3** (0.45 g) in crystalline form.

After chromatographic separation pure **2** (0.20 g; 10.0%) and **3** (0.10 g; 5.0%) were obtained.

1-(1,2,3,4-Tetrahydro-2-carbolin-1-one-2-yl)-4-hexanol (4)

Compound **2** (0.10 g; 0.35 mmol) was dissolved in methanol (8 mL), cooled to 0 °C and sodium tetrahydridoborate(III) (0.10 g; 2.65 mmol) was added in small portions with continuous stirring. After completing the addition, stirring was continued at 0 °C for 30 min then at room temperature for 1 h. The solvent was then evaporated in vacuum, water (20 mL) was added to the residue and the solution was made alkaline (pH 10—11) with 40% sodium hydroxide solution. The aqueous fraction was extracted with dichloromethane, the organic solution dried over magnesium sulfate and evaporated to dryness. The solid residue was rubbed with ether, then filtered off with suction to obtain **4** as a white crystalline product (0.08 g; 79.0%), m.p.: 152—153 °C.

$C_{17}H_{22}N_2O_2$ (286.37). Calcd. C 71.29; H 7.74; N 9.78%. Found C 71.48; H 7.78; N 9.37%.

IR (KBr): ν_{max} 3210 (ind-NH), 1635 cm^{-1} (amide C=O).

UV (methanol): λ_{max} (log ε): 225 (4.3521), 237 (4.2227), 299 nm (4.2355).

^{1}H-NMR ($CDCl_3$): δ 0.93 (3H, t, J = 7.4 Hz, $-CH_3$), 3.03 (2H, t, J = 7.0 Hz, C4—H2), 3.63 (2H, t, $N2-CH_2-$), 3.70 (2H, t, C3—H_2), 9.72 (1H, br. s, NH) ppm.

MS (*m/z*): 286 (44), 269 (1.7), 268 (1.5), 257 (14), 251 (2.3), 228 (4.4), 227 (6.8), 213 (4.4), 212 (4.3), 199 (10), 157 (16), 144 (11), 143 (8.2), 129 (26).

1-(1,2-Dihydro-2-carbolin-1-one-2-yl)-4-hexanol (5)

Compound **3** (0.10 g; 0.35 mmol) was dissolved in methanol (8 mL), cooled to 0 °C and sodium tetrahydridoborate(III) (0.10 g; 2.65 mmol) was added to it in small portions, with continuous stirring. After completing the addition, stirring was continued at 0 °C for 30 min, then at room temperature for 1 h. The solvent was evaporated in vacuum, water (20 mL), was added to the residue and it was made alkaline (pH 10—11) with 40% sodium hydroxide solution. The aqueous fraction was extracted with dichloromethane, the combined organic phases were dried over magnesium sulfate and evaporated to dryness. The solid residue was rubbed with ether then filtered off to obtain **5** as a white crystalline product (0.09 g; 89.5%), m.p. 177—178 °C.

$C_{17}H_{20}N_2O_2$ (284.35). Calcd. C 71.80; H 7.09; N 9.85. Found C 71.83; H 6.91; N 10.02%.

IR (KBr): ν_{max} 3120 (ind-NH), 1660 amide C=O), 1598 cm^{-1} (—CH=CH—).

UV (methanol): λ_{max} (log ε): 237 (4.0667), 256 (3.6532), 264 (3.3710), 283 (3.3180), 294 (3.3180), 332 (3.2201), 346 nm (3.0966).

^{1}H-NMR ($CDCl_3$): δ 0.93 (3H, t, J = 7.5 Hz, $-CH_3$), 3.64 (1H, m, CH—OH), 4.25 (2H, m, N2—CH_2—), 6.96 + 7.09 (2H, d, J = 7 Hz, C3-H + C4—H), 7.24 (1H, ddd, C7—H), 7.46 (1H, ddd, C6—H), 7.62 (1H, d, C5—H), 7.93 (1H, d, C8—H), 10.54 (1H, br. s, NH) ppm.

MS (*m/z*): 284 (50), 267 (9.3), 266 (2.7), 255 (13), 249 (2.3), 226 (5.1), 225 (9.7), 212 (18), 198 (12), 197 (5.7), 184 (100), 167 (15), 129 (7.0).

REFERENCES

[1] Szántay, Cs., Keve, T., Bölcskei, H., Ács, T.: Tetrahedron Lett., **1983,** 5539
[2] Szántay, Cs., Szabó, L., Kalaus, Gy., Kárpáti, E., Szporny, L.: Ger. Offen. 2.520.131; Chem. Abstr., **84,** 90138 (1976)
[3] Oppolzer, W., Hauth, H., Pfäffli, P., Wenger, R.: Helv. Cim. Acta, **60,** 1801 (1977)
[4] Danieli, B., Lesma, G., Palmisano, G.: Gazz. Chim. Ital., **111,** 257 (1981)

Acta Chimica Hungarica 119 (1), pp. 7—16 (1985)

^{13}C- AND ^{1}H-NMR STUDY OF TETRAHYDRO-3,5--DIALKYL-1,3,5-THIADIAZIN-2-THIONES

A LARGE THIONE ANISOTROPY EFFECT

Gábor SZALONTAI* and József DUDÁS

(Research Institute for Heavy Chemical Industries, H-8201 Veszprém, Warta Vince u. 1.)

Received April 13, 1984
Accepted for publication July 24, 1984

^{13}C- and ^{1}H-NMR studies of seven tetrahydro-3,5-dialkyl-1,3,5-thiadiazin-2--thiones were carried out. In the ^{1}H-NMR spectra the diastereotopic protons of the prochiral ring methylene groups remained isochronous even at 195 K indicating a fast ring inversion process. Chemical shift differences of 3.1—3.6 ppm were obtained for H-3' and H-5' protons methine protons attached to the α carbons of the alkyl groups) in the case of the isopropyl and *sec*-butyl derivatives. These differences are attributed to the anisotropic effect of the thione group located in the spatial proximity of H-3'. Supported also by ^{13}C-NMR data, a favoured rotameric form (due to hindered rotation of the $N(sp^2)$-$C(sp^3)$bond) of the 3-alkyl groups has been assumed in these compounds casting doubts on the currently accepted geometry of the thione deshielding cone. The three-bond ^{3}J(HCNH) coupling constants proved to be useful in the determination of the ring stereochemistry.

Introduction

Despite the fact that tetrahydro-3,5-dialkyl-1,3,5-thiadiazine-2-thiones have been widely used as fungicides [1] for long no systematic study on their NMR spectra and stereochemistry has been reported, to our knowledge, so far. Earlier NMR studies [2, 3] on tetrahydro-3,5-dialkyl-1,3,5-thiadiazines **1** showed rapid ring- and nitrogen inversions. According to low temperature

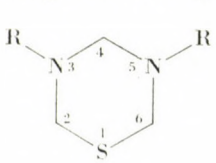

1

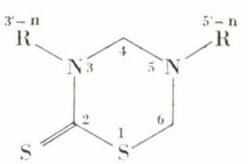

2

	R		R
2a	Me	**2e**	*i*-Bu
2b	Et	**2f**	*s*-Bu
2c	*n*-Pr	**2g**	*n*-Bu
2d	*i*-Pr		

* To whom correspondence should be addressed

measurements [3] the ring inversion barrier lies in the range 38 to 51 kJ mol^{-1} and this barrier decreases as the alkyl group increases in size. The decrease was attributed to the increased steric strain present in the ground state with the increasingly bulky *N*-substituents. In the case of 2-thione derivatives (**2a — g**) the S(1) — C(2) — N(3) — C(4) part of the ring is expected to be planar; ring inversion can occur only through carbons 4 and 6 (Scheme 1).

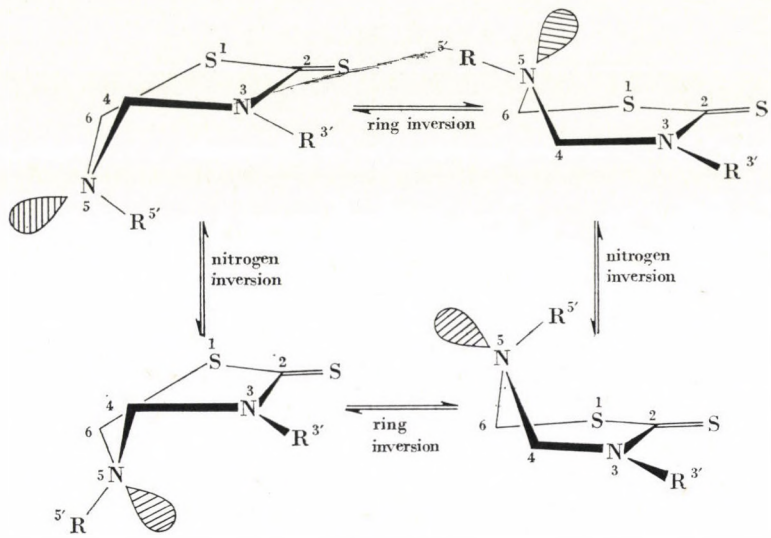

Scheme 1

The more strained nature of ring **2** may increase the interconversion barrier, however, the steric interactions of the R groups existing in all possible conformers may counterbalance this increase.

In this paper we report on the ^{13}C- and ^{1}H-NMR spectra of compounds **2a—g**, their assignments, the strong anisotropic effect of the thione group on H-3' protons, and the possible ring processes.

Proton NMR spectra

The ^{1}H-NMR spectral data of compounds **2a—g** recorded in $CDCl_3$ and C_6D_6 are listed in Table I. At room temperature the H-4 (*a*, *e*) and H-6 (*a*, *e*) methylene protons showed two closely spaced (**2a, b, c, e, g**) or overlapping (**2d, f**) A_2 singulets indicating a fast ring inversion process which renders the otherwise diastereotopic geminal protons isochronous. The correct assignment of these signals to H-4 (*a*, *e*) and H-6 (*a*, *e*) is not obvious. In C_6H_6 the singulets were separated by 0.05—0.25 ppm in all compounds but **2d** and **2f** (see Fig. 1). In the case of **2d** we attempted to separate these, perhaps acci-

Table I

^{1}H-NMR *chemical shifts* ($\delta_{TMS} = 0$ ppm) *of compounds* **2a—g**

Compound		H-4(*a*, *e*)	H-6(*a*, *e*)	H-3'	H-5'	H-3''	H-5''	H-3'''	H-5'''	$\Delta\delta_{H-3'-H-5'}$	$\Delta\delta_{H-3'}$	$CDCl^3$—C^6D^6
2a	a	4.43[c]s	4.38[c]s	3.50 s	2.68 s					0.82		+0.40
	b	3.72 s	3.42 s	3.10 s	2.17 s					0.93		
2b	a	4.43[c]s	4.37[c]s	4.06 q	2.85 q	1.26 m	1.18 m			1.21		+0.40
	b	3.70[c]s	3.44 s	3.66 q	2.34 q	0.92 m	0.73 m			1.32		
2c	a	4.43[c]s	4.40[c]s	3.94 t	2.76 t	1.61 m	1.61 m	0.95 t	0.95 t	1.18		+0.26
	b	3.79[c]s	3.62[c]s	3.68 t	2.40 t	1.45[c]m	1.36[c]m	0.76[c]t	0.73[c]t	1.28		
2d	a	4.42 s	4.42 s	6.23 sp	3.14 sp	1.26 d	1.18 d			3.09		−0.12
	d	3.77 s	3.77 s	6.35 sp	2.95 sp	0.87 d	0.77 d			3.40		
2e	a	4.40 s	4.40 s	3.92 d	2.62 d	2.25 n	1.85 n	1.02 d	0.98 d	1.30		+0.16
	b	3.90 s	3.85 s	3.76 d	2.40 d	2.20 n	1.53 n	0.85 d	0.80 d	1.36		
2f[v]	a	4.45 s	4.45 s	6.13 sx	3.00[e]m	1.60[e]m	0.90[e]t	0.90[e]t	3.13[e]t	3.13		−0.20
	b	3.95 s	3.95 s	6.33 sx	2.75[e]m	1.25[e]m	1.25[e]t	0.75[e]t	0.75[e]t	3.58		
2g[z]	a	4.45 s	4.45 s	4.05 t	2.83 t	1.60 m	1.60 m	1.60 m	1.60 m	1.22		+0.30
	b	3.80 s	3.62 s	3.75 t	2.45 t	1.20 m	1.20 m	1.20 m	1.20 m	1.30		

[a]$CDCl_3$. [b]C_6D_6. [c]May be interchanged. [d]Doublet. [e]Multiplet due to the two diastereomers present. [m]Multiplet. [n]Nonet. [s]Singulet. [sp]Septet. [sx]Sextet. [t]Triplet. [q]Quartet.

[v]R = $-CH^{3'}-(CH_3^{''''}-CH_2^{3''}-CH_3^{3'''}$. [z]R = $-CH_2^{3'}-CH_2^{3''}-CH_2^{3'''}-CH_3^{''''}$

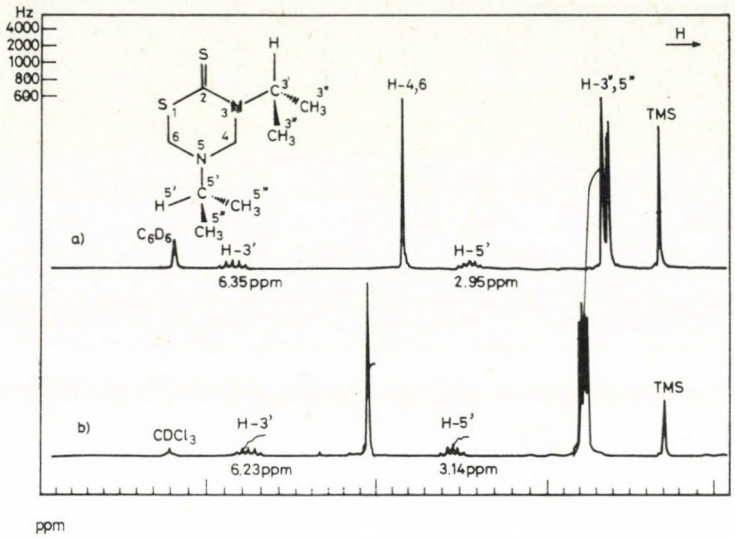

Fig. 1. ^{1}H-NMR spectrum of **2d** (a) in C_6D_6 and (b) in $CDCl_3$

dently, overlapping signals by LIS experiments but without success. We assigned tentatively the lower field signals to H-4 (*a*, *e*) which is in agreement with the ^{13}C-NMR chemical shift order of carbons 4 and 6 (see later), but opposite to that proposed [3] for compound **1**. A possible explanation can be that the thione group may deshield the H-4 (*a*, *e*) protons relative to H-6 (*a*, *e*) the latter being somewhat out of the S(1) — C(2) — N(3) — C(4) plane, irrespectively of the actual conformation. This view is based on the evidence shown by the Dreiding model. In the case of protons H-3' and H-5' (protons attached to carbons α to N-3 and N-5, respectively) the assignments are less ambiguous. The chemical shift difference between them is unexpectedly large in **2d** and **2f**; the 3.40 and 3.58 ppm differences obtained in C_6D_6, respectively, are perhaps among the largest ever observed for such a situation (see Fig. 1). For **2a-c**, **e**, **g** this difference is about 1.20 ppm on average (see Table I for $\Delta\delta_{H-3'-H-5'}$ values). The latter can be readily explained by the deshielding effect of the acidic thioamide nitrogen relative to the amine nitrogen. However, subtracting the same magnitude from the corresponding values of **2d** and **2f**, a low field shift of about 2.0—2.20 ppm of the H-3' protons remains still unaccounted for. Several factors can be considered when looking for possible reasons of this.

(i) We assume that in these compounds the rotation around the N(3) — — C(3) bond is hindered due to the steric repulsion arising between C-3" methyl groups and C-4 (Scheme 2). Furthermore, the N(3) — C(3') bond may have a partial double bond character (N-3 can draw the electrons away from C-3',

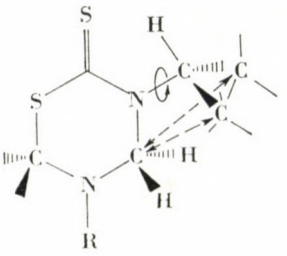

Scheme 2

including partly those of the electron donor methyl groups also), which adds to the rotational barrier and also to the electron deficiency of H-3'.

(ii) If H-3' is fixed in the close vicinity of the C=S bond, its anisotropic effect can be very strong. Ambiguities related to the conventional, *C*, and modified, *M*, geometries of the thione and carbonyl deshielding cone were discussed recently [5]. In Ref. [5] studying two rotameric forms, **A** and **B**, of compound **3**, the lower field H-α signal was assigned to A on the basis of CNDO calculations of H-α 1s electron densities as a function of the H—C_α—S=S dihedral angle (Scheme 3).

In compounds **2d** and **2f** we assume a situation somewhat similar to **3A**; although in these cases the H-3' proton is one bond farther away from the thione group, the spatial distance between them is even smaller than in **3A**. In addition, H-3' should probably be located at the sulphur site of the imaginary straight line passing perpendicularly through the midpoint of the C=S bond (*x* axis in Scheme 4). This was confirmed experimentally by applying the Bhacca—Williams rule [6] for protons of compounds **2a—g**. The $\Delta\delta$H-3'$CDCl_3-C_6D_6$ values (see Table I) were positive for all compounds but **2d** and **2f**, indicating that in these cases the H-3' protons are on the sulphur site, indeed (see Scheme 4).

Considering the assumed rotametric from of **2d** and **2f** for the modified and conventional geometries of the thione deshielding cone, it looks unlikely that the modified one would be valid in this case, unless the thione cone angle were considerably different from that of the carbonyl, as suggested in Ref. [5]

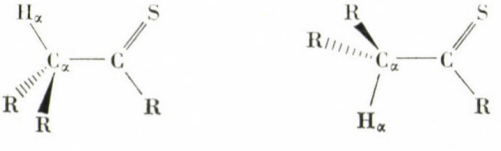

3A **3B**

Scheme 3

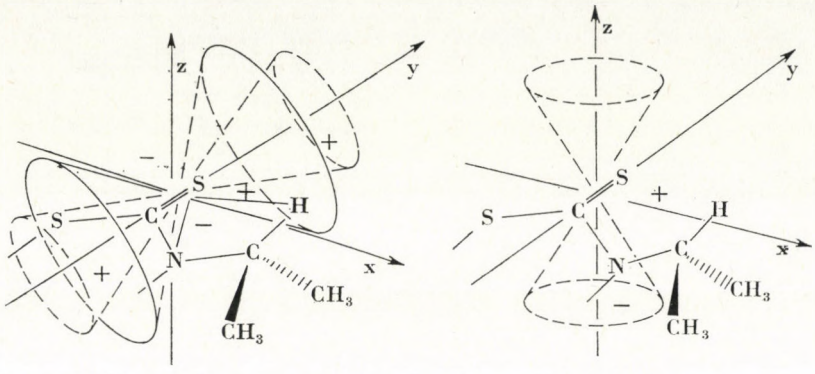

Scheme 4

(see continuous line in Scheme 4) To confirm this, we would need the correct geometry of the favoured conformer.

(iii) Finally, there is a possibility for an intramolecular hydrogen bond between H-3' and one of the sulphur lone pairs which would further deshield H-3'. If so, this hydrogen bond should be rather strong as the high temperature spectra recorded at 373—393 K in DMSO and dioxane, did not show the expected upfield shift of H-3'.

Of these factors the thione anisotropic effect is believed to be dominant; the relative weight of the other two factors, in lack of evidence for the hydrogen bond, cannot be judged.

^{13}C-*NMR spectra*

The C-2 carbon signals appear between 190.8 and 192.6 ppm, as expected. The effect of R groups on these signals is negligible. Contrary to ^{1}H-NMR, the ring methylene carbons, C-4 and C-6 were well separated in the ^{13}C-NMR spectra. Intuitively the C-4 carbons are believed to appear at lower field relative to C-6. To confirm this, the proton coupled spectra were also recorded. These spectra enabled us to make an unambiguous assignment of all carbons and to obtain some insight into the molecular structure and dynamic processes also. The proton coupled spectrum of **2a** is shown in Fig. 2 as an illustrative example.

Several points merit comment. The fine splitting of the lower field triplet (δ 73.0 ppm) is an unresolved multiplet indicating that at least one of the three possible ^{3}J(HCNC) couplings is considerably different from the others in magnitude. At the same time the fine structure of the upper field triplet (δ 60.2 ppm) is a sextet as expected for C-6, provided $^{3}J(H_5, C_5, N_5C_6) \simeq$

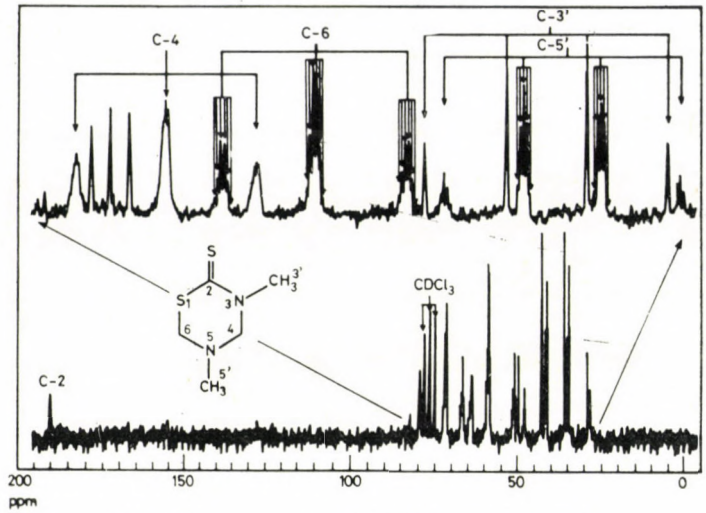

Fig. 2. Proton coupled ^{13}C-NMR spectrum of **2a**

$\simeq {}^3J(H_{4a,e}C_4H_5C_6) \simeq 4.3$ Hz (see Fig. 2). Concerning C-4 this also means that it is the $^3J(H_3, C_3, N_3C_4)$ coupling which is smaller in magnitude, perhaps less positive relative to the other ^3J couplings experienced by C-4. This is in agreement with the expected dihedral angle dependence of these three-bond couplings [7] (see Scheme 5).

As can be seen, from the point of C-6 ring inversion will make the H-4(a, e) protons to exchange sites approximately identical for a Karplus-like relation-

Table II

^{13}C-NMR *chemical shifts* ($\delta_{TMS} = 0$ ppm) *of compounds* **2a—f** *in* $CdCl_3$

Compound	C-2	C-4	C-6	C-3'	C-5'	C-3''	C-5''	C-3'''	C-5'''	C-3''''	C-5''''
2a	191.1	73.0	60.2	40.4	39.1						
2b	190.8	69.0	57.6	46.8	44.4	12.8	11.6				
2c	191.2	70.1	58.1	53.9	51.9	20.7	19.9	11.5	11.2		
2d	191.7	61.7	54.8	49.8	47.6	21.1	18.8				
2e	192.5	71.5	59.5	58.5[c]	58.4[c]	27.3[c]	26.3[c]	20.4[c]	20.2[c]		
2f	192.6	62.3 62.1[c]	54.3 54.6[c]	55.4[c,b]	54.0[cb]	27.2 27.1[c]	26.7 26.6[c]	11.2	9.6	17.3[c]	16.8[c]

[c] May be interchanged. [b] Broadened line. [c] Split into doublet due to the two diastereomers present

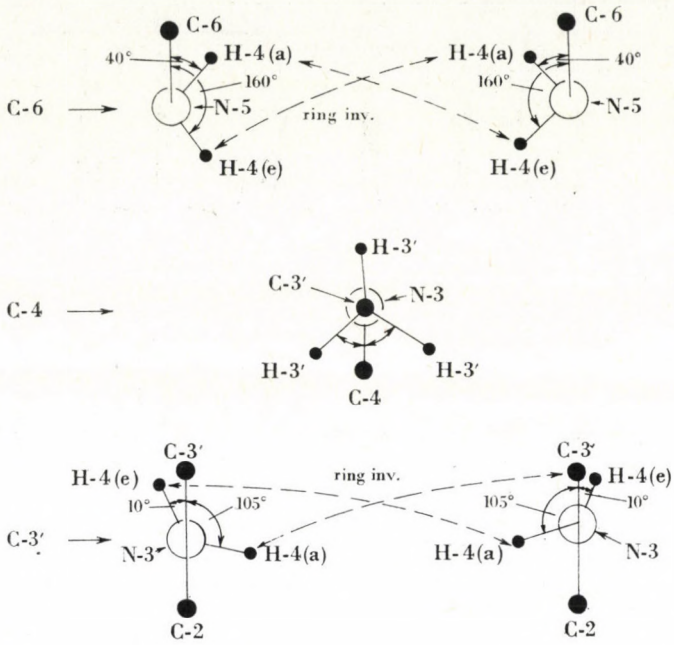

C-5′ *axial* C-5′ *equatorial*

Scheme 5

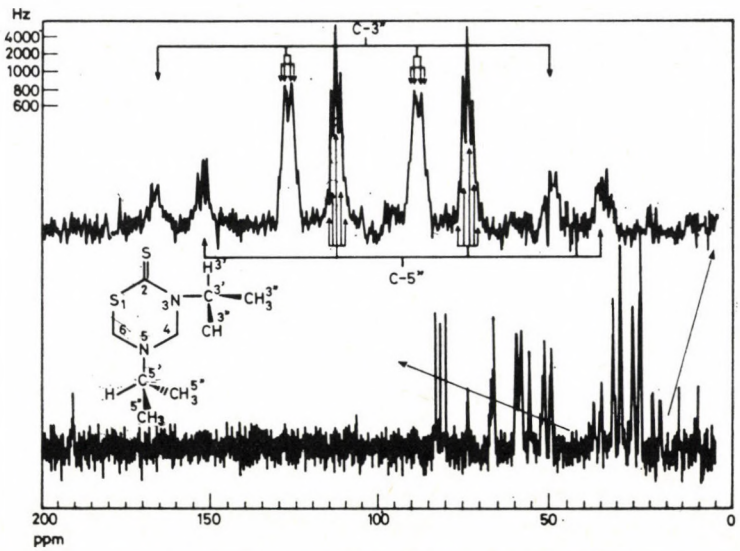

Fig. 3. Proton coupled ^{13}C-NMR spectrum of **2d**

ship. This can explain the observed symmetrical sextet splitting of the C-6 lines. C-3' being fixed in *equatorial* position, C-4 will show a weighted average coupling with the H-3' protons, provided the N(3)—C(3) rotation is free.

Considering C-3', the ring inversion will change the H-4(a, e) protons between non-identical sites (see Scheme5.) which can result in a coupling constant of less than 2 Hz. The observed non-splitting and splitting of the C-3' and C-5' quartets, respectively, in the upfield region of the spectrum (Fig. 2) confirm this assumption.

The same features were observed for all compounds studied. The chemical shifts of C-4 and C-6 in compounds **2d** and **2f** differ significantly from those of the others, they appear at higher field by about 10 and 4 ppm, respectively (Table II). This is a further argument for the preferred rotameric form of the equatorial R group assumed in these compounds (Scheme 3). In a conformation analogous to **3A**, the steric interactions (1,4 — *gauche* interactions) existing between the C-3'' methyl groups and the C-4 carbon (see Scheme 2) may well cause the observed upfield shift of C-4. Similarly, the reason for the 4 ppm upfield shift of C-6 is of steric compression nature.

Another interesting feature of the proton coupled spectrum of **2d** is the different fine splitting pattern of the two methyl quartets (Fig. 3).

The lower field quartet which belongs to carbon C-3'' (proved by selective decoupling experiment) exhibits a multiplet resembling a double quartet, hereas the fine splitting of the upper field quartet C-5'' clearly shows a quintet. These splitting pattern should be governed by the relative magnitude of the ^2J(CCH) and ^3J(CCCH) couplings operational here. Considering the factors [7] which influence their values, we concluded that N-3, being a stronger electron-withdrawer that N-5, makes $^2J(H_3, C_3, C_{3''})$ more positive (i.e. smaller in magnitude, ^2J(HCC) being most probably negative [7]). Thereby C-3'' will appear as a double quartet. At the same time C-5'' appears as a quintet suggesting that in this case $^2J(\mathrm{HCC}) \simeq {}^3J(\mathrm{CCCH}) = 4.5$ Hz. In **2f**, due to the two asymmetric methin carbons (C-3 carons), two diastereomers were expected *(RS, SR* and *SS, RR)*. In accordance with this, the signals of the C-4 and C-6 carbons split into doublets, the C-3' and C-5' signals were broadened and the signals corresponding to C-3'', C-5'', C-3''' and C-5''' were doubled in the proton decoupled spectrum.

Ring conformation

Concerning the ring and nitrogen inversion processes decipted in Scheme 1, we conducted low temperature experiments trying "to freeze out" the possible ring conformers. However, even at 195 K the ^{1}H-NMR spectrum of 2d (recorded at 60 MHz in CS_2) did not show any significant line broadening, that is, the equatorial and axial protons of the prochiral ring methylenes C-4

and C-6 were equivalent, proving that ring inversion is still fast on the NMR time scale. This means a lower inversion barrier (less than 35 kJ mol^{-1}) in comparison with compounds of type 1; this is perhaps due to the steric interactions existing between the R groups in all possible conformers. The N-5 nitrogen inversion is thought to be even faster.

Experimental

Spectroscopy

The recording conditions were as follows: ^{13}C: frequency, 20.1 Hz; instrument, Varian CFT-20; mode, FT; lock, ^{2}H (internal $CDCl_3$); temperature, 302 K; tube size, 10 mm o.d.; solvent and concentration, 100—200 mg for 1.0 mL of $CDCl_3$; standard, internal TMS; pulse conditions, broad band decoupling ($PW = 8$ s, *flip angle* = 42°), aquisition time, 1.024 s; spectral width, 4000 Hz; number of transients, approx. 3000 for the decoupled and 6000 for the coupled spectra; gated decoupling with NOE, accuracy, J $\pm$ 1 Hz, $\pm$0.05 ppm. ^{1}H: frequency, 80 and 60 MHz; instruments, Varian CFT-20 and EM 360 for the variable-temperature experiments; tube size, 5 mm o.d.; solvent and concentration, 50—100 mg for 0.5 mL of $CDCl_3$ and C_6D_6 (CS_2 was used for low and DMSO or dioxane for high temperature experiments); mode, FT and CW, respectively, pulse width in the FT mode (50 s, *flip angle* = 90°); aquisition time, 4.098 s; spectral width, 1000 Hz.

Synthesis

Compounds **2a—g** were synthesized by previously described method [4]. Crystalline reaction products were recrystallized, after drying, from a mixture of chloroform and hexane. Oils were extracted from the reaction mixture with chloroform, dried over $MgSO_4$ and finally the solvent was evaporated under reduced pressure. When necessary, the product was purified by column chromatography.

*

The authors are grateful to Prof. Pál Sohár for stimulating discussions and advice.

REFERENCES

[1] Patents: (a) Union Carbide Corp.: U.S.Pat., 2.838,389. (10 June, 1958); (b) BASF: Ger. Pat., 1,003739. 1957 (Cl 12 p, 10)
[2] Angiolini, L., Jones, R. A. Y., Katritzky, A. R.: Tetrahedron Lett., **1971**, 2209
[3] Angiolini, L., Duke, R. P., Jones, R. A. Y., Katritzky, A. R.: J. Chem. Soc. Perkin Trans. 2, **5**, 674 (1972)
[4] ApSimon, J. W., Graig, W. G., Demarco, P. V., Mathieson, D. W., Nasser, A. K., Sanders, L., Whalley, W. B.: J. Chem. Soc. Chem. Commun., **1966**, 754
[5] Balasubrahmanyan, S. N., Narasimha Bharathi, S., Usha, G. G.: OMR, **21**, 475 (1983)
[6] Williams, D. H., Bhacca, N. S.: Tetrahedron, **21**, 2021 (1965)
[7] Hansen, P. E.: Progress in NMR Spectroscopy, Vol. **14**. pp. 175—296 (1981)

Acta Chimica Hungarica 119 (1), pp. 17—32 (1985)

SIMPLE AND CONDENSED β-LACTAMS, II*

THE SYNTHESIS OF NEW DIETHYL 4-OXOAZETIDINE-2,2-DICARBOXYLATES AND SOME MANIPULATIONS OF THEIR FUNCTIONAL GROUPS AND *N*-SUBSTITUENTS

Gyula SIMIG[1]**, József FETTER[2], Gyula HORNYÁK[1], Károly ZAUER[1], Gábor DOLESCHALL[1], Károly LEMPERT[2], József NYITRAI[2], Zsuzsa GOMBOS[2], Tibor GIZUR[2], Gizella BARTA-SZALAI[1] and Mária KAJTÁR-PEREDY[3]

([1]Research Group for Alkaloid Chemistry of the Hungarian Academy of Sciences, H-1521 Budapest, Gellért tér 4., [2]Department of Organic Chemistry, Technical University Budapest H-1521 Budapest, Gellért tér 4. and [3]Central Research Institute for Chemistry of the Hungarian Academy of Sciences, H-1525 Budapest, P.O.B. 17.)

Received May 22, 1984
Accepted for publication July 24, 1984

A series of new diethyl *N*-aryl- and *N*-aralkyl-4-oxoazetidine-2,2-dicarboxylates **5** has been obtained by the Bose-Sheehan synthesis. The dilactam **7** was similarly synthesized. Partial deethoxycarbonylation of the compounds **5** by Krapcho's method furnished the lactam monocarboxylic esters **9**. Reduction of the ester group of the latter gave the hydroxymethyl derivatives **12**, whose hydroxyl groups were derivatized and replaced to obtain type **13—16** and type **17—27** compounds, respectively. The *N*-substituent of compounds **16c** and **20c** was removed by the peroxydisulfate oxidation method.

The Sheehan—Bose β-lactam synthesis [2, 3] consists, in its original form, in treatment of a dialkyl *aryl*aminomalonate (e.g. **3a**) with chloroacetyl chloride, and base-induced ring closure of the resulting dialkyl *N*-aryl-*N*-chloroacetylaminomalonate (e.g. **4a**) to obtain the corresponding dialkyl 1-aryl-4-oxoazetidine-2,2-dicarboxylate (e.g. **5a**). By replacing chloroacetyl chloride by its homologues and functionally substituted homologues (or those of bromoacetyl chloride), this method is readily extended to the preparation of dialkyl 1-aryl-4-oxoazetidine-2,2-dicarboxylates appropriately substituted in position 3. The starting *aryl*aminomalonates may be replaced by their *alkyl*amino and *aralkyl*amino counterparts; however, the latter are, in general, less readily obtainable from dialkyl halomalonates than the *aryl*amino compounds (see Ref. [1] and references cited therein).

In Part I of the present series the synthesis of some diethyl 3-acetyl-1-aryl- and 3-acetyl-1-aralkyl-4-oxoazetidine-2,2-dicarboxylates, starting with the appropriate diethyl *N*-arylamino- and *N*-aralkylaminomalonates (**1**) and

* For Part I, see Ref. [1]
** To whom correspondence should be addressed

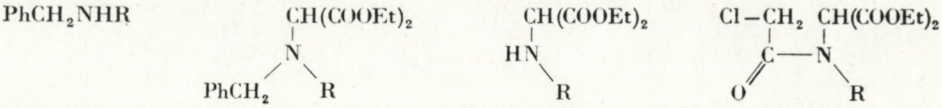

1 (d,f,i)* **2 (d,f,i)*** **3 (b-k)*** **4 (b-f, g', h-k)***

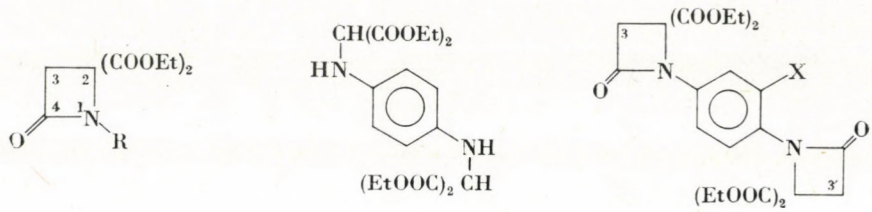

5 (a-f, g', h-k)* **6**

X = H : **7**
X = NO_2: **8**

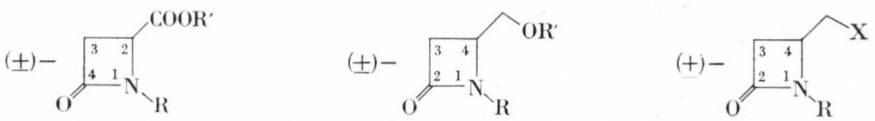

R' = Et : **9 (a-d, h-j)***
R' = H: **10 (e)***
R' = $-CHPh_2$: **11 (e)***

R' = H: **12 (a-c, h)***
R' = $-ONO_2$: **13 (a)*** ****
R' = −Ac: **14 (a)***
R' = −CONHPh : **15 (a)***
R' = $-SO_2Me$: **16 (a-c, j, 1)***

X = Cl: **17 (a)***
X = Br: **18 (a)***
X = I: **19 (a, c, j)***
X = CN: **20 (a, c, j, 1)***
X = $-SCH_2Ph$: **21 (a)***
X = N_3 : **22 (a)***
X = $-N=PPh_3$: **23 (a)***
X = $-N=CHC_6H_4Cl$-4 : **24 (a)***
X = $-{}^{\oplus}NH_3Cl^{\ominus}$: **25 (a)*** ****

: **26 (a)*** ****

X = H: **27 (a)***

a: R = Ph	**h**: R = $-CHPh_2$
b: R = $-CH_2Ph$	**i**: R = $-CH_2-CH_2COOEt$
c: R = $-CH_2C_6H_3(OMe)_2$-2,4	**j**: R = H
d: R = $-CH_2C_6H_3(OMe)_2$-3,4	**k**: R = $-SiMe_3$
e: R = $-CH_2C_6H_4OMe$-4	**l**: R = $-COC_6H_3(OMe)_2$-2,4
f: R = $-CH_2C_6H_2(OMe)_3$-3,4,5	
g: R = $-C_6H_4-NHPh$-4	
g': R = $-C_6H_4-N(COCH_2Cl)Ph$-4	

diketene has been described [1]. With these *N*-substituted diethyl aminomalonates in hand, as well as with other members of this class of compounds (prepared analogously, see Experimental), we have now prepared a series of

* The letters in parentheses indicate new compounds prepared in the course of the present study, or known substances used as starting compounds
** Numbering different from that shown

new diethyl 4-oxoazetidine-2,2-dicarboxylates (**5b—5j**) and studied some possibilities of manipulating their ethoxycarbonyl groups and *N*-substituents.

Among the *N*-substituted diethyl aminomalonates compounds **3d—3i** were new. Compound **3e** · HCl, **3g** and **3h** were obtained by allowing to react diethyl bromomalonate with the appropriate primary aryl- and aralkylamines, in yields ranging from 32 to 65%. Compounds **3d**, **3f** and **3i**, on the other hand, were obtained by reductive debenzylation of the corresponding *N*-benzyl derivatives **2** in yields ranging from 65 to 96%; the latter, in turn, were obtained in yields between 77 and 87% by allowing to react diethyl bromomalonate with the appropriate secondary amines **1**. Chloroacetylation of the compounds **3d—3i** as well as of their known [1] analogues **3b** and **3c** presented no difficulties, see Table I. Chloroacetylation of compound **3g** resulted in the introduction of chloroacetyl groups at both nitrogen atoms, i.e. compound **4g'** was obtained.

The chloroacetyl derivatives **4b—4f**, **4g'**, **4h** and **4i** were cyclized to the corresponding *N*-substituted diethyl 4-oxoazetidine-2,2-dicarboxylates **5** by treatment with triethylamine in benzene or chloroform solution, in most cases by refluxing the reaction mixtures, see Table II. Similarly obtained was, starting with tetraethyl (1,4-phenylenediamino)dimalonate (**6**) [4], compound **7** which could be nitrated to furnish the mononitro derivative **8**.

Direct cyclization of diethyl (chloroacetylamino)malonate (**4j**) [3, 5] to the *N-un*substituted diethyl 4-oxoazetidine-2,2-dicarboxylate **5j** is, both according to literature [3] and our own experience, not feasible. Compound **5j** was therefore obtained either by oxidative ($K_2S_2O_8$) removal of the *N*-substituent of compounds **5c**, **5e** and **5f** in 38—52% yield, or by silylating compound **4j** with *N,O*-bis(trimethylsilyl)acetamide [6] and subjecting the resulting compound **4k** to ring closure under the usual conditions; during work-up the *N*-trimethylsilyl group of initially formed compound **5k** was removed by hydrolysis, and compound **5j** was obtained in an overall yield of 40%.

Partial de(ethoxycarbonylation) of compounds **5a—5d**, **5h** and **5i** to the corresponding racemic monoesters **9** was carried out by Krapcho's method [7], see Table III. Compound **9a** had been obtained before by partial alkaline hydrolysis of compound **5a** and subsequent decarboxylation of the resulting ethyl hydrogen 4-oxo-1-phenylazetidine-2,2-dicarboxylate; the product was described as an oil (in contrast, we have found compound **5a** to be crystalline), and no NMR data were given [2].

Attempts at de(ethoxycarbonylation) of the *N-un*substituted compound **5j** under conditions where its *N*-substituted analogues were successfully de(ethoxycarbonylated), failed to furnish the required monoester **9j**. The latter was therefore prepared by oxidative removal ($K_2S_2O_8$) of the *N*-substituents of compounds **9c** and **9d**.

The ester group of compound **9c** could be selectively hydrolyzed with aqueous-ethanolic sodium hydroxide, the β-lactam ring thereby remaining intact. The resulting carboxylic acid **10c** was subsequently esterified with diazodiphenylmethane to obtain the benzhydrylester **11c**.

Compounds **9a—9c**, **9h** and **9i** were smoothly reduced with $NaBH_4$ in methanol at 0 °C to the corresponding hydroxymethyl derivatives **12**, see Table IV. Compound **12a** had been obtained before by converting acid **10a** [2a] with thionyl chloride into the acid chloride [8], and $NaBH_4$ reduction [9] of the latter in tetrahydrofuran at −78° C, and by B_2H_6 reduction of acid **10a** in tetrahydrofuran [10].

Acetylation with acetyl chloride and phenylcarbamoylation with phenyl isocyanate of compound **12a** furnished the *O*-substituted derivatives **14a** and **15a**, respectively, in good yields. Methylsulfonylation of compounds **12a—12c** with methanesulfonyl chloride in the presence of tertiary amine bases at 0 °C furnished the corresponding derivatives **16**, see Table IV. At elevated temperatures compound **12a** gave, probably via successive replacement of the methylsulfonyl group of the initially formed compound **16a** by chlorine, the chloromethyl derivative **17a**, which had been obtained before by treating compound **12a** with thionyl chloride [10]. The *N-un*substituted derivative **16j** was obtained by oxidative removal ($K_2S_2O_8$) of the *N*-substituent of compound **16c**. In one run the *N*-(2,4-dimethoxybenzoyl)derivative **16l** was obtained as a minor product, in addition to the *N*-unsubstituted compound **16c**.

Reaction of compound **16a** with potassium bromide furnished the bromomethyl derivative **18a**. Similarly obtained were the iodomethyl derivatives **19a**, **19c** and **19j** from the appropriate compounds **16** with sodium iodide. Compound **19j** had been obtained before from the corresponding tosyloxy derivative and sodium iodide [11], and by cycloaddition of allyl iodide and chlorosulfonyl isocyanate [12].

Compound **16a** was allowed to react with a series of nucleophiles including nitrate ions, potassium cyanide, phenylmethanethiol, sodium azide, and pyridine to obtain compounds **13a**, **20a—22a**, and **26a**, respectively. Similarly obtained was, starting with iodide **19c**, the cyanomethyl derivative **20c**. Oxidative removal ($K_2S_2O_8$) of the *N*-substituent of the latter furnished 4-cyanomethylazetidin-2-one (**20j**) (which was identified by comparison with an authentic sample obtained by allowing to react the iodide **19j** with potassium cyanide as described by Tanaka and Miyadera [12]) as the main product, and 4-cyanomethyl-1-(2,4-dimethoxybenzoyl)azetidin-2-one (**19l**) as a minor product.

Catalytic reduction of iodide **19a** furnished 4-methyl-1-phenylazetidin--2-one (**27a**). Finally, the azidomethyl derivative **22a** was converted via the iminophosphorane **23a** and Schiff base **24a** into the aminomethyl derivative, isolated in form of its hydrochloride **25a**.

Experimental

Unless otherwise stated, ^{1}H-NMR spectra were obtained with a Perkin Elmer R 12 spectrometer at 60 MHz. 25.2 MHz ^{13}C- and 100 MHz ^{1}H-NMR spectra were obtained with Varian XL-100 and JEOL FX-100 spectrometers. Except where noted, $CDCl_3$ was used as solvent and Me_4Si as internal reference. IR spectra were recorded with a Spektromom 2000 instrument (Hungarian Optical Works, Budapest).

Benzyl(3,4,5-trimethoxybenzyl)amine (1f)

A mixture of 3,4,5-trimethoxybenzaldehyde (11.8 g; 60 mmol), benzylamine (6.4 g; 60 mmol), dry methanol (80 mL) and dry dioxane (20 mL) was stirred for 20 min at ambient temperature. The mixture was cooled to 0 °C, and $NaBH_4$ (2.25 g; 60 mmol) was added in small portions with continuous stirring at this temperature. Stirring was continued for 20 min at 0 °C, and the mixture was evaporated to dryness. The residue was taken up in ether (40 mL) and water (30 mL) to obtain, after conventional work-up of the ethereal solution, 17 g (98%) of the title compound as an oil which was characterized in form of its crystalline hydrochloride, m.p. 157—159 °C.

$C_{17}H_{22}ClNO_3$ (323.82). Calcd. C 63.06; H 6.85; Cl 10.95; N 4.33. Found C 63.38; H 7.04; Cl 10.44; N 4.60%.

N-Substituted diethyl (benzylamino)malonates (2d, 2f, 2j)

(a) A mixture of benzyl(3,4-dimethoxybenzyl)amine (**1d**) [14] (92.5 g; 0.36 mol), diethyl bromomalonate (86 g; 0.36 mol), triethylamine (36.3 g, 0.36 mol) and ether (200 mL) was stirred for 34 h at ambient temperature. The crystalline product ($Et_3N \cdot HCl$) was filtered off, and the filtrate was evaporated to dryness to obtain 115 g (77%) of crude diethyl *N*-benzyl-*N*-(3,4-dimethoxybenzyl)aminomalonate (**2d**) as an oil.

A 30 g portion of the latter was purified by column chromatography (Kieselgel 60, 0.063—0.200 mm; benzene–acetone, 100 : 1 → 100 : 4) to obtain 25 g (64%) of pure (TLC) **2d**.

$C_{23}H_{29}NO_6$ (415.47). Calcd. C 66.49; H 7.04; N 3.74. Found C 66.65, H 7.02, N 3.40%.

IR (film): 1730, 1240, 1130 cm^{-1}.

^{1}H-NMR: δ 1.3 t + 4.3 q (J = 7 Hz; 2×COOEt), 3.8 s (>C—H), 3.9 s (2×MeO), 4.2 s (2×N—CH_2—Ar), 6.8—7.5 m (8×ArH).

(b) Starting with benzyl (3,4,5-trimethoxybenzyl)amine (**1f**) (16.5 g), diethyl bromomalonate (13.8 g) and triethylamine (5.8 g; 58 mmol, each), 22 g (86%) of diethyl *N*-benzyl-*N*-(3,4,5-trimethoxybenzyl)aminomalonate (**2f**) was similarly obtained as an oil.

$C_{24}H_{31}NO_7$ (445.55). Calcd. C 67.70; H 7.01; N 3.14. Found C 67.50; H 7.24; N 2.88%.

IR (film): 1740, 1240, 1120 cm^{-1}.

^{1}H-NMR δ 1.3 t + 4.15 q (J = 7 Hz; 2×COOEt), 3.78 s (>C—H), 3.8 s (3×MeO), 4.25 s (2×N—CH_2—Ar), 6.6 s (2×ArH), 7.2—7.5 m (5×ArH).

(c) A mixture of ethyl 3-benzylaminopropionate (**1i**) 15 (41.4 g; 0.2 mol) and diethyl bromomalonate (23.9 g; 0.1 mol) was kept for 4 days at ambient temperature to obtain a thick paste which was triturated with ether (200 mL) to furnish 28 g (97%) of **1i** · HBr as a crystalline product. Evaporation to dryness of the ethereal filtrate gave an oil which was taken up in pentane. The insoluble impurities were filtered off, and the filtrate was evaporated to dryness to give 32 g (87%) of diethyl *N*-benzyl-*N*-(2-ethoxycarbonylethyl)aminomalonate (**2i**) as an oil, which was used without further purification in the following step (see below).

IR (film): 1760, 1740, 1720 cm^{-1}.

HCl salt (obtained by treatment with ethereal HCl). m.p. 160 °C.

$C_{19}H_{28}ClNO_6$ (401.86). Calcd. Cl 8.83; N 3.67. Found Cl 9.12; N 3.67%.

N-Substituted diethyl aminomalonates (3d—3i)

(a)Compound **2d** (7.7 g; 18.6 mmol) was reduced in dry ethanolic (100 mL) solution in the presence of an 8% Pd/C catalyst at normal pressure and ambient temperature to obtain, after conventional work-up, 6 g (96%) of diethyl (3,4-dimethoxybenzylamino)malonate (**3d**) as an oil.

HCl salt, m.p. 148—150 °C (from EtOAc).

$C_{16}H_{24}ClNO_6$ (361.82). Calcd. C 53.11; H 6.68; N 3.87. Found C 52.90; H 6.23; N 3.84%.

IR (KBr): 3000—2400, 1740 cm^{-1}.

(b) Similarly obtained were, by hydrogenolysis of the *N*-benzyl groups of compounds **2f** and **2i**, compounds **3f** and **3i**, respectively

Compound **3f**, 60% yield, m.p. 156—157 °C (from EtOH).

$C_{17}H_{25}NO_7$ (355.38). Calcd. C 57.45; H 7.09; N 3.94. Found C 57.76; H 6.65; N 3.63%.

IR (KBr): 3400, 1770, 1250, 1130 cm^{-1}.

^{1}H-NMR: δ 1.3 t + 4.25 q (J = 7 Hz; 2×COOEt), 3.78 s (>C—H), 3.8 s (3×MeO), 4.4 s (N—CH_2—Ar), 6.9 s (2×ArH).

Compound **3i**, 89% yield, oil; IR (film): 3300, 1750—1730 cm^{-1}.

Hydrochloride, 82% yield, obtained by treatment of an ethereal solution of the base with ethanolic HCl, m.p. 156—157 °C (from EtOH–ether).

$C_{12}H_{22}ClNO_6$ (311.77). Calcd. Cl 11.37; N 4.49. Found Cl 11.02; N 4.37%.

(c) 4-Methoxybenzylamine [16] (13 g; 95 mmol) was added to a mixture of diethyl bromomalonate (22.7 g; 95 mmol) and triethylamine (9.6 g; 95 mmol) with vigorous stirring and external ice cooling. The resulting thick paste was stirred for 1 h at about 45 °C. The mixture was diluted with ether (50 mL), the $Et_3N \cdot HBr$ was filtered off and washed with ether, and the combined filtrate and washings were evaporated to dryness The oily residue was taken up in ether (100 mL), and the solution was strongly acidified by dropwise addition of ethanolic HCl to obtain 10 g (32%) of the hydrochloride of diethyl (4-methoxybenzylamino)-malonate (**3e** · HCl), m.p. 87—90 °C (from EtOAc).

$C_{15}H_{22}ClNO_5$ (331.79). Calcd. Cl 10.68; N 4.22. Found Cl 11.10; N 4.27%.

IR (KBr): 3400—2500, 1720 cm^{-1}.

(d) 4-Nitrosodiphenylamine [17] (58.4 g; 296 mmol) was reduced in ethanolic (400 mL) solution with Zn + NH_4Cl (cf. Ref. [18]). The hot solution was filtered into a flask containing diethyl bromomalonate (77 g; 322 mmol), and the mixture was refluxed for 12 h, K_2CO_3 (20 g; 145 mmol) being added during the first 1/2 h. The resulting dark and weakly acidic (pH 6) solution was allowed to cool to obtain 52 g (52%) of crude compound **3g** in the form of crystalline plates, m.p. 80 °C, which gradually decomposed on standing in air and were therefore immediately subjected to chloroacetylation.

IR (KBr): 3350, 1755, 1725 cm^{-1}.

(e) A mixture of diethyl bromomalonate (26.2 g; 109 mmol) and benzhydrylamine (40 g; 218 mmol) was kept, with occasional stirring, for 1 week at ambient temperature. The resulting thick paste was diluted with ether, and the crystalline benzhydrylamine · HBr was filtered off. The filtrate was evaporated to dryness, the residue was taken up in ethanol, and the solution was chilled in a freezer to obtain small amounts of a crystalline product which was filtered off. The filtrate was evaporated to dryness once more to obtain 24.2 g (65%) of diethyl benzhydrylaminomalonate (**3h**), which was used without further purification in the subsequent step (see below).

N-Substituted diethyl chloroacetylaminomalonates (4b—4f, 4h, 4i)

(a) A mixture of diethyl benzylaminomalonate hydrochloride (**3b** · HCl) [1] (30.1 g; 0.1 mol), chloroacetyl chloride (13.6 g; 0.12 mol) and benzene (150 mL) was refluxed for 1 h and evaporated to dryness. The oily residue crystallized when triturated with light petroleum to give 32.5 g (95%) of diethyl *N*-benzyl-*N*-(chloroacetyl)aminomalonate (**4b**), m.p. 53—54 °C (from ether–light petroleum). For the microanalysis results, see Table I.

IR (KBr): 1760, 1740, 1685 cm^{-1}.

^{1}H-NMR: δ 1.2 t + 4.15 q (J = 7 Hz; 2×COOEt), 4.05 s ($ClCH_2CO$), 4.75 s (N—CH_2—Ph), 5.35 a (>C—H), 7.28 s (5×ArH).

(b) Similarly obtained were, starting either with the corresponding compounds **3** or their hydrochlorides, compounds **4c—4f**, **4h** and **4i** (see Table I). IR and ^{1}H-NMR spectra of the products were similar to those of compound **4b**, except for the signals of the groups R in the ^{1}H-NMR spectra.

N-Substituted diethyl 4-oxoazetidine-2,2-dicarboxylates (5b—5f, 5g', 5h and 5i)

(a) A mixture of compound **4b** (34.1 g; 0.1 mol), triethylamine (13.2 g; 0.13 mol) and benzene (100 mL) was stirred for 8 h at ambient temperature, and washed successively with water (100 mL), 10% aqueous HCl (50 mL) and water (100 mL). The dry residue of the organic phase was purified by distillation at reduced pressure to obtain 23 g (75%) of diethyl 1-benzyl-4-oxoazetidine-2,2-dicarboxylate (**5b**), b.p. 149—150 °C/0.1 torr. For the microanalysis results, see Table II.

Table I

N-Substituted diethyl (chloroacetylamino)malonates **4**

Compound	Yield, %	M.p., °C (recryst. from)	Molecular formula Mol. wt.	Calcd/found, % C	H	Cl	N
4b[a]	95	53—54 (ether-LP[b])	$C_{16}H_{20}ClNO_5$ 341.85	56.21 56.13	5.89 5.94	10.37 10.20	4.10 3.94
4c[a]	66[c]	83—84 (EtOH)	$C_{18}H_{24}ClNO_7$ 401.84	53.80 53.63	6.02 6.26	8.82 8.79	3.49 3.56
4d	70[d]	68—70 (EtOH)	$C_{18}H_{24}ClNO_7$ 401.84	53.80 53.83	6.02 5.74	8.82 8.91	3.49 3.43
4e	90	[e]	$C_{17}H_{22}ClNO_6$ 371.82	54.92 54.45	5.96 5.61	9.53 10.03	3.77 3.89
4f	92[d]	90—92 (EtOH)	$C_{19}H_{26}ClNO_8$ 431.87			8.21 8.60	3.24 3.40
4h	42[f]	98—100 [g]	$C_{22}H_{24}ClNO_5$ 417.86			8.49 8.93	3.35 3.15
4i	86	[e, h]					

[a]For the preparation of the starting compounds **3b** and **3c**, respectively, see Ref. [1]
[b] LP = light petroleum
[c]The oily crude product was crystallized from ethanol
[d]The oily crude product crystallized when triturated with light petroleum
[e]Oily product which resisted all attempts at crystallization
[f]The oily crude product crystallized when triturated with an ether–light petroleum mixture
[g]Non-recrystallized product
[h]The crude product was used without further purification in the following ring closure step

Table II

N-Substituted diethyl **4***-oxoazetidine-2,2-dicarboxylates* **5**

Compound	Yield, %	M.p., °C (Recryst. from)	Molecular formula Mol. wt.	Calcd./found, % C	H	N
5b	75	[a]	$C_{16}H_{19}NO_5$ 305.33	62.94 63.29	6.27 6.75	4.59 4.83
5c[b]	89	52—54 (ether)	$C_{18}H_{23}NO_7$ 365.38	59.17 59.24	6.34 6.24	3.83 3.54
5d	86	[c]	$C_{18}H_{23}NO_7$ 365.38	59.17 58.95	6.34 6.27	3.83 3.85
5e	95	[c]	$C_{17}H_{21}NO_6$ 335.35	60.87 60.98	6.31 6.38	4.18 4.48
5f	85	76—77 (ether)	$C_{19}H_{25}NO_8$ 395.41	57.71 57.35	6.37 6.90	3.54 3.66
5g′	57[d]	89—90 (ether)	$C_{23}H_{26}ClN_2O_6$[e] 458.91	60.20 60.52	5.05 5.20	6.12 6.32
5h	79[f]	65[g]	$C_{22}H_{23}NO_5$ 381.41	69.27 69.08	6.08 6.13	3.67 3.41
5i	93	[c, h]	$C_{14}H_{21}NO_7$ 315.32	53.33 53.33	6.71 6.56	4.44 4.34

[a]B.p.: 149—150 °C/1 torr
[b]B.p.: 175—180 °C/1 torr
[c]Oily product which resisted all attempts at crystallization
[d]Overall yield of the successive reactions **3g** → **4g'** → **5g'**
[e]Cl, cald. 7.72, found 8.30%
[f]The oily crude product crystallized when triturated with light petroleum
[g]Non-recrystallized product
[h]B.p. 166—168 °C/0.6 torr

IR (film): 1760—1730 cm^{-1}.

^{1}H-NMR: δ 1.15 t + 4.0 q (J = 7 Hz; 2×COOEt), 3.38 s (3-H_2), 4.6 s (N—CH_2—Ph). 7.25 s (Ph).

(b) Except that the reactions were carried out by refluxing the reaction mixtures, compounds **5c—5f**, **5h** and **5i** were similarly obtained, see Table II. IR and ^{1}H-NMR spectra of the products were similar to those of compound **5b**, except for the signals of the R groups in the ^{1}H-NMR spectra.

(c) A mixture of crude compound **3g** (25 g; 73 mmol), chloroacetyl chloride (22.4 g; 200 mmol) and dry benzene (160 mL) was refluxed for 5 h. The resulting solution of diethyl {*N*-chloroacetyl-*N*-[4-chloroacetylanilino]anilino}malonate (**4g'**) was evaporated to dryness under reduced pressure. The gummy residue was taken up in dry chloroform (200 mL). Triethylamine (36 g; 360 mmol) was added with continuous stirring and external ice-cooling. The mixture was allowed to stand for 16 h at ambient temperature and evaporated to dryness at reduced pressure. The oily residue was vigorously shaken with water, while *conc.* HCl was added until the aqueous phase became slightly acidic. The aqueous phase was discarded and the oil was washed by decantation with water (2×100 mL) and taken up in ether (20 mL). Crystallization of the resulting compound **5g'**, 17.7 g (56.7%), m.p. 89—90 °C (from ether), was induced by scratching. For the microanalytical results, see Table II.

IR (KBr): 1780, 1750 sh, 1740, 1695 cm^{-1}.

Diethyl 4-oxoazetidine-2,2-dicarboxylate (5j)

(a) A mixture of compound **5c** (9.7 g; 26.6 mmol), $K_2S_2O_8$ (28.7 g; 106 mmol), Na_2HPO_4 · · 2 H_2O (37.8 g; 212 mmole), acetonitrile (120 mL) and water (80 mL) was refluxed for 6 h. $K_2S_2O_8$ (14.4 g) and Na_2HPO_4 · 2 H_2O (18.9 g) were added, and refluxing was continued for 6 h. The mixture was allowed to cool, the crystalline salts were filtered off and washed with EtOAc. The aqueous phase of the filtrate was extracted with EtOAc (50 mL), and the combined organic solutions were dried ($MgSO_4$) and evaporated to dryness. The residue was purified by column chromatography (Kieselgel 60, 0.063—0.200 mm; benzene → benzene–acetone, 7 : 3). The fraction (3.1 g) which contained the desired product **5j** was taken up in CH_2Cl_2 (20 mL) and extracted with 5% aqueous $NaHCO_3$ solution (2×15 mL) to remove the contaminant 2,4-dimethoxybenzoic acid and to obtain 2.2 g (38%) of pure compound **5j** as an oil. For the ^{1}H-NMR spectrum, see below.

(b) A mixture of compound **5e** (1 g; 3 mmol), $K_2S_2O_8$ (3.25 g; 12 mmol), Na_2HPO_4 · · 12 H_2O (8.6 g; 24 mmol), acetonitrile (12 mL) and water (2.8 mL) was stirred at 100—110 °C until the starting compound **5e** was consumed (TLC; Kieselgel G; benzene–acetone, 8 : 2). The mixture was allowed to cool, the inorganic salts were filtered off, and the aqueous phase of the filtrate was extracted with EtOAc (3×10 mL). The dry residue of the combined organic solutions was taken up in CH_2Cl_2 (20 mL), the solution was washed with saturated aqueous NaCl solution (20 mL), and the product, resulting from conventional work-up, was purified by TLC (Kieselgel $PF_{254+366}$; benzene–acetone, 8 : 2) to give 0.3 g (47%) of compound **5j** as an oil.

^{1}H-NMR: δ 1.3 t + 4.2 q (J = 7 Hz; 2×COOEt), 3.4 d (J = 1.5 Hz;* 3-H_2), 7.1 br s (NH).

(c) The same product was obtained in 0.2 g (52%) yield by starting with compound **4f** (0.7 g; 1.8 mmol) and proceeding as described in (b).

(d) Freshly distilled *N*,*O*-bis(trimethylsilyl)acetamide [6] (4.1 g; 20 mmol) was added to a solution of diethyl *N*-chloroacetylaminomalonate (**4j**) [5] (2.5 g; 10 mmol) in anhydrous acetonitrile (6 mL) with continuous stirring. The mixture was kept for 7 h at 80—90 °C, and the solvent and the resulting trimethylsilylacetamide were distilled off at reduced pressure. The residue (which consisted mainly of compound **4k**) was refluxed for 1 h with triethylamine (1.3 g; 13 mmol) in anhydrous benzene (10 mL). The mixture was washed with 1*N* HCl, the aqueous phase was saturated with NaCl and extracted with benzene. The combined benzene solutions furnished an oily residue (2.9 g) which was purified by column chromatography (Kieselgel 60, 0.063—0.200 mm; benzene–acetone, 100 : 2) to give 0.86 g (40%) of compound **5j,** identical (^{1}H-NMR) with samples obtained as described in (a)—(c).

* Long-range coupling with NH proton

Tetraethyl 1,1'-(1,4-phenylene)bis(4-oxoazetidine-2,2-dicarboxylate) (7)

A mixture of tetraethyl (1,4-phenylenediamino)dimalonate (**6**) [4] (18.3 g; 43 mmol), chloroacetyl chloride (15 g; 133 mmol) and dry benzene (100 mL) was refluxed for 14 h and evaporated to dryness. Chloroform (20 mL) was added and the mixture was evaporated to dryness once more. The chloroform (80 mL) solution of the resulting crude *N*,*N*'-di(chloracetyl) derivative was treated with triethylamine (36.2 g; 36 mmol) (added dropwise with continuous stirring and ice-cooling). The mixture was kept for 2 h at 0 °C and for 24 h at ambient temperature, and subsequently evaporated to dryness at reduced pressure. The residue was vigorously shaken with water (100 mL) while dil. HCl was added until the aqueous phase became slightly acidic (pH 6—7). Conventional work-up by extraction with benzene furnished a semisolid product which crystallized when triturated with ethanol (15 mL) to give 21 g (97%) of the title compound, m.p. 131—132 °C (from EtOH).

$C_{24}H_{28}N_2O_{10}$ (504.50). Calcd. C 57.14; H 5.59; N 5.59. Found C 56.93; H 5.88; N 5.31%.

IR (KBr): 1765, 1745, 820 cm^{-1}.

^{1}H-NMR: δ 1.27 t + 4.27 q (J = 7.2 Hz; 4×COOEt), 3.52 s (3-H_2 + 3'-H_2), 7.48 s (4×ArH).

Tetraethyl 1,1'-(2-nitro-1,4-phenylene)bis(4-oxoazetidine-2,2-dicarboxylate) (8)

A solution of compound **7** (4.0 g; 7.9 mmol) in dry CH_2Cl_2 (30 mL) was treated with continuous stirring at ambient temperature successively with fuming HNO_3 (d = 1.5; 0.8 g; 13 mmol) and trifluoroacetic anhydride (15 g; 71 mmol). Stirring was continued for 8 h. After being allowed to stand overnight, the mixture was poured into ice-cold water (30 mL). The two phases were separated, the aqueous phase was extracted with CH_2Cl_2 (2×5 mL), and the combined CH_2Cl_2 solutions were washed with water (5 mL). Conventional work-up furnished an oil which gradually crystallized on standing. Recrystallization from a small amount of ethanol furnished 3.2 g (74%) of the title compound, m.p. 83 °C.

$C_{24}H_{27}N_3O_{12}$ (549.48). Calcd. C 52.46; H 4.95; N 7.65. Found C 52.51; H 5.22; N 7.63%.

IR (KBr): 1760, 1735, 1535, 1340 cm^{-1}.

^{1}H-NMR: δ 1.21 t + 1.30 t + 4.23 q + 4.32 q [J = 7.1 Hz; (2+2)×COOEt], 3.34 s + + 3.40 s (3-H_2 + 3'-H_2), 7.5—8.1 m (3×ArH).

Racemic *N*-substituted ethyl 4-oxoazetidine-2-carboxylates (9a—9d, 9h and 9i)

(a) A mixture of diethyl 4-oxo-1-phenylazetidine-2,2-dicarboxylate (**5a**) [2] (151 g; 0.52 mol), NaCl(36.5 g), DMSO (150 mL) and water (19 ml; 1.04 mol) was stirred for 5 h in an oil bath at 170—180 °C, and subsequently poured into water. After extraction with ether (3×200 mL), the aqueous phase was saturated with NaCl and extracted with ether (3×100 mL) to obtain 106.5 g (94%) of ethyl 4-oxo-1-phenylazetidine-2-carboxylate (**9a**) which gradually crystallized, m.p. 34—36 °C. In some runs the crude product **9a** was purified by distillation at reduced pressure, b.p. 120—130 °C/0.2 torr [2].

IR (KBr): 1730 cm^{-1} (br)

^{1}H-NMR (100 MHz): δ 1.35 t + 4.27 q (J = 7.2 Hz; COOEt), 3.12 + 3.39 (AB part of an ABX spectrum, J_{gem} = 15 Hz, J_{vic} = 3 and 6 Hz, respectively; *trans* and *cis* 3-H, respectively), 4.48 dd (J = 6 and 3 Hz; 2-H), 7.0—7.4 m (Ph).

^{13}C-NMR: δ 14.0 + 61.9 + 169.3 (COOEt), 41.5 (C-3), 50.4 (C-2), 116.7 + 124.3 + + 129.1 + 137.5 (Ph), 162.9 (C-4).

(b) Starting with the appropriate compounds **5**, compounds **9b—9d**, **9h** and **9i** were similarly obtained, except that in some cases the products were purified by distillation at reduced pressure (see Table III). IR and ^{1}H-NMR spectra of the resulting products were similar to those of compound **9a**, except for the signals of the R groups in the ^{1}H-NMR spectra.

Ethyl 4-oxoazetidine-2-carboxylate (9j)

(a) A mixture of compound **9c** (6.0 g; 20.5 mmol), $K_2S_2O_8$ (11 g; 41 mmol), $Na_2HPO_4 \cdot$ $\cdot$ 2 H_2O (14.5 g; 82 mmol), acetonitrile (90 mL), and water (60 mL) was refluxed for 6 h. The phases were separated, the aqueous phase was extracted with benzene (100 mL), and the combined organic phases were washed with saturated aqueous NaCl solution (3×30 mL) to obtain, after conventional work-up, an oil. This was further purified by column chromatog-

Table III

N-Substituted ethyl 4-oxoazetidine-2-carboxylates **9**

Compound	Yield, %	M.p., °C (Recryst. from)	Molecular formula Mol. wt.	Calcd./found, % C	H	N
9a	94	34—36[a]				
9b	75	[b]	$C_{13}H_{15}NO_3$			6.00
			233.26			6.01
9c	90	[c]	$C_{15}H_{19}NO_5$	61.42	6.53	4.77
			293.32	61.25	6.87	4.58
9d	81	[d]	$C_{15}H_{19}NO_5$	61.42	6.53	4.77
			293.32	60.85	6.47	4.75
9h	89	[e]				
9i	43	[f]	$C_{11}H_{17}NO_3$	54.30	7.04	5.75
			243.26	54.17	6.97	5.96

[a]The initially formed oily product slowly crystallized. Non-recrystallized material; b.p. 120—130 °C/0.2 torr [2]

[b]Oily product, b.p. 156—160 °C/0.2 torr

[c]Oily product, b.p. 170—176 °C/0.15 torr

[d]Oily product, purified by TLC (Kieselgel $PF_{254+366}$; benzene–acetone, 7 : 3)

[e]Oily product which was used without further purification in the following reduction step

[f]Oily product, b.p. 145 °C/0.6 torr

raphy (Kieselgel 60, 0.063—0.200 mm; benzene → benzene–acetone, 99 : 1), to obtain 1.21 g (41%) of the title compound as an oil.

IR (film): 3250, 1740 cm^{-1}.

^{1}H-NMR: δ 1.3 t + 4.22 q (J = 7 Hz; COOEt), 3.15 m (3-H_2), 4.15 m (2-H), 6.6 br (NH).

(b) Starting with compound **9d** (1.5 g; 5 mmol), and using the same oxidative de(dimethoxybenzylation) method as described in (a), 0.34 g (45%) of compound **9j**, identical (^{1}H-NMR) with the above product, was obtained.

1-(2,4-Dimethoxybenzyl)-4-oxoazetidine-2-carboxylic acid (10c)

An aqueous (60 mL) solution of NaOH (0.88 g; 22 mmol) was added to an ethanolic (25 mL) solution of compound **9c** (5.8 g; 20 mmol). The mixture was stirred for 2 h at ambient temperature, extracted with ether (3×20 mL), acidified with conc. HCl and extracted with CH_2Cl_2 (3×20 mL) to obtain, after conventional work-up of the CH_2Cl_2 solution, a light yellow crystalline product which was recrystallized from benzene to give 4.0 g (75%) of the title compound, m.p. 124—125 °C.

$C_{13}H_{15}NO_5$ (265.26). Calcd. C 58.86; H 5.70; N 5.28. Found C 58.83, H 5.93, N 5.49%.

IR (KBr): 3500—2300, 1735, 1695 cm^{-1}.

^{1}H-NMR (100 MHz):* δ 3.02 + 3.16 (AB part of an ABX spectrum, J_{gem} = 14.3, J_{vic} = 2.8 and 5.4 Hz, respectively; *trans* and *cis* 3-H), 3.79 s (2×MeO), 3.96 dd (J = 5.4 and 2.8 Hz; 2-H), 4.23 + 4.61 (AB, J = 14.5 Hz; N—CH_2—Ar), 6.4—6.55 m (3'-H + 5'-H), 7.15 d (J = 9 Hz; 6'-H), 10.27 br s (COOH).

Benzhydryl ester (11c): A solution of compound **10c** (0.45 g; 1.7 mmol) in CH_2Cl_2 (2 mL) was treated with a solution of diazodiphenylmethane (0.46 g; 2.4 mmol) in CH_2Cl_2 at 0 °C; the mixture was stirred for 1 h at this temperature and allowed to stand for 1 h at ambient temperature, washed with aqueous $NaHCO_3$ solution, dried ($MgSO_4$) and evaporated to dryness. The residue was crystallized from methanol and the crude product was purified by TLC (Kieselgel $PF_{254+366}$; benzene–chloroform–ethyl acetate, 8 : 1 : 1) to obtain 0.25 g (35%) of the ester, m.p. 64—65 °C.

^{1}H-NMR (100 MHz):* δ 2.91 + 3.10 (AB part of an ABX spectrum, J_{gem} = 14.3, J_{vic} = 2.8 and 5.5 Hz, respectively; *trans* and *cis* 3-H), 3.58 s + 3.77 s (2×MeO), 3.97 dd (J = 5.5 and 2.8 Hz, 2-H), 4.17 + 4.62 (AB, J = 14.5 Hz; N—CH_2—Ar), 6.3—6.45 m (3'-H + + 5'-H), 6.95 s ($OCHPh_2$), 7.03 d (J = 9 Hz; 6'-H), 7.32 s (2×Ph).

* Primed locants refer to the dimethoxybenzyl group

N-Substituted 4-hydroxymethylazetidin-2-ones (12c—12c and 12h)

(a) $NaBH_4$ (12.5 g; 0.33 mol) was added to a methanolic (200 mL) solution of compound **9c** (47.6 g; 0.16 mol) with continuous stirring and external ice-cooling. The mixture was stirred until the starting **9c** was consumed (TLC; 1/2 h) and neutralized with dil. HCl. The solvent was distilled off under reduced pressure, and the product was extracted with EtOAc (5×50 mL) to obtain, after conventional work-up, 39.1 g (96%) of ***N*-(2,4-dimethoxybenzyl)-4-hydroxymethylazetidine-2-one (12c)** as an oil, which was used without further purification in the following step (see below).

IR (film): 3350, 1750—1700 cm^{-1}.

^{1}H-NMR:* δ 2.1 br (OH), 2.85 m (3-H_2), 3.65 m (CH_2OH), 3.82 s + 3.85 s (2×MeO), 4.05 m (4-H), 4.38 s (N—CH_2—Ar), 6.55 m (3'-H + 5'-H), 7.25 d (J = 9 Hz; 6'-H).

(b) Starting with the appropriate esters **9**, compounds **12a**, **12b** and **12h** were similarly obtained (see Table IV). The IR and ^{1}H-NMR spectra of the resulting products were similar to those of compound **12c**, except for the signals of the R groups in the NMR spectra.

4-Acetoxymethyl-1-phenylazetidin-2-one (14a)

Acetyl chloride (0.21 g; 2.7 mmol) was added to a solution of compound **12a** (0.40 g, 2.25 mmol) in pyridine (1 mL). The mixture was stirred for 1 h at ambient temperature and, poured into water (5 mL) to obtain, after conventional work-up by extraction with CH_2Cl_2, 0.32 g (54%) of the title compound, m.p. 74—75 °C (from ether–light petroleum).

$C_{12}H_{13}NO_3$ (219.23). Calcd. C 65.74; H 5.98; N 6.39. Found C 65.85; H 5.90, N 6.67%.

^{1}H-NMR: δ 2.04 (Ac), 2.95—3.20 m (3-H_2), 4.15—4.45 m (4-H + —CH_2O—), 7.0—7.4 m (Ph).

Table IV

N-Substituted 4-hydroxymethylazetidin-2-ones **(12)** *and N-substituted 4-(methylsulphonyloxymethyl)azetidin-2-ones* **(16)**

Compound	Yield, %	M.p., °C (recryst. from)	Molecular formula Mol. wt.	Calcd./found, %			
				C	H	N	S
12a[a]	76	100—102	$C_{10}H_{11}NO_2$	67.78	6.26	7.91	
		(EtOAc-LP[b])	177.20	67.52	6.19	8.20	
12b[c]	86	94	$C_{11}H_{13}NO_2$	69.09	6.85	7.33	
		(EtOAc)	191.22	68.32	6.41	6.98	
12c	96[d]						
12h	73	101—102	$C_{17}H_{17}NO_2$	76.38	6.41	5.24	
		(EtOAc-LP[b])	267.32	76.38	6.27	4.96	
16a	87	86—87	$C_{11}H_{13}NO_4S$	51.75	5.13	5.49	12.56
		(EtOH)	255.28	52.18	5.10	5.38	12.41
16b	71	110	$C_{12}H_{15}NO_4S$	53.50	5.61	5.20	
		(EtOAc)	269.38	53.38	5.77	5.47	
16c[e]	73	71—72	$C_{14}H_{19}NO_6S$	51.05	5.81	4.25	9.74
		(ether)	329.36	51.19	6.07	4.19	9.93

[a]Known compound [9, 10], *lit.* [10] m.p. 98 °C (benzene–light petroleum)

[b]LP = light petroleum

[c]The oily crude product crystallized when triturated with light petroleum to which a few drops of EtOH had been added

[d]Oily product which was used without further purification in the following methylsulfonylation step

[e]The oily crude product slowly crystallized

* Primed locants refer to the dimethoxybenzyl group

1-Phenyl-4-(phenylcarbamoyloxymethyl)azetidin-2-one (15a)

A mixture of compound **12a** (0.20 g; 1.13 mmol), phenyl isocyanate (0.22 g; 1.84 mmol and toluene (2 mL) was refluxed for 2 h. When the mixture was allowed to cool, crystallization of the product started and was completed by the addition of light petroleum to obtain 0.22 g (66%) of the title compound, m.p. 191—192 °C (from ethanol).

$C_{17}H_{16}N_2O_3$ (296.32). Calcd. C 68.90; H 5.44; N 9.46. Found C 68.67; H 5.48; N 9.76%.

IR (KBr): 3320, 1755, 1720 cm^{-1}.

N-Substituted 4-(methylsulfonyloxymethyl)azetidin-2-ones (16a—16c)

(a) Methanesulfonyl chloride (11.7 g; 100 mmol) was added dropwise to a solution of compound **12a** (15 g; 85 mmol) in pyridine (40 mL) with continuous stirring and external ice-cooling. The mixture was stirred for 1 h. Water was added slowly with stirring to obtain 18.8 g (87%) of **4-(methylsulfonyloxymethyl)-1-phenylazetidin-2-one (16a)**, m.p. 86—87 °C (from ethanol).

IR (KBr): 1740, 1340, 1140 cm^{-1}.

^{1}H-NMR: δ 2.9 s ($MeSO_2$), 3.1—3.3 m (3-H_2), 4.3—4.6 m (4-H + $-CH_2O-$), 7.2—7.5 m (Ph).

(b) Starting with the appropriate compounds **12**, compounds **16b** and **16c** were similarly obtained (see Table IV). The IR and ^{1}H-NMR spectra of the resulting products were similar to those of compound **16a**, except for the signals of the R groups in the NMR spectra.

4-(Methylsulfonyloxymethyl)azetidin-2-one (16j)

(a) A mixture of compound **16c** (16 g; 48.6 mmol), $K_2S_2O_8$ (26.3 g; 97.4 mmol) and $Na_2HPO_4 \cdot 2\,H_2O$ (34.5 g; 193 mmol), acetonitrile (240 mL) and water (160 mL) was refluxed for 3 h. The two phases were separated, and the aqueous phase was extracted with ether (5×100 mL). Convertional work-up of the combined organic solutions furnished an oily residue which was crystallized from ethanol (50 mL) to give 4.6 g (53%) of the title compound, m.p. 117—118 °C (from ethanol).

IR (KBr): 3210, 1740—1710, 1340, 1170 cm^{-1}.

^{1}H-NMR (DMSO-d_6, internal reference: DMSO-d_5 = 2.50): δ 2.75 m (3β-H), 2.9 m (3α-H), 3.22 s ($MeSO_2$), 3.85 m (4-H), 4.3 m($-CH_2O-$), 8.15 br (NH). The multiplets at 2.75 and 2.9 ppm are the inner peaks of the AB part of an ABX spectrum, which are further split because of long-range coupling with the NH proton (J_{vic} = 2.8 and 4.7 Hz, respectively, $J_{H-C-C-N-H}$ = 1.1 and 2.0 Hz, respectively; since the low-intensity outer peaks of the AB spectrum are concealed by the DMSO-d_5 and the $MeSO_2$ signal, respectively, J_{gem} could not be determined).

^{13}C-NMR (DMSO-d_6):* δ 36.5 q (Me), 39.8 t (C-3), 44.5 d (C-4), 71.7 t ($-CH_2O-$), 166.5 s (C-2).

MS, *m/z* (rel. intensity): 179 (3; $M^{+\cdot}$), 152 (7), 136 (12; M — HNCO), 97 (15; $MeSO_3H_2^+$), 83 (100; M — $MeSO_3H$), 80 (54; $MeSO_2H^{+\cdot}$), 79, 70 (74; M — CH_2OSO_2Me), 65 (34; SO_2H^+), 58 (56), 57 (88; M — $CHCH_2OSO_2Me$), 43 (78; $HNCO^{+\cdot}$) 42 (24; $H_2C{=}C{=}O^{+\cdot}$).

The *S*-enantiomer of compound **16j** has been described by Merck chemists [13]. ^{1}H-NMR (D_2O): δ 2.88 dd (J = 15 and 2.5 Hz; 3β-H), 3.19 dd (J = 15 and 4.5 Hz; 3α-H), 4.12 m (4-H), 4.43 dd + 4.62 dd (J_{gem} = 11.2, J_{vic} = 6 and 3 Hz, respectively; $-CH_2O-$); MS: 179, 136; m.p. 109.5—110.5 °C.

(b) A mixture of compound **16c** (3.3 g; 10 mmol), $K_2S_2O_8$ (10.8 g; 40 mmol), $Na_2HPO_4 \cdot 2\,H_2O$ (14.2 g; 80 mmol), acetonitrile (60 mL) and water (40 mL) was refluxed for 3 h. The mixture was allowed to cool, and the inorganic salts were filtered off and washed with acetonitrile (20 mL). Conventional work-up by extraction with ethyl acetate furnished an oily product which was successively triturated with ether (2×20 mL) and ethanol (1×50 mL) to furnish 1.1 g (61.5%) of the crystalline compound **16j**, identical with the product obtained as described in (a). When the ethanolic filtrate was allowed to stand at room temperature, 0.20 g (5.8%) of 1-(2,4-dimethoxybenzoyl)-4-(methylsulfonyloxymethyl)azetidin-2-one **(16l)**, m.p. 140—141 °C (from benzene), separated.

$C_{14}H_{16}NO_7S$ (342.34). Calcd. C 49.11; H 4.71; N 4.09. Found C 49.38; H 4.77; N 4.32%.

IR (KBr): 1790, 1640, 1360, 1160 cm^{-1}.

^{1}H-NMR: δ 3.0 s ($MeSO_2$), 3.12 m (3-H_2), 3.82 (2×MeO), 4.4 m (4-H + $-CH_2O-$) 6.45—7.5 m (3×ArH).

* Multiplicities refer to the off-resonance spectra

4-Chloromethyl-1-phenylazetidin-2-one (17a)

Methanesulfonyl chloride (23 g; 0.2 mol) was added dropwise to a refluxing solution of compound **12a** (22.5 g; 0.127 mol) in dry pyridine (50 mL). The mixture was refluxed for 1/2 h and poured into water (400 mL). The resulting crystalline product was recrystallized from ethanol to obtain 13.2 g (53%) of the title compound, m.p. 97—98 °C (from ethanol), *lit.* [10] m.p. 96—97 °C (from light petroleum).

IR (KBr): 1740 cm^{-1}.

4-Bromomethyl-1-phenylazetidin-2-one (18a)

A mixture of compound **16a** (5.0 g; 19.6 mmol), KBr (23 g; 200 mmol), ethanol and water (30 ml, each) was refluxed for 12 h. The solvent was evaporated at reduced pressure. Water (50 mL) was added to obtain 3.8 g (80%) of the title compound, m.p. 105 °C (from ethanol).

$C_{10}H_{10}BrNO$ (240.41). Calcd. C 50.02; H 4.20; N 5.83. Found C 49.79; H 4.18; N 5.65%.

IR (KBr): 1745 cm^{-1}.

4-Iodomethylazetidin-2-ones (19a, 19c, and 19j)

(a) A mixture of compound **16a** (18.8 g; 74 mmol), NaI (18.8 g; 125 mmol) and dry acetone (80 mL) was refluxed for 4 h with continuous stirring. Water (100 mL) was added, and the resulting crystalline product was recrystallized from ethanol to obtain 18.1 g (89%) of **4-iodomethyl-1-phenylazetidin-2-one (19a)**, m.p. 100—101 °C.

$C_{10}H_{10}INO_4$ (287.10). Calcd. C 41.83; H 3.51; I 44.20; N 4.88. Found C 41.61; H 3.85; I 44.77; N 5.07%.

IR (KBr): 1735 cm^{-1}.

^{1}H-NMR: δ 2.80 dd (J = 15.2 and 2.7 Hz; 3β-H), 3.27 dd (J = 15.2 and 5.3 Hz; 3α-H), 3.35 + 3.72 (AB part of an ABX spectrum, J_{gem} = 10, J_{vic} = 2.0 and 2.7 Hz, respectively; CH_2I), 4.15 m (4-H), 7.3 m (Ph).

^{13}C-NMR: δ 6.1 (CH_2I), 44.4 (C-3), 51.2 (C-4), 116.7 + 124.2 + 129.3 + 137.1 (Ph), 162.9 (C-2).

(b) A mixture of compound **16c** (37.5 g; 107 mmol), NaI (56.3 g; 376 mmol) and dry acetone (250 mL) was refluxed for 16 h, another portion of NaI (18.8 g; 125 mmol) being added after 8 h. The solvent was evaporated under reduced pressure, the temperature being maintained below 50 °C, and the dry residue was taken up in water and CH_2Cl_2 (100 mL, each). The aqueous layer was extracted with CH_2Cl_2 (3×50 mL) to obtain, after conventional work up of the combined CH_2Cl_2 solutions 40.3 g (98%) of **1-(2,4-dimethoxybenzyl)-4-iodomethyl-azetidin-2-one (19c)** as on oil, IR (film): 1750 cm^{-1}, which was used without further purification in the following step (see below).

(c) A mixture of compound **16j** (0.6 g; 3.4 mmol), NaI (0.88 g; 5.9 mmol) and dry acetone (5 mL) was refluxed for 10 h, another portion of NaI (0.2 g; 1.3 mmol) being added after 5 h. Water (20 mL) was added and the mixture extracted with ether (5×50 mL) to obtain, after conventional work-up, 0.65 g (91%) of **4-iodomethylazetidin-2-one (19j)**, m.p. 110—111 °C (from EtOAc), lit. [11], m.p. 105—107 °C and [12] 106—106.5 °C. The ^{1}H-NMR spectrum of this product was identical with those published in literature for the racemic compound **19j** [11b, 12] and for the *S*-enantiomer [13].

^{13}C-NMR: δ 11.3 (CH_2I), 44.3 (C-3), 47.9 (C-4), 166.6 (C-2).

4-Oxo-1-phenylazetidin-2-ylmethyl nitrate (13a)

A solution of compound **19a** (8.8 g; 31 mmol) and finely pulverized $AgNO_3$ (6.0 g; 35 mmol) in acetonitrile (40 mL) was kept for 1 week at ambient temperature in the dark. The resulting AgI was filtered off and washed with ether (20 mL), and the combined filtrate and washings were evaporated to dryness at reduced pressure. The oily residue was treated with warm ether (1×70 + 2×20 mL), the insoluble material was filtered off and the combined ethereal solutions were evaporated to dryness to obtain 4.6 g (65%) of the crystalline title compound, m.p. 88 °C (from ethanol–acetone, 1 : 1).

$C_{10}H_{10}N_2O_4 \cdot 1/2\ H_2O$ (231.21). Calcd. C 51.49; H 4.79; N 12.12. Found C 52.30; H 4.95; N 11.83%.

IR (KBr): 1750, 1635, 1275 cm^{-1}.

4-Cyanomethylazetidin-2-ones (20a and 20c)

(a) A mixture of compound **19a** (1.0 g; 3.5 mmol), NaCN (0.4 g; 8 mmol) and DMF (5 mL) was stirred for 24 h at 0 °C, and then poured into saturated aqueous NaCl solution. Conventional work up by extraction with ether (3×30 mL) furnished 0.6 g (91%) of **4-cyanomethyl-1-phenylazetidin-2-one (20a)**, m.p. 97—98 °C (*i*-PrOH).

$C_{11}H_{10}N_2O$ (186.21). Calcd. C 70.95; H 5.41; N 15.04. Found C 71.24; H 5.93; N 15.34%.

IR (KBr): 2270, 1750 cm^{-1}.

(b) A mixture of compound **19c** (1.2 g; 3.3 mmol), NaCN (0.35 g; 7 mmol) and DMF (5 mL) was stirred for 48 h at ambient temperature, and then poured into water (30 mL). Conventional work-up by extraction with ether (5×20 mL) furnieshed 0.6 g (70%) of **4-cyanomethyl-1-(2,4-dimethoxybenzyl)azetidine-2-one (20c)** as an oil.

$C_{14}H_{16}N_2O_3$ (260.29). Calcd. N 10.76. Found N 10.71%.

IR (film): 2270, 1750 cm^{-1}.

4-Cyanomethylazetidin-2-one (20j) and its 1-(2,4-dimethoxybenzoyl) derivative (20l)

A mixture of compound **20c** (13.7 g; 52.6 mmol), $K_2S_2O_8$ (56.4 g; 208 mmol), $Na_2HPO_4 \cdot 2\ H_2O$ (75.1 g; 420 mmol), acetonitrile (165 mL) and water (110 mL) was refluxed for 4 h, and allowed to cool. The inorganic salts were filtered off and washed with acetonitrile (2×20 mL). The aqueous phase of the filtrate was extracted with ethyl acetate (3×100 mL), the combined organic solutions were dried ($MgSO_4$) and evaporated to dryness under reduced pressure. The residue (14.2 g) was worked up by column chromatography (Kieselgel 60, 0.063—0.200 mm, 115 g; toluene–acetone, 10 : 2 → 10 : 3) to obtain the following products in the order of decreasing R_f values: 2,4-dimethoxybenzaldehyde (4.1 g; 47%), **4-cyanomethyl-1-(2,4-dimethoxybenzoyl)azetidin-2-one (20l)** (1.8 g; 14.4%) and **4-cyanomethylazetidin-2-one (20j)** (3.3 g; 57%).

Compound **20l**: m.p. 137—138 °C (from benzene).

$C_{14}H_{14}N_2O_4$ (274.27). Calcd. C 61.30; H 5.14; N 10.22. Found C 61.30; H 5.37; N 10.28%.

IR (KBr): 1815, 1680 cm^{-1}.

Compound **20j** proved identical with an authentic product obtained from the iodide **19j** and KCN as described in Ref. [12].

4-Benzylthiomethyl-1-phenylazetidin-2-one (21a)

A mixture of compound **19a** (1.0 g; 3.5 mmol), phenylmethanethiol (0.62 g; 5 mmol), dry triethylamine (0.5 g; 5 mmol) and anhydrous DMF (5 mL) was allowed to stand for 24 h at ambient temperature. Water (30 mL) and acetic acid (1 mL) were added. An oily product separated which was taken up in ether (20 mL). The aqueous phase was extracted with ether (2×20 mL), and the combined ethereal solutions were washed with water (1×50 + 2×25 mL) and dried ($CaCl_2$). The dry residue was triturated with pentane to obtain 0.76 g (77%) of the title compound, m.p. 89 °C (from EtOH).

$C_{17}H_{17}NOS$ (283.38). Calcd. C 72.04; H 6.05; N 4.94; S 11.31. Found C 71.94; H 6.05; N 4.77; S 11.35%.

IR (KBr): 1740 cm^{-1}.

^{1}H-NMR: δ 2.55 + 2.95 (AB part of an ABX spectrum, J_{gem} = 15 Hz, J_{vic} = 8 and 4.7 Hz, respectively; CH—C**H**$_2$—S), 2.8—3.25 m (3-H$_2$), 3.65 s (S—C**H**$_2$Ph), 3.95 m (4-H), 7.2 m (2×Ph).

4-Azidomethyl-1-phenylazetidin-2-one (22a)

A mixture of compound **19a** (6.0 g; 21 mmol), NaN_3 (2 g; 30 mmol) and anhydrous DMF (30 mL) was stirred for 5 h at 100 °C. Water (120 mL) was added, and the mixture was extracted with ether (1×75 + 2×50 mL). The combined ethereal solutions were washed with water (1×100 + 1×60 mL), dried ($CaCl_2$) and evaporated to dryness at reduced pressure. Pentane (50 mL) was added, and the mixture was once more evaporated to dryness under reduced pressure to obtain 4.2 g (98%) of the title compound as an oil which gradually solidified, m.p. 55—56 °C (ether–pentane).

$C_{10}H_{10}N_4O$ (202.21). Calcd. C 59.39; H 4.98. Found C 59.56, N 5.09%.
IR (KBr): 2200w, 2120, 1730 cm^{-1}.
The same product was obtained by the same procedure in 84 and 74% yields starting with compounds **16a** and **17a**, respectively.

(4-Oxo-1-phenylazetidin-2-ylmethyl)ammonium chloride (25a)

A mixture of compound **22a** (4.2 g; 20.8 mmol), Ph_3P (5.8 g; 22 mmol) and benzene (50 mL) was stirred at ambient temperature until, with the evolution of heat and nitrogen gas, a clear solution resulted. This was diluted with hexane (150 mL) and chilled (0 °C) to obtain 8.4 g (92%) of the iminophosphorane **23a**, m.p. 182 °C.

A mixture of the iminophosphorane **23a**, *p*-chlorobenzaldehyde (3.4 g; 24 mmol) and dry benzene (40 mL) was refluxed for 1 1/2 h. The solvent was evaporated under reduced pressure. Pentane was added to the residue, and the mixture was evaporated to dryness once again to obtain a mixture of the Schiff base **24a** and triphenylphosphine oxide.

This was stirred for 5 h with a mixture of *conc.* HCl (7 mL), methanol (25 mL) and water (50 mL), and then allowed to stand for 24 h at ambient temperature. The triphenylphosphine oxide was removed by extraction with ether (3×80 mL), and the aqueous phase was evaporated to dryness at reduced pressure. Benzene (75 mL) was added, and the mixture was evaporated to dryness once again; this operation was repeated. The solid residue was triturated with ether (35 mL). The insoluble material was dried over P_2O_5 and KOH in vacuum, and recrystallized from *i*-PrOH (25 mL) to obtain 3.05 g (68%) of the title compound as its monohydrate, m.p. 120—122 °C and, after resolidification, 180—182 °C.

$C_{10}H_{13}ClN_2O \cdot H_2O$ (230.69). Calcd. C 52.06; H 6.55; Cl 15.37; N 12.14. Found C 52.26; H 6.82; Cl 16.11; N 11.89%.

IR (KBr): 3450, 3200—2500, 1760 cm^{-1}.

N-(4-Oxo-1-phenylazetidin-2-ylmethyl)pyridinium iodide (26a)

A mixture of compound **19a** (7.0 g; 24 mmol) and freshly distilled pyridine (30 mL, 15 mol-equivalents) was refluxed for 5 h and then evaporated to dryness. The residue was triturated with ether to obtain 8.9 g (100%) of the title compound, m.p. 224—225 °C (from 90% aqueous EtOH).

$C_{15}H_{15}IN_2O$ (366.21). Calcd. C 49.19; H 4.13; I 34.65; N 7.65. Found C 49.52; H 4.54; I 35.26; N 8.00%.

IR (KBr): 1745 cm^{-1}.

4-Methyl-1-phenylazetidin-2-one (27a)

Compound **19a** (1.44 g; 5 mmol) was reduced in ethanolic (150 mL) solution in the presence of a 10% Pd/C catalyst at normal pressure and ambient temperature to obtain, after conventional work-up by preparative TLC (Kieselgel $PF_{254+366}$; benzene–acetone, 7 : 3), 0.35 g (43%) of the title compound as a yellowish oil.

IR (film): 1740 cm^{-1}.

^{1}H-NMR: δ 1.48 d (J = 5.9 Hz; 4-Me), 2.62 + 3.23 (AB part of an ABX spectrum, J_{gem} = 15.4, J_{vic} = 2.7 and 5.9 Hz, respectively; 3-H_2), 4.12 m (4-H), 7.2 m (Ph).

*

The authors are grateful to Dr. I. Balogh-Batta and staff for the microanalyses, to Mrs. L. Székely for the IR, to Mrs. Cs. Szücs for the 60 MHz, to Mr. A. Almásy for the JEOL FX-100 NMR spectra and to Dr. J. Møller (Odense, Denmark) for the mass spectrum of compound **16j**. Financial assistance by Gedeon Richter Chemical Works Ltd. (Budapest) and Biogal Pharmaceutical Works (Debrecen) is gratefully acknowledged.

REFERENCES

[1] Simig, Gy., Doleschall, G., Hornyák, Gy., Fetter, J., Lempert, K., Nyitrai, J., Huszthy, P., Gizur, T., Kajtár-Peredy, M.: Tetrahedron, **41,** 479 (1985)
[2] Sheehan, J. C., Bose, A. K.: J. Am. Chem. Soc., **72,** 5158 (1950)

[3] Sheehan, J. C., Bose, A. K.: J. Am. Chem. Soc., **73,** 1761 (1951)
[4] Ruggli, P., Grand, R.: Helv. Chim. Acta, **20,** 373 (1937)
[5] Goodson, J. J., Wharton, C. J., Wigglesworth, R.: J. Chem. Soc., Perkin Trans. I, **1980,** 2721
[6] Birkofer, L., Ritter, A., Giessler, W.: Angew. Chem., **75,** 93 (1963)
[7] Krapcho, A. P.: Synthesis, **1982,** 805, 893, and earlier references cited
[8] Chatterjee, B. G., Moza, P. N.: J. Med. Chem., **9,** 259 (1966)
[9] Kano, S., Ebata, T., Denta, Y., Hibino, S., Shibuya, S.: Heterocycles **8,** 411 (1977)
[10] Ongania, K.-H., Hohenlohe-Oehringen, K.: Chem. Ber., **114,** 1203 (1981)
[11] Brennan, J., Richardson, G., Stoodley, R. I.: (a) J. Chem. Soc. Chem. Commun, **1980,** 49; (b) J. Chem. Soc., Perkin Trans. I., **1983,** 649
[12] Tanaka, T., Miyadera, T.: Heterocycles, **19,** 1497 (1982)
[13] Christensen, B. G., Ratcliffe, R. W., Salzmann, Th. N., to Merck & Co., Inc.: U.S. Pat., 4,174,316 (Nov. 13, 1979; appl. 933,323, Aug. 14, 1978)
[14] Walter, G. N., Klett, M. A.: J. Med. Chem., **9,** 624 (1966)
[15] Stork, G., McElvain, S. M.: J. Am. Chem. Soc., **69,** 931 (1947)
[16] Goldschmidt, H., Polonowska, N.: Ber. dtsch. Chem. Ges., **20,** 2407 (1887); cf. Lycan, W. H., Puntambeker, S. V., Marvel, C. S.: Organic Syntheses. Coll. Vol. II. p. 139 (Ed.: A. H. Blatt), J. Wiley, New York 1963
[17] Goldschmidt, S., Wurzschmidt, B.: Ber. dtsch. chem. Ges., **55,** 3220 (1922)
[18] Ullmann, F. Dahnen, R.: Ber. dtsch. chem. Ges., **41,** 3744 (1908)

Acta Chimica Hungarica 119 (1), pp. 33—38 (1985)

SUBSTITUENT EFFECTS IN KETOFERROCENES

Ágnes G. NAGY

(Department of Chemistry, Central Research Institute for Physics, H-1525 Budapest 114, P.O.B. 49)

Received May 15, 1984
Accepted for publication July 30, 1984

The effect of the carbonyl group on the redox potential and Mössbauer parameters was studied in ketoferrocenes and chalcone analogous ferrocene derivatives. Interaction of electron-donating and electron-withdrawing substituents and the carbonyl group is discussed and the transmission coefficient of the vinylene is shown. The effect of carbonyl group on the electron population of the molecular orbitals is discussed on the basis of Mössbauer measurements.

Introduction

In the early years of ferrocene chemistry it was revealed that reversible one-electron oxidation of ferrocene to the ferricenium cation was a characteristic reaction of the molecule [1, 2]. This reversible oxidation is effected chemically, anodically or photolytically [3, 4]. The ease of oxidation of ferrocene derivatives was found to be related to the electronic character of the substituents in the cyclopentadienyl rings, thus electron-donating substituents decreased the oxidation potential whereas electron-withdrawing groups had the opposite effect [5—9]. Many research teams have provided correlations of redox potentials with various properties of substituted ferrocenes [10—13]. Analysis of the results showed that the oxidation potentials of the ferrocene derivatives were sensitive to structural and to conformation effects. For example, a correlation was found between the change in molecular geometry and the redox potentials as well as in the Mössbauer parameters of bridged ferrocenes [14, 15]. In the present paper the interaction of some substituents is studied by Mössbauer spectroscopy and cyclic voltammetry in several keto derivatives of ferrocene.

Results and Discussion

The oxidation potentials ($E_{1/2}$)and the Mössbauer parameters of the ferrocene derivatives studied are listed in Tables I and II. The formulas of the ketoferrocenes studied are shown in Fig. 1. It can be seen that the $E_{1/2}$ value of 3--aryl-1-ferrocenyl-2-propene-1-one is considerably higher than that of ferrocene.

Table I

Redox potentials of ketoferrocenes

Compound		$E_{1/2}$ (mV)	ΔE (mV)
Ferrocene	**I**	440 ± 1	—
Ferrocenecarbaldehyde	**II**	723 ± 1	283
Monoacetylferrocene	**III**	682 ± 1	242
Ferrocenyl phenyl ketone	**IV**	689 ± 2	249
3-Aryl-1-ferrocenyl-2-propene-1-one	**V**	685 ± 1	245
1-Aryl-3-ferrocenyl-2-propene-1-one	**VI**	563 ± 1	123
Phenylferrocene	**VII**	473 ± 1	33
1-Aryl-2-ferrocenyl-ethylene	**VIII**	435 ± 2	−5

Table II

Mössbauer parameters of ketoferrocenes

Compound		IS (mm/s)	ΔIS × 10^3 (mm/s)	QS (mm/s)	ΔQS × 10^3 (mm/s)
Ferrocene	**I**	0.432 ± 2	—	2.367 ± 2	—
Ferrocenecarbaldehyde	**II**	0.448 ± 1	+16	2.225 ± 2	−142
Monoacetylferrocene	**III**	0.434 ± 2	+2	2.263 ± 4	−104
Ferrocenyl phenyl ketone	**IV**	0.450 ± 1	+18	2.251 ± 1	−116
3-Aryl-1-ferrocenyl-2-propene-1-one	**V**	0.447 ± 1	+15	2.223 ± 1	−144
1-Aryl-3-ferrocenyl-2-propene-1-one	**VI**	0.438 ± 2	+6	2.219 ± 5	−148
Phenylferrocene	**VII**	0.445 ± 1	+13	2.297 ± 3	−70
1-Aryl-2-ferrocenyl-ethylene	**VIII**	0.446 ± 1	+14	2.306 ± 3	−61

The carbonyl group in the α position in relation to the cyclopentadienyl ring increases significantly the redoxpotential of the iron component in the ferrocenyl moiety. Considering the $E_{1/2}$ of monoacetylferrocene (Table I), we can see that the $E_{1/2}$ values of these two compounds are very near to each other, which means that the vinylene group and the phenyl group located far from the ferrocenyl are not able to modify significantly the effect of the carbonyl group on the ferrocenyl moiety (see Fig. 1). The $-CH=CH-C_6H_5$ "substituent" directly bonded to the ferrocenyl moiety decreases the $E_{1/2}$ value of ferrocene by 5 mV (Table I **VIII**); this means that the $-CH=CH-C_6H_5$ group is an electron-donating "substituent". The dominant rule of the carbonyl is also confirmed by the $E_{1/2}$ value of phenylferrocenylketone (689 mV), which surpasses the redoxpotentials of the monoacetylferrocene and the 3-aryl-1-ferrocenyl-2-propene-1-one by only a few mV. The phenyl group itself is a relatively weak electron-withdrawing substituent, which, as a direct substituent, increases the $E_{1/2}$ of ferrocene by 33 mV (see Table I). If we compare the $E_{1/2}$ values of the three ferrocene derivatives (**III**, **IV** and **V** in Table I), it is obvious that in spite of the small ΔE values, the trend of the redox potentials

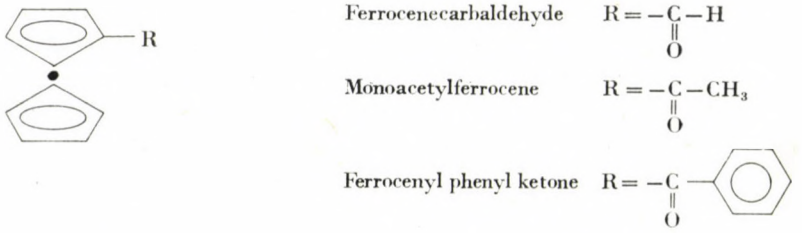

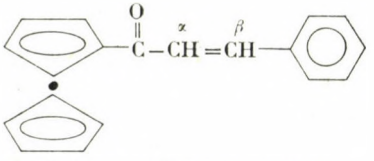

3-aryl-1-ferrocenyl-2-propene-1-one

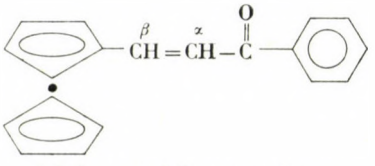

1-aryl-3-ferrocenyl-2-propene-1-one

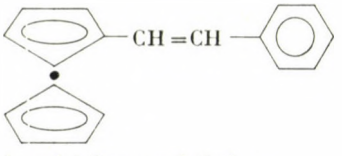

1-aryl-2-ferrocenylethylene

Fig. 1. The ferrocene derivatives studied (In each case the dark dot represents the iron atom)

is in good agreement with the properties of the substituents, i.e. that the phenyl group is an electron-withdrawing substituent and the methyl group is an electron-donating one.

The $E_{1/2}$ of 1-aryl-3-ferrocenyl-2-propene-1-one surpasses the $E_{1/2}$ of the ferrocene by 123 mV (Table I). Consequently, the carbonyl group is able to influence the ferrocenyl moiety even via the double bond. Judging from our measurements, the transmission coefficient of the double bond is 0.501. This value is in good agreement with the transmission coefficient (0.51) obtained by ^{1}H NMR measurements of chalcones [21]. Thus $\sim$50% of the inductive effect of the carbonyl can reach the ferrocenyl through the vinylene radical.

The chemical shifts of H_α and C_α in both compounds (Fig. 1) were found at higher fields than those of H_β and C_β, similar to the chemical shifts found for the benzene chalcones in their H^1 and C^{13} NMR spectra [22, 23]. This is caused by the polarization of the double bond by the carbonyl group. The chemical shifts of C_β in 3-aryl-1-ferrocenyl-2-propene-1-one and H_α and C_α in 1-aryl-3-ferrocenyl-2-propene-1-one are at higher fields than in the analogous benzene chalcones, explainable by the strong electron-donating character of the ferrocenyl group [24].

In our previous work on the keto derivatives of bridged ferrocenes it was suggested that consideration be given to the different contributions of the bridges without ketone to the redox potentials [17]. In the case of monoacetylferrocene, for example, the ΔE value is 287 mV if, instead of the ferrocene $E_{1/2}$, the potential of ethylferrocene is considered for the calculation of ΔE value. The ethyl group thus donates 55 mV [17]. The ΔE value of 287 mV for the monoacetylferrocene is near to that of the carbonyl in ferrocenylcarbaldehyde and fits well with the set of ΔE values obtained in the keto derivatives of bridged ferrocenes [17]. In reality, such treatment of the results is possible only in a few cases because the reduced pair of ketoferrocenes is not always available.

If one compares the ΔE values and the Mössbauer parameters of phenylferrocene, stilbene analogous ferrocene and the ketoferrocenes, it can be concluded that the carbonyl plays a significant role in the electron density distribution of these compounds. The quadrupole splittings (QS) for all of these compounds (Table II) are found to be smaller than the QS of ferrocene whereas the isomer shifts (IS) are a little higher than the IS value of ferrocene. The effect of the $-CH=CH-C_6H_5$ and the phenyl groups on the QS is illustrated by compounds **VII** and **VIII**. The ΔQS values are only -70 and -61 mm/s respectively. As shown in Table II the decrease in the QS values in the carbonyl-containing derivatives is higher than these values. (This does not mean, of course, that the effects of CO and $-CH=CH-C_6H_5$ or $-C_6H_5$ on the Mössbauer parameters are regarded as being additive. The QS values of **II** and **V** also contradict the additivity.) A similar effect of the carbonyl on the Mössbauer parameters was observed for the keto-derivatives of bridged ferrocenes as well [25]. These observations support the assumption that the electron-withdrawing effect of the carbonyl increases the population of the $\varepsilon_1(d_{xz}, d_{yz})$ molecular orbital (MO) [26]. According to MO calculations for ferrocene, the contribution of the ε_1 population to the QS value is -2.7 mm/s; the contribution of $\varepsilon_2(d_{xy}, d_{x^2-y^2})$ is $+5.4$ mm/s [27, 28, 29]. Consequently, a decrease in the ε_2 population should be accompanied by a decrease in IS because of the decreased shielding effect of d electrons on the s electron density at the nucleus [30]. Since the IS values of these compounds are higher than that of ferrocene, it is probable that the ε_2 is not involved in the effect of the carbonyl group.

Experimental

Methods

The Mössbauer spectra of the compounds were recorded at room temperature by means of a constant acceleration spectrometer using a ^{57}Co source in a chromium matrix. The Mössbauer parameters were evaluated by the least squares method. Metallic iron was used for the calibration of the velocity scale. From three to five measurements were made for each sample. The relative errors of QS and IS values are given in Table II.

Electrode pontential measurements

Electrode potentials for the one-electron oxidation of the ferrocenes to their respective cations were measured by cyclic voltammetry [16]. A three-electrode cell was used in which the working and auxiliary electrodes were platinum and the reference electrode was Ag/AgCl (sat). The solutions were 0.1 mol/dm^3 tetrabutylammonium perchlorate in acetonitrile which had been dried over molecular sieves. The potentiostat (type OH-105) was a Radelkis (Hungary) products. The measurement were made at a scan rate of 66 mV/s. Ferrocene and phenylferrocenylketone were used as internal standards to eliminate systematic error. The utilization of internal standard increases the accuracy of cyclic voltammetry [17, 18].

Materials

Ferrocene analogues of chalcones were prepared by base catalyzed aldol condensation according to Ref. [19]. These compounds were purified by repeated crystallization from ethanol. Purities of compounds were checked by their melting points, thin layer chromatography (TLC) and IR spectra. The monoacetylferrocene was prepared by the method of Rosenblum [20]. It was purified by sublimation. Purity was checked by its melting point and TLC. Except for phenylferrocene and **VIII**, all the other compounds were purchased from Ventron Corporation (FRG). The phenylferrocene and the stilbene analogues ferrocene were donated by Prof. S. Toma.

*

The author is indebted to Professor S. Toma (Comenius University, Bratislava, Czechoslovakia) for donating the phenylferrocene and compound **VIII** and to Miss A. Szuja for her technical assistance.

REFERENCES

[1] Kuwana, T., Bublitz, D., Hoh, G.: J. Am. Chem. Soc., **82,** 5811 (1960)
[2] Masson, J. G., Rosenblum, M.: J. Am. Chem. Soc., **82,** 4206 (1960)
[3] Rosenblum, M.: Chemistry of the Iron Group Metallocenes, Part I. Interscience, New York 1965
[4] Gubin, S. P., Perevalova, E. G.: Dokl. Akad. Nauk SSSR, **143,** 1351 (1962); Perevalova, E. G., Gubin, S. P., Smirnova, S. A., Nesmeyanov, A. N.: ibid., **147,** 384 (1962)
[5] Hoh, G. L. K., McEven, W. E., Kleinberg, J.: J. Am. Chem. Soc., **83,** 3949 (1961)
[6] Hall, D. W., Hill. E. A., Richards, J. H.: J. Am. Chem. Soc., **90,** 4972 (1968)
[7] Hall, D. W., Russell, C. D.: J. Am. Chem. Soc., **89,** 2316 (1967)
[8] Little, W. F., Reilley, C. N., Johnson, J. D., Sanders, A. P.: J. Am. Chem. Soc., **86,** 1382 (1964)
[9] Little, W. F., Reilley, C. N., Johnson, J. D., Lynn, K. N., Sanders, A. P.: J. Am. Chem. Soc., **86,** 1376 (1964)
[10] Henning, H., Gürtler, O.: J. Organometal. Chem., **11,** 307 (1968)
[11] Gorton, J. E., Lentzner, H. L., Watts, W. E.: Tetrahedron, **27,** 4353 (1971)
[12] Barr, T. H., Watts, W. E.: Tetrahedron, **24,** 3219 (1969)
[13] Lentzner, H. L., Watts, W. E.: Chem. Commun., **1970,** 906
[14] Nagy, Á. G., Dézsi, I., Hillman, M.: J. Organometal. Chem., **117,** 55 (1976)
[15] Hillman, M., Nagy, Á. G.: J. Organometal. Chem., **184,** 433 (1980)
[16] Adams, R. N.: Electrochemistry at Solid Electrodes. Dekker. Inc., New York 1969
[17] Fujita, E., Gordon, B., Hillman, M., Nagy, Á. G.: J. Organometal. Chem., **218,** 105 (1981)
[18] Gritzner, G., Rechberger, P.: J. Electroanal. Chem., **114,** 129 (1980)
[19] Toma, S.: Collect. Czech. Chem. Commun., **34,** 2771 (1969)

[20] Rosenblum, M., Woodward, R. B.: J. Am. Chem. Soc., **80,** 5443 (1958)
[21] Silver, N. L., Boykin, D. W.: J. Org. Chem., **355,** 759 (1970)
[22] Solcaniová, E., Toma, S., Gronowitz, S.: Org. Magn. Reson., **8,** 439 (1976)
[23] Solcaniová, E., Toma, S., Fiedlerová, A.: Org. Magn. Reson., **14,** 181 (1980)
[24] Solcaniová, E., Toma, S.: Org. Magn. Reson., **14,** 138 (1980)
[25] Nagy, Á. G.: J. Organometal. Chem., **270,** 327 (1984)
[26] Neshvad, G., Roberts, R. M. G., Silver, J.: J. Organometal. Chem., **236,** 349 (1982)
[27] Turta, K. I., Stukan, R. A., Goldanskii, V. I., Volykenai, N. A., Sirotkina, E. I., Bolesova, I. N., Iozaeva, L. S., Nesmeyanov, A. N.: Teor. Eksp. Khim., **7,** 1971 (1970)
[28] Shustorovich, E. M., Dyatkina, M. E.: Dokl. Akad. Nauk SSSR, **131,** 113 (1960)
[29] Shustorovich, E. M., Dyatkina, M. E.: Dokl. Akad. Nauk SSSR, **133,** 141 (1966)
[30] Vértes, A., Korecz, L., Burger, K.: Mössbauer Spectroscopy. Akadémiai Kiadó, Budapest 1979

Acta Chimica Hungarica 119 (1), pp. 39—47 (1985)

THE MASS SPECTRA OF NITROGEN-CONTAINING STEROIDS, III*

BISQUATERNARY SALTS OF PIPERAZINOANDROSTANES

Marianna MÁK[1], József TAMÁS[1]** and Zoltán TUBA[2]

([1]Central Research Institute for Chemistry, Hungarian Academy of Sciences, H-1025 Budapest, Pusztaszeri út 59—67, and [2]Chemical Works of Gedeon Richter Ltd., H-1103 Budapest, Gyömrői út 19/21.)

Received March 21, 1984
Accepted for publication August 6, 1984

The applicability of the electron impact technique to elucidate structural problems of bisquaternary ammonium salts is demonstrated by describing the mass psectrometric features of 2β,16β-bis(4',4'-dimethyl-1'-piperazino)-3α,17β-diacetoxy-5α-androstane dibromide (Arduan®, **1a**) and its isomers and derivatives (eight bis-quaternary salts altogether). The mass spectrometric behaviour of these compounds was found to be very similar to that of the monoquaternary ammonium salts.

The evaporation of the sample is always preceded by quantitative "in situ" dealkylation and the mass spectrum gives information about the structures of the evaporated products; the mass spectra of the bases resulting from the decomposition are characteristic of the positional isomerism, and significant differences are observed even among the stereoisomers.

This technique — completed with the determination of the relative amounts of the decomposition products — seems to be suitable to establish the number and the positions of the quaternary centres and to decide the nature of the quaternary groups in compounds of this type.

Introduction

Mass spectrometry has long been used for the study of monoquaternary salts of various amines [1—3]. These compounds, as crystalline salts, can be evaporated in the electron impact (EI) ion source only at relatively high temperatures, after suffering thermal decomposition. Hence the EI technique provides direct information only about the mixture of the evaporated decomposition products. As this thermal decomposition process for ammonium salts is generally very simple and the volatile products are characteristic of the original compound, conclusions can also be drawn from the results obtained as to the structure of the salt [1].

Some recent special ionization methods, such as the field desorption (FD) technique [4, 5], secondary ion mass spectrometry (SIMS) [6, 7], laser desorption technique (LD) [8, 9], fast atom bombardment (FAB) [10], field desorption in conjunction with collisionally activated dissociation (FD CAD)

* Part II: M. Mák, J. Tamás, A. Vedres and Cs. Szántay: Acta Chim. Acad. Sci. Hung., **111**, 397 (1982)

** To whom correspondence should be addressed

[11—15], make the direct ionization of the intact salts possible, without prior evaporation.

The only bisquaternary ammonium salt, the EI mass spectrum of which has already been published is c(I)-curanine dichloride [16], although knowledge of the mass spectrometric behavior of this group of compounds may be of great importance in the structural analysis of compounds with two or more amine functions and of their derivatives.

This paper demonstrates the utility of the EI technique to elucidate structural problems of bisquaternary ammonium salts. Different bis(4',4'--dialkyl-1'-piperazino)diacetoxy-5α-androstane dibromides ($K^{++}(Br^-)_2$; **1—3**) were chosen as model compounds, among which **1a** is well known, because of its high neuromuscular blocking activity [17], under the name pipecuronium bromide (ARDUAN®). Using the model system selected, the EI technique proved to be suitable to afford detailed information about the structure of these salts, and to study the effects of the positional and stereoisomers and of the nature of the 4'-alkyl group on the mass spectra.

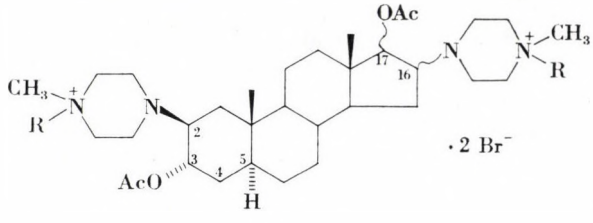

1

	R	16-H	17-H
1a	CH_3	α	α
b	CH_3	α	β
c	CH_3	β	β
d	CD_3	α	α
e	C_3H_5	α	α
f	C_3H_7	α	α

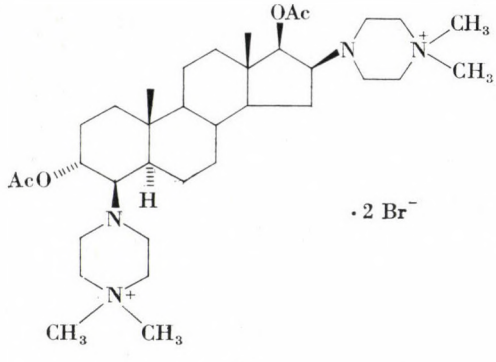

2

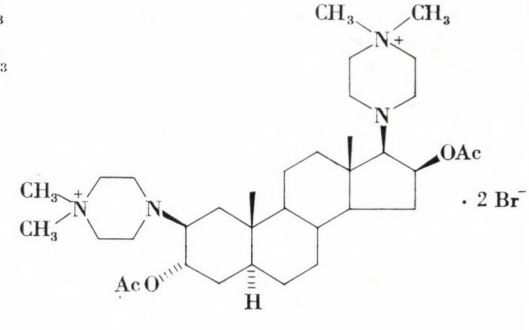

3

Results and Discussion

In the mass spectrum of **1a** (Fig. 1) two products formed by thermal dealkylation from the doubly-charged cation (K^{++}) of the salt can be detected. These products are CH_3Br (*m/z* 94, 96) and the amine base itself ($K^{++}(Br^-)_2$—

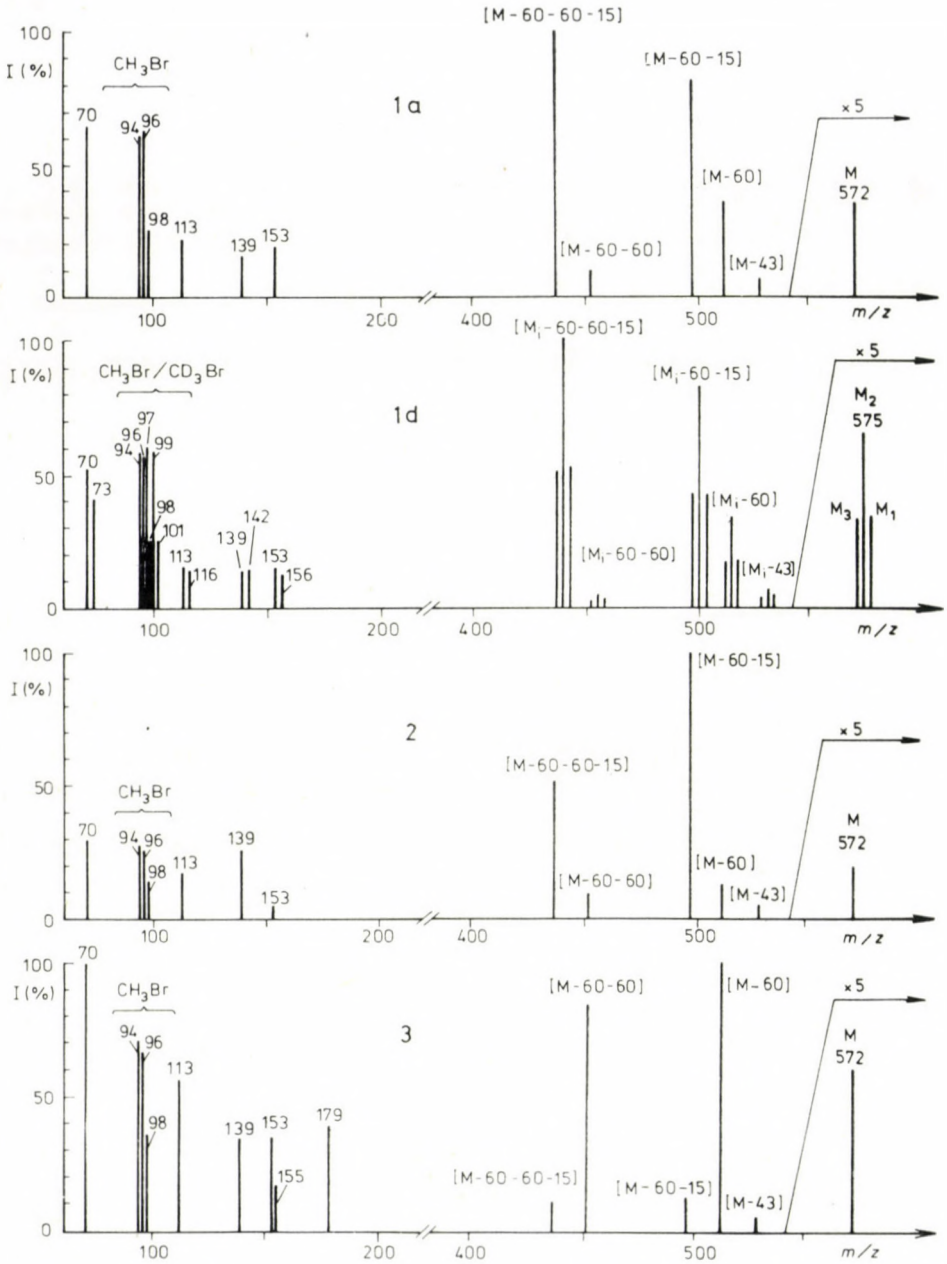
1a
I (%)
CH3Br
70
94
96
98
113
139
153
[M-60-60-15]
[M-60-15]
[M-60]
[M-60-60]
[M-43]
M
572
×5
m/z
1d
CH3Br/CD3Br
97
99
73
101
142
116
156
[Mi-60-60-15]
[Mi-60-15]
[Mi-60]
[Mi-60-60]
[Mi-43]
M2
575
M3
M1
2
[M-60-60-15]
[M-60-15]
[M-60]
[M-60-60]
[M-43]
3
179
155
[M-60-60]
[M-60]
[M-60-15]
[M-43]

Fig. 1

$-2CH_3Br$: m/z 572). The main fragmentation processes of this ionized base (supported by metastable transitions) comprise the loss of an acetic acid molecule from the molecular ion (mainly the C_{17}-substituent is lost), followed by elimination of a CH_3 group (mostly from the C_{13} position) and/or the loss of another acetic acid molecule, of which the OAc part originates from the C_3-position. All the $(M\text{-}60]^+$, $[M\text{-}60\text{-}15]^+$, $[M\text{-}60\text{-}60]^+$ and $[M\text{-}60\text{-}15\text{-}60]^+$ ions arising in this way are of significant abundance. Further abundant ions occur at m/z 152, 139 and 113 (containing the 4'-methylpiperazino moiety) and the ion at m/z 70 is due to their further decomposition:

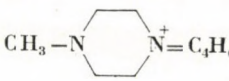

m/z 153

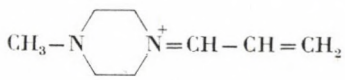

m/z 139

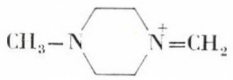

m/z 113

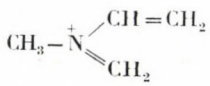

m/z 70

Accordingly, the EI mass spectrum of the **1a** bisquaternary salt does not differ from that expected for its monoquaternary analogue.

The mass spectra of isomers **2** and **3** are largely similar to that of **1a**. The overwhelming majority of the peaks are common; however, the differences noticed in their abundance clearly indicate the structural differences of the corresponding bases. For example, the $CH_3^{\cdot}$ loss subsequent to an acetic acid elimination from $M^{+\cdot}$ is an especially favoured process for **1a** and **2** due to the high stability of the product ion:

$[M\text{-}60]^{+\cdot}$ $[M\text{-}60\text{-}15]^+$

(1a, 2)

In the case of compound **3**, however, the same process would not lead to an ion of stable structure. For this reason, this compound produces a new, charac-

teristic fragmentation process, leading to an ion at m/z 179:

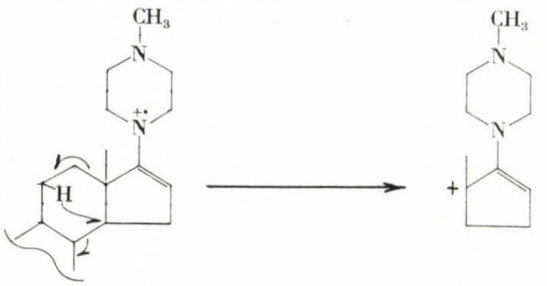

$[M\text{-}60]^{+\cdot}$ m/z 179

(3)

The relative abundances in the mass spectra of the stereoisomeric compounds **1a**, **1b** and **1c** (Table I) were also found to be different — though only to a slight extent — and in this way they can be distinguished.

In the light of the above data, the EI mass spectra of the bis(4',4'--dimethyl-1'-piperazino)diacetoxyandrostane dibromides are characteristic of the base and the CH_3Br forming the quaternary salt, but do not differ from those expected for the corresponding monoquaternary salts.

The mass spectra of the so-called "mixed" 4',4'-dialkyl derivatives (**1d**, **1e** and **1f**) exhibit striking differences. In the mass spectrum of **1d** (Fig. 1) a series of molecular peak M' of CH_3Br and CD_3Br, as well as those of the three different bases (M_1 to M_3) can be observed, where

$$M_1 = K^{++}(Br^-)_2 - 2\ CH_3Br$$

$$M_2 = K^{++}(Br^-)_2 - CH_3Br - CD_3Br$$

$$M_3 = K^{++}(Br^-)_2 - 2\ CD_3Br.$$

The simultanenous occurrence of all these three isotopic forms suggests the presence of the bisquaternary salt **1d**; at the same time, the equivalent amounts of CH_3Br and CD_3Br indicate the equivalent number of the CD_3 and CH_3 groups connected to the quaternary centres thereby revealing their equivalent position. Fig. 1 also shows that the abundance ratios of the molecular ions of M_1^+, M_2^+ and M_3^+ and those of the corresponding fragments are in good agreement with the statistical ratios (1 : 2 : 1) obtained by probability calculation.

From the mass spectra of compounds **1a**—**1d**, **2** and **3** and from the abundance ratios observed for **1d** it can be concluded that it is only the demethylation process, as thermal decomposition, that proceeds during the EI

Table I

The 70 eV *mass spectra of* **1a**, **1b** *and* **1c**

Ions		Relative abundances (*B* %)		
		1a	**1b**	**1c**
m/z	*M*—X	16-H : α 17-H : α	16-H : α 17-H : β	16-H : β 17-H : β
572	[*M*]	7.2	6.3	7.9
512	[*M*-60]	39	38	51
497	[*M*-60-15]	86	94	82
452	[*M*-60-60]	9.2	11	5.7
437	[*M*-60-60-15]	100	100	100
139		15	14	14
113		20	12	13
94	[*M'*]($CH_3{}^{79}Br$)	61	39	47
70		58	45	48

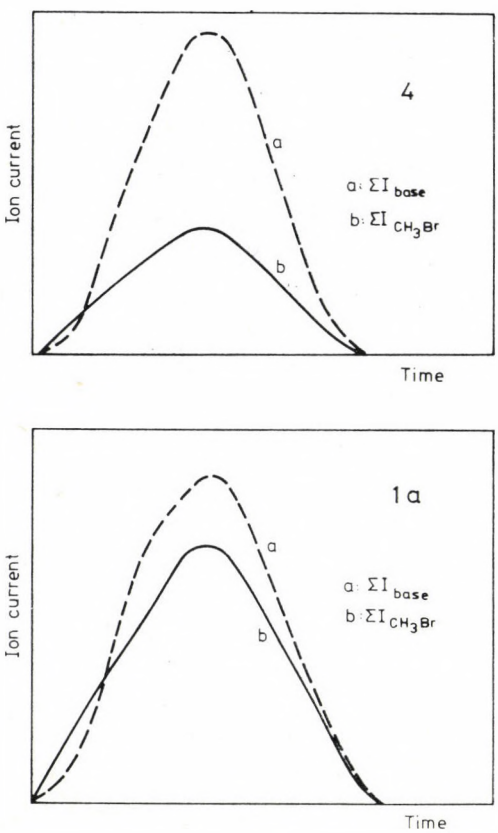

Fig. 2

investigation of these bisquaternary salts. For example, there is no HBr peak due to Hofmann degradation, nor any product resulting from bromine incorporation into the base, in contrast with observations made with tropylium and tetrazolium salts [20].

The observed exclusivity of the dealkylation process was also supported by quantitative measurements. For this purpose we compared the relative amount of CH_3Br molecules and the corresponding base being present in the vapour phase during total evaporation in the case of a bisquaternary

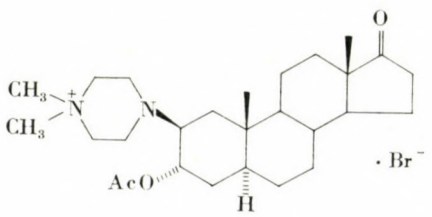

4

compound (**1a**) and the monoquaternary salt (**4**). For this comparison the ion current — time curves of these molecular ions were recorded. The observed intensity values were weighted with the total ion current ratios of the base and methyl bromide arising thermally from the given compound. The obtained curves (Fig. 2) show the abundance of the ions of CH_3Br on this scale compared to that of the bases to be twice as big as that obtained in the case of the monoquaternary salt (**4**). (The ratio of the corresponding areas under the curves is 1.95 : 1). This method seems to be applicable to decide between the mono- and bisquaternary character of the compounds of similar behaviour to **1a**, i.e. when the mass spectrum itself is not informative in this respect.

Compounds **1e** and **1f** show analogous behaviour to **1d** (Table II). In this case, however, two alkyl halides and three bases of different molecular weight are produced via dealkylation, all of which can be observed in the spectra. It is also conspicuous that the abundance ratios of the molecular ions of either the two alkyl halides or the three different bases are not equal to the mole-ratios expected from simple statistical prediction. This phenomenon can be rationalized with accepting that

(a) the products of thermal decomposition, owing to the different stability of the $R^{\cdot}$ and $CH_3^{\cdot}$ radicals result in mole-ratios different from the statistical one;

(b) the molecular ions of the two alkyl bromides and of the bases are of different stability.

Taking into account the further fragmentation of the molecular ions, the relative frequency of the formation of the halides in the case of **1e** and **1f** falls in the sequence: $CH_2{=}CH{-}CH_2{-}Br \gg CH_3Br > CH_3{-}CH_2{-}CH_2{-}Br$.

Table II

The 70 eV mass spectra of **1e** *and* **1f**

Ions	Relative abundances (B %)	
	1e (R:CH_2=CH—CH_2—)	**1f** (R:CH_3—CH_2—CH_2—)
M_1 [$K^{++}(Br^-)_2$—$2CH_3Br$]	0.2	4.2
M_2 [$K^{++}(Br^-)_2$—CH_3Br—RBr]	1.5	3.8
M_3 [$K^{++}(Br^-)_2$—2RBr]	2.8	1.3
[M_1-60]	0.4	20
[M_2-60]	5.8	20
[M_3-60]	19	4.6
[M_1-60-15]	1.2	60
[M_2-60-15]	19	49
[M_3-60-15]	63	8.3
[M_1-60-60]	0.4	13
[M_2-60-60]	3.9	6.9
[M_3-60-60]	10	1.3
[M_0-60-60-15]	1.6	100
[M_2-60-60-15]	25	55
[M_3-60-60-15]	100	9.2
m/z 167	—	9.0
165	6.3	—
141	—	7.0
139	18	9.0
113	18	6.0
70	74	30
[M']($CH_3{}^{79}Br$)	18	210
[M'']($R^{79}Br$)	24	31

In accordance with this, it is the twice deallylated base (M_3) that dominates among the bases for **1e**. Furthermore, in the case of **1f**, the twice demethylated M_1 gives rise to the most abundant peaks. An exact analysis of the factors influencing the relative amounts of the products would require a more detailed study of numerous salts. From results described above, however, it already seems very probable that the much favoured formation of allyl bromide for **1e** is due to the relatively weak bond between the allyl group and the quaternary nitrogen atom.

The fact that the thermal decomposition prior to evaporation of the compounds **1**—**3** studied yielded exclusively steroid bases and alkyl bromides is utilizable to localize the quaternary centres of these salts. Namely, if the 1'-nitrogens were quaternarized, dealkylation would lead to other products too, first of all to diacetoxydibromoandrostane. The lack of this compound is sufficient to unambiguously reveal the 4'-positions of the quaternary centres. In addition, alteration of the quaternary centres would lead to significant changes in the relative amounts of the two alkyl bromides. For instance, in case of the 1'-quaternary isomers of **1d**, **1e** or **1f**, the formation of CH_3Br would not be expected.

Experimental

The preparation of the compounds studied is described in Ref. [17].

The mass spectra and the ion current — time curves were recorded using an AEI MS-902 type instrument operating at an ionizing electron energy of 70 eV. To evaporate the samples, they were placed immediately near the electron beam (in-beam technique). The temperature of the ion source was maintained at 200 to 220 °C.

REFERENCES

[1] Budzikiewicz, H., Djerassi, C., Williams, D. H.: Mass Spectrometry of Organic Compounds, pp. 330. Holden-Day, San Francisco 1967
[2] Veith, H. J., Hesse, M.: Helv. Chim. Acta, **52,** 2004 (1969)
[3] Ohashi, M., Barron, R. P., Benson, W. R.: J. Am. Chem. Soc., **103,** 3943 (1981)
[4] Sammons, M. C., Bursey, M. M., White, C. K.: Anal. Chem., **47,** 1165 (1975)
[5] Veith, H. J.: Org. Mass Spectrom., **11,** 629 (1976)
[6] Day, R. J., Unger, S. E., Cooks, R. G.: J. Am. Chem. Soc., **101,** 501 (1979)
[7] Unger, S. E., Ryan, T. M., Cooks, R. G.: Anal. Chim. Acta **118,** 169 (1980)
[8] Schueler, B., Krueger, F. R.: Org. Mass Spectrom., **14,** 439 (1979)
[9] Stoll, R., Röllgen, F. W.: Org. Mass Spectrom., **14,** 642 (1979)
[10] Fenselau, C., Cotter, R. J.: in Frontiers of Chemistry (ed. by Laidler, K. J.), Pergamon Press, New York 1982
[11] Gierlich, H. H., Röllgen, F. W., Borchers, F., Levsen, K.: Org. Mass Spectrom., **12,** 387 (1977)
[12] Veith, H. J.: Org. Mass Spectrom., **13,** 280 (1978)
[13] Fischer, M., Veith, H. J.: Helv. Chim. Acta, **61,** 3038 (1978)
[14] Veith, H. J.: Adv. Mass Spectrom., **8,** 768 (1980)
[15] Veith, H. J.: Org. Mass Spectrom., **18,** 154 (1983)
[16] Hesse, M.: Indolalkaloide, Teil **1**, p. 95., Verlag Chemie, Weinheim 1974
[17] Tuba, T., Bor, M., Szeberényi, Sz., Kárpáti, E., Szporny, L., Szepesi, G.: Hung. Pat., 165600 (G. B. Pat. 1398 050; FRG Pat. 2 337 882)
[18] Tamás, J., Mák, M.: Kémiai Közlemények, **46,** 509 (1976)
[19] Mák, M., Tamás, J., Tuba, Z.: Acta Chim. Acad. Sci. Hung , **111,** 381 (1982)
[20] Tamás, J., Hegedüs-Vajda, J., Messmer, A.: Acta Chim. Acad. Sci. Hung., **99,** 193 (1979)

Acta Chimica Hungarica 119 (1), pp. 49—55 (1985)

REACTIONS WITH 4,5-DIPHENYLIMIDAZOLIDINE-2-THIONE, II*

Hamdy Ali HAMMOUDA[1]**, Sanaa Osman ABD-ALLAH[1] and Hanafi Hassan ZOOROB[2]

([1]Chemistry Department, Faculty of Science, Cairo University, Giza and [2]Mansoura University, Mansoura, A. R. Egypt)

Received April 17, 1984
In revised form July 2, 1984
Accepted for publication August 6, 1984

4,5-Diphenylimidazolidine-2-thione (**I**) added acrylonitrile to give the *N*-cyanoethyl derivative, **II**. Hydrolysis of **II** by alkali gave the carboxyethyl derivative, **V**, while by acids the imidazo[2,1-*b*][1,3]-thiazine derivative, **IV** was obtained. Compound **I** gave also *N*-Mannich bases, **VIII**. Dehydrogenation of **I** and desulfurization by various methods were investigated. Oxidation of the *S*-alkyl and *S*-aryl derivatives to a sulfoxide, **XIV** and to sulfones, **XV** were also tried.

In continuation of our recent interest in the chemistry of imidazolidinethiones [1—3], this paper deals with some reactions of 4,5-diphenylimidazolidine-2-thione (**I**) [1]. Thiourea, its analogues and derivatives may readily add to the activated olefinic bond of acrylonitrile [4]. Thiourea units incorporated into cyclic structures are also capable of this reaction [5, 6]. Because of the ambient reactivity of the thiourea moiety, particularly in its anionic form, either *N*-(2-cyanoethyl) [5, 7] or *S*-(2-cyanoethyl) derivative [4] is generally obtained. Compound **I** added to acrylonitrile to give the 1-(2-cyanoethyl) derivative, **II**. That *N*-cyanoethylation took place was proved by the hydrolysis of **II**. Boiling of **II** in acetic acid-hydrochloric acid mixture afforded the imidazo[2,1-*b*][1,3] thiazinone derivative, **IV**.

On the other hand, alkaline hydrolysis of **II** afforded the acid **V** and not **VI** [2]. The latter (**VI**) would have been obtained if compound **II** were an *S*-(2-cyanoethyl) derivative. Compound *V* is not dehydrated to **IV** on boiling in acetic acid-hydrochloric acid mixture. This may lead to the assumption that **IV** is formed via the hydrolysis of an intermediate imine (**III**), which might be formed by an intramolecular nucleophilic addition.

A more rigorous proof for the structure assigned to **II** was obtained from the fact that 1-(2-cyanoethyl)-4,5-diphenyl-2-methylthio-2-imidazoline (**VII**) could be prepared by the methylation of **II** and also by the cyanoethylation of the *S*-methyl derivative, **XIIIa**.

* Part I: See Ref. [2]
** To whom correspondence should be addressed

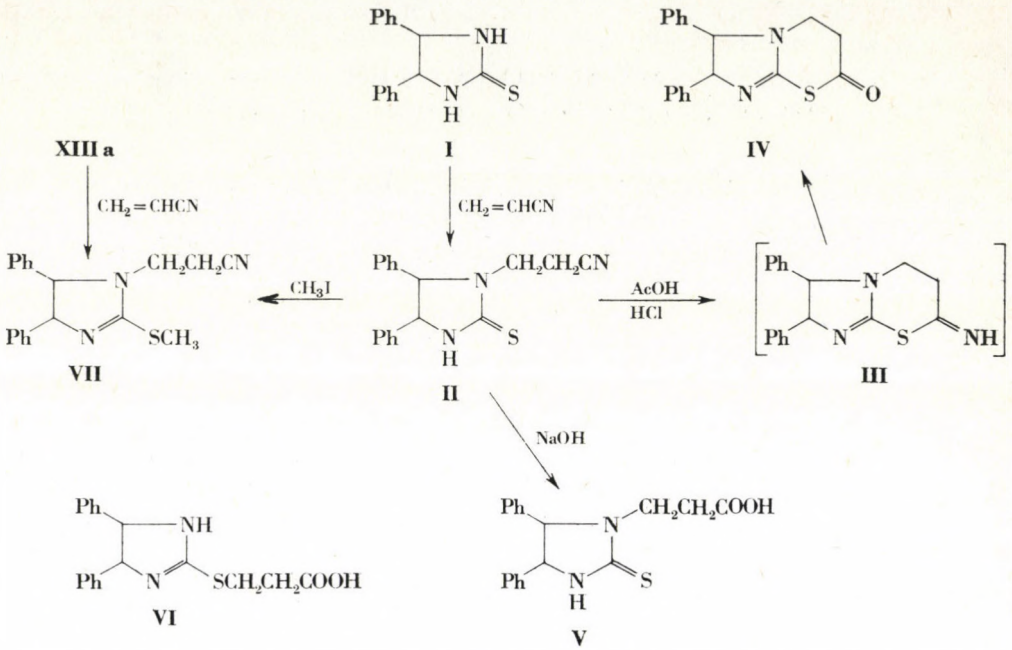

Imidazoline-2-thiones and imidazolidine-2-thiones behave differently in the Mannich reaction. Most of them react exclusively in the thione form to give 1,3-bis Mannich bases [8], however, reaction at other sites has also been reported [9]. Compound **I** reacted with formaldehyde and piperidine or morpholine to give the 1-aminomethyl derivatives, **VIIIa, b.**

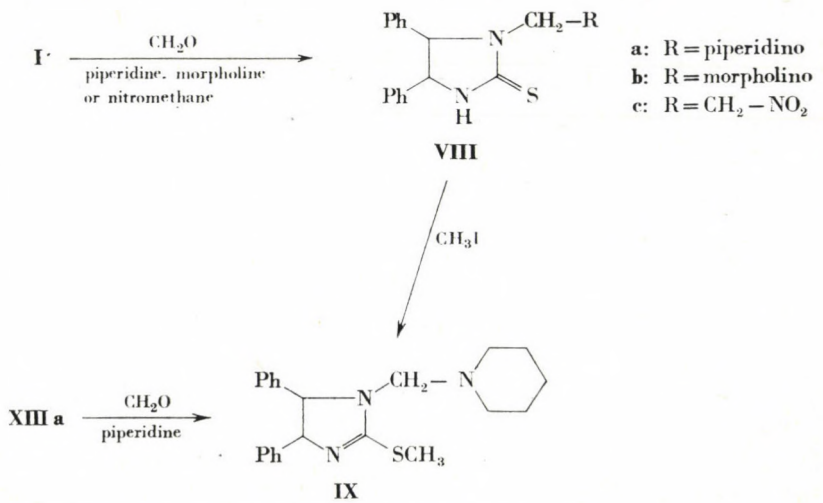

In support of structure **VIII** is the formation of 4,5-diphenyl-2-methylthio-1-piperidinomethyl-2-imidazoline (**IX**) by the methylation of **VIIIa** and

also by the reaction of **XIIIa** with formaldehyde and piperidine. The IR spectrum of **IX** has no absorption bands for the NH or SH group. Compound **I** reacted also with formaldehyde and nitromethane to give the 1-(2-nitroethyl) derivative, **VIIIc**.

The oxidation of imidazolidine-2-thiones has been studied and was later reviewed by Hofmann [10]. We reported [1] on the oxidative chlorination of **I** and will describe here other types of oxidation of **I** and its *S*-substituted derivatives. When compound **I** was heated with sulfur at 200—220 °C, hydrogen sulfide evolved and 4,5-diphenyl-2-mercaptoimidazole (**X**) [11] was formed. This method has been used for the dehydrogenation of some dihydropyrimidine derivatives [12]. Treatment of **I** with potassium permanganate gave the disulfide (**XI**).

The replacement of sulfur in **I** by oxygen could be achieved in several ways. Thus, refluxing of **I** with selenium dioxide in acetic acid afforded 4,5-diphenylimidazolidone (**XII**) [13]. Mercuric oxide was also used. Whereas the 2-methylthio derivative, **XIIIa** showed abnormal stability to acid hydrolysis, the 2-carboxymethylthio derivative, **XIIIe** was hydrolysed by boiling in 2*N* sulfuric acid to give **XII**.

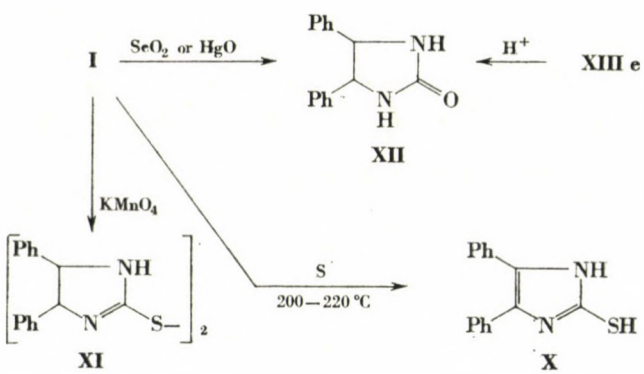

The *S*-alkyl derivatives, **XIIIa—c** behaved differently towards the oxidation by nitric acid. Whereas the imidazoline ring in the *S*-methyl and *S*-ethyl derivatives (**XIIIa, b**) was destroyed and benzil was formed, the *S*-benzyl derivative (**XIIIc**) showed stability and only the sulfur atom was oxidized to a sulfoxide group affording **XIV**.

On the other hand, treatment of compounds **XIIIa—d** in hot acetic acid with potassium permanganate afforded the sulfones (**XVa—d**). Moreover, the benzylsulfoxide (**XIV**) was further oxidized to the benzylsulfone (**XVc**) by the action of 3% potassium permanganate solution.

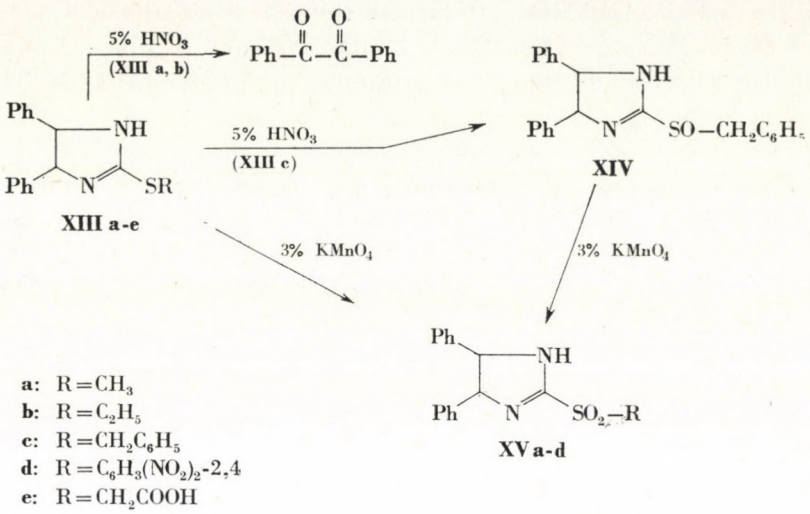

Experimental

M.p.'s (uncorrected) were determined on a Fisher-Johns melting point apparatus. IR spectra were taken in KBr with a Pye-Unicam SP 1000 Spectrometer. ^{1}H-NMR spectra were recorded on a Varian 390 90 MHz Spectrometer using TMS as internal reference.

1-(2-Cyanoethyl)-4,5-diphenylimidazolidine-2-thione (II)

A mixture of **I** (2.54 g; 10 mmol), acrylonitrile (2 mL), KOH (0.1 g), pyridine (15 mL) and water (3 mL) was refluxed for 6 h, cooled and poured into water. The aqueous layer was decanted and the oily residue was triturated with a little ethanol to give **II** as a white solid, crystallized from benzene–benzine (60—80 °C), m.p. 112 °C; yield 63%.

IR: 3380 cm^{-1} (NH), 2240 (C≡N).

$C_{18}H_{17}N_3S$ (307.4). Calcd. C 70.33; H 5.57; N 13.67; S 10.43. Found C 70.05; H 5.70; N 13.86; S 10.17%.

2,3-Diphenyl-2,3,5,6-tetrahydro-7*H*-imidazo[2,1-*b*][1,3]thiazin-7-one (IV)

A mixture of **II** (1 g), acetic acid (10 mL) and conc. hydrochloric acid (10 mL) was refluxed for 2 h and left to cool. The crystalline solid was collected and recrystallized from aqueous ethanol to give **IV**, m.p. 145 °C; yield 58%.

IR: 1700 cm^{-1} (C=O).

^{1}H-NMR (DMSO-d_6): δ 3.1—3.6 ppm (m, 4H, $2CH_2$), 5.2 (m, 2H, H-2 and H-3), 6.9—7.2 (m, 10H, aromatic).

$C_{18}H_{16}N_2OS$ (308.4). Calcd. C 70.10; H 5.23; N 9.08. Found C 70.30; H 5.34; N 8.90%.

1-(2-Carboxyethyl)-4,5-diphenylimidazolidine-2-thione (IV)

A solution of **II** (1 g) in ethanol (50 mL) was mixed with 10 mL of 10% NaOH solution and the mixture refluxed for 3 h, concentrated and acidified with dilute hydrochloric acid. The solid that separated was filtered off and crystallized from aqueous ethanol to give **V**, m.p. 168 °C; yield 70%.

IR: 3380 cm^{-1} (NH), 2900—2500 (dimeric COOH), 1700 (C=O).

$C_{18}H_{18}N_2O_2S$)326.4). Calcd. C 66.23; H 5.56; N 8.58. Found C 66.01; H 5.80; N 8.72%.

1-(2-Cyanoethyl)-4,5-diphenyl-2-methylthio-2-imidazoline (VII)

(*a*) A solution of **II**)1.53 g; 5 mmol) and methyl iodide (0.5 mL; 8 mmol) in absolute ethanol (50 mL) was refluxed for 4 h, concentrated and cooled. The solid that separated on adding ether was filtered off, dissolved in ethanol and the solution made alkaline with NH_4OH. The solid which precipitated on dilution was collected and crystallized from aqueous ethanol to give **VII**, m.p. 93 °C; yield 64%.

^{1}H-NMR (DMSO-d_6): δ 2.55 ppm (s, 3H, CH_3), 2.9—3.5 (m, 4H, $2CH_2$), 5.4 (m, 2H, H-4 and H-5), 6.9—7.3 (m, 10H, aromatic).

$C_{19}H_{19}N_3S$ (321.5). Calcd. C 71.00; H 5.96; N 13.07. Found C 71.28; H 6.05; N 13.11%.

(*b*) A mixture of **XIIIa** (1.34 g; 5 mmol), acrylonitrile (1 mL), KOH (0.05 g), pyridine (7 mL) and water (1 mL) was refluxed for 6 h and worked up as described for **II** to give 0.9 g (56%) of a product identical by m.p. and mixed m.p. with **VII** prepared according to (*a*).

1-Aminomethyl-4,5-diphenylimidazolidine-2-thione (VIII)

A solution of **I** (1 g; 4 mmol), piperidine or morpholine (1 mL; 12 mmol) and 37% aqueous formaldehyde (2 mL) in methanol (30 mL) was refluxed for 4 h. The product that separated on cooling was filtered off and crystallized to give **VIIIa, b.**

VIIIa was crystallized from aqueous ethanol, m.p. 208 °C; yield 74%.

IR: 3400 cm^{-1} (NH), 2940 (νCH_2).

$C_{21}H_{25}N_3S$ (351.5). Calcd. C 71.76; H 7.17; N 11.95; S 9.12. Found C 71.55; H 7.29; N 12.11; S 9.25%.

VIIIb was crystallized from ethanol; m.p. 213 °C; yield 70%.

$C_{20}H_{23}N_3OS$ (353.5). Calcd. C 67.96; H 6.56; N 11.89; S 9.07. Found C 68.21; H 6.70; N 11.75; S 9.31%.

4,5-Diphenyl-1-(2-nitroethyl)imidazolidine-2-thione

(VIIIc) was similarly prepared using nitromethane. It was crystallized from aqueous ethanol, m.p. 190 °C; yield 70%.

IR: 1550 cm^{-1} (ν as NO_2), 1350 (ν s NO_2).

$C_{17}H_{17}N_3O_2S$ (327.4). Calcd. V 62.36; H 5.23; N 12.83; S 9.79. Found C 62.55; H 5.25; N 12.65; S 10.01%.

Formation of IX

(*a*) **IX** was obtained in 62% yield from **VIIIa** and methyl iodide, as described for **VII**, m.p. 125 °C (from methanol).

$C_{22}H_{27}N_3S$ (365.5). Calcd. C 72.29; H 7.44; N 11.50; S 8.77. Found C 72.10; H 7.30; N 11.65; S 8.91%.

(*b*) **IX** was obtained in 60% yield fro m **XIIIa**, formaldehyde and piperidine, as described for **VIII**, m.p. and mixed m.p. with **IX** pre pared under (*a*) 124 °C.

4,5-Diphenyl-2-mercaptoimidazole (X)

An intimate mixture of **I** (1 g) and powdered sulfur (2 g) was heated at 200—220 °C until hydrogen sulfide ceased to evolv e (ca. 1 h). The cooled reaction mixture was triturated several times with carbon disulfide an d the solid residue was crystallized from acetic acid to give *X*, yield 75%, m.p. and mixed m.p. with an authentic sample [11] 320 °C.

2,2'-Dithiodi-(4,5-diphenyl-2-imidazoline) (XI)

A solution of potassium permanganate (1.74 g; 11 mmol) in 30 mL of water was added, over a period of 1 h, to a solution of **I** (2.54 g; 10 mmol) in 100 mL of acetic acid while shaking at 0—5 °C. The brown solid thus obtained was collected, washed with water and dried. It was purified by washing with hot DMF, m.p. above 340 °C; yield 88%.

IR: 3390 cm^{-1} (NH), 470 (S—S).

$C_{30}H_{26}N_4S_2$ (506.7). Calcd. C 71.11; H 5.17; N 11.06. Found C 71.33; H 5.15; N 11.10%.

4,5-Diphenylimidazolidone (XII)

(*a*) A mixture of **I** (0.5 g) and mercuric oxide (1 g) or selenium dioxide (0.6 g) in acetic acid (20 mL) was refluxed for 2 h and filtered while hot. The filtrate was diluted with water and neutralized with NH_4OH to give a colourless solid which was crystallized from aqueous ethanol; yields 67 and 80%, m.p. 245 °C (not depressed when admixed with an authentic sample [13].

(*b*) Compound **XIIIe** [1] (1 g) was refluxed in 50 mL of 2*N* sulfuric acid for 2 h and then cooled to give **XII** (m.p. and mixed m.p.).

Action of 5% nitric acid on XIIIa—c

A mixture of **XIIIa—c** [2] (1 g), acetic acid (10 mL), water (16 mL) and 70% nitric acid (2 mL) was refluxed for 5 h, cooled and diluted with water.

XIIIa,b gave yellow needles, crystallized from ethanol and characterized as benzil (m.p. and mixed m.p. 95 °C), yield 80%.

XIIIc gave 2-benzylsulfinyl-4,5-diphenyl-2-imidazoline (**XIV**), crystallized from aqueous ethanol, m.p. 157 °C (dec.); yield 70%.

IR: 3380 cm^{-1} (NH), 1040 (S=O).

$C_{22}H_{20}N_2OS$ (360.5). Calcd. C 73.30; H 5.59; N 7.77; S 8.89. Found C 73.51; H 5.62; N 7.90; S 9.03%.

2-(2,4-Dinitrophenylthio)-4,5-diphenyl-2-imidazoline (XIIId)

A mixture of **I** (2.54 g; 10 mmol), 2,4-dinitrochlorobenzene (2.03 g; 10 mmol) in absolute ethanol (30 mL) was refluxed for 4 h and then cooled. The solid that separated on adding ether was filtered off, dried and dissolved in ethanol. Basification with NH_4OH and dilution gave yellow crystals of **XIIId**, recrystallized from ethanol, m.p. 240 °C; yield 78%.

$C_{21}H_{16}N_4O_4S$ (420.5). Calcd. C 59.99; H 3.84; N 13.33; S 7.63. Found C 60.25; H 3.96; N 13.50; S 7.65%.

2-Alkyl (aryl) sulfonyl-4,5-diphenyl-2-imidazolines (XVa—d)

A 3% potassium permanganate solution (27 mL) was gradually added to a solution of **XIIIa—d** (5 mmol) in acetic acid (20 mL). The mixture was heated on a water bath for 1 h, cooled and filtered. The black cake was digested by boiling in dioxan. Filtration and addition of water gave white crystals which were collected and crystallized to give **XVa—d** in 60—65% yields.

XVa, m.p. 195 °C (aqueous dioxan).

IR: 3390 cm^{-1} (NH), 1310 and 1290 (ν as SO_2) and 1130 (ν s SO_2).

^{1}H-NMR ($CDCl_3$): δ 2.6 ppm (s 3H, CH_3), 5.2 (s, 2H, H-4 and H-5), 6.8—7.4 (m, 11H, aromatic + NH).

$C_{16}H_{16}N_2O_2S$ (300.4). Calcd. C 63.98; H 5.37; N 9.33; S 10.67. Found C 64.25; H 5.42; N 9.21; S 10.83%.

XVb, m.p. 205 °C (aqueous dioxan).

$C_{17}H_{18}N_2O_2S$ (314.4). Calcd. C 64.94; H. 5.77; N 8.91; S 10.20. Found C 65.19; H 5.87; N 8.97; S 10.14%.

XVc, m.p. (170 °C (aqueous dioxan).

$C_{22}H_{20}N_2O_2S$ (376.5). Calcd. C 70.19; H 5.35; N 7.44; S 8.52. Found C 70.34; H 5.40; N 7.65; S 8.85%.

XVd, m.p. 183 °C (acetic acid).

$C_{21}H_{16}N_4O_6S$ (452.5). Calcd. C 55.75; H 3.56; N 12.38; S 7.09. Found C 55.93; H 3.63; N 12.48; S 7.15%.

Oxidation of XIV

To a solution of **XIV** (0.3 g) in acetic acid (20 mL) was added gradually 15 mL of 3% potassium permanganate solution. The reaction mixture was heated on a water bath for 30 min and filtered while hot. The filtrate was diluted and cooled to give **XVc** (m.p. and mixed m.p. 170 °C).

REFERENCES

[1] Ali, M. I., El-Sayed, A. A., Hammouda, H. A.: J. Prakt. Chem., **318,** 168 (1976)
[2] Hammouda, H. A., Abd-Allah, S. O., Hussain, S. M., Yousef, N. M.: Gazz. Chim. Ital., **114,** 201 (1984)
[3] Abd-Allah, S. O., Hammouda, H. A., Eid, H. A., Metwalli, N. H.: Indian J. Chem. (in the press)
[4] Kataev, E. G., Barinova, L. K.: Dokl. Acad. Nauk SSSR, **141,** 1373 (1961); Chem. Abstr., **56,** 12727h (1962)
[5] Novacek, A., Lissnerova, M.: Coll. Czech. Chem. Commun., **33,** 604 (1968)
[6] Shvachkin, Yu. P., Rapanovich, I. I., Azarova, M. T.: Khim., **20,** 73 (1965); Chem. Abstr., **62,** 13002c (1965)
[7] Efros, A. M.: Zh. Obshch. Khim. **28,** 617 (1958); Chem. Abstr., **52,** 17242 (1958)
[8] I. G. Farbenind, A. G.: Ger. Pat. 575,114; Chem. Abstr., **27,** 3483 (1933)
[9] Heath, H., Lawson, A., Rimington, C.- J. Chem. Soc., **1951,** 2217
[10] Hofmann, K.: Chemistry of Heterocyclic Compounds-Imidazole and Its Derivatives, Part **I** (Ed. A. Weissberger) p. 234, Interscience Publishers, New York 1953
[11] Biltz, H., Krebs, P.: Justus Liebigs Ann. Chem., **391,** 191 (1912)
[12] Hitchings, G. H., Russel, P. B., Whittaker, N.: J. Chem. Soc., **1956,** 1019
[13] Biniecki, S., Moll, M.: Acta Pol. Pharm., **31,** 731 (1974)

Acta Chimica Hungarica 119 (1), pp. 57—63 (1985)

A POSSIBILITY OF ESTIMATION OF THE CHANGES IN THE SIZE OF PARTICLES CONTAINING MÖSSBAUER ATOMS

Todor M. PEEV[1] and Attila VÉRTES[2]*

([1]Higher School of Chemical Technology, Department of Physical Chemistry, 8010 Bourgas, Bulgaria and [2]L. Eötvös University, Laboratory of Nuclear Chemistry, 1088-Budapest, Puskin u. 11—13)

Received May 24, 1984
Accepted for publication August 15, 1984

Analytical dependences were obtained to determine the decrease in the particle size and surface by using Mössbauer experimental data.

The shape and some parameters of Mössbauer spectra depend on the particle size. Examples of the existence of a connection between spectra parameters and particles size have been described for Fe_2O_3 [1], α- and β-FeOOH [2], F_3O_4 [3] and fine despersed tin [4]. Investigations have been carried out taking into account the change in the internal magnetic fields [1—3], the change in the magnetic properties of substances [3] and the recoil-free fraction f' [4].

The present work is an attempt to determine the changes in the radius and the surface of a particle in chemical interactions, using the ratios between the areas of partial Mössbauer spectra. The ratio of the areas is equivalent to the change in the quantity of a substance containing Mössbauer atoms (iron, tin or others).

Theoretical considerations

A decrease in the radius of a spherical particle in chemical interactions

The theoretical considerations for estimating the decrease in the particle radius were drawn on the basis of a model analogous to that of Jander [5] concerning reactions in the solid phase. According to that model, the reaction rate is determined by a one-way diffusion through the layer formed on the surface of a spherical particle. The model is valid at a low degree of transformation, i.e. when the initial particle does not react completely. The following assumption was made: the chemical interaction proceeds uniformly all over the surface of the spherical particle. The influence of the energy heterogeneity is neglected.

* To whom correspondence should be addressed

The total Mössbauer spectrum of the reacting particle will consist of the spectrum of the metal or substance from the spherical particle, and that of the compounds from the surface layer resulting from the chemical interaction. In order to express the areas of the partial spectra (A_i), the equation for low thickness absorbers suggested in ref. [6] was used:

$$A_i = k \cdot f_i' \cdot n_i \tag{1}$$

where n_i is the number of atoms of the resonance nuclei; f_i' is the recoil-free fraction of the given compound determining the particle spectrum; k is a factor which includes resonance cross section, time of measuring, radiation intensity etc. Allowing for certain approximation, factor k is assumed to be the same in all experiments.

Let's suppose that the spherical particle with radius r and volume

$$V = \frac{4}{3}\pi r^3 , \tag{2}$$

consists of n nuclei conditioning the resonance. The spectrum having area $A = kf'n$ corresponds to it.

At a given moment of the chemical interaction x the volume of the initial particle decreases and will be:

$$V_x = \frac{4}{3}(r - \Delta r_x)^3 \tag{3}$$

The resonance nuclei which have not reacted yet are $n - \Delta n_x$, and the area $A_x = k \cdot f' \cdot (n - \Delta n_x)$ corresponds to them.

The volumes of the particles are proportional to the number of the resonance nuclei. Using (1), they can be expressed as

$$V \sim n = \frac{A}{k \cdot f'}$$

$$V_x \sim n - \Delta n_x = \frac{A_x}{k \cdot f'} \tag{4}$$

The nuclei Δn_x, forming part of the composition of the newly formed surface compounds whose number is i, determine part of the area of the total spectrum which is $\sum_{i \neq x} \frac{A_i}{k \cdot f_i'}$. The total area of Mössbauer spectrum at a given moment x is

$$\frac{A_x}{k \cdot f_i'} = \sum_{i \neq x} \frac{A_i}{k \cdot f_i'} \tag{5}$$

This area is equivalent to $\frac{A}{k \cdot f'}$, (2), (3) and (5) give

$$\frac{V_x}{V} = \frac{(r - \Delta r_x)^3}{3} = \frac{\frac{A_x}{k \cdot f'}}{\frac{A_x}{k \cdot f'} + \sum \frac{A_i}{k \cdot f_i'}} \tag{6}$$

Using (6), the following expression can be written

$$\Delta r_x = r \left[1 - \frac{1}{1 + \sum_{i \neq x} \frac{f'}{f_i'} - \frac{A_i}{A_x}} \right]^{1/3} \tag{7}$$

Provided the recoil-free fractions of the substance from the initial particle and the surface layer substances resulting from the chemical interaction were equal, the total spectrum area A would be equal to the denominator of expression (7), and then

$$\Delta r_x = r \left[1 - \left(\frac{A_x}{A} \right) \right]^{1/3} \tag{8}$$

It follows from (7) and (8) that the decrease in the radius of a spherical particle Δr_x could be determined if the radius of the initial particle, the area of the partial and/or total Mössbauer spectra and the corresponding recoil-free fractions were known.

Determination of the surface of the spherical particle

The surface of the spherical particle at a given moment of the chemical interaction may be determined after calculating Δr_x.

On the other hand, employing the well-known expression relating the volume V to the surface S of a sphere $\left(V = \frac{1}{6} \sqrt{\frac{S^3}{\pi}} \right)$, and equation (6), it follows that

$$S_x = \left[\frac{S}{1 + \sum_{i \neq x} \frac{f'}{f_i'} - \frac{A_i}{A_x}} \right]^{2/3} \tag{9}$$

where S and S_x are the surface of the initial particle and its surface at a given moment.

If $f' = f'_i$, then (9) can be simplified to give

$$S_x = S\left(\frac{A_x}{A}\right)^{2/3} \tag{10}$$

The surface can be determined making use of the same data as for estimating Δr_x.

Equations (7—10) can be used to determine the decrease in the radius of the particles in monodisperse systems provided the number of the particles in the system under study remains constant at each stage of the chemical interaction.

The dependences obtained can be applied to polydisperse systems. Then the average values $\Delta\bar{r}_x$ and $\bar{S}_x$ can be determined. A good reason for this assumption is the fact that the relative change in the resonance effect magnitude $\frac{\Delta\varepsilon}{\varepsilon}$ is less dependent on the particle radius in polydisperse systems than in monodisperse ones [7].

Determination of the decrease in foil thickness

The approach suggested above may also be applied to determine the decrease in the thickness of a metal foil which interacts chemically, a non-metallic layer being formed on its surface. Provided the energy heterogeneity is neglected, and the reaction proceeds on one surface only, the decrease in the foil thickness Δh_x will be

$$\Delta h_x = h\left[1 - \frac{1}{1 + \sum\limits_{i \neq x} \frac{f'}{f'_i} \cdot \frac{A_i}{A_x}}\right] \tag{11}$$

where h is the foil initial thickness; A_x is the area of the partial spectrum of the foil that has not yet reacted; A_i stands for the areas of the spectra conditioned by the surface compounds. At equal values for f', $A_i + A_x = A$, where A may be either the area of the total spectrum or the area conditioned by a sample having thickness h. Then equation (11) can be rewritten as:

$$\Delta h_x = h\left(1 - \frac{A_x}{A}\right) \tag{12}$$

If both surfaces take part in the reaction, then Δh_x will include the decrease in the thickness of both surfaces.

Results

Dependences (7) and (9) were used to determine the decrease in the radius and the surface of particles when Fe-powder (commercial product of Merck) reacts with aluminophosphates, chromophosphates and alumino-chromophosphates at 548 K. The particles were assumed to be spherical. Their sizes are determined using an electron microscope. The particle size follows a Gaussian distribution. The average arithmetical radius of the particles $\bar{r} = 1.37$ μm and the dispersion 0.32 were determined on the basis of the measured values for the diameter of the particles and statistical analysis. Particles of that size, may be assumed to form a monodisperse system [7], i.e. the size of each particle is of the same order of magnitude.

The preparation of the samples for Mössbauer experiments and the measurements of the spectra have been described in refs. [8] and [9]. The samples were designated as follows:

1. Fe-powder + aluminophosphate
2. Fe-powder + chromophosphate
3. Fe-powder + alumino-chromophosphate

Mössbauer spectra of samples 1, 2 and 3 after 6 hours of thermal treatment are shown in Fig. 1. The spectra are an overlap of the partial spectra of α-Fe, Fe(II)-phosphates and Fe(III)-phosphates. The absence of temperature dependence in the spectra parameters (width and intensity of the peaks)

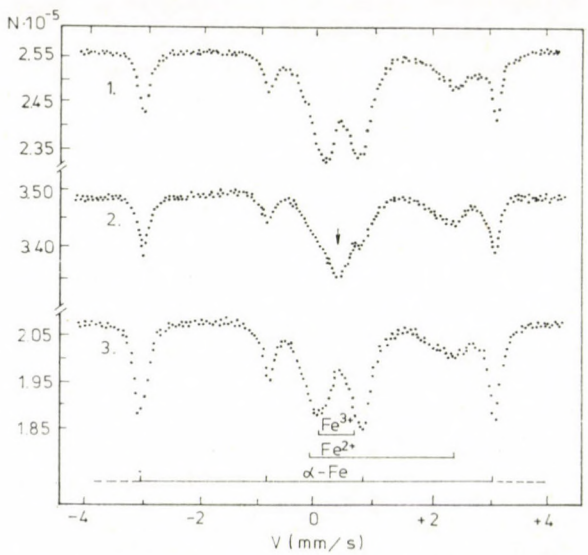

Fig. 1. Mössbauer spectra of samples 1, 2 and 3 treated at 548 K for 6 hours

Table I

Average values for $\bar{\Delta r}_x$ and the surface $\bar{S}_x$

Sample	Time of treatment, min	$\frac{A_i}{A_x}$	$\bar{\Delta r}_x$ μm	$\bar{S}_x$ μm²
1	5	0.30	0.150	18.67
	15	1.27	0.394	11.97
	360	1.56	0.437	10.93
2	5	0.23	0.121	19.59
	15	0.61	0.177	17.85
	360	0.92	0.329	13.61
3	5	0.14	0.079	20.94
	15	0.32	0.157	18.44
	360	0.75	0.290	14.64

established in refs. [8] and [9] indicates the presence of stable structures in the boundary layer.

The formation of a boundary layer of Fe-phosphates is connected with a decrease in the average radii ($\bar{\Delta r}_x$) and the surface ($\bar{S}_x$) of iron particles. In order to determine $\bar{\Delta r}_x$ and $\bar{S}_x$, data concerning the areas of Mössbauer spectra were used similarly to the spectra in Fig. 1. Beside the assumptions made so far (1.1, 1.2 and that α-Fe particles are spherical), it is also assumed that the recoil-free fractions of F(II)-phosphates and Fe(III)-phosphates are the same, $f_i' = 0.59$, and the recoil-free fraction of Fe-powder is $f' = 0.82$. The numerical values for f_i' and f' are reported in ref. [10]. The calculated values for $\bar{\Delta r}_x$ according to ref. [7], and $\bar{S}_x$ according to ref. [9], provided $\bar{r} = 1.37$ μm and $\bar{S} = 23.58$ μm², are shown in Table I.

The $\bar{S}_x$ values calculated according to equation (9) and the expression $S_x = 4\pi(r - \Delta r_x)^2$ coincide. On the other hand, the values for $\bar{\Delta r}_x$ and $\bar{S}_x$ after thermal treatment of 360 min correspond to the final changes of these quantities. As the kinetic examinations of these samples in ref. [9] show, a surface layer is formed under these conditions which prevents diffusion and the chemical interaction ceases.

Conclusions

A possibility of determining the changes in the particle size is suggested. In the method described, the quantities Δr_x, S_x and Δh_x are calculated on the basis of transmission Mössbauer spectra data. This method may be particularly useful in quantitative and qualitative studies of corrosion processes, solid phase reactions etc. The calculated values for $\bar{\Delta r}_x$ and $\bar{\Delta h}_x$ may be related to the thickness and the composition of the boundary layers formed.

REFERENCES

[1] Kündig, V., Bömmel, H., Constabaris, G., Linquist, R.: Phys. Rev., **142,** 273 (1966)
[2] Kubsch, H., Fritzsch, E., Schneider, H. A.: Proc. Intern. Conf. Mössbauer Spectroscopy, Bratislava, Czechoslovakia, **1,** 233 (1973)
[3] Mørup, S., Topsøe, H.: Appl. Phys., **11,** 63 (1976)
[4] Suzdalev, I. P., Gen, M. Ya., Goldanskii, V. I., Makarov, E. F.: J. E. T. F., **51,** 118 (1966)
[5] Jander, W.: Z. anorg. allgem. Chem., **163,** 1 (1927)
[6] Meisel, W., Kreysa, G.: Z. anorg. allgem. Chem., **393,** 31 (1973)
[7] Gamma methodi v rudnoi geologii. Ed. Otschura, A. P. Nedra, Leningrad 1976
[8] Peev, T. M., Iovkov, G. M., Vértes, A., Nagy S.: J. de Physique. Colloq. Cl, suppl. n° 1., **41,** Cl 393 (1980)
[9] Peev, T. M., Vértes, A., Iovkov, G. M., Nagy, S.: Radiochem. Radioanal. Lett., **46,** 405 (1981)
[10] Kerler, W.: Z. Physik, **167,** 194 (1962)

Acta Chimica Hungarica 119 (1), pp. 65—69 (1985)

POLAROGRAPHIC STUDY OF MIXED LIGAND (*n*-BUTYLTHIOGLYCOLATE-OXALATE) COMPLEXES OF CADMIUM(II), LEAD(II) AND THALLIUM(I)

Kevalchand GUPTA* and Kalpana Kumari SHARMA

(Post Graduate Department of Chemistry, Govt. College, Kota-Rajasthan, India 324002)

Received June 6, 1984
Accepted for publication August 15, 1984

Precise nature of complexation of cadmium, lead and thallium with mixed ligand (*n*-butylthioglycolate and oxalate) has been investigated by polarographic method. Triton X-100 (0.001%) was used as wave maximum suppressor and potassium nitrate solution ($\mu = 1.0\ M$) as the supporting electrolyte. It has been found that only one mixed ligand entity MA_iX_j is formed, where i is three for Cd(II) and Pb(II) and one for Tl(I), j is one for all complexes. A and X are the *n*-butylthioglycolate and oxalate ligands, respectively. The composition and stability constants of the mixed ligand complexes formed have been evaluated.

Introduction

A survey of the literature reveals that mercapto acids, their esters and other sulphur containing organic compounds with active-SH group have gained importance in the field of pharmaceutical, biological and analytical chemistry [1—4]. These ligands are also significant in co-ordination chemistry [5—7]. As a part of our investigation of mixed ligand complexes of mercaptans and carboxylic ligands [8—11] with various metal ions, the composition and stability constants of mixed ligands (*n*-butylthioglycolate-oxalate) complexes of Cd(II), Pb(II) and Tl(I) have been studied by polarographic technique, for which no reference could be traced out in the literature.

Experimental

The sodium salt of *n*-butylthioglycolate (95%, Evan Chemetics, Inc., New York) and sodium salt of oxalic acid (B.D.H. Chemicals Ltd., AnalaR) were used as complexing agents. All other reagents used were of AnalaR grade (BDH Chemicals Ltd.). Freshly prepared solution of *n*-butylthioglycolate in methanol 50% was used and other stock solutions were prepared in doubly distilled air-free conductivity water. Triton X-100 (0.001%) was used as a wave maximum suppressor and potassium nitrate solution. ($\mu = 1.0\ M$) as the supporting electrolyte. A manual polarograph (Southern instruments Ltd., Surrey) with a scalamp galvanometer was used for recording current-voltage curves. The capillary characteristics in potassium nitrate solution ($\mu = 1.0\ M$) at $E_{d.e.} = -0.7$ V with respect to a saturated calomel electrode

* Mailing address: Opp. Girl's H. S. School, Jain Mandir Road, Kota — 324002, India.

(SCE) were $m^{2/3} t^{1/6} = 2.4436$ mg$^{2/3}$ s$^{-\frac{1}{2}}$ ($h = 45$ cm). All measurements were made with the cell immersed in a thermostatic bath. Dissolved air was removed by bubbling hydrogen through the cell and the necessary corrections for the potential drop and charging current were made as usual.

Results and Discussion

The reduction of each metal ion in mixed ligand system was studied at 30 °C by recording polarograms of two different sets.

Set I: 0.5 mM $Cd(NO_3)_2$ or $Pb(NO_3)_2$ or $TlNO_3$, 0.001% Triton X-100 and KNO_3 ($\mu = 1.0$ M) with constant oxalate concentration [$C_X = 20.0 \times \times 10^{-3}$ M with Cd(II) and $C_X = 8.0 \times 10^{-3}$ M with Pb(II) and Tl(I)] and varying concentration of *n*-butylthioglycolate [$C_A = 8.0 \times 10^{-3} M$ to $40.0 \times \times 10^{-3}$ M with Cd(II) and $C_A = 4.0 \times 10^{-3}$ M to 20.0×10^{-3} M with Pb(II) and Tl(I)].

Set II: 0.5 mM $Cd(NO_3)_2$ or $Pb(NO_3)_2$ or $TlNO_3$, 0.001% Triton X-100 and KNO_3 ($\mu = 1.0$ M) with constant *n*-butylthioglycolate concentration [$C_A = 20.0 \times 10^{-3}$ with Cd(II) and $C_A = 8.0 \times 10^{-3}$ M with Pb(II) and Tl(I)] and varying concentration of oxalate [$C_X = 8.0 \times 10^{-3}$ M to $40.0 \times \times 10^{-3}$ M with Cd(II) and $C_X = 4.0 \times 10^{-3}$ M to 20.0×10^{-3} M with Pb(II) and Tl(I)].

All the plots of log $[i/(id - i)]$ versus-$E_{d.e.}$ yielded straight lines with slopes, which agree with the theoretical value corresponding to $n = 2$ for Cd(II) and Pb(II) and $n = 1$ for Tl(I), respectively. The mean values of the slopes (Cd(II) = 0.0297, Pb(II) = 0.0300, Tl(I) = 0.0598) showing the reversibility of the reduction. Rectilinear plots of id vs $h^{\frac{1}{2}}$ passing through the origin, established the diffusion controlled nature in each case. The $E^{\frac{1}{2}}$ values from the log plots of the above mentioned current-voltage curves and corresponding diffusion current values have been recorded (see Tables I, II and III). The pH of the solution remained at pH 5 within the all concentration range of mixed ligand employed in the present studies. It was found that the nature and behaviour of the wave remains almost the same at lower pH range (2 pH to 6 pH) while at higher pH (8 pH to 12 pH) metal precipitated. The $E^{\frac{1}{2}}$ values of the metal ion in mixed ligand systems are more negative than that of the free metal ion, since the ion must be first liberated from the complex, this requires certain amount of energy. From the shift in half wave potential of the complexed metal ion and the concentration of the complex forming agents, both the stability constants of complex and its composition can be calculated.

Souchay and Faucherre [12] derived an equation where a metal ion complexes with two ligand species simultaneously in solution. If the complexing reaction of the following type is considered:

$$\mathrm{M} + i\mathrm{A} + j\mathrm{X} \rightarrow \mathrm{MA}_i\mathrm{X}_j \qquad (1)$$

Table I

Cadmium(II) mixed ligand system

$C_A(M)$	0.000	0.008	0.010	0.020	0.030	0.040	0.020	0.020	0.020	0.020
$C_X(M)$	0.000	0.020	0.020	0.020	0.020	0.020	0.008	0.010	0.030	0.040
30 °C *id* (μA)	4.730	3.540	3.470	3.330	2.930	2.660	3.580	3.510	3.160	2.970
$-E^{\frac{1}{2}}$(V)	0.592	0.966	0.974	1.001	1.016	1.026	0.988	0.992	1.006	1.010
$K_{MA_iX_j}$*	—	20.486	20.465	20.469	20.467	20.447	20.398	20.459	20.470	20.491

* Mean value = 20.461 and standard deviation = 0.030

Table II

Lead(II) mixed ligand system

$C_A(M)$	0.000	0.004	0.006	0.008	0.010	0.020	0.008	0.008	0.008	0.008
$C_X(M)$	0.000	0.008	0.008	0.008	0.008	0.008	0.004	0.006	0.010	0.020
30 °C *id* (μA)	4.200	4.160	4.110	4.000	3.850	3.660	4.120	4.050	3.840	3.730
$-E^{\frac{1}{2}}$ (V)	0.412	0.702	0.718	0.730	0.740	0.768	0.722	0.728	0.734	0.742
$K_{MA_iX_j}$*	—	18.934	18.940	18.966	19.020	19.059	18.999	19.026	19.015	18.986

* Mean value = 18.934 and standard deviation = 0.048

Table III

Thallium(I) mixed ligand system

$C_A(M)$	0.000	0.004	0.006	0.008	0.010	0.020	0.008	0.008	0.008	0.008
$C_X(M)$	0.000	0.008	0.008	0.008	0.008	0.008	0.004	0.006	0.010	0.020
30 °C *id* (μA)	3.510	2.920	2.730	2.620	2.460	2.350	2.770	2.690	2.420	2.230
$-E^{\frac{1}{2}}$(V)	0.486	0.626	0.638	0.646	0.652	0.672	0.628	0.638	0.650	0.668
$K_{MA_iX_j}$*	—	6.862	6.900	6.917	6.933	6.975	6.907	6.903	6.904	6.920

* Mean value = 6.933 and standard deviation = 0.030

with the restriction that a single mixed ligand entity MA_iX_j is formed, then the shift in the $E^{\frac{1}{2}}$ of the polarographic wave of the metal ion as a function of the concentration of the added reagents A and X is given by

$$\Delta E^{\frac{1}{2}} = \frac{2.303\,RT}{nF}\log\left[\frac{D_{free}}{D_{Comp}}\right]^{\frac{1}{2}} - \frac{2.303\,RT}{nF}\log K_{MA_iX_j} - i\,\frac{2.303\,RT}{nF}\log C_A - j\,\frac{2.303\,RT}{nF}\log C_X . \qquad (2)$$

The ratio $D_{free}/D_{Comp.}$ was obtained from the values of the limiting current measured at $C_A = C_X$ and extrapolated to $C_A = C_X = \infty$ respectively. From plots of ΔE versus $\log C_A$ (C_X kept constant) values for i and from those

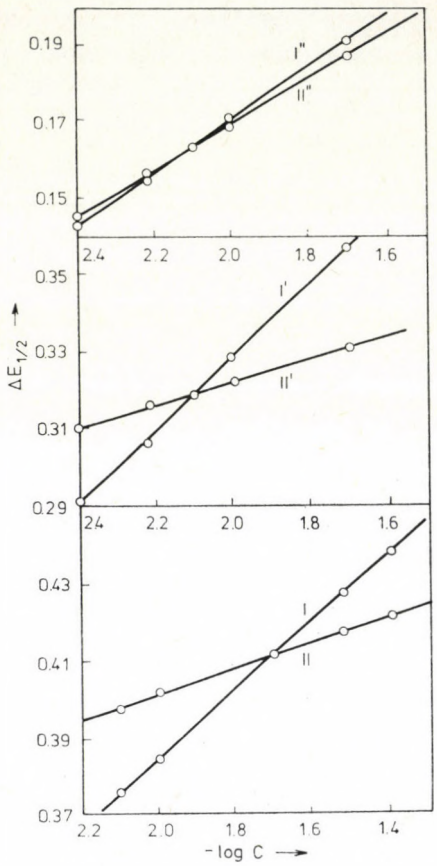

Fig. 1. Plots of $\Delta E^{\frac{1}{2}}$ versus — log C_A (I) and versus — log C_X (II) respectively, at 30 °C for Cd(II) containing systems. The meanings of I' and II' are the same for systems containing Pb(II), and tohse of I" and II" for systems containing Tl(I)

of $\Delta E^{\frac{1}{2}}$ versus log C_A (C_X kept constant) values for j can be obtained since on differentiation.

$$\left[\frac{\partial(\Delta E^{\frac{1}{2}})}{\partial(\log C_A)}\right]_{C_X} = -\,i\,\frac{2.303\,RT}{nF} \tag{3}$$

$$\left[\frac{\partial(\Delta E^{\frac{1}{2}})}{\partial(\log C_X)}\right]_{C_A} = -\,j\,\frac{2.303\,RT}{nF} \tag{4}$$

plots of (I) $\Delta E^{\frac{1}{2}}$ versus log C_A (C_X kept constant), (II) $\Delta E^{\frac{1}{2}}$ versus log C_X (C_A kept constant) yielded straight lines. Figure 1, curves I and II for Cd(II) curves I' and II' for Pb(II) and curves I" and II" for Tl(I) containing systems and thus establish the formation of a single mixed ligand entity MA_iX_j.

The co-ordination numbers "i" and "j" of ligand A and X were determined from the graphs shown in Figure 1 and were found to be $i = 2.94$ for

Cd(II), 3.18 for Pb(II) and 1.16 for Tl(I) and $j = 1.13$ for Cd(II), 0.98 for Pb(II) and 1.02 for Tl(I). Values of i and j were used in equation (2) for the calculation of the stability constant $K_{MA_iX_j}$ which were found to be 20.461 for Cd(II), 18.934 for Pb(II) and 6.913 for Tl(I).

The present investigation suggests the formation of only one kind of mixed ligand species $(Cd\ A_3X)^{-6}$, $(Pb\ A_3X)^{-6}$ and $(TlAX)^{-4}$ with the mixed ligand (*n*-butylthioglycolateoxalate) system.

*

The authors wish to express their sincere thanks to prof. R. P. Tiwari, vice principal and Head of the Chemistry Department and to Prof. M. M. Khatri, Principal for providing research facilities.

REFERENCES

[1] Sos, J., Csalay, L., Fecher, I., Gati, T., Harmos, Gy., Kemeny, T., Perenyi, L.: Schweizmed Wochschr., **86,** 1077 (1956); C. A., **52,** 2281 i (1958)
[2] Schroeder, H. A., Menhard, E. M., Perry, M. H. (Jr.): J. Lab. Clin Med., **45,** 431 (1955)
[3] Kyuma, Terao, Takashi, Sakashita, (to Takeda Pharmaceutical Industries Co.) Japanese Patent, 4948 (September 30, 1953), Chem. Abs., **48,** 11010 i (1954)
[4] Seiichiio, Y.: Fukuoka Acta Med., **45,** 234 (1954)
[5] Saxena, R. S., Gupta, K. C.: J. Polarography. Soc., **14,** 24 (1968)
[6] Saxena, R. S., Gupta, K. C.: Z. Naturforsch., **24** , 135 (1969)
[7] Saxena, R. S., Singh, P.: Indian J. Chem., **8,** 76 (1976)
[8] Gupta, K. C., Kaur, T.: J. Inorg. Nucl, Chem., **41,** 1602 (1979)
[9] Gupta, K. C., Kaur, T.: Electrochim. Acta, **24,** 1133 (1979)
[10] Gupta, K. C., Sharma, Kalpana K.: Analyst, **107,** 1512, (1982)
[11] Gupta, K. C., Sharma, Kalpana, K.: Bull. Chem. Soc. Jpn, **56,** 1867 (1983)
[12] Souchay, P., Faucherre, J.: Bull. Soc. Chim. France, **1947,** 529

BOOK REVIEWS

Adcances in Polymer Science, Vol. 52/53 H. H. Kausch (editor): Crazing in Polymers

(Springer Verlag, Berlin, Heidelberg New York, Tokyo, 1983)

This volume consists of six parts, each of them dealing with different aspects of crazing.

E. J. Kramer: *Microscopic and Molecular Fundamentals of Crazing* (26 Figures, 133 References, 56 pages)

Crazes are small crack-like defects formed usually under tensile stress. Their two surfaces are bridged by many small fibrils with diameters in the range 5 to 30 nm. This crazing is a process of plastic deformation, and as such it is the most important source of fracture toughness in polymer glasses. The improved impact toughness produced by rubber modification of polystyrene is an example of the practical application of crazing nucleation.

Craze nucleation, craze growth, craze hydromechanics are described with their theoretical background and experimental results.

The microstructure of crazes may be studied by either diffraction methods or directly by TEM. Small angle X-ray scattering gives information on the fibril structure averaged over many crazes in bulk samples, the TEM micrograph can detect the fibrillar nature of the craze.

On the SAXS patterns the high angle tail of the curve obeys Porod's law, and from this and from the Q invariant the mean fibril diameter can be calculated. The same pattern also gives information on the arrangement of fibrils.

Crazing is strongly influenced by the molecular entanglements, and calculations are presented how the craze fibril breakdown is influenced by the entanglement density of the polymer.

M. Detenmaier: *Intrinsic Crazes in Polycarbonate: Phenomenology and Molecular Interpretation of a new Phenomenon* (29 Figures, 193 References, 48 pages)

Ordinary crazes (called craze-I or extrinsic type of craze) are described in the literature. The phenomenon is frequently controlled by foreign particles and surface grooves which both act as stress concentrators. In multiphase systems, such as rubber-modified polymers, the rubber particles act as stress concentrators. The intensive light scattering from crazes gives rise to the phenomenon of stress-whitening.

The intrinsic craze phenomena (called crazes-II) have been reported for amorphous single phase polymers. Chain ends, weak molecular mass substances or additives may generate defects which allow local plastic deformation to occur. Such intrinsic craze phenomenon was investigated in bisphenol-A polycarbonate, drawn to high stresses and strains close to the glass temperature region, T_g.

Intrinsic crazing is a post-yield phenomenon, it could be distinguished from the type I by optical and by SAXS methods. A molecular interpretation is given and a detailed description, how SAXS can be used for revealing craze microstructure. It is hoped that this research direction opens some new paths to a better understanding of the phenomenon of cavitational plasticity in polymers.

W. Döll: *Optical Interference Measurements and Fracture Mechanics Analysis of Crack Tip Craze Zones* (57 Figures, 143 References, 64 pages)

In glassy thermoplastics the craze zone contains molecular chains of the polymer, which are drawn out of their amorphous arrangement in the bulk material into bundles under

the action of the principal tensile stress component acting normal to the crack plane. Crazes have a lower density and a lower refractive index than the bulk polymer. Their sizes and shapes can be measured by optical interference, provided that some conditions are fulfilled.

Using the results of fracture mechanics, quantitative information can be derived about the craze stress from interference optical measurements. The review explains the fundamental aspects of the fracture behaviour of glassy thermoplastics. The optical interference method is described, and the results obtainable in this way are discussed. One section considers the behaviour of cracks and crazes in specimens subjected to quasistatic loading. The last section examines the role of crazing associated with fatigue crack growth.

J. A. Sauer and C. C. Chen: *Crazing and Fatigue Behavior in One- and Two-Phase Glassy Polymers* (50 Figures, 74 References, 54 pages)

Crazing involves orientation of polymer chain segments in the direction of the principal stress, together with caviation or voiding. It tends to develop at stress concentration sites. The review investigates deformation and fracture mechanisms in glassy polymer systems subject to alternating stresses, comparing and contrasting their behavior with that observed under monotonic loading. Craze initiation, strain softening due to shear deformation and fatigue life and fracture surface morphology are studied as a function of the applied stress and test frequency. The deformation and fracture response are investigated, under static and dynamic conditions, of several rubber-modified glassy polymers and their behavior is compared with that of the corresponding unmodified polymers. Two polymer systems are considered: PS and its rubber-modified varieties, such as medium impact polystyrene (MIPS) and high impact polystyrene (HIPS); the other system is styrene-acrylonitrile (SAN) based copolymers of varying acrylonitrile contents and of varying molecular mass, together with a rubber-modified version of this polymer, viz. acrylonitrile-butadienestyrene (ABS).

K. Friedrich: *Craze and Shear Bands in Semi-Crystalline Thermoplastics* (39 Figures, 151 References, 50 pages)

The crystalline and amorphous phases are arranged within a polymer solid depending strongly on the strain and thermal history. Unstrained polymers usually crystallize in a spherulitic manner, the spherulites being point-nucleated semicrystalline entities which grow in a spherically symmetrical form. The spherulites are composed of radiating lamellar crystals in which the molecular axis is perpendicular to the growth direction. The lamellae are folded chain crystals. As a rule, the chains in the crystal lattice are oriented at 90° to the lamellar plane. Some of the chains do not immediately reenter the crystal core of the same lamella by forming a tight loop, but remain in the amorphous surface layer as free chain ends (ciliae), or reenter forming loose loops. Spherulite size, size distribution can be varied by the thermal history and nucleating agents. Different local cooling conditions can lead to differences in the morphology across the specimen thickness.

Polymers which have been crystallized under high melt strains have a microstructure similar to that of a fiber cold-drawn. Highly oriented semicrystalline fibers have a microfibrillar structure with lateral dimensions of 20 to 40 nm, containing folded chain crystallites as the most important structural elements. In addition, they contain amorphous regions with coiled chains and chain ends (ciliae). Loading such a microfibrillar structure in the direction of orientation results in the shear loading of the microfibrils, the dilatational loading of the amorphous regions and the stretching of molecules connecting adjacent crystallites, the so-called inter- and intrafibrillar tie molecules.

The formation of crazes in semicrystalline polymers is a common response to an applied tensile stress. The crazing behavior is modified by the morphology of the crystalline polymer. In some cases the plastic deformation is confined to the weak spherolitic boundaries, resulting in interspherulitic craze formation and subsequent boundary fracture. Stress whitening after neck formation in tensile bars of crystalline polymers under plane stress conditions may be associated with some kind of craze-II formation, in analogy to the corresponding observations in amorphous materials.

Shear banding is controlled by a shear stress which encourages lateral movements without voiding.

A. S. Argon, R. E. Cohen, O. S. Gebizlioglu and C. E. Schwier: *Crazing in Block Copolymers and Blends* (33 Figures, 68 References, 60 pages)

The control of crazing by the incorporation of compliant heterogeneities can impart very substantial toughness to a normally brittle glassy polymer.

Several factors are important in the achievement of acceptable toughness: the size of the heterogeneities, their internal structure, the need to graft the rubbery heterogeneities to

the glassy matrix to achieve good adhesion, and a sufficiently high molecular weight in the glassy phase to form craze matter with high mechanical integrity. A summary is given of investigations of the sources of toughtening in both pure di-block copolymers and blends of di-blocks with additional homopolymer to coarsen the microstructure, and to form particulate heterogeneities.

The book is an excellent summary about our knowledge in the field of crazing in polymers. The microstructure of crazes and the role of crazes in deformation and fracture of amorphous and crystalline polymers gives a key to understand the physical and mechanical properties of polymers.

Géza BODOR

Research Institute for Plastics Industry, Budapest

Advances in Polymer Science, Vol. 54 Spectroscopy: NMR, Fluorescence, FT-IR

(Springer Verlag, 1984. 166 pp.)

The Springer Publishing Co. has surpassed its 50th volume in the series "Advances in Polymer Science". In this series invited critical review articles are published dealing with new developments in all fields of Polymer Science, in English.

Volume **54** contains three reviews, which are not closely related, therefore they are discussed separately.

(1) E. D. von Meerwall: *Self-diffusion in Polymer Systems Measured with Field Gradient Spin Echo NMR Methods* (11 Figures and 79 References)

Nuclear Magnetic Resonance (NMR) has two main goals in the study of polymers: it is a tool for characterization the chemical structure, and its is used to measure molecular motion in polymer solutions, melts and in different networks.

The latter can be measured either by observing the width of the spectral features or by measuring NMR relaxation times, the spin-spin relaxation time T_2 and the spin-lattice relaxation times T_1 or $T_{1\sigma}$. (Regrettably, the literature uses T_2 and T_1 instead of t_2 and t_1 for a time expression. T is supposed to denote temperature in physical chemistry notations.)

This article reviews diffusion measurements in polymer systems made with the Steady Gradient Spin Echo (SGSE) method and its Pulsed-Gradient (PGSE) variant.

These methods are useful in three areas, in examining the diffusion of polymers in their own melt and in concentrated solutions, in dilute and semidilute solutions, and the diffusion of penetrants and diluents in polymer hosts.

Theories which attempt to predict absolute diffusion rates based on molecular and dynamic parameters do not appear yet to be sufficiently mature. The measured parameters are, in general, merely empirically correlated with the molecular and structural attribute. According to the early results, there is a tendency to use field gradient spin echo methods for routine rheological characterization and for rapid self-diffusion measurements.

(2) S. N. Semerak and C. W. Frank: *Photophysics of Excimer Formation in Aryl Vinyl Polymers* (9 Tables and 213 References)

Excimer formation and energy migration processes are characterized mainly in aryl vinyl polymers, and the excimer probe was used to study the polymer structure quantitatively.

In the first part of the review, the major photophysical species and processes are summarized, occurring in some polymers under the experimental conditions applicable to solid blends.

The effects of oxygen in photophysics are summarized, and the effects of the rigidity of the host matrix relative to solution are discussed.

The molecular structure of PS, P2VN and the photobehaviour of the naphthalenophanes are reviewed.

In the second part, evidence for and against migration of singlet state energy in aryl vinyl polymers are presented. The most likely mechanism of the energy migration is discussed.

Specific conclusions relevant to the photophysics of PS and P2VN are deduced. The fields of application of this technique are the analysis of the thermodynamics of multicomponent systems and the kinetics of phase separation.

(3) J L. Koenig: *Fourier Transform Infrared Spectroscopy of Polymers* (29 Figures and 344 References)

This is a summary of the theory and application of Fourier transform infrared spectroscopy to the characterization of polymers.

The basis theory, the sampling techniques and the spectral operations are described.

The digitized spectra can be treated by sophisticated data processing techniques greatly increasing the utility of infrared spectra for qualitative and quantitative purposes.

The following data processing techniques are discussed: absorbance subtraction, the ratio method, factor analysis, the least square curve fitting for quantitative analysis.

A detailed summary is given on the experimental techniques in FT-IR: transmission measurements, diffuse reflectance spectroscopy, internal reflexion spectroscopy, external reflexion spectroscopy, reflexion-absorption spectroscopy, emission spectroscopy and photoacoustic spectroscopy are discussed.

Using the FT-IR techniques, the structural defects could be determined. Different conformational structures could be isolated by variation of the annealing conditions or by varying the measurement temperature or the pressure applied.

In polymer chemistry FT-IR is used for oxidation studies, for the determination of irradiation damage of polymers. In polymer structure analysis FT-IR has been very significant in the field of polymer blends, polymer surfaces, and in determining structural changes induced by mechanical deformation.

Short time phenomena can be detected, as the FT-IR speed of measurement is by two orders of magnitude shorter than when using a dispersive instrument. This allows the monitoring of short-time changes for a variety of processes in polymers, such as kinetics, crystallization, heating, orientation and relaxation.

Géza Bodor

Research Institute for Plastics Industry, Budapest

Modern Trends in Analytical Chemistry, Part A and B

Edited by E. Pungor, G. E. Veress, I. Buzás, Akadémiai, Kiadó, Budapest 1984, 198 pages

The volume comprises the lectures and the discussion of the lectures of two Symposia, held at Mátraháza (Hungary) in 1982.

The first part, Part *A*, summarizes the lectures of the symposium on Electrochemical Detection in Flow Analysis. The main object of the symposium was the reporting and discussion of recent results achieved in the domain of the development of electrochemical sensors of novel type. W. Kemula and W. Kutner (Warsaw, Poland) reported in their plenary lecture on amperometric detectors used in liquid chromatography, W. E. Morf and W. Simon (Zürich, Switzerland) on clinical potentiometric detectors, H. A. Mottola, Ch. M. Wolff, A. Iob and R. Gnanasekaran (Stillwater, USA) on enzyme electrodes, H. Poppe and H. W. Lan Rooijen (Amsterdam, The Netherlands) on research in conjunction with the noise and stability of solid electrodes.

In the part containing further 21 lectures, topics such as various modes of application of ion-selective electrodes, autmatic method of polarographic series analysis, the elegant evaluation by Fourier transformation of triangle-programmed continuous titration, automation of titration, and novel voltammetric electrodes are covered.

Details of the discussions, following the single lectures are also rather valuable, because several questions are answered, which may arise in the reader.

In summary, the subject covered by the symposium gives an excellent cross-section of trends characteristic of research in conjunction with flow systems analysis.

The second part of the book, Part *B*, contains the application of computers in chemical analysis, its modern trends, the description of the methods of pattern recognition applicable in analytical chemistry, and recent progress achieved in this field.

H. Malissa (Vienna, Austria) emphasized in his plenary lecture the role of computer techniques in analytical chemistry, and summarized the fields of application. H. C. Smit (Amsterdam, The Netherlands) gave a plenary lecture on the methods of parameter estimation J. T. Clarc and G. Székely (Bern, Switzerland) on the pattern recognition methods of structure identification, L. A. Gribow (Moscow, USSR) — an expert of international renown of spectrum evaluation — on the problems of computerized structure identification of multiatomic mol-

ecules, J. Kwiatowski and W. Riepa (Dortmund, FGR) on the optimization of spectrum library search.

One part of the discussions dealt with the applications of pattern recognition and with the results of applications, while the other part with the comparative evaluation of pattern recognition methods.

Both parts of the conference, Part *A* as well as Part *B*, report on the results of the most advanced research trends of analytical chemistry.

Therefore, all those active in research and development work in the field of analytical chemistry, and all those who use modern analytical methods will peruse with pleasure this book, which gives in a clear form, in well organized chapters, information on the latest advances in the development of continuous electrochemical detectors, and in the application of pattern recognition.

Ilona Buzás deserves credit for careful compilation.

János INCZÉDY

Veszprém University of Chemical Engineering, Dept. of Analytical Chemistry, Veszprém

Structure and Bonding, Vol. 55

Transition Metal Complexes — Structures and Spectra.
Springer-Verlag, Berlin—Heidelberg—New York—Tokio, 1983

Vol. **55** of the series contains for reviews:

(1) M. H. Gubelmann, A. F. Williams: The Structure and Reactivity of Dioxygen Complexes of the Transition Metals (pp. 1—65);

(2) M. Bacci: The Role of Vibronic Coupling in the Interpretation of Spectroscopic and Structural Properties of Biomolecules, (pp. 67—99);

(3) F. Valach, B. Koreň, P. Sivy, M. Melnik: Crystal Structure Non-Rigidity of Central Atoms for Mn(II), Fe(II), Fe(III), Co(II), Co(III), Ni(II), Cu(II) and Zn(II) Complexes (pp. 101—151);

(4) F. Mathey, J. Fischer, J. H. Nelson: Complexing Modes of the Phosphole Moiety (pp. 153—201).

(1) The study of dioxygen complexes of the transition metals is generally accepted to have begun with the report by Fremy in 1852. A satisfactory explanation of his results had, however, to await the development of a general theory of coordination compounds and Pauling and Coryell proposed the first of many theoretical models to explain the iron dioxygen interaction in haemoglobin in 1936. The increasing availability of physical methods coupled with a better understanding of the electronic structures has given considerable encouragement to the study of these compounds in recent years.

This article gives a review of the complexes in which a dioxygen ligand is bonded to a transition metal. The structure, the electronic structure, and the reactivity — these three aspects of the compounds are discussed in details. The structural part collects the recent X-ray crystal structure data and the other structural ones obtained by other methods. The electronic structure is first considered in qualitative terms, and this model is compared with the results of calculations and with spectroscopic data. The reactivity of the complexes is discussed separately for each structural class in terms of the electronic structure. The review gives a clear summary of current knowledge of these compounds for workers interested in their application to catalysis and in their role in biochemical systems (529 references).

(2) The expression "vibronic coupling" is widely spread in the literature nowadays, although it is rather vague and sometimes misleading. The word "vibronic" derives from the contraction of two adjectives, "vibrational" and "electronic", and in its more common meaning, indicates a dynamic interaction between vibrational and electronic motions. Another frequently used definition of vibronic coupling is "the breakdown of the Born-Oppenheimer approximation".

The aim of the author is to review several biomolecules, the spectroscopic and structural properties of which have been so far interpreted in the light of the Jahn-Teller effect. After a brief outline of the Jahn-Teller effect, the whole problem in critically re-examined separating the systems for which the experimental evidence of the effect is clear, from those where its effectiveness is still debated. Some suggestions are also given for a proper inclusion

of the vibronic coupling in future analysis on biomolecules. The importance of this article is that the first widely attention is paying in it to the role of such a coupling in biological systems (169 references).

(3) The metal atom in crystal structures of coordination compounds is surrounded by adjacent atoms located in the apices of a convex polyhedron. Usually, polyhedra of coordination compounds are deformed by some holosymmetric form. Such a non-rigidity of complexes in the solid state mainly depends on the properties of the central atom, ligands and of the crystal as a whole. The review deals with the conception of crystal structure non-rigidity for central atoms of some selected complexes by the using of statistical distributions of interatomic distances central atom — nearest ligand atom (M—L; M=Mn(II), Fe(II), Fe(III), Co(II), Co(III), Ni(II), Cu(II) and Zn(II)). The dispersion of these empirical distributions has been introduced as a measure of non-rigidity of central atoms — based on the vector equilibrium principle. Starting from the distribution of M—L distances for certain types of central and ligand atoms, the contribution of atoms of the inner coordination sphere to the vector equilibrium of crystal structures is discussed. The compounds are classified both with respects to the geometry of their inner coordination sphere and to their crystal structure aspect. Such a statistical approach with a sufficiently great number of crystal structure data of different nearest surroundings of central atoms of the same type allows us to suppose some averaging of contributions of more distant atoms. By the consideration it is possible to determine the contribution of the central atom to the crystal structures (72 references).

(4) The growing interest aroused by phospholes in coordination chemistry can be attributed to three main reasons. The first one is a question: what is the influence of the partial delocalization of the phosphorus lone pair upon the complexing ability of phospholes. This is namely related to the widely discussed question of phosphole aromaticity. The second one is the discovery of phosphametallocenes. Apart from their interest as phosphorus analogs of η^5-cyclopentadienyl complexes, phosphametallocenes are the only λ^3-phosphorus-carbon heterocycles for which an extensive chemistry of electrophilic substitutions at carbon has been demonstrated. The third one lies in the tremendous variety of complexing modes found for the phosphole nucleus. Another less obvious, but compelling reason is that phospholes are now readily available on a large scale. In the paper there are also included a section on arsole and stibole complexes, and a brief comparison between azametallocenes and their phosphorus analogs. The review gives a complete coverage of the literature up to October 1981 (116 references).

Vol. **55** includes an Author index of the Volumes **1—55** also.

Sándor PAPP

Veszprém University of Chemical Engineering
Department of General and Inorganic
Chemistry,
Veszprém

Polymers — Properties and Applications, Vol. 8. W. L. Hawkins: Polymer Degradation and Stabilization

(119 pages, 33 figures, 16 tables, 133 references)

The monograph is organized in six main chapters. The first of these (B) deals with the non-inhibited degradation of polymers. It discusses non-oxidative thermal decomposition, oxidative degradation initiated in different ways, recent research results on the oxidation of some polymers, and mentions briefly hydrolytic degradation.

In the next four chapters (C—F) stability is dealt with. The methods of increasing the thermal stability (C) are briefly discussed, those of increasing thermooxidative stability (D) are treated more extensively, and the following two chapters (E and F) summarize knowledge concerning stability to radiation and to ozone. The last chapter (G) describes some methods of testing.

Though the title suggests a comprehensive coverage of the subject, this is impossible in a book of this size. Thus, the discussion is restricted to the description of the mechanism of degradation processes induced by heat, radiation, oxygen, and their combination, and of the inhibition of these processes. Within this field prominence is given to thermo- and photo-oxidation and the problem of their suppression, so that the domain discussed in detail is, in spite of the general formulation of the title, rather narrow.

The mode of discussion does not follow some concept consequently applied; the volume cannot be regarded as a summary on handbook level of already settles, accepted knowledge, as the narrowed-down and non-uniform discussion and the not adequately exact description of certain definitions and reaction mechanisms make it unsuitable for this purpose. It cannot be considered a critical survey of recent knowledge either, since it hardly mentions the results of several research schools. In recent times several monographs have been published on similar subjects; compared with these, the work reviewed here offers a rather small amount of new knowledge.

Margit IRING

Central Research Institute for Chemistry of the Hungarian Academy of Sciences, Budapest

Jürgen Fuhrhop, Gustav Penzlin: *Organic Synthesis. Concepts, Methods, Starting Materials*

Verlag Chemie, Weinheim, 1983. XI and 355 pp.

Both the practice and the theory of organic synthesis have developed enormously in the past ten to fifteen years. After Corey's pioneering theoretical considerations on retrosynthetic analysis and on computer-aided organic synthesis, followed by the related theoretical works of many brilliant researchers, the art of the design of the synthesis of complex organic molecules became a widely discussed aspect of modern organic chemistry. Complex synthetic processes were systematically analysed, new concepts and methods developed, and these have been treated in many excellent reviews and books. It is therefore an especially remarkable achievement that the present authors. Professor Jürgen Fuhrhop and Dipl. Chem. Gustav Penzlin, both of the Freie Universität, Berlin, have produced such an original and effective treatment of this topic.

The book consists of four main chapters. The first three discuss the various aspects of the theory of the syntheses. All these three chapters have an introduction and a summary, and the symbols and concepts used are defined.

Chapter **1**, "Synthons in the synthesis of carbon chains and carbocycles" (pp. 1—86), deals with d^1-synthons, d^2-synthons, d^3-synthons, etc., umpolung, synthons of different oxidation stages, 1,2-, 1,3-, 1,4-, 1,5- and 1,6-difunctional compounds, synthons with different ring sizes, and bridged hydrocarbons.

In Chapter **2** (pp. 87—152), "Selective functional group interconversions (FGI)", the main titles are: reduction, oxidation, olefin synthesis, synthesis of carboxylic acid derivatives, nitrogen heterocycles, protection of functional groups.

Chapter **3** (pp. 153—196), "*Retro*-synthetic analysis of simple organic compounds", is especially interesting, if it is proper to single out one part of this quite excellent book. This chapter provides an introduction to the planning of syntheses using the synthon approach. An original aspect of the chapter is that a systematic survey of commercially available organic starting materials is given. These "inexpensive" starting materials are listed in Tables 4—15 on pp. 156—174. Difunctional, trifunctional and oligofunctional open-chain reagents, silicon- and phosphorus reagents, nonaromatic carbocyclic reagents, and oligocyclic (in fact mainly bicyclic) hydrocarbon derivatives (over 700 chemicals) are tabulated. Further Tables in Chapter **4** survey the most important inexpensive natural substances, which can also serve as starting materials. For example, in Table 19 "Inexpensive sugars and sugar derivatives", in Table 20 "Inexpensive steroids", and in Table 21 "Inexpensive alkaloids" are listed.

In connection with this unusual feature of the book, not only the symbols, but all the important basic expressions used are exactly defined. Thus, it is explained, for instance, what compounds are considered "simple". The definition here is as follows: "A simple molecule is one that may be obtained by four or less synthetic reactions from inexpensive commercial compounds". The authors call a compound "inexpensive" if it costs less than or around one German mark per gram. In the selected lists in the Tables, the approximate prices of the chemicals are given in German marks per 10 g. The main sources are the Aldrich-Europe Merck and Fluka catalogues. Only those compounds that cannot be purchased inexpensively are considered synthetic target molecules in this book.

The remaining part of Chapter **3** (pp. 175—196) is devoted to a discussion of *retro*-synthetic analysis („antithesis"). Numerous useful and instructive examples are given.

Chapter 4. "Methods in the construction of complex molecules" (pp. 197—299), deals with the most characteristic reactions of different substance classes. Reactions specific for each class of compounds are described, and entire total syntheses are given only in some cases. The following main substance classes are treated: oligonucleotides, peptides, macroheterocycles, porphyrins, chlorophyll *a* and corrins, carbohydrates as starting materials, prostaglandins, steroids, alkaloids, synthetic drugs, antibiotics, and finally "esoteric" polycyclic hydrocarbons, i.e. unusual, highly-condensed polycyclic hydrocarbons which do not relate to natural hydrocarbons or fulfil society needs. In this last part the syntheses of such beautiful but really uncommon molecules as dodecahedrane $[(CH)_{20}]$ and kekulene $[(C_{48}H_{24})]$ are discussed.

A large section deals with the design of syntheses, and the main features of the syntheses of more complex molecules are discussed. The application of retrosynthetic analysis in the design of more complex molecules is used throughout. The widely applied modern concepts of organic synthesis, the synthon approach, and strategies to achieve regioselectivity and stereoselectivity in carbon-carbon bond formation and functional group transformation are discussed thoroughly. Strategies to enforce thermodynamically unfavoured reactions are also included.

The book is exceptionally well edited. The text is very concise, some 200 abbrevations are used, and an enormous amount of material has been condensed into the 299 pages of text. Some 800 references are listed in alphabetical order (pp. 301—318). Then follows a very detailed subject index (pp. 319—355), unusual today, which helps greatly in the search for a given topic or a compound. The index also includes the page where the price of the starting material is given! The last two inside cover pages list the some 200 abbreviations (mainly reagents and groups) applied, which made possible such a compact text.

To summarize: this book is a brand new treatment of the concepts and methods of modern organic synthesis from a theoretical point of view, and also includes useful data and a compilation on the starting materials. The book discusses the up-to-date theoretical considerations used in modern organic synthesis. The examples are well selected and the discussions are on a high theoretical level. The reviewer considers it highly original and one of the best edited books on the concepts and theory of organic synthesis. This volume is a must for all organic chemists dealing with synthesis!

Gábor BERNÁTH

Institute of Pharmaceutical Chemistry,
University Medical School, Szeged

William H. Watson: (Ed.) *Stereochemistry and Reactivity of Systems Containing π-Electrons*

Verlag Chemie International, Deerfield Beach, Florida 1983. pp. XIII and 439.

This volume, which is the third in the series "Methods in Stereochemical Analysis" (Series Editor: Alan P. Marchand), contains the Proceedings of the symposium "Stereochemistry and Reactivity in Pi Systems" held on May 19—22, 1982 in Fort Worth, Texas, in recognition of Professor Paul Bartlett's many years of leadership in physical organic chemistry.

The book contains 12 lectures and, with the exception of one lecture, the generally very active discussions following the presentations are also reported. For each lecture a detailed list of references is given.

Most of the lectures were devoted to the problem of "pyramidalization" of sp^2 hybridized carbon atoms, and reactions of norbornene and more highly condensed analogues, e.g. *syn*-sesquinorbornenes and other polycyclic compounds, were treated.

The following lectures are included in the volume: K. N. Houk: Theoretical studies of alkene pyramidalizations and addition stereoselectivites, L. A. Paquette: Long-range stereoelectronic control by norbornyl frame works of cycloaddition and electrophilic processes. P. D. Bartlett et al.: Structural and geometric factors in the reactivity of π-systems. R. Gleiter and M. G. Böhm: Regio- and stereoselectivity in Diels-Alder reactions. Theoretical considerations. P. Vogel: Exocyclic dienes, tetraenes, and hexaenes. Diels-Alder reactivity, regioselectivity and stereoselectivity. F. D. Greene: Findings new and old in olefin-electrophile reactions. W. Adam et al.: The di-π-methane rearrangement revisited. H. O. House: Enones with distorted double bonds. K. J. Shes: Synthesis and chemistry of bridgehead alkenes.

The topics of the last three papers are somewhat different from the earlier-mentioned ones. These are: C. S. Foote et al.: Singlet oxygen: new and old mysteries. P. J. Wagner:

Conformational mobility and photochemistry. W. E. Noland: Cyclizative condensation and addition reactions of indoles and indenes.

The deviation of sp^3 hybridized carbon atoms from planarity causes many theoretically interesting reactions. Numerous interesting features of the Diels-Alder reactions are discussed.

In the book special emphasis is laid on mechanistic and stereochemical reasoning to reactions of compounds containing π-systems. The reactivities of some unusual polycyclic bridged compounds are very thoroughly discussed and the theoretical conclusions drawn from the treated reactions are of great interest.

For the final, camera-ready copy, the whole manuscript was retyped, which helped greatly towards the uninformity of the book. However, the original drawings of the formules remained unchanged, so that in the individual chapters these are somewhat different, though on the whole they are clear-cut. The subject index covers a somewhat modest five typed pages, and no name register is given.

This book will be particularly valuable to all investigators working with molecules containing π-systems, and to researchers interested in theoretical organic chemistry, stereochemistry and the reactions of norbornene and related polycyclic compounds.

Gábor BERNÁTH

Institute of Pharmaceutical Chemistry,
University Medical School, Szeged

PRINTED IN HUNGARY

Akadémiai Kiadó és Nyomda, Bndapest

Text

The text of the paper should be concise. The description of new compounds (in the Experimental) must include the complete analytical data. Special attention must be paid to structural formulas given within the text. Complicated (non-linear) formulas should be drawn on separate sheets of paper and their position in the text should be clearly marked. The numbering of formulas and equations (in parentheses on the right-hand side) is only needed if they are referred to in the text. Units should conform to the International System of Units (SI). In nomenclature the rules of the I.U.P.A.C. are accepted as standard. Symbols for physical quantities are printed in italic type and should, therefore, be underlined in the manuscript.

References

References should be numbered in order of appearance in the text (where the reference number appears in brackets) and listed at the end of the paper. The reference list, too, should by typed double-spaced. Journal titles are to be abbreviated as defined by the Chemical Abstracts Service Source Index.

Examples:

[1] Brossi, A., Lindlar, H., Walter, M., Schneider, O.: Helv. Chim. Acta, **41**, 119 (1958)
[2] Parr, R. G.: Quantum Theory of Molecular Electronic Structure, Benjamin, New York 1964
[3] Warshel, A.: in Modern Theoretical Chemistry, Vol. 7, Part A (Ed. G. A. Segal), Plenum Press, New York 1977

Tables

Each table should be given a Roman number and a brief informative title. Structural formulas should not be used in column headings or in the body of tables.

Figures

Figures should be numbered consecutively with Arabic numerals. Their approximate place should be indicated in the text on the margin. All figures must be identified on the back by the author's name and the figure number in pencil. Standard symbols (such as circles, triangles, squares) are to be used on line-drawings to denote the points determined experimentally. Line-drawings must not contain structural formulas and comments. Spectra or relevant segments thereof, chromatograms, and X-ray diffraction patterns will be reproduced only if concise numerical summaries are inadequate to replace them. Drawings and graphs should be prepared in black ink on good-quality white or tracing paper. Photographs should be submitted on glossy paper as high-contrast copies. Xerox or similar copies are not suitable for reproduction, but may be used for duplicate copies.

Redrawn illustrations will be sent to the authors for checking. No corrections of figures will, therefore, be accepted in the proofs.

Submission of manuscript

After having completed the corrections suggested by the referees and editors, the final manuscript should be submitted in duplicate, in a form ready for publication. If the corrected manuscript is not returned to the editors *within six weeks*, the intended publication of the paper will be regarded as withdrawn by the authors.

Page charge will not be assessed for the publication, however, authors from overseas countries must contribute to the postage of correspondence by sending, together with the manuscript, international postal coupons to the value of U.S. $ 10.—

Proofs and reprints

A set of proofs will be sent to the submitting author. The proofs must be returned within 48 hours of receipt. Late return may cause a delay in the publication of the paper. 100 reprints will be supplied to the authors free of charge.

Periodicals of the Hungarian Academy of Sciences are obtainable at the following addresses:

AUSTRALIA
C.B.D. LIBRARY AND SUBSCRIPTION SERVICE
Box 4886, G.P.O., *Sydney N.S.W. 2001*
COSMOS BOOKSHOP, 145 Ackland Street
St. Kilda (Melbourne), Victoria 3182

AUSTRIA
GLOBUS, Höchstädtplatz 3, *1206 Wien XX*

BELGIUM
OFFICE INTERNATIONAL DE LIBRAIRIE
30 Avenue Marnix, *1050 Bruxelles*
LIBRAIRIE DU MONDE ENTIER
162 rue du Midi, *1000 Bruxelles*

BULGARIA
HEMUS, Bulvar Ruszki 6, *Sofia*

CANADA
PANNONIA BOOKS, P.O. Box 1017
Postal Station "B", *Toronto, Ontario M5T 2T8*

CHINA
CNPICOR, Periodical Department, P.O. Box 50
Peking

CZECHOSLOVAKIA
MAD'ARSKÁ KULTURA, Národní třida 22
115 66 Praha
PNS DOVOZ TISKU, Vinohradská 46, *Praha 2*
PNS DOVOZ TLAČE, *Bratislava 2*

DENMARK
EJNAR MUNKSGAARD, Norregade 6
1165 Copenhagen K

FEDERAL REPUBLIC OF GERMANY
KUNST UND WISSEN ERICH BIEBER
Postfach 46, *7000 Stuttgart 1*

FINLAND
AKATEEMINEN KIRJAKAUPPA, P.O. Box 128
SF-00101 Helsinki 10

FRANCE
DAWSON-FRANCE S. A., B. P. 40, *91121 Palaiseau*
EUROPÉRIODIQUES S. A., 31 Avenue de Versailles, *78170 La Celle St. Cloud*
OFFICE INTERNATIONAL DE DOCUMENTATION ET LIBRAIRIE, 48 rue Gay-Lussac
75240 Paris Cedex 05

GERMAN DEMOCRATIC REPUBLIC
HAUS DER UNGARISCHEN KULTUR
Karl Liebknecht-Straße 9, *DDR-102 Berlin*
DEUTSCHE POST ZEITUNGSVERTRIEBSAMT
Sraße der Pariser Kommüne 3–4, *DDR-104 Berlin*

GREAT BRITAIN
BLACKWELL'S PERIODICALS DIVISION
Hythe Bridge Street, *Oxford OX1 2ET*
BUMPUS, HALDANE AND MAXWELL LTD.
Cowper Works, *Olney, Bucks MK46 4BN*
COLLET'S HOLDINGS LTD., Denington Estate
Wellingborough, Northants NN8 2QT
WM. DAWSON AND SONS LTD., Cannon House
Folkstone, Kent CT19 5EE
H. K. LEWIS AND CO., 136 Gower Street
London WC1E 6BS

GREECE
KOSTARAKIS BROTHERS INTERNATIONAL BOOKSELLERS, 2 Hippokratous Street, *Athens-143*

HOLLAND
MEULENHOFF-BRUNA B.V., Beulingstraat 2,
Amsterdam
MARTINUS NIJHOFF B.V.
Lange Voorhout 9–11, *Den Haag*
SWETS SUBSCRIPTION SERVICE
347b Heereweg, *Lisse*

INDIA
ALLIED PUBLISHING PRIVATE LTD., 13/14
Asaf Ali Road, *New Delhi 110001*
150 B-6 Mount Road, *Madras 600002*
INTERNATIONAL BOOK HOUSE PVT. LTD.
Madame Cama Road, *Bombay 400039*
THE STATE TRADING CORPORATION OF INDIA LTD., Books Import Division, Chandralok
36 Janpath, *New Delhi 110001*

ITALY
INTERSCIENTIA, Via Mazzé 28, *10149 Torino*
LIBRERIA COMMISSIONARIA SANSONI, Via Lamarmora 45, *50121 Firenze*
SANTO VANASIA, Via M. Macchi 58
20124 Milano
D. E. A., Via Lima 28, *00198 Roma*

JAPAN
KINOKUNIYA BOOK-STORE CO. LTD.
17-7 Shinjuku 3 chome, Shinjuku-ku, *Tokyo 160-91*
MARUZEN COMPANY LTD., Book Department,
P.O. Box 5050 Tokyo International, *Tokyo 100-31*
NAUKA LTD. IMPORT DEPARTMENT
2-30-19 Minami Ikebukuro, Toshima-ku, *Tokyo 171*

KOREA
CHULPANMUL, *Phenjan*

NORWAY
TANUM-TIDSKRIFT-SENTRALEN A.S., Karl Johansgatan 41–43, *1000 Oslo*

POLAND
WĘGIERSKI INSTYTUT KULTURY, Marszałkowska 80, *00-517 Warszawa*
CKP I W, ul. Towarowa 28, *00-958 Warszawa*

ROUMANIA
D. E. P., *Bucureşti*
ILEXIM, Calea Grivitei 64–66, *Bucureşti*

SOVIET UNION
SOJUZPECHAT — IMPORT, *Moscow*
and the post offices in each town
MEZHDUNARODNAYA KNIGA, *Moscow G-200*

SPAIN
DIAZ DE SANTOS, Lagasca 95, *Madrid 6*

SWEDEN
ALMQVIST AND WIKSELL, Gamla Brogatan 26
101 20 Stockholm
GUMPERTS UNIVERSITETSBOKHANDEL AB
Box 346, *401 25 Göteborg 1*

SWITZERLAND
KARGER LIBRI AG, Petersgraben 31, *4011 Basel*

USA
EBSCO SUBSCRIPTION SERVICES
P.O. Box 1943, *Birmingham, Alabama 35201*
F. W. FAXON COMPANY, INC.
15 Southwest Park, *Westwood Mass. 02090*
THE MOORE-COTTRELL SUBSCRIPTION AGENCIES, *North Cohocton, N. Y. 14868*
READ-MORE PUBLICATIONS, INC.
140 Cedar Street, *New York, N. Y. 10006*
STECHERT-MACMILLAN, INC.
7250 Westfield Avenue, *Pennsauken N. J. 08110*

YUGOSLAVIA
JUGOSLOVENSKA KNJIGA, Terazije 27, *Beograd*
FORUM, Vojvode Mišića 1, *21000 Novi Sad*

Index: 26.007

Acta Chimica Hungarica

VOLUME 119, NUMBERS 2—3, JUNE/JULY 1985

EDITOR-IN-CHIEF
F. MÁRTA

MANAGING EDITOR
GY. DEÁK

ASSISTANT EDITOR
L. HAZAI

EDITORIAL BOARD
M. T. BECK, R. BOGNÁR, GY. HARDY, K. LEMPERT,
B. LENGYEL, K. POLINSZKY, E. PUNGOR, G. SCHAY,
Z. G. SZABÓ, P. TÉTÉNYI

Akadémiai Kiadó, Budapest
ACTA CHIM. HUNG. ACHUDC 119 (2—3) 83—284 (1985) HU ISSN 0231—3146

ACTA CHIMICA HUNGARICA

A JOURNAL OF THE HUNGARIAN ACADEMY OF SCIENCES

Acta Chimica publishes original reports on all aspects of chemistry in English.

Acta Chimica is published in three volumes per year, each volume consisting of four issues, by

AKADÉMIAI KIADÓ

Publishing House of the Hungarian Academy of Sciences
H-1054 Budapest, Alkotmány u. 21.

Manuscripts and editorial correspondence should be addressed to

Acta Chimica
H-1450 Budapest P.O. Box 67

Subscription information

Orders should be addressed to

KULTURA Foreign Trading Company
H-1389 Budapest P.O. Box 149

or to its representatives abroad

Acta Chimica is indexed in Current Contents

NOTICE TO AUTHORS

Acta Chimica publishes original papers on all aspects of chemistry in English. Before preparing a manuscript for submission to this journal authors are advised to consult recent issues.

Form of manuscript

Manuscripts, tables and illustrations should be submitted in triplicate. Manuscripts should be typewritten double spaced (25 lines, 50 characters per line including spaces). The *title page* should include (1) the title of the paper, (2) the full names of the author(s) in the sequence to be published; apply an asterisk to designate the name of the author to whom correspondence should be addressed, (3) name and address of the institution where the work was done. If the paper is part of a series, reference to the previous communication must be given as a footnote.

Abstract

A summary is printed at the head of each paper. This should not exceed 200 words and should state briefly the principal results and major conclusions of the work. It should be suitable for use by abstracting services.

CONTENTS

PHYSICAL AND INORGANIC CHEMISTRY

Reaction centre shift in metal catalyzed reactions, **P. Tétényi, Z. Paál** 83

Homologation of hexane isomers catalyzed by platinum, **M. A. Dobrovolszky, Z. Paál, P. Tétényi** 95

Support effect in cluster derived catalysts, **Z. Schay, I. Bogyay, L. Guczi** 105

Base catalyzed reactions of cobalt carbonyls related to hydroformylation, **A. Sisak, F. Ungváry, L. Markó** 115

Palladium catalysts poisoned by metal ions, **T. Mallát, S. Szabó, J. Petró** 127

Enantio- and stereo-selective hydrogenation of ketones with phosphinerhodium catalytic systems, **Sz. Tőrös, B. Heil, L. Kollár, L. Markó** 135

Reduction of carbon monoxide on cobalt(I) complexes, **J.-L. Costa, A. Demonceau, J. Drapier, A. Hubert, A. Noels, P. Teyssié** 147

Physico-chemical characterization of reversed micelles CTAB—1-Hexanol — Water containing Co(II) ions, **I. Ravet, N. Lufimpadio, A. Gourgue, J. B. Nagy** 155

Physico-chemical characterization of uranium-antimony mixed oxide catalysts, **S. Maroie, H. Collette, Z. Gabelica, J. Verbist, J. B. Nagy** 167

Intra- and intermolecular methyl-transfer of *m*-xylene on H-zeolites, **I. Bankós, J. Papp, D. Kalló** 179

Hydrogenation of ethylene by $Pt/H_xVMoO_{5.5}$ bronzes obtained by hydrogen spillover, **C. Ancion, G. Poncelet** 185

The $V_6O_{13}(001)$ surface studied by LEIS, **J. P. Landuyt, R. De Gryse, J. Vennik** 193

Hydroisomerization and hydrocracking of methylnonanes over Pt/HZSM-5, **J. A. Martens, M. Tielen, P. A. Jacobs** 203

Kinetic study of *n*-hexane conversion over Pt/Al_2O_3 catalyst, **J. Margitfalvi, M. Hegedüs, P. Szedlacsek, F. Nagy** 213

Competitive hydrogenation of a nitrile function and of an olefinic unsaturation on Raney nickel, **J. L. Dallons, G. Jannes, B. Delmon** 223

Synthesis and characterization of faujasite-type zeolites, I. Multinuclear NMR characterization of liquid and solid intermediate phases formed during synthesis of zeolite Y, **N. Dewaele, P. Bodart, Z. Gabelica, J. B. Nagy** 233

The ruthenium(II)-tris-(1,4,5,8-tetraazaphenanthrene) dication: a new photocatalyst in redox cycles for hydrogen production, **A. Kirsch-De Mesmaeker, D. Maetens, R. Nasielski-Hinkens** 245

Metathesis and oligomerization of propene over molybdena-alumina catalysts, **J. Engelhardt, D. Kalló** 249

High resolution magic angle spinning ^{29}Si-NMR characterization of zeolites, **J. B. Nagy, Z. Gabelica, G. Debras, P. Bodart, E. G. Derouane, P. A. Jacobs** 265

Characterization of X-ray amorphous ZSM-5 zeolites by thermal analysis and high resolution solid state multinuclear NMR spectroscopy, **Z. Gabelica, J. B. Nagy, G. Debras, E. G. Derouane** 275

PRINTED IN HUNGARY

Akadémiai Kiadó és Nyomda, Budapest

THE PAPERS OF THIS ISSUE WERE PRESENTED AT THE SECOND BELGIAN-HUNGARIAN COLLOQUIUM ON CATALYSIS AT DE HAAN, BELGIUM, OCTOBER 10-13, 1983

Acta Chimica Hungarica 119 (2—3), pp. 83—94 (1985)

REACTION CENTRE SHIFT IN METAL CATALYZED REACTIONS+

Pál TÉTÉNYI* and Zoltán PAÁL

(Institute of Isotope of the Hungarian Academy of Sciences, H-1525 Budapest, P.O. Box 77)

Received June 8, 1984
Accepted for publication July 18, 1984

It is disputed whether single metal atoms (like in homogeneous catalysis) or rather multiatomic "ensembles" are active in heterogeneous catalysis. Examples are enumerated where the reaction centre is "shifted" during the reaction and some of the products must have been formed via the interaction of the reactant with more than one surface site. These are: hydrogenolysis of propane as compared to that of ethane; hydrogenolysis of polymethylbutanes; hydrogenolysis involving skeletal rearrangement; aromatization with addition and abstraction of a C_1 unit formation and opening of the cyclopentane ring; one-step formation of cyclopentane from cyclohexanol. These reactions verify that active *ensembles* operate at least in reactions involving C—C bond rupture, not excluding also those where the intermediate is bonded by a π-type adsorption.

Introduction

Since Balandin's early work [1] there were disputes whether and how the parts of reactant molecule not interacting directly with the catalyst surface influence the catalytic process. This problem is related to another basic question of heterogeneous catalysis: whether does it exist a strict analogy between heterogeneous and homogeneous metal catalysis in that respect whether single metal atoms are active in both cases (surrounded by other metal atoms as ligands in the first and various ligands in the second case) or bulk metal creates such conditions which differ principally from separate metal atoms. Both views have supporters in the recent literature [2—4]. The recognition of the ensemble requirement in catalysis [3] gives arguments for the second view. Knor's theory on the interplay of localized and delocalized electrons [4] gives, according to our view, a good theoretical background to these assumptions although present knowledge does not permit us to bridge the gap between approximative calculations and real catalysis.

The present paper enumerates chemical arguments for the specific nature of metals as catalysts by treating such reactions where the given product could not have been formed without the interaction of the reacting molecule by more than one site of the catalyst. These cases can be generalized as "reaction

+ This paper was presented at the 2nd Belgian—Hungarian Colloquium on Catalysis at De Haan, Belgium, October 10—13, 1983.

* To whom correspondence should be addressed.

centre shift" processes. The following examples will show that the above term cannot be regarded as a strict category of reactions: instead, we want to point out how frequently this phenomenon can be met with various classes of catalytic processes. The reactions to be discussed are sometimes side processes with low yields, this, in turn, underlines how important the careful analysis of the full product spectrum may be.

The examples to be discussed will include:

— hydrogenolysis reactions of alkanes (several types);

— C_5-ring closure and opening of alkanes;

— the formation of cyclopentane from cyclohexanol.

1. Hydrogenolysis reactions

Most of our examples will be taken from the variety of hydrogenolysis reactions involving carbon-carbon bond rupture. It is generally accepted that this reaction is preceded by the rupture of more than one C—H bond, i.e. the surface intermediate is a species attached to the catalyst through several C—M bonds [5, 6].

a) *Hydrogenolysis of ethane and propane*

The simplest example of reaction centre shift is supplied by the comparison of the hydrogenolysis of ethane and propane [6]. Whereas the 1,2- (or, more likely, 1,1,2-) adsorption is important in ethane hydrogenolysis, the possibility of 1,2,3- (or a π-allylic) interaction of propane and higher hydrocarbons with the catalyst facilitates the reaction (Fig. 1). The difference of the activation energy values is lower with nickel where the stability of surface π-complexes is lower. The E_a value of neopentane is closer to that of ethane because the quaternary carbon atom separates the C-1 and C-3 carbon atoms.

b) *Hydrogenolysis with skeletal rearrangement*

Another example is offered by such hydrogenolysis reactions where the structure of the products cannot be explained by simple C—C bond rupture of the parent molecule. For example, it was reported that *n*-butane appears when neopentane undergoes hydrogenolysis over palladium black [7]. Its selectivity was low: 2—4% and increased with increasing hydrogen partial pressure (Fig. 2). It was assumed that neopentane isomerizes first, then the product isopentane loses one of its methyl groups, probably without desorption. In fact, a fairly good parallelism was observed between the yields of isopentane and *n*-butane.

A similar phenomenon was observed when neohexane (2,2-dimethylbutane) reacted over four Group VIII metals (Pt, Pd, Rh, Ir): skeletal isomers and also *n*-pentane were found among the products [8]. The selectivity of *n*-pentane formation decreased at higher temperatures (Fig. 3) and lower hydrogen pressures. At the same time, these conditions favoured higher total hydrogenolysis yields and selectivities. Again, the selectivities of skeletal isomers (twice as much 2,3-dimethylbutane than 3-methylpentane) were parallel to that of *n*-pentane. These isomers should have been produced via bond

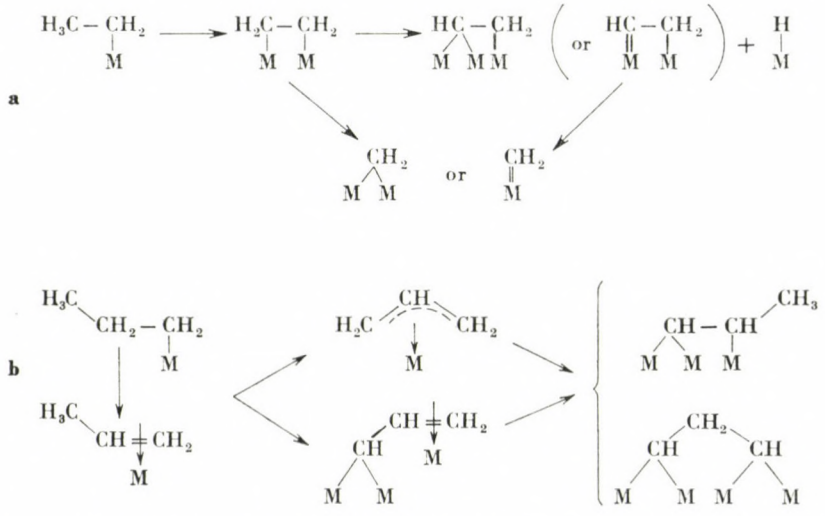

Fig. 1. Proposed reaction pathways of ethane (a) and propane (b) hydrogenolysis

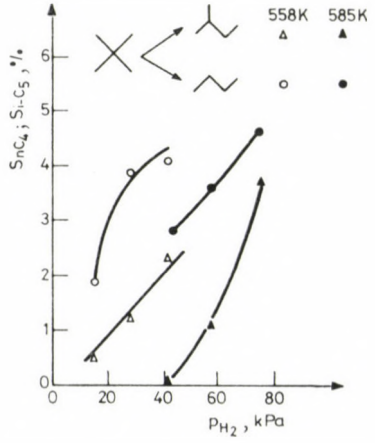

Fig. 2. Selectivity of *n*-butane and isopentane formation from neopentane, as a function of hydrogen pressure. Catalyst: Pd-black, static-circulation system

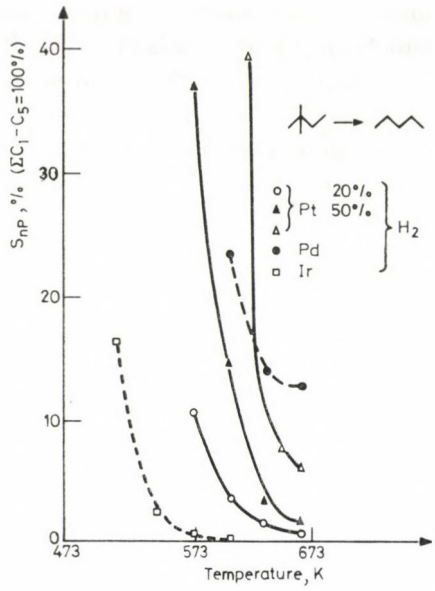

Fig. 3. Selectivity of *n*-pentane formation from 2,2-dimethylbutane, as a function of the temperature. Pulse system

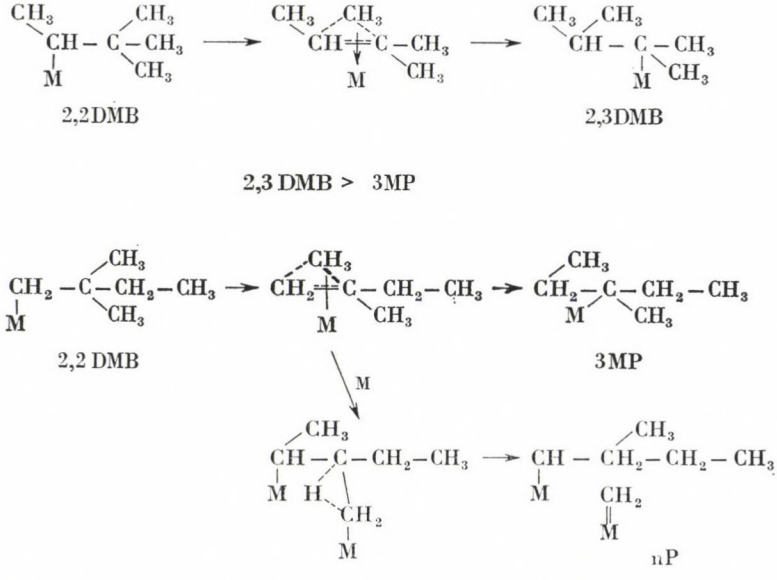

Fig. 4. Proposed pathway of bond shift isomerization of 2,2-dimethylbutane with and without degradation

shift isomerization. Since it is not likely that the low amounts of reaction products would readsorb and react once again during the short contact times, we have to assume that isomerization and hydrogenolysis take place simultaneously or at least, during one sojourn of the molecule on the catalyst surface. Of the several mechanisms suggested, that of McKervey—Rooney—Sammann [9] is able to explain adequately the isomerization of alkanes with quaternary carbon atoms. Figure 4 shows the route of 2,3-dimethylbutane and 3-methylpentane formation. In the latter case, obviously there is a possibility for a two-step reaction shifting of the centre to another carbon atom of the alkane, and resulting in the formation of *n*-pentane. This process should require slightly more hydrogen than common hydrogenolysis.

The occurrence of degradative isomerization obtains further evidence in the hydrogenolysis of radioactive 3-[^{14}C]-methylpentane. *n*-Pentane formed from this alkane should be inactive; whereas isopentane and 2-methylpentane should keep the original molar radioactivity of the parent molecule. Actually, the *n*-pentane fragment contained always some radioactivity. Its molar value corresponded to 10—25% of the molar radioactivity of isopentane or 2-methylpentane. Lower isomerization yield was accompanied by less radioactivity in *n*-pentane. This point to the occurrence of reaction I in Scheme 1, in addition to direct splitting via reactions II and III which the latter pathways produce "normal" *n*-pentane and isopentane fragments:

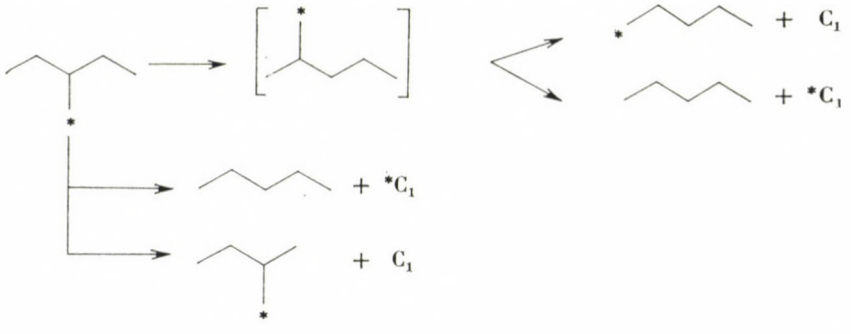

c) *Hydrogenolysis of alkanes with quaternary carbon atoms*

In the first example, quoted the difference of 1,2- 1,3- and also 1,2,3-adsorption in hydrogenolysis was pointed out. The question arises naturally whether the chemisorption of still further carbon atoms could lead to hydrogenolysis reactions. This question was studied by reacting 2,2,3,3,-tetramethylbutane (containing two adjacent quaternary carbon atoms) and also the related 2,2-dimethyl- and 2,2,3-trimethyl-butanes [10].

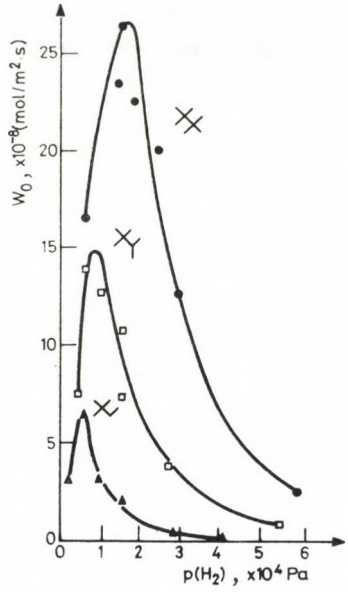

Fig. 5. Initial rate of rupture of the bond between the quaternary carbon atom and its most substituted neighbouring carbon atom as a function of hydrogen pressure

The total yields of hydrogenolysis increased with increasing branching of the hydrocarbon, i.e. in the sequence: 2,2-dimethylbutane < 2,2,3-trimethylbutane < 2,2,3,3-tetramethylbutane. The yield of the product of middle C—C bond rupture increased in the same order. The importance of demethylation, in turn, showed an opposite sequence (Fig. 5a and b) [10].

The only possible way of reactive chemisorption is a 1,4-adsorption in the case of tetramethylbutane; due to the similarity of their behaviour we have to assume that the same is the situation with the other two substituted butanes, too. Such an adsorption was found to be active in hydrogenolysis [11]. We have to underline two features of this reaction. First, the reacting bond is not in direct interaction with the catalyst surface: this is the clearest form of reaction centre shift. Second, as a consequence, the energetics of the bonds formed between the reactant and the catalyst [1] do not influence in this

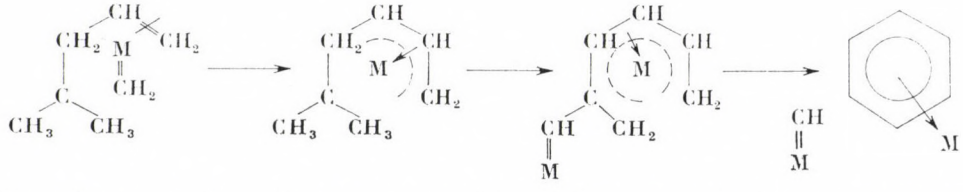

Fig. 6. Suggested pathway for aromatization of 2-methylpentane, via C_1 addition—abstraction

Table I

Dissociation energies of the $C_{(2)}-C_{(3)}$ *bond and its relative reactivity in* Pt*-catalyzed hydrogenolysis of substituted butanes* [10]

Alkane	C—C bond energy* (kJ/mol)	Relative reactivity
2,2-Dimethylbutane	322	1.00
2,2,3-Trimethylbutane	306	2.82
2,2,3,3-Tetramethylbutane	283	4.06

* After Ref. [12].

Catalyst: Pt-black, reactivities are compared at their maximum values which is observed at different hydrogen pressures for each alkane. $T = 603$ K, $p(H_2) = 5-20$ kPa, p(alkane) = = 1.23 kPa.

particular case the rate of the reaction. Therefore, the relative reactivities are strictly related to the energy of the C—C bond to be cleaved (Table I [12].

As discussed in detail earlier [10], the above reaction can take place even over nickel black catalyst, which is a typically end demethylating metal. Nevertheless, the relative amounts of methane and other fragment show without doubt that apart from end demethylation, a not negligible middle bond rupture occurs, especially with 2,2,3,3-tetramethylbutane.

d) *Addition-abstraction of methylene groups*

Several metal catalysts — especially those promoting multiple hydrogenolysis — catalyze chain lengthening reactions of alkanes [13]. The product of this reaction appears often as an aromatic hydrocarbon.

Sárkány et al. observed a peculiar sort of this reaction [14]. They reacted the mixture of ^{14}C labelled benzene and unlabelled 2-methylpentane and monitored the specific radioactivities of the resulting benzene and toluene fractions. At lower temperatures, when the fragmentation of benzene did not occur, the toluene fraction was practically nonradioactive and the radioactivity of benzene was significantly diluted with inactive benzene product. In the case of alkylating of the existing aromatic ring, the toluene should reflect the specific radioactivity of benzene. Inactive toluene, in turn, means that it is formed from 2-methylpentane which is alkylated by its own nonradioactive fragments. This toluene was largely demethylated, this reaction being a favourable process over Ni catalyst [15]. Thus, a simultaneous addition and abstraction of C_1-units to the alkane molecules occurred. This so-called "external C_1-shift" may be the pathway of benzene formation over metals which are not active catalysts for the other pathways of skeletal rearrangement. The above facts were confirmed with other alkane isomers, too [14, 16].

A suggested pathway for this reaction centre shift process is shown in Fig. 6. Here the π-complex formed after the accepted mechanism of homologa-

tion is shown; this species would undergo aromatization without desorption, according to the polyenic mechanism [17]; this π-like adsorption could, possibly, facilitate the loss of methyl group *before* ring closure, essentially by the same type of adsorption of the C_6-unit as in the case of the aromatic ring [15].

2. Rupture and formation of the cyclopentane ring

It has been found that the rupture of C—C bonds of cyclopentane rings is a process requiring a lower energy of activation and occurring with much higher rates over four particular metals: Pt, Pd, Ir, Rh [18]. It should, therefore, involve a type of C—C bond breaking other than that observed in hydrogenolysis. The other characteristic of this process is that — as distinct from alkane hydrogenolysis [8] — the cleavage of the C—C bond of the ring adjacent to an alkyl substituent is strongly hindered [18, 19]. Selectivity values for the rupture of various bonds are shown in Table II. A third feature of C_5-ring opening is that its reverse process, i.e. C_5-cyclization takes place with high yields under the same conditions and on the same catalysts, whereas we saw that alkane buildup is far from being a common process and occurs with rather low yields only as homologation by addition of C_1 units to the chain.

C_5-ring opening should, therefore involve a — reversible — type of C—C bond breaking different from that observed in hydrogenolysis. Therefore,

Table II

Selectivity of ring opening, b/a over various metals

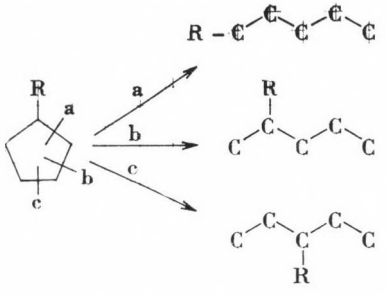

Alkane feed	Ratio *b/a* if the catalyst is			Ref.
	Pt	Ir	Rh	
Methylcyclopentane	9.8	32.4	6.5	[18]
	7.9	6.9	21.5	[19]
Ethylcyclopentane	3.7	10.5	7.5	[19]

Ref. [18]: pulse system, H_2 carrier gas, $T = 603$ K, Pt; 468 K, Ir; 543 K, Rh, metal blacks.

Ref. [19]: flow system, H_2 added, $T = 533-583$ K, metals on active charcoal.

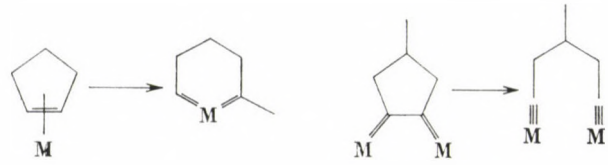

Fig. 7. Intermediate for C_5 ring opening proposed by Gault and co-workers [20]

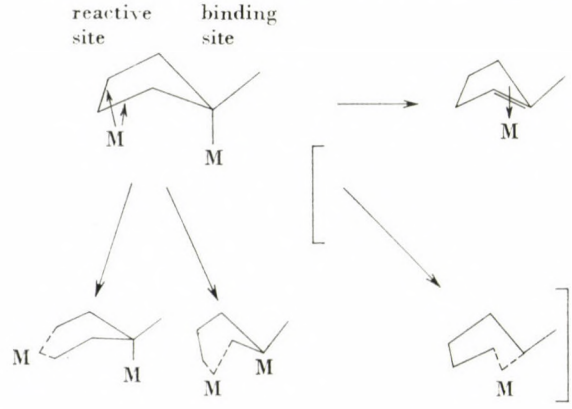

Fig. 8. "Dual site" mechanism of C_5 ring opening involving flatly adsorbed intermediate

an intermediate analogous to alkane hydrogenolysis [20] (Fig. 7) cannot explain all the features shown above. We propose, instead, a flat adsorption of the C_5 ring to be destroyed or produced (Fig. 8) [21]. This could explain not only all the peculiar features mentioned but also the sensitivity of the process to the structure of the reactant which must not have been observed if the reacting carbon atoms were the only ones interacting with the surface. A tertiary carbon atom (which loses its hydrogen more easily than secondary or primary ones [12]) facilitates the adsorption which also keeps the molecule in a proper geometry on the surface. With a methyl substituent, the distance between the atoms of the catalyst surface facilitates ring opening in "*b*" or "*c*" positions in a more pronounced way than with an ethyl substituent where the primary binding may be shifted further in the side chain. Here the *b*/*a* selectivity is lower (Table II).

Such a "dual site" interaction may also operate in C_5 ring closure. The rate of this reaction has maxima as a function of the hydrogen partial pressure [22, 23]. The value measured at the maxima increases in the following order: *n*-pentane < 3-methylpentane < 3-ethylpentane, even if we divide the rate of 3-ethylpentane cyclization by 3 because of the triple statistical possibilities of its ring closure. Apparently, the same effect (i.e. a 1,3-interaction of the

future side ethyl group with the surface) increases the lifetime of the surface intermediate with proper geometry quite significantly as compared with the other hydrocarbons.

This reaction has two requirements. One is the proper geometry of the catalyst: too large (Au) and too small (Co, Ni) atoms do not have the proper geometry for the dual site mechanism. The other is the proper (not too small) hydrogen coverage of the metal, which prevents multiple dissociation, leading, for example, to hydrogenolysis.*

3. CO elimination from cyclohexanol accompanied with cyclization

Dehydrogenation of cyclohexanol to cyclohexanone or to phenol [24] is accompanied with small amounts of fragments. Adsorption processes leading to these products could be monitored by IR spectroscopy [25]. The following spectral characteristics were observed over Pt (as well as Ni and Rh):

a) the formation of surface carbonyls;

b) interaction of the adjacent C atoms with the surface;

c) CO elimination from the molecule.

Process *a* means that the molecule interacts with the surface through its polar oxygen atom. This is the main feature of dehydrogenation of cyclohexanone. Further dehydrogenation to phenol should require type *b* interactions, whereas type *c* should mean fragmentation which should occur in the vicinity of the oxygen atom.

Both processes *b* and *c* mean the shift of the original centre of attack to another atom of the molecule. The pathway of phenol formation has been discussed in detail earlier [24]; here a feature of degradation reactions will be discussed. A small amount of cyclopentane was detected among the products even on nickel which does not promote cyclization of *n*-pentane. Neither can cyclopentane be formed via cyclohexane → methylcyclopentane → cyclopen-

Table III

The ratio of n-pentane to cyclopentane produced from cyclohexanol and n-pentane, respectively

Feed	Carrier gas	Cyclopentane/*n*-pentane × 10^3 at T (K)		
		513	573	633
Cyclohexanol	H_2	6	22	40
	N_2	86	85	166
n-Pentane	H_2	1.2	5.3	2.1

* Kramer and Zuegg [27] attribute selective ring opening to metal sites and nonselective opening to sites on the borderline of the metal support. It is obvious that the distance between the two active sites is more important in the former than in the latter case.

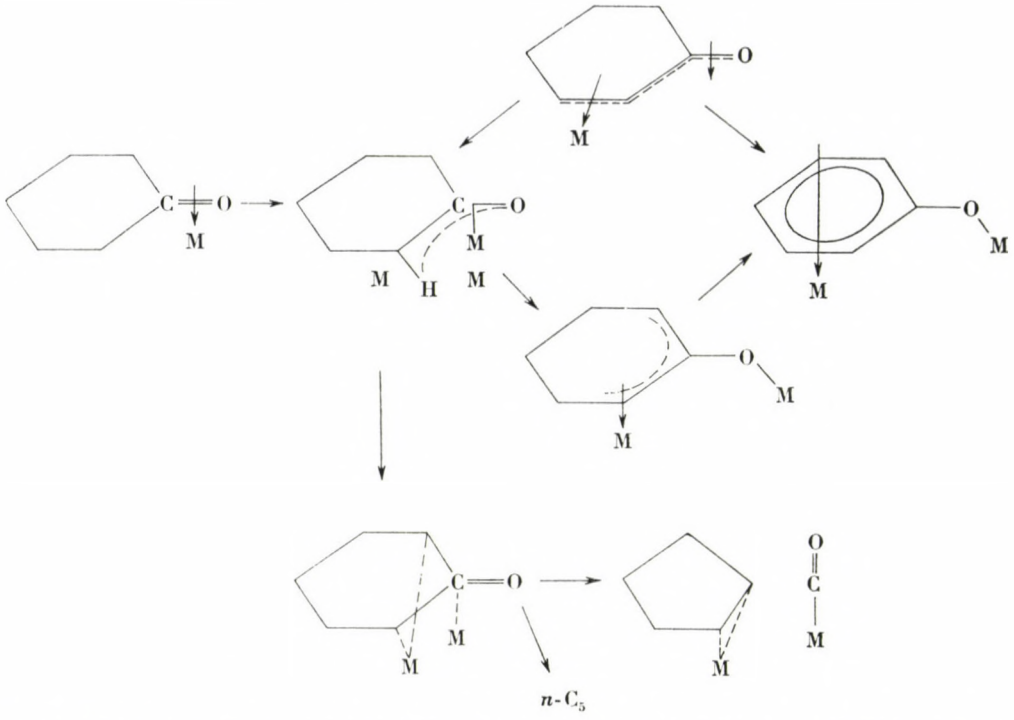

Fig. 9. Proposed pathway of dehydrogenation and degradation reactions of cyclohexanol

tane route, since none of the first two products are formed from cyclohexanol. The ratio *n*-pentane/cyclohexanol is higher than with *n*-pentane feed (Table III). Again, more cyclopentane is formed from cyclohexanol in hydrogen than in nitrogen although the C_5-cyclization of alkanes does not occur at all without hydrogen [18].

Thus, we regard it as justified to assume that upon adsorption of the oxygen containing group (which probably has a ketonic character after adsorption) the centre of reaction is shifted to the two α-carbon atoms in a way that a new C—C bond can be formed between the two ends of the hydrocarbon fragment. The interaction of the reacting molecule with the catalyst ensures here the proper geometry for this cyclization even with Ni catalyst (Fig. 9).

Conclusions

The above examples certify that there are such reactions where the products could only be formed by interaction of the reactant molecule with more than one atom of the catalyst. No doubt that there are processes where the interaction involves strictly one catalyst atom. Mostly hydrogenation reactions where the reactive adsorption form involves probably π- or π-allyl complexes belong to this group (2, 26). These are the most frequent reactions in homoge-

neous catalysis, too. However, the simplest example of reaction centre shift was interpreted in terms of π-allylic interaction of adsorbed propane with metal surface thus facilitating hydrogenolysis. The π-character of the adsorption cannot, therefore, exclude reaction centre shift, neither interaction with more than one surface atom (cf. toluene demethylation). The "localized—free electron interplay" shoulde be considered here [3].

As far as ligands are concerned, no doubt other components present on the catalyst surface may also have some role in directing the reaction into the proper pathway. Here hydrogen can be mentioned: we have demonstrated how sharply the selectivity can vary as a function of the hydrogen pressure, with almost every example discussed. To sum up: we argue for the specific character of metal catalyst being not equivalent with single metal atoms. This, however, does not mean that any relationship is excluded, and analogies may help to solve of problems of both homogeneous and heterogeneous catalysis.

*

The authors wish to express their sincere gratitude to Dr. A. Sárkány, Dr. I. Manninger and Dr. M. Dobrovolszky for carrying out the experiments on which the present paper has been based, as well as for valuable discussions.

REFERENCES

[1] Balandin, A. A.: Adv. Catalysis, **19,** 1 (1969)
[2] Rooney, J. J.: Faraday Disc. Chem. Soc., **72,** 80 (1981)
[3] Knor, Z.: in "Surface and Defect Properties of Solids" (M. W. Roberts, and J. M. Thomas, Eds. Vol. **6,** p. 139. The Chemical Society, London, 1977; Knor, Z.: Acta Chim. Hung. (in press)
[4] Sachtler, W. M. H.: Faraday Disc. Chem. Soc., **72,** 7 (1981)
[5] Anderson, J. R., Avery, N. R.: J. Cat., **5,** 446 (1966)
[6] Tétényi, P., Guczi, L., Paál, Z., Sárkány, A.: Kém. Közlemények, **47,** 363 (1977)
[7] Sárkány, A., Guczi, L., Tétényi, P.: Acta Chim. Acad. Sci. Hung., **96,** 27 (1978)
[8] Paál, Z., Tétényi, P.: React. Kinet. Catal. Lett., **12,** 131 (1979)
[9] McKervey, M. A., Rooney, J. J., Samman, N. G.: J. Catal., **30,** 330 (1973)
[10] Zimmer, H., Tétényi, P., Paál, Z.: J. Chem. Soc. Faraday Trans. I, **78,** 3573 (1982)
[11] Leclercq, G., Leclercq, L., Maurel, L.: J. Catal., **50,** 87 (1977)
[12] Benson, S. W.: Thermochemical Kinetics, Wiley, New York 1968
[13] O'Donohoe, C., Clarke, J. K. A., Rooney, J. J.: J. Chem. Soc., Faraday Trans. I., **76,** 346 (1980)
[14] Sárkány, A., Pálfi, S., Tétényi, P.: Acta Chim. Acad., Sci. Hung., **111,** 633 (1982)
[15] Grenoble, D. C.: J. Catal., **56,** 32 (1979)
[16] Sárkány, A., Tétényi, P.: submitted
[17] Paál, Z., Tétényi, P.: J. Catal., **30,** 350 (1973)
[18] Paál, Z., Tétényi, P.: Nature, **267,** 234 (1977)
[19] Bragin, O. V., Olferyeva, T. G., Preobrazhenskii, A. V., Liberman, A. L., Kazanskii, B. A.: Dokl. Akad. Nauk SSSR, **202,** 339 (1972)
[20] Amir-Ebrahimi, V., Gault, F. G.: J. Chem. Soc. Faraday Trans. I, **76,** 1735 (1980)
[21] Paál, Z., Dobrovolszky, M., Tétényi, P.: J. Catal. **45,** 189 (1976)
[22] Zimmer, H., Paál, Z., Tétényi, P.: Acta Chim. Acad. Sci. Hung., **111,** 513 (1982)
[23] Zimmer, H., Paál, Z.: Paper accepted at the 8th ICC, Berlin 1984
[24] Dobrovolszky, M., Tétényi, P., Paál, Z.: J. Catal., **74,** 31 (1982)
[25] Szilágyi, T., Sárkány, A., Mink, J., Tétényi, P.: J. Catal., **66,** 191 (1980)
[26] Rooney, J. J., Webb, G.: J. Catal., **3,** 488 (1964)
[27] Kramer, R., Zuegg, H.: Proc. 8th Int. Congress on Catalysis v. 5. p 275. Verl. Chem. Weinheim—Deerfield Beach—Basel.

Acta Chimica Hungarica 119 (2—3), pp. 95—104 (1985)

HOMOLOGATION OF HEXANE ISOMERS CATALYZED BY PLATINUM+

Mária A. Dobrovolszky, Zoltán Paál* and Pál Tétényi

(Institute of Isotopes of the Hungarian Academy of Sciences, H-1525 Budapest, P.O. Box 77)

Received June 8, 1984
Accepted for publication July 18, 1984

The homologation of *n*-hexane, 3-methylpentane, hexadienes and *n*-heptane were studied over Pt-black (and some supported Pt) and compared to the reactions of C_8 hydrocarbons. The composition of C_8-aromatics was used to evaluate the possible pathways. The ratio of internal to terminal addition was about 0.25; this way, the C_8-composition from *n*-hexane could be explained. The appearance of branched chain saturated buildup products from 3-methylpentane and methylcyclopentane complicates their homologation and confirms the possibility of addition of C_1 units to internal C-atoms, too. The mechanism of O'Donohoe et al. [8, 9] was found to be valid.

Introduction

As distinct from well-known hydrogenolysis (degradation) reaction of hydrocarbons [1], their homologation, i.e. buildup process has not been studied until recently over metallic catalysts. Preliminary studies reported propane formation from ethane over W, Rh, Pt films [2]. Toluene was observed among the products of *n*-hexane transformation over Ni/Al_2O_3 [3, 4]. Guczi et al. [5, 6] found toluene produced from *n*-hexane via benzene alkylation. They claimed that cracking of benzene would be responsible for creating C_1 units able to carry out alkylation. No toluene was observed on Pt [5, 6]. Péter and Clarke [7] observed benzene formation from *n*-pentane over Rh and Rh—Cu films. O'Donohoe et al. [8, 9] observed one- and two-step chain growth of *n*-alkanes over W and other metal films. The amount of products was strongly influenced by the length and shape of the feed molecule. The reactivity of branched chain alkanes was about one order of magnitude lower than that of *n*-alkanes. Hardly any homologues were observed with neopentane and cyclopentane feed. Homologation was also observed over sintered Pd and Rh films; here chain lengthening was followed by rapid 1,6-dehydrocyclization. Hydrogen pressure was another important factor, low pressures favouring the reaction. These authors found the reaction to be related to the metathesis of olefins [9]. The criterion of its occurrence are high concentrations of both

+ This paper was presented at the 2nd Belgian—Hungarian Colloquium on Catalysis at De Haan, Belgium, October 10—13, 1983.

* To whom correspondence should be addressed.

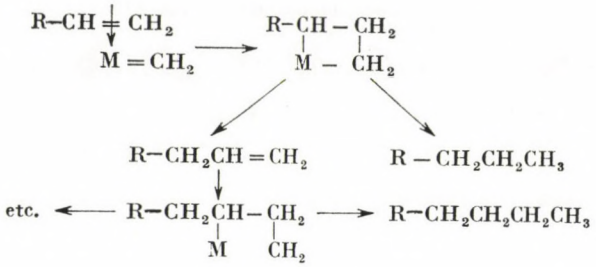

Scheme 1

linear surface methylene groups ($CH_2 = M$) and migrating 1-olefins. These two precursors would then give a surface metalecyclobutane intermediate which would be hydrogenated to an alkane homologue or would isomerize to give another 1-olefin capable of reacting with another methylene group (Scheme 1). Both these authors and Sárkány et al. [10, 11] found hardly any or no activity with Pt-films and blacks. These latter authors studied the homologation of pentanes, cyclopentane and isohexanes over Ni-black and Ni/SiO_2. They also found lower activity with branched chain feed but observed the formation of small amounts of benzene and 2-methylpentane from cyclopentane. Since product distribution indicates that carbene addition to internal carbon atoms or to internal double bonds would be hindered, they assumed a ring opening of cyclopentane prior to chain growth.

The inactivity of platinum was attributed to its poor carbene formation ability [9]. Sárkány et al. [12] found a fairly good correlation between the activity of several Group VIII metals in homologation and ethane hydrogenolysis. They stated that homologation should be a general phenomenon under the conditions of "deep" fragmentation. Their radiotracer studies with [^{14}C] benzene showed that the reaction involves chain lengthening followed by aromatization instead of alkylation of the benzene ring.

Carbene-alkyl addition occurs predominantly at the end of the carbon chain, although cyclopentane was not quite unreactive over Pd [9] and Ni [11]. A considerable part of chain lengthening products of pentane appears as benzene since homologation is favoured by the same hydrogen-deficient conditions like aromatization. Also, benzene formation from methylpentanes may involve a CH_x addition-abstraction mechanism where homologation to toluene is followed by demethylation [12].

As opposed to other reports, Margitfalvi et al. [13] found a homologation activity over Pt/Al_2O_3 catalyst. They constructed another mechanism for the interpretation of toluene formation from *n*-hexane. They claim that the appearance of toluene (and also, that of C_8 and still higher aromatics) in the product would be due to the hydro-depolymerization of a polycyclic aromatic

polymer deposited over the surface of the catalyst during its ageing. The preference of this mechanism over carbene addition is supported by the facts that (i) no open chain homologues were observed and (ii) no higher toluene yields were observed over catalysts with enhanced olefin formation; although this would be expected according to the insertion mechanism. The flash desorption of the aged catalysts resulted in the appearance of a number of higher aromatic compounds.

The present work reports homologation experiments over Pt-black catalysts. Normal-hexane, 3-methylpentane and also methylcyclopentane were used as a feed; the product distribution will be used to draw conclusions about the possible reactivities of various carbon atoms, as well as about the general mechanism of chain lengthening over platinum catalyst.

Experimental

The experiments were carried out in a pulse system [14]. The reactor was coupled before a Packard—Becker Model 419 gas chromatograph. Nitrogen and hydrogen were used as carrier gases.

Analysis were carried out on a 2 m column packed with 14% Squalane on Chromosorb P. A temperature programme from room temperature up to 353 K was used; heating the column commenced after the peak of benzene appeared on the chromatogram. Hydrocarbons were FLUKA or Merck GC grade samples. Catalysts: Pt [14], Pt/SiO_2 [15] and Pt/Al_2O_3 (+Sn or Pb added) [16] were described earlier.

Results and Discussion

Homologation was observed at or above 633 K. Typical product selectivities in H_2 are seen in Table I (also for Pt/SiO_2 [15]). Whereas mostly aromatic homologues were found in nitrogen, several other peaks were detected in hydrogen. They could be identified according to their retention times as various heptanes and alkylcyclopentanes. Their amount was much higher with 3-methylpentane. Such products also appeared with methylcyclopentane feed. On the basis of a few runs performed not every product could be identified here. The distribution of C_7 products is shown in Table II.

The formation of isoalkane homologues has not been reported until now. These products indicate the possibility of chain growth in internal position, too. This hypothesis is verified also by the analysis of composition of C_8 aromatics. These gave three separate peaks: ethylbenzene (EBz), *p*- plus *m*-xylene ($p + m$X) and *o*-xylene (oX). Their distribution can give suggestions about the ratio of terminal and internal chain growth.

The possible formation of isomers from *n*-hexane is compiled in Fig. 1. All the C_8 skeletons formed this way are summarized in Table III. (Care should

be taken that the alkane skeleton shown does not mean necessarily *saturated* surface species!) The cyclization of these C_8 isomers gives various C_8 aromatics as shown in Table III. Their actual distribution does not, however, correspond to this value calculated on the basis of random addition (Table IV). Neither does it fit the value obtained with terminal addition only. Thus, we have to assume that addition to both primary (terminal) or secondary (internal) carbon atoms occurs but their reactivity is different. Quite good agreement is obtained assuming that the reactivity of internal C-atoms is 0.25 as compared to that of those at the end of the carbon chain (Table IV).

The comparison of the ratio of ethylbenzene: $(m + p)$-xylene: *o*-xylene obtained over supported platinum catalysts deserves attention. The values obtained in hydrogen, over $Pt—Sn/Al_2O_3$ correspond to a situation where the

Table I

Selectivities of various products formed from C_6 saturated hydrocarbons

	Feed[a]			
	*n*H	3MP	MCP	*n*H[b]
Conversion (%)	41.74	23.15	21.31	83.4
Selectivity (%)				
CH_4	20.1	15.0	12.7	43.7
$C_2—C_5$	36.5	30.1	21.7	
C_6 nonaromatic	13.2	50.8	59.7	29.4
Bz	28.9	1.6	2.8	26.1
C_7 nonaromatic	0.20	0.91	0.94	0.07
Toluene	0.8	0.7	0.8	0.5
C_8 nonaromatic	—	0.10	0.55	—
C_8 aromatic	0.57	0.75	1.08	0.30

[a] Catalyst 0.134 g Pt-black, carrier gas H_2, $T = 673$ K; *n*H = *n*-hexane; 3MP = 3-methylpentane; MCP = methylcyclopentane; Bz = benzene.
[b] Pt/SiO_2, $T = 673$ K, catalyst as in Ref. [15].

Table II

C_7 product selectivities

Feed	C_7 yield (%)	Selectivity (%)					
		2-MH*x*	3-MH*x* +2,3DMP	3EP	*n*Hp	1,2DMCP +EPC	Toluene
n-Hexane	0.39	3	19		3	6	69
	0.26	—	21		5	—	74
	0.48	4	20		5	2	70
3-Methylpentane	0.97	4	29	12	5	3	46
	0.94	3	32	10	5	5	44
	0.80	3	38	15	4	7	34

$T = 673$ K, pulse system, carrier gas: H_2. Results of parallel runs.

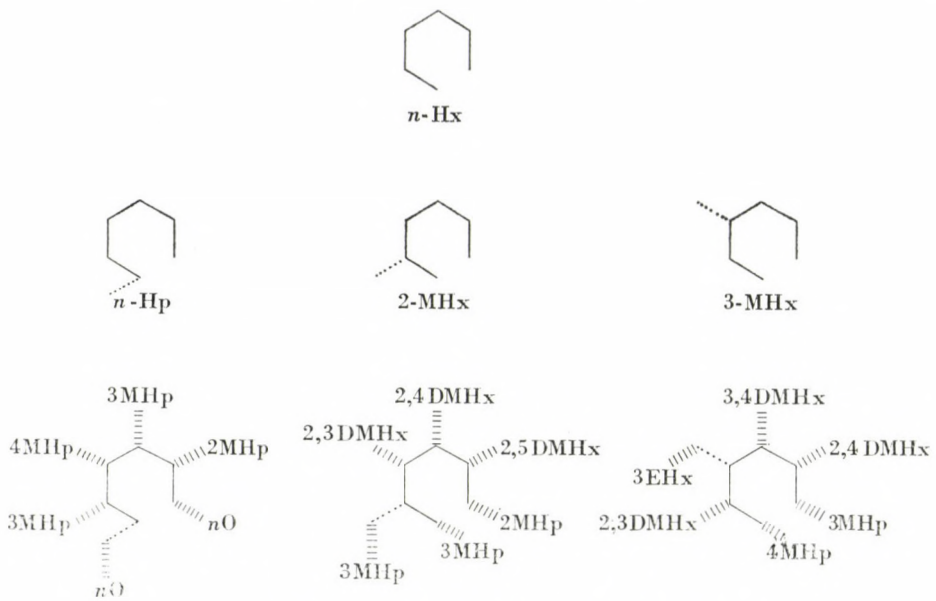

Fig. 1. Possible pathways of chain growth of *n*-hexane

Table III

The statistics of formation of C_8*-aromatics from n-hexane*

C_8-skeleton	C-atoms involved in chain lengthening[a]	Stat. weight of formation	C_8-aromatics formed and stat. weight of cyclization[b]
n-octane	P + P	4	2.(1/2 EBz) + 1/2 *o*-X
3-ethylhexane	S + P	2	2 EBz
2-methylheptane	S + P	6	2 *m*-X
3-methylheptane	S + P	10	1/3 EBz + 1/3 *o*-X + + 1/3 *p*-X
4-methylheptane	S + P	4	2 *m*-X
2,3-dimethylhexane	S + S	4	2 *o*-X
2,4-dimethylhexane	S + S	4	2 *m*-X
2,5-dimethylhexane	S + S	2	4 *p*-X
3,4-dimethylhexane	S + S	2	1 *o*-X

[a] P = primary; S = secondary, irrespective of the fact whether the C-atom taking up a new C_1-unit is new or had been present originally in *n*-hexane.

[b] EBz = ethylbenzene; *o*-X, *m*-X, *p*-X = *ortho*, *meta* and *para*-xylene, respectively.

The relative amounts of individual C_8-aromatics are obtained by multiplying the statistical weight of the C_8-skeleton formation by the statistical weight of its cyclization. The results are:

EBz: 4 + 4 + 10/3 = 11.33
m-X: 12 + 8 + 8 = 28
p-X: 10/3 + 8 = 11.33 EBz: (*m* + *p*)-X : *o*-X = 1 : 3.58 : 1.42
o-X: 2 + 10/3 + 8 + 2 = 15.33.

Table IV

Distribution of C_8-aromatics produced from n-hexane

Assumption	Ratio EBz: $(m + p)$—X: o-X
Experimental value over	
Pt-black[a]	1 : 1.07 ± 0.16 : 0.62 ± 0.12
Pt/Al_2O_3, H_2[b]	1 : 2.93 ± 0.64 : 1.57 ± 0.69
Pt/Al_2O_3, N_2[c]	1 : 3.01 ± 0.33 : 1.37 ± 0.22
$Pt\text{-}Sn/Al_2O_3$[b],	1 : 2.36 ± 0.23 : 1.04 ± 0.25
Pt/SiO_2[d]	1 : 2.00 ± 0.06 : 0.99 ± 0.06
Calculated values:	
1. Terminal addition only	1 : 0 : 0.5
2. Random addition	1 : 3.58 : 1.42
3. The addition to secondary C-atoms has a lower reactivity	
$s = 0.25$[e]	1 : 1.17 : 0.59
4. As above, but	
$s = 2/3$[e]	1 : 2.31 : 0.99
5. As above, but	
$s = 0.5$	1 : 2.04 : 0.80

[a] Average of 11 runs, $T = 673$ K.
[b] Average of 9 runs, $T = 773$ K, 0.5 μL pulses into hydrogen. After Ref. [16].
[c] Average of 10 runs, with no regeneration in between, $T = 723$ K.
[d] Average of 2 runs, H_2 carrier gas, $T = 673$ K. More ethylbenzene is formed in nitrogen. Catalyst as described in Ref. [15].
[e] s = the ratio of the reactivity of secondary C-atoms to that of primary C-atoms.

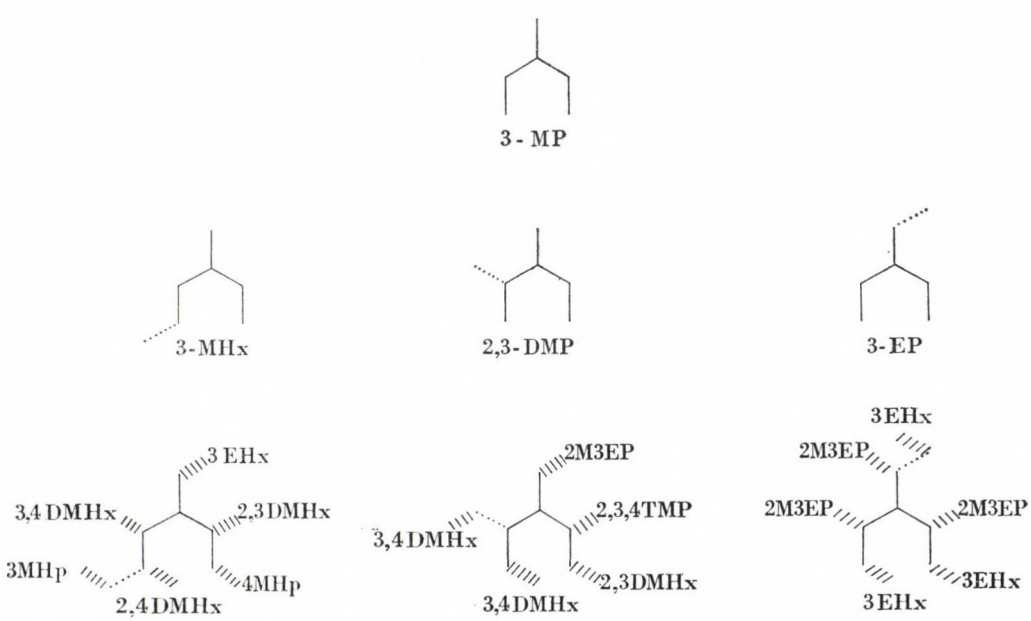

Fig. 2. Possible pathways of chain growth of 3-methylpentane

Table V

Distribution of C_8-aromatics produced from 3-methylpentane

Assumption	Ratio EBz: $(m + p)$-X: o-X
Experimental value[a]	1 : 2.07 ± 0.50 : 0.735 ± 0.30
1. Terminal addition only	1 : 0.44 : 0.06
2. Random addition	1 : 0.81 : 1
3. $s = 0.25$[b]	1 : 0.56 : 0.36
4. C_5-cyclization and ring expansion is also active and random addition	1 : 1.20 : 0.51
5. As above but $s = 0.25$[b]	1 : 1.14 : 0.21
6. Only 3-methylhexane is active in further chain growth; random addition	1 : 1.64 : 0.46
7. As above, but $s = 0.25$[b]	1 : 1.67 : 0.45

[a] Average of 6 runs.
[b] See footnote b to Table IV.

reactivity of internal carbon atoms in 2/3 of that of terminal C-atoms ($s = 2/3$). With Pt/Al_2O_3 somewhat higher s-values can be estimated; in nitrogen carrier gas, the composition corresponds almost to random addition, with somewhat less m- and p-xylene formed. Perhaps the bifunctional character of these catalysts contributes to this effect, although we are far from equilibrium values EBz: $(m + p)$ — X : o-X = 1 : 6.1 : 2.1. Pt/SiO_2 [15] which is nonacidic, occupies an intermediate position ($s \sim 0.5$); Pt/C also produced homologues.

A similar consideration for isomer formation from 3-methylpentane is shown in Fig. 2. Calculations analogous to that shown in Table I do not give, however, good fits with the measured values (Table V). Here, however, the homologation process may give also saturated isomers which may undergo C_5-cyclization. Cyclopentanes, in turn, may give aromatics by ring opening and reclosure [17] or by bond shift type ring expansion [18, 19]. Xylenes and ethylbenzene were actually found during the conversion of propylcyclopentane over nonacidic supported Pt [22]. The appearance of C_8 aromatics from methylcyclopentane points to their not negligible role in creating the C_8-composition observed. It is impossible, however, to consider all possible reaction pathways with its correct statistical weight. Somewhat better agreement is obtained assuming that 3-methylhexane is the only heptane isomer participating in C_8 formation; other species must contribute mainly to $(m + p)$-xylene and also to o-xylene via C_5-cyclic species (Table V).

The side methyl group represents the only primary C-atom in methylcyclopentane. Its growth would produce propylcyclopentane which could give ethylbenzene via ring expansion (which should be faster than skeletal isomerization [19]). Its C_5-ring closure to pentalane could lead to m-xylene. The observed distribution, EBz : $(m + p)$ — X : o-X = 1 : 1.48 ± 0.38 : 0.64 ±

$\pm$ 0.11 (average of 3 runs) points also to more complicated routes involving various cyclopentanes formed via C_1-unit addition to the C-atoms of the ring. Whereas this confirms the possibility of homologation of secondary C-atoms, the complex character of all routes makes it impossible to estimate their individual role.

The question may arise to what extent the ready C_7 or C_8-molecules (alkanes or aromatics) may isomerize further, influencing thus the C_8-composition. Table VI shows selectivity values obtained with C_7 and C_8 feeds. This effect may only have a secondary importance. Ethylbenzene showed no isomerization at all. Low amounts of $(m + p)$-xylenes are formed from *n*-octane and even less from 1,7-octadiene. This also points to the fact that enhanced *m*-xylene formation from *n*-heptane may not have originated from *n*-octane cyclization to pentalane [20] which, would give mainly *m*-xylene (see later, Scheme 2). The importance of this route may be judged from the *m*-xylene produced from *n*-octane. Since double bonds are not favourable for C_5-cyclization (to which also pentalane formation belongs), is not surprising that less *m*-xylene is formed from octadiene. It is also seen that the ratio of ethylbenzene to *o*-xylene at *n*-octane cyclization is lower than the value of 2 : 1 expected on the basis of pure statistics. Thus, these values must also carry a correction or the calculations outlined in Tables III and IV. It is also confirmed that propylcyclopentane does not give exclusively ethylbenzene as expected with ring expansion reaction only (Scheme 2). This is in good agreement with data reported for acidic Pt/Al_2O_3 and does not fit well to values obtained over alkaline catalyst [22].

Table VI

Typical selectivities of various products formed from C_7 *and* C_8 *saturated hydrocarbons*

Feed	Conversion (%)	Selectivity (%)						Ratio[b] EBz: $(m + p)$—X: *o*-X
		$\Sigma < C_6$	ΣC_6	Saturated C_7	Toluene	Non-aromatic C_8 products	Aromatic C_8 products	
n-Heptane	33.9	59.9	13.0	14.7	11.5	0.1	0.9	1 : 2.12 : 0.78
n-Octane	47.3	64.8	14.5	6.5	3.3	4.0	7.0	1 : 0.18 : 0.23
4-MHp	97.8	28.2	6.2	2.4	3.5	56.0	3.5	1 : 0.10 : 0.23
Propylcyclopentane	48.6	44.7	18.2	6.6	3.2	24.9	2.2	1 : 1.39 : 0.15[d]
Ethylbenzene	27.2	42.9	36.8	—	20.2	—	—[c]	1 : 0 : 0

Catalyst: Pt-black, $T = 673$ K, pulse system, carrier gas: H_2
[a] Values from typical single runs
[b] Average of 3 runs
[c] Xylenes
[d] Comparison with literature data [22]:
Pt/Al_2O_3, acidic, 0.1 MPa — 1 : 1.24 : 0.20
2.7 MPa — 1 : 1.32 : 0.46
$PtAl_2O_3$ + K, 0.1 MPa — 1 : 0.19 : 0.14
H_2/hydrocarbon ratio: 10 : 1

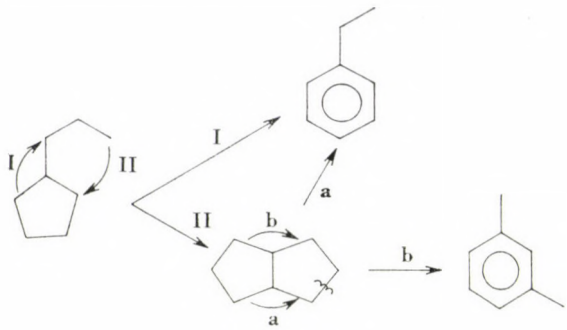

Scheme 2

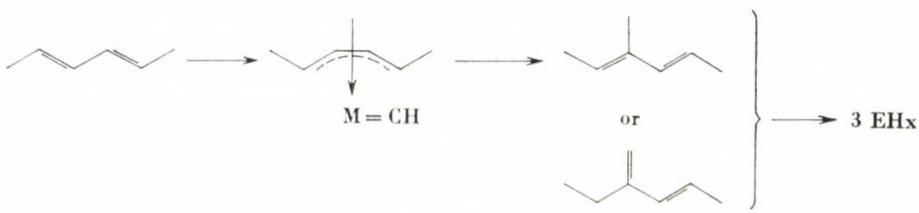

Scheme 3

The existence of a "ready" C=C bond in the molecule may enhance carbene addition (Table VII). Thus, for example, 1,5-hexadiene should produce more 2-methyl-heptane and 2,5-dimethylhexane (cf. Fig. 1) than *n*-hexane. These isooctanes form more *m*- and *p*-xylene, and indeed, the ratio EBz: : $(m + p)$X : *o*-X is 1 : 1.52 : 0.76. With 2,4-hexadiene feed, addition to C_3 seems to predominate; this gives 3-ethylhexane and much ethylbenzene. The measured ratio EBz : $(m + p)$ — X : *o*-X is 1 : 0.70 : 0.36. It is not excluded that the conjugated double bond behaves like one single "unsaturated unit" to which only one C_1 addition is possible; further chain growth may occur "continuing" this first addition. This gives rise to much ethyl side group (Scheme 3).

Table VII

Homologation of hexadienes (HD)

Feed	Selectivity (%)[a]				Ratio, EBz: $(m + p)$—X: *o*-X[b]
	C_7-sat.	Toluene	C_8-sat	C_8-arom.	
1,5-HD	0.13	0.36	0.01	0.26	1 : 1.52 : 0.76
c-t-2,4-HD	0.20	0.38	0.09	0.36	1 : 0.70 : 0.36

[a] First run after regeneration. Conversion: nearly 100%, mainly hydrogenation and double bond isomerization.

[b] Average of 3 runs.

To sum up: three characteristics of Pt-catalyzed homologation could be recognized on the basis of the present studies:

1. The appearance of relatively high amounts of saturated homologues in addition to aromatics.

2. The formation of *iso*-homologues and the reactivity of methylcyclopentane shows that a so far unique reaction of C_1 addition to internal C—C bonds has been recognized. Their activity is about 4 times less then that of terminal C—C bonds.

3. Stepwise homologation has been shown up to C_8 molecules; presumably this may go on to give further products. Their degradation may contribute to lower aromatics, but certainly is not the main pathway of buildup reactions here [13].

Separate radiotracer studies [21] show that only deep fragmentation of *n*-hexane produces carbenes active in homologation, since all of its C atoms have equal probability to participate in chain lengthening. End demethylation is more important with 3-methylpentane. With the above additions we found the mechanism of homologation put forward in the literature by O'Donohoe et al. [8, 9] to be valid.

REFERENCES

[1] Anderson, J. R.: Adv. Catal., **23,** 1 (1977)
[2] Anderson, J. R. and Baker, B. G.: Proc. Roy. Soc., *A***271,** 402 (1963)
[3] Paál, Z., Rozengart, M. I.: Acta Chim. Acad. Sci. Hung., **49,** 395 (1966)
[4] Paál, Z., Rozengart, M. I.: Acta Chim. Acad. Sci. Hung., **54,** 287 (1967)
[5] Guczi, L., Kálmán, J., Matusek, K.: React. Kinet. Catal. Lett., **1,** 51 (1974)
[6] Guczi, L., Matusek, K., Tétényi, P.: React. Kinet. Catal. Lett., **1,** 291 (1974)
[7] Péter, A., Clarke, J. K. A.: J. Chem. Soc. Faraday Trans. I., **72,** 1201 (1976)
[8] O'Donohoe, C., Clarke, J. K. A., Rooney, J. J.: J. Chem. Soc., Chem. Comm., **1979,** 648
[9] O'Donohoe, C., Clarke, J. K. A., Rooney, J. J.: J. Chem. Soc. Faraday Trans. I., **76,** 345 (1980)
[10] A. Sárkány, P. Tétényi: J. Chem. Soc. Chem. Comm., **1980,** 525
[11] Sárkány, A., Pálfi, S., Tétényi, P.: React. Kinet., Catal. Lett., **15,** 1 (1980)
[12] Sárkány, A., Pálfi, S., Tétényi, P.: Acta Chim. Acad. Sci. Hung., **111,** 633 (1982)
[13] Margitfalvi, J., Hegedüs, M., Göbölös, S., Kwaysser, E., Koltai, L., Nagy, F.: Acta Chim. Acad. Sci. Hung., **111,** 573 (1982)
[14] Zimmer, H., Paál, Z., Tétényi, P.: Acta Chim. Acad. Sci. Hung., **111,** 513 (1982)
[15] Altham, J. A., Webb, G.: J. Catal., **18,** 133 (1970)
[16] Paál, Z., Dobrovolszky, M., Völter, J., Lietz G.: Applied Catal. (in press)
[17] Amir-Ebrahimi, V., Choplin, A., Parayre, P., Gault, F. G.: Nouv. J. Chim., **4,** 431 (1980)
[18] Paál, Z., Tétényi, P.: J. Catal., **29,** 276 (1973)
[19] Kane, A. F., Clarke, J. K. A.: J. Chem. Soc. Faraday Trans. I, **76,** 1640 (1980)
[20] Paál, Z.: Adv. Catal., **29,** 273 (1980)
[21] Paál, Z., Dobrovolszky, M., Tétényi, P.: J. Chem. Soc. Faraday Trans. I (in press)
[22] Davis, B. H.: Proc. 8th Internat. Congress on Catalysis, Berlin, 1984, Verlag Chemie, Weinheim, 1984, Vol. II, p. 469.

Acta Chimica Hungarica 119 (2—3), pp. 105—113 (1985)

SUPPORT EFFECT IN CLUSTER DERIVED CATALYSTS+

Zoltán SCHAY, István BOGYAY and László GUCZI*

(Institute of Isotopes of the Hungarian Academy of Sciences, H-1525 Budapest, P.O. Box 77)

Received June 8, 1984
Accepted for publication August 15, 1984

Iron-ruthenium catalysts prepared from $Fe_3(CO)_{12}$, $Ru_3(CO)_{12}$, $Fe_2Ru(CO)_{12}$ and $H_2FeRu_3(CO)_{13}$ deposited on Al_2O_3 and TiO_2 from hexane solution have been investigated in the CO/H_2 reaction. The cluster support interaction has been followed in each step of preparation. The interaction already starts during impregnation as part of CO is stripped off from the clusters. On evacuation additional CO is removed, depending on the cluster and the support. $Fe_2Ru(CO)_{12}$ is the most unstable on both Al_2O_3 and TiO_2 supports, while $H_2FeRu_3(CO)_{13}$ has a high stability. The amount of CO recovered in temperature programmed decomposition also depends on the cluster-support pair. When the decomposition is interrupted at 570 K same CO is left in the cluster and activates it for the CO/H_2 reaction. The selectivity for CH_4 is about 0.7 for Al_2O_3 supported clusters and drops to about 0.5 for TiO_2 supported ones. Changes in reaction rate and selectivity are discussed in light of metal-support interaction.

Introduction

Previously [1—3] we have reported the properties of Cab-O-Sil HS 5 supported iron-ruthenium catalysts. Results clearly showed that catalysts derived from carbonyl clusters are more active than that prepared from inorganic salts. In the coimpregnated $Fe_3(CO)_{12}$ + $Ru_3(CO)_{12}$ catalysts interaction develops between Fe and Ru during decomposition. In that work we wanted to minimize the cluster-support interaction and focussed our attention to the metal-metal interaction. For preparation of highly active catalysts anchoring of the clusters to the support is necessary [4], when an interaction between the cluster and support develops. Al_2O_3 is one of the most preferred supports [5] but since the discovery of SMSI (strong metal support interaction) on TiO_2 [6, 7] considerable effort has been made to explain the increase in catalytic activity in terms of metal support interaction.

Recently Burch et al. [8] emphasized the importance of the interface between the metal and the partially reduced TiO_2 support. They proposed that the new active sites created at the interface are active for CO + H_2 reaction on Ni/TiO_2 catalysts.

+ This paper was presented at the 2nd Belgian—Hungarian Colloquium on Catalysis at De Haan, Belgium, October 10—13, 1983.

* To whom correspondence should be addressed.

In the present work the interaction between the metal carbonyl clusters and Al_2O_3 and TiO_2 supports is studied. The interaction is followed in each step of the catalyst preparation, and activity and selectivity in the CO + H_2 reaction will be discussed in light of the metal-support interaction.

Experimental

Catalysts

Cab—O—Sil HS 5, Al_2O_3 (Woelm) and TiO_2 (Degussa P25) have been used for catalyst preparation. For catalysts Fe + Ru the support was impregnated with aqueous solution of $Fe(NO_3)_3$ and $RuCl_3$ and dried overnight at 400 K. Before the catalytic tests they were calcined in a reactor in oxygen for 1 hr at 570 K additionally for 1 hr at 770 K reduced in hydrogen at 770 K for 1 hr. The metal load was 0.5 wt% Fe and 0.5 wt% Ru. Catalysts Fe_3 + + Ru_3, Fe_2Ru and $FeRu_3$ were prepared by impregnation of the support with *n*-hexane solution of $Ru_3(CO)_{12}$ + $Fe_3(CO)_{12}$, $Fe_2Ru(CO)_{12}$ and $H_2FeRu_3(CO)_{13}$, respectively. Hexane was frozen out and the supported carbonyl cluster was evacuated overnight at room temperature. Total metal load was 1 wt% and the Fe_3 + Ru_3 catalyst contained 0.5 wt% Fe and 0.5 wt% Ru. Details of the preparation have been reported elsewhere [3]. Clusters were decomposed for 0.5 hr in situ the reactor in He at 770 K, in H_2 at 570 K or in H_2 at 770 K, denoted by He/770, H_2/570 and H_2/770, respectively.

Methods

For measuring CO evolution during impregnation and MS-10 mass spectrometer was connected to a closed circulation reactor which was modified to allow in situ impregnation. For details see [9].

Temperature programmed decomposition (TPDC) and temperature programmed reduction (TPR) were carried out in a flow system in He and in 1% H_2 in Ar at 20 K min^{-1} heating rate. Thermal conductivity detector and flame ionization detector was used to measure CO and hydrocarbons simultaneously.

Catalytic reactions were carried out with a 2 : 1 mixture of H_2/CO in a continuous flow type tubular reactor working at atmospheric pressure in a differential regime at a conversion level below 1%. The experimental conditions were the following: amount of the catalyst 0.05—0.2 g, the gas flow rate 5—30 ml min^{-1}, temperature 470—600 K. Reaction products were analysed on a Packard 427 gas chromatograph, using *n*-octane on Porasil C column. For details see [3].

Selectivities were calculated by $S_i = C_i / \sum_i C_i$ where C_i is the concentration of the *i*-th species in mole L^{-1}. Reaction rates were calculated from the hydrocarbons produced and given for the CO converted in mole $g^{-1}\,s^{-1}$ units.

Results

The first step in the preparation of supported carbonyl clusters is the impregnation, when interaction between the support and the cluster develops. As a consequence of this interaction the bonding of CO ligands is influenced and CO evolution is observed.

Amounts of the CO evolved during the impregnation step are given in Table I. For Cab—O—Sil the interaction between the support and the clusters is very weak and there is hardly any CO stripped off from the cluster. The interaction is very strong with Al_2O_3 and TiO_2. It is important to notice that

Table I

CO stripped off during impregnation

Support	Cab—O—Sil		Al_2O_3				TiO_2			
Cluster	Fe_3	Ru_3	Fe_3	Ru_3	Fe_2Ru	$FeRu_3$	Fe_3	Ru_3	Fe_2Ru	$FeRu_3$
Average number of CO molecules stripped off from one cluster	0.1	<0.05	1.1	0.4	1.2	<0.05	0.7	0.2	1.5	—

$Fe_3 = Fe_3(CO)_{12}$
$Ru_3 = Ru_3(CO)_{12}$
$Fe_2Ru = Fe_2Ru(CO)_{12}$
$FeRu_3 = H_2F3Ru_3(CO)_{13}$
1 wt% total metal load

Table II

Total amounts of CO *and* CH_4 *measured in* TPDC *and* TPR *of the supported clusters*

	Carrier gas Detected product		He		1% H_2 in Ar CH_4 (μmol g^{-1})
			CO + CH_4	CH_4 (μmol g^{-1})	
Support	Cluster	CO in the impregnated catalyst (μmol g^{-1})			
Cab–O–Sil	Fe_2Ru	564	276	156	228
	$FeRu_3$	362	304	150	221
Al_2O_3	$Fe_3 + Ru_3$	556	208	2	24
	Fe_2Ru	564	52.8	20	40
	$FeRu_3$	362	300	—	50.4
TiO_2	$Fe_3 + Ru_3$	556	254	12	25.2
	Fe_2Ru	564	26	9.6	60
	$FeRu_3$	362	198	—	58

$Fe_3 = Fe_3(CO)_{12}$
$Ru_3 = Ru_3(CO)_{12}$
$Fe_2Ru = Fe_2Ru(CO)_{12}$
$FeRu_3 = H_2FeRu_3(CO)_{13}$

$Fe_3(CO)_{12}$ and especially $Fe_2Ru(CO)_{12}$ easily give off one CO molecule, whereas $Ru_3(CO)_{12}$ is more stable. The tetrametal cluster, $H_2FeRu_3(CO)_{13}$, shows a remarkable stability during impregnation.

TPDC curves measured in He for the supported clusters are given in Fig. 1. The initial decomposition at low temperature is always followed by an additional process over 570 K. In this second step the residual CO content of the cluster reacts with OH groups left on the surface after pretreatment and CH_4 is formed. In Figs 2 and 3 only FID signals in He and in 1% H_2 in Ar are given and the curves clearly show that hydrocarbons are formed.

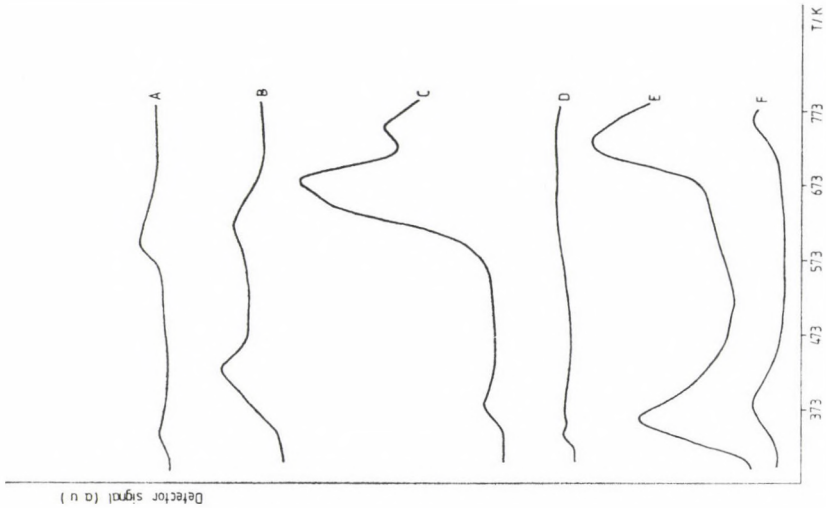

Fig. 1. Temperature programmed decomposition in He carrier gas using thermal conductivity detector; a) $Fe_2Ru(CO)_{12}/TiO_2$; b) $H_2FeRu_3(CO)_{13}/TiO_2$; c) $Fe_3(CO)_{12} + Ru_3(CO)_{12}/TiO_2$; d) $Fe_2Ru(CO)_{12}/Al_2O_3$; e) $H_2FeRu_3(CO)_{13}/Al_2O_3$; f) $Fe_3(CO)_{12} + Ru_3(CO)_{12}/Al_2O_3$

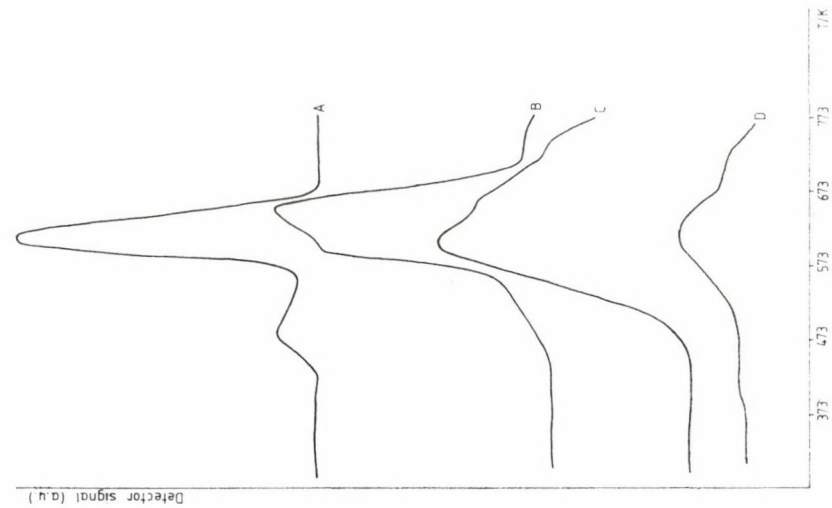

Fig. 2. Temperature programmed decomposition in He carrier gas using flame-ionization detector; a) $Fe_2Ru(CO)_{12}/TiO_2$; b) $Fe_3(CO)_{12} + Ru_3(CO)_{12}/TiO_2$; c) $Fe_2Ru(CO)_{12}/Al_2O_3$; d) $Fe_3(CO)_{12} + Ru_3(CO)_{12}/Al_2O_3$

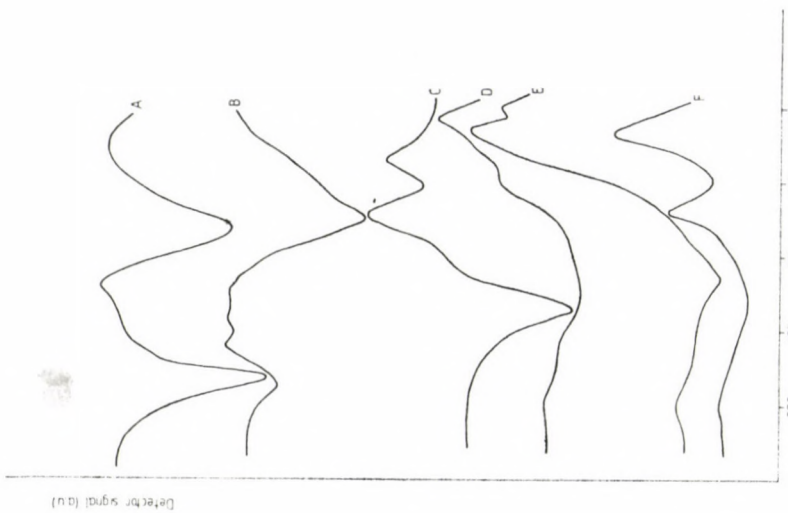

Fig. 4. Temperature programmed reduction in 1% H_2 in Ar carrier gas using thermal conductivity detector; a) $Fe_2Ru(CO)_{12}/TiO_2$; b) $H_2FeRu_3(CO)_{13}/TiO_2$; c) $Fe_3(CO)_{12}$ + $Ru_3(CO)_{12}/TiO_2$; d) $Fe_2Ru(CO)_{12}/Al_2O_3$; e) $H_2FeRu_3(CO)_{13}/Al_2O_3$; f) $Fe_3(CO)_{12}$ + $Ru_3(CO)_{12}/Al_2O_3$

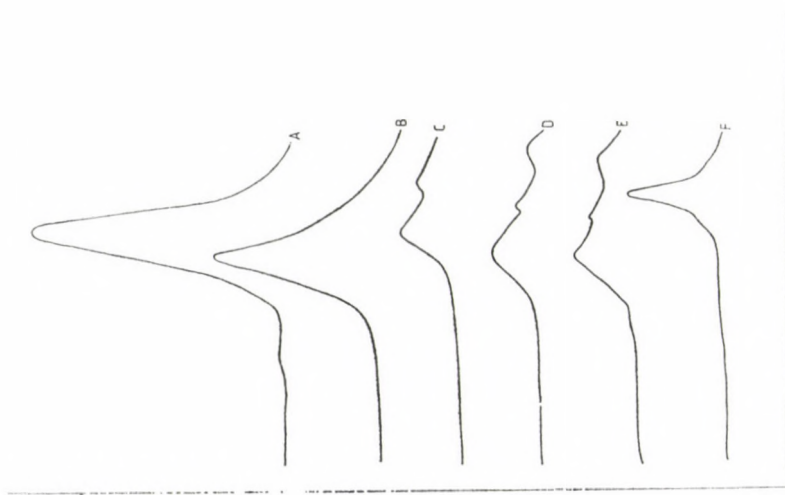

Fig. 3. Temperature programmed reduction in 1% H_2 in Ar carrier gas using flame-ionization detector; a) $Fe_2Ru(CO)_{12}/TiO_2$; b) $H_2FeRu_3(CO)_{13}/TiO_2$; c) $Fe(CO)_{12}$ + $Ru_3(CO)_{12}/TiO_2$; d) $Fe_2Ru(CO)_{12}/Al_2O_3$; e) $H_2FeRu_3(CO)_{13}/Al_2O_3$; f) $Fe_3(CO)_{12}$ + $Ru_3(CO)_{12}/Al_2O_3$

Mass spectrometry revealed, that besides CH_4 some CO_2 is also formed simultaneously.

The TPR curves in Fig. 4 indicate that the clusters are partially oxidized on impregnation, as there is a low temperature reduction peak in addition to the high temperature peak, the latter being responsible for the reduction of CO to CH_4.

Both the TPDC and TPR curves reveal the complex behaviour of the cluster support interaction, The curves are completely different for the clusters

Table III

The effect of the support on the reaction rate and selectivity at 554 K

Support	Cluster	Decomposition	Reaction rate*	S_{C_1}	S_{C_2}	$S_{C_2=}$	S_{C_3}	$S_{C_3=}$	S_{C_4+}
Cab–O–Sil[a]	Fe + Ru	H_2/770	1.4	0.57	0.03	0.19	0.01	0.15	0.05
	$Fe_3 + Ru_3$	He/570	19	0.68	0.02	0.12	<0.01	0.16	<0.01
		H_2/770	52	0.69	0.03	0.16	<0.01	0.10	0.02
	Fe_2Ru	He/570	43	0.69	0.03	0.11	0.01	0.10	0.05
		H_2/770	10	0.73	0.02	0.10	0.01	0.12	0.03
	$FeRu_3$	He/570	22	0.77	0.02	0.09	0.01	0.10	0.02
		H_2/770	13	0.74	0.04	0.06	<0.01	0.10	0.05
Al_2O_3	Fe + Ru	H_2/770	4.5	0.61	0.06	0.12	0.01	0.11	0.10
	$Fe_3 + Ru_3$	He/770	29	0.69	0.11	0.02	0.04	0.06	0.07
		H_2/770	26	0.46	0.09	0.06	0.04	0.10	0.24
		H_2/570	17	0.74	0.04	0.06	0.09	0.08	0.07
	Fe_2Ru	He/770	7.3	0.77	0.04	0.05	0.01	0.07	0.04
		H_2/770	0.1	0.75	0.06	0.06	0.01	0.07	0.03
		H_2/570	12	0.75	0.05	0.05	0.01	0.08	0.04
	$FeRu_3$	He/770	34	0.61	0.09	0.04	0.02	0.10	0.12
		H_2/770	31	0.58	0.09	0.05	0.03	0.11	0.15
		H_2/570	55	0.72	0.09	0.02	0.02	0.07	0.08
TiO_2	Fe + Ru	H_2/770	28	0.51	0.06	0.09	0.01	0.14	0.17
	$Fe + Ru_3$	He/770	116	0.52	0.04	0.07	0.01	0.14	0.22
		H_2/770	57	0.53	0.05	0.08	0.01	0.14	0.19
		H_2/570	95	0.47	0.03	0.06	0.01	0.11	0.31
	Fe_2Ru	He/770	131	0.44	0.03	0.06	0.01	0.15	0.29
		H_2/770	121	0.47	0.03	0.06	0.01	0.15	0.30
		H_2/570	101	0.50	0.05	0.06	0.01	0.14	0.24
	$FeRu_3$	He/770	0.23	0.52	0.02	0.12	<0.01	0.05	0.30
		H_2/770	0.35	0.73	0.02	0.16	<0.01	0.08	<0.01
		H_2/570	20	0.54	0.05	0.08	0.01	0.13	0.18

* 10^8 mol s^{-1} g^{-1}

[a] Data reproduced from Refs [2, 3].

$Fe_2Ru(CO)_{12}$ and $H_2FeRu_3(CO)_{13}$ indicating a different support-cluster interaction. Quantitative data for the curves are given in Table II. It is noted that for $Fe_2Ru(CO)_{12}$ supported on TiO_2 and Al_2O_3 only a small fraction of the CO in the original cluster can be detected. It is remarkable that the Cab—O—Sil supported clusters give more CH_4 than the TiO_2 and Al_2O_3 supported ones. The carbon balance is also better for Cab—O—Sil, and rather poor for TiO_2, in agreement with data in Table I.

Results for the catalytic tests are summarized in Table III. For better comparison data are given for an average temperature of 554 K and 15 mL min^{-1} flow rate in steady state. Values for the Cab—O—Sil supported catalysts are also reproduced [2, 3] to make comparisons easier. Data in Table III clearly show that the reaction rate is higher for the cluster derived $Fe_3 + Ru_3$ catalysts than for the Fe + Ru catalysts prepared from inorganic salts, although there is no marked difference in the selectivities. Reaction rate and selectivity depends on the pretreatment. In general for the Al_2O_3 supported, cluster derived catalysts the $H_2/570$ pretreatment results in more CH_4 and less C_4^+ compared to the $H_2/770$ pretreatment. The TiO_2 supported catalysts produce less CH_4 and more C_4^+ than the Al_2O_3 supported ones, and the reaction rate is also higher. Besides changes in the selectivity the $H_2/570$ pretreatment results in higher reaction rates. The reaction rate is unusually low for Al_2O_3 supported $Fe_2Ru(CO)_{12}$ and for TiO_2 supported $H_2FeRu_3(CO)_{13}$ pretreated at 770 K both in He and H_2.

These changes in the reaction rate and selectivity indicate changes in the cluster support interaction.

Discussion

It is generally accepted that the final catalytic properties of supported bimetallic catalysts strongly depend on the preparation [10]. In our case an interaction between the carbonyl clusters and the support starts already during the impregnation step. IR spectroscopy [11] has proved that this interaction is in some cases very strong and even leads to splitting of the Fe—Ru bond for the Al_2O_3 supported $Fe_2Ru(CO)_{12}$ cluster. The CO evolution is also on indication of the interaction and the values clearly show that it is weak with Cab—O—Sil and rather strong with Al_2O_3 and TiO_2. The interaction also depends on the structure of the cluster and the $H_2FeRu_3(CO)_{13}$ cluster seems to be very stable during the impregnation step.

The next step in the preparation of the catalysts is the decomposition of the carbonyl clusters. The coordination sphere of the cluster is already disturbed during impregnation and therefore parts of the CO ligands are mobile. ^{13}CO exchange studies [12] also give evidence for the mobility of the CO ligands.

In the first stage of the decomposition up to 570 K the Fe—Ru bonds are also disturbed and Fe, originally in zero valent state is oxidized to Fe^{2+} and Fe^{3+} [13, 14]. Part of the iron can be reduced according to the TPR curves. When the decomposition is interrupted at 570 K some CO is left in the partially decomposed clusters and activates the cluster for the CO + H_2 reaction. The partially decomposed clusters are more active than the fully decomposed ones. In the coimpregnated $Fe_3(CO)_{12}$ + $Ru_3(CO)_{12}$ catalysts an interaction between the two clusters already starts to operate as the selectivities significantly differ from the selectivities of the individual clusters.

On increasing the temperature over 570 K during the decomposition the remaining CO reacts with surface OH groups, or with hydrogen in TPR, to form methane. The amount of CH_4 is again an indication of the cluster support interactions. The interaction is very strong with Al_2O_3 therefore most of the CO is activated and the cluster decomposes at relatively low temperatures, below 570 K, without CH_4 formation. For TiO_2 more active CO is left in the cluster and therefore more CH_4 forms than for Al_2O_3. The interaction also depends on the type of the cluster and in some pairs of support-cluster results in catalysts of very low reactivity. The $Fe_2Ru(CO)_{12}/Al_2O_3$ and the $H_2FeRu_3(CO)_{13}/TiO_2$ decomposed at 570 K both show reasonable reaction rates, but after further decomposition in He or in H_2 at 770 K the reaction rate drastically decreases. This is most probably caused by strong metal support interaction. For the Cab—O—Sil supported clusters interaction is weak therefore no such deactivation is observed and in the final state of the catalysts only the overall composition and not the type of the clusters determines the catalytic properties [2]. For TiO_2 and Al_2O_3 the cluster support interaction is dominating and this results either in stabilization of the metal dispersion or if it is very strong in deactivation of the catalyst.

Changes in selectivity can also be explained by differences in support metal interaction. For Cab—O—Sil supported catalysts the overall metal composition and the iron ruthenium interaction determines the selectivity, whereas pretreatment and chemical form of the metals in the impregnation step have only marginal effects [15] indicating a weak metal support interaction.

For Al_2O_3 the effect of pretreatment on selectivities depends on the type of the cluster. For Fe_2Ru there is no effect, only the reaction rate changes by a factor of 100, as the cluster already decomposes during the impregnation step. The $FeRu_3$ and Fe_3 + Ru_3 cluster derived catalysts produce more CH_4 and less C_4^+ on H_2/570 than on H_2/770 pretreatment. This can only be explained by changes in the cluster support interaction as the reaction rate is only slightly effected. The stronger interaction which is developed at high temperature pretreatment results in less hydrogen available for the reaction and therefore the chain lengthening and olefin formation is preferred.

For TiO_2 supported clusters the chain lengthening is favoured even more than for Al_2O_3 supported ones. The decomposition of Fe_2Ru is more pronounced as more CO is stripped off during impregnation and only about 5% of the original CO content could be detected in TPDC when the impregnated catalyst was evacuated overnight. In contrast to Al_2O_3 the reaction rate is high, indicating a different interaction. This interaction has also the character of the strong metal support interaction and reduces the hydrogen available for the reaction and results in high $S_{C_4^+}$ values. The $FeRu_3$ cluster also decomposes on evacuation as only about 50% of the original CO content was detected in TPDC. This interaction is different to the previous one as the reaction rate is very low and on changing the pretreatment from $H_2/570$ to $H_2/770$ a further decrease in the reaction rate and $S_{C_4^+}$ is experienced. The role of Ti^{3+} defects in the cluster-support interaction is probable but at present we do not have direct evidence for their effect on the iron-ruthenium carbonyl clusters.

For both Al_2O_3 and TiO_2 supported clusters the cluster-support interaction depends on the structure of the iron-ruthenium carbonyl cluster, and results in changes not only in the reaction rate but in the selectivities as well.

REFERENCES

[1] Guczi, L., Schay, Z., Matusek, K., Bogyay, I., Stefler, G.: Proc. 7th Intern. Congress on Catalysis, Part *A*, p. 211 Kodansha Ltd., Tokyo and Elsevier Sci. Publ. Co. Amsterdam 1981
[2] Guczi, L., Schay, Z., Lázár, K., Vizi, A., Markó, L.: Surf. Sci., **106,** 516 (1981)
[3] Schay, Z. Guczi, L.: Acta Chim. Acad. Sci. Hung., **111,** 607 (1982)
[4] Yermakov, Yu. I.: Proc. 7th Intern. Congress on Catalysis, Part *A*, p. 57, Kodansha Ltd., Tokyo and Elsevier Sci. Publ. Co. Amsterdam 1981.
[5] Kuznetsov, V. L., Bell, A. T., Yermakov, Y. I.: J. Catal., **65,** 374 (1980)
[6] Tauster, S. J., Fung, S. C., Garten, R. L.: J. Amer. Chem. Soc., **100,** 170 (1978)
[7] Tauster, S. J., Fung, S. C.: J. Catal., **55,** 29 (1978)
[8] Burch, R., Flambard, A. R.: J. Catal., **78,** 384 (1982)
[9] Lázár, K., Matusek, K., Mink, J., Dobos, S., Guczi, L., Vizi-Orosz, A., Markó, L., Reiff, W. M.: J. Catal., **87,** 163 (1984)
[10] Imelik, B., Naccache, C., Coudurier, G., Praliaud, H., Meriaudeau, P., Gallezot, P., Martin, G. A., Vedrine, J. C.: in Metal-Support and Metal-Additive Effects in Catalysis, Elsevier Sci. Publ. Co. Amsterdam 1982
[11] Böszörményi, I., Dobos, S., Guczi, L. (to be published)
[12] Guczi, L., Böszörményi, I., Dobos, S., Lázár, K., Takács, L., Schay, Z.: X. Intern. Symp. on the Reactivity of Solids, Dijon, 27 Aug.—1 Sept., 1984
[13] Böszörményi, I., Dobos, S., Guczi, L., Markó, L., Lázár, K., Reiff, W. M., Schay, Z., Takács, L., Vizi-Orosz, A.: Proc. 8th Intern. Congress on Catalysis Vol. **V,** 183, Verlag Chemie, Weinheim 1984
[14] Lázár, K., Guczi, L., Reiff, W. M.: J. Catal. (in press)
[15] Schay, Z., Lázár, K., Mink, J., Guczi, L.: J. Catal., **87,** 179 (1984)

Acta Chimica Hungarica 119 (2—3), pp. 115—125 (1985)

BASE CATALYZED REACTIONS OF COBALT CARBONYLS RELATED TO HYDROFORMYLATION+

Attila SISAK*, Ferenc UNGVÁRY and László MARKÓ

(Research Group for Petrochemistry of the Hungarian Academy of Sciences, Veszprém, and Institute of Organic Chemistry, University of Chemical Engineering, H-8201 Veszprém, P.O.B. 158)

Received June 8, 1984
Accepted for publication August 15, 1984

The hydrogemation of $Co_2(CO)_8$ to $HCo(CO)_4$ could be efficiently catalyzed by some nitrogen and phosphorus bases and halide ions. In the case of pyridine about 300 fold acceleration could be achieved at 50 °C, $p_{H_2} = 70$ bar and $p_{CO} = 5$ bar. A radical pathway is suggested on the basis of the half order for both $Co_2(CO)_8$ and pyridine. The carbonylation of $Co_4(CO)_{12}$ to $Co_2(CO)_8$ proved to be about 10^4 times faster in the presence of 40 mol% pyridine (based on $Co_4(CO_{12})$ at 50 °C and $p_{CO} = 0.87$ bar. The reaction was found to be of first order for both $Co_4(CO)_{12}$ and pyridine and minus first order for CO. A mechanism containing $Co_4(CO)_{11}(py)$ as reactive intermediate is proposed.

Introduction

In the practice of the industrially important cobalt carbonyl catalyzed hydroformylation of olefins high temperatures (100—150 °C) and high pressures (200—300 bar of $1:1 = CO:H_2$) are employed. Kinetic data for the assumed steps of the catalysis show (Table I) that the formation of $HCo(CO)_4$ from $Co_2(CO)_8$ by H_2 could be the "bottle neck" in the catalytic cycle. The drastic conditions are presumably necessary only to achieve a high rate of this relatively slow reaction (Eq. 1).

$$Co_2(CO)_8 + H_2 \xrightarrow{r_1} 2\ HCo(CO)_4 \qquad (1)$$

In the so called stoichiometric hydroformylation (Eq. 2) high pressures of H_2 (200 bar) are used at room temperature to prepare 2 mols of aldehyde from each mol $Co_2(CO)_8$ [5]. Adding of CO slows down the reaction dramatically and does not lead to a catalytic cycle. Obviously, at room temperature also the regeneration of $Co_2(CO)_8$ from $Co_4(CO)_{12}$ is very slow (see Table I).

$$Co_2(CO)_8 + 2\ H_2 + 2\ RCH{=}CH_2 \rightarrow 2\ RCH_2CH_2CHO + 1/2\ Co_4(CO)_{12} \qquad (2)$$

$$Co_4(CO)_{12} + 4\ CO \xrightarrow{r_2} 2\ Co_2(CO)_8 \qquad (3)$$

+ This paper was presented at the 2nd Belgian—Hungarian Colloquium on Catalysis at De Haan, Belgium, October 10—13, 1983.

* To whom correspondence should be addressed.

Table I

Comparison of rates at 25 °C for some reactions relevant to the cobalt catalyzed hydroformylation of olefins

Reaction	Rate[a] ($M \cdot s^{-1}$)	E_a (kJ · mol^{-1})	Ref.
$Co_2(CO)_8 + H_2 \rightarrow 2\ HCO(CO)_4$	10^{-10}	123	[1]
$Co_4(CO)_{12} + 4\ CO \rightarrow 2\ Co_2(CO)_8$	10^{-11}	55	[2]
$HCo(CO)_4 +$ olefin $+ CO \rightarrow RCOCo(CO)_4$	10^{-6}—10^{-5}[b]	55—65[b]	[3]
$RCOCo(CO)_4 + H_2 \rightarrow RCHO + HCo(CO)_4$	10^{-8}	119	[4]
$RCOCo(CO)_4 + HCo(CO)_4 \rightarrow RCHO + Co_2(CO)_8$	10^{-7}		[4]

[a] Calculated for [Co] = 0.01 *M*, $p_{H_2} = p_{CO} = 1$ bar, [olefin] = 0.50 *M* in heptane solution from published kinetic data.
[b] Depending on the olefin.

The effect of additives, primarily bases, on catalytic hydroformylation has been already studied and in most cases an inhibition or only a moderate activation was found [6, 7]. In these works, however, relatively large amounts of additives (above 1 mol/mol Co) were used, which inevitably led to side reactions producing catalytically inactive species, e.g. $[Co(CO)_4]^-$ [8].

In this communication we report on the catalytic influence of small amounts of bases on reactions (1) and (3) and present some kinetic data. Part of this work has already been published [10].

Results

We have found that both slow reactions represented by Eq. 1 and Eq. 3 could be accelerated by adding catalytic amounts of bases. The hydrogenation of $Co_2(CO)_8$ to $HCo(CO)_4$ in toluene is catalyzed by tertiary amines, imines and — very efficiently — by some nitrogen heterocycles, tertiary phosphines (with $pK_a \geq 5$) and halide ions (Table II). In the case of pyridine the equilibrium conversion is reached in 10 minutes at 50 °C and $p_{H_2} = 70$ bar, $p_{CO} =$ $= 5$ bar if 28 mol % pyridine (based on $Co_2(CO)_8$) is added. Furthermore, the $Co_2(CO)_8$ conversion shows a maximum as a function of the [additive]/[Co] ratio in the case of three additives : pyridine, PBu_3 and $P(OBu)_3$ (Fig. 1).

The acceleration of $Co_2(CO)_8$ hydrogenation is more than 300 fold under the optimum conditions mentioned as compared to the rate observed in the absence of pyridine [10]. For convenience, however, the kinetic measurements were performed with lower amounts of added pyridine. The results are listed in Table III. The reaction proved to be of half order for both $Co_2(CO)_8$ and pyridine in the concentration range of 0.07—0.3 M, and 0.004—0.016 *M*, respectively (Figs 2 and 3). The hydrogenation rate was inversely proportional

Table II

Hydrogenation of $Co_2(CO)_8$ *in the presence of various additives. Reaction conditions:* 50 °C, p_{H_2} = 70 bar, p_{CO} = 5 bar, *toluene solution*, $[Co_2(CO)_8]$ = 0.105 *M*, [additive] = 0.011 *M*, *reaction time* 30 min

Additive[a]	$HCo(CO)_4$ (% of Co)	Additive	$HCo(CO)_4$ (% of Co)
None	<0.5	PPh_3	1.4
DMF	2.6	PPh_2Me	1.4
quin	14.8	PBu_3	17.1
8-OHquin	18.6	$PMe(i\text{-}Pr)_2$	18.6
py	17.6	$P(i\text{-}Pr)_3$	14.5
2-Mepy	17.9	$P(c\text{-}Hex)_3$	20.0
2,4-Me_2py	16.7	diphos[b]	15.7
2,6-Me_2py	<0.5	$P(OPh)_3$	0.7
NMe_2Ph	6.2	$P(OBu)_3$	12.9
$NEt(c\text{-}Hex)_2$	2.7	$AsPh_3$	2.1
PhCH=NPh	<0.5	$SbPh_3$	<0.5
Me(*i*-Bu)C=NPh	13.7	$K_2[CoCl_4]$[b,c,d]	21.6
Me(*i*-Bu)C=NCH_2Ph	2.7	$K_2[CoBr_4]$[b,c,d]	18.8
bipy[b]	1.4	$K_2[CoI_4]$[b,c,d]	15.2
phen[b]	6.7	NBu_4Br	12.9

[a] Key to abbreviations: DMF, *N*,*N*-dimethylformamide; quin, quinoline; py, pyridine; bipy, 2,2-bipyridine; phen,1,10-phenantroline; diphos, 1,2-bis(diphenylphosphino)ethane.
[b] [Additive] = 0.006 *M*.
[c] In CH_2Cl_2 solution.
[d] K^+ ions were solvatized by 18-crown-6, see ref. [9].

Table III

Initial rates of H_2 *uptake* (r_1) *in the hydrogenation of* $Co_2(CO)_8$ *at* 50 °C *in toluene solution*

$[Co_2(CO)_8]$ (*M*)	$[py] \cdot 10^2$ (*M*)	p_{H_2} (bar)	p_{CO} (bar)	$r_1 \cdot 10^5$ ($M \cdot s^{-1}$)
0.218	—	16.8	3.7	0.16
0.070	0.40	18.6	4.0	1.10
0.072	1.61	18.2	4.0	2.71
0.142	1.59	16.5	3.6	3.99
0.147	1.60	38.3	8.3	5.65
0.155	0.79	19.8	4.3	3.11
0.216	1.57	19.3	4.2	4.78
0.227	1.20	18.7	4.1	4.40
0.293	1.58	18.7	4.1	5.43
0.211	1.58	8.8	5.5	1.18
0.215	1.61	19.5	8.3	3.08
0.215	1.61	23.0	14.2	1.84
0.215	1.61	25.0	2.5	6.19
0.216	1.62	35.3	4.6	12.3

to p_{CO} above 3 bar. The dependence on p_{H_2} seemed to be more complex: the apparent order lay higher that 1 (Fig. 4).

The carbonylation of $Co_4(CO)_{12}$ at atmospheric pressure does not occur at 50 °C in the absence of pyridine. In the presence of pyridine the reaction

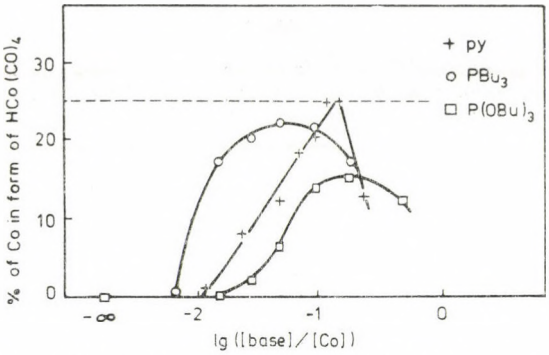

Fig. 1. Conversion of $Co_2(CO)_8$ to $HCo(CO)_4$ vs. lg([B]/[Co]) (50 °C, $p_{H_2} = 70$ bar, $p_{CO} = 5$ bar $[Co_2(CO)_8]_0 = 0.115$ *M*, toluene solution, reaction time: 10 min). The dotted line shows the equilibrium value measured in the case of pyridine

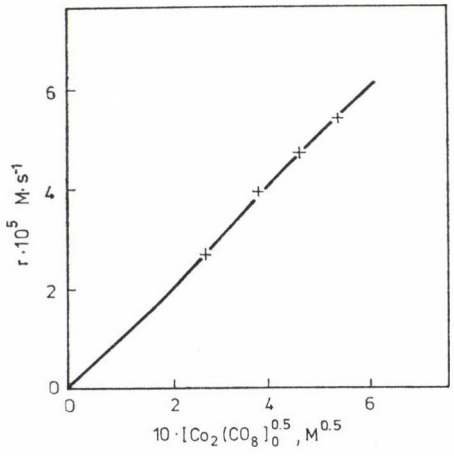

Fig. 2. Initial rates of $Co_2(CO)_8$ hydrogenation vs. $[Co_2(CO)_8]_0^{1/2}$ (50 °C, $p_{H_2} = 18$ bar, $p_{CO} = 4$ bar, $[py]_0 = 0.016$ *M*, toluene solution)

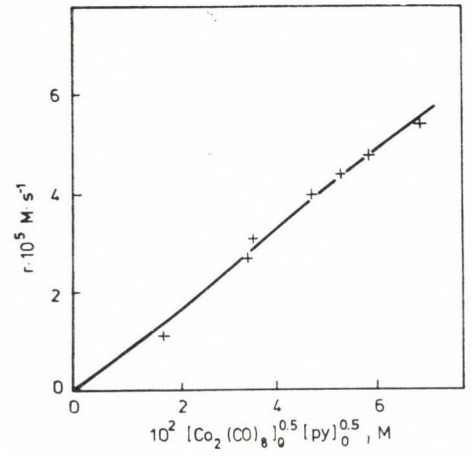

Fig. 3. Initial rates of $Co_2(CO)_8$ hydrogenation vs. $[Co_2(CO)_8]_0^{1/2} \cdot [py]_0^{1/2}$ (50 °C, $p_{H_2} = 18$ bar, $p_{CO} = 4$ bar, toluene solution)

was studied both under atmospheric and under higher CO pressures. A typical time course obtained at 50 °C and $p_{CO} = 0.87$ bar in toluene is shown in Fig. 5. Because of a fast and small CO evolution observed at the start of the reaction the kinetic evaluation was based on the maximum rate of CO absorption. The results are summarized in Table IV. We found a first order dependence both in $Co_4(CO)_{12}$ and pyridine in the concentration range of 0.01—0.06 *M* (Fig. 6). Surprisingly CO pressure has a negative effect on the reaction rate. Rising the p_{CO} from 0.87 bar to 17.5 bar the rate of CO uptake dropped nearly

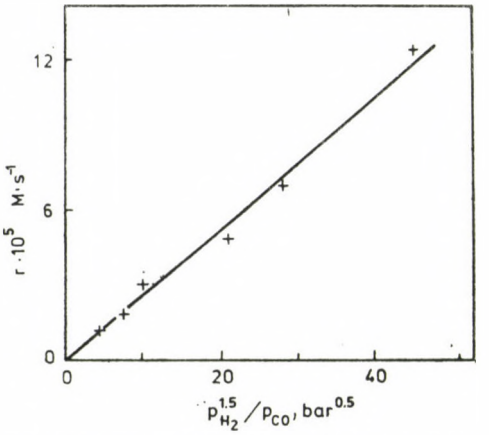

Fig. 4. Initial rates of $Co_2(CO)_8$ hydrogenation vs. $p_{H_2}^{1.5}/p_{CO}$ (50 °C, $[Co_2(CO)_8]_0 = 0.21$ *M* $[py]_0 = 0.016$ *M*, toluene solution)

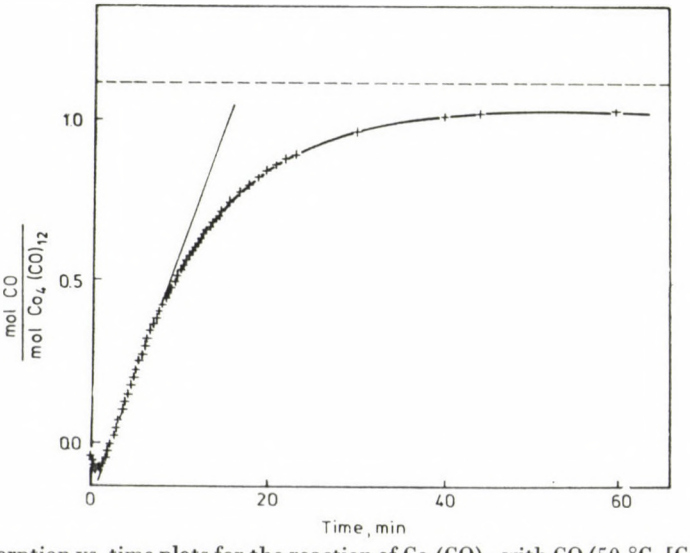

Fig. 5. CO absorption vs. time plots for the reaction of $Co_4(CO)_{12}$ with CO (50 °C, $[Co_4(CO)_{12}]_0 = 0.041$ *M*, $[py]_0 = 0.016$ *M*, $p_{CO} = 0.872$ bar, toluene solution). The dotted line represents the amount of CO for equilibrium composition calculated from literature data [11]

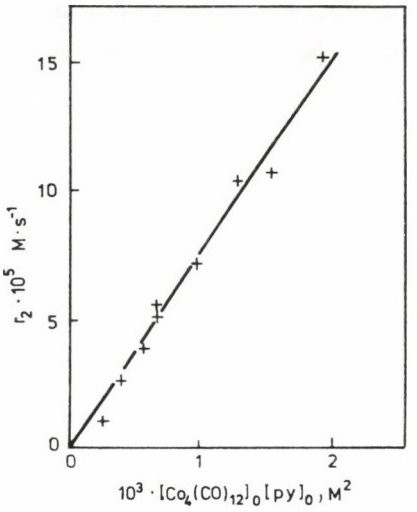

Fig. 6. CO absorption rates vs. $[Co_4(CO)_{12}]_0 \cdot [py]_0$ (50 °C, $p_{CO} = 0.86$ bar, toluene solution)

in the same proportion which suggests a minus first order dependence in CO. At the end of CO uptake the ratios of $Co_2(CO)_8/Co_4(CO)_{12}$ corresponded to the equilibrium values which could be calculated from published data [11]. The initial rate of CO evolution at the beginning at 30 °C was found to be first order in both $Co_4(CO)_{12}$ and pyridine. The result of an experiment performed under argon indicated a slight negative effect of CO on the rate of this initial step (see Table IV). In this case a new $Co_4(CO)_{12}$ derivative could be detected by IR spectroscopy in the reaction mixture, which could not be isolated, however. The IR spectrum (ν(C=O) in toluene: 2086 (m), 2038 (vs, broad), 2029 (sh), 2004 (w), 1990 (sh), 1850 (m, br), 1838 (m)) strongly suggests, that the new complex has a structure related to the known $Co_4(CO)_{11}(PR_3)$ compounds [12]. Under CO also other unknown products absorbing in the same IR region could be detected, but they could not be separated from $Co_2(CO)_8$ and the above $Co_4(CO)_{11}(py)$.

The effect of other bases on the carbonylation of $Co_4(CO)_{12}$ was studied under atmospheric conditions at 50 °C, and at the ratio [base]/[Co] = 1/10. Triethylamine accelerated the CO uptake much less than pyridine, but the $Co_4(CO)_{12} - Co_2(CO)_8$ equilibrium could be achieved within 8 hours. Phosphorus ligands, however, gave the known $Co_4(CO)_{11}(PR_3)$ complexes immediately, and the rate of the CO uptake dropped quickly. A $Co_4(CO)_{12}$—$Co_2(CO)_8$ equilibrium could be achieved in the case of PBu_3 within 3 hours, but the amount of absorbed CO was lower due to the formation of $Co_4(CO)_{11}(PBu_3)$.

The complex $Co_4(CO)_{11}(P(OEt)_3)$ did not absorb any CO even in the presence of equimolar pyridine.

Table IV

Kinetic data for carbonylation of $Co_4(CO)_{12}$ *at* 50 °C *and* $p_{CO} = 0.86 \pm 0.01$ *bar in toluene solution*

$[Co_4(CO)_{12}] \cdot 10^2$ (M)	$[py] \cdot 10^2$ (M)	$r_i \cdot 10^{5a}$ ($M \cdot s^{-1}$)	$r_1 \cdot 10^{5b}$ ($M \cdot s^{-1}$)
2.1	1.9	n.d.	2.7
2.1	1.3	n.d.	1.0
3.1	1.9	n.d.	3.9
3.7	4.3	n.d.	11.7
4.1	—	—	0.0[c]
4.1	0.8	n.d.	0.3
4.1	1.7	>10	5.2
4.0	2.5	n.d.	7.2
4.0	3.2	n.d.	10.8
4.0	4.8	n.d.	15.2
3.9	7.8	n.d.	11.0[d]
5.0	3.1	n.d.	10.7
6.0	3.7	n.d.	10.3[e]
4.1	1.7	n.d.	1.4[f]
2.1	1.7	n.d.	0.27[g]
4.1	1.7[h]	0.8	0.66
4.1	1.7[i]	>40	5.2
4.1	1.7[j]	>40	~1
1.2	2.4	1.7[k]	n.d.
1.7	3.6	4.3[k]	n.d.
2.3	4.7	7.1[k]	0.31
2.4	2.4	3.6[k]	0.17
2.4	2.4	8.3[k,l]	—

[a] Initial rate of the fast CO evolution. [b] Maximum rate of the CO uptake. [c] CO uptake was not detectable. From published kinetic data [2] a value of $8.10^{-10}\ M \cdot s^{-1}$ can be calculated. [d] Precipitation of $[Co(py)_6]\ [Co(CO)_4]_2$ was observed. [e] Precipitation of metallic cobalt was observed. [f] $p_{CO} = 3.10$ bar [g] $p_{CO} = 17.5$ bar. [h] NEt_3, [i] PBu_3, [j] $P(OEt)_3$ was used instead of py. [k] at 30 °C. [l] Under argon.

Discussion

The formation of $HCo(CO)_4$ from $Co_2(CO)_8$ and H_2 in hydrocarbon solvents was already studied in detail [1, 12]. The reaction proved to be of first order for both $Co_2(CO)_8$ and H_2, and of minus first order for CO. A mechanism corresponding to the 16- and 18-electron rule of Tolman [14] was proposed. The efficient acceleration of $Co_2(CO)_8$ hydrogenation by bases at low [B]/[Co] ratios, and the obtained fractional orders suggest a rather different pathway under such conditions presumably a radical one. Such pathways were proposed recently for several fast reactions of metal carbonyls [3, 15]. The simplest mechanism which correlates with our kinetic data is shown in Scheme 1.

$$Co_2(CO)_8 \underset{k_{-1}}{\overset{k_1}{\rightleftharpoons}} 2 \cdot Co(CO)_4$$

$$\cdot Co(CO)_4 + B \underset{k_{-2}}{\overset{k_2}{\rightleftharpoons}} \cdot Co(CO)_3B + CO$$

$$\cdot Co(CO)_3B + H_2 \xrightarrow[\text{slow}]{k_3} \rightarrow \rightarrow HCo(CO)_4 + B + \ldots$$

Scheme 1

Two steady-state assumptions can be made:
a) $k_{-1} \gg k_2$, $k_{-2} \gg k_2$. This results in the following rate expression:

$$-\frac{d\,p_{H_2}}{dt} = r = \frac{k_2 \cdot K_1^{1/2} \cdot k_3 [Co_2(CO)_8]^{1/2} \cdot [B] \cdot p_{H_2}}{k_{-2} \cdot p_{CO} + k_3 \cdot p_{H_2}}$$

($K_1 = k_1/k_{-1}$)
b) $k_2 \gg k_{-1}$, $k_2 \gg k_{-2}$. The derived rate expression in this case is the following:

$$r = \frac{k_1 \cdot k_3 [Co_2(CO)_8] \cdot p_{H_2}}{k_{-2} \cdot p_{CO}}$$

Consequently, for a base weekly associated with $\cdot Co(CO)_4$ a first order dependence, for a strongly associated one a zero order dependence is to be expected: Pyridine represents presumably an intermediate case ($k_2 \sim k_{-2}$). Thus, the fractional orders obtained may be explained by the proposed mechanism.* The slowest step is probably the reaction of molecular H_2 with the $\cdot Co(CO)_3B$ radical. A few paramagnetic Co(O) species are known to react with H_2 [16]. The observed order of H_2, however, differs from 1 which would be expected on the basis of Scheme 1, and obviously more work is needed to elaborate a more detailed mechanism.

The decrease of $Co_2(CO)_8$ conversion above $[B]/[Co] = 10^{-1}$ (see Fig. 1) suggests that further reactions between the base and the starting and product complexes lead to species which are not able to activate H_2. The following side reactions may be expected

— disproportionation of $Co_2(CO)_8$ into $[CoB_6]^{2+}[Co(CO)_4]_2^-$ or $[Co(CO)_3B_2]^+$ $[Co(CO_4)]^-$ [8],

— substitution of $Co_2(CO)_8$ leading to $Co_2(CO)_7B$ (I) [17] and $Co_2(CO)_6B_2$ [8],

— reaction of $HCo(CO)_4$ with B to give $HCo(CO)_3B$ [18], or HB^+ $[Co(CO)_4]^-$ (II) [19].

* We have not investigated the kinetics for other ligands yet. The conversion data plotted in Fig. 1 suggest, however, that $P(OBu)_3$ and PBu_3 could represent the cases a) and b), respectively, in the range of $[B]/Co] = 10^{-2}$ to 10^{-1}.

$Co_4(CO)_{13} \underset{\longleftarrow\!\!\!\!\!\!\!\!\!\!\!\!\!\!\!\!}{\overset{+CO,\ very\ slow}{\longrightarrow\!\!\!\!\!\!\!\!\!\!\!\!\!\!\!\!}} Co_2(CO)_8$ [2]

$-CO\uparrow\downarrow + CO$, fast

$Co_4(CO)_{12}$

$-py\uparrow\downarrow + py$, fast

$Co_4(CO)_{12}(py)$

$+CO\uparrow\downarrow - CO$, very fast

$[Co_4(CO)_{11}(py)]_a \underset{\longleftarrow\!\!\!\!\!}{\overset{slow}{\longrightarrow\!\!\!\!\!}} [Co_4(CO)_{11}(py)]_b \underset{\longleftarrow\!\!\!\!\!\!\!\!\!}{\overset{CO}{\longrightarrow\!\!\!\!\!\!\!\!\!}}$ products

Scheme 2

The products (I) and (II) could be detected by IR spectroscopic analysis of the reaction mixtures in the case of phosphorus ligands and tertiary amines, respectively (see Experimental).

Bor and coworkers have determined the kinetics and mechanism [2] and the equilibrium [11] of the reaction of $Co_4(CO)_{12}$ with CO in hexane solution. They have found that the reaction is first order in $Co_4(CO)_{12}$ and the order in CO changed between one (at low pressures and high temperatures) and two (at high pressures and low temperatures) [2]. In our experiments the presence of pyridine caused not only a dramatic acceleration of the rate by a factor of about 10^4 but a different order in CO as well. Obviously in the presence of pyridine a different mechanism accounts for the faster carbonylation. We assume that pyridine and CO are in competition for $Co_4(CO)_{12}$ is fast equilibria leading to $Co_4(CO)_{12}(py)$ and $Co_4(CO)_{13}$, respectively. Both equilibria are far on the side of $Co_4(CO)_{12}$. $Co_4(CO)_{13}$ is an intermediate of the uncatalyzed $Co_2(CO)_8$ formation as suggested by Bor [2]. $Co_4(CO)_{12}(py)$ looses CO in a fast equilibrium and gives a relatively stable, detectable intermediate $[Co_4(CO)_{11}(py)]_a$ which presumably has the pyridine substituent at the basal plane in the axial position [12]. The succeeding step, a rearrangement of this latter species into $[Co_4(CO)_{11}(py)]_b$ should be rate determining but still much faster, than the transformation of $Co_4(CO)_{13}$. This mechanism would account for the observation that CO uptake is much faster in the presence of pyridine at low CO pressures. At higher pressures the catalyzed route is hindered and the uncatalyzed becomes more and more pronounced. This proposal depicted in Scheme 2 is in accordance with the observed kinetic picture. The first, CO evolution step in the pyridine catalyzed carbonylation is more than one order of magnitude faster than the dissociation of CO in $Co_4(CO)_{12}$, which was investigated by Darensbourg and coworkers [12]. Thus a pathway through $Co_4(CO)_{11}$ can be excluded. In the presence of phosphorus bases instead of

pyridine the intermediate $[Co_4(CO)_{11}(base)]_a$ becomes very stable [12], therefore the carbonylation rate is slowed down.

Our observations on the base catalyzed hydrogenation of $Co_2(CO)_8$ are in accordance with the rules of Heimbach and coworkers [20], namely, that the required concentration of a controlling ligand is determined by the steady-state concentration of the intermediate (in our case $\cdot Co(CO)_4$) reacting with that ligand. The optimal ligand concentration is additionally influenced by thermodynamic and kinetic parameters, which depend, of course, on the ligand properties. Different optimum ligand concentrations are therefore to be expected for different ligands. In the case of $Co_4(CO)_{12}$ carbonylation the ligand reacts with the starting complex, therefore a higher [py]/[Co] ratio is required.

Experimental

Toluene and pyridine were dried by standard methods and distilled under carbon monoxide. $Co_2(CO)_8$ was recrystallized first from CH_2Cl_2 and then twice from heptane. $Co_4(CO)_{12}$ was prepared by refluxing $Co_2(CO)_8$ in toluene under CO and then recrystallized from heptane. $Co_4(CO)_{11}(P(OEt_3))$ was obtained by the method of Poilblanc and coworkers [22].

Hydrogenations of $Co_2(CO)_8$

Screening experiments for the effect of various bases were described earlier [10]. IR spectra of the compounds detected in addition to $HCo(CO)_4$ (cm^{-1}, $\nu(C{=}O)$ region, toluene): $pyH^+[Co(CO)_4]^-$:1936 (s), 1903 (vs), $Et(c\text{-}Hex)_2NH^+[Co(CO)_4]^-$: 1995 (w), 1925 (s), 1893 (vs), $[Me(i\text{-}Bu)C{=}HNCH_2Ph]^+[Co(CO)_4]^-$: 1997 (w), 1931 (s), 1898 (vs), $Co_2(CO)_7PPh_2Me$: 2077 (m), 2022 (m), 1987 (s), 1954 (w), $Co_2(CO)_7P(OBu)_3$, 2081 (m), 2025 (m), 1989 (s), 1963 (m), $Co_2(CO)_7AsPh_3$: 2079 (m) 2023 (m), 1900 (s), 1956 (w). Kinetic runs were performed in a thermostated 50cm^3 stainless steel autoclave equipped with a magnetic stirrer, a calibrated Bourdon-type manometer of $\pm 2.5\%$ accuracy, and a high pressure six-way stainless steel micro valve. The required amount of crystalline $Co_2(CO)_8$ and the solvent was added into the autoclave under CO. The autoclave was closed, flushed and pressurized with a mixture of H_2 and CO. The required amount of pyridine was injected into the bore of the stainless steel valve. The stirrer was started, and the autoclave was thermostated at 50 °C for 30 minutes to reach the equilibrium of the two phases and the complete dissolution of $Co_2(CO)_8$. Then the hydrogenation was started by turning the valve using toluene as flushing solvent. The total pressure increased by about 0.5 bar during the injection. The hydrogenation rate was followed by means of the manometer for 10 to 120 minutes. The initial rate was determined generally on the basis of the pressure drop in the first 2 minutes, and was reproducible within $\pm 5\%$.

Carbonylation of $Co_4(CO)_{12}$

Atmospheric runs were performed in a gasometric apparatus. The reaction was started by injecting the pyridine stock solution into the stirred and thermostated solution of $Co_4(CO)_{12}$ in toluene. The reaction was followed volumetrically. Initial rates of CO evolution and maximum rates of CO absorption were reproducible within $\pm 10\%$. The kinetic runs under pressure were performed in a low pressure gasometric apparatus described earlier [3], or by the method used for the hydrogenation of $Co_2(CO)_8$.

REFERENCES

[1] Ungváry, F.: J. Organomet. Chem., **36,** 363 (1972)
[2] Bor, G., Dietler, U., Pino, P., Poë, A.: J. Organometal. Chem., **154,** 301 (1978)
[3] Ungváry, F., Markó, L.: Organometallics, **1,** 1120 (1982). Ungváry, F.: Acta Chim. Acad. Sci. Hung., **111,** 117 (1982)

[4] Ungváry, F., Markó, L.: Organometallics, **2,** 1608 (1983)
[5] Pino, P., Ercoli, R., Calderazzo, F.: Chim. Ind. (Milan), **37,** 782 (1955)
[6] Pino, P., Piacenti, F., Bianchi, M.: Reaction of Carbon Monoxide and Hydrogen with Olefinic Substrates: The Hydroformylation (Oxo) Reaction, p. 43—135, in Wender, I., Pino, P. (Eds.): Organic Syntheses via Metal Carbonyls Vol. **2.,** Wiley, New York 1977
[7] Hasek, H., Wayman, V.: U. S. Patent 2 820.059, 1958, assigned to Eastman Kodak Co.; Chem. Abstr., **53,** 13040 (1959): Botteghi, C., Braca, M., Marchetti, M., Saba. A.: J. Organomet. Chem., **161,** 555 (1978); Murata, K., Matsuda, A.: Bull. Chem. Soc. Jpn., **53,** 214 (1980)
[8] Calderazzo, F., Ercoli, R., Natta, G.: Metal Carbonyls, Preparation, Structure and Properties p. 80—99, in Wender, I., Pino, P. (Eds.): Organic Syntheses via Metal Carbonyls Vol. **1.,** Wiley, New York 1968
[9] Braterman, P. S., Walker, B. S., Robertson, T. H.: J. Chem. Soc. Chem. Commun., **1977,** 651
[10] Sisak, A., Ungváry, F., Markó, L.: Organometallics, **2,** 1244 (1983)
[11] Bor, G., Dietler, V. K.: J. Organomet. Chem., **191,** 295 (1980)
[12] Darensbourg, D. J., Peterson, B. S., Schmidt, R. E., Jr.: Organometallics, **1,** 306 (1982)
[13] Iwanaga, R.: Bull. Chem. Soc. Jpn., **35,** 774 (1962)
[14] Tolman, C. A.: Chem. Soc. Rev., **1,** 337 (1972)
[15] Brown, T. L.: Ann. N. Y. Acad. Sci., **333,** 80 (1980)
[16] James, B. R.: Homogeneous Hydrogenation, p. 188—193 Wiley, New York 1973
[17] Szabó P., Fekete, L., Bor, G., Nagy-Magos, Z., Markó, L.: J. Organomet. Chem., **12,** 245 (1968)
[18] Heck, R. F.: J. Am. Chem. Soc., **85,** 657 (1963); Van Boven, M., Alemdaroglu, N., Penninger, J. M. L.: J. Organomet. Chem., **84,** 65 (1975)
[19] Fachinetti, G., Balocchi, L., Secco, F., Venturini, M.: Angew. Chem., **215,** 93 (1981)
[20] Heimbach, P., Schenkluhn, H.: Topics Curr. Chem., **92,** 45 (1980)
[21] Labroue, D., Poilblanc, R., Inorg. Chim. Acta, **6,** 387 (1972)

Acta Chimica Hungarica 119 (2—3), pp. 127—133 (1985)

PALLADIUM CATALYSTS POISONED BY METAL IONS+

Tamás MALLÁT[1]*, Sándor SZABÓ[2] and József PETRÓ[1]

([1]Department of Organic Chemical Technology, Technical University, H-1521 Budapest, Műegyetem rkp. 3. and [2]Central Research Institute of Chemistry H-1025 Budapest, Pusztaszeri út 59—67.)

Received June 8, 1984
Accepted for publication August 15, 1984

The poisoning effect of Sn^{2+}, Pb^{2+}, Cd^{2+} and Fe^{3+} on graphite supported and unsupported palladium was studied by catalytic, electrochemical and x-ray diffraction measurements. Deactivation and change in selectivities were due to the deposition of metal (Sn, Pb or Cd) on the surface of palladium.

Introduction

The toxicity of metal ions towards platinum type catalysts was thoroughly investigated by Maxted [1] more than thirty years ago. It has been found that those metals are poisonous in which the d-orbitals next to valency orbitals are occupied by single or pairs of d-electrons.

Seven poisonous metal ions have positive metal/metal ion standard potentials (Table I). It was found earlier during alloy catalyst preparation that "forming a strong adsorptive bond" (as claimed by Maxted) is only the first step: in hydrogen atmosphere (at 1 bar, 25 °C) these metal ions are easily reduced to adsorbed metals on the surface of palladium and moreover a bulk alloy can be formed [2—4]. After all this is the basis of alloy catalyst preparation by consecutive reduction at room temperature and atmospheric pressure.

The ions having a negative standard potential (Table I) can be reduced as well if the bond between palladium and foreign metal atoms is strong enough, i.e. the potential shift according to the different energies of Me-Pd or Me-Me bonds results in a higher potential than H/H^+ potential in the same solution. There is a great development in electrochemistry in studying this phenomenon, called "undervoltage deposition" or "ad-atom theory" [e.g. 5—7].

We have selected four metal ions — Pb^{2+}, Sn^{2+}, Cd^{2+} and Fe^{3+} — and investigated if there is any correlation between the poisoning phenomenon

+ This paper was presented of the 2nd Belgian—Hungarian Colloquium on Catalysis at De Haan, Belgium, October 10—13, 1983.

* To whom correspondence should be addressed.

Table I

Standard potentials of metal/metal ion systems, found poisonous by Maxted [1]

E°		E°	
Me^{n+}	Me/Me^{n+}	Me^{n+}	Me/Me^{n+}
Au^+	1.7	Pb^{2+}	−0.13
Hg^{2+}	0.85	Sn^{2+}	−0.14
Ag^+	0.80	Ni^{2+}	−0.23
Hg_2^{2+}	0.80	Co^{2+}	−0.27
Cu^+	0.52	Tl^+	−0.34
Cu^{2+}	0.34	In^+	−0.34
Bi^{3+}	0.20	Cd^{2+}	−0.40
		Fe^{2+}	−0.44
		Zn^{2+}	−0.76
		Mn^{2+}	−1.05

and the metal deposition on the surface of palladium catalyst. (Fe^{3+} ions can easily be reduced to Fe^{2+} ions on the surface of palladium in a solution saturated with hydrogen.)

Experimental

The supported palladium catalyst contained 10 wt% metal on graphite activated by hot HNO_3 (BET surface area 62 $m^2 \cdot g^{-1}$). The graphite was impregnated first with a 94 $g \cdot dm^{-3}$ H_2PdCl_4 solution, then with a 20 wt% Na_2CO_3 solution at 80 °C and 5 Kpa. The dry powder was heated in a hydrogen flow at 100 °C for 30 min, then washed with distilled water on a filter and dried at 60 °C in air. Dispersity of palladium was 0.3 by a CO chemisorption measurement.

For the preparation of unsupported palladium 13 g $PdCl_2$ in 30 cm^3 concentrated HCl was dropped into a solution of 60 g $NaHCO_3$ in 500 cm^3 water, at 60 °C. After 0.5 h stirring the mixture was shaken in hydrogen atmosphere. The catalyst was filtered, washed thoroughly with distilled water and dried at room temperature, above NaOH. Dispersity of palladium was 0.125 by an electrochemical measurement [8].

Acetates (Pb^{2+}, Cd^{2+}) or chlorides (Sn^{2+}, Fe^{3+}) were used as poisoning salts.

For the x-ray and electrochemical measurements 0.4 g palladium catalyst was shaken in hydrogen for an hour in an aqueous solution of 0.37 g $Pb(OAc)_2 \cdot 3H_2O$, 0.47 g $Cd(OAc)_2 \cdot 2H_2O$ or 0.38 g $SnCl_2 \cdot 2H_2O$. (The latter was injected in a HCl solution in hydrogen atmosphere to the palladium.) The poisoned catalyst was filtered and washed with distilled water first in hydrogen, then in argon atmosphere, and dried in air. Activities were measured in the liquid phase hydrogenation of heptene-1, phenyl-acetylene or benzaldehyde, at room temperature and atmospheric pressure. 50 mg catalyst and 5 cm^3 solution containing the proper amount of poisonous metal ion were used. The reactant was injected after 25 min shaking in hydrogen atmosphere (180 oscillations/min). The activity was considered as the initial value of hydrogen consumption in unit time, referred to 1 g of catalyst.

For measuring the selectivities (in the reaction of phenyl-acetylene to styrene and benzaldehyde to benzyl-alcohol) the reaction was stopped after 1 equivalent of hydrogen uptake and the liquid was analyzed on a gas chromatograph.

The platinum sheet bottomed cell and electrochemical equipment used in the experiments were described earlier [9]. The cell construction allowed cell solutions to be changed in the main compartment under the exclusion of air. The potential was measured with respect to a hydrogen electrode in the same supporting electrolyte. During experiments the main compartment of the cell was continuously rinsed with purified nitrogen to deoxygenate the electrolyte.

Before polarization the dry powder (5 mg) was put on the platinum sheet electrode, the cell was purged with nitrogen for 14 hr, with hydrogen for 3/4 hr, then filled up with perchloric

acid electrolyte saturated with hydrogen. Nitrogen was introduced to remove excess hydrogen (1 hr). Anodic polarization commenced from 0.03 V with 1 mVs^{-1} sweep rate up to 1.2 V. The electric circuit was broken, the electrolyte was removed, the cell was rinsed thoroughly and filled up with oxygen-free electrolyte. The catalyst was saturated with hydrogen by a cathodic polarization, excess hydrogen removed with nitrogen and the program proceeded similarly.

1 mol · dm^{-3} perchloric acid solution was prepared from triply distilled water and MERCK analytical grade reagent.

The lattice parameters were measured on a Philips PW 1050 high-angle x-ray powder diffractometer (K_α = 154.18 pm, scanning rate: 1° (2) min^{-1}).

Results and Discussion

The effect of Sn^{2+} ions on the activity and selectivity of Pd/graphite catalyst is shown in Table II as a function of the ratio Sn^{2+} ions to surface Pd atoms. Disregarding the small initial maxima we got typical poisoning "curves" in all three hydrogenation reactions. Sn^{2+} ions had a marked effect on the selectivities in the hydrogenation of phenyl-acetylene to styrene and benzaldehyde to benzyl alcohol.

The formation of metal deposition on the surface of palladium was studied by electrochemical and x-ray diffraction measurements. These experiments were carried out on unsupported Pd to make the results unambiguous. (In the case of Pb^{2+} ion poisoning the catalytic experiments were carried out on unsupported Pd and the electrochemical polarization on Pd/graphite to check the effect of graphite support. It was found that the poisoning phenomenon was essentially the same, but the large double layer capacity of activated graphite caused some difficulties in the interpretation of polarization curves.)

On the curve of Pd poisoned by excess Sn^{2+} ions (Fig. 1, curve 1) the first peak at around 0.1 V is the ionization of dissolved hydrogen. The second, large peak at around 0.33 V is the anodic oxidation of Sn deposited on the surface of Pd. Above 0.7 V the rising curve shows the oxygen adsorption on Pd.

The curve of the second run (after washing with $HClO_4$ and hydrogen saturation) is characteristic of Pd [8]: there is adsorbed hydrogen instead of Sn on the surface of Pd (Fig. 1, curve 2). It means that during Sn^{2+} ion poisoning (in hydrogen atmosphere) metallic Sn is deposited on the surface of Pd. It seems likely that metal deposition is the real cause of catalyst deactivation.

It is interesting that we could not find any sign of Sn in the catalyst by x-ray diffraction measurements: the peaks of Pd remained uneffected by poisoning.

The second example is the Pb^{2+} ion poisoning of Pd (Table III). Both activities and selectivities are decreased by increasing the ratio of Pb^{2+} ions to surface Pd atoms. It was found by a classical analytical method that all the Pb^{2+} ions disappeared from the liquid phase during the 25 min hydrogen saturation (before the reactant was injected) below 1.0 Pb^{2+}/Pd_s atomic ratio.

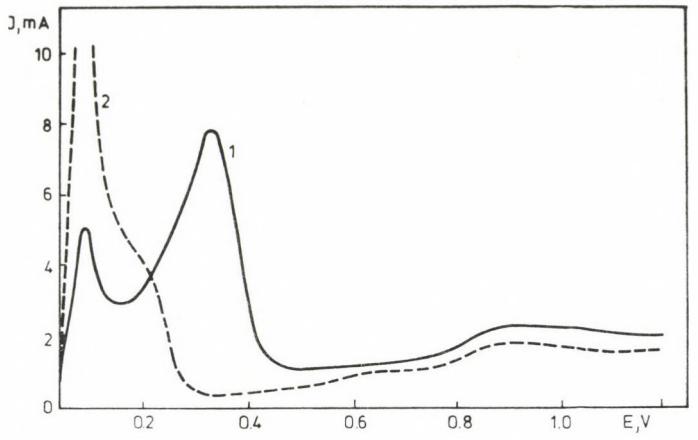

Fig. 1. Potentiodynamic polarization of Pd catalyst poisoned by excess Sn^{2+} ions, 1 — first sweep, 2 — second sweep after changing electrolyte ($m = 5$ mg, $v = 1$ mVs^{-1})

Table II

Effect of Sn^{2+} *on the activity and selectivity of* Pd/*graphite catalyst* (in methanol)

$\frac{[Sn^{2+}]}{[Pd_s]}$	activities cm³ H_2/min, g catalyst			selectivities %	
	heptene	phenylacetylene	benzaldehyde	to styrene	to benzylalcohol
0	410	160	240	96	95
0.06	395	170	250	92	91
0.3	250	115	110	87	81
0.6	180	46	54	76	69
1.2	66	18	27	62	60
1.8	22	12	19	—	—
3.0	17	12	12	—	—

Table III

Effect of Pb^{2+} *on the activity and selectivity of* Pd/*graphite catalyst*

$\frac{[Pb^{+2}]}{[Pd_s]}$	activities cm³ H_2/min, g catalyst			selectivities %	
	heptene in MeOH	phenylacetylene in MeOH	benzaldehyde in AcOH	to styrene	to benzylalcohol
0	410	160	135	96	96
0.034	385	150	125	95	92
0.17	330	110	74	94	93
0.34	220	55	25	90	89
0.68	120	25	7	88	84
1.0	54	22	8	—	—
1.7	15	13	5	—	—

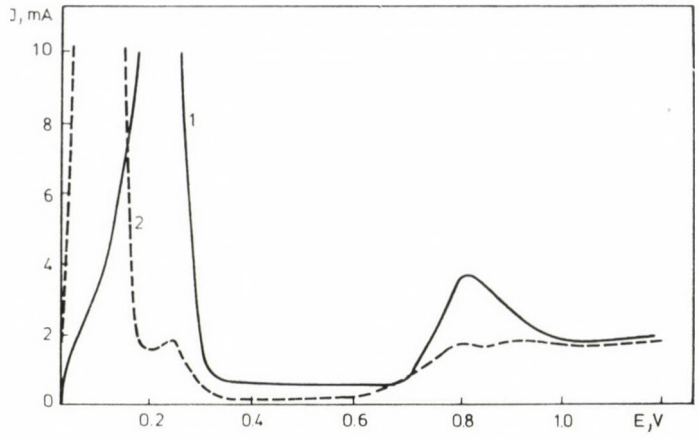

Fig. 2. Potentiodynamic polarization of Pd catalyst poisoned by excess Pb^{2+} ions, 1 — first sweep, 2 — second sweep after changing electrolyte ($m = 5$ mg, $v = 1$ mV · s^{-1})

Deposition of discharged Pb on Pd is proved by electrochemical investigations. Curve 1 on Fig. 2 shows the anodic oxidation of Pd catalyst poisoned by excess Pb^{2+} ions. The peak at around 0.8 V represents the deposited Pb on the surface [10]: the bulk of the grains remained unchanged and dissolved hydrogen.

After rinsing the catalyst and the cell with deoxygenated electrolyte and saturation with hydrogen the sweep was repeated (Fig. 2, curve 2). There was no Pb on the surface and the curve was characteristic of Pd.

The approximate amount of adsorbed hydrogen and that of Pb deposited can be calculated from the areas under the curves, supposing a 1 : 1 H_a : Pd_s ratio [8] and that Pb is oxidized to Pb^{2+}. It was found that the ratio of adsorbed Pb to adsorbed H was 0.95 which is close to 1.0 found by classical analysis on graphite supported Pd.

The 0.1 shift of the peak of dissolved hydrogen on curve 1 can be attributed to the surface Pb "layer" representing a barrier. Although formally it was found that 1 Pb atom substitutes approximately 1 adsorbed hydrogen atom one cannot claim that there is a monoatomic layer on the surface of Pd. One adsorbed foreign metal atom replaces usually more than one adsorbed hydrogen atom, according to the electrochemical investigations on Pt [11—13].

We could not find a solution for the above problems by an x-ray diffraction measurement. The peaks of Pd remained unchanged (the difference between the average lattice constant and that of literature was less than 0.1 pm) and there were five peaks of low intensity, which could not be identified by the ASTM system.

The investigation of poisoning effect of Cd^{2+} ions led to similar conclusions. The increasing amount of Cd^{2+} ions resulted in a considerable decrease

Table IV

Effect of Cd^{2+} *on the activity and selectivity of* Pd/*graphite catalyst, in methanol*

$\frac{[Cd^{2+}]}{[Pd_s]}$	activities cm^3 H_2/min, g catalyst			selectivities %	
	heptene	phenylacetylene	benzaldehyde	to styrene	to benzylalcohol
0	410	160	240	96	95
0.063	385	140	180	93	97
0.32	250	85	73	87	96
0.63	120	30	22	78	92
1.3	58	18	15	58	90
1.9	24	9	14	—	—
3.2	10	13	6	—	—

in activities and selectivities (Table IV). The limit of metal deposition was 0.55 Cd^{2+}/Pd_s: above this value Cd^{2+} ions were present as well during hydrogenation reactions.

The interpretation of the electrochemical polarization curves (Fig. 3) is not so simple as before. The Cd adsorption region (0.25—0.6 V) is partly overlapped by the hydrogen adsorption region (0.15—0.3 V), but the difference between the anodic oxidation of Cd^{2+} -poisoned Pd (curve 1) and Pd (curve 2) is obvious.

The presence of a new phase could be proved by x-ray diffraction measurements, but the two peaks of low intensity could not be identified. The bulk of Pd remained unalloyed in this case, too.

The changes in activity and selectivity of graphite supported Pd in the presence of Fe^{3+} ions are small or insignificant (Table V). In fact, Fe^{3+} ion can be considered as an activator in the reduction of phenyl-acetylene.

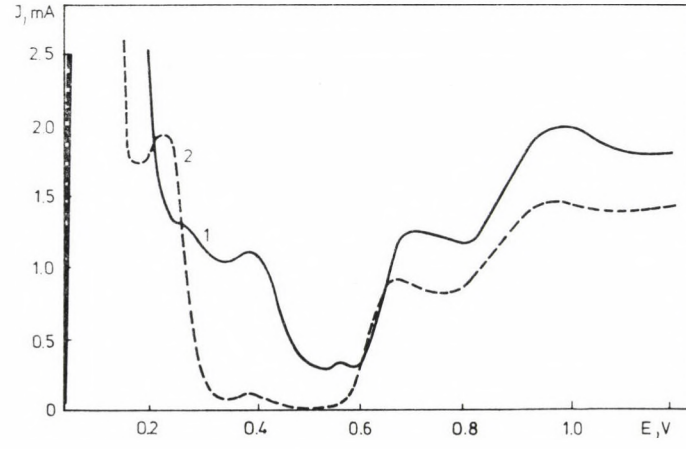

Fig. 3. Potentiodynamic polarization of Pd catalyst poisoned by excess Cd^{2+} ions, 1 — first sweep, 2 — second sweep after changing electrolyte ($m = 5$ mg, $v = 1$ mV $\cdot$ s^{-1})

Table V

Effect of Fe^{3+} *on the activity and selectivity of* Pd/*graphite catalyst*

$\frac{[Fe^{3+}]}{[Pd_s]}$	activities cm³ H_2/min, g catalyst			selectivities %	
	heptene in MeOH	phenylacetylene in MeOH	benzaldehyde in AcOH	to styrene	to benzylalcohol
0	410	160	135	96	96
0.25	—	—	125	—	97
0.64	405	165	115	95.5	96.5
1.3	415	180	120	96	96.5
3.8	410	200	115	96	96.5
6.4	415	200	—	96	—

In accordance with the catalytic investigations metal deposition could not be found either by classical analytical or electrochemical methods. There are indications in the literature [5, 14, 15] both about the activity-enhancing effect of Fe^{3+} ions on Pt catalysts and that Fe^{3+} ions do not adsorb on the surface of Pt.

Summarising the results we can say that the explanation of metal ion poisoning, given by Maxted [1] is a formal one. It was proved, that only the surface deposition of foreign metal atoms effect a real poisoning of Pd. It is not clear yet, how many outer atomic layers of Pd take part in the process.

The electrochemical polarization experiments offer a simple and effective method for catalyst regeneration. The potential of Pd saturated with oxygen is above 1 V, above the ionization potential of poisoning metals deposited on the surface. So it is enough to blow air in the slurry in the pressence of $HClO_4$ or H_2SO_4 (HCl dissolves Pd as well), and change the liquid a few times to remove poisoning ions and recover the active Pd catalyst.

*

Acknowledgement is due to F. Hange for the X-ray investigations.

REFERENCES

[1] Maxted, E. B.: Advances in Catalysis, **3,** 129 (1951)
[2] Szabó, S.: J. Electroanal. Chem., **77,** 193 (1977)
[3] Petró, J., Mallát, T.: Acta Chim. Acad. Sci. Hung., **95,** 253 (1977)
[4] Mallát, T., Petró, J., Schaffer, M.: Acta Chim. Acad. Sci. Hung., **98,** 175 (1978)
[5] Takamura, K., Sakamoto, M.: J. Electroanal. Chem., **113,** 273 (1980)
[6] Kolb, D. M., Przasnyski, M., Gerischer, H.: J. Electroanal. Chem., **54,** 25 (1974)
[7] Szabó, S., Nagy, F.: J. Electroanal. Chem., **160,** 299 (1984)
[8] Mallát, T., Petró, J.: Acta Chim. Hung., **112,** 173 (1983)
[9] Szabó, S., Nagy, G., Móger, D.: Acta Chim. Acad. Sci. Hung., **93,** 33 (1977)
[10] Adzhich, R. R., Spasojevich, M. D., Despich, A. R.: J. Electroanal. Chem., **92,** 31 (1978)
[11] Bowles, B. J.: Electrochim. Acta, **15,** 737 (1970)
[12] Furuya, N., Motoo, S.: J. Electroanal. Chem., **98,** 195 (1979)
[13] Szabó, S., Nagy, F.: Israel J. Chem., **18,** 162 (1979)
[14] Freifelder, M.: Practical catalytic hydrogenation. Wiley, Interscience, New York, London, Toronto 1971
[15] Rylander, P. N.: Catalytic hydrogenation over platinum metals, Acad. Press, New York, London 1967

Acta Chimica Hungarica 119 (2—3), pp. 135—145 (1985)

ENANTIO- AND STEREO-SELECTIVE HYDROGENATION OF KETONES WITH PHOSPHINERHODIUM CATALYTIC SYSTEMS+

Szilárd Tőrös*, Bálint Heil, László Kollár and László Markó

(Research Group for Petrochemistry of the Hungarian Academy of Sciences, University of Chemical Engineering, H-8200 Veszprém, P.O. Box 158)

Received June 8, 1984
Accepted for publication August 15, 1984

Rhodium-phosphine catalytic systems prepared "in situ" were successfully used for the hydrogenation of a wide range of ketones (including aminoketones) with high selectivity. Both enantioselectivity and stereoselectivity depend mainly on the ratio of monohydrido- and dihydrido phosphinerhodium complexes and this ratio can be influenced by adding a suitable base as additive.

Introduction

Many chiral transition metal complexes showing catalytic activity were discovered in the last ten years and their application has lead to the development of several homogeneous catalytic asymmetric reactions. The best results were obtained in hydrogenation of dehydroaminoacids using rhodium catalysts but many pharmaceutically interesting compounds with biological activity were obtained also by the enantioselective reduction of ketones.

In this paper we summarize our results achieved in the hydrogenation of ketones using rhodium-phosphine catalytic systems with or without bases as additives and based on these results we propose a general mechanistic picture for these hydrogenations. Some parts of our work have been already published earlier [1—8].

Results and Discussion

We have found several years ago [1] that the catalysts prepared "in situ" from $[Rh(diene)Cl]_2$ and chiral phosphines give better optical yields than the cationic complexes $[Rh(diene)(PR_3)_2]^+A^-$ prepared separately if the same phosphines are applied (Table I). Using DIOP as phosphine component we obtained α-phenylethanol with about 50% optical purity, but the reaction

+ This paper was presented at the 2nd Belgian—Hungarian Colloquium on Catalysis at De Haan, Belgium, October 10—13, 1983.

* To whom correspondence should be addressed.

Table I

Asymmetric hydrogenation of acetophenone

Catalyst	Solvent	Temp., °C	p_{H_2} bar	Reaction time, h	Chemical yield, %	Optical yield, %	Ref.
[Rh(NBD)((R)—P(CH_2Ph)MePh)$_2$]$^+$$ClO_4^-$	EtOH	20	1	24—80		*R*-(+) 8.6	[9]
[Rh(NBD)(—)-DIOP]$^+$$ClO_4^-$	MeOH-*i*PrOH	30	1			*R*-(+) 3.2—8.1	[10]
[Rh(HD)Cl]$_2$ + (*S*)-P(CH_2Ph)MePh	MeOH/C_6H_6	30	1	60	60	*S*-(—) 27.2	[1]
[Rh(HD)Cl]$_2$ + (+)-DIOP	MeOH/C_6H_6	30	1	173	10	*R*-(+) 51.4	[1]
[Rh(NBD)Cl]$_2$ + (—)-DIOP	MeOH	50	70	6	6	*S*-(—) 38	[2]
[Rh(NBD)Cl]$_2$ + (—)-DIOP + 0.5 Et_3N	MeOH	50	70	6	14	*R*-(+) 53	[2]
[Rh(NBD)Cl]$_2$ + (—)-DIOP + 5 Et_3N	MeOH	50	70	6	99	*R*-(+) 11	[2]
[Rh(NBD)Cl]$_2$ + (+)-DIOP + 2 Et_3N	C_6H_6	50	70	6	64	*S*-(—) 80	[3]

DIOP = 2,3-*O*-isopropylidene-2,3-dihydroxy-1,4-bis(diphenylphosphino)butane
NBD = 2,5-norbornadiene
HD = 1,5-hexadiene

was very slow. The next significant development was the observation, that the addition of Et_3N to this "in situ" system increased the reaction rate significantly and resulted in the formation of the opposite antipode [2]. This dramatic effect of Et_3N aroused our interest and we started systematic investigations to clarify its mechanism.

As can be seen on Figure 1 the conductivity of the "in situ" catalytic system in methanol is high under argon but its ionic character decreases during prehydrogenation which saturates the diene component (2 moles of hydrogen are absorbed). Adding Et_3N to this catalytic solution the conductivity increases again and comes close to that of equivalent $Et_3N \cdot HCl$. At the same time the system absorbs a third mole of hydrogen.

Catalytic experiments at various Et_3N/Rh ratios (Figure 2) showed that increasing the Et_3N/Rh ratio in methanol there is a maximum in enantioselectivity, but further amounts of base decreased the optical purity of the secondary alcohol considerably. In contrast to this the chemical yield steadily increased with the Et_3N/Rh ratio [2]. The cationic catalyst could also be modified with Et_3N. The effect of other N-bases was very similar to that of Et_3N. Using NaOMe as a base a high optical yield could be achieved only within a narrow range.

The formation of catalysts and the effect of bases was studied by ^{31}P NMR (Figure 3). In the spectrum of the "in situ" system prepared in methanol

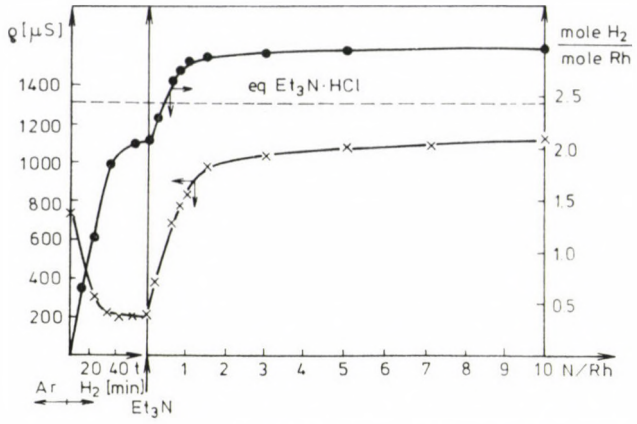

Fig. 1. Conductivity of the $[Rh(NBD)Cl]_2$ + DIOP + Et_3N catalytic system

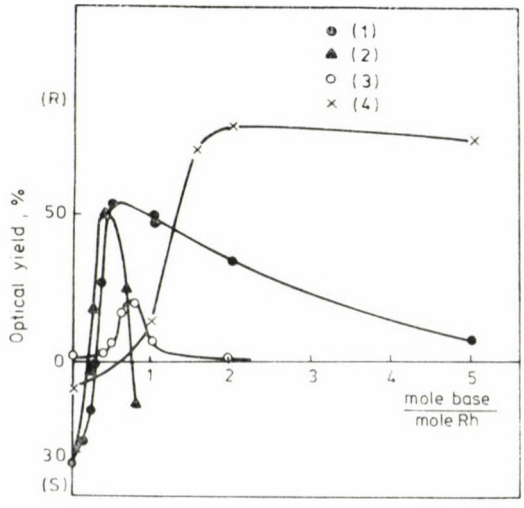

Fig. 2. Enantioselective hydrogenation of acetophenone in presence of catalysts modified with bases; (1) $[Rh(NBD)Cl]_2$ + (−)-DIOP + Et_3N (in methanol), (2) $[Rh(NBD)Cl]_2$ + (−)-DIOP + NaOMe (in methanol), (3) $[Rh(NBD)(-)DIOP]^+ClO_4^-$ + Et_3N (in methanol), (4) $[Rh(NBD)Cl]_2$ + (−)-DIOP + Et_3N (in benzene)

under argon only one doublet appeared. The chemical shift and the rhodium-phosphorus coupling constant (150 Hz) corresponded to data published by Slack for ionic complexes [11]. After prehydrogenation this doublet disappeared and a new intensive doublet represented the main amount of the catalyst. Its fairly large coupling constant (190 Hz) refers to a low coordination number of the rhodium atom, and the fact, that there is no P—P coupling proves the symmetrical position of the two phosphorus atoms.

Adding 1 mole of Et_3N to the catalytic solution a third doublet with a coupling constant of 124 Hz could be observed. The rather small coupling constant points to a higher coordination number of the complex. A similar spectrum developed in the presence of small amounts of NaOMe and the 124 Hz doublet appeared also in the spectrum of the ionic complex after

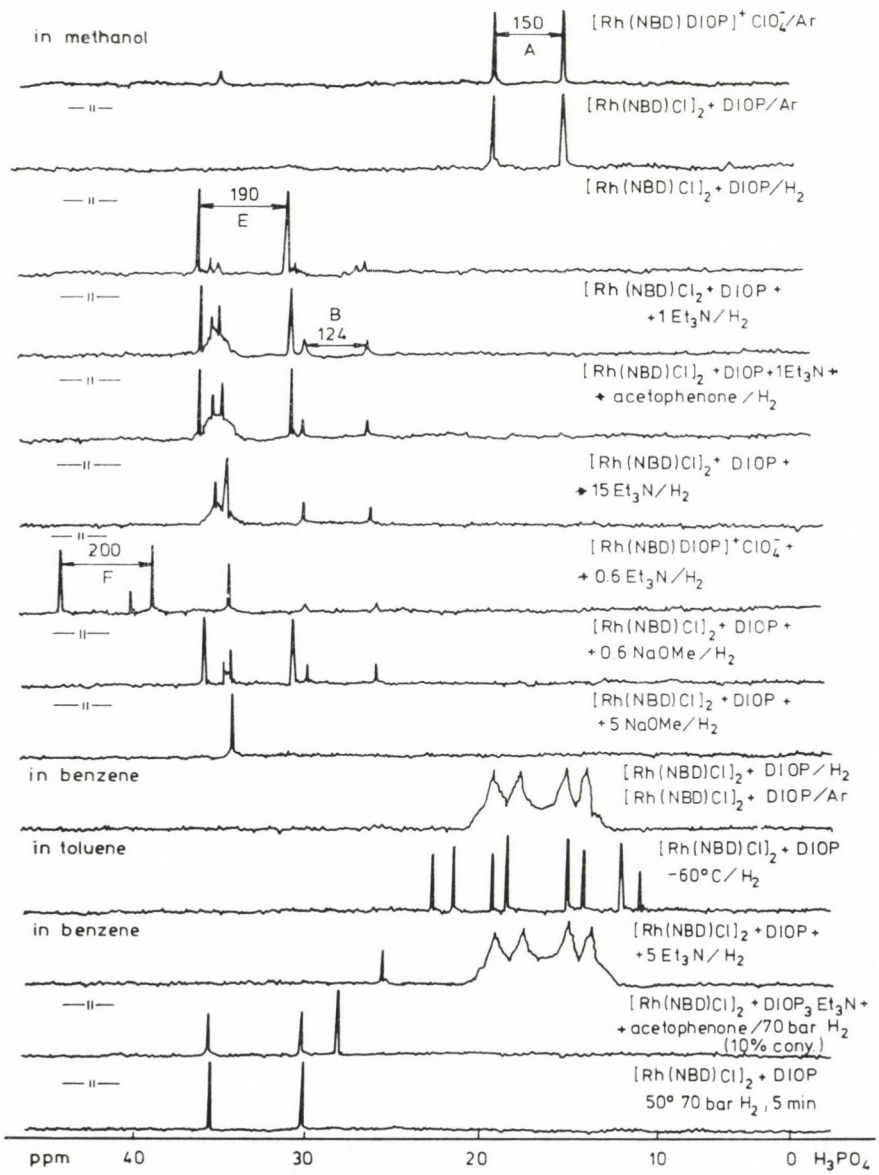

Fig. 3. ^{31}P NMR investigations

prehydrogenating in the presence of a small amount of Et_3N. Increasing the amount of Et_3N or NaOMe an intensive singlet developed.

Hydrogenation experiments have shown that the solvent has a dramatic influence on the enantioselectivity of the catalyst. Optical yields could be significantly increased by using benzene instead of methanol as solvent (Figure 2) [3]. Accordingly ^{31}P NMR investigations were carried out also in benzene (and toluene) but were less conclusive. The system proved to be complicated because several complexes were present simultaneously and there was a fast ligand exchange between the complexes. On adding Et_3N only a new singlet appeared which, however, was not identical with the singlet observed in methanol. In a sample taken under hydrogenation conditions, the 190 Hz doublet appeared and the singlet gradually shifted to the left as conversion increased. The same doublet appeared without acetophenone, if the catalytic system was prehydrogenated at 50° and under 70 bar hydrogen.

The complexes and equilibria we suppose to be present in our catalytic system on the basis of these facts can be seen on Figure 4. According to the ^{31}P NMR and conductivity data in methanol the main part of the catalyst is present under argon in an ionic form (complex A). After prehydrogenation the equilibria are shifted towards covalent derivatives. Within these dihydrido complexes represent only a small fraction. Adding equivalent amounts of bases the monohydrido complex B is formed from the "in situ" systems by HCl elimination and from the ionic systems by deprotonation. We suppose that this monohydride is responsible for high enantioselectivity. Using larger amounts of tertiary amines or NaOMe this selective catalyst is gradually destroyed by RO^- ions leading to catalytically active but achiral complexes.

In benzene under argon a mixture of complexes C and D is present. After prehydrogenation under pressure these are transformed into the same complex which is the main species in methanol. Accordingly this complex contains no solvent and thus only the dimeric structure corresponding to E fits these requirements.

Our results reported above clearly show that in the presence of Et_3N (or generally bases) Rh(I) hydrides are formed and these have to be regarded as the principal catalytic species in such reaction mixtures. These catalysts differ considerably from the Rh(III) hydrides $[H_2RhP_2]^+$ or H_2RhP_2Cl present in the cationic [12] or "in situ" [1] catalyst systems reported earlier. Thus, for example, even PPh_3 yields an active catalyst for ketone hydrogenation under such conditions [4]. Furthermore, the activity of these systems is increased by increasing the P/Rh ratio from 2 to 3 [5] suggesting that trisphosphine complexes are the active species. All these phenomena point to a profound change in mechanism going from Rh(III) to Rh(I) hydrides. Accordingly, we successively explored the practical possibilities of this new catalyst

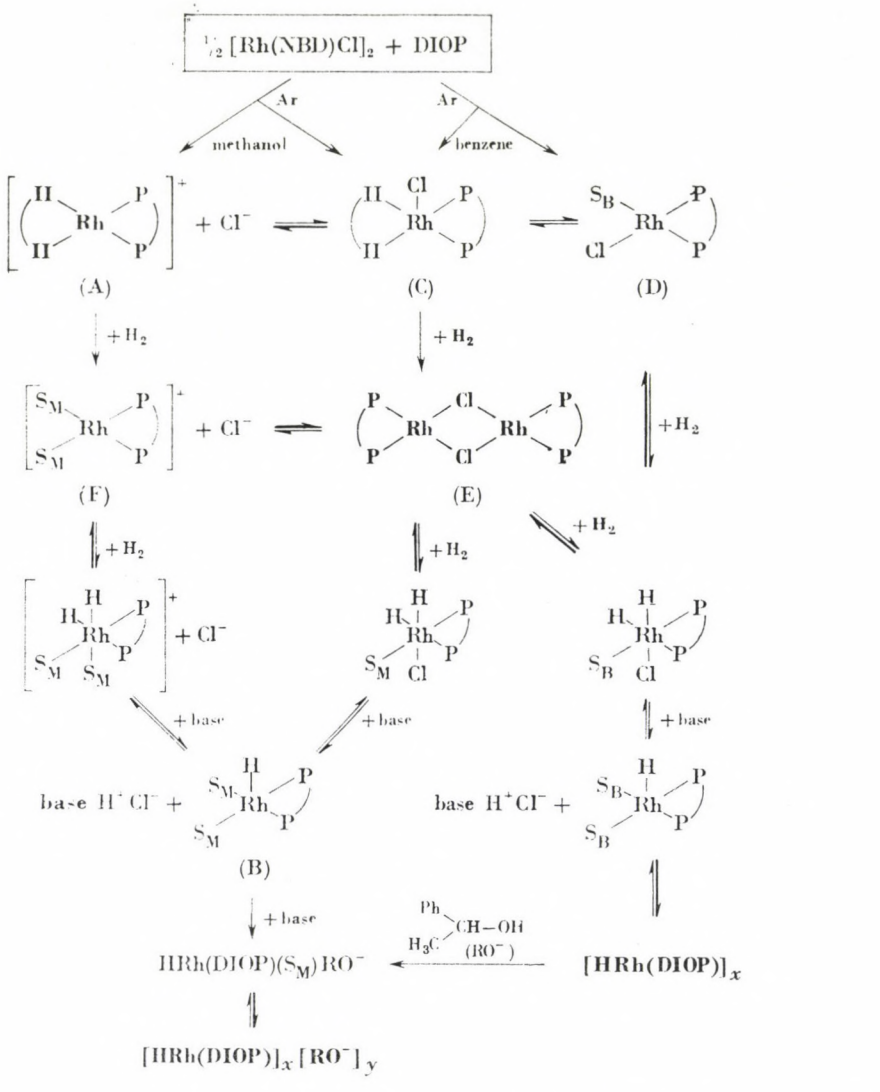

Fig. 4. Complexes and equilibria in the $[Rh(NBD)Cl]_2$ + DIOP system

system and continued our work to gain more insight into the mechanism of ketone hydrogenation.

First we tested our catalytic system for the hydrogenation of several simple ketones. In the case of alkyl aryl ketones relatively high optical yields (55—84%) were achieved if benzene was used as a solvent [3].

It is well known that the optically active β-amino-α-phenyl-ethanol derivatives are biologically active compounds. Therefore we applied our catalyst also for the reduction of aminoketones. We have found that the $[Rh(NBD)Cl]_2$ + DIOP system catalyzes the hydrogenation of α-(*N*,*N*-dialkylamino]-alkyl aryl ketones with enantioselectivities of up to 95% [6].

Up till this we concentrated our efforts on enantioselective hydrogenation but a somewhat different type of selectivity, that of stereoselectivity in the hydrogenation of cyclic ketones seemed also worth-while to explore. As we shall see these experiments significantly contributed to our understanding of the reaction.

A few results obtained with 4-*t*-butylcyclohexanone and some cyclic ketones which have practical importance are compiled in Table II. It can be seen, that with "in situ" prepared PBu_3-containing rhodium catalysts always the thermodynamically more stable (*trans* or β) alcohol was formed irrespectively whether Et_3N was added to the reaction mixture or not. In the case of 4-*t*-butylcyclohexanone the $[Rh(NBD)Cl]_2$ + PPh_3 catalyst, however, was dramatically changed by an addition of Et_3N and the *cis* alcohol became the main product. Similar changes in stereoselectivity were observed during the hydrogenation of androstane derivatives and nortropinones, but in the latter case the use of Et_3N was unnecessary because the substrate itself played the role of the base.

Later we have found, that even the PBu_3-containing system can be transformed by sufficiently strong bases into a catalyst which provides the *cis* alcohol as the main product. This fact is illustrated by Figure 5 which shows the effect of additive basicity on stereoselectivity of hydrogenation (the half-neutralization potential is characteristic for the basicity of the additives [13]).

According to equation (1) Rh(III)dihydrido complexes — formed after prehydrogenation — can be transformed by a base (B) into Rh(I)mohohydrido complexes:

$$H_2RhL_nCl + B \rightleftharpoons HRhL_n + HB^+ + Cl^- \qquad (1)$$

Since the position of the equilibrium depends on the acidity of the Rh(III)-dihydride and the basicity of the base, the complexes containing more basic phosphines (like PBu_3) are less readily deprotonated and only small amounts of Rh(I) monohydrides will be formed in the presence of weak bases. This explains the ineffectivity of Et_3N. In experiments with stronger bases like KOH, KOMe or NaOH, the equilibrium is more strongly shifted to the right and Rh(I) monohydrido complexes become the predominant catalytic species. On the other hand, if PPh_3 is used as ligand, already Et_3N or acetophenone benzylimine are bases strong enough to shift the equilibrium to the right.

We propose the following explanation for the difference in stereoselectivity when working with H_2RhP_2Cl or $HRhP_3$ as catalyst. Rhodium(I) is a soft

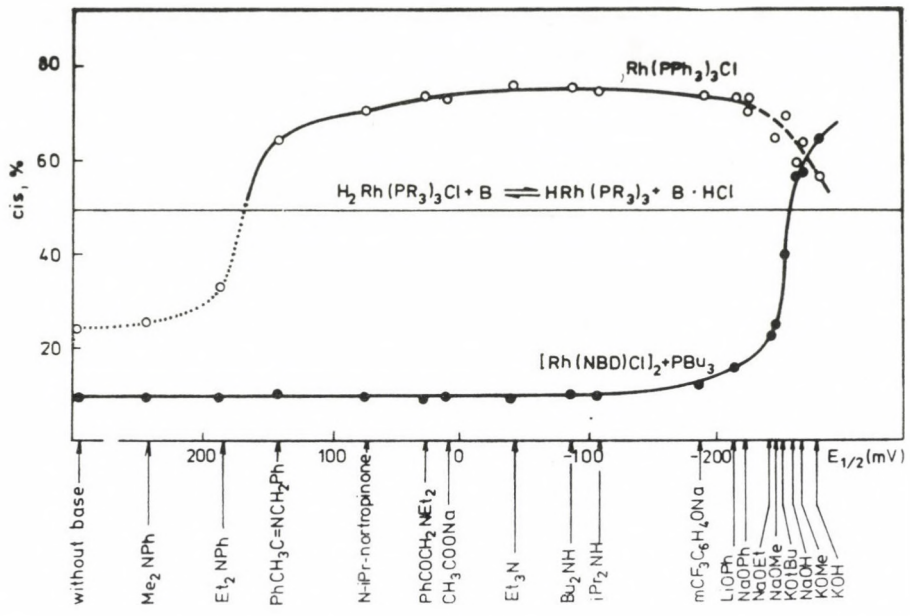

Fig. 5. Stereoselective hydrogenation of 4-*t*-butyl-cyclohexanone in presence of catalysts modified with bases

Lewis-acid and will tend to coordinate the ketone carbonyl group like an olefin as a π-ligand. Due to steric reasons this type of coordination favors an *equatorial* attack and because of the softness of Rh(I) will lead after H-transfer to a σ-complex with a carbon-rhodium bond. Since the large $Rh(PR_3)_3$ group tends to occupy the *equatorial* position mainly the α alcohol will be formed (Figure 6). On the other hand Rh(III) is a hard Lewis-acid and will coordinate the ketone through its oxygen atom. Following hydrogen transfer a σ-complex with an oxygen-rhodium bond will be formed. Steric requirements will force the large $ORhH(PR_3)_2Cl$ broup into equatorial position and this results in the predominant formation of β alcohol.

Summarizing our results we can say that in the case of stereoselectivity the ratio of monohydrido- and dihydrido complexes is the dominant factor and that this ratio can be regulated by choosing a suitable base as additive. A similar rule is expected to govern enantioselectivity.

To confirm this assumption we hydrogenated acetophenone using a $[Rh(NBD)Cl]_2$ + (*S*)—(—)P(CH_2Ph)MePh catalyst modified by additives of different basicity. As can be seen in Table III, Et_3N was ineffective in the case of this more basic phosphine, but in the presence of KOH a change in configuration could be observed. Comparing this result with the effect of Et_3N on the DIOP-based catalyst it is again obvious, that the position of

Table II

Stereoselective hydrogenation of various cyclic ketones [7, 8]

Ketone	Catalyst	Rh : P : N	k_{obs}, min^{-1}	Conversion %	Relative amount of alcohol isomers, %	
					cis or α	*trans* or β
4-*t*-Butylcyclohexanone	$[Rh(NBD)Cl]_2 + PBu_3$	1 : 2.2	$3.7 \cdot 10^{-2}$	98.9	9.9	90.1
	$[Rh(NBD)Cl]_2 + PBu_3 + Et_3N$	1 : 2.2 : 5	$3.5 \cdot 10^{-2}$	97.5	9.6	90.4
	$[Rh(NBD)Cl]_2 + PPh_3$	1 : 3.2	$4.6 \cdot 10^{-5}$	2.1	28.5	71.5
	$[Rh(NBD)Cl]_2 + PPh_3 + Et_3N$	1 : 3.2 : 5	$5.1 \cdot 10^{-3}$	95.4	72.7	27.3
	$HRh(PPh_3)_4$	1 : 4	$7.1 \cdot 10^{-3}$ [a]	89.6	80.3	19.7
	$HRh(PBu_3)_4$	1 : 4	$4.2 \cdot 10^{-5}$ [b]	2.1	62.8	37.2
5-α-Androstan-3,17-dione	$[Rh(NBD)Cl]_2 + PBu_3$	1 : 2.2	$6.4 \cdot 10^{-3}$	88.6[b]	7.6	92.4
	$[Rh(NBD)Cl]_2 + PPh_3 + Et_3N$	1 : 3.2 : 5	$7.6 \cdot 10^{-4}$	12.8[b]	65.7	34.3
Tropinone	$[Rh(NBD)Cl]_2 + PBu_3$	1 : 2.2	$3.5 \cdot 10^{-3}$	75.0	14.3	85.7
	$[Rh(NBD)Cl]_2 + PPh_3 + Et_3N$	1 : 3.2 : 5	$4.1 \cdot 10^{-3}$	81.7	95.2	4.8
N-Ph-nortropinone	$[Rh(NBD)Cl]_2 + PBu_3$	1 : 2.2	$2.2 \cdot 10^{-3}$	54.5	12.6	87.4
	$[Rh(NBD)Cl]_2 + PPh_3 + Et_3N$	1 : 3.2 : 5	$2.1 \cdot 10^{-3}$	58.0	93.6	6.4
N-*i*Pr-nortropinone	$[Rh(NBD)Cl]_2 + PBu_3$	1 : 2.2	$2.8 \cdot 10^{-3}$	58.9	11.9	88.1
	$[Rh(NBD)Cl]_2 + PPh_3 + Et_3N$	1 : 3.2 : 5	$6.1 \cdot 10^{-3}$	96.2	97.6	2.4
	$[Rh(NBD)Cl]_2 + PPh_3$	1 : 3.2	$5.8 \cdot 10^{-3}$	83.5	97.5	2.5

50 °C, 1 bar H_2, reaction time 6 h; 1 mmole ketone in 5 mL benzene/methanol = 3/7.
[a] Benzene/methanol = 1/1; [b] product: 5-α-androstan-3-ol-17-one.

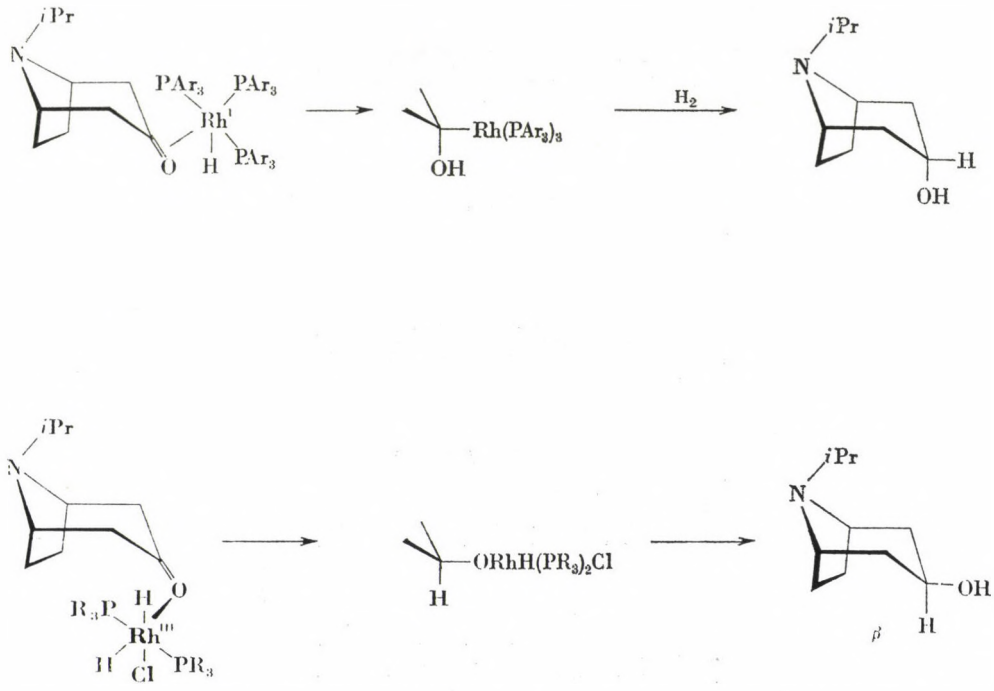

Fig. 6. Mechanism of α and β alcohol formation by hydrogenation of *N*-*i*Pr-nortropinone

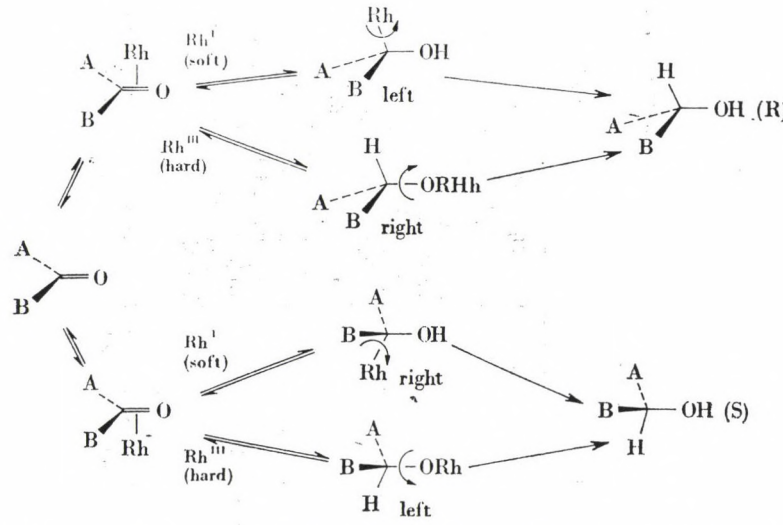

Fig. 7. Possible structure of σ-complexes formed as intermediates in enantioselective hydrogenation of ketones

Table III

Asymmetric hydrogenation of acetophenone with $[Rh(NBD)Cl]_2$ + (*S*)-(−)-$P(CH_2Ph)MePh$ *catalyst modified with bases*

Base (B)	Reaction time, h	Chemical yield, %	Optical yield, %
—	62	76	(*S*)-(−) 37
Et_3N	18	20	(*S*)-(−) 35
KOH	18	13	(*R*)-(+) 11

50°, 1 bar H_2; solvent methanol; Rh : P : B = 1 : 3 : 5

equilibrium between the mono- and dihydrido complexes strongly depends on the basicity of the phosphine.

We propose the following explanation for the change of configuration in enantioselective hydrogenation. There are two enantiotopic faces of the carbonyl group by which the catalyst may coordinate onto the prochiral ketone (Figure 7). Depending on whether the rhodium is a hard Rh(III) or a soft Rh(I) these diastereomeric π-complexes will transform into diastereomeric alkoxy- or alkyl-rhodium species, respectively. Assuming that the chirality of the phosphine ligand tends to favor the same chirality on the carbon atom irrespective of whether a Rh—O—C or Rh—C bond is formed, the resulting alcohol will have the opposite configuration in these two cases. Obviously this latter assumption cannot be strictly valid but since catalysts containing DIOP or $P(CH_2Ph)MePh$ both change their enantioselectivity under the influence of an appropriate base it may serve as a useful working hypothesis. Further it may be concluded, that in general optical selectivity should be higher with Rh(I) hydrides because in this case rhodium is nearer to the new chiral atom formed in the reaction.

REFERENCES

[1] Heil, B., Tőrös, Sz., Vastag, S., Markó, L.: J. Organomet. Chem., **94,** C47 (1975)
[2] Heil, B., Tőrös, Sz., Bakos, J., Markó, L.: I. Organomet. Chem., **175,** 229 (1979)
[3] Tőrös, Sz., Heil, B., Kollár, L., Markó, L.: J. Organomet. Chem., **197,** 85 (1980)
[4] Tőrös, Sz., Kollár, L., Heil, B., Markó, L.: J. Organomet. Chem., **253,** 375 (1983)
[5] Heil, B., Markó, L., Tőrös Sz.: in L. H. Pignolet (ed.), Homogeneous Catalysis with Metal Phosphine Complexes, Plenum, New York (1983) p. 317
[6] Tőrös, Sz., Kollár, L., Heil, B., Markó, L.: J. Organomet. Chem., **232,** C17 (1982)
[7] Tőrös, Sz., Kollár, L., Heil, B., Markó, L.: J. Organomet. Chem., **225,** 377 (1983)
[8] Kollár, L., Tőrös, Sz.: Magy. Kém. Lapja, **38,** 223 (1983)
[9] Bonvicini, P., Levi, A., Modena, G., Scorrano, G.: Chem. Commun., **1972,** 1188
[10] Levi, A., Modena, G., Scorrano, G.: Chem. Commun., **1975,** 6
[11] Slack, D. A., Baird, M. C.: J. Organomet. Chem., **142,** C69 (1977)
[12] Schrock, R. R., Osborn, J. A.: Chem. Commun., **1970,** 567
[13] Halmos, E., Vizi-Orosz, A., Tőrös, Sz.: XVIIIth West-Hungarian Analytical Conference, Aug. 1983. Pécs p. 57.

Acta Chimica Hungarica 119 (2—3), pp. 147—154 (1985)

REDUCTION OF CARBON MONOXIDE ON COBALT(I) COMPLEXES+

Jean-Louis COSTA, Albert DEMONCEAU, Julien DRAPIER, André HUBERT*, Alfred NOELS and Philippe TEYSSIÉ

(Laboratory of Macromolecular Chemistry and Organic Catalysis, University of Liège, Sart Tilman 4000 Liège, Belgium)

Received June 8, 1984
Accepted for publication August 15, 1984

The hydrogenation of carbon monoxide has been investigated in the presence of reduced cobalt species under different conditions of pressure (atmospheric pressure in a high-boiling solvent, 1.4 bar in a circulator with continuous trapping of the products, 150 bars in autoclaves) at 200—250 °C.

These carbon monoxide reductions led to the formation of mixtures of olefinic and paraffinic hydrocarbons whose distribution depends on the reaction conditions.

At low pressure, unusual selectivities in olefins were observed, the C_3 fraction being generally important. The factors governing these selectivities are briefly discussed.

Introduction

Hydrogenation of carbon monoxide on transition-metal-based catalysts is of major industrial importance in relation with the energy crisis (synthesis of fuel from syngas).

Among the most efficient catalysts in this field (Fe, Rh, Ru, Co, . . .), the cobalt-based catalysts are of particular interest as they are quite active and efficient for the production of hydrocarbons from syngas and for the homologation of methanol to ethanol [1].

Particularly interesting was the selectivity towards olefins observed under very low pressure (close to one bar) with reduced cobalt catalysts ($Co(acac)_2$ + triethylaluminium) in a high-boiling solvent, reported by Petit and Mortreux [2].

It is noteworthy that these authors added butadiene as a ligand to stabilize the catalytic centre.

The participation of cobalt(I) complexes as the active catalytic species was therefore suspected in such cobalt catalyzed CO hydrogenation. Similarly, complexes of Fe and Rh in low oxidation states have indeed been frequently proposed in the literature as the active species in Fischer—Tropsch catalysis [3] (e.g. Fe(I) and Rh(I)).

+ This paper was presented of the 2nd Belgium—Hungarian Colloquium on Catalysis at De Haan, Belgium, October 10—13, 1983.

* To whom correspondence should be addressed.

We have therefore compared the catalytic performances of reduced cobalt species (prepared according to Petit and Mortreux procedures) to a preformed cobalt(I) complex (π-cyclooctenyl-π-1,5-cyclooctadiene cobalt(I) (Co(COD)). The catalytic activity of that complex was studied both in a liquid phase (high-boiling solvent) and in a supported system, under different conditions of pressure (1 to 150 bars) and processes (in circulators with continuous trapping of the products or in autoclaves).

Experimental

Analytical procedure

The gas phases were analysed by GLC using different analytical columns: Spherocarb (9 feet, 1/8 inch) for CO, CO_2, CH_4; Al_2O_3 capillary PLOT column (30 meters, isothermal 60 °C) for all hydrocarbons C_1-C_5; FFAP and Silicone SE-30 (9 feet, 1/8 inch) for higher hydrocarbons.

Identification of the gases was based both on chromatographic methods (retention times) and mass spectrometry coupled to a GLC apparatus.

Catalysts

π-cyclooctenyl-π-1,5-cyclooctadiene Co(I) was purchased from Emser Werks A.G., or prepared according to a reported procedure [4].

Supports

Bentonite Tixoton is a commercial clay (presenting base character) available from Süd Chemie A.G. (München). Bentonite Tixoton is dried before use by azeotropic distillation of water with benzene using a Dean-Stark trap. The solvent is then evaporated under reduced pressure and bentonite is next dried under vacuum (0.2 mm) overnight (ca. 18 hr) at 150 °C. Bentonite is finally heated in a furnace at 400 °C for 2 hours.

Triton Kaowool (alumina silicate fibres) is available from Morganite Ceramic Fibres Ltd., Tebay Road, Bromborough, WIRRAL, Merseyside L62 3PH UK (composition of the standard fibre (%): Al_2O_3 (44.8); SiO_2 (54.4); Fe_2O_3 (0.05); TiO_2 (0.04); MgO (0.02); alkalis (Na_2O, K_2O) (0.03); B_2O_3 (0.01); Cl (20 ppm); trace inorganics (0.2—0.3).

Preparation of supported catalysts

Impregnation of supports was effected by slow evaporation of a catalyst solution in pentane, followed by drying overnight in vacuum (<1 mm) at 25 °C.

Preparation of cobalt catalysts in a solvent by reduction of cobalt(II) trifluoroacetate with Dibal-H (diisobutylaluminium hydride) was run in a high-boiling solvent (typically terphenyl) in the presence of 1,5-cyclooctadiene (COD) with a (COD) to metal ratio equal to 4.

Operating conditions

Low pressure (1—1.4 bar) experiments were run in a glass reactor heated at 200 to 250 °C with continuous trapping of the reaction products in a cool trap (liquid nitrogen), the syngas being recycled continuously by mean of a pump [2]. The total amount of gases was measured after each period of six hours by volumetry.

High pressure experiments were carried out in stainless steel autoclaves (PROLABO) (125 mL). The dried catalyst (contained in a glass jacket under nitrogen) was introduced into the autoclave which was closed under a stream of nitrogen as quickly as possible after removal of the glass stopper of the jacket. A pressure of carbon monoxide (50 bars) was then applied to the autoclave, followed by hydrogen (100 bars). The reactor was then shaken at the required temperature (electrical heating) during 40 hours. The gases were collected in a reservoir after cooling at room temperature and analysed by GLC.

Results and Discussion

A. Experiments under low pressure with recycling of syngas

1. *Reactions in solution:* by using a solution of π-cyclooctenyl-π-1,5-cyclooctadienecobalt(I) (0.001 mole) as catalyst in terphenyl, we observed the formation of a mixture of alkanes and olefins. If methanation is the main reaction, it is noteworthy that the proportion of olefins relatively to the corresponding alkanes is higher than unity up to the C_5 fraction, being particularly high for the C_3 hydrocarbons. The ethylene to ethane ratio is, however, comparatively low (even smaller than 1) but it increases when the catalyst is used for a second run (to reach a constant value after a few hours) (Fig. 1).

When they are used in a solvent, the Co(COD) catalyst as well as reduced cobalt systems prepared in situ by reduction of cobalt(II) species, affords a rather similar pattern as far as the relative alkanes and olefins distribution is concerned (Fig. 2); the olefins to alkanes ratio remains higher than unity in the C_3-C_5 fractions but is substantially lower than one for the C_2 hydrocarbons. This trend seems to be very general with these systems and supports the hypothesis that olefins are primary products in Fischer-Tropsch reactions[3].

2. *Experiments with recycling* of syngas on a *supported* (bentonite Tixoton) Co(COD) catalyst under low pressure (1.4 bar) afforded results very similar to those obtained in solution. Olefins are formed together with alkanes. The catalyst remains active during long periods of time (it is still active after 18

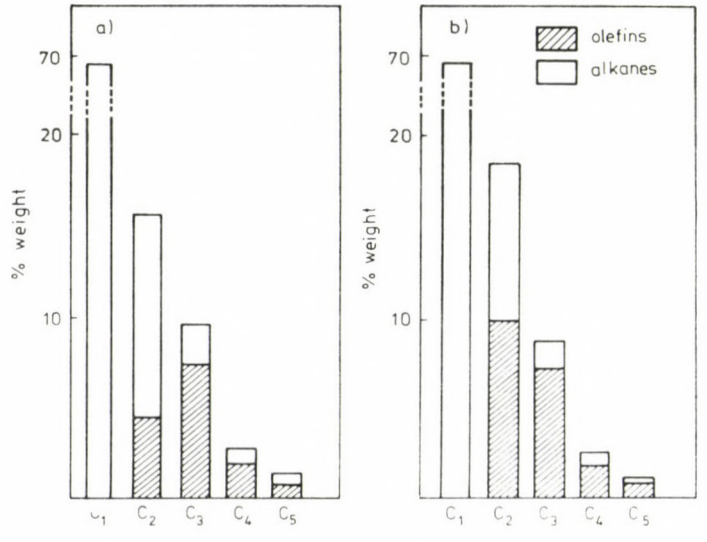

Fig. 1. Evolution of olefins to alkanes selectivity with the number of utilisations of a Co(COD) catalyst : Co(COD) : (0.001 mole); solvent : terphenyl (30 mL); P : 1 bar (circulator); CO/H_2 : 0.5; T : 200 °C; (a) first run : 5h, % olefins/alkanes (besides CH_4) : 49% (b) second run : 5h, % olefins/alkanes : 63%

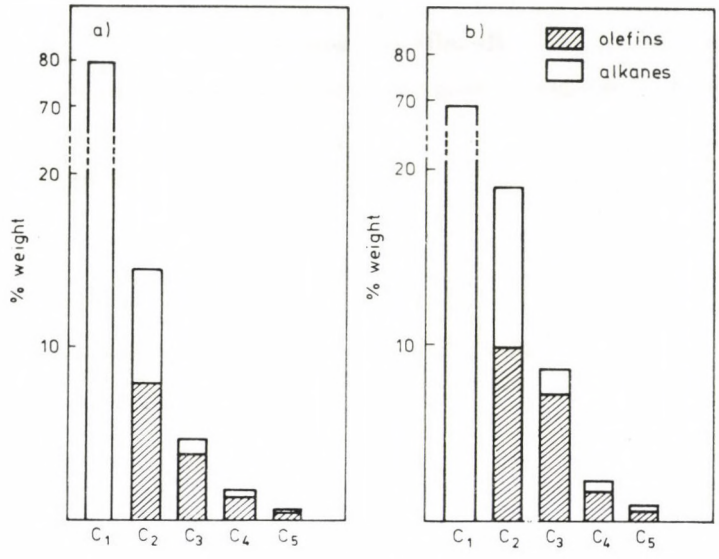

Fig. 2. Comparison between (a) a cobalt catalyst prepared by reduction of cobalt(II) trifluoro acetate and (b) Co(COD) (a preformed Co(I) complex). (a) catalyst : reduction of Co(II) trifluoroacetate (0.001 mole) with Dibal-H (0.005 mole) in the presence of 1,5-cyclooctadiene (0.01 mole). (b) catalyst : π-cyclooctenyl-π-1.5-cyclooctadienecobalt(I) (0.001 mole). Solvent : terphenyl (30 mL); P : 1 bar (circulator); CO/H_2 : 0.5; $T = 200$ °C; $t = 5$h

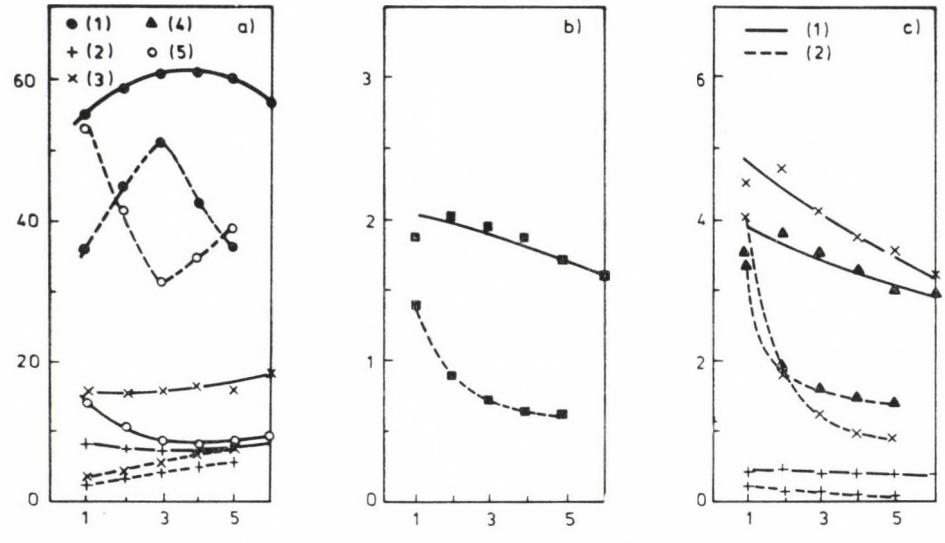

Fig. 3. Selectivity evolutions with the number of utilisations of a Co(COD) catalyst. *N:* number of utilisations (6 hours each) of the catalyst. (a) Evolution of the C_1, C_2 and C_3 hydrocarbons (and CO_2) distribution of the gas phase against *N*. (1) : CH_4, (2) : C_2, (3) : C_3, (4) : C_4, (5) : CO_2. (b) Evolution of $\Sigma(C_2-C_4)^=$ to $\Sigma(C_2-C_4)$ ratio against *N*. (c) Evolution of the olefin(s) to alkane(s) ratios for C_2, C_3 and C_4 against *N* (same symbols as in Fig. 3a). *P* : 1.4 bar (circulator); CO/H_2 : 0.5; *T* : 250 °C. (1) : 0.001 mole of Co(COD)/5 g bentonite Tixoton. (2) : 0.001 mole of Co(COD)/0.5 g bentonite Tixoton then mixing of this charged support with 4.5 g of bentonite (the local concentration of cobalt is higher than in the above case but the total amounts of metal and of support are the same)

uses of 6 hours each) but the product distribution changes significantly with time (Fig. 3, a—c):

a) namely the *olefins to alkanes* ratio (Fig. 3, b—c) decreases steadily. The drop of the olefin production is quite general as it is observed for the C_2, C_3 and C_4 fractions, the effect being, however, particularly important in the C_2 case. This result could perhaps be related to a higher hydrogenation rate for ethylene than for higher olefins.

b) Moreover, the relative *distribution of the hydrocarbons* (olefins + alkanes) according to their molecular weight, changes significantly with the number of catalyst utilisations. In fact, each component of the hydrocarbon fractions shows a particular evolution trend: the relative concentration of methane (calculated on $C_1 + C_2 + C_3 + C_4 + C_5 + CO_2$) presents a maximum; the C_2 fraction does not change appreciably (it increases however when the local concentration of cobalt is increased—see below) whereas the C_3 fraction increases slightly. In opposition, the CO_2 production goes down with time.

All these modifications of selectivity are strongly accelerated when the local concentration of cobalt is increased (Fig. 3, dotted curves). This is a very general observation which is apparent as well for the relative distribution of the chains (C_1—C_3) as for the evolution of the olefins to alkanes ratio (or the production of CO_2). This effect may therefore be related to a modification of the particle sizes with time: large particles promoting both the formation of higher alkanes and the hydrogenation of the olefins.

Moreover, in opposition to the experiments performed in the presence of a solvent, the *distribution of hydrocarbons* (olefins + alkanes) presents a minimum for the C_2 fraction (Fig. 3, a).

B. Experiments under high pressure of syngas ($P_0 = 150$ bars)

Beside the pressure conditions, the main difference between these experiments and those run at low pressure (with recycling of syngas) is the fact that the catalyst remains in contact with the products formed in the reaction (including water) whereas these products were continuously trapped in the low pressure experiments. The observation that the catalyst is appreciably deactived even after one single use could in fact be due to reactions with the products formed [ΔP after 40 hours: 33 bars, second run under the same conditions: 16 bars (Table I)].

Oppositely, the catalyst remains active after several uses (more than 18) in the recycling device ($P = 1.4$ bar) (see above A-2) when the products (particularly water and organic liquids which could act as deactivators) are continuously removed.

Table I

Modification of the catalyst efficiency during successive utilisations (a)

Product	Composition of the gas phase (%) weight (b)	
	first run	second run
Methane	60.7	52.2
Ethane	7.6	11.7
Ethylene	0.12	traces
Propane	13.3	16.9
Propene	0.43	0.15
Butane	9.2	10.9
Isobutane	0.27	0.09
Butenes	0.33	0.11
n-Pentane	6.3	6.2
2-Methylbutane	0.23	0.08
Neopentane	0.00	0.00
Pentenes (c)	0.22	0.07
Unidentified	1.3	1.6

(a) Catalyst: Co(COD) : (0.001 mole) or bentonite Tixoton (5 g)
Conditions: $P = 150$ bars, $CO/H_2 = 0.5$, $T° = 245$ °C, $t = 40$ h (each utilisation)
(b) % of hydrocarbons calculated from the total ($C_1 - C_5$); average of at least two runs
(c) 1-pentane + *t*-2 pentene + *c*-2 pentene.

Table II

Influence of the temperature on the distribution of hydrocarbons in the gas phase

Product	Composition of the gas phase (% weight)			
	235 °C	245 °C	250 °C	265 °C
Methane	62.0	66.0	70.0	81.0
Ethane	3.5	4.2	4.8	4.5
Ethene	0.05	0.03	0.02	traces
Propane	12.6	10.6	8.8	6.6
Propene	2.1	1.7	1.4	0.05
Butane	9.9	8.9	7.4	4.6
Isobutane	0.13	0.10	0.08	0.08
1-Butene	0.56	0.49	0.46	0.06
trans-2-Butene	0.75	0.71	0.70	0.32
cis-2-Butene	0.51	0.43	0.40	0.15
Isobutene	0.05	0.04	0.03	0.03
n-Pentane	6.0	5.1	4.4	2.0
2-Methylbutane	0.06	0.05	0.05	traces
Neopentane	0.00	0.00	0.00	0.00
1-Pentene	0.19	0.18	0.15	0.02
trans-2-Pentene	0.36	0.36	0.34	0.18
cis-2-Pentene	0.26	0.24	0.22	0.08
Unidentified	0.98	0.87	0.75	0.33

Catalyst: Co(COD) : (0.001 mole) supported on Triton Kaowool (2 g); $P_0 = 150$ bars (autoclaves); $CO/H_2 : 0.5$; $t = 40$ h.

The most noteworthy difference with the low pressure experiments (performed with continuous trapping of the reaction products) is the low concentration of olefins (0.1—10%) relatively to alkanes. Obviously the hydrogenation of the olefins is favoured in this case as they remain in close contact with the cobalt catalyst during the whole experiment. Moreover, the composition of

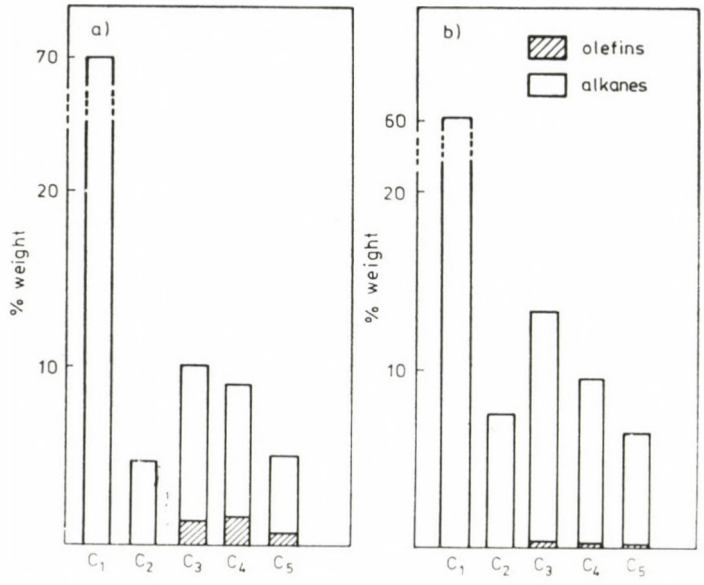

Fig. 4. Distribution of the hydrocarbons in the gas phase. Catalyst : Co(COD) : (0.001 mole); support : (a) Triton Kaowool (2 g), (b) Bentonite Tixoton (5 g); P_0 : 150 bars (autoclaves); CO/H_2 : 0.5; T : (a) 250 °C, (b) 245 °C; t : 40 h

the gas phase is markedly affected within a relatively narrow range of temperature (235—265 °C). (Table II): the more striking feature being an increase of methanation reaction by raising the temperature (together with extensive CO_2 formation by water gas shift reaction).

A common feature of these supported Co(COD) catalysts used under high pressure ($P_0 = 150$ bars) is, besides the almost complete absence of olefins, the abnormal low value of the C_2 fraction (Fig. 4) observed on different supports (Triton Kaowool, Bentonite Tixoton, glass beads, $Mg(OH)_2$ . . .).

Different proposals have been invoked to account for such a discrepancy [2b].

In some cases, it seems to be related to oxygenates [3, 6] formation from ethylene (this explanation is however not probable in our case as no oxygenates have been detected in most cases). In fact, hydrogenolysis of ethylene to methane as well as the preferential participation of ethylene in the formation of higher hydrocarbons can also be responsible for such an effect. For example, Pettit

has explained the formation of C_3 hydrocarbons by the homologation of ethylene according to a carbenoid mechanism [5]. This problem is under investigation in our laboratory.

Conclusion

1. Even at low pressure (1.4 bar), catalysts based on low oxidation state cobalt derivatives [(Co(I) species] are active for CO hydrogenation.

2. Light olefins and alkanes are formed as gaseous products. The olefins to alkanes ratio strongly depends on the operating conditions: experiments performed with recycling of the gas and continuous trapping of the products yield olefin rich mixtures. Oppositely, in static experiments (autoclave at 150 bars), when the products of the reaction remain in contact with the catalyst, the alkanes are preferentially formed: olefins seem to be probable primary product in these reactions.

3. The life of the catalyst strongly depends on the above set of conditions: under trapping conditions (recycling of the gas under 1.4 bar), the catalyst remains active for a long reaction time (more than 100 hours) but the selectivity towards olefin formation goes down noticeably with time. Moreover, these modifications of selectivity are accelerated by increasing base concentration of cobalt. Oppositely, the catalyst is readily deactivated when the reaction is performed in an autoclave (150 bars), the catalyst remaining in contact with the reaction products.

4. In the presence of supported catalyst, the C_2 hydrocarbons are generally formed in smaller quantities than that expected from a Schulz-Flory distribution (Figs 3 and 4). A Schulz—Flory type distribution is, however, observed in low pressure experiments run in the presence of solvent (Figs 1 and 2).

*

We are particularly indebted to the Commission of the European Communities (Contract n° EED-2-326B) and to the FNRS (Belgium) for their generous financial support and one of us (J.L. Costa) to IRSIA (Belgium) for a fellowship.

REFERENCES

[1] C_1-Based Chemical from Hydrogen and Carbon Monoxide. Ed. M. T. Gillies. Noyes Data Corporation Park Ridge, New Jersey USA 1982
[2] (a) Blanchard, M., Vanhove, D., Petit, F., Mortreux, A.: J. Chem. Soc., Chem. Comm., **1980,** 908; (b) Vanhove, D., Blanchard, M., Petit, F., Mortreux, A.: Nouv. J. Chim., **5,** 205 (1981)
[3] Satterfield, C. N.: International Symposium on "Conversion of Energy-carriers and Production of Chemicals from the Synthesis Gas". Utrecht, May 11, 1983
[4] Gosser, L. W., Cushing Jr., M. A.: Inorg. Synthesis, **17,** 112 (1977)
[5] Brady, R. C., Pettit, R.: (a) J. Am. Chem. Soc., **102,** 6181 (1980); (b) J. Am. Chem. Soc., **103,** 1287 (1981)
[6] Takeuchi, A., Katzer, J. R., Schuit, C. C. A.: J. Catal., **82,** 477 (1983)

Acta Chimica Hungarica 119 (2—3), pp. 155—166 (1985)

PHYSICO-CHEMICAL CHARACTERIZATION OF REVERSED MICELLES CTAB — 1-HEXANOL — WATER CONTAINING Co(II) IONS+

Isabelle RAVET, Ndongala LUFIMPADIO, Alain GOURGUE and Janos B. NAGY*

(Facultés Universitaires de Namur, Laboratoire de Catalyse, 61, rue de Bruxelles, B-5000 — Namur, Belgium)

Received June 8, 1984
Accepted for publication August 15, 1984

Reversed micellar systems composed of CTAB, 1-hexanol and water and containing Co(II) ions were characterized by ^{13}C- and ^{19}F-NMR and UV-visible spectroscopies.

The ^{13}C-NMR results have shown that the Co(II) ions are solubilized in the inner water core of the micelles, in the vicinity of the interface, and that 1-hexanol molecules participate to the first coordination shell of the ions. The UV-visible spectroscopy has shown the simultaneous presence of octahedral and tetrahedral complexes, the former being favoured at high water content. The average size of the micellar water cores, as determined by ^{19}F-NMR, increases in the presence of Co(II) ions and with increasing water concentration.

Finally the Co(II) ions were reduced with $NaBH_4$ in the reversed micellar solutions leading to very small monodisperse cobalt boride particles.

Introduction

Reversed micelles are formed by self-association of surfactant molecules in non-aqueous media [1]. In the ternary system CTAB — 1-hexanol — water, the domain of existence of reversed micelles is shown in Figs 1, 2.

Due to the great influence of paramagnetic ions on the ^{13}C-NMR chemical shift, the ^{13}C-NMR technique is quite useful to study the interactions of Co(II) ions with the micellar components. For example, the sites of solubilization of the Ni(II) and Fe(III) ions were readily determined [3, 4]. The former has been shown to be close to the interface while the latter was essentially dissolved in the interior of the inner water core.

UV-visible absorption measurements complement quite well the ^{13}C-NMR data, the absorption energies of the Co(II) ions being very sensitive to the types of ligands and the nature of the complexes. These latter can be either octahedral or tetrahedral depending on the nature of the solvent [5].

+ This paper was presented at the 2nd Belgian—Hungarian Colloquium on Catalysis at De Haan, Belgium, October 10—13, 1983.

* To whom correspondence should be addressed.

The size of the inner water core is determined by an indirect method, based on ^{19}F-NMR of 6-fluoro-1-hexanol used as a probe, in small amount, in the reversed micellar system [6].

Finally, it is shown that monodisperse Co_2B can be prepared by reducing the Co(II) ions by $NaBH_4$ under nitrogen atmosphere. The use of reversed micelles is thus quite promising for the preparation of monodisperse metallic particles of colloidal size [3, 4, 7, 8].

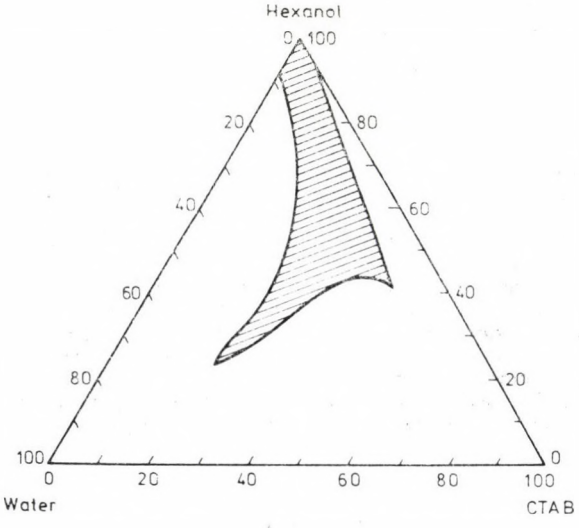

Fig. 1. Domain of existence of reversed micelles following ref. [2]

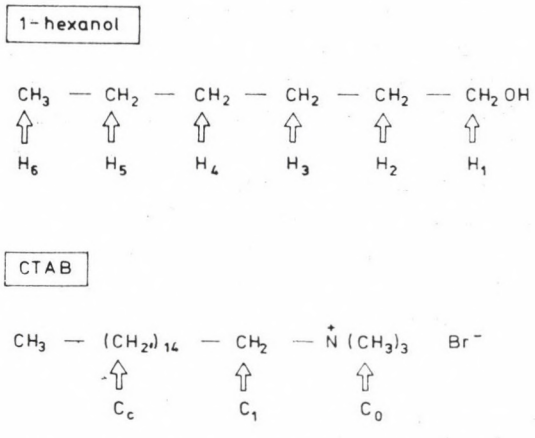

Fig. 2. Nomenclature of 1-hexanol and CTAB carbon atoms

Experimental

Materials

The commercial products, 1-hexanol (Aldrich, 98%), CTAB (Serva, p.a.), $CoCl_2 \cdot 6H_2O$ (Merck p.a.) and $NaBH_4$ (Aldrich, >99%), have been used without further purification. The 6-fluoro-1-hexanol has been synthesized according to the Pattison method [9].

The reversed micellar solutions used in this study were prepared with a constant 1-hexanol/CTAB weight ratio (= 1.25) and varying water content (10 to 20 wt. %).

^{13}C-NMR

The interactions between the Co(II) ions and the micellar components were studied by ^{13}C-NMR spectroscopy. The spectra were recorded on a Bruker WP-60 spectrometer, at room temperature and with broadband proton decoupling, at 15.08 MHz. To avoid the problem of volume susceptibility corrections, we used the methyl carbon of the 1-hexanol molecule as internal reference. The stabilization of the magnetic field was carried out using a deuterium lock of D_2O contained in the external part of two concentric tubes, the inner tube being filled with the micellar solution.

UV-visible spectroscopy

The nature of the cobalt complexes in the reversed micelles was studied by UV--visible spectroscopy. The spectra were recorded on a Varian Cary 219 spectrophotometer at 25 °C. The corresponding micellar solution without cobalt was used as reference.

^{19}F-NMR

The approximate sizes of the micellar water cores were determined by ^{19}F-NMR of 6-fluoro-1-hexanol used as label compound in the micellar solution (ca. 1—5 wt. %). The spectra were recorded on a Bruker CXP-200 spectrometer, at 188 MHz. The stabilization of the magnetic field was carried out using a deuterium lock of CD_3OD contained in a solution of 6-fluoro-1-hexanol in 1-hexanol (ca. 2 vol.%), used as external reference.

Electron microscopy

The average size of the metallic particles obtained by reducting the Co(II) ions with $NaBH_4$ and deposited on silica gel was determined by means of a Philips EM 301 electron microscope working in the transmission mode.

Results and Discussions

Co(II)-micellar interactions and site of solubilization

The nature of the interactions between the Co(II) ions and the micellar components and the location of the solubilized Co(II) ions were studied by ^{13}C-NMR. The nomenclature of the 1-hexanol and CTAB carbon atoms is shown in Fig. 2. Results obtained for a typical micellar solution are shown in Fig. 3.

The presence of only one resonance line for each carbon atom is characteristic of a rapid exchange of the molecules between several sites (interface, organic phase, vicinity of a paramagnetic Co(II) ion, . . .).

The results show that for the CTAB carbon atoms, the chemical shifts increase with increasing Co(II) ion concentration but decrease rapidly within the hydrocarbon chain. The more influenced carbon atom, due to the proximity

of paramagnetic ions, is C_0 of the CTAB polar headgroup. This indicates that the interaction between the Co(II) ions and the CTAB molecules is mostly of dipolar type and that the Co(II) ions are located in the polar part of the micelles, close to the interface.

For the 1-hexanol molecules, the chemical shifts increase with the Co(II) ion concentration (as in the case of CTAB), but the carbon atom in β-position (H_2) is the most influenced one. It follows that the interaction between Co(II)

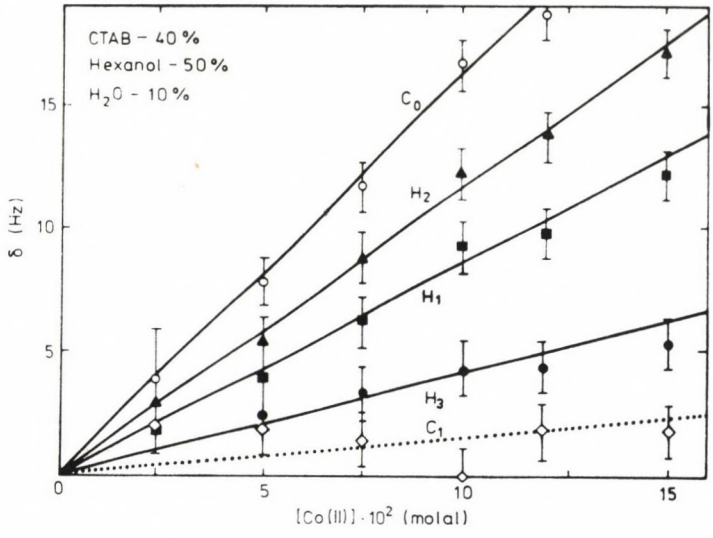

Fig. 3. ^{13}C-NMR chemical shift variations as a function of the Co(II) ions concentration

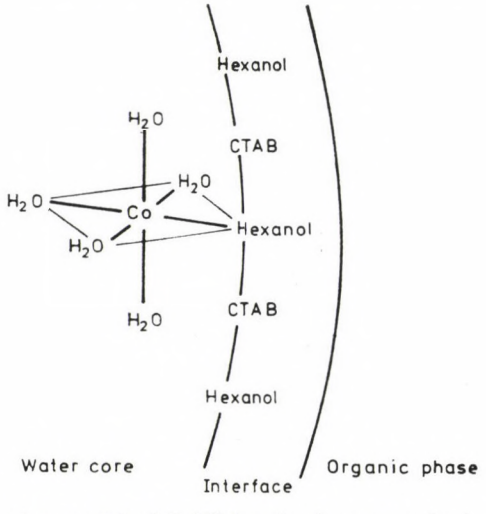

Fig. 4. Solubilization model of Co(II) ions in the reversed micellar water core

ions and 1-hexanol molecules include an important contribution of the contact type. It is therefore assumed that hexanol molecules participate to the first coordination shell of the solubilized Co(II) ions.

The greater effect observed for the CTAB C_0 atom compared to H_2 of the hexanol is due to the averaging under rapid exchange. The proportion of influenced molecules is more important in the case of CTAB where almost all of the molecules are located in the interface, close to the paramagnetic ions, while the greater part of the hexanol molecules are in the organic phase.

From the ^{13}C-NMR chemical shifts of 1-hexanol and CTAB carbon atoms, we conclude that the Co(II) ion dissolved in the reversed micellar solutions are solubilized in the water cores, in the vicinity of the interface. There is a direct interaction between Co(II) ions and 1-hexanol molecules, forming Co-hexanol complexes, Figure 4 shows this model of solubilization of Co(II) ions in the water core.

Nature of the Co(II)-complexes

The nature of Co(II) complexes formed in micellar solutions was studied by UV-visible spectroscopy. Figure 5 shows a typical spectrum of a micellar solution containing Co(II) ions. We observe two different absorption bands: one at $\lambda_{max} = 688$ nm and another at $\lambda_{max} = 512$ nm, respectively attributed to a tetrahedral and an octahedral cobalt species.

The importance of the band of the tetrahedral cobalt species is only due to a much greater value of the corresponding molar absorption coefficient ($\sim$800 L mol^{-1} cm^{-1}) compared to the octahedral complex (4.76 L mol^{-1} cm^{-1}). The calculated relative amount of the tetrahedral complex is rather weak (0—2.5% of the total Co(II) amount).

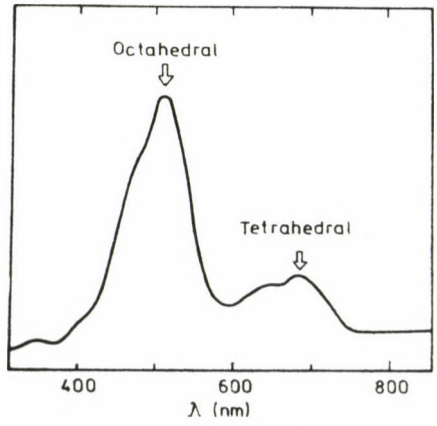

Fig. 5. Typical UV-visible spectrum of Co(II) ions in a reversed micellar system

Figure 6 shows the variation of the absorbance of the cobalt complexes with respect to Co(II) ions and water concentrations. We observe that the concentrations of the two complexes increase with increasing [Co(II)], but for a given value of this concentration the absorbance due to the tetrahedral complex decreases quite rapidly with increasing water content. Hence, the octahedral complex is favoured for high water content in the micellar system. This behaviour can be explained by a specific solvation process of the Co(II) ions. In fact, in the case of low water content, there are not enough water molecules available to solvate completely the Co(II) ions. Consequently, some of them are transformed into tetrahedral complexes. With increasing amount of water, the concentration of "free" water molecules also increases which favours the formation of octahedral complex.

In water, the octahedral cobalt complex, $Co(H_2O)_6^{2+}$, absorbs at 510 nm, while in the micellar solution we found a band at 512 nm; this small difference is attributed to the coordination by hexanol molecules (shown also by ^{13}C-NMR). Thus the octahedral complex in the micellar water core can be of the form $(Co(H_2O)_{6-x}\ Hexanol_x)^{2+}$ where x is very small.

Tetrahedral complexes of the types $CoBr_4^{2-}$ or $CoCl_xBr_{4-x}^{2-}$ are formed in micellar solution of the system CTAB — chloroform — water containing Co(II) ions. The maximum of the absorption band is at 719 nm [5]. On the other hand, in pure 1-hexanol, the tetrahedral complex $CoCl_2\ Hexanol_2$ adsorbs at 656 nm and in HBr, $CoBr_4^{2-}$ absorbs at 710 nm. As in our micellar solutions, the tetrahedral complex absorbs at 688 nm, we can assume that it has an intermediate composition, i.e. $Co\ Cl_x\ Br_{3-x}\ Hexanol$ with $0 \leq x \leq 3$.

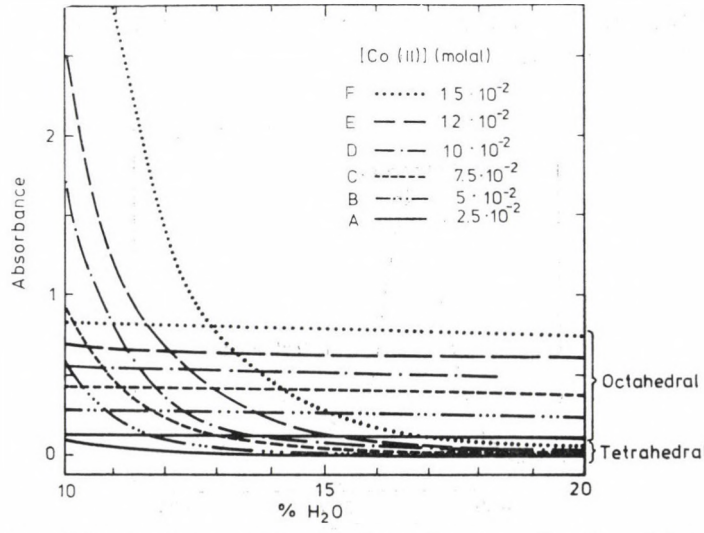

Fig. 6. Variation of the absorbance of the Co(II) complexes as a function of the water content for different Co(II) concentrations

Determination of the micellar size

The approximate sizes of the micellar water core were determined by means of ^{19}F-NMR of 6-fluoro-1-hexanol the behaviour of which is similar to that of the 1-hexanol molecules [6].

This probe is distributed in the water core, the interface and the bulk organic phase. Because of fast exchange between these phases, the observed chemical shift (δ_{obs}) of 6-fluoro-1-hexanol is related to the amounts present in each phase by the following equation:

$$\delta_{obs} = X\delta_w + Y\delta_I + Z\delta_H$$

where δ_w, δ_I and δ_H are the chemical shifts of 6-fluoro-1-hexanol in water, interface and 1-hexanol respectively, with the corresponding mole fractions X, Y and Z.

Because of the very low solubility of 1-hexanol in water, $X \simeq 0$. Moreover, 6-fluoro-1-hexanol in 1-hexanol is used as reference and δ_H is therefore

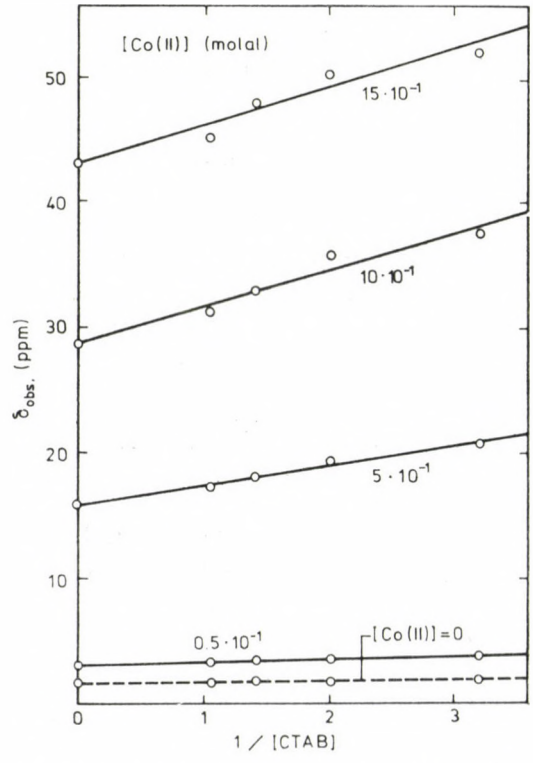

Fig. 7. Variation of the observed chemical shift versus 1/(CTAB) for different Co(II) concentrations in normal micelles

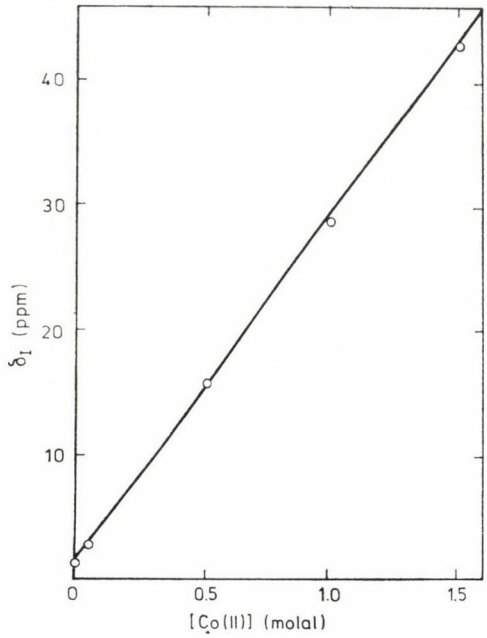

Fig. 8. Variation of δ_I as a function of the Co(II) concentration

equal to zero. The relationship is then simplified to:

$$\delta_{obs} = Y\delta_I$$

δ_I is determined from normal micelles formed by CTAB in aqueous solutions with 2 wt.% of 6-fluoro-1-hexanol. The observed chemical shifts in solutions with different CTAB concentrations are related, in the fast exchange approximation, to δ_I, δ_w and the CMC of the surfactant according to [10]:

$$\delta_{obs} = \delta_I + \frac{CMC}{[CTAB]}(\delta_w - \delta_I)$$

From the variation of δ_{obs} as a function of 1/[CTAB], the intercept of the straight line yields δ_I. The results obtained in presence of different Co(II) concentrations are shown in Fig. 7 and the intercept values are given in Fig. 8, giving the following relationship:

$$\delta_I(ppm) = 1.67(\pm 0.11) + 27.51(\pm 0.14)\ [Co(II)]$$

In the reversed micellar system, the Co(II) ions are not dispersed in the water core but they are located in an envelope in the vicinity of the inter-

face as it was shown by ^{13}C-NMR and UV-visible spectroscopy measurements. The Co(II) local concentration is more important than the global concentration, with a correction factor given by [3]:

$$F_{corr} = \frac{r_M^3}{r_M^3 - (r_M - r_{Co})^3}$$

where r_M is the radius of the micellar water core,
and r_{Co}, the thickness of the envelope containing the Co(II) ions, is taken equal to 3.2 Å, on the basis of the coordination shell of the ions.

The knowledge of the δ_I value enables us to calculate, from the observed chemical shift, the molar fraction of probe molecules (and therefore that of 1-hexanol) in the interface.

Assuming a monodisperse distribution of spherical reversed micelles, the average radius of the inner water cores is given by

$$r_M = \frac{3V}{S_T}$$

where V is the total volume of water in the micellar solution and S_T is the total area of the interface. (Let us note that r_M is needed to calculate δ_I and the determination of the average radius must then be an iterative process.)

S_T is the sum of the areas occupied by the molecules of 1-hexanol and of CTAB; if we assume that all the CTAB molecules are located in the interface and that the cross section of the CTAB and 1-hexanol molecules are equal to 34 Å^2 and 21 Å^2, respectively [3]:

$$S_T = n_{Hex}^{int} \times 21\ \text{Å}^2 + n_{CTAB} \times 34\ \text{Å}^2$$

$$\text{where} \quad n_{Hex}^{int} = Y \frac{(W_{Hex}/100) \times 6.02 \times 10^{23}}{M_{W(Hex)}}$$

$$n_{CTAB} = \frac{(W_{CTAB}/100) \times 6.02 \times 10^{23}}{M_{W(CTAB)}}$$

with W_{Hex} and W_{CTAB} being the weight % concentrations of 1-hexanol and CTAB.

Figure 9 shows the variation of r_M as a function of Co(II) concentration for a typical micellar composition. The average size of the water cores increases with increasing Co(II) concentration. This increase is a direct consequence of the increase of the interfacial free energy of 1-hexanol when Co(II) ions are present in the water core. It leads to a diminution of the number of alcohol molecules in the interface and hence the total interface area decreases.

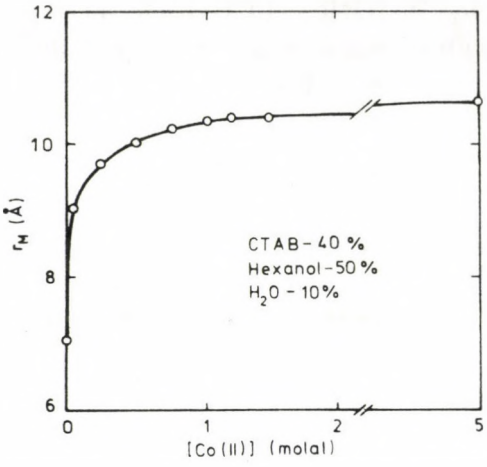

Fig. 9. Variation of the water core radius as a function of Co(II) concentration for one typical micellar composition

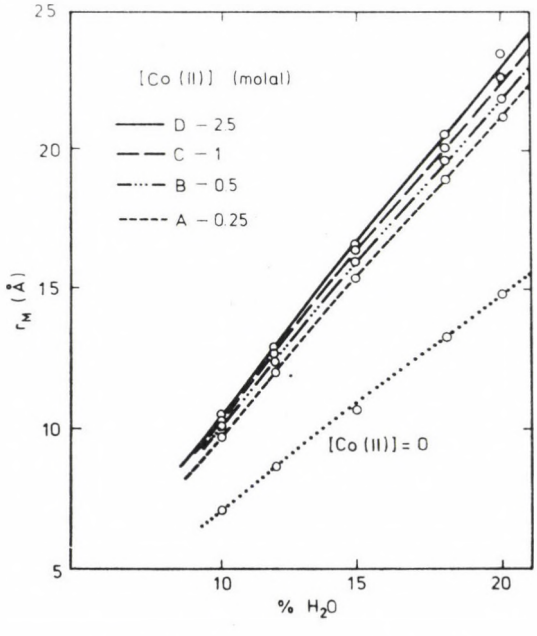

Fig. 10. Average radius of the micellar water core as a function of water concentration

Table I

Average particle sizes of cobalt boride

$[Co(II)] \times 10^2$ (molal)	$\bar{d}$ (Å)
2.5	42
5.0	22
10.0	29
15.0	62

Nevertheless the most important effect on the average size of the water cores is due to the water content of the micellar solutions, as shown in Fig. 10: the micellar radius increases with increasing water concentration because of the decrease of the aggregates surface to volume ratio.

Preparation of small cobalt boride particles

Small cobalt boride particles were prepared by reducing, with sodium borohydride, the Co(II) ions dissolved in the micellar water core.

After degassing with nitrogen, the micellar solution is transferred into a glove box under nitrogen atmosphere. An excess of sodium borohydride is then added at 0 °C. The black solution obtained is vigorously stirred and the particles are deposited on silicagel. The average particle size was examined by electron microscopy. Table I gives the results obtained for different Co(II) initial concentrations in a typical micellar solution (CTAB : 38, 1-hexanol : 47, water : 15 wt.%).

The average particle size varies between 22 and 52 Å. Oppositely when the particles are prepared in ethanol or water, their size is much larger: 2500 Å in the former and 3500 Å in the latter. It is thus concluded that reversed micelles constitute a very adequate medium to obtain very small colloidal particles. Preliminary investigations on the nature of the particles by ferromagnetic resonance indicate that they are essentially Co_2B.

Conclusions

The cobalt ions introduced in a reversed micellar solution of the ternary system CTAB — 1-hexanol — water, are solubilized in the water core, in the vicinity of the interface where they form octahedral and tetrahedral complexes. The average size of the micellar water cores increases with increasing water content and with increasing Co(II) concentration. The reduction of $CoCl_2$ by $NaBH_4$ in micellar solution leads to very small monodisperse cobalt boride particles.

REFERENCES

[1] Fendler, J. H., Fendler, E. J.: "Catalysis in Micellar and Macromolecular Systems", Academic Press, New York 1975
[2] Ahmad, S. I., Friberg, S.: J. Am. Chem. Soc., **94,** 5196 (1972)
[3] Gourgue, A.: Ph. D. Thesis, Facultés Universitaires de Namur 1981
[4] Lufimpadio, N.: Ph. D. Thesis, Facultés Universitaires de Namur 1983
[5] Sunamoto, J., Hamada, T.: Bull. Chem. Soc. Jpn., **51,** 3130 (1978)
[6] Nguyen, T., Ghaffarie, H. H.: J. Chim. Phys., **76,** 513 (1979)
[7] Boutonnet, M.: Ph. D. Thesis, Université Louis Pasteur, Strasbourg 1977
[8] Kurihara, K., Kizling, J., Stenius, P., Fendler, J. H.: J. Am. Chem. Soc., **105,** 2574 (1983)
[9] Pattison, F. L. M., Howell, W. C., NcNamara, A. J., Schneider, J. C., Walker, J. F.: J. Org. Chem., **21,** 739 (1956)
[10] Lindman, B., Wennerström, H.: "Micelles amphiphile aggregation in aqueous solution" Topics in Current Chemistry, **87,** 1 (1980), Springer Verlag, Berlin

Acta Chimica Hungarica 119 (2—3), pp. 167—178 (1985)

PHYSICO-CHEMICAL CHARACTERIZATION OF URANIUM-ANTIMONY MIXED OXIDE CATALYSTS+

Serge MAROIE[1,2*], Hervé COLLETTE[1,2], Zélimir GABELICA[2], Jacques VERBIST[1] and Janos B. NAGY[2**]

([1]Laboratoire de Spectroscopie Electronique, [2]Laboratoire de Catalyse, Facultés Universitaires Notre-Dame de la Paix, 61, rue de Bruxelles, B-5000 Namur, Belgium)

Received June 8, 1984
Accepted for publication August 15, 1984

The characterization of uranium-antimony oxides has been investigated by using thermal analysis (TG-DTA-DTG), X-ray diffraction (XRD) and X-ray photoelectron spectroscopy (XPS).

The mechanism of formation of $USbO_5$ and USb_3O_{10} could be inferred from thermal analysis data. The XRD results evidenced a slow and continuous transformation of $USbO_5$ into USb_3O_{10} with increasing calcination time, for both precursors (mixture of Sb and U oxides, where Sb/U = 1 or 3).

By contrast, the Sb/U ratio of the precursor does influence the nature of the surface species which could be identified by XPS as either USb_3O_{10} or Sb_2O_4.

Introduction

The conversion of alkenes into products containing either oxygen or other heteroatoms produces intermediates which are important for the petrochemical industry. In the middle of the sixties, a catalyst based on a complex uranium antimonate system was developed for commercial use [1]. Several physical methods of analysis [2—4] were used in an attempt to clarify relationships between the structure and the physical or catalytic properties of this system. The catalyst was found to consist of discrete phases $USbO_5$ and USb_3O_{10} rather than of a simple mixture of oxides. These two compounds exhibit very different catalytic properties in the oxidation and ammoxidation of propene. From the catalytic point of view, USb_3O_{10} is more important; it transforms selectively propene into acrolein or acrylonitrile. $USbO_5$ produces mainly waste products (CO_2, H_2O, ...). It is thus of prime importance to prepare USb_3O_{10} in its purest form.

The aim of the present work is to evaluate, by several physico-chemical techniques, the amount of the different species obtained in the bulk catalyst

+ This paper was presented at the 2nd Belgian—Hungarian Colloquium on Catalysis at De Haan, Belgium October 10—13, 1983.

* Senior Assistant of the NFSR (Belgium).

** To whom correspondence should be addressed.

or present on its surface after the precursors have been calcined in various ways. Emphasis was put on the systematic influence of calcination time, temperature, atmosphere and composition of the precursors.

Experimental

Catalysts

The precursors were prepared by reaction of NH_4OH (25%, Merck) with a mixture of $UO_2(CH_3COO)_2 \cdot 2H_2O$ and Sb_2O_3 dissolved in concentrated HCl (37%, Merck). The precipitate was filtered, washed with water and finally dried at 140 °C for 20 h. The active catalytic phases were obtained after thermal treatment of the precursors under conditions defined in the results section. Depending on the initial Sb/U atomic ratio, the two precursors were named I (Sb/U = 1) or II (Sb/U = 3). The pure mixed oxides $USbO_5$ and USb_3O_{10} were prepared as described previously [2].

Physico-chemical characterization

The Sb/U atomic ratio of the catalyst was determined by X-ray fluorescence. XRD patterns were run at room temperature, by means of a Philips PW1730 powder diffractometer, using CuKα radiation. XPS spectra were obtained on a Hewlett Packard 5950A spectrometer, using monochromatized AlKα radiation ($h\nu = 1486.6$ eV). The samples were pelletted and deposited on a gold-plated sample holder. A STA-780 Thermal Analyzer (TG-DTA-DTG) from Stanton Redcroft was used to study the formation of the mixed oxides, i.e. the precursors I or II. The sample (about 0.05 g) was heated from room temperature to 950 °C, at a heating rate of 20 °C-min^{-1} under dry air or dry nitrogen (30 mL-min^{-1}). Weight changes (in %) were referred to the weight of the initial precursor.

Atomic composition determined by XPS

XPS is a technique which may give semiquantitative information by using the relationship.

$$\frac{I_x}{I_y} = \frac{N_x \sigma_x \lambda_x T_x \left(1 + \frac{1}{2}\beta_x \left(\frac{3}{2}\sin^2 \alpha - 1\right)\right)}{N_y \sigma_y \lambda_y T_y \left(1 + \frac{1}{2}\beta_y \left(\frac{3}{2}\sin^2 \alpha - 1\right)\right)}$$

where I_x and I_y are the peak area of a considered level for species x and y, N_x and N_y the corresponding atomic concentration, σ_x and σ_y the photoionisation cross sections [5] of the respective core levels, β_x and β_y the asymmetry parameter factors [6]; T and λ are the analyser transmission factor and the mean escape depth of the ejected electrons respectively, both being a function of the electron kinetic energy [7]. α is the angle between incident X-rays and emitted electrons (73° in the Hewlett Packard spectrometer). We have considered the following photoelectron peaks U $4f_{7/2}$, Sb $3d_{5/2}$, Sb $3d_{3/2}$, O 1s. An overlap occurs between the Sb $3d_{5/2}$ and the O 1s peaks, hence the O 1s intensity was obtained from

$$I\ \mathrm{O\ 1s} = (I\ \mathrm{Sb\ 3d_{5/2}} + I\ \mathrm{O\ 1s})_{\mathrm{exp}} - (I\ \mathrm{Sb\ 3d_{5/2}})_{\mathrm{theor.}}$$

$(I\ \mathrm{Sb\ 3d_{5/2}})_{\mathrm{theor.}}$ is computed from $(I\ \mathrm{Sb\ 3d_{3/2}})_{\mathrm{exp.}}$ multiplied by the ratio of the respective photoionisation cross sections:

$$(I\ \mathrm{Sb\ 3d_{5/2}})_{\mathrm{theor.}} = (I\ \mathrm{Sb\ 3d_{3/2}})_{\mathrm{exp.}} \times 1.438$$

Sb/U atomic concentration ratio is then given by

$$\frac{N_{\mathrm{Sb}}}{N_{\mathrm{U}}} = \frac{(I\ \mathrm{Sb\ 3d_{3/2}})_{\mathrm{exp}}}{(I\ \mathrm{U\ 4f_{7/2}})_{\mathrm{exp}}} \times 2.15$$

Results and Discussion

1. *Formation of $USbO_5$ and USb_3O_{10} followed by thermal analysis Calcination of the precursors I and II under air flow*

The TG and DTA curves are presented in Fig. 1 and the numerical values in Tables I and II. For both precursors, three domains can be distinguished between room temperature and 950°.

Domain 1. The weight loss can be attributed to dehydratation of the precursors accompanied by the reduction of UO_3 to U_3O_8. The proposed chemical equations are

$$[3\ UO_3 \cdot 3/2\ Sb_2O_3] \rightarrow [U_3O_8 \cdot 3/2\ Sb_2O_3] + 1/2\ O_2 \text{ (precursor I)} \quad (1)$$

and

$$3\ [UO_3 \cdot 3/2\ Sb_2O_3] \rightarrow [U_3O_8 \cdot 9/2\ Sb_2O_3] + 1/2\ O_2 \text{ (precursor II)} \quad (2)$$

The theoretical weight losses, obtained from eqs. (1) and (2), respectively, 1.24 and 0.74%. These values are to be compared to the experimental ones, which are somewhat lower (0.9 and 0.59%). This indicates that only a partial reduction occurs in this temperature range, in good agreement with the results of

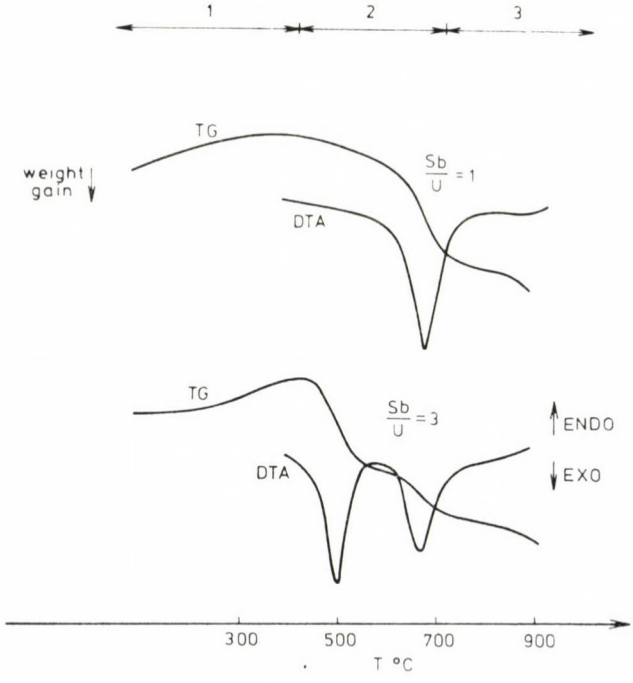

Fig. 1. TG-DTA curves for precursors I (Sb/U = 1) and II (Sb/U = 3) under air flow

Table I

TG-DTA *data for precursor I* (Sb/U = 1) *calcined under air flow*

Temperature range (°C)	Weight (%) loss (—) or gain (+)	DTA
(1) 50—450	—0.9	
(2) 450—705	—2.1	EXO (670 °C)
(3) 705—960	+1.2	

Table II

TG-DTA *data for precursor* II (Sb/U = 3) *calcined under air flow*

Temperature range (°C)	Weight (%) loss (—) or gain (+)	DTA
(1) 50—450	—0.59	
(2) 450—530	+2.03	EXO (500 °C)
530—690	+1.34	EXO (600 °C)
(3) 690—960	+0.94	

Grasselli and Suresh [2]. Actually the reaction becomes complete only at temperatures higher than 750 °C [8].

Domain 2. The weight and the exothermicity of the reaction are characteristic of an oxidation process. Only on exothermic peak is detected by DTA for precursor I, but two for precursor II. The different behaviours can be explained as follows.

In this temperature range, Sb_2O_3 can be oxidized to Sb_2O_4, which penetrates the lattice of uranium oxides to form $USbO_5$ mixed oxide.

For precursor I, these two reactions occur in combination and we can illustrate them by equations (3) and (4).

$$[UO_3 - 1/2Sb_2O_3] + 1/4\ O_2 \rightarrow [UO_3 - 1/2\ Sb_2O_4] \rightarrow USbO_5 \qquad (3)$$

$$2\ [U_3O_8 - 3/2\ Sb_2O_3] + 3/2\ O_2 \rightarrow 2\ [U_3O_8 - 3/2\ Sb_2O_4]$$

$$2\ [U_3O_8 - 3/2\ Sb_2O_4] + O_2 \rightarrow 6\ USbO_5$$

$$2\ [U_3O_8 - 3/2\ Sb_2O_3] + 5/2\ O_2 \rightarrow 6\ USbO_5 \qquad (4)$$

The corresponding theoretical weight gains are 1.85% (3) and 3.1% (4), respectively. The experimental value of 2.1% again suggests that only a partial reduction of UO_3 to U_3O_8 occurs.

In precursor II, Sb_2O_3 is in excess with respect to UO_3 and U_3O_8. The well defined transition in the 450—530 °C range corresponds to the oxidation of Sb_2O_3 in Sb_2O_4. This amount of Sb_2O_4 does not react directly to form $USbO_5$.

The second step, which occurs in the 530—690 °C range, can be attributed as for precursor I to the simultaneous oxidation of Sb_2O_3 and its penetration into the lattice of uranium oxides. Furthermore the second exothermic peak coincides with that of precursor I, confirming the above interpretation. At the end of this step, $USbO_5$ and the earlier formed Sb_2O_4 slowly react to produce USb_3O_{10}. A small amount of Sb_2O_4 is always found at the end of the calcination process, as revealed by XRD. The two steps can be described by equations (5) and (6):

$$[UO_3 \cdot 3/2\ Sb_2O_3] + \frac{3}{4} O_2 \rightarrow USbO_5 + Sb_2O_4 \tag{5}$$

$$\left[U_3O_8 \cdot \frac{9}{2} Sb_2O_3\right] + \frac{11}{4} O_2 \rightarrow 3\ USbO_5 + 3\ Sb_2O_4 \tag{6}$$

The experimental weight gain (3.37%) corresponds well to the theoretical values (3.32% from eq. 5; 4.08% from eq. 6).

Domain 3. At about 700 °C, the formation of USb_3O_{10} takes place, following the equation

$$USbO_5 + Sb_2O_4 + 1/2\ O_2 \rightarrow USb_3O_{10} \tag{7}$$

which describes the phenomenon for both precursors I and II.

For precursor I, we must assure that part of Sb_2O_4 produced in *domain 2* does not react immediately to form $USbO_5$, but reacts further with the produced $USbO_5$ to form USb_3O_{10}. Indeed, the experimental weight gain is not negligible (1.2%) compared to the theoretical value (2.14% for a complete reaction).

Moreover, the formation of USb_3O_{10} is rather slow, as evidenced by a continuous weight gain observed when precursor II is maintained at 900 °C. The experimental weight gain (1%), lower than the theoretical value, confirms this ascertainment. The proposed scheme for the formation of $USbO_5$ and USb_3O_{10} under air is illustrated in Fig. 2.

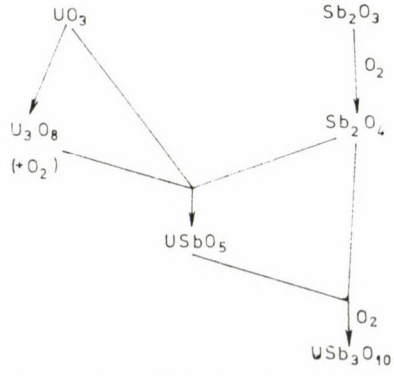

Fig. 2. Formation of $USbO_5$ and USb_3O_{10} under air

Calcination of the precursors I and II under nitrogen flow

The TG and DTA curves are presented in Fig. 3 and the numerical values are given in Tables III and IV.

The important weight loss, observed above 680 °C for both precursors is attributed to the sublimation of Sb_2O_3 under a non oxidizing (N_2) atmosphere.

The equations describing these losses are for precursors I and II, respectively,

$$3\left[UO_3 \cdot \frac{1}{2}Sb_2O_3\right] \rightarrow U_3O_8 + \frac{3}{2}Sb_2O\nearrow + \frac{1}{2}O_2\nearrow \quad (8)$$

$$3\left[UO_3 \cdot \frac{3}{2}Sb_2O_3\right] \rightarrow U_3O_8 + \frac{9}{2}Sb_2O_3\nearrow + \frac{1}{2}O\nearrow \quad (9)$$

The experimental values, 34.5% and 61.2%, respectively, for precursors I and II agree quite well with the theoretical predictions based on equations (8) and (9) (34.1% and 62%).

The sublimation of Sb_2O_3 occurs in two steps, which are easily distinguished in the case of precursor I. Part of Sb_2O_3 is probably stabilized by the other components present in the mixture with, as a consequence, an increase of its sublimation temperature. Indeed, under our conditions, a small amount of $USbO_5$ can always be detected at the end of the calcination. Therefore a small part of Sb_2O_3 is oxidized (either by residual oxygen, or oxygen stemming from the reduction of UO_3 into U_3O_8); this is clearly detected in the DTA curve of precursor I by the exothermic peak at 660 °C. In precursor II we must admit that the greater weight loss due to reduction hides the oxidation

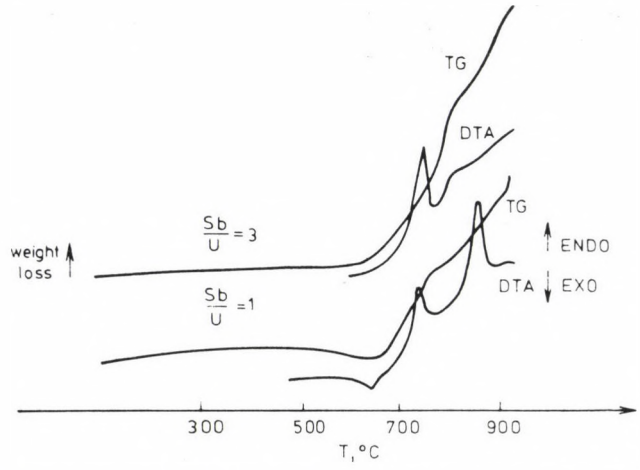

Fig. 3. TG-DTA curves for precursors I (Sb/U = 1) and II (Sb/U = 3) under nitrogen fow

Table III

TG-DTA *data for precursor* I (Sb/U = 1) *calcined under nitrogen flow*

Temperature range (°C)	Weight (%) loss (—) or gain (+)	DTA
(1) 50—485	—0.81	
(2) 485—680	+0.12	EXO (670 °C)
(3) 680—960	—34.5	ENDO (755 °C)
		ENDO (875 °C)

Table IV

TG-DTA *data for precursor* II (Sb/U = 3) *calcined under nitrogen flow*

Temperature range (°C)	Weight (%) loss (—) or gain (+)	DTA
290—960	—62	ENDO (770 °C)
		ENDO (860 °C)

process. It is important to mention, that USb_3O_{10} could never be detected (See below). This absence of USb_3O_{10} formation clearly demonstrates that $USbO_5$ is an intermediate step in the synthesis of this compound.

The proposed scheme of formation of $USbO_5$ under nitrogen is given in Fig. 4.

2. *Influence of calcination time on the concentration of various components*

Evolution of bulk content of $USbO_5$, USb_3O_{10} and Sb_2O_4 versus calcination time is followed by X-ray diffraction. The calcination is conducted at 900 °C under static or flowing air. The results are given in Figures 5, 6 and 7. The formation and decay of the different species was determined by the sub-

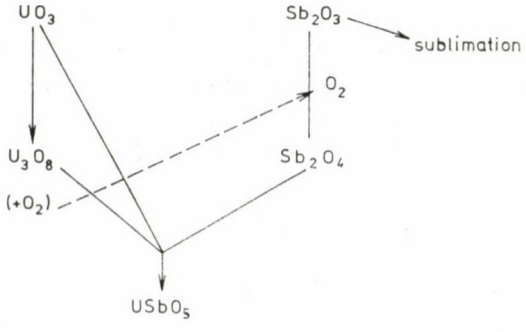

Fig. 4. Formation of $USbO_5$ under nitrogen atmosphere

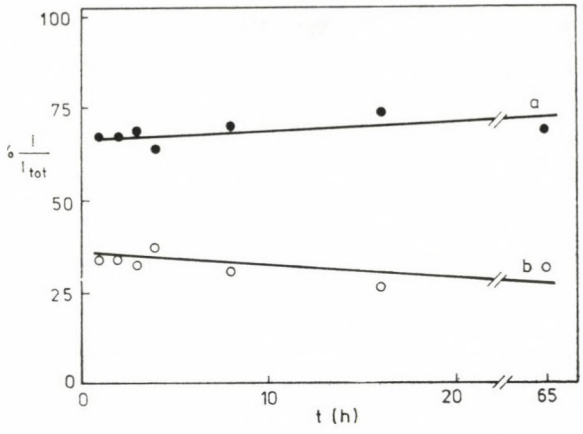

Fig. 5. Compositional makeup (by XRD) as a function of calcination time at 900 °C. Precursor I (Sb/U = 1(— air flow; a = USb_3O_{10}; b = $USbO_5$

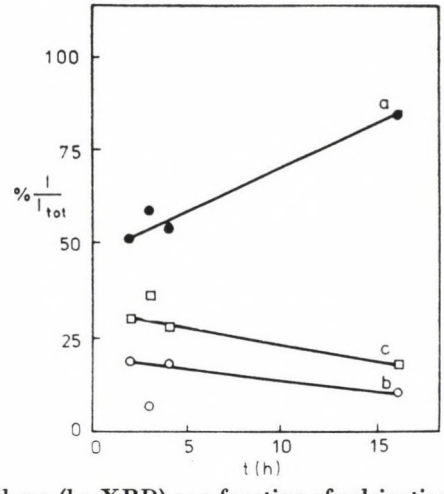

Fig. 6. Compositional makeup (by XRD) as a function of calcination time at 900 °C. Precursor II (Sb/U = 3) — static air; a = USb_3O_{10}; b = $USbO_5$; c = Sb_2O_4

sequent variation of the area ratio of the following diffraction lines: USb_3O_{10}, d = 3.18 Å; $USbO_5$, d = 3.26 Å; Sb_2O_4, d = 3.08 Å. We must keep in mind that this procedure allows one to evaluate the relative amounts of the various components but not their concentrations.

From the X-ray diffraction study, the following conclusions may be drawn.

Calcination of precursor I under static air

$USbO_5$ and USb_3O_{10} are detected, and diffraction lines are not well resolved for calcination times lower than 4h. In every case, $USbO_5$ is the major constituent.

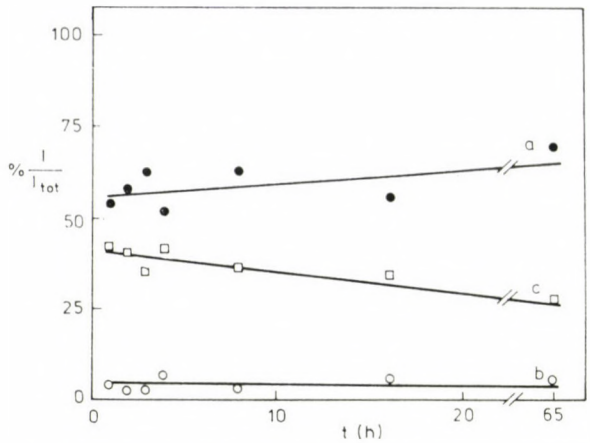

Fig. 7. Compositional makeup (by XRD) as a function of calcination time at 900 °C. Precursor II (Sb/U = 3) — air flow; a = USb_3O_{10}; b = $USbO_5$; c = Sb_2O_4

Calcination of precursor I under flowing air (Fig. 5)

As in the previous case, only $USbO_5$ and USb_3O_{10} are detected. But now USb_3O_{10} is the major constituent, and a slow transformation of $USbO_5$ into USb_3O_{10} is detectable.

Calcination of precursor II under static and flowing air (Figs 6 and 7)

$USbO_5$, USb_3O_{10} and Sb_2O_4 are detected in both cases. A continuous transformation of $USbO_5$ into USb_3O_{10} occurs with the calcination time. However the dynamic conditions (air flow) do affect the $USb_3O_{10}/USbO_5$ ratio by favouring the formation of USb_3O_{10} which is rather slow under static conditions.

In summary, for both precursors I and II we have evidenced a slow and continuous formation of USb_3O_{10}, the latter is favoured under flowing air condition. On the other hand, no maximum in the USb_3O_{10} concentration versus calcination time could be detected, when the precursor is calcined at 900 °C. We only observe a decomposition of USb_3O_{10} at 1100 °C, in a better agreement with Grasselli and Suresh [2] than with Delobel et al. [3] who detected a maximum USb_3O_{10} concentration after having maintained isothermally the residue at about 900 °C for 2—4 h. This time dependence was never reproduced in our preparation.

3. *Surface composition of the catalyst*

The evolution of Sb surface concentration versus calcination time under air flow is followed by XPS for precursors I and II. The results are compared with those obtained for pure $USbO_5$ and USb_3O_{10}.

Table V

Sb *surface concentration for pure* $USbO_5$ *and* USb_3O_{10} (XPS)

	$\left(\frac{Sb}{Sb+U}\right)\%_{exp.}$	$\left(\frac{Sb}{Sb+U}\right)\%_{theor.}$
USb_3O_{10}	80.4	75
$USbO_5$	49.5	50

The results for the latters are summarized in Table V. The agreement with theoretical expectations is excellent for $USbO_5$ and quite good for USb_3O_{10}. To explain the slight difference for the latter we must recall that pure USb_3O_{10} is prepared by dissolving the excess Sb_2O_4 in concentrated boiling HCl. It is possible that after this treatment, a thin layer of Sb_2O_4 always recovers the material. The resulting higher Sb surface concentration, not detected by X-ray diffraction, can be evidenced by XPS.

Atomic Sb surface concentrations, for both precursors I and II after various calcination times at 900 °C are presented in Fig. 8. For precursor II, we observe a slight decrease of the Sb concentration. This can be caused by sublimation of Sb_2O_4. At our calcination temperature, this process is very slow. It was reported to became effective only at 1100 °C under atmospheric pressure [9].

For precursor I, the Sb surface concentration is close to the one measured in pure USb_3O_{10} (75%). Following the XRD results, we would nevertheless expect an intermediate value between USb_3O_{10} and $USbO_5$ if no surface segregation occurred. It is therefore concluded that a pure USb_3O_{10} phase

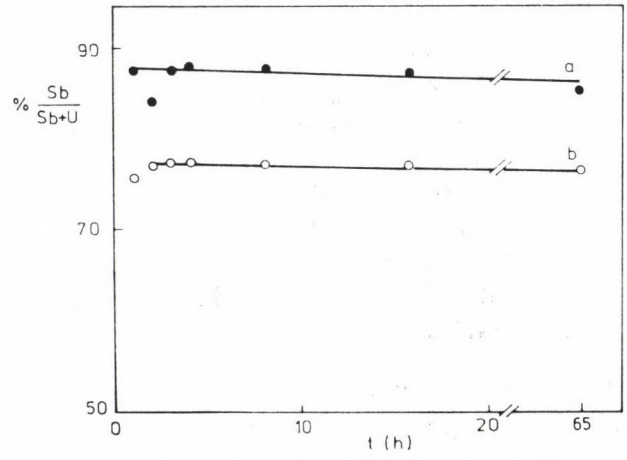

Fig. 8. Surface composition (by XPS) as a function of calcination time at 900 °C under air flow; a = precursor II; b = precursor I

Table VI

Widths of XPS Sb 3d *peaks* (eV) *for* USb_3O_{10}, Sb_2O_4 *and calcined precursor* II (Sb/U = 3)

	Sb $3d_{5/2}$	Sb $3d_{3/2}$
USb_3O_{10}	1.6	1.5
Sb_2O_4	1.8	1.7
Prec. II	1.7	1.6

recovers the catalyst. This finding is of paramount importance from a catalytic point of view. Recalling that the catalytic reactions of oxidation and ammoxidation of propene involve only the oxygen atoms standing in the outer monolayer of the catalysts [3], it is thus possible to prepare a selective catalyst starting with a Sb/U ratio equal to 1 if the calcination is conducted under air flow. $USbO_5$ leading to waste products in the catalytic process, is not disturbing because it mainly stands in the bulk of the particle.

For precursor II, the Sb surface concentration is always higher than that calculated for pure USb_3O_{10}. It was shown that the formation of USb_3O_{10} is never complete, even after a long calcination time. The excess of Sb concentration at the surface is due to Sb_2O_4. Indeed, an analysis of the Sb 3d lineshape reveals that the widths of Sb 3d lines are intermediate between those of pure USb_3O_{10} and pure Sb_2O_4 (Table VI), revealing the simultaneous presence of both materials. In order to obtain a better catalytic activity, it is necessary to remove the excess of Sb_2O_4, which does not exhibit interesting oxidative properties (no adsorption of hydrocarbons occurs on Sb_2O_4, see ref. [10]). This excess of Sb_2O_4 forms a layer at the surface of USb_3O_{10}, as revealed from HCl dissolution experiments; this explains the difficulty to obtain an outer layer of the particle made of pure USb_3O_{10}.

Conclusion

The preparation of USb_3O_{10} and $USbO_5$ mixed oxides was thoroughly investigated by thermal analysis, X-ray diffraction and XPS. TG-DTA data revealed that $USbO_5$ is an intermediate product in the formation of USb_3O_{10}, from a mixture of U and Sb oxides chosen as precursors. However, the formation of the former compound is independent of the initial Sb/U atomic ratio of the precursor.

XRD data showed that the transformation of $USbO_5$ into USb_3O_{10} is slow and is favoured for calcination under flowing air.

XPS analysis revealed that, after calcination of a precursor where Sb/U = = 1, the surface of the catalyst is recovered only by USb_3O_{10}, without any

trace of Sb_2O_4. It is possible to prepare the pure catalyst in a layered form. By contrast, the catalyst prepared by calcination of a precursor of Sb/U = 3, is mainly recovered by Sb_2O_4. These findings can be of paramount importance for the preparation of good and selective catalysts.

*

S. Maroie is grateful to NFSR (Belgium) for financial support.

REFERENCES

[1] Callahan, J. L., Gertisser, B. (Standard Oil Co.): U.S. Pat. 3, 198, 750 (Aug. 3, 1965); Callahan, J. L., Gertisser, B. (Standard Oil Co.): U.S. Pat. 3, 308, 151 (Mar 7, 1967)
[2] Grasselli, R. K., Suresh Dev, D.: J. Catal., **25,** 273 (1972)
[3] Delobel, R., Baussart, H., Leroy, J. M., Grimblot, J., Gengembre, L.: J. Chem. Soc. Faraday Trans. I, **79,** 879 (1983)
[4] Baussart, H., Delobel, R., Le Bras, M., Le Maguer, D., Leroy, J. M.: J. Chem. Soc. Faraday Trans. I, **78,** 485 (1982)
[5] Scofield, J. M.: J. Electr. Spectr., **8,** 129 (1976)
[6] Reilman, R. F., Mrezane, A., Manson, S. T.: J. Electr. Spectr., **8,** 389 (1976)
[7] Seah, M. P.: Surf. Interface Anal., **2,** 222 (1980)
[8] Pascal, P.: Nouveau Traité de Chimie Minérale, tome XI (Masson et Cie, Paris, 1958)
[9] Berry, F. J.: Adv. Catal., **30,** 97 (1981)
[10] Simons, Th. G., Houtman, P. N., Schuit, G. C. A.: J. Catal., **23,** 1 (1971)

Acta Chimica Hungarica 119 (2—3), pp. 179—183 (1985)

INTRA- AND INTERMOLECULAR METHYL-TRANSFER OF *m*-XYLENE ON H-ZEOLITES+

Imre BANKÓS, János PAPP and Dénes KALLÓ*

(Central Research Institute for Chemistry, Hungarian Academy of Sciences, H-1525 Budapest, P.O. Box 17)

Received June 8, 1984
Accepted for publication September 6, 1984

The isomerization (I) and disproportionation (D) of *m*-xylene was studied on acidic zeolite catalysts of different structures, namely on H-ZSM-5, H-Y, FAU and H-MOR. Pronounced shape selectivity on the H-ZSM-5 catalyst was clearly demonstrated by the high I/D and *p*-xylene/*o*-xylene ratios. Under the given experimental conditions bimolecular reaction results mainly in disproportionation with the exception of mordenite catalyst, where in the intermolecular reaction isomerization is preferred.

Introduction

Xylene isomerization proceed on acidic solid catalysts both through intramolecular and intermolecular methyl transfer [1]. The reaction pathways are different.

Carbenium ions formed by proton addition to the aromatic nucleus on the acidic sites, and 1, 2 methyl shift takes place in the aryl carbenium ion resulting in monomolecular isomerization [2].

Hydride abstraction may proceed also on stronger acidic sites [3], and methyl-benzylic cations forms which reacts with xylene resulting diaryl methane intermediate, which decomposes either to xylene isomers or to toluene and trimethyl benzene. Bimolecular isomerization and disproportionation thus take place simultaneously. Xylene disproportionation can thus be suppressed by inhibiting the formation of diaryl methane intermediates. To attain this the following methods can be used:

1. Application of zeolite catalysts with pores in which the large diaryl methane intermediates can not be formed.

2. The formation of methyl-benzylic cation precursors is impeded:

a) by poisoning or eliminating the strongest acidic sites capable of hydride abstraction from the methyl group [4],

b) by increasing the partial pressure of hydrogen which shifts back the equilibrium of hydride abstraction reaction (see ref. [5]),

+ This paper was presented at the 2nd Belgian—Hungarian Colloquium on Catalysis at De Haan, Belgium, October 10—13, 1983.

* To whom correspondence should be addressed.

c) by adding iso-paraffin in "catalytic amounts" and thus the formation of less stable primary methyl benzylic cation is suppressed by more stable tertiary carbenium ions.

We investigated the isomerization (I) and disproportionation (D) of *m*-xylene similarly to Gnep and co-workers [6] on H-ZSM-5, H-MOR, H-Y, FAU i.e. on H-zeolite catalysts of different structure and acidity.

The change of I/D ratio for the three catalysts of different character and the effect of hydrogen on the selectivity will be discussed.

Experimental

The catalytic measurements were carried out at 623 K for H-Y, FAU after having stabilized the activity, at 623 K for H-ZSM-5 the activity of which did not change with time and at 543, 563 K for H-MOR where no deactivation could be observed at all, in contrary to higher temperature where its deactivation is very fast [6]. The total pressure was 2.0 MPa. The partial pressure of hydrogen was 1.0, 1.5, 1.71 and 1.85 MPa. *m*-Xylene was fed into a flow reactor filled with 1.5 g catalyst at a rate between 2 and 10 mL/h. The product was cooled and separated into gas and liquid phases. The liquid product was analyzed by GC.

Synthetic Na-MOR (Norton Co., USA) and Na-ZSM-5 (produced in GDR) were exchanged for ammonium and deammoniated at higher temperature in the reactor. The third catalyst sample was H-Y, FAU (EKA AB, Sweden). Zeolite powders were pelletized without binder. After crushing and sieving the grain fraction of 0.8—1.25 mm was used as catalyst.

Results and Discussion

Conversion up to the thermodynamic equilibrium for *m*-xylene isomerization could be achieved under reaction conditions given above. In Figs 1a and 1b the experimentally determined conversion curves are shown for H-ZSM-5 and H-Y, FAU, respectively. Figure 1 and more clearly the data in Table I unambiguously demonstrate the pronounced dependence of the product distribution, i.e. isomerization/disproportionation ratio (I/D) and *p*-xylene/*o*-xylene formation on the type of zeolite. The disproportionation was considerable and nearly equal amounts of *o*- and *p*-xylene formed on H-Y, FAU. On H-ZSM-5 the I/D ratio is, however, by one order of magnitude higher and the formation of *p*-xylene is more favourable. All these observations can be explained by the theory of shape selectivity recognized by Weisz [8] and developed by Csicsery [9]. Both zeolites have three dimensional pore system. The critical pore sizes are, however, different: for H-Y, FAU 0.74 nm, for H-ZSM-5 0.54×0.56 and 0.51×0.55 nm [10]. These pore size differences are responsible for the differences in selectivities. The formation of large diaryl methane intermediate is inhibited in H-ZSM-5 whereas in H-Y, FAU not. Disproportionation takes place presumably on the outer crystal surface of the former. In H-ZSM-5 the mobility of *p*-xylene with a critical diameter of 0.67 nm is appreciably greater than of *m*-xylene which was a critical diameter of 0.74 nm.

Disproportionation is plotted against isomerization in Fig. 2. Although selectivities are very different for the three catalysts, a general tendency can be observed. The disproportionation increases with the isomerization conversion far above linearity, i.e. by increasing the space time the I/D ratio decreases (see data in Table I). Different reaction order for disproportionation and isomerization can thus be concluded.

In the case of H-zeolites not only the accessibility of acid sites or with other words the steric factors are decisive in the catalytic behaviour (life time, selectivity, etc.) but also the strength of acid sites.

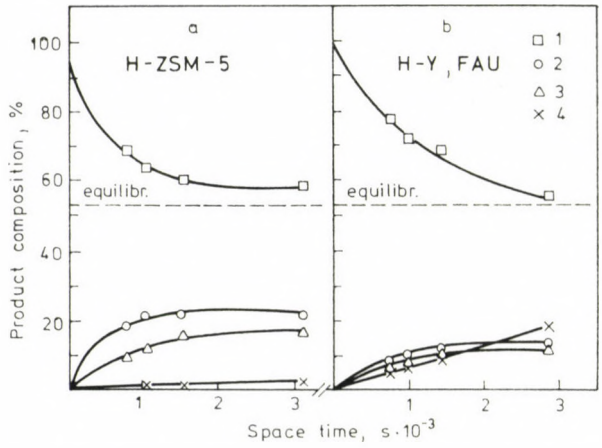

Fig. 1. Selectivity of *m*-xylene transformation on H-ZSM-5 and H-Y, FAU catalysts. Conversion isotherms of *m*-xylene (1), *p*-xylene (2), *o*-xylene (3) and disproportionation products (4). Reaction conditions: 623 K; $P = 2.0$ MPa, $p_{m-x} = 0.5$ MPa

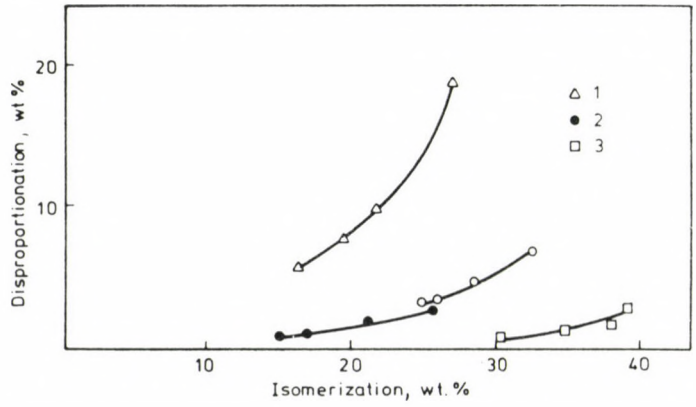

Fig. 2. Selectivity of *m*-xylene transformation on H-Y, FAU at 623 K (1), on H-MOR at 543 K (2), at 563 K (*o*), on H-ZSM-5 at 623 K (3); $P = 2.0$ MPa, $p_{m-x} = 0.5$ MPa

The acid strength of the three catalysts studied can be characterized by the isosteric adsorption heat of ammonia. The greater is its negative value the stronger is the average acidity of the sites. These are —158, —138, —120 kJ mol^{-1} for H-ZSM-5, H-MOR, H-Y, FAU respectively [11]. Acid sites active

Table I

The ratio of isomerization (I) *to disproportionation* (D) *conversions, and the ratio of p-xylene to o-xylene formation as a function of space velocity* (LHSV, h^{-1})

Catalysts		LSHV [h^{-1}]			
		1.1	2.5	3.6	4.7
H-Y, FAU	I/D	1.46	2.28	2.55	2.88
	$\frac{p-x}{o-x}$	1.17	1.17	1.19	1.14
H-MOR	I/D	4.8	11.20	14.30	20.80
	$\frac{p-x}{o-x}$	1.31	1.29	1.29	1.28
H-ZSM-5	I/D	14.0	22.5	32.16	37.8
	$\frac{p-x}{o-x}$	1.73	2.52	2.51	2.54

In thermodynamic equilibrium at 623 K $p-x/o-x = 1.018$ [7]. Reaction conditions are the same as in Fig. 1, the temperature for H-MOR is 563 K.

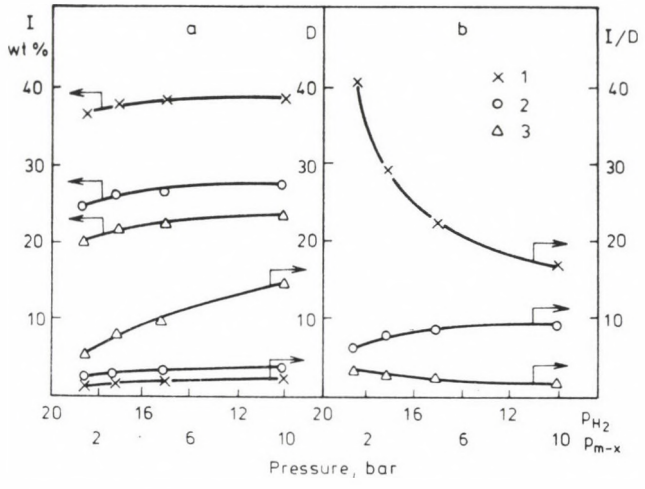

Fig. 3. Isomerization (I), Disproportionation (D) conversions and the ratio of isomerization to disproportionation as a function of partial pressure of hydrogen on H-ZSM-5 at 623 K (1), on H-MOR at 563 K (2), on H-Y, FAU at 623 K (3), LHSV = 2.5 h^{-1}

for disproportionation, i.e. on which hydride abstraction may proceed are present on all the samples but in different numbers. Therefore, xylene disproportionation has been slowed down on all samples by increasing the partial pressure of hydrogen. Increasing p_{m-x} and simultaneously decreasing p_{H_2} both the isomerization and the disproportionation conversions increases (Fig. 3a). The selectivity changes are, however, different (Fig. 3b): I/D ratio decreases for H-ZSM-5 and at the same rate for H-Y, FAU whereas it increases for H-MOR. If isomerization increases less than disproportionation with increasing p_{m-x} and decreasing p_{H_2} (i) its unimolecular route dominates, and (ii) the active sites of weaker acidity are almost completely covered by π-complexes at even low *m*-xylene partial pressures. When, however, I/D increases as for H-MOR (i) bimolecular isomerization seems probable, and/or (ii) the coverage with π-complexes increases with p_{m-x}.

In order to avoid the complex effects of antibate changes of partial pressures p_{m-x} and p_{H_2}, experiments were carried out on each sample at 0.5 MPa p_{m-x} when p_{H_2} was in turn 1.0, 2.0, 3.0 MPa. The increase of p_{H_2} resulted in decreasing disproportionation conversion for all catalyst samples. The suppression of the disproportionation by hydrogen is a proof the hydride abstraction equilibrated reaction.

REFERENCES

[1] Allem, R. H., Yats, L. D., Erley, D. S.: J. Am. Chem. Soc., **82,** 853 (1960)
[2] Lien, A. P., McCauley, S. A.: J. Am. Chem. Soc., **74,** 6246 (1952)
[3] Poutsma, M. L.: Zeolite Chemistry and Catalysis, Ed. J. A. Rabo ACS Monograph 171, Washington, 1976, p. 437
[4] Ratnasamy, R., Sivasankar, S., Vishnoi, S.: J. Catal. **69,** 428 (1981)
[5] Gnep, N. S., Guisnet, M.: Appl. Catal., **1,** 329 (1981)
[6] Gnep, N. S., Tejada, J., Gusinet, M.: Bull. Soc. Chim. France, **1982,** No 1—2
[7] Szakács, S., Papp, J., Lejtovicz, J., Kalló, D.: React. Kinet. Catal. Lett., **21,** 365 (1982)
[8] Weisz, P. B., Frilette, V. J.: J. Phys. Chem., **64,** 382 (1960)
[9] Csicsery, S. M.: "Zeolite Chemistry and Catalysis" Ed. Rabo, J. ACS Monograph 171, Washington, 1975. p. 680
[10] Meier, W. M., Olson, D. H.: Atlas of Zeolite Structure Types, Structures Comission of the International Zeolite Association, Zürich, 1978
[11] Auroux, A., Bolis, V., Wierzchowski, P., Gravelle, P. C., Vedrine, J. C.: J. Chem. Soc., Faraday Trans. I., **75,** 2544 (1979)

Acta Chimica Hungarica 119 (2—3), pp. 185—192 (1985)

HYDROGENATION OF ETHYLENE BY $Pt/H_xVMoO_{5.5}$ BRONZES OBTAINED BY HYDROGEN SPILLOVER+

Colette ANCION and Georges PONCELET*

(Groupe de Physico-Chimie Minérale et de Catalyse, Université Catholique de Louvain, Place Croix du Sud 1, B-1348 Louvain-La-Neuve, Belgium)

Received June 8, 1984
Accepted for publication September 6, 1984

A crystalline mixed molybdenum-vanadium oxide with composition $VMoO_{5.5}$, prepared by thermal decomposition of an oxalic precursor, was impregnated with a platinum salt and exposed to molecular hydrogen. The resulting hydrogen bronze, $H_xVMoO_{5.5}$, was put in contact with ethylene and the formation of ethane was followed as a function of time, at several temperatures and for different insertion rates. The total amount of hydrogen given to the accepting molecule is higher for the mixed bronze than for either the pure H_xMoO_3 and $H_xV_2O_5$ bronzes.

Introduction

The term "bronze" has been given to a class of compounds with general formula M_xTO_n where M is an alkaline or alkaline earth element and TO_n, a transition metal oxide.

Recently, increased attention has been paid to those bronzes where the inserted element is atomic hydrogen. The most thoroughly investigated bronzes have been H_xWO_3, H_xMoO_3 and, more recently, $H_xV_2O_5$.

Three methods of preparation of hydrogen bronzes have been reported in the literature: the wet chemical method, in which nascent hydrogen is generated in the presence of the oxide [1, 2]; the electrochemical approach, through cathodic reduction in aqueous solution, and the hydrogen spillover method [3—7]. In this last method, molecular hydrogen is dissociated on Pt particles deposited on the surface of the oxide and the H atoms invade the host lattice, according to the so-called spillover process.

The mechanism of formation of those bronzes and their physical and chemical properties have been described by several authors [8—22].

Recently, these bronzes have been used as hydrogen reservoirs to carry out hydrogenation of alkenes, the hydrogen being re-donated to the accepting molecule by a "reverse spillover" process [23].

The present study aims to report preliminary results obtained on a mixed hydrogen vanadium molybdenum bronze prepared by spillover.

+ This paper was presented at the 2nd Belgian—Hungarian Colloquium on Catalysis at De Haan, Belgium, October 10—13, 1983.

* To whom correspondence should be addressed.

Experimental

Preparation of the mixed oxide

The mixed oxide phase $VMoO_{5\cdot5}$ has been prepared using the following procedure : 5.14 g of ammonium metavanadate is dissolved in 1 liter of a 0.15 *M* oxalic acid solution. After complete dissolution, 7.2 g of ammonium heptamolybdate is added. The V/Mo atomic ratio in the final solution is 1.077.

The volume of the solution is reduced by evaporation on a sand bath until the volume is approximately 200 mL. The resulting slurry is then freeze-dried and the powder obtained is calcined at 400 °C for 48 h under air. Under these conditions, the organic content is oxidized, yielding a well-crystallized solid. A few other mixtures with a diffreent molar percentages of MoO_3 in the final solution between 50 and 75% were prepared and treated in a similar way.

Characterization

The X-ray diffraction patterns of the solids with different compositions of V-Mo, prepared using the procedure described, above, are illustrated in Fig. 1.

This figure shows that $VMoO_{5\cdot5}$ is obtained as a pure phase from the mixtures containing 65 and 66.7 mol % $M.O_3$. For higher and lower molar percentages the X-ray diagrams show additional peaks due either to MoO_3 or to V_2O_5.

Figure 2 compares the diagram of the so-called $VMoO_{5\cdot5}$ (as established from the chemical analysis data [24] to that of $V_9Mo_6O_{40}$ synthesized by fusion at 650 °C of a V_2O_5—MoO_3 mixture, according to the method of Jarhman et al. [25]. The X-ray peaks are located at the same diffraction angles but they have different relative intensities. The values of the interplanar distances, indexes and lattice parameters of $VMoO_{5.5}$ have been reported elsewhere [24]. All the results given hereafter were obtained with the pure $VMoO_{5.5}$ phase, i.e. prepared from the mixture containing 65 mol % MoO_3.

Formation of the hydrogen bronze

The formation of the bronze and the hydrogenation reactions with ethylene were carried out in a recirculation glass apparatus.

$VMoO_{5.5}$ was impregnated according to the method described elsewhere [26] with an amount of $H_2PtCl_6 \cdot 6\ H_2O$, such that 1% Pt was deposited on the surface. The impregnated oxide was heated at 200 °C for 2 h in vacuum in order to decompose the salt, and then was put in contact with 200 torr of hydrogen at 60 °C. The platinum was reduced and the atoms invaded the oxide lattice. The pressure drop was measured and the consumption of hydrogen was assigned to the bronze formation, the amount corresponding to reduction of $Pt^{4+} \rightarrow Pt^{\circ}$ being negligible with respect to the amount of hydrogen inserted in the oxide lattice.

At the end of the insertion, the temperature was reduced to 25 °C and the excess hydrogen evacuated. Ethylene was then introduced (approximately 50 torr) and the temperature of the reactor adjusted to the desired value. The reaction was followed by analyzing at intervals of time the composition of the gas phase, using a gas chromatograph.

At the end of the reaction, the apparatus was evacuated and the bronze back-titrated at 60 °C with hydrogen (200 torr).

Expression of the results

x, the insertion rate, is given by the number of m at g of H inserted per mole of the oxide.

The kinetic curves are represented by the number of millimoles of ethane produced per g of oxide (nC_2H_6/g) as a function of time.

Results

Bronze formation

Figure 3 shows the evolution of the hydrogen taken up by $Pt/VMoO_{5.5}$ versus time. The different curves correspond to the kinetics established for the same Pt-impregnated oxide but at different time intervals between

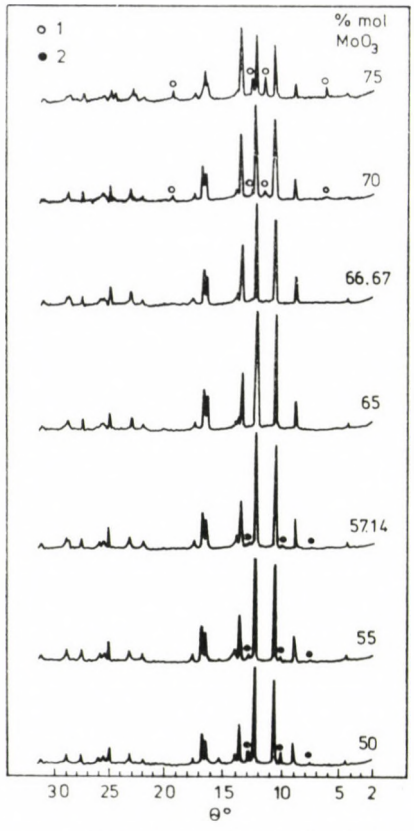

Fig. 1. X-ray diffraction patterns of the mixed phases obtained from mixtures with different compositions (1: MoO_3; 2: V_2O_5)

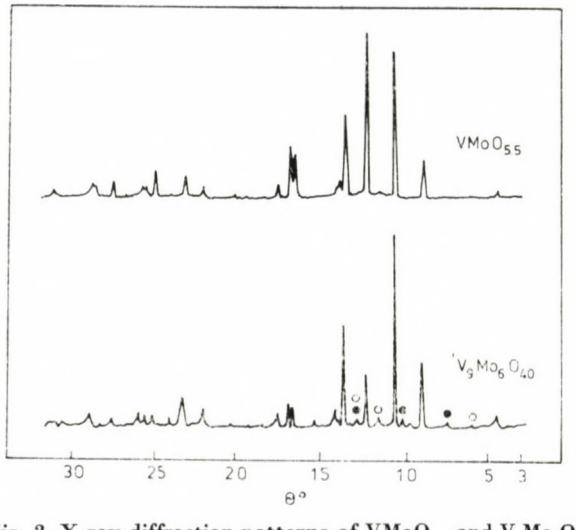

Fig. 2. X-ray diffraction patterns of $VMoO_{5.5}$ and $V_9Mo_6O_{40}$

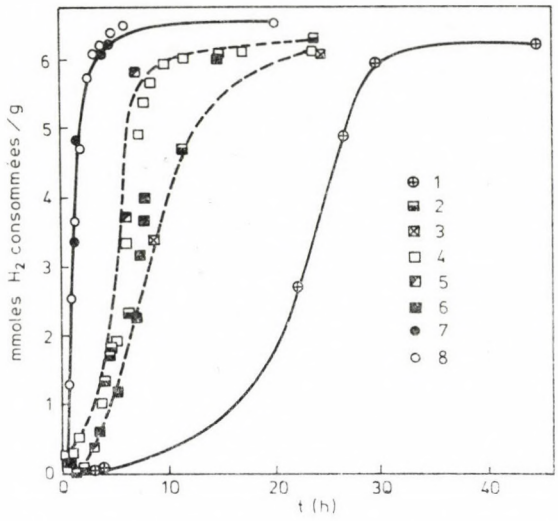

Fig. 3. Kinetics of hydrogen insertion observed at different time intervals between the impregnation and the formation of the bronze : 1: 1 day; 2: 12 days; 3: 15 days; 4: 18 days; 5: 20 days; 6: 75 days; 7: 126 days; 8: 262 days

the impregnation step and the formation of the bronze. If the interval is one day, the bronze is completely formed after 40 h; when the insertion is carried out 18 days after the impregnation, then the insertion is completed within 10 h.

This observation has not been yet explained. The X-ray diagrams do not show any perceptible structural modification occurring with increasing time between impregnation and insertion. However, this does not rule out possible local surface modifications (interactions, better dispersion) induced by the Pt salt, which cannot be picked up by this technique. Surface spectroscopic techniques like ESCA might clear up this point.

The maximum insertion rate reached for $H_xVMoO_{5.5}$ is 3.2, which is to be compared with 1.6, in H_xMoO_3 [27] and 3.65, in the $H_xV_2O_5$ [26] prepared in a similar way.

Recovery of the occluded hydrogen

A fraction of the hydrogen dissolved in the oxide lattice is very labile. We have found that around 10% of the total hydrogen content can be removed by treating the bronze at 60 °C under high vacuum.

During the hydrogenation of ethylene, molecular hydrogen is found in the gas phase; the higher the reation temperature, the larger being the amount.

Figure 4 shows the evolution of the ethane produced as a function of time for 3 different initial ethylene pressures ($P^i_{C_2H_4}$, in torr). In spite of the

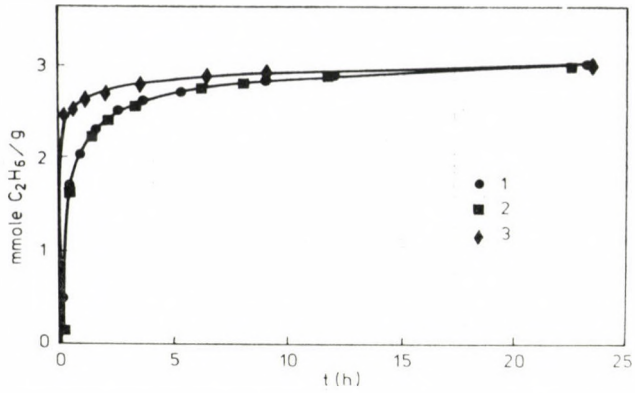

Fig. 4. Influence of the initial pressure of ethylene ($P^i_{C_2H_4}$) on the production of ethane: 1: 51 torr; 2: 84 torr; 3: 138 torr

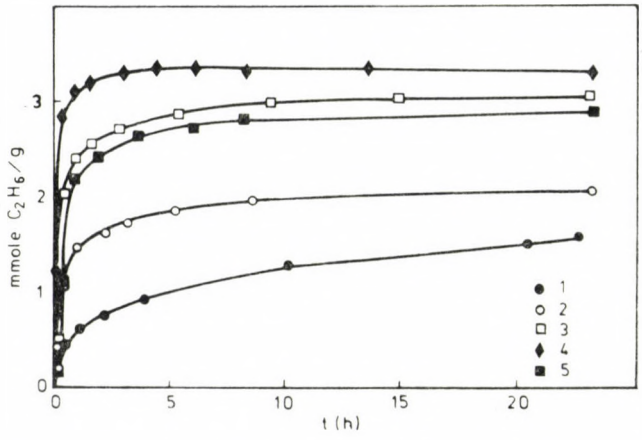

Fig. 5. Influence of temperature on the formation of ethane: 1: 40 °C; 2: 60 °C; 3: 120 °C; 4: 150 °C; 5: 180 °C

differences observed during the first period of the reaction, the final amounts of C_2H_6 produced are identical. These results indicate, as was the case for $H_{1.6}MoO_3$ [27] and $H_{3.6}V_2O_5$ [26], that the reaction order with respect to the ethylene pressure is zero.

The kinetic curves of ethane production at different temperatures are shown in Figure 5. The amount of ethane at the plateau passes through a maximum at a reaction temperature of 150 °C. At higher temperatures less ethane is formed but H_2O and CH_4 are also produced.

The amounts of hydrogen reinserted during back-titration with hydrogen are slightly higher than the corresponding quantities of ethane produced.

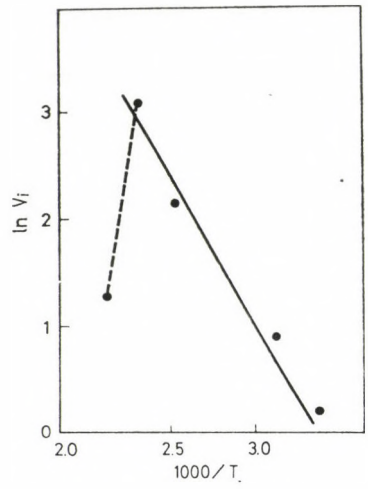

Fig. 6. Arrhenius plot for the conversion of ethylene into ethane

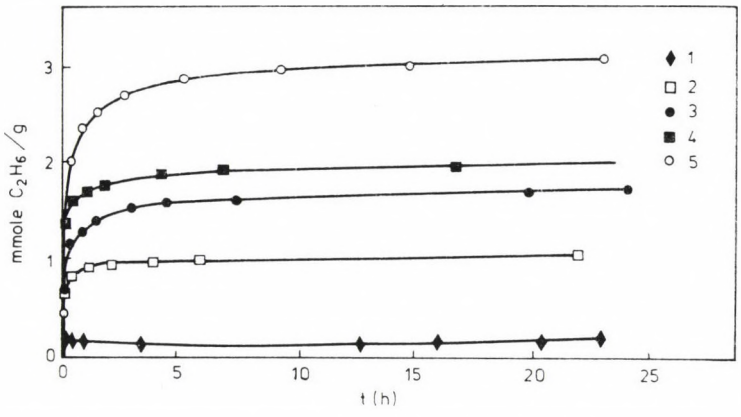

Fig. 7. Kinetics of ethane production at 120 °C ($P^i_{C_2H_4} = 50$ torr) for bronzes with different insertion rates: 1: 0.578; 2: 1.249; 3: 1.897; 4: 2.291; 5: 3.072

The activation energy has been calculated from the Arrhenius' plot, as illustrated in Fig. 6, where V^i, the initial rates of hydrogenation of ethylene have been determined graphically.

The calculated value of E_A is 6.4 kcal/mole in the temperature range between 40 and 150 °C. The corresponding values obtained under similar conditions in $H_xV_2O_5$ and H_xMoO_3 are 12.3 and 16.4 kcal/mole, respectively [27, 26].

As can be expected from Fig. 5, the value corresponding to the reaction performed at 180 °C does not obey the linear relationship.

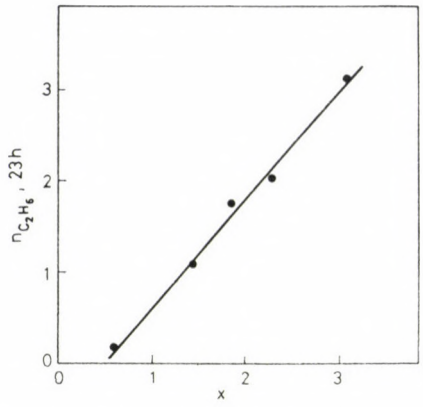

Fig. 8. Relationship between the ethane formed after 23 h at 120 °C, $n_{C_2H_6}$ (mmoles/g) and x (matg H/mmole of oxide)

In another set of experiments, we have investigated the influence of x_{in} on the recovery of hydrogen in the presence of ethylene.

Accordingly, bronzes with initial insertion rates of 0.578, 1.249, 1.897, 2.291 and 3.072 were prepared following the usual procedure and put into contact with ethylene ($P^i_{C_2H_4} \simeq 50$ torr) at 120 °C. The evolution of the ethane produced versus reaction time is shown in Fig. 7. If the amounts of C_2H_6 observed after 23 h of reaction are plotted against x_{in}, a linear relationship is obtained, as illustrated in Fig. 8. The extrapolation of this relationship to $nC_2H_6 = 0$ gives a x_{in} value of 0.5. This might correspond to the fraction of the inserted hydrogen that is irreversibly fixed in the oxide lattice.

The fraction of hydrogen given back by the bronze at the end of the reaction represents 40 to 44% of the total hydrogen content of the freshly prepared bronze, for $x_{in} \geq 1.25$. Only 15% is recovered when $x_{in} = 0.578$.

This fraction (40%) is significantly larger than that found for $H_xV_2O_5$, for which values of 20% and 30% were reported from experiments carried out at 120 and 160 °C, respectively [26]. Still lower figures were reported for H_xMoO_3 [27].

In conclusions, the mixed oxide $VMoO_{5.5}$ is able to form a hydrogen bronze $Pt/H_xVMoO_{5.5}$ with a x value of 3.2. In the presence of ethylene, over 40% of the total hydrogen inserted is given back, which is higher than the fractions recovered for either of the pure bronzes $H_{1.6}MoO_3$ and $H_{3.6}V_2O_5$.

*

C.A. is indebted to I.R.S.I.A. for a doctoral grant. The authors gratefully acknowledge a financial support from SP.P.P.S. (Service de Programmation de la Politique Scientifique).

REFERENCES

[1] Glemser, O., Lutz, G.: Z. Anorg. Allg. Chem., **264,** 17 (1951)
[2] Birtill, J. J., Dickens, P. G.: J. Solid State Chem., **29,** 367 (1979)
[3] Khoobiar, S.: J. Phys. Chem., **68,** 411 (1964)
[4] Kohn, H. W., Boudart, M.: J. Catal., **32,** 304 (1964)
[5] Bond, G. C., Tripathi, J. B. P.: J. Less Common Met., **36,** 31 (1974)
[6] Sermon, P. A., Bond, G. C.: Trans. Faraday Soc., **72,** 770 (1976)
[7] Bond, G. C., Tripathi, J. B. P.: Trans. Faraday Soc., **72,** 933 (1976)
[8] Vannice, M. A., Boudart, M., Fripiat, J. J.: J. Catal., **17,** 359 (1970)
[9] Dickens, P. G., Moore, J. H., Neil, N. H.: J. Solid State Chem., **7,** 241 (1973)
[10] Wiseman, P. J., Dickens, P. G.: J. Solid State Chem., **6,** 377 (1973)
[11] Dickens, P. G., Murphy, D. J., Halstead, T. K.: J. Solid State Chem., **6,** 370 (1973)
[12] Wright, C. J.: J. Solid State Chem., **20,** 89 (1977)
[13] Cirillo, A., Fripiat, J. J.: J. Phys. (Paris), **39,** 247 (1978)
[14] Birtill, J. J., Dickens, P. G.: Mater. Res. Bull., **13,** 311 (1978)
[15] Dickens, P. G., Birtill, J. J., Wright, C. J.: J. Solid State Chem., **28,** 185 (1979)
[16] Tinet, D., Canesson, P., Estrade, H., Fripiat, J. J.: J. Phys. Chem. Solids, **41,** 583 (1979)
[17] Tinet, D., Fripiat, J. J.: J. Chim. Phys., **76,** 867 (1979)
[18] Schöllhorn, R.: Angew, Chem. Int. Ed. Engl., **19,** 983 (1980)
[19] Taylor, R. E., Silva-Crawford, M. M., Gerstein, B. C.: J. Catal., **62,** 401 (1980)
[20] Taylor, R. E., Ryan, L. M., Tindall, P., Gerstein, B. C.: J. Chem. Phys., **73,** 5500 (1980)
[21] Slade, R. C. T., Halstead, T. K., Dickens, P. G.: J. Solid State Chem., **34,** 183 (1980)
[22] Cirillo, A. C., Ryan, L., Gerstein, B. C., Fripiat, J. J.: J. Chem. Phys., **73,** 3060 (1980)
[23] Sermon, P. A., Bond, G. C.: Catal. Rev. Sci. Eng., **8,** 211 (1973)
[24] Ancion, C., Marcq, J. P., Poncelet, G., Kéravis, D., Gatineau, L., Fripiat, J. J.: C. R. Acad. Sc. Paris, **296,** 1509 (1983)
[25] Jarhman, R. H., Dickens, P. G., Jacobson, A. J.: Mater. Res. Bull., **17,** 325 (1982)
[26] Marcq, J. P., Poncelet, G., Fripiat, J. J.: J. Catal., **87,** 339 (1984)
[27] Marcq, J. P., Wispenninckx, X., Poncelet, G., Kéravis, D., Fripiat, J. J.: J. Catal., **73,** 309 (1982)

Acta Chimica Hungarica 119 (2—3), pp. 193—202 (1985)

THE V_6O_{13}(001) SURFACE STUDIED BY LEIS+

Jean Paul LANDUYT*, Roger DE GRYSE and Joost VENNIK

(Laboratorium voor Kristallografie en Studie van de Vaste Stof, Rijksuniversiteit Gent, Krijgslaan, 281, B-9000 Gent, Belgium)

Received June 8, 1984
Accepted for publication September 6, 1984

A LEIS study of the V_6O_{13}(001) surface will be presented as a function of oxygen coverage. The experiments to be discussed are performed on both V_6O_{13} single crystals or on freshly cleaved and converted (reduced) V_2O_5 samples. It is shown that under UHV conditions (O_2 partial pressure $\ll 10^{-8}$ Pa and at temperatures around 750 K, the topmost layer of the stable V_6O_{13}(001) surface is a mixed V—O layer. The oxygen layer as it appears on the converted V_2O_5 sample or after adsorption from the gas phase, has to be considered as an absorbed phase, rather than a regular lattice oxygen. Consequently, the vanadium atoms of the topmost V—O layer at the V_6O_{13} surface can be considered to represent adsorption-desorption sites for atomic oxygen.

An important potassium surface segregation was also observed and investigated by means of LEIS and SIMS experiments. Auger spectroscopy proves to be very unsensitive in detecting this segregation. From the same study, it follows that the most probable potassium site of the V_6O_{13}(001) surface is an interstitial site close to or within the topmost V—O layer.

Introduction

V_6O_{13} is one of the lower oxides which are liable to determine the selectivity and activity of V_2O_5 based catalysts [1—3]. It is generally accepted that the surface vanadyl oxygen is the active species. In search for direct physical evidence for its presence and role at the surface, a LEIS (Low Energy Ion Scattering) study of the V_6O_{13} (001)-surface has been performed at elevated temperatures ($T = 750$ K). Indeed, due to its high surface sensitivity, LEIS offers attractive and unique perspectives to tackle this type of problems.

It is shown that vanadyl sites are present on top of the vanadium atoms of the outermost VO layer. These sites become populated at a significently high partial pressure of oxygen or during the initial state of the transition $V_2O_5 \rightarrow V_6O_{13}$.

During this study a surface segregation of potassium was observed. As potassium is frequently added to industrial V_2O_5-based catalysts, this surface segregation might be of interest for the catalytical behaviour of the V_2O_5/V_6O_{13} system. The experimental evidence for this segregation and a model for the surface structure with incorporated potassium are presented.

+ This paper was presented at the 2nd Belgian—Hungarian Colloquium on Catalysis at De Haan, Belgium, October 10—13, 1983.

* To whom correspondence should be addressed.

Experimental

The experiments are performed using a home-built angular dependent LEIS apparatus. The ion source is equipped with a Wien-type mass-filter. The sample is mounted on a manipulator allowing the adjustment of both the angle of incidence ψ and the azimuth φ. The 127° electrostatic energy analyzer can be rotated around the sample, defining in this way the total scattering angle Θ. The sample can be heated indirectly up to $\pm$1000 K. The temperature is monitored with a thermocouple in direct contact with the sample.

In order to obtain meaningful results, the experimental conditions had to be chosen in such a way the radiation damage is annealed continuously. Most of the experiments were performed at 750 K; in this way LEED did not show any deterioration of the V_6O_{13} surface structure. As reported in the literature [8], similar experiments performed on Ni single crystals, show that due to the continuous surface recovery, at least short range order remains unaltered under the effect of ion bombardment.

The choice of this temperature range is not detrimental to the interpretation of the results. Indeed the catalytic processes take place in the same temperature range.

The experiments were carried out using V_6O_{13} single crystals of two different origins. The first kind is obtained by the topotactical growth of a V_6O_{13} layer on top of a freshly cleaved (in situ) V_2O_5 crystal. The growth (reduction) of this V_2O_{15} layer is initiated by ion irradiation and proceeds spontaneously under the given circumstances of temperature and ambient pressure (UHV). These (V_6O_{13}) single crystals, grown by a chemical vapour deposition method, were used. Both kinds of samples reveal essentially the same LEIS spectra and the same LEED periodicity.

Vanadyl sites at the V_6O_{13}(001)-surface

In the *c*-direction the V_6O_{13} lattice can be considered as a stacking of alternatively pure oxygen (O) and mixed vanadium—oxygen (VO) layers in the following way ... VO—VO—O—VO—O—VO—VO— ... [4]. Figure 1 illustrates the structure of such a VO layer. The results of the following LEIS experiments allow us to determine how this sequence is terminated at the surface, as is explained elsewhere [5] in more detail.

Presence of vanadyl sites at the surface

Figure 2a shows the LEIS spectrum of a V_2O_5 sample immediately after starting the transition $V_2O_5 \rightarrow V_6O_{13}$. Two contributions are observed in this spectrum, a peak due to single scattering from oxygen and an other one, corresponding to double scattering phenomena along oxygen chains. It can be concluded that at a freshly cleaved (in situ) and converted sample the vanadium atoms are screened. Since for a free and unhindered vanadium atom, one expects the scattering cross section to be larger than for oxygen, the vanadium atoms can only be screened if in this initial stage of transition oxygen is present on top of the outermost VO layer. This oxygen will be called vanadyl oxygen in analogy with V_2O_5; this point is further justified in the following paragraph. If the sample is kept at 750 °K, the LEIS spectrum changes gradually. The oxygen signal and especially the double scattering peak from oxygen is reduced and a peak situated at the energy position corresponding

with vanadium scattering, appears. During the whole process, the LEED pattern corresponds to the periodicity of V_6O_{13}.

Figure 2b shows the final LEIS spectrum. The VO layer is no longer screened. This can only be explained by assuming that the vanadyl oxygen on top of the VO-layer is no longer present.

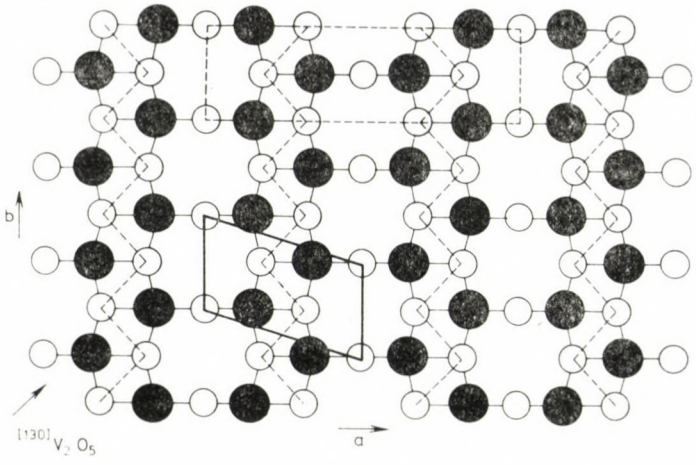

Fig. 1. Projection on the *c*-plane (001) of a V—O layer as it appears in V_6O_{13}. The bold, drawn parallellogram shows the two-dimensional unit mesh. Dark spheres represent the V atoms, open circles the O atoms

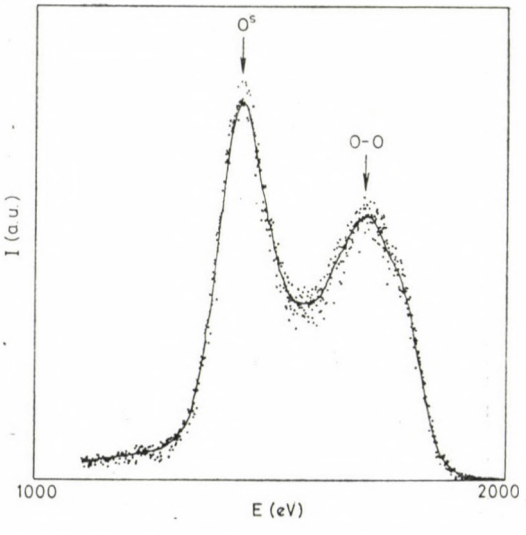

Fig. 2a. Ne^+—V_6O_{13} LEIS spectrum obtained under UHV conditions at a freshly cleaved and converted V_2O_5(001) surface. Experimental conditions: $E_i = 2$ keV; $I_p = 3 \times 10^{-3}$ A m^{-2}; $T = 750$ K; $\Theta = 30°$; $\Psi = 15°$; Φ [130]

Similar experiments along other low index directions produce essentially the same spectra and consequently lead to the same conclusions.

The samples, at a final stage of transition, thus contain no or only very little vanadyl oxygen, whereas at freshly cleaved surfaces oxygen can be present as is shown. The vanadyl sites can thus be considered to be adsorption sites. In the case of stable V_6O_{13} at 750 K and in UHV these sites are not occupied.

The possible presence of vanadyl oxygen is related to the oxygen loss during the transitions $V_2O_5 \rightarrow V_6O_{13}$. During this process an oxygen excess is generated at the interface V_2O_5/V_6O_{13}. The excess oxygen leaves the sample via vanadyl sites. At a freshly cleaved sample the transition occurs close to the surface. Consequently the diffusion towards it is rather easy and consistent, hence the vanadyl sites are occupied. When, however, the transition continues in depth, the interface V_2O_5/V_6O_{13} moves further and further away from the surface and as a consequence the oxygen supply rate decreases. After a certain period the V_6O_{13} layer becomes sufficiently thick for the surface layer to reach equilibrium. In this case the vanadyl sites remain unoccupied, and the vanadium in the VO layer becomes visible.

Position of the vanadyl oxygen

The most probable position of the vanadyl oxygen is on top of the vanadium of the V—O layer, as in the V_2O_5-structure. This can be confirmed by the so called "blocking effect", which is a very well known effect in MEIS and

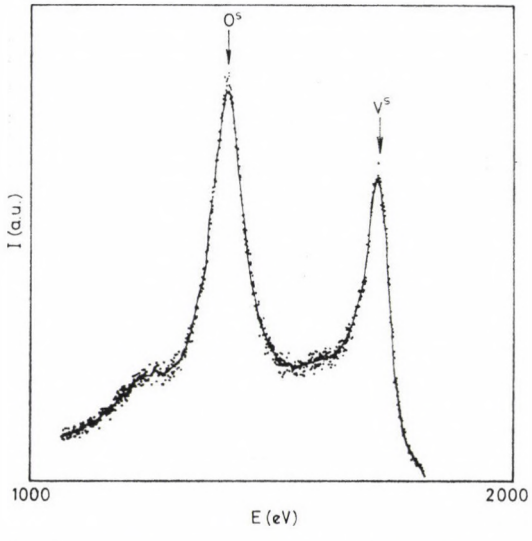

Fig. 2b. Ne^+—V_6O_{13} LEIS spectrum obtained under identical experimental conditions as given in Fig. 2a (300 h after the onset of the transition from V_2O_5 into V_6O_{13})

HEIS (medium- and high-energy-ion-scattering): ions scattered by vanadium in the direction of a vanadyl oxygen cannot reach the detector (Fig. 3), hence the vanadium signal vanishes. In Fig. 4 the V/O ratio (ratio of the intensity of both signals) is shown as a function of the total scattering angle Θ, the angle of incidence being kept constant at 12° along the $[130]_{V_2O_5}$ direction. Ne^+-scattering showed the vanadyl sites to be occupied. The ratio exhibits a distinct minimum at $\Theta = 100°$, i.e. when the outgoing trajectory is perpendicular to the surface. It is consequently concluded that the vanadyl oxygen is indeed situated on top of the vanadium atoms of the outermost V—O layer

Reversible oxygen exchange

If, as it appears from the previous experiments, the sample loses lattice oxygen via the vanadyl oxygen sites, it should be possible to observe the reverse transition at a sufficiently high partial pressure of O_2. The sample can in this case adsorb the oxygen at the vanadyl sites. Dziembay [6] performed a similar experiment with a mixture of V_2O_5 and V_6O_{13} powders.

To study the reoxidation of V_6O_{13} to V_2O_5 in the UHV apparatus, and without compromising too much the available pumping speed, oxygen was blown over the sample through a small tube. The partial oxygen pressure in the UHV system was $1 \cdot 10^{-4}$ Pa, however, the local pressure at the position of the sample should be substantially higher. The precise value was not determined.

It turned out that all previously mentioned processes are reversible. For example, starting from a situation corresponding with the LEIS spectrum of

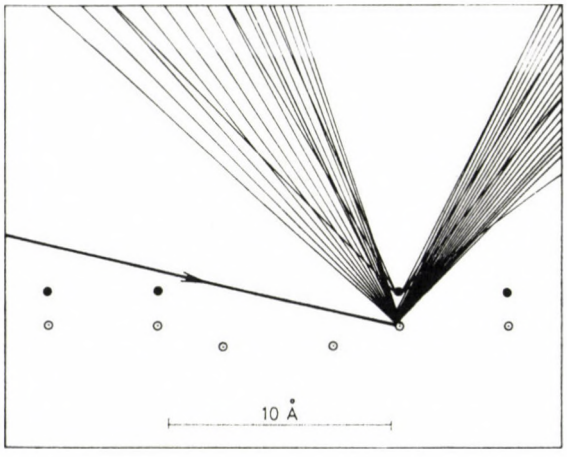

Fig. 3. Blocking configuration as obtained from trajectory simulations of He^+ ions (2000 eV) incident along a V—O chain (Molière approximation of the Thomas—Fermi—Firsov potential). Dark circles represent vanadyl oxygen whereas dotted circles represents vanadium atoms

Fig. 2b, reoxidation yields the spectrum of Fig. 2a. The blocking experiments also reveal that the vanadium atoms become screened again. It is even possible to obtain again V_2O_5 at the surface, as could be shown by LEED. Indeed, before the transition the observed diffraction pattern exhibits a rectangular unit mesh with sharply defined spots (corresponding with the V_2O_5 structure). After the transition to V_6O_{13} is started, the unit mesh changes into a parallellogram, corresponding to the change in surface periodicity. Furthermore, the spots are much more diffuse and less intense, probably due to the introduced defects. Under a higher oxygen partial pressure the V_2O_5 rectangular pattern appears again after some time, with the original brightness and sharpness. This can be explained by assuming that the V_2O_5 substrate acts as a nucleus and that the V_2O_5 layer grows from below towards the surface, consuming the V_6O_{13} layer.

Similar reoxidation experiments were performed on pure V_6O_{13} single crystals. It turned out that in this case, even after several days of oxygen

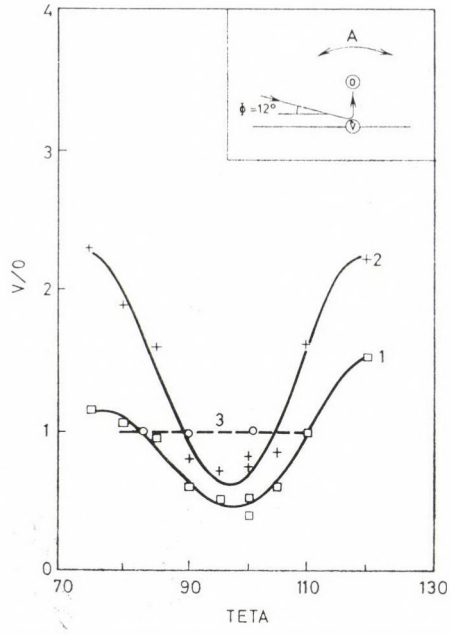

Fig. 4. The amplitude ratio V/O of the vanadium and oxygen signals. (He^+-V_6O_{13} blocking experiment) as a function of total scattering angle under constant angle of incidence ($\Psi = 12°$). Experimental conditions: $E_i = 2$ keV; $I_p = 1.5 \times 10^{-2}$ A m^{-2}; $T = 750$ K; $\Psi = 12°$; Φ [130]. Curves 1 and 2 were obtained under full oxygen coverage whereas curve 3 corresponds to a sample with a depleted V—O layer. For curves 1 and 3, the V/O ratio is directly obtained from the peak amplitudes measured at the appropriate energies in the experimental spectra. For curve 2, the V/O ratio is obtained by correcting the oxygen signal. This corrected amplitude is obtained by subtracting a "background" estimation from the measured peak amplitude. For the vanadium signal, no correction was applied as at the high energy side of the vanadium peak, the signal drops down to a very low value showing little or no background effects at these energies. The insert schematically shows the blocking geometry as used in these experiments

exposure, no transition from V_6O_{13} to V_2O_5 could be observed. This experiment gives more evidence for the discussed model in which the V_2O_5 substrate behaves as a reoxidation nucleus in the case of the topotactically grown V_6O_{13} layer.

Potassium enriched surfaces

Potassium is frequently added to industrial V_2O_5 based catalysts, in order to improve the selectivity and activity of the respective catalysts. Table I shows the bulk concentration of some typical contaminants of V_2O_5 and V_6O_{13} samples, similar to those used for the present experiments. This table illustrates the low bulk contamination. However, in the LEIS energy distributions a potassium contribution can be observed, due to a surface segregation of this element.

Surface segregation

In the LEIS spectra taken at elavated temperatures ($T > 600$ K) a peak is observed corresponding with the energy position of potassium. The V_2O_5—V_6O_{13} system has been studied intensively, using e.g. Auger spectroscopy [7]. However, potassium was never observed, not even at higher temperatures. In order to clarify this point additional SIMS experiments were performed. For this purpose and to avoid surface contamination by the primary ion beam the mass-filtered ion beam of the LEIS experiment was used.

The two potassium lines (39 and 41 amu) are the most important features in the spectrum. The presence of potassium is also ascertained by the thermal desorption of potassium at sufficiently high temperatures ($T > 600$ K).

The amplitude of the K signal in both the LEIS and SIMS experiments, can only be explained by a segregation of potassium to the surface.

The absence of a K contribution in the Auger spectra is probably due to some kind of electron stimulated desorption (ESD). Indeed it was shown that the irradiation with an e-beam (2 keV) enhances the spontaneous emission of K^+-particles. At the moment a model explaining this behaviour is under

Table I

Concentration of impurities in weight ppm as determined by neutron activation analysis

	Pt	Mn	Na	K
V_2O_5	65.6	0.13	9.77	9.64
V_6O_{13}	16.3	1.06	7.38	97.0

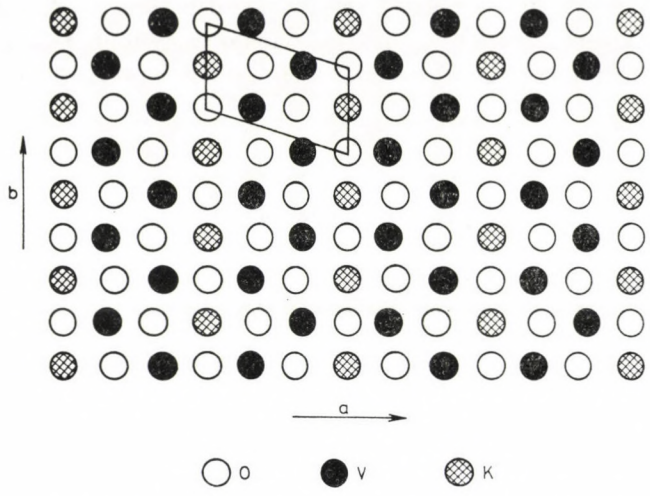

Fig. 5. Projection on the *c*-plane (001) of the outermost VO layer of V_6O_{13}. The two-dimensional unit mesh of V_6O_{13} is shown. Open circles represent the oxygen atoms, dark spheres the vanadium atoms and cross hatched spheres the proposed potassium sites

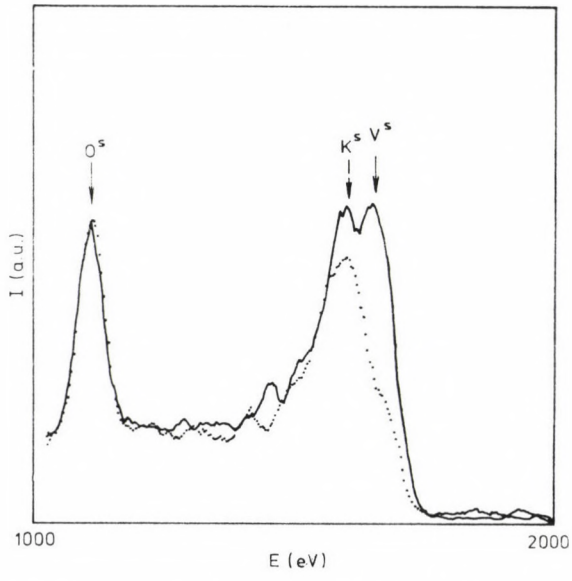

Fig. 6. He^+-LEIS spectrum obtained under blocking conditions; — dotted line : nearly full oxygen coverage of the vanadyl sites, — bold line : unoccupied vanadyl sites. As is shown, the *K* signal is not suppressed by the presence of oxygen. Experimental conditions: $E_i = 2000$ eV; $\Theta = 100°$; $\Psi = 12°$; $T = 775$

investigation. It is assumed that the binding energy of potassium at the surface is lowered by the injection of electrons, enhancing in this way the emission of potassium.

Surface structure

In order to obtain some information about the position of the potassium at the surface, LEED and angular dependent LEIS experiments on samples with depleted vanadyl sites were performed. The LEIS experiment did not reveal blocking or shadowing effects involving the potassium atoms. This indicates that the potassium should be in or near the outermost VO layer. On the other hand the periodicity of the LEED picture remains unaltered as a function of the surface concentration of potassium, and no superstructures are observed. However, in interpreting LEED experiments one should be aware of the discussed perturbing effect of the *e*-beam.

Monovalent elements such as Li, Na, K, Cu or Ag form with V_2O_5 α-bronzes with the general formula M_x V_2O_5 [9—11], consisting of a V_2O_5 matrix with M interstitials. As V_6O_{13} has similar interstitial sites, and taking into account the previous discussed angular dependent experiments, it has to be assumed that the potassium is at an interstitial site in or near the outermost VO layer (cf. Fig. 5).

A semi-quantitative estimation [12] of the potassium concentration at the surface, reveals that at the point of saturation ($\pm$700 K) the concentration of vanadium is twice as high as for potassium atoms. From Fig. 1 it follows that each V_6O_{13} unit cell contains 2 vanadium atoms and one interstitial site. Consequently it is concluded that the unit cell can accommodate one K atom. As such, the most probable site should be as indicated in Fig. 5 showing the structure of the outermost VO layer.

Finally shadowing and blocking measurements where performed in order to determine whether vanadyl sites are present on top of the potassium atoms. As shown in Fig. 6 no oxygen blocking effects related to the K atoms are observed. As a consequence it is assumed that vanadyl sites exist only on top of the vanadium atoms.

Conclusion

LEIS has proven to be an effective tool for studying the surface structure of the V_6O_{13}(001) surface. It follows that under U.H.V. conditions (O_2 partial pressure $\ll 10^{-8}$ Pa) and at the given temperatures ($\pm$750 K) the V_6O_{13} surface consists of a mixed V—O layer. If oxygen is supplied to the surface, it could be deduced from blocking experiments that atomic oxygen adsorbs on top of the vanadium atoms of the topmost V—O layer. Consequently, these vanadium atoms represent adsorption-desorption sites for atomic oxygen.

The topmost (O) layer as it appears at a freshly cleaved and converted V_2O_5 sample or after adsorption from the gas phase shoud be regarded as an adsorbed phase, rather than as regular lattice oxygen. As such the discussed experiments give strong support to the idea that the "vanadyl oxygen" is the active species in the oxidation-reduction mechanism which is responsible for the catalytic activity of the $V_6O_{13}(001)$ surface. At the highest temperatures an important *K* surface segregation has been observed at the V_6O_{13} (001) surface. It could be concluded that these K atoms occupy an interstitial site in or very near to the terminating V—O layer. The most probable position is found to be in the least dense oxygen rows (parallel to the *b*-direction) surrounded symmetrically by four oxygen and four vanadium atoms from the given V—O plane. It was also deduced from blocking experiments that no vanadyl sites are present on top of the potassium atoms.

*

This work is part of a research project suported by IIKW (Interuniversitair Instituut voor Kernwetenschappen, Deel Vaste Stof).

REFERENCES

[1] Schaefer, H.: Ber. Bunsenges, **71,** 222 (1967); Praliaud, H., Mathiey, M. V.: J. Chem. Phys., **73,** 509 (1976); Gasior, M., Grzybowska, G., Haber, J., Machej, T., Ziolkowski, J.: J. Catal., **58,** 15 (1979); Andersson, A., Ludin, S. T.: J. Catal., **58,** 383 (1979)
[2] Fiermans, L., Vandenbroucke, L., Vanden Berghe, R., Vennik, J., Dalmai, G.: J. Microsc. Spectrosc. Electron,. **4,** 543 (1979)
[3] Mars, P., Van Krevelen, D. W.: Chem. Eng. Sci., **3,** 41 (1954)
[4] Fiermans, L., Clauws, P., Dekeyser, W.: Can. Mineralogist, **16,** 353 (1978) and references therein
[5] De Gryse, R., Landuyt, J. P., Vermeire, A., Vennik, J.: Appl. Surf. Sci., **6,** 430 (1980)
[6] Dziembay, R., Piwowarczyk, J.: J. Sol. Chem., **21,** 387 (1977); Dziembay, R.: J. Sol. Chem., **16,** 161 (1978); Dziembay, R., Ciembroniewics, G., Kabicki, R.: React. Kinet. Catal. Lett., **12,** 89 (1979)
[7] Fiermans, L., Vennik, J.: Surface Sci., **24,** 541 (1971); Fiermans, L., Vennik, J.: Surface Sci., **35,** 42 (1973)
[8] Heiland, W., Taglauer, E.: Rad. Effects, **19,** 1 (1973)
[9] Hagenmuller, P., Galy, J., Pouchard, P., Casalot, A.: Mater. Res. Bull., **1,** 45 (1966)
[10] Clauws, P.: Verhand. Kon. Acad. België, **42,** 159 (1980)
[11] Sperlich, G.: Z. Physik, **250,** 335 (1972)
[12] De Gryse, R., Landuyt, J. P., Vandenbroucke, L., Vennik, J.: Surface and Interface Analysis, **4,** 168 (1982)

Acta Chimica Hungarica 119 (2—3), pp. 203—212 (1985)

HYDROISOMERIZATION AND HYDROCRACKING OF METHYLNONANES OVER Pt/HZSM-5+

Johan A. MARTENS, Mia TIELEN and Peter A. JACOBS*

(Centrum voor Oppervlaktescheikunde en Colloïdale Scheikunde, Katholieke Universiteit Leuven, Kardinaal Mercierlaan 92, B-3030 Leuven, Heverlee, Belgium)

Received June 8, 1984
Accepted for publication September 6, 1984

The hydrocracking and hydroisomerization of *n*-decane and the methylnonanes over Pt/HZSM-5 are investigated. Detailed product distributions are reported at low and high conversions. The differences in the products obtained from the different tested alkanes are discussed in terms of the classical bifunctional mechanism.

Introduction

Detailed compositions of the hydroisomerization and hydrocracking products from *n*-decane over Pt/CaY, Pt/ultrastable Y, Pt/HZSM-5 and Pt/HZSM-11 zeolites have been reported [1—4]. The common features or these reactions are:

— hydroisomerization and hydrocracking are consecutive events,

— at low cracking conversions, the distribution of the cracked products by carbon number is symmetric around the C5 fraction as a result of pure primary cracking of the feed isomers,

— methane and ethane are not formed.

In terms of the classical bifunctional mechanism, presented for the first time by Coonradt and Garwood [5], such behaviour is only possible when the two functions are in balance. In that case, enough hydrogenation-dehydrogenation capacity is present in the catalyst, compared to its acidity, so that the rearrangement of the carbenium ions becomes rate limiting. As a result, a steady concentration of olefins is competing with the carbenium ions for the acid protons. This competitive sorption together with the acid strength of the protons determined the life-time of the carbenium ion and consequently the reaction selectivities.

Chen and Garwood reported reactant shape selectivity in the catalytic cracking (CC) of small paraffins over ZSM-5 [6] and showed that ZSM-5 has a pore system which differentiates catalytically molecules having a straight

+ This paper was presented at the 2nd Belgian—Hungarian Colloquium on Catalysis at De Haan, Belgium, October 10—13, 1983.

* To whom correspondence should be addressed.

chain, a methyl and a dimethyl substitution. They found the first order rate constant for CC to decrease in the order:

$$C6 > 2MC5 > 3MC5 \gg 2,3DMC4 > 2,2DMC4$$

$$C7 > 2MC6 > 3MC6 \gg 2,3DMC5 > 2,4DMC5$$

ZSM-5 has a constraint index [CI] of 8.3 [7]. This reflects a considerable higher activity for the cracking of C6, compared to 3MC5. Moreover, this CI is strongly temperature dependent. The selectivity in CC for C6 against 3MC5 is ascribed to steric hindrance within the ZSM-5 pores rather than to molecular screening. This is based on the fact that 3MC5 and C6 are both readily sorbed by ZSM-5, but 3MC5 has a lower packing density in the zeolite channels. The difference in selectivity for CC between 3MC5 and 2MC5 could also to some extent at least be the result of a difference in steric hindrance.

The sorption capacity of ZSM-5 for 2-methylnonane and 3-methylnonane is nearly half of that for 4-methylnonane and 5-methylnonane at a relative pressure of 0.5 [4]. On the contrary, the diffusion coefficients of the methylnonane isomers in precatalytic temperature conditions are very similar [4].

In this work the catalytic behaviour of HZSM-5, loaded with Pt and therefore acting as a bifunctional catalyst is investigated in the reaction of the different methylnonane isomers. Detailed product distributions are reported and the results are compared with those from *n*-decane.

Experimental

Materials

The ZSM-5 zeolite was synthetized and transformed into the NH_4 form as reported elsewhere [8]. The atomic ratio Si/Al in the synthesis mixture was 37.4. The crystal dimensions on the average were 15 μ, as determined by SEM. The zeolite was loaded with 1% by weight with Pt by impregnation with $Pt(NH_3)_4Cl_2$. The catalyst was pelletized and the 0.3—0.5 mm fraction was used. The purity of the feed hydrocarbons, as determined by capillary GLC is given in Table I. Product distributions were corrected under the assumption that the feed impurities underwent no reaction. Hydrogen had a purity of at least 99.9%.

Table I

Experimental conditions for the hydroconversion of alkanes over Pt/HZSM-5

Feed molecule	Purity %	H_2/feed molar ratio	WHSV $g\,g^{-1}\,h^{-1}$
Cl0	99.9	151	0.31
2MC9	98.6	120	0.39
3MC9	98.6	107	0.43
4MC9	97.8	109	0.43
5MC9	98.0	105	0.44

Methods

Hydrocracking experiments were performed in a continuous flow tubular reactor. The hydrocarbons were fed and converted at atmospheric pressure. The hydrogen/hydrocarbon molar ratios and the space velocities for the hydrocarbons are given in Table I.

The catalyst was activated by calcining in situ in flowing oxygen at 673 K, followed by reduction at the same temperature in hydrogen. The whole conversion domain was covered by varying the reaction temperature. Product separation was done using capillary GC with a 50 m OV101 fused silica column. Sample injection was on-column and temperature programming between 10 and 150 °C.

Results

Figure 1 shows the reaction selectivity for hydroisomerization and hydrocracking as a function of the reaction temperature for the different alkanes tested. The slope of the hydroisomerization and hydrocracking curves is sharper for C10, compared to those of the MC9 reactants. At low conversions, the isomerization curve is close to the cracking curve for 2MC9 and 4MC9. For 3MC9 and 5MC9, hydroisomerization precedes hydrocracking. In the reaction of C10, hydrocracking at all conversions is the main reaction.

The maximum of the hydroisomerization curve for the respective feeds increases in the following order:

$$5MC9 > 3MC9 > 4MC9 > C10 > 2MC9$$

In Table II, the hydroisomerization products at the maximum hydroisomerization conversion are separated according to their branching structure.

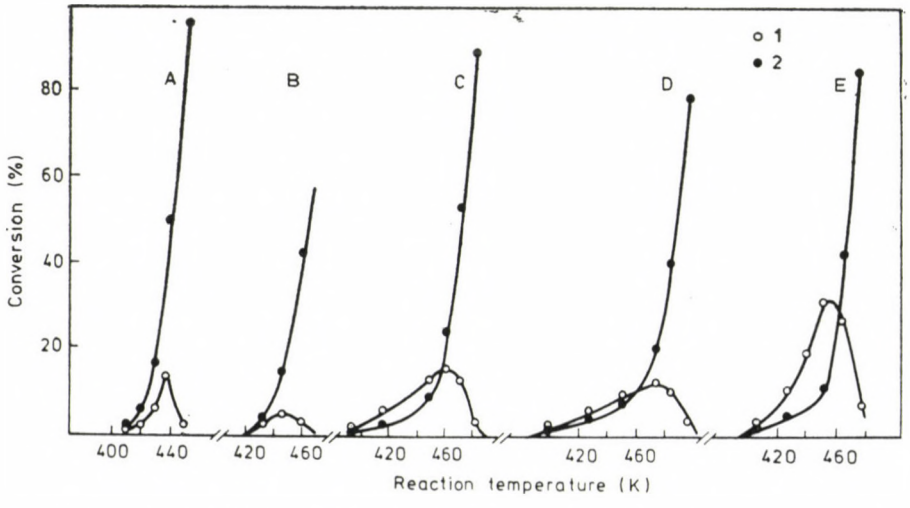

Fig. 1. Overall reaction selectivity for hydroisomerization (1) and hydrocracking (2) for the conversion of (A) C10, (B) 2MC9, (C) 3MC9, (D) 4MC9 and (E) 5MC9 over Pt/HZSM-5

Table II

Distribution of the hydroisomerization products from n-decane and different methylnonanes over Pt/HZSM-5 *at the maximum hydroisomerization conversion*

Feed	Cl0	Monobranched* isomers	Dibranched isomers
Cl0	—	95	5
2MC9	10	64	26
3MC9	4	69	27
4MC9	1	72	27
5MC9	4	84	12

* Other than the feed.

Table III

Distribution of the monobranched hydroisomerization products from n-decane and different methylnonanes over Pt/HZSM-5 *at* 5% *hydroisomerization conversion*

Feed	3EC8	4EC8	2MC9	3MC9	4MC9	5MC9
Cl0	0	0	58	23	13	6
2MC9	2	0	—	78	14	6
3MC9	3	3	47	—	32	15
5MC9	3	7	22	29	40	—

Table IV

Distribution of the monobranched hydroisomerization products from n-decane and different methylnonanes over Pt/HZSM-5 *at the maximum hydroisomerization conversion*

Feed	3EC8	4EC8	2MC9	3MC9	4MC9	5MC9
Cl0	0	0	55	25	14	7
2MC9	3	1	—	66	21	9
3MC9	5	5	34	—	41	15
4MC9	3	3	24	46	—	24
5MC9	6	7	17	28	42	—

Monobranched isomers include MC9 and EC8. All observed dibranched structures are dimethyl-branched.

Tables III and IV give the distribution of the monobranched isomers which are the main hydroisomerization products in each reaction (Table II). At low hydroisomerization conversion (Table III) it was not possible to measure this composition for the reaction of 4MC9 since the small chromatographic peak of 5MC9 was overlapped by the intense reactant 4MC9 peak. At higher conversion (Table IV) this was no longer a problem. In Tables V and VI, the cracked product distributions are presented at small and large cracking conversions, respectively.

Table V

Distribution of the cracked products from n-decane and different methylnonanes at small cracking conversions over Pt/HZSM-5 (mol/100 mol of feed cracked)

		Cracked product distribution (mol/100 mol cracked)											
Feed	cracking conv. (%)	Sum	C3	iC4	C4	iC5	C5	2MC5	3MC5	C6	2MC6	3MC6	C7
C10	5	200	40	12	30	11	25	8	2	31	9	3	29
2MC9	7	206	35	20	32	21	24	19	4	23	11	4	13
3MC9	7	204	29	18	31	26	26	18	6	23	9	7	11
4MC9	5	209	26	30	35	25	33	18	4	22	7	3	6
5MC9	6	206	23	27	32	29	29	20	5	24	8	3	6

Table VI

Distribution of the cracked products from n-decane and different methylnonanes at high cracking conversions over Pt/HZSM-5 (mol/100 mol of feed cracked)

		Cracked product ditribution (mol/100 mol cracked)												
Feed	Cracking conv. (%)	SUM	C3	iC4	C4	iC5	C5	2,3DMC4	2MC5	3MC5	C6	3DMC5	2MC6	3MC6	C7
C10	95	209	49	20	30	15	20	—	17	4	22	—	13	5	14
2MC9	45	223	50	20	34	17	32	0	15	4	23	0	10	5	13
3MC9	90	219	56	33	31	19	24	0	20	6	18	0	5	4	3
4MC9	78	229	60	41	32	15	32	0	17	5	23	0	2	1	1
5MC9	84	223	56	37	32	19	27	0	18	6	20	0	3	2	3

Discussion

Overall conversion

In Figure 1 it can be seen that the slope of the cracking and the isomerization curves is smaller for the reaction of any MC9 than for the reaction of C10. Nevertheless, the activation energy for cracking and isomerization, in a kinetic regime where the surface reaction is rate controlling, should be identical on the same catalyst. This smaller activation energy therefore has to be explained by diffusional restrictions of the methylnonanes in the pores of the HZSM-5, especially at lower reaction temperatures.

Hydroisomerization

The reaction of MC9 gives more dibranched isomers than the reaction of C10 (Table II). C10 is also a product from any MC9 feed.

The hydroisomerization of C10 over Pt/HZSM-5 yields high amounts of 2MC9 at the expense of the other MC9 (Tables III and IV). This is in line with the previously reported data [2], [4]. It was stated that this high selectivity for 2MC9 is a result of transition state shape selectivity.

In principle the hydroisomerization of any MC9 molecule can proceed as follows:

— either via a methyl shift,

— or first via PCP intermediates into C10 and then again via a PCP intermediate into another MC9.

Indeed C10 is always present as a product (Table II). If isomerization involves branching of C10, a product distribution similar to that of the reaction of C10 is expected. From Table III it is clear that isomerization of MC9 proceeds via methyl shift. 2MC9 isomerizes subsequently into 3MC9, 4MC9 and 5MC9. At higher conversions, this sequence is unchanged (Table IV). The reaction of 3MC9 yields more 2MC9 than 4MC9. This is in contrast with the results over Pt/CaY, where a methyl shift towards the center of the molecule is faster than towards the end [9]. At the maximum hydroisomerization conversion, however, 4MC9 is the main product. 4MC9 gives more 3MC9 than 5MC9 at high conversions. 5MC9 transforms into 4MC9, 3MC9 and 2MC9.

The formation of EC8 is dependent on the kind of MC9 used as feed (Tables III and IV). 3EC8 is favoured in the reaction of 2MC9, whereas 4EC8 is the main product from 5MC9. 3MC9 yields equal amounts of 3EC8 and 4EC8. This confirms the formation of EC8 via bulky alkyl shifts from 3MC9, 4MC9 and 5MC9-type carbenium ions. It can be depicted as follows:

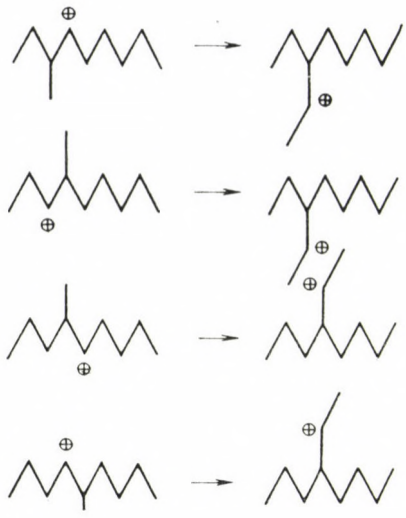

3EC8 and 4EC8 can also be interconverted by ethyl shift:

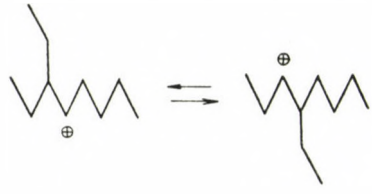

The equilibrium ratio 3EC8/4EC8 is 0.5 [10]. Since at high conversions (Table IV) this equilibrium is never observed, this kind of ethyl shift should be slow.

Hydrocracking

In Table V, large differences in the cracked product distributions at low conversions are observed when C10 or the MC9 are used as feed. The cracking of any MC9 gives more *i*C4, *i*C5, 2MC5 and less C3, C6 and C7 than cracking of C10.

If only primary cracking of the feed isomers is operative, a symmetric cracked product distribution around the C_5 fraction has to be observed and 200 mol of cracked products should be obtained from the β-scission of 100 mol of feed. Only C10 at low conversions is cracked via this pathway (Table V). All the MC9 give more than 200 mol cracked products per 100 mol feed cracked.

Secondary cracking of the largest cracked fragments results in an asymmetric distribution among C5. A C3 and C4 fragment result from the β-scission of C7. Eventually, C6 cracks into two C3 fragments. In Figure 2(A), the differ-

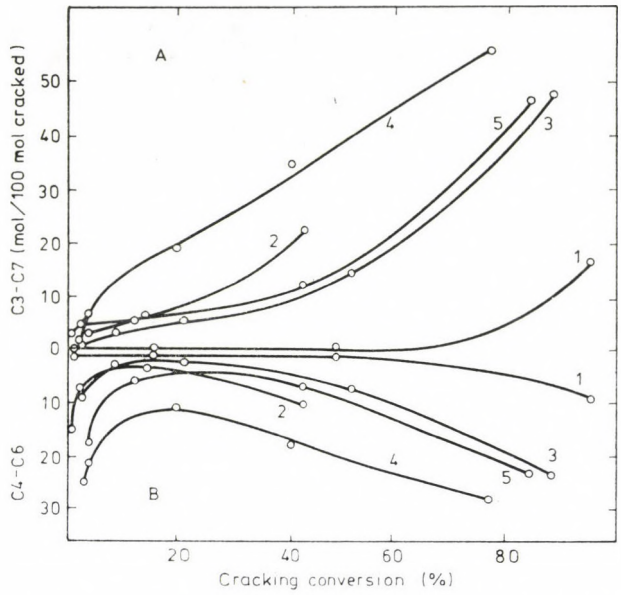

Fig. 2. Difference between C3 and C7 fractions (A) and between C4 and C6 fractions (B) for the hydrocracking of (1) C10, (2) 2MC9, (3) 3MC9, (4) 4MC9 and (5) 5MC9 over Pt/HZSM-5 in function of the cracking conversion (mol/100 mol cracked)

ence between the C3 and C7 fractions is presented, expressed in mol/100 mol of feed cracked, against the cracking conversion. Figure 2(B) presents the same for the C4 and C6 fractions. If only primary cracking is operative, the respective yields of C4 and C6 and also of C3 and C7 should be equal. This situation is only encountered for C10 up to 60% total conversion.

Secondary cracking of the C7 and eventually C6 fractions results in a difference between the C3 and C7 fractions which is twice the difference between C4 and C6. In Figure 2 this is observed for all cases *only at high cracking conversions* ($>20\%$).

At low conversions for any MC9 used as feed the difference in C4 and C6 yields is much larger than between C3 and C7 yields. This cannot be explained by a bifunctional mechanism involving cracking of feed isomers and subsequent secondary isomerization and cracking of the cracked products. From Table V it is seen that this difference is mainly the result of an excess *i*C4, since the absolute amount of C4 is the same for all reactions. Also the amount of *i*C5 is larger for the reaction of a MC9 than for C10.

Studies on CC of ^{13}C labelled hydrocarbons led to the conclusion that the formation of *i*C4 and *i*C5 has to be explained by a continuous breakage and reformation of polymeric chains, attached to the zeolite framework [11], [12]. An analogous explanation can be given here. At low temperatures, small

olefins polymerize on the acid protons and the resulting bulky hydrocarbon chain cracks preferentially into iC_4 and iC_5 olefins which are hydrogenated at the Pt sites. According to Weisz' intimacy criterion [13], this acid catalysed reaction sequence is possible in the case of a shortness of long chain olefins, competing for the acid protons. At higher temperatures a normal secondary cracking pattern develops. The diffusion limitation of the long chain olefins is lowered as is the carbenium ion life time.

A comparison between Table VI and Table V indicates that only the C_7 fraction is cracked a second time. The amount of the C_6 fraction remains more or less the same at higher conversions.

Secondary isomerization

Secondary isomerization of C6 and C7 is important at high conversions for the reaction of C10.

On the same catalyst, the same cracking mechanism are probably operative in the reaction of C10 and any MC9, yielding the same cracked fragments. The composition of the C6 fraction obtained from the reaction of a MC9 at low conversion is very similar to the composition of this fraction in the reaction of C10 at high conversion (Table VI). This indicates that secondary isomerization of the cracked products is operative from the start on in the reaction of MC9. This is consistent with a longer life time of the carbenium ions, due to diffusional retardation of feed olefins. Also the traces of dibranched C6 and C7 are explained by a higher secondary isomerization activity, rather than cracking of very bulky tribranched feed isomers.

Conclusions

Pt/HZSM-5 acts as an ideal bifunctional catalyst at low conversions of C10. At high conversion, secondary isomerization and cracking is observed. In contrast to this, acidic reactions predominate on the same catalyst at low conversions for any MC9, as indicated by a higher selectivity for *i*C4 and *i*C5. At higher temperatures, a normal secondary cracking pattern develops, the latter being more severe than for the reaction of C10.

*

J. A. Martens and P. A. Jacobs acknowledge respectively a grant as Research Assistant and a permanent research position as Senior Research Associate from N.F.S.R. (Belgium).

Abbreviations

MC9	: methylnonanes	2MC6	: 2-methylhexane
EC8	: ethyloctanes	3MC6	: 3-methylhexane
C3	: propane	2,3DMC5	: 2,3-dimethylpentane
C4	: butane	2,4DMC5	: 2,4-dimethylpentane
*i*C4	: isobutane	C7	: heptane
C5	: pentane	2MC9	: 2-methylnonane
*i*C5	: isopentane	3MC9	: 3-methylnonane
2MC5	: 2-methylpentane	4MC9	: 4-methylnonane
3MC5	: 3-methylpentane	5MC9	: 5-methylnonane
2,2DMC4	: 2,2-dimethylbutane	3EC8	: 3-ethyloctane
2,3DMC4	: 2,3-dimethylbutane	4EC8	: 4-ethyloctane
C6	: hexane	PCP	: protonated cyclopropane

REFERENCES

[1] Weitkamp, J.: Am. Chem. Soc. Symp. Ser., **20,** 1 (1975)
[2] Jacobs, P. A., Uytterhoeven, J. B., Steyns, M., Froment, G., Weitkamp, J.: Proc. 5th Int. Conf. Zeolites (Ed. L.V.C. Rees), Heyden, London, 607 (1980)
[3] Steyns, M., Froment, G., Jacobs, P., Uytterhoeven, J. B., Weitkamp, J.: Ind. Eng. Chem. Prod. Res. Dev., **20,** 654 (1981)
[4] Jacobs, P. A., Martens, J. A., Weitkamp, J., Beyer, H. K.: Faraday Disc. Chem. Soc., **72,** 353 (1982)
[5] Coonradt, H. L., Carwood, W. E.: Ind. Eng. Chem. Prod. Res. Dev., **3,** 38 (1964)
[6] Chen, N. Y., Garwood, W. E.: J. Catal., **52,** 453 (1978)
[7] Frillette, V. J., Haag, W. O., Lago, R. M.: J. Catal., **67,** 218 (1981)
[8] Jacobs, P. A., von Ballmoos, R.: J. Phys. Chem., **86,** 3050 (1982)
[9] Weitkamp, J., Farag, H.: Proc. Symp. Zeolites, Szeged, Hungary, September 11—14, 1978; Acta Physica et Chemica, **1978,** 327
[10] Stull, R. D., Westrum, E. F., Sinke, G. C.: The Thermodynamics of Organic Compounds, Wiley, New York 1969
[11] Bolton, A. P., Ladd, I. R., Weeks, T. J., Jr.: Proc. Intern. Congr. Catalysis, 6th, London, 1976, Chemical Society, **1977,** 316
[12] Fajula, F., Gault, F. G.: J. Catal., **68,** 312 (1981)
[13] Weisz, P. B.: Adv. Catal., **13,** 137 (1962)

Acta Chimica Hungarica 119 (2—3), pp. 213—222 (1985)

KINETIC STUDY OF *n*-HEXANE CONVERSION OVER Pt/Al_2O_3 CATALYST+

József MARGITFALVI*, Mihály HEGEDÜS, Péter SZEDLACSEK and Ferenc NAGY

(Central Research Institute for Chemistry, Hungarian Academy of Sciences, H-1025 Budapest, Pusztaszeri út 59—67.)

Received June 8, 1984
Accepted for publication September 12, 1984

An experimental approach is described to study the steady-state and transient kinetics of hydrocarbon reactions at high temperatures, close to those used in industrial practice. As a case study *n*-hexane conversion was investigated at 480 °C. The initial rates of formation of the main reaction products such as hydrogenolysis products, isohexanes, methylcyclopentane (MCP) and benzene and of *n*-hexane conversion were measured at different *n*-hexane partial pressures.

Positive pressure dependences were obtained for *iso*-hexanes and MCP. However, the initial rates of formation of hydrogenolysis products had a slight maximum vs. *n*-hexane partial pressure, while benzene formation showed a strong negative dependence. These two reaction products resulted in an overshoot type of response in the transient kinetic curves. Monotonic increase type of responses were obtained for isohexanes and MCP.

It is suggested that the reaction selectivity is controlled by the hydrocarbon coverage. The formation of *iso*-hexanes and of MCP is favored by high coverages, while the formation of benzene and hydrogenolysis products is enhanced by low coverages.

Introduction

In the last fifteen years the study of catalytic hydrocarbon reactions involved in naphtha reforming and aromatization received much scientific and industrial interest [1—4]. Despite the tremendous efforts made in this field, there are only scarce kinetic data measured at high temperatures, i.e. under conditions close to those of industrial processes.

This fact can be attributed to the problem of fast catalyst ageing. This process is related to the formation of a carbonaceous over-layer on the catalyst surface [5]. The higher the reaction temperature, the higher is the rate of formation of this surface carbon (often called coke), consequently, the extent of catalyst ageing is higher and the reliability of the kinetic data is lower.

In this paper we are going to demonstrate that the long slug pulse technique, with parallel determination of the steady-state condition for the majority of reaction products, can be used to study the steady-state and transient

+ This paper was presented at the 2nd Belgian—Hungarian Colloquium on Catalysis at De Haan, Belgium, October 10—13, 1983.

* To whom correspondence should be addressed.

reaction kinetics at high temperatures. In order to demonstrate the application of this method, we are presenting our experimental data obtained in the course of a study of *n*-hexane conversions on a Pt/Al_2O_3 catalyst.

Experimental

The conversion of *n*-hexane was studied on 0.5% Pt/Al_2O_3 catalyst. The dispersion of the catalyst measured by pulse hydrogen chemisorption was 23.0%, its chlorine content was 1.1%.

A conventional quartz tube reactor equipped with a preheater was used. The partial pressure of *n*-hexane was controlled by the temperature in the saturator before the reactor. The reactor inlet was connected with a four-port valve. A constant hydrogen flow was kept through the reactor. This hydrogen flow was periodically interrupted by means of the four-port valve introducing a slug of the mixture of hydrogen and *n*-hexane.

The reactor effluents were analyzed in two ways:

(i) The total reactor effluent was connected to a FID and the total ion current was monitored. In this way the quasi steady state condition of the reactor could be determined.

(ii) The concentrations of the individual components were measured by means of G. C. analysis using a six-port valve for sample introduction.

The conditions of gas chromatographic analysis were as follows. Column: 3.8 m long Chromosorb P HMDS, coated with 9.75% silicone DC410. Column temperature: 65 °C. Gas flow rate: 0.58×10^{-3} dm^3/sec.

The time required for G. C. analysis was 16 minutes including determination of toluene.

The purity of *n*-hexane was 99.8%. The main impurities were 2-methylpentane (2MP) and 3-methylpentane (3MP). The conversion of *n*-hexane was studied at atmospheric pressure in the pressure range of *n*-hexane 0.40—16.4 kPa. In the kinetic measurements the amount of catalyst (W) was between 0.01 to 0.20 g. The flow rate of the reaction mixture (V) varied between $0.5—2.5 \times 10^{-3}$ dm^3/sec.

In this work emphasis is laid on the determination of the rates of formation of the main reaction products such as light hydrocarbons (hydrogenolysis products), 2-methylpentane and 3-methylpentane (isohexanes), methylcyclopentane and benzene. The rates of formation of these products are expressed in terms of moles of converted *n*-hexane [mol(CH)]. The initial rates were calculated by using a curve fitting program and calculating the slope at zero contact time. In these calculations the yields of the reaction products (Y_j) were used, where the sum of yields gave the total conversion of *n*-hexane.

Results and discussion

Application of the slug-pulse technique

The pulse reaction technique has been widely used to study hydrocarbon reactions at high temperatures, where the ageing process makes it difficult to use conventional techniques, i.e. circulating or continuous-flow reactors [6—7].

It is known that results obtained by the pulse method can be different from those measured by conventional techniques. However, upon increasing the pulse width [8] results obtained by pulse method can approach those measured by the continuous-flow technique.

A further advantage of the long pulse technique is that if there is a possibility to analyze not the whole pulse but only its definite volume, it is possible to get information within the entire pulse width including the transient periods at the start and at the end of the pulse.

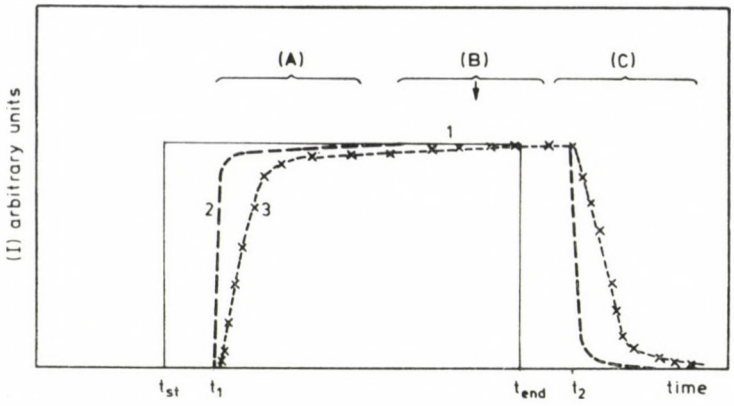

Fig. 1. Form of the pulse; (1) the theoretical rectangular pulse, (2) experimentally observed response without catalyst, (3) experimentally observed response in the presence of catalyst, (A) transient conditions; (B) steady state conditions

In order to demonstrate this, let us consider the reactor without catalyst with a rectangular hydrocarbon pulse as shown in Fig. 1. The time of the start of the hydrocarbon pulse is t_{st}, its end is t_{end}, which should correspond to the opening and closing of the four-port valve before the reactor, respectively. The theoretical form of the pulse [curve (1)] is slightly distorted and there is a short delay in the hydrocarbon response [curve (2)]. The delay $t_1 - t_{st}$ and $t_2 - t_{end}$ can be attributed to the dead volumes in the gas lines before and after the reactor up to the product analyzer (the six-port valve or the FID detector); the pulse distortion is related to the hydrocarbon adsorption in the gas line, to the non-ideal form of the hydrocarbon slug, and to the diffusion of the hydrocarbon into the pure hydrogen at the front and the end of the slug.

Upon introducing a catalyst, the form of the pulse is further changed due to: (i) the adsorption of the reactant hydrocarbon on the catalyst, (ii) surface reactions, and (iii) adsorption and further reactions of the primary reaction products. Curve 3 represents the response curve in the presence of a working catalyst. In this curve three parts can be distinguished: two transent periods at the start and the end of the pulse and a quasi-steady state period between them. In the transient periods the amount of the effluents leaving the ractor is not equal to the amount of the reactant at the inlet of the reactor, while in the quasi-steady state the overall material balance is maintained. However, it does not mean a real steady state for each reaction product. For a complex set of reactions (where the number of products is n), as for instance conversion of *n*-hexane, there is a more narrow interval of time in which a real steady state is maintained for each of the n-th reaction products. In our reactor system we considered to achieve this steady state

condition when the yields of the main reaction products were constant in time within 5—10%. The time to achieve this period was 35—50 s, depending on the experimental conditions. Based on these data the width of the pulse was arbitrarily selected as 60 s in all the experiments.

All steady state kinetic data correspond to conversions measured at the end of the pulse, i.e. the time on stream is 60 s. It is a general observation that after subsequent pulses of hydrocarbon the activity of the Pt/Al_2O_3 catalyst decreases, however, after a given number of pulses there are no further changes in the activity and selectivity data. Under our experimental conditions, usually 15—20 pulses were needed to achieve this period of constant activity. This period was used to study the steady-state kinetics by varying either the flow rates of the reactants in the same experiment or upon carrying out an independent run with a different amount of catalyst.

The period of constant activity was also used to obtain transient kinetic data. In these experiments, keeping constant the width of one pulse, the time of sampling (i.e. the opening of the six-port valve for G.C. analysis in the reactor outlet line) was varied up to 90 s. In this way we were able to obtain direct information on the product distribution within the pulse. In the transient kinetic experiments terminologies given by Kobayashi [9—11] were used.

Steady state kinetic studies

General observations

Our primary approach was directed to distinguish the kinetic and diffusion controlled regimes varying either the amount of the catalyst [W, g(cat)] or the flow rates of the reactants (V, $dm^3\ sec^{-1}$) at a given *n*-hexane partial pressure. From these data it was concluded that in the range of the ratio W/V [g(cat) sec dm^{-3}] between 10 to 100 the conversion of *n*-hexane was kinetically controlled in our *n*-hexane partial pressure range.

For the characterization of different reaction routes involved in *n*-hexane conversion of Pt/Al_2O_3 catalyst, the yields (Y_j) and selectivities (S_j) ($S_j = Y_j/\sum_j Y_j$) of the main reaction products were measured at different contact times. These data are shown in Fig. 2.

As can be seen from Fig. 2a the relationship between the conversion of *n*-hexane to hydrogenolysis products (Y_H) and the residence time is linear. The selectivity for hydrogenolysis products (S_H) increased only slightly at higher residence times. These data indicate that the main part of the hydrogenolysis products is formed directly from *n*-hexane, i.e. hydrogenolysis products can be considered as primary products of *n*-hexane conversion.

From Fig. 2b it can be suggested that isohexanes and methylcyclopentane are primary products, however, as their selectivity values decrease at

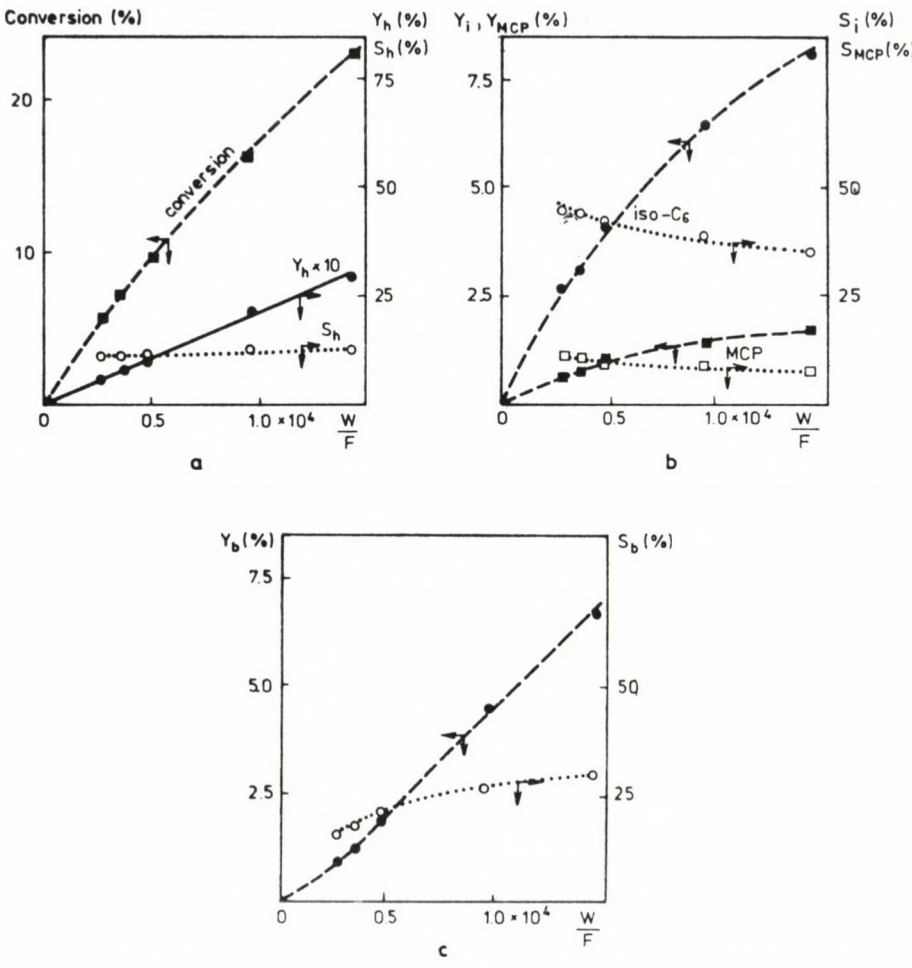

Fig. 2. *n*-Hexane conversion, product yields (Y_i) and selectivity (S_j) data as a function of residence time (W/F, g_{cat} s [mol(CH))$^{-1}$]. Reaction temperature 480 °C. *n*-Hexane pressure 16.4 kPa. Amount of catalyst 0.05 g; $\sum_i' Y_j$ = conversion, $S_j = Y_j / \sum_i' Y_j$

higher residence times, it is suggested that they are further converted, probably, to benzene. This suggestion is supported by the form of the kinetic curve of benzene formation. As is shown in Fig. 2c, the kinetic curve has a definite *S*-character, which clearly indicates that in the formation of benzene, parallel to a direct route for its formation, different consecutive reactions are involved. Based on the fact that the calculated initial rates of benzene formation were not zero, we came to the conclusion that a direct route for aromatization of *n*-hexane should also exist. In our work, in order to eliminate the influence of

these consecutive reactions, the initial rates of formation of different reaction products and of *n*-hexane conversions were calculated from the kinetic curves and these data were used to obtain further information on *n*-hexane conversion.

Rate dependence on n-hexane partial pressure

In these series of experiments the partial pressure of *n*-hexane was changed in the range from 0.4 to 16.4 kPa. The initial rates of *n*-hexane conversion and of formation of hydrogenolysis products, isohexanes, methylcyclopentane and benzene are plotted against *n*-hexane partial pressure and shown in Fig. 3.

As can be seen, upon increasing the partial pressure of *n*-hexane, the rates of formation of isohexanes and methylcyclopentane show a constant increase in the whole partial pressure range. At higher partial pressures the formation of methylcyclopentane appeared to be almost independent of *n*-hexane partial pressure, while the initial rate of formation of isohexanes increased slightly even in this partial pressure range.

The rates of formation of hydrogenolysis products showed a slight but well defined maximum vs. *n*-hexane partial pressure. Contrary to these data, the initial rates of benzene formation show a strong negative rate dependence in the whole pressure range studied.

From these data it can be concluded that different rate expressions will describe the rates of formation of these reaction products, i.e. different mechanisms should exist for these reactions.

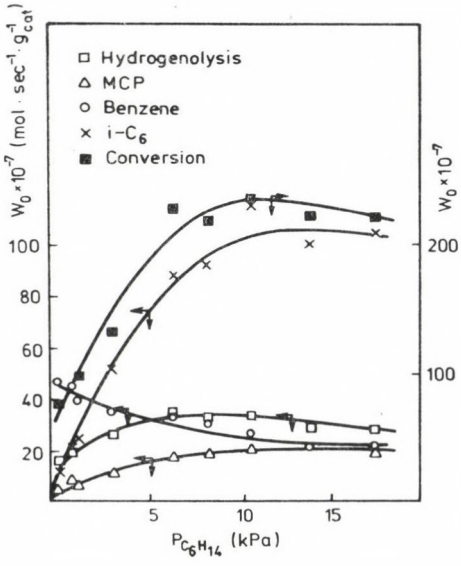

Fig. 3. Initial rates of *n*-hexane conversion and of product formation as a function of *n*-hexane partial pressure. Reaction temperature 480 °C

The negative rate dependence of benzene formation and the maximum obtained in the rates of formation of hydrogenolysis products indicate that the formation of these two products is hindered by the amount of *n*-hexane adsorbed on the catalyst, i.e. the higher the *n*-hexane partial pressure, the lower the number of sites available for the formation of the precursors of benzene and hydrogenolysis products. These data clearly demonstrate that from the point of view of site requirement the precursors of the main reaction products can be divided into two types: (i) precursors with large site requirement, responsible for the formation of benzene and hydrogenolysis products, (ii) precursors with small site requirement, responsible for the formation of isohexanes and methylcyclopentane.

Transient response curves

The transient response curves have been obtained under the following experimental conditions: reaction temperature 480 °C, *n*-hexane partial pressure 16.4 kPa, amount of catalyst (W) 0.1 g, flow rate (V) 0.5×10^{-3} dm^3 sec, the conversion of *n*-hexane under steady state condition was 23.7%.

As can be seen from Fig. 4, there are significant differences between the response curves of different reaction products. On the (inc. 0) part of the responses [9], i.e. after introduction of *n*-hexane, the benzene and hydrogenolysis products resulted in an overshoot type of response, while a monotonic increase type with a small delay was observed in the formation of isohexanes and methylcyclopentane. On the (dec. 0) part of the response [9], i.e. after disconnecting the *n*-hexane inlet into the reactor hydrogenolysis products, isohexanes and methylcyclopentane showed a monotonic decrease, while benzene and MCP indicated a false start type [9].

The distribution of the hydrogenolysis products is shown in Fig. 5. All of the these products, including isobutanes and isopentanes had an overshoot type of response. As far as the formation of 2MP and 3MP takes place by a monotonic increase type, it can be suggested that on the Pt/Al_2O_3 catalyst, there are at least two types of surface reactions responsible for the formation of hydrocarbons with branched chain.

One of the most interesting results in these series of experiments is the distinction between the formation of hydrogenolysis products and benzene. Beside the similarities found for these two products, i.e. maxima on the rate dependence on *n*-hexane partial pressure (see Fig. 3), and the overshoot type responses (Fig. 4), we obtained a very pronounced difference, the absence of the false start type response for hydrogenolysis products. This fact may indicate that either hydrogen is involved in different ways in the formation of benzene and hydrogenolysis products, or inhibition of the surface intermediates of benzene and of hydrogenolysis products to the reaction have different extent or mode.

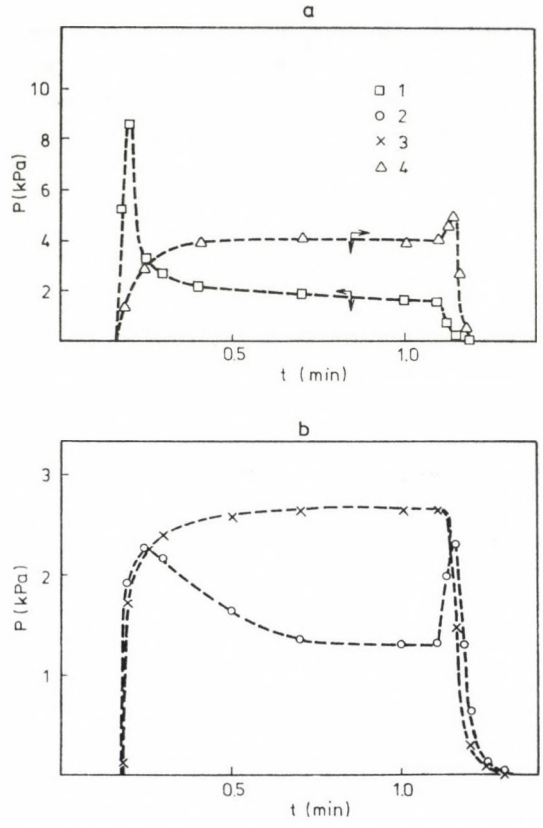

Fig. 4. Transient response curves of different reaction products. Reaction temperature 480 °C. Amount of catalyst 0.1 g. *n*-Hexane pressure 16.4 kPa. Gas flow rate 0.5×10^{-3} dm^3/s; (1) hydrogenolysis products, (2) benzene, (3) isohexanes, (4) MCP

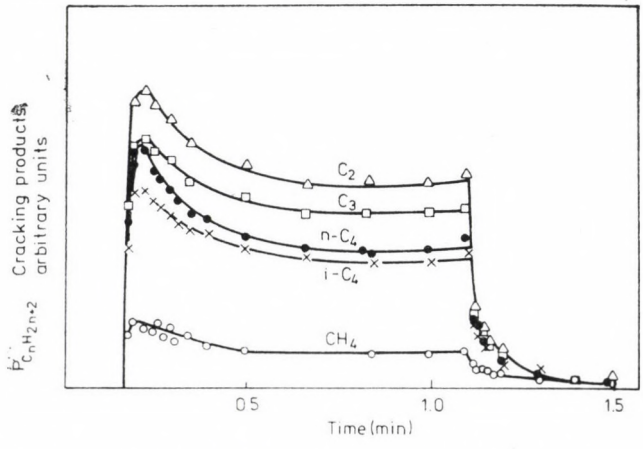

Fig. 5. Transient response curves of hydrogenolysis products. Experimental conditions: see *Fig. 4.* Partial pressures under steady state conditions (in kPa): $P_{CH_4} = 0.11$, $P_{C_2H_6} = 0.41$, $P_{C_3H_8} = 0.27$, $P_{n\text{-}C_4} = 0.20$, $P_{i\text{-}C_4} = 0.21$

Conclusions

Results obtained in this study clearly demonstrated the complexity of *n*-hexane conversions. Analogously to earlier findings, viz. that hydrocarbon reactions involved in naphtha reforming and aromatization are strongly influenced by the hydrogen partial pressure [4], we observed a very strong dependence on hydrocarbon partial pressure too. It is even more interesting that the influence of *n*-hexane partial pressure appeared to be significantly different for the main reaction products studied. Upon increasing the *n*-hexane partial pressure, the type of changes in the initial rates was different. The values of the ratio $\Delta w_0/\Delta P_{C_6H_{14}}$ were positive for isohexanes and partly for MCP, while they were negative for benzene and hydrogenolysis products. At higher *n*-hexane partial pressure the values of this ratio increased in the following order: benzene < hydrogenolysis products < MCP < *iso*-hexanes. From these data as well as from the hydrogen partial pressure dependences [4] it is suggested that the strength of chemisorption of the precursors of these products increases in the opposite direction.

The observed differences in the transient kinetic response curves of the main reaction products resulted in further evidence that the mechanism of formation of these reaction products is different.

Both steady state and transient kinetic results obtained in this work clearly demonstrated that on our Pt/Al_2O_3 catalyst the routes of *n*-hexane conversions are strongly influenced by the hydrocarbon coverage. At low hydrocarbon coverage there is a sufficient number of sites on Pt needed for reactions with high site requirements, i.e. under these conditions, as was evidenced, the formation of benzene and hydrogenolysis products prevailed. However, upon increasing the hydrocarbon coverage, the number of sites required for these reactions decreases, as is evidenced by the maxima on the dependence of the rate of formation of benzene and of hydrogenolysis products on *n*-hexane partial pressure (Fig. 3) and by the overshoot response type of these products in the transient kinetic curves (Fig. 4).

We consider that the increase of the site equirement can be related to the increase in the number of those carbon atoms of the adsorbed *n*-hexane which are bound to the platinum sites. It also indicates the higher extent of dehydrogenation of these surface species.

From data obtained in this work the following reaction scheme can be suggested.

This scheme only slightly differs from that given by Paál et al. [12] and it contains same part of our earlier scheme proposed in connection with the formation of different types of surface carbon [13]. Formation of surface species (A) and (B) are favoured at higher and lower *n*-hexane coverages, respectively. The differences between them are as follows: (i) (A) is a weakly

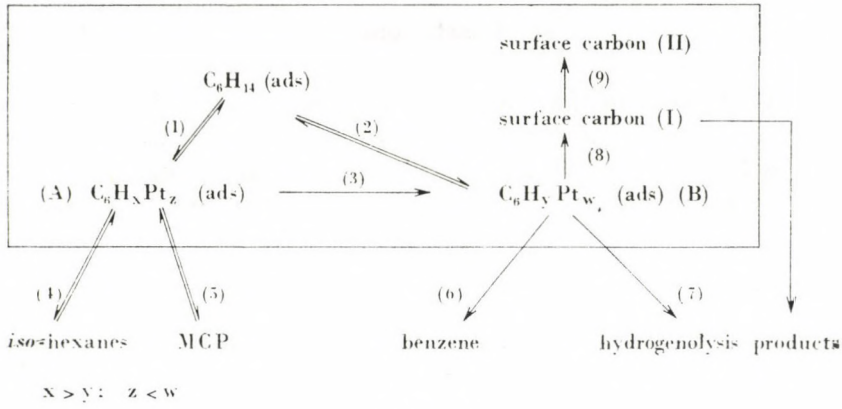

Scheme 1

bound surface species with a lower extent of dehydrogenation, (ii) (B) has higher site requirements and is bound to the surface more strongly.

Surface reactions (1), (2) and (6) were suggested earlier [12]. Based on experimental data observed at higher contact times, i.e. formation of benzene from isohexanes and MCP, we propose route (3) as an alternative possibility.

Reaction routes for surfaces species (B) will depend both on the extent of its dehydrogenation and its geometry (benzene formation would favour a "cisoid" configuration [4]). The reactivity of this species, as was demonstrated in our earlier paper [13], strongly depends on the availability of surface and gas phase hydrogen.

The similarity in the formation of hydrogenolysis products and benzene found in recent work supports routes (6) and (7). Routes (8) and (9) were proposed and evidenced in our previous work [13].

In order to give further details on the reaction mechanism more comprehensive kinetic studies are needed, which are in progress in our Laboratories.

REFERENCES

[1] Sinfelt, J. H.: "Bifunctional Catalysis" Advan. Chem. Engn., **5**, 37—74, Drew, T. B. et al., Eds., Academic Press, New York 1964
[2] Ciapetta, F. G., Wallace, D. N.: Catal. Rev., **5**, 67 (1971)
[3] Sinfelt, J. H.: in "Catalysis, Science and Technology", Anderson, J. R., Boudart, M., Eds., Vol. **1**, 257—300, Springer, Berlin 1981
[4] Paál, Z.: Adv. Catal., **29**, 273 (1980)
[5] Davies, S. M., Zaera, F., Somorjai, G. A.: J. Catal., **77**, 439 (1982)
[6] Paál, Z., Tétényi, P.: Acta Chim. Acad. Sci. Hung., **54**, 175 (1967)
[7] Hattori, T., Murakami, Y.: J. Catal., **10**, 114 (1968)
[8] Hattori, T., Murakami, Y.: J. Catal., **31**, 127 (1973)
[9] Kobayashi, M.: Chem. Engn. Sci., **37**, 393 (1982)
[10] Kobayashi, M.: Chem. Engn. Sci., **37**, 403 (1982)
[11] Kobayashi, H., Kobayashi, M.: Catal. Rev., **10**, 139 (1974)
[12] Paál, Z., Székely, G., Tétényi, P.: J. Catal., **58**, 108 (1979)
[13] Margitfalvi, J., Hegedüs, M., Gőbölös, S., Kwaysser, E., Koltai, L., Nagy, F.: Acta Chim. Acad. Sci. Hung., **111**, 573 (1982)

Acta Chimica Hungarica 119 (2—3), pp. 223—232 (1985)

COMPETITIVE HYDROGENATION OF A NITRILE FUNCTION AND OF AN OLEFINIC UNSATURATION ON RANEY NICKEL+

Jean Luc DALLONS[1,2], Georges JANNES[1]* and Bernard DELMON[2]

([1]C.E.R.I.A., I.I.F.-I.M.C., avenue E. Gryzon 1, B-1070 Bruxelles, [2]Université Catholique de Louvain, Groupe de Physico-Chimie Minérale et de Catalyse, place Croix du Sud 1, B-1348 Louvain-la-Neuve)

Received June 8, 1984
Accepted for publication September 12, 1984

The selectivity in the competitive hydrogenation of the carbon-carbon double bond and the carbon-nitrogen triple bond has been studied on Raney nickel.

This selectivity is different in the case of intramolecular competition (bifunctional molecules) and intermolecular competition (two monofunctional molecules).

For intermolecular competition, the adsorption factor is decisive: nitriles are hydrogenated and olefins are unreactive. In the case of bifunctional molecules, the olefinic unsaturation reacts first. Therefore, a more intricate mechanism must be assumed.

Introduction

As is well known, a catalyst may exhibit different activities in the hydrogenation of various functions. A reactivity order may be given starting with the more reducible function: this corresponds to the highest rate observed in the presence of the catalyst when a monofunctional molecule is hydrogenated alone. At first sight, it seems tempting to use this scale to explain the intramolecular selectivity of this catalyst for the hydrogenation of bifunctional molecules. Such a scale for instance may be built for group VIII b metals that are better catalysts for the hydrogenation of C=C bonds than for C=O or C≡N bonds. Hence, when observing that unsaturated ketones or aldehydes [1, 2] or unsaturated nitriles [3—9] lead to the saturated ones, the authors do not discuss that apparently normal selectivity.

In a broader research, Germain and coworkers [10] studied the competitive hydrogenation of aldehydes or ketones and olefins on copperchromite catalyst. They drew the conclusion that the scale of reactivity obtained in competitive hydrogenation of monofunctional compounds may be extended to non-conjugated bifunctional molecules. A conjugated molecule is an exception for these workers: it seems to act as a specific entity.

Nevertheless, the saturation of the olefinic bond in the hydrogenation of unsaturated dinitriles for the manufacture of saturated diamines is not an

+ This paper was presented at the 2nd Belgian—Hungarian Colloquium on Catalysis at De Haan, Belgium, October 10—13, 1983.

* To whom correspondence should be addressed.

easy reaction [11]. In our opinion, it is not simply due to a steric effect. This investigation is aimed at a better understanding of the competitive hydrogenation of a nitrile function with an olefinic unsaturation either in the same molecule or in two monofunctional compounds.

Experimental

The catalyst

The preliminary results were obtained on a Raney nickel prepared by the "Dominguez" method [12]. It consists in adding the Ni—Al alloy (50—50% by weight) to a stirred solution of sodium hydroxide (10% by weight), keeping the temperature at 95 °C. After washing with water, we stored this catalyst under methanol.

The specific surface area was determined by adsorption of nitrogen at 96 K by a gravimetric B.E.T. method. The sample was maintained under vacuum for 8 hours at room temperature and then outgassed at 100 °C until constant weight was reached [13]. This catalyst developed a surface area of 81 $m^2 g^{-1}$.

The further experiments were carried out on a Raney nickel prepared by the "Grenoble" method [14]. The Ni—Al alloy (50—50% by weight) is treated with boiling concentrated (6 *M*) sodium hydroxide solution without stirring, then washed with increasingly dilute sodium hydroxide solutions (3 *M*, 2 *M* and *M*). The catalyst is kept under a molar solution of sodium hydroxide.

The specific area was determined by adsorption of nitrogen at 96 K by a volumetric B.E.T. method. The catalyst is outgassed at a temperature of 100 °C at a pressure of 10^{-3} Torr over 4 hours [15]. This Raney nickel developed a surface of 65 $m^2 g^{-1}$. This preparation yields a catalyst with a lower surface area, but the reproducibility of the catalytic properties is better.

Moreover, when stored under sodium hydroxide solution, Raney nickel retains a longer activity [16].

Kinetic measurements

All the hydrogenation experiments were done in a well stirred autoclave (Labor-Druckrührwerk Ingenieurbüro SFS Zürich) under a constant hydrogen pressure of 10 bar. The apparatus allows the introduction of the reactants under pressure and is equipped with sampling and flushing attachments, and a thermocouple probe.

In a preliminary stage of the work, we have studied the experimental conditions to be free of diffusion control. In this way, the catalyst (0.3 g), weighted by pycnometry, is introduced under solvent in the reactor. The stirring rate is 750 rpm. The introduction of the compound to be hydrogenated is taken as the zero time of the experiment.

Analysis

Products analysis was performed by gas chromatography. Several phases were used according to the reaction to be studied.

a. Propionitrile in the presence of an amine : 2 m glass column filled with 10% Carbowax 20 M + 5% KOH on Chromosorb W 60—80 mesh.

b. Cyclohexene and competition between cyclohexene and propionitrile : 2 m glass column filled with 10% Carbowax 20 M on Chromosorb W 60—80 mesh.

c. Acrylonitrile and 3-butenenitrile : 2 m glass column filled with 20% D.E.G.S. on Chromosorb W 60—80 mesh.

1-butanol (a, b) and 1-pentanol (c) were used as internal standards.

Products

All the products were laboratory reagents. The solvents were treated with Raney nickel in order to trap sulfur compounds, and freshly distilled before use.

Results

In order to study the competition between a nitrile function and an olefinic unsaturation, we have firstly hydrogenated monofunctional molecules alone: then we have engaged them in a competitive reaction. Finally, the hydrogenation of conjugated or unconjugated unsaturated nitriles was considered. In each case, the influence of amines and that of different solvents was tested. The addition of amines is justified by the fact that on nickel, the main product of the hydrogenation of nitriles is the primary amine with the formation of some 20% of secondary amine [17].

a. *Propionitrile hydrogenation*

We have first hydrogenated a saturated nitrile alone and in the presence of a primary (Fig. 1) or a secondary (Fig. 2) amine. These results were obtained on a Raney nickel prepared by the "Dominguez" method [12].

b. *Cyclohexane hydrogenation*

On the other hand, we have reduced cyclohexene on Raney nickel (Fig. 3). The reaction rate was much lower when propylamine was added in the reaction mixture. These experiments and the following ones were performed on a Raney nickel prepared by the "Grenoble" method [14].

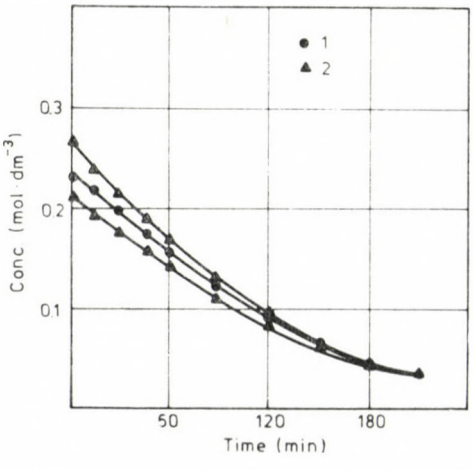

Fig. 1. Propionitrile hydrogenation. Solvent: methanol. Temperature : 70 °C. Hydrogen pressure : 10 bar. Raney nickel : 0.3 g. (1) propylamine added (2.5% vol.); (2) propionitrile alone

c. *Competitive reaction of cyclohexene with propionitrile*

When propionitrile was engaged in competition with cyclohexene, it was only the nitrile that underwent hydrogenation. Figure 4 shows also that the rate of nitrile hydrogenation was not affected by the presence of cyclohexene. After the complete disappearance of the nitrile, but in the presence of the amine formed, cyclohexene was not reduced.

This competitive reaction was made in many solvents such as cyclohexane, benzene, methanol, dioxane without any apparent modifications.

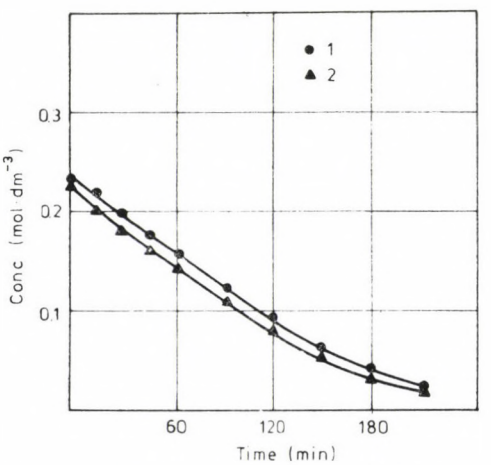

Fig. 2. **Propionitrile hydrogenation. Solvent: methanol. Temperature : 70 °C. Hydrogen pressure : 10 bar. Raney nickel : 0.3 g. (1) dipropylamine added (2.5% vol.); (2) propionitrile alone**

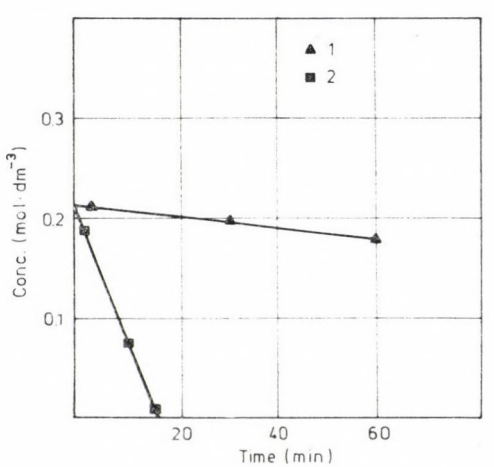

Fig. 3. **Cyclohexene hydrogenation. Solvent : methanol. Temperature : 70 °C. Hydrogen pressure : 10 bar. Raney nickel : 0.3 g. (1) propylamine added (2.5% vol.); (2) cyclohexene alone**

d. *Acrylonitrile hydrogenation*

Acrylonitrile is a molecule which contains an olefinic double bond conjugated with a cyano group. In this case, the catalyst was selective for the hydrogenation of the carbon-carbon unsaturation (Fig. 5). No unsaturated amine formation was detected. The reaction carried out in methanol and in isooctane gave the same results. The addition of a primary amine had no remarkable effect.

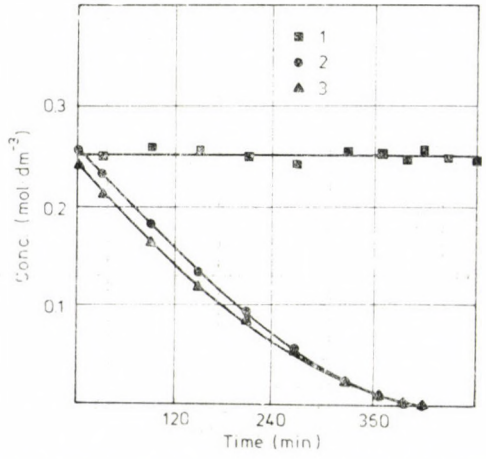

Fig. 4. Competitive hydrogenation of propionitrile and cyclohexene. Solvent : methanol. Temperature : 70 °C. Hydrogen pressure : 10 bar. Raney nickel : 0.3 g. (1) cyclohexene in a competitive reaction, (2) propionitrile alone, (3) propionitrile in a competitive reaction

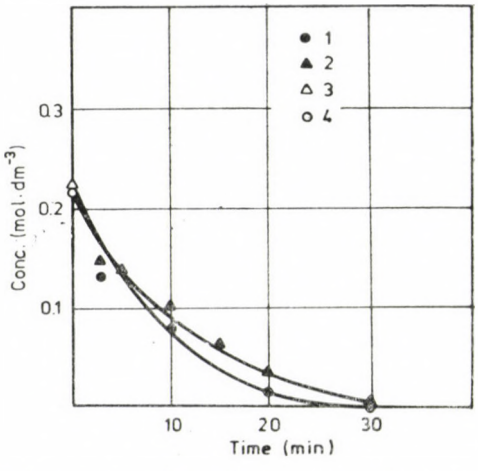

Fig. 5. Acrylonitrile hydrogenation. Solvent: isooctane. Temperature: 50 °C. Hydrogen pressure: 10 bar. Raney nickel: 0.3 g. (1) propylamine added (2.5% vol.), (2) acrylonitrile alone, (3, 4) concentrations determined by mass balance

e. *3-butenenitrile hydrogenation*

The same selectivity for the carbon-carbon double bond was observed in the hidrogenation of this nonconjugated nitrile (Fig. 6): no unsaturated amine formation was detected. Again, a solvent effect (e.g. methanol-isooctane) or an amine addition effect was not measurable.

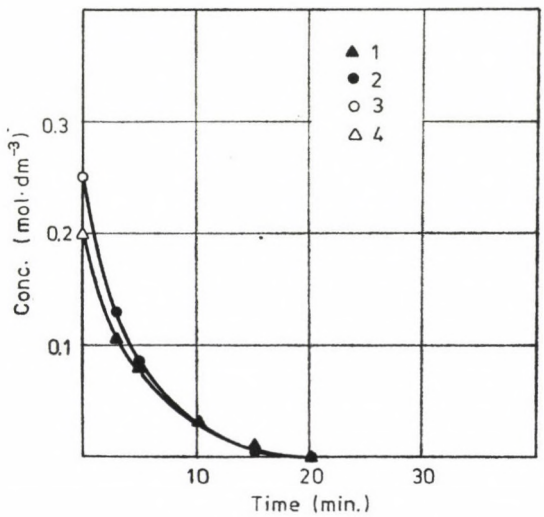

Fig. 6. 3-butenenitrile hydrogenation. Solvent: isooctane. Temperature: 50 °C. Hydrogen pressure: 10 bar. Raney nickel: 0.3 g. (1) propylamine added (2.5% vol.), (2) 3-butenenitrile alone, (3, 4) concentrations determined by mass balance

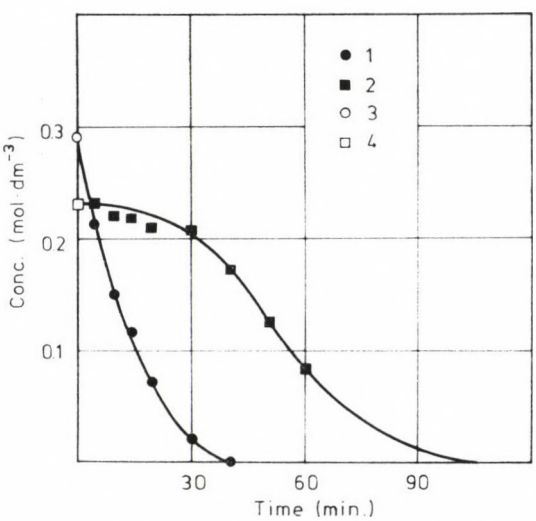

Fig. 7. Hydrogenation of acrylonitrile and 3-butenenitrile. Solvent: cyclohexene. Temperature: 50 °C. Hydrogen pressure: 10 bar. Raney nickel: 0.3 g. (1) acrylonitrile, (2) 3-butenenitrile, (3, 4) concentrations determined by mass balance

f. *Competitive hydrogenation of acrylonitrile and 3-butenenitrile*

In Figure 7, we can see that the selectivity of the catalyst was in favour of acrylonitrile hydrogenation. Nevertheless, 3-butenenitrile underwent noticeable hydrogenation from the beginning of the reaction.

Discussion

The hydrogenation of monofunctional molecules such as propionitrile and cylohexene shows that an olefin is more easily reduced than a nitrile.

On the other hand, propylamine and dipropylamine are not poisons for Raney nickel in the case of propionitrile hydrogenation, contrary to cyclohexene hydrogenation. We can conclude that an amino group is more strongly adsorbed than an olefinic unsaturation but more weakly adsorbed than a carbon-nitrogen triple bond. All the more, a nitrile should be more strongly adsorbed than an olefin.

This is confirmed by the competitive hydrogenation of propionitrile with cyclohexene where the olefin remains unreduced. The fact that cyclohexene is still not hydrogenated after the complete reduction of propionitrile is evidence for the influence of amines on the adsorption of olefins (Fig. 4).

We can propose a scale of affinity for the surface $C \equiv N > NH_2 > C=C$. The difference of affinity should be high enough to explain why the solvent has no effect on the selectivity.

The experimental results are just the opposite in the case of unsaturated nitriles.

We have seen that the selectivity is in favour of carbon-carbon double bond hydrogenation and is not disturbed by the presence of amine or by a change of solvent. We can deduce from the previous results that molecules such as acrylonitrile or 3-butenenitrile must be adsorbed at their cyano group. The fact that the olefinic unsaturation is hydrogenated first should depend on a complex mechanism. In the case of a conjugated unsaturated nitrile such as acrylonitrile, we propose two possible mechanisms.

The first should be that after the adsorption of the carbon-nitrogen triple bond, the carbon-carbon double bond is in the immediate vicinity of the catalyst surface. The vibrational amplitudes of atoms normal to faces are larger for a surface atom than for a bulk atom and this effect should facilitate raising a surface atom above the surface plane [18]. We suggest that the adsorption of acrylonitrile should look like the following:

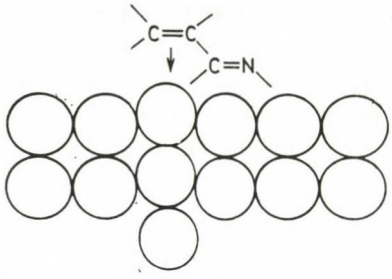

An alternative explanation should rest on tunnelling of hydrogen atoms from the hydrogen-rich surface to neighbouring olefinic unsaturations.

Another mechanism should be that the first hydrogenation of the nitrile function gives the primary imine, which can be isomerized into saturated nitrile as we can see in the following scheme:

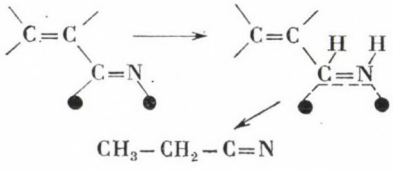

At present we have no argument to support one of these mechanisms.

In the case of 3-butenenitrile, the formation of butyronitrile can be explained by two reaction paths:

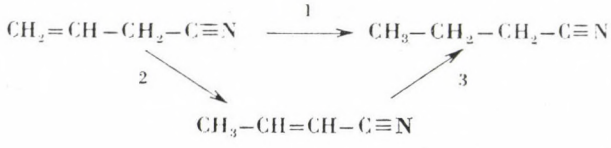

If 3-butenenitrile undergoes isomerization into 2-butenenitrile (step 2), the system reverts to the former case: the hydrogenation of a conjugated nitrile. Work under progress is aimed at the identification of a possible conjugated intermediate species. However, if direct hydrogenation (step 1) is important, simultaneous adsorption of the two functions, or at least vicinity of the olefinic unsaturation and the surface must be assumed.

For both unsaturated nitriles, hydrogenation of the nitrile function is not observed, but it should in any case be negligible at this temperature in the reaction time considered.

The result observed in the competitive hydrogenation of acrylonitrile and 3-butenenitrile cannot be explained by a higher reactivity of the conjugated C=C—C≡N group: in the separate hydrogenation of these two molecules, we observe a higher rate for 3-butenenitrile (Figs 5 and 6). Hence, we suppose that the conjugated C=C—C≡N group acts as a specific entity in the adsorption on the surface and has a higher adsorption coefficient than the nonconjugated nitrile. The idea of considering conjugated functions as a special entity has already been advanced by Germain and coworkers [10].

Conclusions

Hydrogenation of monofunctional molecules alone raises a possible comparison of reaction rate constants on the catalyst surface, provided that the products of the reaction and hydrogen do not compete with the reactant for the same sites. This means that, when fully covering the surface, a functional group will react faster or slower depending only on the rate constant of the reaction.

Results obtained when putting such monofunctional molecules in competition lead to the possible comparison between adsorption constants. The role of adsorption may be decisive in competitive reactions: a molecule, which has the smaller rate constant but a greater adsorption constant, can completely exclude another monofunctional molecule from the catalyst surface, preventing it from reacting. Adsorption is then the selectivity-determining step.

In the case of bifunctional compounds, the situation is more intricate. The reaction occurs as if the group with the greatest adsorption constant were bringing the molecule on the surface and then it were the group with the greatest rate constant which were hydrogenated.

*

Acknowledgements are made to Dr J. M. Piérard, directeur of the I.I.F. — I. M.C. for his interest in our work, and to the Province of Brabant for its financial support.

We owe all our thanks to Dr. B. K. Hodnett for his participation in the initial part of this work and the fruitful discussions we had together. The valuable help of P. Berteau is gratefully acknowledged.

REFERENCES

[1] Campelo, J. M., Garcia, A., Luna, D., Marinas, J. M.: Bull. Soc. Chim. Belg., **91,** 131 (1982)
[2] Noller, H., Lin, W. M.: React. Kinet. Catal. Lett., **21,** 479 (1982)
[3] Paul, R.: Bull. Soc. Chim. Fr., **7,** 296 (1940)
[4] Rylander, P. N.: Catalytic Hydrogenation over Platinum Metals. Academic Press, New York 1967
[5] Schreifels, J. A., Maybury, P. C., Swartz, Jr., W. E.: J. Org. Chem., **46,** 1263 (1981)
[6] Barnett, C.: Ind. Eng. Chem., Prod. Res. Develop,. **8,** 145 (1969)

[7] Russel, T. W., Hoy, R. C., Cornelius, J. E.: J. Org. Chem., **37,** 3552 (1972)
[8] Schreifels, J. A., Maybury, P. C., Swartz Jr., W. E.: J. Catal., **65,** 195 (1980)
[9] Tihanyi, T., Varga, K., Hannus, I., Kirics, I., Fejes, P.: React. Kinet. Catal. Lett., **18,** 449 (1981)
[10] Jenck, J., Germain, J. E.: J. Catal., **65,** 141 (1980)
[11] Drake, C. A., Campbell, R. W., Will, H. W., Vanderveen, J. W., Marwill, S. J.: Chem. Eng. Prog., 83, December 1982
[12] Dominguez, X. A., Lopez, I. C., Franco, R.: J. Org. Chem., **26,** 1625 (1961)
[13] Freel, J., Pieters, W. J. M., Anderson, R. B.: J. Catal., **14,** 247 (1969)
[14] Sane, S.: Thèse, Université Scientifique et Médicale de Grenoble (1981)
[15] Delannay, F., Damon, J. P., Masson, S., Delmon, B.: Applied Catal., **4,** 169 (1982)
[16] Chaudhary, V. R., Chaudhari, S. K.: J. Chem. Tech. Biotechnol., **32,** 925 (1982)
[17] Dallons, J. L.: Ing Chim. (Brux.), **65** (307), 3 (1983)
[18] Kung, N. H., Pellett, R. J., Burwell, Jr., R. L., J. Am. Chem. Soc., **98,** 5603 (1976)

Acta Chimica Hungarica 119 (2—3), pp. 233—244 (1985)

SYNTHESIS AND CHARACTERIZATION OF FAUJASITE-TYPE ZEOLITES, I

MULTINUCLEAR NMR CHARACTERIZATION OF LIQUID AND SOLID INTERMEDIATE PHASES FORMED DURING SYNTHESIS OF ZEOLITE Y+

Nicole DEWAELE, Philippe BODART, Zelimir GABELICA and Janos B. NAGY*

(Facultés Universitaires de Namur, Laboratoire de Catalyse, 61, Rue de Bruxelles, B-5000 Namur, Belgium)

Received June 8, 1984
Accepted for publication October 11, 1984

XRD, SEM, EDX and multinuclear solid and liquid state NMR techniques have been used to characterize the intermediate phases obtained during the synthesis of zeolite Y. The latter crystallizes at 100 °C from an aluminosilicate hydrogel having the composition $20Na_2O \cdot Al_2O_3 \cdot 20SiO_3 \cdot 700H_2O$. Solid state ^{23}Na-, ^{27}Al- and ^{29}Si-NMR allowed us to follow the incorporation of these atoms into the zeolite framework. High resolution NMR investigations of the same nuclei in the remaining solutions were very useful for the determination of the nature and the concentrations of the soluble aluminosilicate species. This combined solid and liquid state analysis yielded a deep insight into the mechanism of zeolite Y formation.

Introduction

During the last thirty years, increasing attention has been devoted to the synthesis and the multiple uses of new and/or improved zeolitic materials [1, 2]. Zeolites are defined as hydrated crystalline aluminosilicates with the chemical formula: $M_xD_y\,[Al_{x+2y}\,S_{n-(x+2y)}O_{2n}] \cdot m\,H_2O$ (M and D standing for mono- and divalent cations). They involve an ordered arrangement of SiO_4 (and AlO_4) tetrahedra interconnected through shared oxygen atoms. This arrangement gives rise to open structures forming channels and cages of molecular dimensions. The extra negative charges produced by the replacement of Si-atoms by trivalent Al-atoms are neutralized by positive counterions.

Due to its large pore volume, zeolite Y is of particular interest in catalysis, mainly in hydrocarbon conversions. Indeed, the structure of this zeolite consists of an arrangement of 24-hedra (sodalite cages) linked by double 6-ring units in a diamond-like structure. The large cavities so generated are interconnected through 12-membered ring windows (8Å diameter). The typical composition of zeolite Y, expressed as oxide mole ratio, is: $SiO_2/Al_2O_3 > 3$ [3, 4].

+ This paper was presented at the 2nd Belgian—Hungarian Colloquium on Catalysis at De Haan, Belgium, October 10—13, 1983.

* To whom correspondence should be addressed.

In order to control more efficiently the various physico-chemical and morphological properties of zeolites that influence in various ways their catalytic properties, a better understanding of the synthesis procedures of these materials is needed. The aim of this paper is to describe in detail the nucleation and growth processes of zeolite Y. This was achieved by characterizing by different physico-chemical techniques a series of intermediate (solid and liquid) phases that progressively appear during the crystallization of this zeolite.

Experimental

Synthesis procedure

Synthesis of zeolite Y was based on procedures proposed by Breck [4]. An aqueous aluminosilicate gel having a molar composition of $20Na_2O \cdot Al_2O_3 \cdot 20SiO_2 \cdot 700H_2O$ was prepared from sodium hydroxide (Merck P.A), silica gel (Davison grade 950) and sodium aluminate (Riedel de Haën). After 30 minutes stirring, the gel was divided in several portions, poured into polypropylene autoclaves and left at room temperature for 24 h. The autoclaves were then heated at 100 °C under autogeneous pressure in static conditions, and progressively removed from the oven after regular periods of time (0 to 26.5 h). After cooling to room temperature, each intermediate solid phase was filtered, washed thoroughly with cold water and dried at 120 °C for 20 h. Both solid (gel + zeolite) and liquid (filtrate) phases were characterized by various physico-chemical techniques.

Characterization of the samples

X-ray powder diffraction (XRD) patterns were recorded on a Philips P.W. 1349/30 diffractometer using monochromatic CuK_α radiation. This technique allowed us to identify the crystalline species within the solid phases and, hence, the degree of crystallinity of the latter, using the characteristic reflections of zeolite Y occurring at 2Θ values of 6.2, 15.6, 23.5, 29.4 and 31.2 degrees. 100% crystallinity has been assigned to the most crystalline sample [5].

SEM micrographs were obtained with a Jeol JSM-35 electron microscope; crystal morphologies, sizes and their distribution, as well as the possible presence of amorphous phases and/or impurities were determined. Si, Al and Na contents of the solid phases were measured by energy dispersive X-ray analysis (EDX) following the procedure previously described [6].

NMR spectra were obtained at room temperature, using a BRUKER CXP 200 spectrometer operating in the Fourier transform mode. High resolution magic angle spinning (HRMAS) solid state ^{29}Si-NMR spectra were recorded at a frequency of 39.7 MHz using an r.f. field of 49.3 Oe [7]. The Delrin conical rotor was spun at a rate of 3.1 kHz. Time intervals between the pulse sequences were 3.0 s. Tetramethylsilane (TMS) was used as external reference for chemical shift measurements (δ in ppm). Solid state ^{27}Al-NMR spectra [8] were obtained in static conditions, at a frequency of 52.1 MHz, using $Al(H_2O)_6^{3+}$ as external reference. Time intervals between pulse sequences were 0.1 s. Solid state ^{23}Na-NMR spectra [9] were recorded at 52.9 MHz, in static conditions, using 0.2 s time intervals between pulse sequences. Chemical shifts were measured with respect to aqueous $NaClO_4$, used as external reference. Liquid state ^{27}Al- and ^{23}Na-NMR spectra [10] have been obtained in the same conditions as the solid state spectra. Liquid state ^{29}Si-NMR spectra [11] were recorded at 39.7 MHz with a 6 s time interval between pulse sequences. Teflon tubes, spun at a frequency of 40 Hz, were used for all the liquid phase ^{29}Si-NMR measurements.

Results and Discussion

Characterization of the solid intermediate phases

The variation of XRD crystallinity with crystallization time shows a classical sigmoidal curve, as usually observed for zeolites growing in non-seeded systems [12—14]. At longer crystallization times, zeolite Y transforms into the more stable zeolite P and analcime.

Crystallites of zeolite Y appear octahedral in shape, as generally reported for the material [15]. Figure 1 shows the parallel evolution of XRD crystallinity and the average crystal size measured by SEM. Figure 2 compares particles size distributions for three different cyrstallization times. The observed uniform distribution suggests that the crystallization process is preceded by a single nucleation step [12].

The composition of the solid phase determined by EDX remains constant throughout the whole synthesis process, the atomic ratios Si/Al and Al/Na being 1.74 ($\pm$0.03) and 1.02 ($\pm$0.02) respectively. Thus, prior to crystallization, the initial gel has a composition (Si, Al and Na contents) similar to that of the final zeolite.

Figure 3 shows the HRMAS solid state ^{29}Si-NMR spectra of the intermediate phases obtained at various crystallization times. The spectra corresponding to the amorphous phase (1, 2 and 4 hours) consist of a broad line centered at δ = —90 ppm. As crystallization proceeds, the amorphous phase is reorganized and the five resonance lines characterizing zeolite Y become clearly resolved. They appear at δ = —84.6, —89.1, —94.5, —99.5 and —103.4 ppm and correspond to Si atoms having respectively 4, 3, 2, 1 and 0 Al-atoms in their second coordination sphere [7]. These values are close to those recorded for the initial amorphous phases, suggesting that the silicon environments in the amorphous phases and in the zeolite structure are very similar.

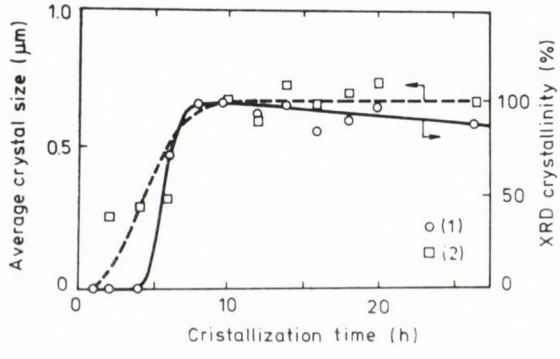

Fig. 1. Comparative evolution of XRD crystallinity (1) and of average crystal size (2) with crystallization time

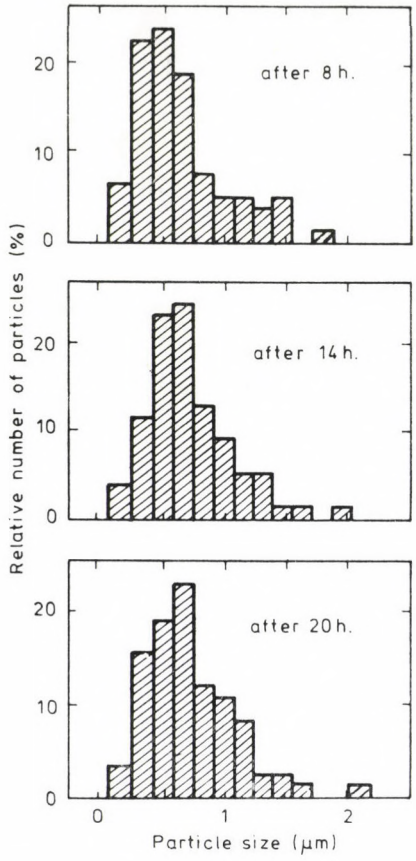

Fig. 2. Particles size distributions of various intermediate phases obtained during the crystallization of zeolite Y

Figure 4 compares the variations of XRD crystallinity and the total intensity of the ^{29}Si-NMR spectrum during crystallization. Although the composition of the solid phase remains constant, an increase of the ^{29}Si-NMR signal with XRD cristallinity is detected. This variation is related to the T_1 relaxation times of silicon atoms, probably different in the amorphous and in the crystalline phases [7].

A single resonance line appears at about $\delta = 56$ ppm in the solid state ^{27}Al-NMR spectra. It shows that Al-atoms occupy tetrahedral positions during the whole crystallization process [9]. The intensity of the line slowly increases during crystallization. As no variation in the Al-concentrations was detected by EDX, this suggests that only the most symmetrical Al-species are detected by NMR in the amorphous phases. Asymmetrical species can give rise to a very broad undetectable NMR line [10]. Furthermore, the corresponding line-

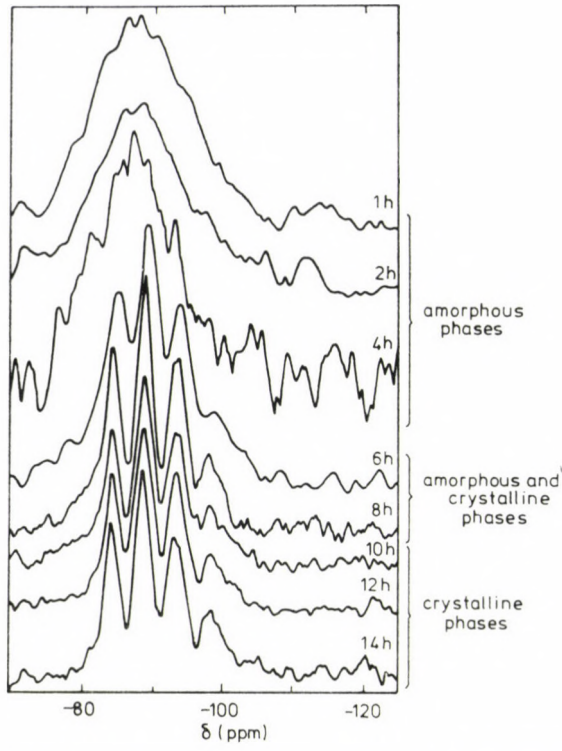

Fig. 3. Evolution of HRMAS solid state ^{29}Si-NMR spectrum of the intermediate phases during crystallization of zeolite Y

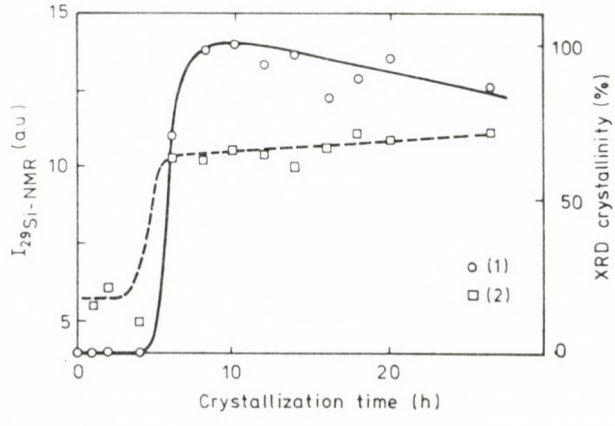

Fig. 4. Evolution of XRD crystallinity (1) and of ^{29}Si-NMR line intensity (2) of the solid phase during crystallization of zeolite Y

widths decrease during the process, showing the progressive Al-incorporation in the more organized zeolitic lattice (Figure 5).

The solid state ^{23}Na-NMR spectra mainly exhibit one resonance line occurring at about $\delta = -20$ ppm. As already observed in solid state ^{27}Al-NMR,

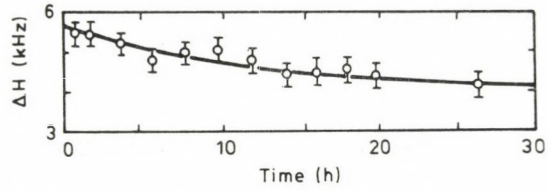

Fig. 5. Variation of solid state ^{27}Al-NMR linewidth (ΔH) with synthesis time

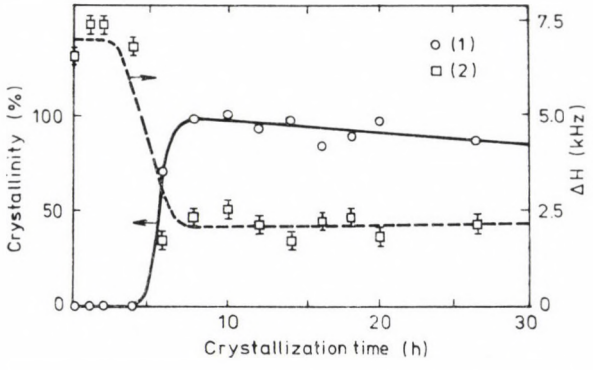

Fig. 6. Comparative evolution of XRD crystallinity (1) and solid state ^{23}Na-NMR linewidth (2), during crystallization time

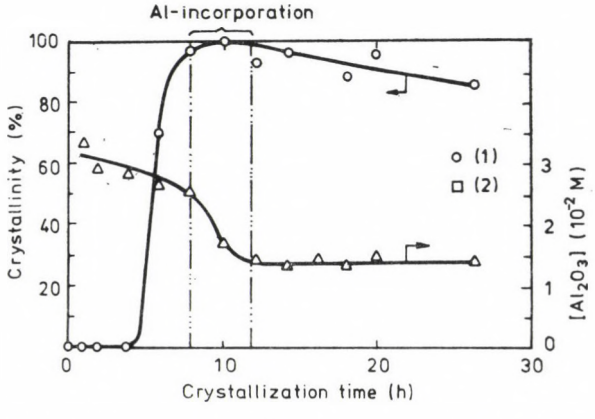

Fig. 7. Evolution of the Al_2O_3 content of the liquid phase (1) and of XRD crystallinity (2), as a function of synthesis time

the total intensity of this line slowly increases as the crystallization proceeds. The rapid decrease of the linewidth with increasing crystallinity illustrates the progressive incorporation of sodium ions from an amorphous solid into an ordered (crystalline) phase where the chemical shift distribution is narrower (Figure 6).

As a conclusion, the ^{29}Si-NMR line intensities and the ^{23}Na-NMR linewidths appear to be the best solid state NMR parameters to follow the progressive crystallization of amorphous intermediate phases into zeolite Y. The constant composition of the solid phases and the constant ^{23}Na-, ^{27}Al- and ^{29}Si-NMR chemical shifts throughout the whole process suggest that crystallization probably occurs directly from a rearrangement of the hydrogel and does not involve an important contribution of ion transportation through the liquid phase, from the gel to the growing crystallites.

Characterization of the liquid intermediate phase

Table I sums up the evolution of pH, density and Na_2O, SiO_2 and Al_2O_3 concentrations (obtained from liquid state NMR measurements) of the solutions, with the XRD crystallinity of the corresponding solid phases.

pH, density and SiO_2 and Na_2O concentrations remain essentially constant during all the crystallization process, while the Al_2O_3 content sharply decreases at the end of the process (Table I, Figure 7).

In alkaline medium, silicates and aluminosilicates are present in different monomeric or polymeric entities. The various Si-species are symbolized as $Q_x(n\text{Al})$, where Q represents the central Si-atom, x, the number of T-atoms (Si or Al) linked to it via an oxygen bridge and n, the number of Al-atoms in the second coordination sphere of the central Si. For instance, the $Q_2(1\text{Al})$

Table I

Evolution of pH, *density and composition of the liquid phase with* XRD *crystallinity of the solid phase, during zeolite* Y *synthesis*

Crystallization time (h)	pH	Density	$[SiO_2]$ (M)	$[Na_2O]$ (M)	$[Al_2O_3]$ $(10^{-2}\ M)$	XRD crystallinity of corresponding solid phase (%)
1	13.5	1.2	1.4	1.7	3.3	0
2	13.5	1.2	1.4	1.7	2.9	0
4	13.5	1.2	1.3	1.8	2.8	0
6	13.5	1.2	1.2	1.6	2.6	70
8	13.5	1.2	1.2	1.7	2.5	98
10	13.5	1.2	1.3	1.7	1.7	100
12	13.5	1.1	1.2	1.5	1.4	93
14	13.5	1.2	1.3	1.6	1.3	97
16	13.5	1.2	1.5	1.6	1.4	83
18	13.5	1.2	1.5	1.6	1.3	89
20	13.6	1.2	1.3	1.7	1.5	96
26.5	13.6	1.2	1.3	1.6	1.4	87

species corresponds to:

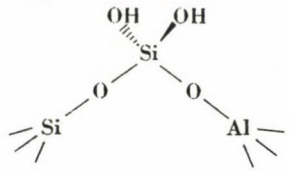

Liquid state ^{29}Si-NMR can discriminate between the different species. Figure 8 shows the typical chemical shift values for the various Si-spaces in aluminosilicates [11, 16—18].

Figure 9 gives the spectrum of the intermediate phase obtained after 6 h of heating at 100 °C. $Q_0(\delta = -72$ ppm), Q_1(OAl) ($\delta = -80$ ppm), Q_2(OAl) in cyclic trimer ($\delta = -82$ ppm) or in chains ($\delta = -90$ ppm) are among the main species that appear in solution. Q_2(2Al) as well as Q_3(2Al) and Q_4 species also contribute to the lines at $\delta = -80$ ppm and $\delta < -87$ ppm, respectively. As the chemical shifts remain constant, the nature of the species in solution mostly remain unchanged during the process.

Figure 10 shows the variation of the relative intensities measured for each species. Due to the Al-depletion of the solution during crystallization, a slow increase of the lines corresponding to Q_0 and Q_2(OAl)*(cyclic trimer) and a parallel decrease of the contribution of the other species are observed. At the end of the crystallization process, the line intensities recorded correspond to those measured in the case of a silicate solution of same concentration (Table II).

Figure 11 shows a typical ^{27}Al-NMR spectrum of an intermediate liquid phase. Up to five different lines can be distinguished, corresponding to Al-atoms with 0, 1, 2, 3 and 4 Si-atoms in their second coordination sphere (Table III) [19]. The main Al-bearing species in the intermediate liquid phases are Al(2Si), Al(3Si), and Al(4Si). As the aluminium of the solution is depleted,

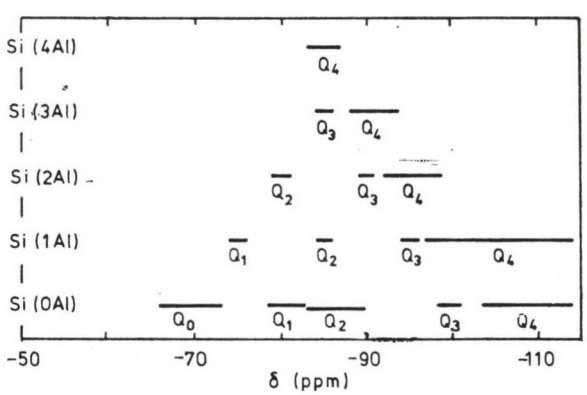

Fig. 8. ^{29}Si-NMR chemical shifts in various aluminosilicates [11, 17—19]

Table II

Comparison of the ^{29}Si-NMR line intensities of the liquid phase obtained at the end of zeolite Y crystallization, with the intensities recorded for silicate solutions of similar compositions

Composition: Si/Na	^{29}Si-NMR line intensities (%)				Ref.
	$\delta = -72$ ppm	$\delta = -80$ ppm	$\delta = -82$ ppm	$\delta = -90$ ppm	
2.56	45	26	16	13	(a)
2.4	44	34	21	—	[17]
2.5	53	24	12	10	[11]

(a) Liquid phase obtained after 26.5 h of crystallization.

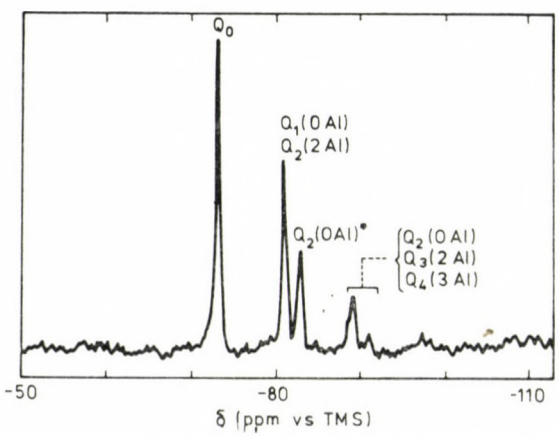

Fig. 9. Typical ^{29}Si-NMR spectrum of a liquid intermediate phase obtained during zeolite Y synthesis

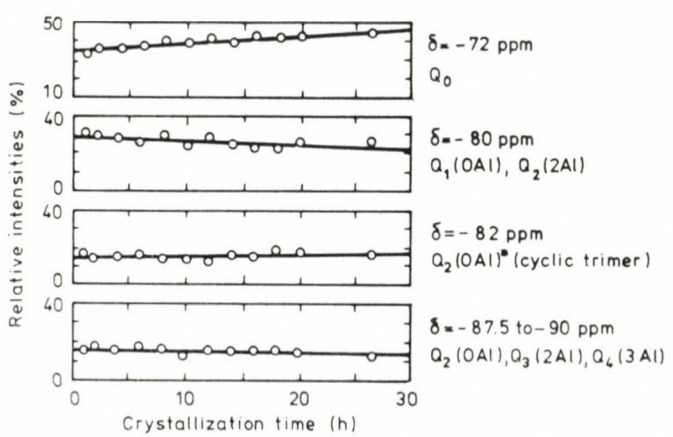

Fig. 10. Variation of the ^{29}Si-NMR line intensities of the liquid phase during crystallization of zeolite Y

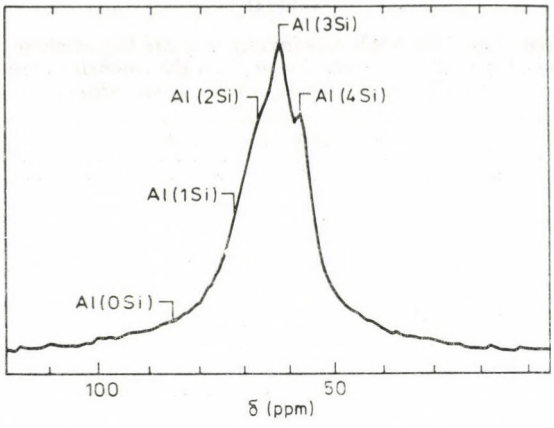

Fig. 11. Typical ^{27}Al-NMR spectrum of a liquid phase obtained during zeolite Y synthesis, after 2 h crystallization

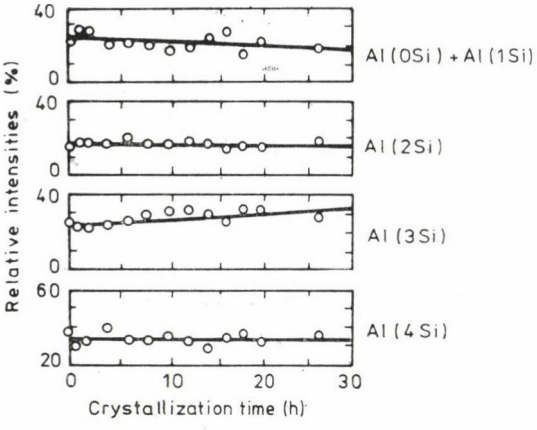

Fig. 12. Evolution of the various ^{27}Al-NMR line intensities of the liquid phase during zeolite Y synthesis

Table III

^{27}Al-NMR *chemical shifts of the different aluminic species in aqueous aluminosilicates solutions* [19]

Aluminic species	δ (ppm)	Symbol
$Al(OH)_4^-$	80	Al(0Si)
$Al(OH)_3(OSi\equiv)^-$	74	Al(1Si)
$Al(OH)_2(OSi\equiv)_2^-$	69	Al(2Si)
$Al(OH)_1(OSi\equiv)_3^-$	64	Al(3Si)
$Al(OSi\equiv)_4^-$	59	Al(4Si)

the Si-rich species are progressively favoured, with a resulting increase of the proportion of Al(3Si) and a decrease of the contribution of Al(0Si) and Al(1Si) (Figure 12).

The ^{23}Na-NMR spectrum of the liquid phase consists of a sharp resonance line occurring at $\delta = -3.6$ ppm. It is characteristic of a hydrated sodium ion. No significant change was detected during crystallization.

As a conclusion, liquid state multinuclear NMR allows us to determine the nature of the species in solution and their concentrations. As nearly no change in composition was detected during the first part of zeolite Y crystallization, it is supposed that the nucleation process directly occurs within the solid gel and that the crystallites start to grow by involving a straightforward reorganization of this hydrogel. At the end of the process, aluminium species are progressively incorporated from the solution into the growing crystallites.

Conclusions

Classical physico-chemical techniques (XRD, SEM, EDX) combined with liquid and solid state multinuclear NMR investigations proved to be a powerful tool to follow the evolution of the intermediate phases progressively formed during crystallization of zeolite Y. The composition of the solid intermediate phases was shown to be constant during all the crystallization process. Furthermore, in the liquid phase, Na_2O and SiO_2 concentrations, as determined by NMR, were also found constant during the process while the Al_2O_3 concentration decreased only at the end of the crystallization. Solid state ^{23}Na-, ^{27}Al- and ^{29}Si-NMR have shown that the chemical shifts of the initial gel phase as nearly the same as those measured in the crystalline phases. This indicates that Na-, Al- and Si environments in the initial (amorphous) and final (crystalline) solid phases are similar. Consequently, the crystallization of zeolite Y probably occurs through a reorganization of the hydrogel, confirming some previous findings [20]. However, the Al concentration changes and the depletion of some species [Al(1Si(, Q_2(2Al) in the liquid phase imply some participation of the solution species, at least at the end of crystal growth.

*

The authors thank Mr. G. Daelen for his skilful help in taking the NMR spectra and Mr. F. Vallette for technical assistance. P. Bodart acknowledges IRSIA (Belgium) for financial support.

REFERENCES

[1] Breck, D. W.: Zeolite Molecular Sieves, Wiley, New York 1974
[2] Barrer, R. M.: Hydrothermal Chemistry of Zeolites, Academic Press, London 1982
[3] Meier, W. M., Olson, D. H.: Atlas of Zeolite Structure Types, Structure Commission of the International Zeolite Association, 1978, p. 37

[4] Breck, D. W.: U. S. Pat. 3,130,007 (1964)
[5] Ref. [2], p. 176
[6] Gabelica, Z., Blom, N., Derouane, E. G.: Appl. Catal., **5**, 227 (1983)
[7] Gabelica, Z., B. Nagy, J., Bodart, P., Debras, G., Derouane, E. G., Jacobs, P. A.: in "Zeolites: Science and Technology" (F. R. Ribeiro et al., eds.) pp. 193—210, Martinus Nijhoff, Den Haag 1984
[8] B. Nagy, J., Gabelica, Z., Debras, G., Derouane, E. G., Gilson, J.-P., Jacobs, P. A.: Zeolites, **4**, 133 (1984)
[9] Bodart, P., Gabelica, Z., B. Nagy, J., Debras, G.: in "Zeolites: Science and Technology" (F. R. Ribeiro et al., eds.) pp. 211—226, Martinus Nijhoff, Den Haag 1984
[10] Dewaele, N.: Mémoire de licence, Facultés Universitaires de Namur, Namur 1983
[11] Engelhardt, G., Jancke, H., Hoebbel, D., Wieker, W.: Z. Chem., **14**, 109 (1974)
[12] Ref. [2], p. 145
[13] Culfaz, A., Sand, L. B.: Adv. Chem. Ser., **121**, 140 (1973)
[14] Ueda, S., Murata, H., Koizumi, M., Nishimura, H.: Am. Mineral., **65**, 1012 (1980)
[15] Ref. [2], p. 139
[16] Harris, R. K., Newman, R. H.: J. Chem. Soc., Faraday Trans. II, **73**, 1204 (1977)
[17] Marsmann, H. C.: Z. Naturforsch., Teil B, **29**, 495 (1974)
[18] Engelhardt, G., Hoebbel, D. Tarmak, M., Samoson, A., Lippmaa, E.: Z. Anorg. Allg. Chem., **484**, 22 (1982)
[19] Mueller, D., Hoebbel, D., Gessner, W.: Chem. Phys. Lett., **84**, 25 (1981)
[20] Polak, F., Stobiecka, E.: Bull. Acad. Pol. Sci., **26**, 899 (1978)

Acta Chimica Hungarica 119 (2—3), pp. 245—247 (1985)

THE RUTHENIUM(II)-TRIS-(1,4,5,8-TETRAAZA-PHENANTHRENE) DICATION: A NEW PHOTOCATALYST IN REDOX CYCLES FOR HYDROGEN PRODUCTION+

Andrée KIRSCH-DE MESMAEKER*, Daniel MAETENS and Raymonde NASIELSKI-HINKENS

(Université Libre de Bruxelles, Fac. Sciences, CP 160, Chimie Organique, 50 Av. F.D. Roosevelt, B-1050 Bruxelles, Belgium)

Received June 8, 1984
Accepted for publication October 11, 1984

A new Ru complex, the ruthenium(II)-tris-(1,4,5,8-tetraazaphenanthrene) dication, has been tested as photocatalyst of methyl viologen radical cation production ($MV^{\cdot+}$), in the presence of a sacrificial agent. The excited state of this complex is reductively quenched by irreversibly oxidized reducing agents (sacrificial agents). The so-produced reduced complex is able to reduce MV^{2+} with a quantum yield better than with $Ru(bpy)_3^{2+}$ (bpy ≡ 2,2'-bipyridine).

Introduction

The $Ru(bpy)_3^{2+}$ (bpy ≡ 2,2'-bipyridine) has been extensively studied during the last few years because of its potential use for H_2 production [1—6]. It has been shown that in the presence of methyl viologen (MV^{2+}) as electron relay, and triethanolamine (TEOA) as sacrifical agent, the $Ru(bpy)_3^{2+}$ excited state is oxidatively quenched by MV^{2+} to produce $Ru(bpy)_3^{3+}$ and the methyl viologen radical cation ($MV^{\cdot+}$). The sacrificial compound (TEOA) is irreversibly oxidized by the Ru^{3+} to regenerate the starting complex. The quantum yield of $MV^{\cdot+}$ production ($\Phi MV^{\cdot+}$) is equal to 0.19 (5.7×10^{-5} *M* $Ru(bpy)_3^{2+}$, 0.2 *M* TEOA, 0.06 *M* MV^{2+}) [7]. When colloidal Pt is added to the system, $MV^{\cdot+}$ reduces the protons with regeneration of MV^{2+} and H_2 evolution [2, 5, 6].

Very recently, Crutchley and Lever [7] synthesized a new ruthenium complex, $Ru(bpz)_3^{2+}$ (bpz ≡ bipyrazine), and tested it as a photocatalyst of $MV^{\cdot+}$ production, in the presence of sacrificial TEOA; in this case, $\Phi MV^{\cdot+}$ reaches 0.77 (6×10^{-5} *M* Ru bpz_3^{2+}, 0.6 *M* TEOA, 0.02 *M* MV^{2+}). However, in this system, the $Ru(bpz)_3^{2+*}$, contrary to the $Ru(bpy)_3^{2+*}$, is reductively quenched by TEOA, with formation of $Ru(bpz)_3^{+}$, capable of reducing MV^{2+}.

This shows that the complexes in the excited state behave differently depending on the nature of the ligand and play either the role of a reductant

+ This paper was presented at the 2nd Belgian—Hungarian Colloquium on Catalysis at De Haan, Belgium, October 10—13, 1983.

* To whom correspondence should be addressed.

(Ru bpy_3^{2+}) or of an oxidant (Ru bpz_3^{2+}) with different $\Phi MV^{\cdot+}$ values. In connection with this last result, it seemed of interest to test the potentialities of a still little explored ligand: the 1,4,5,8-tetraazaphenanthrene (TAP). The $Ru(TAP)_3^{2+}$ has thus been prepared [9] and tested as photocatalyst in redox cycles for H_2 production, with consumption of an electron donor.

Results and Discussion

In order to use the $Ru(TAP)_3^{2+}$ as a photocatalyst, it is important to know its electrochemical and photochemical properties. We have shown that $Ru(TAP)_3^{2+}$ behaves similarly compared to the $Ru(bpy)_3^{2+}$ in cyclic voltammetry, with all the waves shifted positively by about +0.5 V, which makes the complex more oxidizing [4]. Based only on the energy of the luminescence maximum and on the oxidation and reduction potentials in the ground state, the redox potentials in the excited state can be estimated to be

$$E^\circ(RuTAP_3^{2+*/3+}) < -0.21 \text{ V (SCE)}$$

$$E^\circ(RuTAP_3^{2+*/1+}) > +1.38 \text{ V (SCE)}$$

and indicate that, opposite to the $Ru(bpy)_3^{2+}$, the $Ru(TAP)_3^{2+*}$ is a weak reducing agent and a very strong oxidant. In agreement with this conclusion, the luminescence quenching by reductants such as hydroquinone (H_2Q), TEOA or cysteine (RSH) is almost diffusion controlled ($k_{qH_2Q} = 4.5\times10^9\ M^{-1}\ s^{-1}$, pH 5; $k_{qTEOA} = 0.3\times10^9\ M^{-1}\ s^{-1}$, pH 9; $k_{qRSH} = 2.2\times10^9\ M^{-1}\ s^{-1}$, pH 9), whereas there is no quenching by MV^{2+}.

The photolysis of the complex in the presence of a reductant has been studied in order to observe reduced species, capable of reducing MV^{2+}. The photodechelation ($\Phi \leq 10^{-3}$) which occurs in H_2O without reductant is completely quenched in the presence of a reversibly oxidized reducing agent such as hydroquinone and the system becomes photostable. On the other hand, with cysteine or TEOA, irreversibly oxidized reductants, at least 2 photoproducts are formed in degassed aqueous solutions. One of them is a reduced entity able to be reoxidized into the starting complex, in the presence of O_2 or MV^{2+}; the other one is probably a dechelated complex species, insensitive to O_2 and MV^{2+} ($\lambda_{max} = 490$ nm). When the photolysis is performed in the presence of cysteine or TEOA *and* MV^{2+}, able to trap the reduced complex before its dechelation, $MV^{\cdot+}$ is produced. The $\Phi MV^{\cdot+}$ values have been determined under vacuum, by illumination of the complex at 430 nm and by monitoring the $MV^{\cdot+}$ production at 605 nm. With cysteine (5×10^{-5} *M* $RuTAP_3^{2+}$, 0.1 *M* RSH, 0.06 *M* MV^{2+}, pH 7), $\Phi_{MV^{\cdot+}} = 0.20$ and with TEOA (5×10^{-5} *M* $RuTAP_3^{2+}$, 0.1 *M* TEOA, 0.02 *M* MV^{2+}, pH 9.5), $\Phi_{MV^{\cdot+}} = 1.11$. It has to be

noticed that with TEOA, one absorbed quantum can produce two $MV^{\cdot+}$, since the produced radical cation of TEOA is deprotonated in basic solution to give rise to a reducing radical, able to reduce MV^{2+}. The maximum quantum yield is thus 2 with TEOA [2].

In conclusion, based on the $\Phi MV^{\cdot+}$, the three-component system "$RuTAP_3^{2+}$ + TEOA + MV^{2+}" is more efficient than with $Ru(bpy)_3^{2+}$ and even slightly better than with $Ru(bpz)_3^{2+}$, in the same experimental conditions. However, the instability of the photoreduced $RuTAP_3^{2+}$, as evidenced by photolysis of the complex with cysteine or TEOA, would present a slight disadvantage compared to the $Ru(bpy)_3^{2+}$, for H_2 production with an electron relay and colloidal Pt.

REFERENCES

[1] Kirch, M., Lehn, J. M., Sauvage, J. P.: Helv. Chim. Acta, **62,** 1345 (1979)
[2] Kalyanasundaram, K., Kiwi, J., Grätzel, M.: Helv. Chim. Acta, **61,** 2720 (1978)
[3] De Laive, P. J., Sullivan, B. P., Meyer, T. J., Whitten, D. G.: J. Am. Chem. Soc., **101,** 4007 (1979)
[4] Abruña, H. D., Teng, A. Y., Samuels, G. J., Meyer, T. J.: J. Am. Chem. Soc., **101,** 6745 (1979)
[5] Kiwi, J., Grätzel, M.: Nature, **281,** 657 (1979)
[6] Kiwi, J., Borgarello, E., Pelizzetti, E., Visca, M., Grätzel, M.: Angew. Chem. Int. Ed., **19,** 646 (1980)
[7] Crutchley, R. J., Lever, A. B. P.: J. Am. Chem. Soc., **102,** 7128 (1980)
[8] Nasielski-Hinkens, R., Benedek-Vamos, M.: J. Chem. Soc., Perkin Trans. 1, **1975,** 1229
[9] Kirsch-De Mesmaeker, A., Nasielski-Hinkens, R., Maetens, D., Paulwels, D., Nasielski, J.: Inorg. Chem., **23,** 377 (1984)

Acta Chimica Hungarica 119 (2—3), pp. 249—264 (1985)

METATHESIS AND OLIGOMERIZATION OF PROPENE OVER MOLYBDENA-ALUMINA CATALYSTS+

József ENGELHARDT* and Dénes KALLÓ

(Central Research Institute for Chemistry of the Hungarian Academy of Sciences, H-1525 Budapest, P.O. Box 17)

Received June 8, 1984
Accepted for publication October 15, 1984

Metathesis of propene at 313 K and its oligomerization at 470—550 K were studied over a molybdena-alumina catalyst pretreated under various conditions. Activity of the catalyst decreased in both reactions as a result of elution with nitrogen at high temperature (823 K) after reduction with hydrogen. Ammonia was found to be an effective poison in both reactions. Hydrogen adsorbed at high temperature on reduced catalyst poisoned metathesis but did not influence oligomerization. Conversion in oligomerization of propene and selectivity in formation of C_6 alkenes varied in an identical way under various conditions.

Introduction

Since the discovery of olefin metathesis reactions [1, 2], molybdena-alumina catalysts — often with a CoO promoter — are widely used in these processes. The behaviour of the catalysts can be influenced significantly by different pretreatments. In metathesis of propene, the activity of a MoO_3/Al_2O_3 catalyst increases upon reduction with hydrogen or carbon monoxide [3—5]. The hydrogen adsorbed on the catalyst reduced under identical conditions has an even more significant influence on the behaviour of the catalyst [6, 7]. The rate of metathesis increases when hydrogen is adsorbed at low temperatures, but the hydrogen adsorbed at higher temperatures decreases the metathetic activity of the catalyst.

Polymerization of ethene was described on a MoO_3/Al_2O_3 catalyst pre-reduced with hydrogen [8, 9]. It has been found that the rate of polymerization is hardly influenced by hydrogen adsorbed whether at low or at high temperature [10]. The isomerization rate of 2-butenes, however, is usually high over catalysts holding hydrogen bound at high temperature [11]. Catalysts which are equally active in metathesis and double bond isomerization can be used in production of higher molecular weight olefins from e.g. propene

+ This paper was presented at the 2nd Belgian—Hungarian Colloquium on Catalysis at De Haan, Belgium, October 10—13, 1983.

* To whom correspondence should be addressed.

(metatethic oligomerization, "metol" reaction) [12, 13]. It is the goal of this paper to shed some light on how the activity of MoO_3/Al_2O_3 catalyst in metathesis and oligomerization of propene is influenced by various pretreatments.

Experimental

Catalysts

Catalysts consisted of 10 mass % MoO_3 (referred to the support) on Ketjen CK 300 Al_2O_3 (particle size 0.2—0.4 mm) [14] and 15 mass % MoO_3 on the same carrier (1/16" pellets). They are denoted by C 310 and C 315, respectively. Preparation of the catalysts involved impregnation of the support (incipient wetness technique) with an adequate amount of molybdic acid (Merck, commercial grade) dissolved in dilute ammonium hydroxide, then drying at room temperature by evacuation, heating to 823 K in dry air stream, and calcination under these conditions for 24 h. Surface of support and catalysts calculated from nitrogen adsorption isotherms were 214 and 205 $m^2 g^{-1}$, respectively.

Reactants

Commercial oxygen was passed through a trap cooled with liquid nitrogen and an adsorber containing activated clinoptilolite to remove water contamination. High purity nitrogen was purified further with Ridox Reagent (Fischer Scientific Co.) and by cooling with liquid nitrogen to remove traces of oxygen and water. Ultrapure hydrogen was prepared by diffusion using a Matheson hydrogen purifier. Ammonia (Matheson, anhydrous) was outgassed after freezing with liquid nitrogen. Polymerization grade propene (Tisza Chemical Works) was redistilled after outgassing.

Equipment and procedures

Propene metathesis experiments were carried out at 313 K either in a flow, or in a closed recirculation system using a U-shaped quartz reactor attached to a combined system equipped with greaseless "O" ring taps. The reactor and the recirculation system could be evacuated separately to 1×10^{-2} Pa using two-stage mercury diffusion pumps and traps cooled with liquid nitrogen. Change of pressure in the recirculation system was measured with a mercury manometer. The same charge of catalyst (1 g) was used repeatedly in each experiment. The composition of the reaction mixture was determined by gas chromatographic analysis on a 3 m long column containing 20% dibenzylamine/Chromosorb P; flame ionization detector was used.

Propene oligomerization experiments were carried out in a flow system at 470—550 K, atmospheric pressure using a quartz reactor. The same charge of catalyst (33 g) was used repeatedly in each experiment. Liquid products were collected in a trap cooled to 263 K. Flow rate of propene before the reactor and after the cold trap was measured by rotameters. Composition of the liquid product was determined by gas chromatographic analysis on a 6 m long 24% squalane/Chromosorb P column. Components were identified using reference materials and on the basis of retention indices given by Soják et al. [15] and Rijks and Cramers [16].

Infrared spectroscopic study of C 310 was carried out using a Perkin Elmer 577 double-beam grating spectrometer. A film of 12 mg cm^{-2} "thickness" was pressed and placed into a cell equipped with a calcium fluoride window. The film in the cell was treated with different gases and by evacuation. The infrared spectra were recorded at room temperature in the frequency range of 1000—3000 cm^{-1}.

Activation of the catalysts

Basic activation and regeneration of the catalysts started by heating to 823 K in streaming oxygen followed by calcination for 2 h and by evacuation at 823 K for 0.5 h. Then it was reduced with hydrogen at 823 K, atmospheric pressure for 2 h (CAT-H). In certain cases activation was carried out only with oxygen (CAT-O). Both types of activation were followed by various pretreatments described below. Oxidation and reduction of the catalyst was carried out by recirculation of gases in the combined system and with streaming gases in the flow system.

Results

Effect of hydrogen adsorbed on reduced catalyst

Metathesis of propene was carried out over 1 g of C 310 (CAT-H) at 313 K, 100 kPa in a flow system. The catalyst was evacuated at 823 K for 1 h after reduction, then hydrogen was recirculated through it again at various temperatures and 100 kPa for 0.25 h. The reactor was cooled rapidly to 313 K in hydrogen, and the feed of propene was started without any evacuation of the catalyst. The rate of metathesis calculated from the amount of ethene and 2-butene formed over catalysts pretreated under various conditions is plotted against reaction time in Fig. 1.

Initial increase of the activity of catalyst was observed in each case. The activity maxima decrease upon increasing the temperature of second hydrogen treatment. This treatment above 453 K resulted in a lower activity than that of the catalyst without additional hydrogen treatment (curve 1); below 373 K, however, this treatment led to a higher activity. The catalyst treated with hydrogen at 823 K (curve 2), like the catalyst without evacuation at 823 K after reduction [7] appeared to be almost totally inactive in metathesis of propene.

Experiments were carried out under identical conditions as above, but instead of hydrogen treatment at various temperatures, the catalysts were

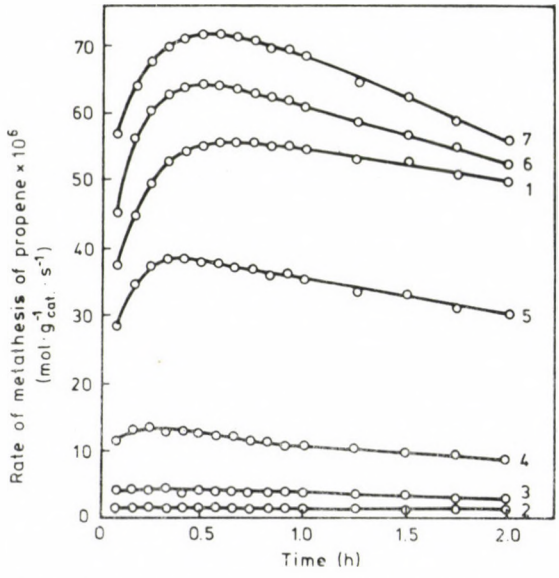

Fig. 1. Rate of metathesis of propene over 1 g of C 310 (CAT-H). Flow system, 313 K, 100 kPa. Pretreatment of catalyst by evacuation for 1 h at 823 K, and: no additional pretreatment (1); recirculation of atmospheric hydrogen for 0.25 h at 823 (2); 673 (3); 523 (4); 453 (5); 373 (6); and 313 K (7)

Table I

Relative rate of metathesis of propene over molybdena-alumina (CAT-H) evacuated at different temperatures for 1 h

Temperature of evacuation (K)	Relative rate of metathesis (%)
823	100
723	25
673	4
623	2.5

evacuated at different temperatures for 1 h after reduction. The maximum rates of metathesis related to that obtained over catalysts evacuated at 823 K are collected in Table I. As can be seen, the activity of the catalyst evacuated even at 723 K is significantly lower than that of the catalyst evacuated at 823 K.

Effect of nitrogen

Experiments were carried out over C 310 (CAT-H) and (CAT-O) under similar conditions as above. After activation, the catalysts were either evacuated at 823 K for 1 h, or atmospheric nitrogen was recirculated through them at the same temperature for 1 h and through a trap cooled with dry ice-acetone. One hour runs were interrupted by nitrogen recirculation through the reactor at 313 K for 0.5 h and through a cold trap. The rate of metathesis over such catalysts is plotted against time in Fig. 2.

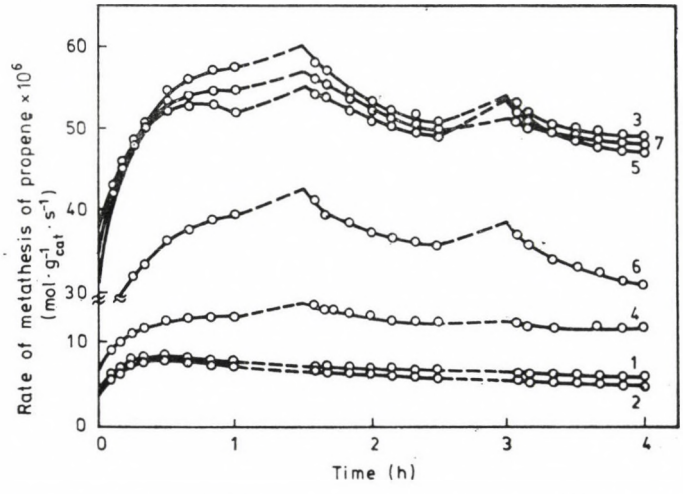

Fig. 2. Rate of metathesis of propene over 1 g of C 310. Flow system, 313 K, 100 kPa. Pretreatment of catalysts after activation carried out for 1 h at 823 K: evacuation of CAT-O (1); recirculation with nitrogen of CAT-O (2); evacuation of CAT-H (3); recirculation with nitrogen of CAT-H followed by evacuation (4); evacuation of CAT-H followed by recirculation with nitrogen (6); evacuation of CAT-H followed by recirculation with nitrogen at 313 K (7)

Table II

Relative rate of metathesis of propene over molybdena-alumina (CAT-H) treated with ammonia at 823 K then treated in various ways

Treatment after poisoning with ammonia	Relative rate of metathesis[a]
Evacuation at 313 K	0
Evacuation at 723 K	0
Evacuation at 823 K	39
Reactivation[b]	100

[a] Rate values referred to that obtained over unpoisoned catalyst.
[b] Activation with oxygen for 2 h, then with hydrogen for 2 h and evacuation for 1 h at 823 K.

The activity of CAT-O was the same after evacuation (curve 1) as after nitrogen elution (curve 2). The change in activity after interruptions was insignificant. The activity of CAT-H, however, was significantly higher after evacuation (curve 3) than after elution with nitrogen (curve 4). Interestingly, the nitrogen elution during the interruptions did not result in activity decrease, even some increase of metathesis rates was observed.

The activity of CAT-H eluted with nitrogen was closer to that of CAT-O than to that of CAT-H evacuated. One obvious explanation for this would be the presence of oxygen impurity in nitrogen, which to some extent could reoxidize the catalyst. But, as can be seen in Fig. 2, the activity of CAT-H eluted with nitrogen and then evacuated (curve 5) was nearly as high as that of the catalyst without nitrogen treatment (curve 3). This means that the drop of activity cannot be attributed to reoxidation but to poisoning by nitrogen itself.

When the sequence of elution with nitrogen and evacuation was reversed, i.e. the catalyst was first evacuated, then eluted with nitrogen, a less significant activity drop was observed (curve 6) than in the case of nitrogen treatment after reduction directly. No decrease of the activity was observed, however, when after evacuation the catalyst was eluted with nitrogen at 313 K (curve 7).

Effect of ammonia

Experiments for metathesis of propene were carried out under identical conditions as above, but the catalysts were poisoned by ammonia. After reduction with hydrogen for 2 h and evacuation for 1 h at 823 K, ammonia was recirculated through the catalyst for 0.25 h at the same temperature, 25 kPa pressure. This was followed by evacuation at different temperatures for 1 h. The maximum metathetic reaction rates related to those obtained over unpoisoned catalyst are collected in Table II. Catalyst evacuated at 313 K

was inactive in propene metathesis. Even the catalyst evacuated at 823 K regained only a fraction of its activity. The activity of the catalyst was restored, however, by reactivation, i.e. by reoxidation and reduction.

Infrared spectra

The film of catalyst reduced with hydrogen and evacuated at 823 K was exposed to ammonia at room temperature, 26.6 kPa. The band at 1440 cm^{-1} characteristics of ammonium ions disappeared after evacuation at 573 K for 0.5 h. No such bands appeared when freshly reduced films were exposed to nitrogen at 823 K.

Selectivity in metathesis of propene

Selectivity in propene metathesis over molybdena-alumina is mainly influenced by isomerization of 2-butenes and oligomerization of ethene:

$$2C_3H_6 \rightleftharpoons C_2H_4 + 2-C_4H_8 \quad (1)$$

$$2-C_4H_8 \rightleftharpoons 1-C_4H_8 \quad (2)$$

$$2C_2H_4 \rightarrow 1-C_4H_8 \quad (3)$$

$$1-C_4H_8 + 2-C_4H_8 = C_3H_6 + 2-C_5H_{10}. \quad (4)$$

Experiments were carried out over 1 g of C 310 (CAT-O) and (CAT-H) at 313 K, 100 kPa initial pressure in recirculation system. Hydrocarbon uptake by the catalyst in the course of reaction was determined from pressure drop. Hydrocarbon uptake partly resulted from adsorption, but a fraction of it can be regarded as due to oligomerization. For comparison, experiments with ethene were carried out as well. The hydrocarbon uptake against time is plotted in Fig. 3.

Continuous increase of the hydrocarbon uptake from ethene and the simultaneous appearance of butene and liquid hydrocarbons in the products [14] indicate that CAT-H, independently of its pretreatment, is active in ethene oligomerization under the given conditions. The much less significant rate of uptake in case of propene shows that oligomerization of propene besides metathesis is insignificant under these conditions. 1-Butene in the products can originate from 2-butene isomerization as well as from ethene dimerization.

Selectivity in propene metathesis was calculated by Eq. (5).

$$S = \frac{[C_2H_4] + [2-C_4H_8]}{[\Sigma \text{ products}]} \cdot 100 \quad (5)$$

The values obtained in the above experiments are plotted against time in Fig. 4. Significantly higher selectivity in metathesis of propene was observed over CAT-O than CAT-H. Accordingly, the rate of oligomerization of ethene was higher over catalysts reduced with hydrogen than over the unreduced one (Fig. 3). While activity in metathesis over a reduced catalyst can be influenced significantly by hidrogen adsorbed at various temperatures, activity in ethene oligomerization and selectivity in metathesis of propene are influenced less significantly by such treatments.

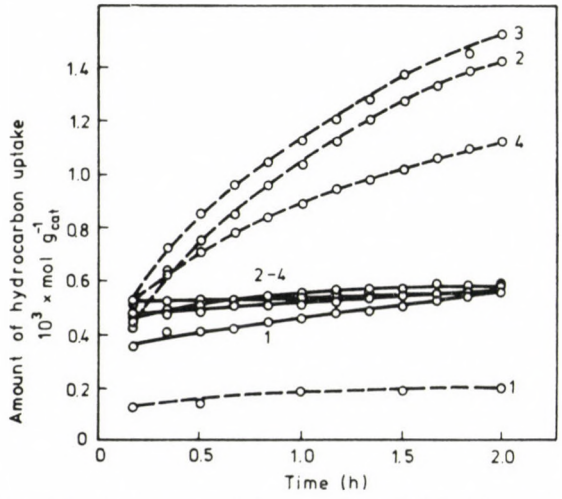

Fig. 3. Amount of total hydrocarbon uptake over 1 g of C 310 in experiments with ethene (dotted lines) and propene (solid lines) carried out in recirculation system at 313 K, 100 kPa initial pressure. CAT-O (1); CAT-H evacuated at 823 K (2); CAT-H evacuated at 823 K and treated again with hydrogen at 313 K (3); CAT-H evacuated at 823 K and treated again with hydrogen at 823 K (4)

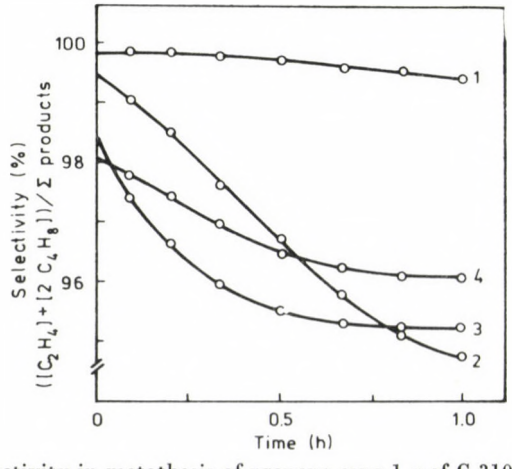

Fig. 4. Selectivity in metathesis of propene over 1 g of C 310. See Fig. 3

Oligomerization of propene over catalyst 310

Experiments were carried out in flow system over 1 g of C 310 (CAT-H) at 473 K and 100 kPa. After reduction, the catalyst was evacuated at 313 or at 823 K. Products in the gas phase were analyzed. The composition of products (except ethene and butenes) is plotted against time in Figs 5 and 6. As can be seen, the concentration of 2-pentenes in the products over catalysts evacuated at 313 K decreases and that of C_6-alkenes increases with time. No such increase of selectivity for C_6-alkenes was observed over catalysts evacuated at 823 K. In this case 2-pentene remained the main product (besides ethene and butenes) in the period studied.

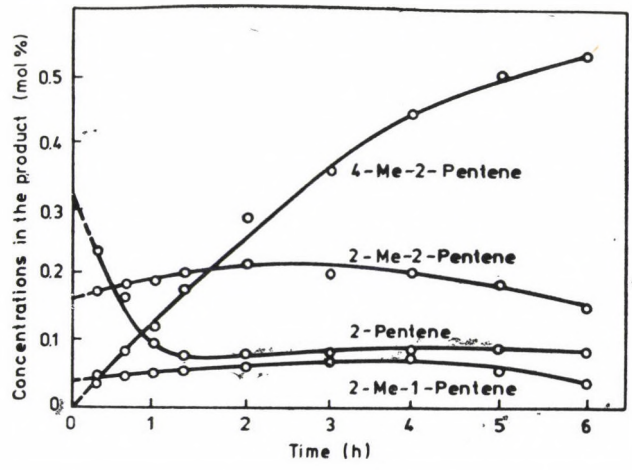

Fig. 5. Composition of propene oligomerization products. Flow system (13×10^{-3} mol propene/h), 473 K, 110 kPa, 1 g of C 310. CAT-H evacuated at 313 K

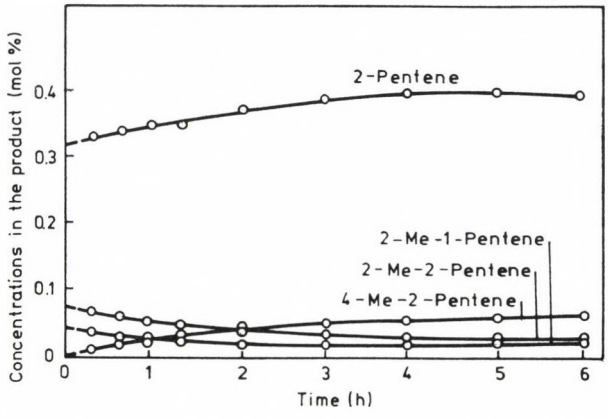

Fig. 6. See Fig. 5. C 310. CAT-H evacuated at 823 K

Oligomerization of propene over C 315

Over C 315 (33 g) experiments were carried out in a flow system equipped with a cold trap for collection of liquid products. The catalyst was reduced at 823 K in flowing hydrogen for 2 h, then cooled in hydrogen to reaction temperature. Before starting the feed of propene, the catalyst was evacuated for 1 min. Space time (W/F) was defined as follows:

$$W/F = \frac{\text{catalyst mass (g)}}{\text{feed rate of propene (mol/s)}} \tag{6}$$

Conversion was calculated on the basis of the amount of liquid products formed in unit time:

$$C\% = \frac{\text{rate of formation of liquid product mass } t^{-1} \text{ (g h}^{-1}\text{)}}{\text{feed rate of propene mass } t^{-1} \text{ (g h}^{-1}\text{)}} \tag{7}$$

The catalyst was eluted with hydrogen and cooled to room temperature after 5 h on stream. Next day it was heated to reaction temperature in hydrogen and the process was repeated as before. The change of the conversion with time in a 5-day run at 525 K, 2.7×10^6 g_{cat} s $mol^{-1}_{propene}$ space time is plotted in Fig. 7.

The activity of the catalyst increased during the five-hour periods, and increased in the successive days as well. After a 3-day run the activity reached a constant level. This stabilized catalyst was used in further experiments. Average daily composition of the liquid product formed in the 5-day run is shown in Table III. As can be seen, both the conversion and the selectivity related to the formation of C_6 alkenes increased over successive days.

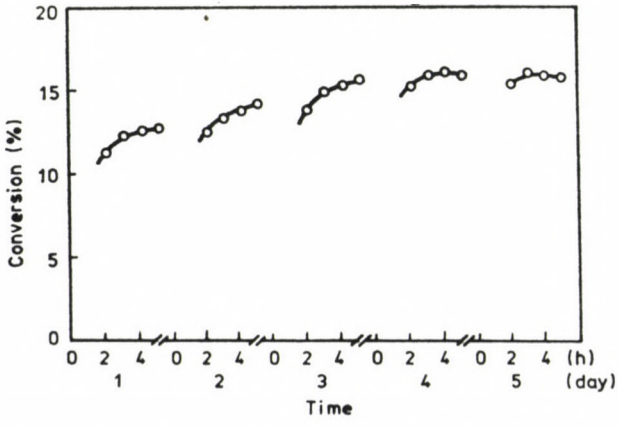

Fig. 7. Oligomerization conversion of propene over 33 g of C 315 at 523 K, 100 kPa; flow system, space time 2.7×10^6 g_{cat} s $mol^{-1}_{propene}$

Table III

Composition of the liquid product[a] *formed over* 33 g *of* C 315 *at* 523 K, 100 kPa, $W/F = 2.7 \times 10^6$ g_{cat} s $mol^{-1}_{propene}$

No. of days	1	2	3	4	5
alkenes					
	mass %				
C_5	24.6	22.3	20.5	19.7	18.0
C_6	46.7	48.4	53.2	54.0	53.6
C_7	18.4	19.3	13.0	12.8	13.6
C_8	7.0	5.2	6.3	5.4	5.4
C_9	2.2	3.0	4.5	5.0	5.4
C_{10}	1.1	1.8	2.5	3.1	4.0

[a] Average daily composition.

Experiments were carried out over the stabilized catalyst at various temperatures and feed rates. The mean conversions of 3—5 hour experiments are plotted against space time in Fig. 8. The initial rate of oligomerization calculated from conversion isotherms in Fig. 8 is 2.2×10^{-8} and 6.0×10^{-8}, mol g_{cat}^{-1} s^{-1} at 493 and 523 K, respectively.

The concentrations of C_6 and $C_9 + C_{10}$ alkenes in the products at various temperatures and feed rates are plotted against the conversion in Fig. 9. Selectivity for C_6 alkenes increases, while the concentration of $C_9 + C_{10}$ alkenes decreases with the conversion.

Effect of nitrogen in propene oligomerization

Similar experiments were carried out at 523 K over the stabilized catalyst but nitrogen was periodically admixed in different concentrations to the feed of propene. Rate of oligomerization calculated from conversions after restabili-

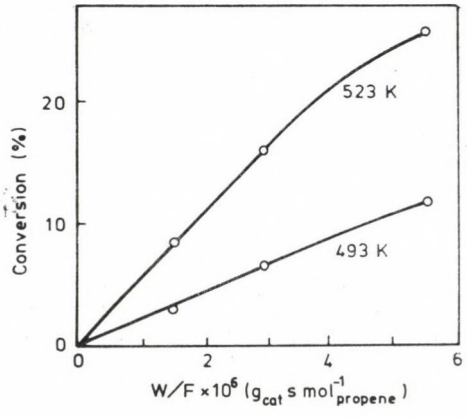

Fig. 8. Conversion curves of propene oligomerization at different temperatures

zation is plotted against partial pressure of propene in Fig. 10. The rate of oligomerization is proportional to the partial pressure of the reactant. Although after experiments with dilute propene, the same activity was obtained as before (see the two points at 100 kPa partial pressure), the shape of the curve of Fig. 10 indicates that the oligomerization is inhibited by nitrogen diluent.

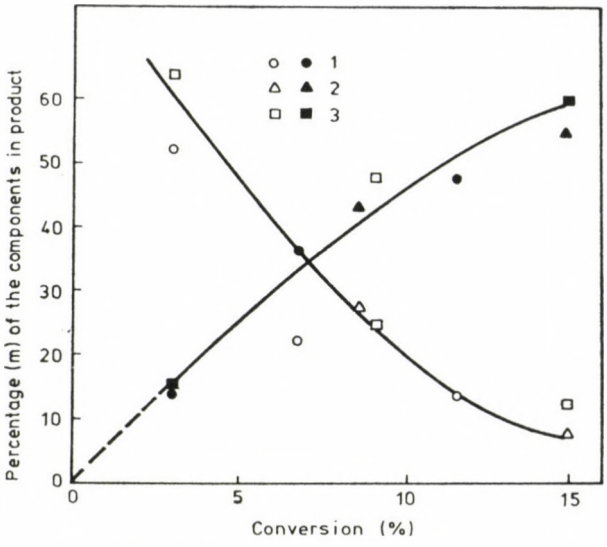

Fig. 9. Concentration of C_6 (full symbols) and $C_9 + C_{10}$ (empty symbols) alkenes in the propene oligomerization products at 493 (1), 523 (2) and 553 K (3) as the function of conversion

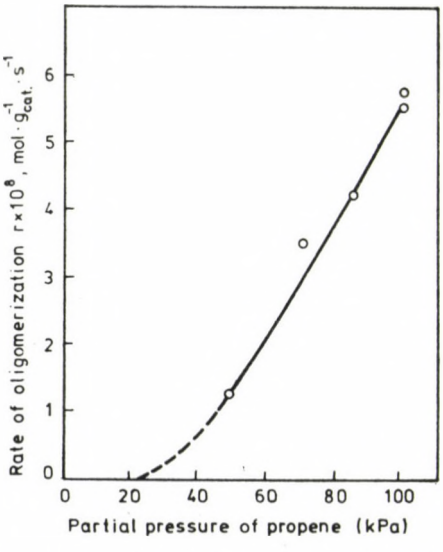

Fig. 10. Dependence of the propene oligomerization rate on partial pressure of the reactant. 33 g of C 315, 523 K, N_2 as diluent

Table IV

Propene oligomerization conversion at 523 K *over* 33 g *of* C 315 *eluted with nitrogen after reduction*

Temperature of nitrogen elution	Relative conversion (%)
None	100
423 K	67
523 K	47
823 K	0

Like in other experiments, selectivity correlated for the formation of C_6 alkenes, decreased with decreasing conversion.

Experiments were carried out with undiluted propene at 523 K over 33 g of C 315 freshly reduced with hydrogen. After reduction, the catalyst was eluted with nitrogen for 1 h at various temperatures. Conversions obtained after 4 h on stream and related to that obtained over a catalyst not treated with nitrogen are shown in Table IV. Like metathesis, oligomerization of propene slowed down upon treating the catalyst with nitrogen. The higher the temperature of nitrogen treatment the lower the catalyst activity in oligomerization.

Discussion

Metathesis of propene effected by hydrogen bound on the catalyst

Formation of surface species like **I** was described by Hall et al. [17] upon reduction and evacuation of molybdena-alumina catalysts.

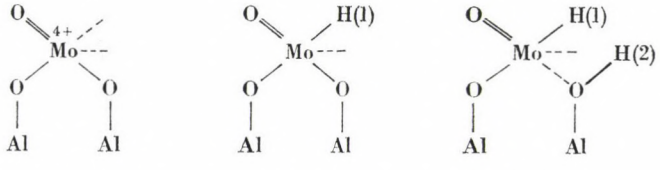

I II III

Hydrogen adsorbed at low temperatures can be bound in position 1 to form oxy-molybdena species like **II**. At higher temperatures hydrogen may be bound both in positions 1 and 2 to form species like **III** [18]. On the basis of butene isomerization experiments it was assumed [18] that hydrogen in position 1 enhances the formation of Mo-alkyl species, the common intermediates for isomerization, oligomerization and metathesis:

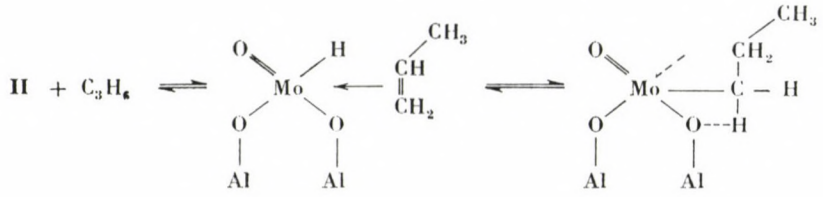

(8)

IV

Hydrogen in Mo-alkyl species close to the molybdenum ion may be attracted by oxygen in the sublayer. If hydrogen abstraction is completed, Mo-alkylidene species may form which serve as initiators in metathesis:

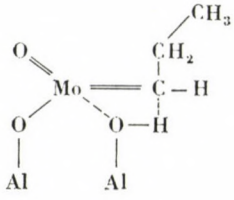

V

When there are already OH groups in the sublayer, as in species **III**, hydrogen abstraction from Mo-alkyl intermediate, consequently, transformation to the Mo-alkylidene intermediate of metathesis is hindered.

From this it follows that the greater fraction of species **II** is transformed to species **III**, the lower is the metathetic activity of a molybdena-alumina reduced to an identical degree. It can be seen in Fig. 1 that the activity of catalysts in propene metathesis decreases upon increasing the temperature of second hydrogen treatment. At higher temperatures of treatment the enhancement of the reaction by hydrogen in position 1 is counterbalanced by the hindrance caused by hydrogen in position 2.

Once hydrogen is bound at high temperature, it is rather stable; activity of the catalyst in metathesis of propene was only partly regained by evacuation at 723 K when hydrogen was preadsorbed at 823 K (Table I). This suggests that the catalyst used in oligomerization of propene without effective evacuation after reduction has only a very low metathetic activity.

Oligomerization of propene

Olefin mixtures with a broad range in the number of carbon atoms in the molecule can be produced through combination of metathesis and double bond shift reactions [13]. High activity in metathesis and isomerization of

butenes was attained by molybdena-alumina catalyst reduced with hydrogen then evacuated at high temperature [19]. This catalyst proved to be less effective in the dimerization of propene than that holding hydrogen bound at high temperature, consequently, being less active in metathesis (see Figs 5—6).

When the reactants are linear olefins, products formed in the metol reaction may contain linear olefins only:

$$\begin{array}{l} CH_2{=}CH-CH_3 \overset{C_3H_6}{\rightleftharpoons} CH_2{=}CH_2 + CH_3-CH{=}CH-CH_3 \\ \qquad\qquad\qquad\qquad\qquad\qquad\qquad\qquad\qquad\qquad \Big\updownarrow \text{isomerization} \\ CH_3-CH_2-CH{=}CH-CH_3 + CH_2{=}CH_2 \overset{C_3H_6}{\rightleftharpoons} CH_2{=}CH-CH_2-CH_3 \\ \qquad\qquad \Big\updownarrow \text{isomerization} \\ CH_3-CH_2-CH_2-CH{=}CH_2 \overset{C_3H_6}{\rightleftharpoons} CH_2{=}CH_2 + CH_3-CH_2-CH_2-CH{=}CH-CH_3 \\ \qquad\qquad\qquad\qquad\qquad\qquad\qquad\qquad\qquad\qquad \Big\updownarrow \text{isomerization} \\ \qquad\qquad\qquad\qquad\qquad\qquad \text{etc.} \overset{C_3H_6}{\rightleftharpoons} CH_3-CH_2-CH_2-CH_2-CH{=}CH_2 \end{array} \qquad (9)$$

In practice, the process would be more complicated by the actual formation of a variety of internal double bond isomers of C_5 and higher olefins and by the cross metathesis of any of the olefins present.

2-Pentene in the products indicates the existence of metathesis reaction. Over catalysts evacuated at 823 K after reduction (Fig. 6), the formation of 2-pentene besides ethene and 2-butene is dominant. Over catalysts not evacuated after reduction (Fig. 5), however, formation of 2-pentenes decreases and the formation of methylpentenes increases with time on stream. This is an indication that propene oligomerization on this catalyst is not due to successive metathesis and double bond shift reactions.

Branched alkyl chains may be formed by skeletal isomerization of products, but more probably in non-metathetic oligomerization. One likely way for non-metathetic oligomerization of propene is by analogy to oligomerization by nickel complexes [20]:

As can be seen, like in metathesis, the initial step in oligomerization is the insertion of π-bonded propene into Mo—H bonds (eq. 10). Oligomerization, however, does not require the formation of alkylidene species, but insertion of a second or further propene molecules into the Mo—C bond of species **IV**. Therefore, oligomerization is not hindered by hydrogen bound in position 2 at high temperature.

Non-metathetic oligomerization of propene may lead to the formation of olefins with 6, 9, 12, etc., carbon atoms in one molecule. A continuous product distribution was, however, found containing components with 7, 8, 10 carbon atoms as well (Table III). This non-selectivity in oligomerization can presum-

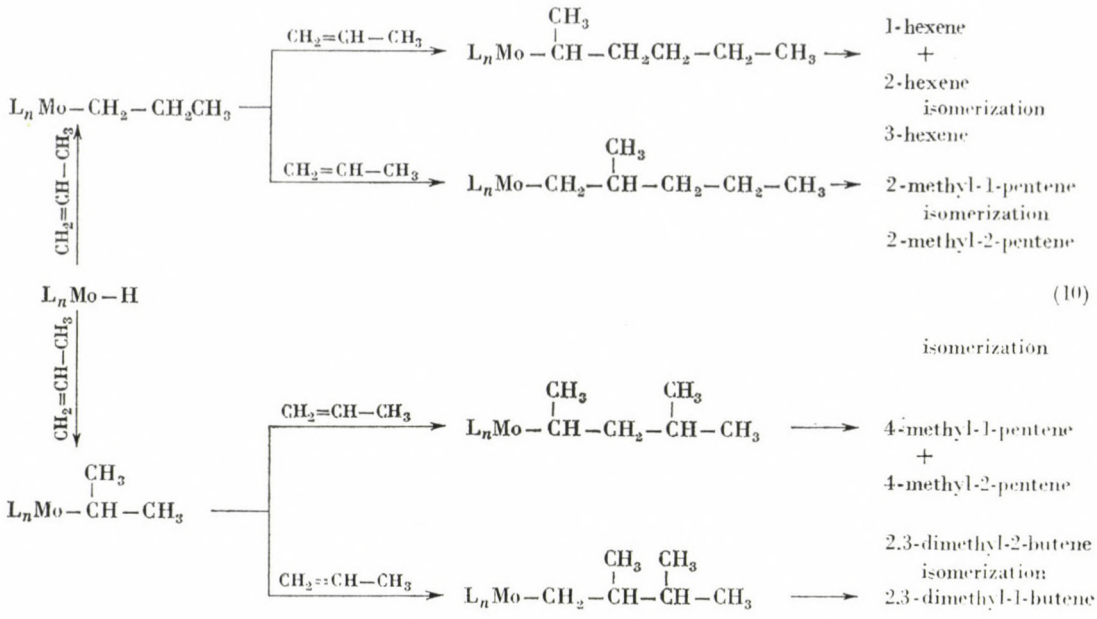

ably be accounted for by the low, but not negligible metathetic activity of the catalyst.

More detailed studies including the identification of the structure of the heavier product molecules are necessary, in order to shed light on the role of metathesis and non-metathetic oligomerization in the transformation of propene over molybdena-alumina.

Metathesis of propene effected by treatment of the catalyst by nitrogen and ammonia

Figure 2 shows that the activity of catalyst activated by oxygen is not influenced by elution with nitrogen at any temperature. The activity of catalyst reduced with hydrogen decreases significantly to the effect of elution with nitrogen at high temperature, but remains unchanged if the elution is carried out at low temperature. The decrease of activity is more significant when more hydrogen is bound to the catalyst at the beginning of elution (curve 4 vs. curve 6). Thus, the formation of ammonia from nitrogen and hydrogen bound to the catalyst was assumed.

Fixation of dinitrogen by molybdenum containing complexes and formation of ammonia from molybdenum-bound dinitrogen was described under reducing conditions at room temperature [21, 22]. The observation that ammonia is an effective catalyst poison (Table II) would support the assump-

tion that ammonia may form in the presence of nitrogen over the reduced catalyst holding hydrogen. Infrared spectroscopic studies, however, failed to show the presence of ammonia on the reduced catalyst after nitrogen treatment.

We have to remind that the presence of ammonia has not been observed in the infrared spectrum of the catalyst after ammonia exposure followed by evacuation at 573 K. Metathetic activity, however, cannot be revealed even after evacuation at 723 K when ammonia was preadsorbed on the catalyst (Table II). Presumably, less than 1% of the surface oxy-molybdenum species is active in metathesis [23]; if adsorption of ammonia takes place selectively on these species, it cannot be detected by IR spectroscopy.

Catalysts, containing molybdenum were found to be active in ammonia synthesis, under the given conditions (atmospheric pressure), however, concentration of ammonia in the gas phase could be below the limit of detectability. On the basis of the above speculation, formation of ammonia from nitrogen on reduced molybdena-alumina holding preadsorbed hydrogen cannot be ruled out, although it has not received experimental verification.

REFERENCES

[1] Banks, R. L., Bailey, G. C.: Ind. Eng. Chem., Prod. Res. Develop., **3,** 170 (1964)
[2] More recent reviews of olefin metathesis: a) Rooney, J. J., Stewart, A.: in "Catalysis", ed. C. Kemball (Specialist Periodical Reports), Vol. **1,** p. 277, The Chemical Society, London 1977; b) Katz, T. J.: in "Advances in Organometallic Chemistry", ed. Stone, F. G. and West, R., Vol. **16,** p. 283. Academic Press, New York 1977; c) Grubbs, R. H.: in "Progress in Inorganic Chemistry", ed. Lippart, S. J., Vol. **24,** p. 1. Wiley-Interscience, New York, 1978; d) Banks, R. L.: Chemtechn., **9,** 494 (1979); e) Calderon, N., Lawrence, J. P., Ofstead, E. A.: in "Advances in Organometallic Chemistry" ed. Stone, F. G. West, R., Vol. **17,** p. 449, Academic Press, New York 1979; f) Banks, R. L.: in "Catalysis" ed. Kemball, C. (Specialist Periodical Reports), Vol. **4** p. 100, The Royal Society of Chemistry, London 1981
[3] Nakamura, R., Echigoya, E.: Nippon Kagaku Kaishi, **13,** 244 (1973)
[4] Giordano, N., Padovan, M., Vaghi, A.: J. Catal., **38,** 1 (1975)
[5] Engelhardt, J.: Magy. Kém. Foly., **83,** 311 (1977)
[6] Engelhardt, J.: Magy. Kém. Foly., **83,** 452 (1977)
[7] Engelhadt, J.: Rec. Trav. Chim. Pays-Bas, **96,** M101 (1977)
[8] Hashimoto, K., Watanabe, S., Tarama, K.: Bull. Chem. Soc. Japan, **49,** 12 (1976)
[9] Hashimoto, K., Watanabe, S., Tarama, K.: Bull. Chem. Soc. Japan, **49,** 3408 (1976)
[10] Engelhardt, J.: J. Mol. Catal., **8,** 119 (1980)
[11] Engelhardt, J., Kalló, D.: J. Catal., **71,** 209 (1981)
[12] Crain, D. L., Reusser, R. E.: Amer. Chem. Soc. Prepr. Div. Pet. Chem., **17,** E80 (1970)
[13] Warwel, S., Hachen, G., Kirchmeyer, H., Ridder, H., Winkelmüller, W.: Tenside Detergens, **19,** 321 (1982)
[14] Engelhardt, J.: J. Catal., **62,** 243 (1980)
[15] Soják, L., Hrivnák, J., Mayer, P., Janák, J.: Anal. Chem., **45,** 293 (1973)
[16] Rijks, J. A., Cramers, C. A.: Chromatographia, **7,** 99 (1974)
[17] Millman, W. S., Crespin, M., Cirillo, Jr. A. C., Abdo, S., Hall, W. K.: J. Catal., **60,** 404 (1979)
[18] Engelhardt, J., Kalló, D., Zsinka, I.: J. Catal., **88,** 317 (1984)
[19] Engelhardt, J., Goldwasser, J., Hall, W. K.: J. Mol. Catal., **15,** 173 (1982)
[20] Commereuc, D., Chauvin, Y., Léger, G., Gaillard, J.: Rev. Inst. Franc. Petrol, **37,** 639 (1982)
[21] Haight, Jr. G. P., Scott, R.: J. Am. Chem. Soc., **86,** 743 (1964)
[22] Brulet, C. R., van Tamelen, E. E.: J. Am. Chem. Soc., **97,** 911 (1975)
[23] Brenner, A., Burwell, Jr. R. L.: J. Catal., **52,** 364 (1978)

Acta Chimica Hungarica 119 (2—3), pp. 265—274 (1985)

HIGH RESOLUTION MAGIC ANGLE SPINNING ^{29}Si-NMR CHARACTERIZATION OF ZEOLITES+

Janos B. NAGY[1]*, Zelimir GABELICA[1], Guy DEBRAS[1], Philippe BODART[1], Eric G. DEROUANE[1] and Peter A. JACOBS[2]

([1]Facultés Universitaires de Namur, Laboratoire de Catalyse, 61, rue de Bruxelles, B-5000 Namur, Belgium, [2]Centrum voor Oppervlakte Chemie, Katholieke Universiteit Leuven, Kardinaal Mercierlaan, B-3030 Leuven, Belgium)

Received June 8, 1984
Accepted for publication October 15, 1984

High resolution magic-angle-spinning solid state ^{29}Si-NMR was used to characterize various synthetic and natural zeolites. Emphasis is put on the determination of the silicon-aluminium ordering in the zeolitic framework. It is concluded that aluminium atoms occupy preferential sites in mordenite, ZSM-5 and ZSM-11 zeolites and possible in ZSM-39 zeolite. The Si/Al ratios determined from the NMR data are in good agreement with results obtained by other analytical techniques. Finally, defect silanol groups can be detected using cross-polarization NMR pulse sequences.

Introduction

Zeolites are hydrated crystalline alumino-silicates. Their framework consists of a lattice of corner sharing SiO_4 tetrahedra partially substituted by AlO_4^- units giving rise to open structures with channels and cavities of molecular dimensions. The negative electric charges generated by this substitution are compensated by positive counterions (Na^+, K^+, NH_4^+, . . .) located in the cavities of the structure.

X-ray diffraction has been considered for a long time as the most important tool to study the alumino-silicates. Nevertheless it is very difficult to discriminate between the silicon and aluminium atoms by this technique. This shortcoming has led to the near impossibility of determining the short-range order and silicon-aluminium distribution in the alumino-silicate framework. Fortunately, those tasks are well suited for high resolution magic-angle-spinning solid state ^{29}Si-NMR spectroscopy [1].

The ^{29}Si-NMR spectra of aluminium-rich zeolites generally exhibit up to five lines corresponding to the five possibilities for the linkage of an SiO_4 tetrahedron through oxygen bridges to $n$$AlO_4$ tetrahedra (n = 0—4). An interval of ca. 5 ppm usually separates two neighbouring NMR lines belonging to each Si(nAl) configuration [2]. The percentage of each Si(nAl) unit is evaluated by measuring the corresponding line intensity. The assignment of the lines to

+ This paper was presented at the 2nd Belgian—Hungarian Colloquium on Catalysis at De Haan, Belgium, October 10—13, 1983.

* To whom correspondence should be addressed.

the various silicon-aluminium orderings is achieved by examining their intensity variations for different Si/Al ratios. The samples are obtained either by direct synthesis or by different dealumination processes.

Silicon-aluminium orderings have been assessed for several natural and synthetic zeolites such as faujasite [3—7], zeolite ZK-4 [8, 9], mordenite [7, 10, 11] and pentasil materials [7, 11—15].

In the present paper we show how specific aluminium distribution characterizes the framework of ZSM-5, ZSM-11, mordenite and possibly ZSM-39 zeolites. In addition, the detection of defect silanol groups in ZSM-5 is emphasized by using the cross-polarization NMR pulse sequences.

Experimental

Materials

Mordenite was supplied by the Norton Company. Zeolite Y was received from Union Carbide Corporation. The other zeolites ZSM-5, ZSM-11 and ZSM-39 were obtained by syntheses according to procedures published in the current or patent literature. X-ray diffractograms confirmed that all phases were crystallographically pure. The zeolites were transformed into their final form via classical ion-exchange techniques. Organic cations or bases occluded in some zeolite precursors were removed by calcination. The mordenite samples were dealuminated by treatment with aqueous HNO_3 in various concentrations at different temperatures. NH_4Y was dealuminated with $SiCl_4$ at 773 K. The Al, Si and Na contents of each sample were determined by Proton Induced Gamma Ray Emission (PIGE) [16] or by Energy Dispersive X-ray Analysis (EDX) [17].

NMR measurements

All NMR spectra were recorded at room temperature on a Bruker CXP-200 spectrometer operating in the Fourier transform mode.

The magic-angle-spinning spectra were obtained by 'one-cycle' type measurements [18]. An r. f. field of 49.3 Oe was used for the $\pi/2$ pulses of ^{29}Si ($\nu = 39.7$ MHz). The Delrin conical rotor was spun at a rate of 3.1 kHz. The intervals between pulse sequences were 3.0 s or 6.0 s. 2000—20,000 free induction decays were accumulated prior to Fourier transformation. The cross-polarization magic-angle-spinning spectra were recorded using a single contact sequence [19]. The contact time was 10 ms and the time intervals were 3.0 s. Chemical shifts (in ppm) were measured with respect to tetramethylsilane (TMS) used as external reference.

Results and Discussion

Effect of dealumination on silicon-aluminium ordering

In connection with the determination of Al-ordering and the assignment of the zeolite structure, the effect of dealumination is of special importance. The progressive elimination of tetrahedral Al atoms from the faujasitic zeolite framework is followed by ^{29}Si-NMR. The computed Si/Al ratios are in good agreement with those determined by different analytical methods [7, 11, 20, 21].

The faujasitic structure is built up of 24 corner sharing tetrahedra (TO_4 with T = Si or Al), forming a sodalite cage. These cages are joined tetrahedrally

Table I

Si/Al *ratios and relative line intensities* (%) *in zeolite* Y, *mordenite and their aluminium deficient forms*

Sample	Si/Al[a]	Si/Al[b]	Relative intensities (%) of various Si(*n*Al) configurations				
			Si(4Al)	Si(3Al)	Si(2Al)	Si(1Al)	Si(0Al)
NaY	2.4	2.3	2.9	15.0	39.4	37.3	5.4
Dealuminated HY	14.5	—	—	—	—	—	100
Na-Mordenite	5.5	5.5	—	—	13.2	44.7	42.1
H-Mordenite (2)	6.7	8.9[c]	—	—	10.1	24.7	65.2
H-Mordenite (4)	23.5	25.3[c]	—	—	4.3	7.2	89.5
H-Mordenite (5)	30.0	32.2[c]	—	—	2.3	7.8	89.9

[a] EDX values.
[b] ^{29}Si-NMR values : Si/Al in the lattice.
[c] Presence of extra-lattice octahedral Al [24], which is not computed by NMR.

through six-membered rings by hexagonal prisms to form a cubic diamond lattice. All the T-sites are crystallographically equivalent.

Figure 1 illustrates the effect of dealumination on the H—Y zeolite. Table I compares the Si/Al ratios calculated from NMR intensities and derived from EDX analysis. The NMR Si/Al ratios were computed considering that Loewenstein's rule [22] on the Si—O—Al ordering is obeyed:

$$\mathrm{Si/Al} = \frac{I_{\mathrm{total}}}{\sum_{0}^{4} 0.25\, n I_{\mathrm{Si}(n\mathrm{Al})}}$$

where $I_{\mathrm{Si}(n\mathrm{Al})}$ stands for the relative intensity of the line due to silicon atoms surrounded by n Al atoms.

In NaY zeolite, the five NMR lines at —83, —88, —93, —98 and —104 ppm correspond, respectively, to Si atoms with 4, 3, 2, 1 and 0 neighbouring Al-atoms, denoted usually as Si(nAl). The dealumination by $SiCl_4$ leads to a highly siliceous and crystalline material where the Si(0Al) line predominates (Si/Al = 14.5). From the relative intensities of the NMR lines (Table I), Al distribution in the zeolitic framework can be proposed. The silicon-aluminium distribution is consistent with Loewenstein's rule which excludes Al—O—Al linkages. Moreover, the details of this distribution provide evidence for a high degree of ordering in the faujasite framework [6], especially when electrostatic interactions are taken into account [4]. For compact structures (i.e. Si/Al = 1.40) aluminium atoms have to occupy the meta positions in the six-membered alumino silicate rings. In the four-membered ring, opposite corners are of course occupied by aluminium atoms. For Si/Al = 2.3, the occupation of para positions of the six-membered ring by aluminium atoms has also to be taken into account and the number of possible schemes rapidly increases.

Figure 1 shows that the Si(0Al) configurations do not coincide in NaY zeolite (Si/Al = 2.3) and in the corresponding dealuminated sample: $\delta =$ $=$ —104 ppm for the former and —108 ppm for the latter. This difference is due to an effect of second-nearest (tetrahedral) neighbours. The aluminium atoms in the second (tetrahedral) coordination shell induce a low field shift in the NaY zeolite sample.

Mordenite structure is composed of an assembly of six-membered ring sheets of tetrahedra linked together through single four-membered rings to form a three dimensional structure. Dealumination of Na-mordenite by acid leaching removes about 80% of the initial amount of tetrahedral Al-atoms (Table I and Fig. 2) [10]. The Na-mordenite is characterized by NMR lines corresponding to Si(2Al) at —98 ppm, Si(1Al) at —105 ppm and Si(0Al) at —110 ppm, the Al atoms occupying preferentially the four-membered rings [10, 11], as it was also suggested by crystallographic analysis [23]. The highly dealuminated mordenite essentially exhibits the Si(1Al) and Si(0Al) lines. The Si/Al ratios computed from the NMR data are in good agreement with the EDX values.

If one takes into account the presence of defect silanol groups ($\equiv$ Si—OH), which also give rise to an NMR line near $\delta =$ —105 ppm, and assuming that

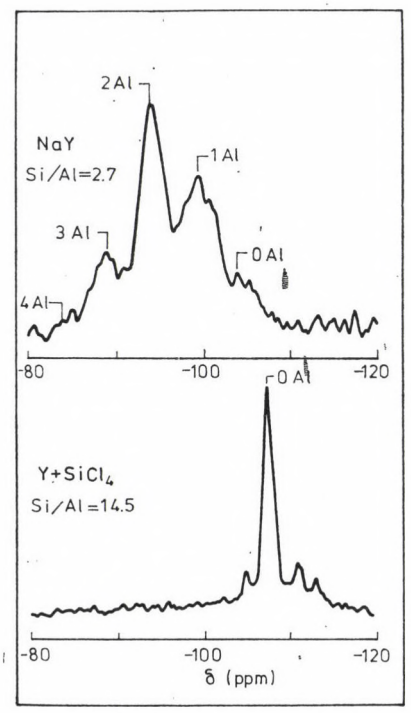

Fig. 1. Effect of dealumination on the ^{29}Si-NMR spectra of NaY zeolite

dealumination destroys the four-membered ring removing both Al atoms from it, the theoretical distribution of the Al atoms in the mordenite structure can be calculated. Excellent agreement is found between the theoretical and experimental distributions [24]. It is thus clearly shown that the variation in intensity of the ^{29}Si-NMR lines during progressive dealumination of mordenite can be explained, if silicon-aluminium ordering exists in the zeolitic framework. The Al atoms preferentially occupy the four-membered rings.

Silicon-aluminium orderings in zeolites synthesized with various Si/Al ratios

The high resolution ^{29}Si-NMR spectra of H-ZSM-5 and H-ZSM-11 pentasil zeolites have been systematically studied for Si/Al ratios varying from 25 to 1000 [7, 11, 13]. They essentially show three resonances at —105 ppm (3), —113 (1) and —115 (2) ppm (Fig. 3). The —105 ppm line can be clearly identified as corresponding to a Si atom linked to one Al atom through an oxygen bridge, Si(1Al), because its intensity decreases with increasing Si/Al ratio.

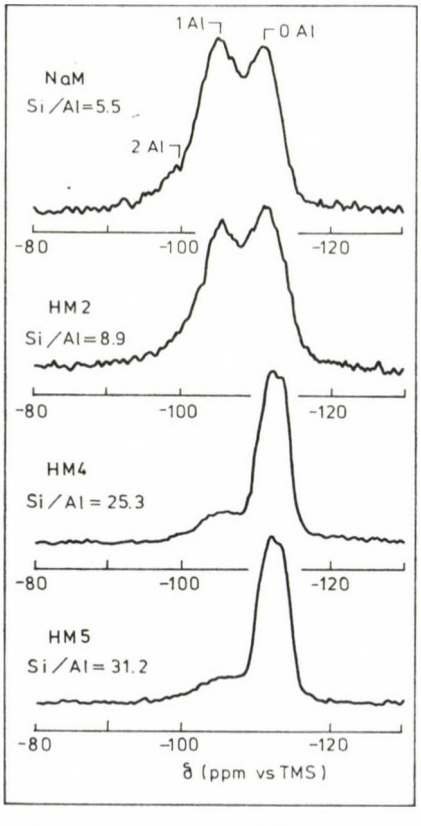

Fig. 2. Effect of dealumination on the ^{29}Si-NMR spectra of Mordenite

This decreasing intensity is accompanied by a parallel increase of the —113 ppm line, while the —115 ppm line remains constant in both H-ZSM-5 and H-ZSM-11 zeolites (Fig. 4). In addition, the intensity ratio I(—115)ZSM-11/I(—115)ZSM-5 is equal to 2. This ratio can be explained if the —115 ppm line is attributed to Si(0Al) atoms located in four-membered rings. Indeed these atoms are twice as abundant in ZSM-11 as in the ZSM-5 unit cell structure:

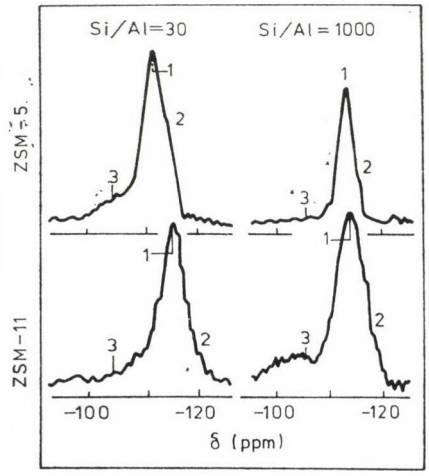

Fig. 3. High resolution solid state ^{29}Si-NMR spectra of H-ZSM-5 and ZSM-11 zeolites with different Si/Al ratios

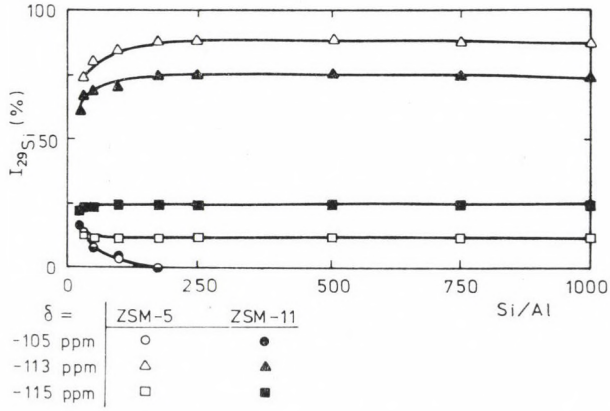

Fig. 4. Variation of ^{29}Si-NMR line intensities as a function of Si/Al ratios in H-ZSM-5 and H-ZSM-11 zeolites

four in ZSM-5 and eight in ZSM-11. This assignment implies that Al atoms are specifically [25, 26] located in the five-membered rings where the energy is probably lower than in the strained four-membered rings and that they are

not statistically distributed throughout the pentasil framework. Finally, the —113 ppm line is attributed to Si(0Al) in the five-membered rings.

The enhanced resolution spectrum of a very pure H-ZSM-5 (Si/Al = = 1000) shows up to eight different NMR lines (Fig. 5A). This multiplicity stems from crystallographically non-equivalent Si(0Al) configurations. The intensities can be split on a basis of 24 non-equivalent sites in the repeat unit of the ZSM-5 structure [27]. Some of these probably originate from the high strain characterizing the structural building units of these pentasil materials [14]. The unambiguous assignment of all these NMR lines still needs further investigation. Nevertheless, the most intense lines at —112.7 and —113.2 ppm can be tentatively attributed to Si atoms surrounded by a set of 5-5-5-5-5-6 and of 5-5-5-5-5-10 membered rings, respectively, because these types of atoms represent about 50% of the cases [28]. The occurrence of three magnetically different Si atoms in the four-membered rings (at —114.1 (1), —115.3 (2) and —116.3 (1) ppm) reveals the existence of strain in these rings.

Finally, the presence of defect Si—OH groups can also be detected using cross-polarization MAS ^{29}Si-NMR technique. Figure 5B illustrates the spectrum of a fully hydrated H-ZS-5M zeolite (Si/Al = 1000) obtained with cross-polarization. The relative enhancement of the intensity at ca. —103 ppm shows unambiguously the presence of silanol groups [29, 30].

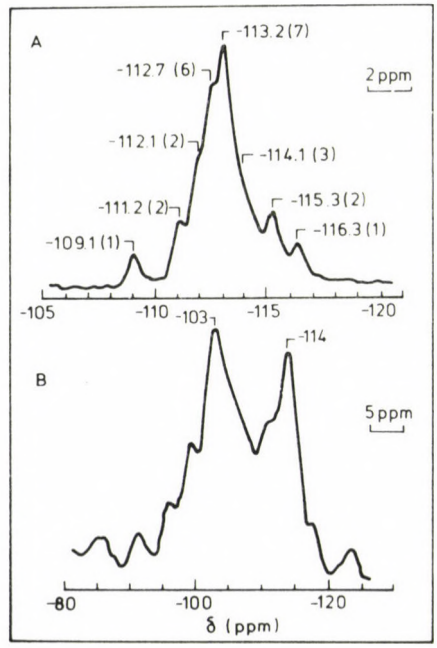

Fig. 5. Influence of cross-polarization on the magic-angle spinning ^{29}Si-NMR spectra of fully hydrated H-ZSM-5 zeolite (Si/Al = 1000); A) without and B) with cross-polarization

Table II

Distribution of T *atoms in the unit-cell of* ZSM-39

T-atom	Ring structure	Number of T-atoms/u.c.	Number of neighbouring T-atoms of type		
			T_1	T_2	T_3
T_1	shared between five-membered rings	8	8	4	0
T_2	in five-membered rings	32	1	0	3
T_3	shared between five- and six-membered rings	96	0	1	3

The framework of ZSM-39 zeolite consists of an arrangement of 12- and 16-hedra in which three types of tetrahedrally coordinated T atoms (T1, T2 and T3) were identified (Table II) [39].

The ^{29}Si-NMR spectrum of ZSM-39 shows three well resolved resonances at = —109, —115 and —120 ppm (Fig. 6) [7, 11, 32]. The number of relevant Si(nAl) configurations is restricted to Si(1Al) and Si(0Al), due to the high Si/Al ratio. The strongest NMR line at δ = —120 ppm is assigned to Si(0Al) located in the most abundant T3-sites. The two other resonance lines are therefore attributed to Si(0Al) in sites T1 and T2 and to Si(1Al) configurations.

It is known that the presence of an Al atom in the second coordination shell of zeolitic Si atoms shifts the resonance line by ca. 5 ppm to lower fields [2]: the configuration $Si(1Al)_{T3}$ will thus contribute to the —115 ppm line. Assuming that $Si(1Al)_{T2}$ also contribute to this resonance line, $Si(1Al)_{T2}$ should appear at δ = —109 ppm. Finally, the δ = —109 ppm line should also include the $Si(0Al)_{T1}$ configuration.

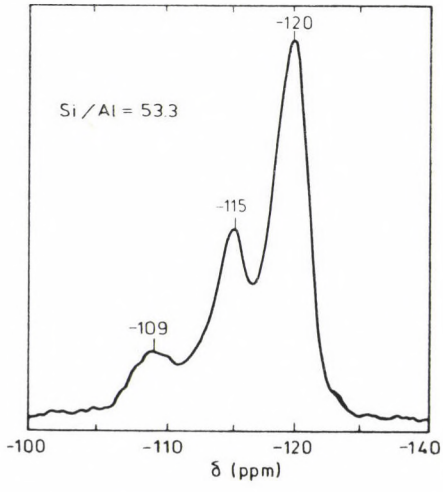

Fig. 6. High resolution solid state ^{29}Si-NMR spectrum of ZSM-39 zeolite

Table III

Comparison between the relative theoretical intensities calculated for different Al-*sitings in the lattice and the experimental* NMR *results for* H-ZSM-39 (Si/Al = 53.3)

δ(ppm)	Relative theoretical intensities (%) assuming Al-siting in				Relative experimental intensities (%)
	T_1	T_2	T_3	Statistical	
−104	0.0	1.8	0.0	0.5	0
−109	11.6	4.2	7.8	7.2	10
−115	16.5	27.5	27.6	27.0	29
−120	71.9	66.5	64.6	65.3	61

Table III compares the experimental intensities with those calculated by assuming a specific location of the Al atoms on T1, T2 or T3 sites or their statistical distribution between all the T sites in the lattice. For the statistical distribution, intensities of the NMR lines are calculated from the sum of intensities obtained for a specific location of Al on sites T1, T2 or T3 multiplied by the probability of an Al atom being located on the same sites. This probability is computed as the ratio (Number of sites Ti)/(Total number of T atoms), per unit cell.

The best agreement between theoretical and experimental values is obtained for specific location of Al atoms on sites T3, shared between five- and six-membered rings. However, the statistical contributions are equally probable since T3 is the most abundant site in the zeolite structure. ^{29}Si-NMR spectra of lower Si/Al ratio samples are needed to differentiate between the two distributions.

Conclusions

High resolution magic-angle-spinning ^{29}Si-NMR is a powerful tool to characterize zeolitic samples. Usually several NMR lines, each belonging to an Si(*n*Al) configuration, are resolved. In addition, various Si(0Al) configurations can also be distinguished in zeolites due to different crystallographic environments. The Si/Al ratios calculated from the NMR values are in good agreement with those obtained by other analytical methods. Silicon-aluminium ordering can easily be computed from the relative line intensities.

Therefore, samples with different Si/Al ratios are prepared either by dealumination or by direct synthesis. For mordenite, ZSM-5 and ZSM-11 zeolites and probably for ZSM-39 zeolite, the Al atoms occupy only preferential sites in the zeolitic framework. This preferential siting can have a definite influence on physico-chemical properties such as acidity or adsorption capacity. Finally, proton-enhanced MAS ^{29}Si-NMR spectra identify unambiguously the presence of silanol groups at defect lattice sites.

*

The authors are indebted to Mr. G. Daelen for his skilful help in taking the NMR spectra. P. A. Jacobs acknowledges a research position as "Senior Research Associate" from NFWO-FNRS (Belgium) and P. Bodart thanks IRSIA (Belgium) for financial support.

REFERENCES

[1] Lippmaa, E., Samoson, A.: Bruker Report, **1,** 6 (1982)
[2] Lippmaa, E., Mägi, M., Samoson, A., Tarmak, M., Engelhardt, G.: J. Am. Chem. Soc., **103,** 4992 (1981)
[3] Engelhardt, G., Lohse, V., Lippmaa, E., Tarmak, M., Mägi, M.: Z. Anorg. All. Chem., **482,** 49 (1981)
[4] Klinowski, J., Ramdas, S., Thomas, J. M., Fyfe, C. A., Hartman, J. S.: J. Chem. Soc., Faraday Trans. 2, **78,** 1025 (1982)
[5] Thomas, J. M., Ramdas, S., Millward, G. R., Klinowski, J., Audier, M., Gonzalez-Calbert, J., Fyfe, C. A.: J. Solid State Chem., **45,** 368 (1982)
[6] Melchior, M. T., Vaughan, D. E. W., Jacobson, A. J.: J. Am. Chem. Soc., **104,** 4859 (1982)
[7] Gabelica, Z., B. Nagy, J., Bodart, P., Debras, G., Derouane, E. G., Jacobs, P. A.: NATO Advanced Study Institute on Zeolites: Science and Technology (Ribeiro, F. R., et al., eds.), pp. 193—210, Martinus Nijhoff, Den Haag 1984
[8] Melchior, M. T., Vaughan, D. E. W., Jarman, R. H., Jacobson A. J.: Nature (London), **298,** 455 (1982)
[9] Thomas, J. M. Fyfe, C. A., Klinowski, J., Gobbi, G. C.: J. Phys. Chem., **86,** 3061 (1982)
[10] Debras, G., B. Nagy, J., Gabelica, Z., Bodart, P., Jacobs, P. A.: Chem. Lett., **1983,** 199
[11] B. Nagy, J., Gabelica, Z., Debras, G., Bodart, P., Derouane, E. G., Jacobs, P. A.: J. Molec. Catal., **20,** 327 (1983)
[12] B. Nagy, J., Gilson, J.-P., Derouane, E. G.: J. Chem. Soc., Chem. Commun., **1981,** 1129
[13] B. Nagy, J., Gabelica, Z., Derouane, E. G., Jacobs, P. A.: Chem. Lett., **1982,** 2003
[14] Jacobs, P. A., Tielen, M., B. Nagy, J., Debras, G., Derouane, E. G., Gabelica, Z.: in Proc. 6th int. Zeolite Conference, Reno, 1983 (in press)
[15] Fyfe, C. A., Gobbi, G. C., Klinowski, J., Thomas, J. M., Ramdas, S.: Nature (London), **296,** 530 (1982)
[16] Debras, G., Derouane, E. G., Demortier, G., Gilson, J.-P., Gabelica, Z.: Zeolites, **3,** 37 (1983)
[17] Gabelica, Z., Blom, N., Derouane, E. G.: Appl. Catal., **5,** 227 (1983)
[18] Ernst, R. R., Anderson, W. A.: Rev. Sci. Instrum., **37,** 93 (1966)
[19] Mehring, M.: High Resolution NMR Spectroscopy in Solids, NMR Basic Principles and Progress Vol. **11a**, Springer, Berlin 1976
[20] Klinowski, J., Thomas, J. M., Audier, M., Vasudevan, S., Fyfe, C. A., Hartmann, J. C.: J. Chem. Soc., Chem. Commun., **1981,** 570
[21] Maxwell, I. E., van Erp. W. A., Hays, G. R., Couperus, T., Huis, R., Clague, A. D. H.: J. Chem. Soc., Chem. Commun., **1982,** 523
[22] Loewenstein, W.: Am. Mineral., **39,** 92 (1954)
[23] Gramlich, V.: Ph. D. Diss. ETH. N° 4633, Zürich (1971)
[24] Bodart, P., Gabelica, Z., B. Nagy, J., Jacobs, P. A.: to be published
[25] Fripiat, J. G., Berger-André, F., André, J.-M., Derouane, E. G.: Zeolites, **3,** 306 (1983)
[26] Derouane, E. G., Fripiat, J. G.: in Proc. 6th Int. Zeolite Conference, Reno, 1983 (in press)
[27] Fyfe, C. A., Gobbi, G. C., Klinowski, J., Thomas, J. M., Ramdas, S.: Nature, **296,** 530 (1982)
[28] Olson, D. H., Kokotailo, G. T., Lawton, S. L., Meier, W. M.: J. Phys. Chem., **85,** 2238 (1981)
[29] B. Nagy, J., Gabelica, Z., Derouane, E. G.: Chem. Lett., **1982,** 1105
[30] Engelhadrt, G., Lohse, U., Samoson, A., Mägi, M., Tarmak, M., Lippmaa, E.: Zeolites, **2,** 59 (1982)
[31] Schlenker, J. L., Dwyer, F. G., Jenkins, E. E., Rohrbaugh, W. J., Kokotailo, G. T., Meier, W. M.: Nature, **294,** 340 (1981)
[32] Bodart, P., B. Nagy, J., Debras, G., Gabelica, Z., Derouane, E. G., Jacobs, P. A.: Bull. Soc. Chim. Belg., **92,** 711 (1983)

Acta Chimica Hungarica 119 (2—3), pp. 275—284 (1985)

CHARACTERIZATION OF X-RAY AMORPHOUS ZSM-5 ZEOLITES BY THERMAL ANALYSIS AND HIGH RESOLUTION SOLID STATE MULTINUCLEAR NMR SPECTROSCOPY+

Zelimir GABELICA*, Janos B. NAGY, Guy DEBRAS** and Eric G. DEROUANE

(Facultés Universitaires de Namur, Laboratoire de Catalyse, 61, rue de Bruxelles, B-5000 Namur, Belgium)

Received June 8, 1984
Accepted for publication October 15, 1984

The potential use of combined DTA and high resolution solid state NMR techniques to characterize very small X-ray amorphous ZSM-5 zeolite particles admixed within a true amorphous Si—Al gel phase, is discussed.

^{13}C-NMR proved, along with DTA, a rapid and accurate technique to' detect traces of TPA ions occluded within the lattice of small ZSM-5 nuclei. ^{27}Al- and ^{29}Si-NMR, related to the Si—Al distribution within a zeolitic lattice, provided valuable additional information on slight modifications and reorganizations that occur in the early stages of the nucleation process and appeared very sensitive to the structural Si—Al ordering that characterizes the beginning of the growth process.

Introduction

In recent years, zeolite ZSM-5 has been the staring point to unique and remarkable catalysts for a variety of reactions. This material can be prepared via a large number of synthesis routes which greatly affect in various ways not only its crystallographic structure but also the final size and shape of the crystallites and hence its shape selective properties. Most of these operational recipes have been described, but rarely explained, in the patent literature. Nevertheless, several recent papers and review articles published in the current literature provide useful background information on factors that affect the hydrothermal synthesis of ZSM-5 and the consequent physicochemical properties of the final crystalline material [1—12].

Although smaller crystallites with larger outer surface are expected to be less shape selective than larger crystals [13], particular efforts have been undertaken to obtain the crystals as small as possible in order to minimize intracrystalline diffusion which often proved to be the rate-limiting step for a variety of reactions [14], especially when conducted on a large scale, in

+ This paper was presented at the 2nd Belgian—Hungarian Colloquium on Catalysis at De Haan, Belgium, October 10—13, 1983.

* To whom correspondence should be addressed.
** Present address: Labofine S. A., Zoning Industriel, B-6520 Feluy, Belgium.

industrial processes [15]. Very small ZSM-5 particles, characterized by an ultimate diameter of 0.005 to 0.1 μm, could be obtained through a high speed stirring of the gel precursor at 110 °C. Unexpectedly, aging is retarded during the use of this material as catalyst in hydrocarbon processing [16].

It is expected that most of these ZSM-5 particles are sufficiently small in size to appear amorphous in XRD examinations.

Various other procedures leading to the formation of amorphous aluminosilicates from gels containing Al_2O_3, SiO_2, Na_2O, H_2O and an organic template such as trimethylenetetramine [17] or tetrapropylammonium (TPA) cation [18—22], have been proposed. With TPA, a medium porous solid having 3.8 nm pore diameter is formed under specific operational conditions [22]. However, X-ray and electron diffraction techniques [22] combined with thermogravimetry and SEM [20, 21], as well as the absence of IR absorption peaks characterizing ZSM-5 [20–22], have confirmed that these materials are truly amorphous and not consisting of tiny particles of ZSM-5. As expected, this amorphous catalyst does not show shape selective properties [22], although its activity is closer to that of ZSM-5 than to that of conventional amorphous silica-aluminas.

Another kind of amorphous ZSM-5 type zeolitic material was reported to form under a long examination of pure crystalline ZSM-5 with a high resolution electron microscope [23]. During the examination, the zeolite becomes gradually "quasi-crystalline" or "semi-amorphous". This material is actually composed of imperfectly ordered ZSM-5 sub-unit fragments and still exhibits marked cation exchange and catalytic properties. Such various degrees of a quasi-crystallinity could be analyzed by direct (real-space) imaging [23].

We have recently developed another synthesis procedure that yields genuine but very small ZSM-5 particles, stabilized in the early stages of the crystallization process of a hydrogel prepared by using nearly monomeric Na silicate. The formation of these crystallites implies a mechanism involving a straightforward solid gel phase transformation process. They appear too small to be detected by XRD, while several other techniques confirm their ZSM-5 type structure [2, 8, 12, 24—27]. This procedure contrasts with the more classical synthesis involving the use of lower Si/Al ratios and polymeric silica. In such a gel indeed, a small number of nuclei is formed and they grow at a relatively high rate to yield rapidly ZSM-5 particles, which are large enough to be quantitatively detected by a variety of methods, e.g. XRD, during the crystallization process.

At that point, some fundamental questions arise: what is the actual chemical nature (structure) of an "amorphous zeolite", provided that the latter term is unambigously defined? How can an amorphous zeolite be formed and stabilized? Which is the most reliable technique to characterize such species?

The first two questions can find partial answer upon close and extensive investigation of the various rearrangements that occur simultaneously or successively within a Si—Al—Na—TPA hydrogel, as soon as the ingredients are admixed. Obviously, ingredient ratios strongly influence the molecular or polymeric species present in the mixture, as well as the rates at which these species are interconverted, by hydrolysis, to the ordered three-dimensional network of the zeolitic product. A close control of these rates or of (poly)-aluminosilicate distribution can sometimes help to stabilize a true ZSM-5 precursor. Numerous other factors that affect simultaneously the rates of nucleation of ZSM- have been recently reviewed and discussed [1—9]. More specifically, valuable information on ZSM-5 precursor species could be derived from studies of TPA-silicate or TPA-aluminosilicate solutions, by high resolution NMR techniques. ^{29}Si-NMR revealed that silicate condensation to polysilicate is favoured in presence of TPA [28] and double Si five-ring intermediates, the structure of which is recognized in the ZSM-5 building unit [29], have been identified in the early stages of the aging process of slurries containing silica, alumina, NaOH and TPAOH [10]. Derouane et al. [30], as well as Romannikov et al. [7], were also able to identify similar TPA-aluminosilicate complexes by ^{27}Al-NMR.

To answer the third question, we shall examine systematically the ability of some experimental methods ot identify unambiguously the X-ray amorphous zeolitic phases previously prepared and recognized to be true ZSM-5 particle [2].

Our procedure consists in isolating intermediate phases progressively formed during crystallization of appropriate gels. The latter, composed of low oligomeric and monomeric silicate and aluminate species, which intimately interact with the numerous structure-directing TPA species, will favour a rapid formation of ZSM-5 through a straightforward hydrogel transformation (or surface nucleation) process. The so obtained mixtures consist of microdomains of (TPA)-ZSM-5 particles dispersed within a non-zeolitic aluminosilicate phase. Although amorphous to X-rays, they could be easily detected by infrared [31—33] and Raman [34] spectroscopy and by high resolution solid state ^{27}Al- [24], ^{29}Si-[24, 26], and ^{13}C-NMR [24, 25]. Their ZSM-5-type structure was confirmed by specific (shape selective) catalytic tests such as the hydrocracking of long chain paraffins [31]. Thermal analysis was also shown to be a very accurate technique to discriminate between TPA loosely bound to an amorphous gel and those interacting strongly with a (very small) ZSM-5 framework [2, 12].

The aim of the present paper is to emphasize the advantage to use high resolution solid state multinuclear NMR, with DTA as complementary technique, to detect quantitatively the amount of X-ray amorphous ZSM-5 zeolite present within a true amorphous aluminosilicate gel-like phase. It is essential that each of these techniques detects with the highest certainty some

properties that unambiguously and exclusively characterize the unaltered ZSM-5 framework, even if the size of the crystallites is below the X-ray detection limit. Each set of techniques gives two different kinds of information. DTA and ^{13}C-NMR are supposed to detect TPA units entrapped within the framework of the ZSM-5 precursors, while ^{27}Al- and ^{29}Si-NMR parameters are more related to the structure and ordering of the T atoms through the ZSM-5 lattice.

Experimental

Formation and stabilization of X-ray amorphous ZSM-5 particles

A hydrogel is prepared by mixing appropriate amounts of aqueous Al sulfate, sulfuric acid and TPABr with soluble aqueous Na silicate and NaCl. Ingredient ratios, final molar composition of the gel and detailed conditions are given elsewhere [2, 5, 8]. The gel must be aged first in acidic medium before its pH is adjusted to about 10 by further adding Na silicate or NaOH. A small amount of XRD amorphous ZSM-5 was shown to be already present in such a gel after a stirring period of about 12 h in basic medium. The acidic pH induces a rapid rearrangement of the silica species appropriate to form the first ZSM-5 nuclei. Furthermore, the TPA cations, well dispersed within the gel, can interact intimately with the aluminosilicate anions that apper in the basic medium, as to yield very small ZSM-5 units even at room temperature, during the homogenization procedure (gel stirring). They probably remain stable during the first steps of the heating, after which they become viable crystallization centers, leading to larger ZSM-5 particles. These mechanisms were discussed in detail previously [2, 8].

The gel mixture was divided into several portions which were sealed in identical 15 m Pyrex tubes prior to autoclaving. They were heated at 140 °C under autogeneous pressure, with occasional shaking, for given periods of time, and progressively removed from the oven in order to isolate materials with increasing degrees of crystallinity. After cooling, each sample (gel + zeolite) was filtered, washed and dried for 12 h, prior to various analyses. This preparation was referred to as synthesis B [2]. For comparison, we have also examined intermediate phases obtained from another type of crystallization procedure (here called procedure A), where no X-ray amorphous ZSM-5 could be found. The procedure A is described and discussed elsewhere [2, 8].

Analytical techniques

The Si, Al and Na contents of all the intermediate and final phases (procedures A and B) were determined by three different surface or bulk analytical methods [5, 35, 36].

The percentage of ZSM-5 in the phases synthesized was evaluated by X-ray diffraction (XRD), differential thermal analysis (DTA) and NMR techniques.

Powder XRD patterns were recorded using a Philips PW 1349/30 X-ray diffractometer with monochromatic Cu Kα radiation. The degree of crystallinity of each phase was obtained by the summation method, considering the intensities of eight of the most characteristic ZSM-5 peaks [2].

Simultaneous TG-DTA analyses of intermediate and final phases were performed in a dry air flow, in a STA-870 thermoanalysis system (Stanton Redcroft), as described elsewhere [2, 12]. Several parameters that can be directly related to the percentage of crystallinity of a phase which is a mixture of ZSM-5 and aluminosilicate gel, have been defined [12].

Two of them, namely weight losses due to the oxidative decomposition of zeolitic TPA species and the magnitude of the corresponding DTA exotherms can be chosen to characterize the intermediate phases.

Being more sensitive to the very small traces of TPA, the DTA information was preferred. We have demonstrated recently that high resolution magic-angle-spinning (HRMAS) solid state ^{13}C-, ^{27}Al- and ^{29}Si-NMR spectroscopy can be successfully used to characterize ZSM-5 zeolites by probing the carbon atoms belonging to occluded TPA species [9, 24, 25], or directly aluminium [24, 38] or silicon [24, 26, 27, 39] atoms constituting the zeolitic lattice. All the NMR spectra were obtained at room temperature, using a Bruker CXP-200 high power instrument in the Fourier transform mode. Detailed conditions as well as the parameters used to scan the ^{27}Al-, ^{29}Si- [40] and ^{13}C-NMR spectra [37] are given elsewhere [24—27, 37, 39, 40].

Results and Discussion

Parameters characterizing zeolitic TPA (^{13}C-NMR, DTA)

HRMAS-^{13}C-NMR spectra of the carbon atoms constituting the propyl chains of TPA units exhibit three typical resonances [24, 25, 37]. However, the relative intensities, positions and widths of these lines depend on the structural environment of the TPA entities so that "free TPA ions" (as in solution or in a solid ionic TPABr lattice) can be easily distinguished from TPA occluded within a ZSM-5 lattice [24]. It has been shown that the intensity of each line is proportional to the amount of the "zeolitic TPA" present, and thus, to the amount of ZSM-5 in an intermediate (ZSM-5 + gel) phase.

Similarly, this amount can be directly computed by measuring the surface area of the DTA exothermic peak that characterizes the oxidative decomposition of the "zeolitic TPA" during the heating of the corresponding (TPA)-ZSM-5 precursor [12]. Table I gives some characteristics of the various intermediate phases obtained from A and B procedures, as well as the corresponding XRD, DTA and ^{13}C-NMR "crystallinites", normalized to 100 for each corresponding final phase.

Figure 1 compares the variation of these crystallinities as a function of synthesis time for both types of procedures. For procedure A, neither a ^{13}C-NMR nor a DTA signal is detected at zero XRD crystallinity (sample 1, 48 h), con-

Table I

Characteristics of some intermediate and final phases isolated from ZSM-5 synthesis procedures A *and* B

Synthesis		Bulk Si/Al at ratio	% crystallinity		^{13}C-NMR		^{27}Al-NMR		^{29}Si-NMR
Type	time (h)		XRD	DTA	I_{tot} (a.u.)[(a)]	$\Delta H^{(b)}$ (Hz)	I_{tot} (a.u.)[(a)]	ΔH (Hz)	I_{tot} (a.u.)[(a)]
A	48	1.8	0	0	0	—	—	4000	36
	136	5.0	45	50	46	400	—	3500	46
	192	10.0	86	92	87	300	(c)	3000	89
	264	12.1	96	—	97	230	—	2800	—
	312	13.2	100	100	100	200	—	2700	100
B	14	33.6	0	34	30	—	50	2950	57
	20	32.0	0	34	30	400	52	3100	54
	26	34.2	0	34	—	—	53	3050	50
	32	34.1	0	38	—	—	57	3000	52
	38	34.3	0	42	—	—	61	3000	—
	42	36.3	0	43	32	400	65	3100	59
	49	36.3	12	49	32	300	67	2800	93
	64	32.0	38	63	50	180	71	2100	96
	110	36.1	100	100	100	140	100	1800	100

(a) Normalized to 100 for each XRD 100% crystalline phase.

(b) First carbon atom from the propyl chain, in $^{+}N(\overset{1}{C}H_2-\overset{2}{C}H_2-\overset{3}{C}H_3)_4$.

(c) Not normalized because of the decreasing Al content.

firming the absence of any occluded TPA. A possible excess of TPA impregnating the gel was already eliminated by washing. The detailed mechanistic study of procedure A [8] has confirmed that a limited number of ZSM-5 nuclei formed in the beginning, at the expense of the amorphous Al-rich phase, will grow at a rather high rate, so that the resulting relatively large crystallites can be detected by the three techniques. Indeed, XRD, DTA and ^{13}C-NMR intensities all follow a classical sigmoid curve, as a function of synthesis time (Fig. 1).

By contrast, XRD does not detect any ZSM-5 in the beginning of procedure B, while both ^{13}C-NMR and DTA do detect some TPA species strongly occluded in the small ZSM-5 nuclei or crystallites, already formed within the gel. These ^{13}C-NMR and DTA intensities stay nearly constant for about 45 h, confirming that a large number of nuclei is formed within the hydrogel, due to the high concentration of the relative aluminate and silicate species which are in intimate interaction with the TPA structure-directing cations. After 45 h, the size of the crystallites begins to be detectable by XRD. The three "crystallinities" then increase in a parallel way, illustrating that more and more TPA templates are progressively entrapped within the growing crystallites.

For both procedures, the linewidth of carbon C_1, chosen as example, becomes narrower as the crystallization proceeds (Fig. 1). This narrowing reflects the progressive reorganization of the Si—Al framework around the propyl chains. In the beginning of procedure B, the ZSM-5 nuclei can be so small that some TPA, only partly incorporated into the zeolite framework, still can interact with various heterogeneous environments of the Si—Al gel, resulting in the broadening of the C_1 NMR line.

Parameters characterizing the ZSM-5 framework (^{27}Al- and ^{29}Si-NMR)

The ^{27}Al-NMR chemical shifts recorded in all cases within the range of 52—65 ppm with respect to $[Al(H_2O)_6]^{3+}$ taken as reference [24], confirm that in both procedures, Al keeps its tetrahedral coordination in both the gel precursors [30] and in crystalline ZSM-5 [39].

The ^{27}Al-NMR linewidth remains large and nearly constant during the time interval in which the XRD amorphous ZSM-5 is stabilized in procedure B (Table I and Fig. 2). It shows a sharp decrease as soon as the crystals begin to grow. Bearing in mind that the average Si/Al ratio in all the intermediate phases remains constant (Table I), the marked decrease of ΔH reflects the progressive migration of the Al atoms from the random, distorted environment in the gel, to an ordered ZSM-5 lattice, where the electric field gradients are reduced [38]. It is also interesting to observe that the overall ^{27}Al-NMR intensity progressively increases during crystallization, despite the fact that the Si/Al ratio does not change during synthesis. It is therefore assumed that

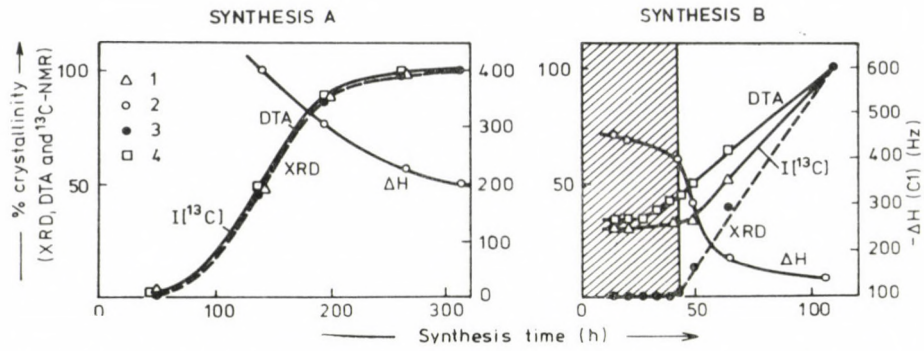

Fig. 1. Variation of ^{13}C-NMR parameters: (1) = total intensity; (2) = C_1 linewidth, ΔH, and of the percentage of crystallinity: (3) = XRD; (4) = DTA, for A- and B-type intermediate phases, as a function of synthesis time

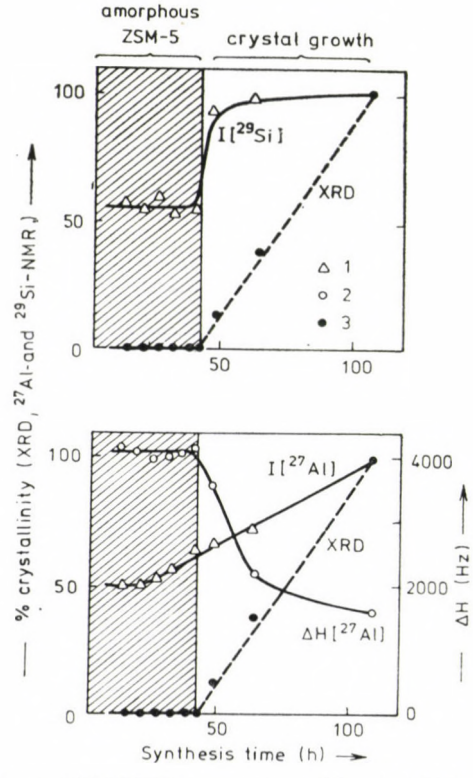

Fig. 2. Variation of ^{27}Al- and ^{29}Si-NMR parameters: (1) = total intensities; (2) = ^{27}Al-NMR linewidth, ΔH, and of the percentage of crystallinity; (3) = XDR, for B-type intermediate phases, as a function of synthesis time

about half of the Al present in a gel-rich phase is not detected, because the corresponding ^{27}Al-NMR line is broadened beyond detection. Obviously, the variation of the ^{27}Al-NMR intensity illustrates qualitatively the Al incorporation within an ordered lattice but by no means should it be used as a quantitative measure of the amount of zeolite (amorphous or not) admixed with a Si/Al gel.

^{29}Si is the best nucleus to study by NMR the structural behaviour of zeolites and, in particular, of ZSM-5 [10, 24, 26, 27, 39, 40]. A complete study of the Si—Al progressive orderings in synthesis A has been achieved by following in detail the variation of the ^{29}Si-NMR line intensities belonging to each Si(nAl) configuration, as a function of crystallization time, during which the overall Si/Al ratios of the intermediate phases increase [24].

In procedure B, where the Si content remains constant in all the intermediate phases, the ^{29}Si-NMR intensity does not vary during the time interval in which the X-ray amorphous ZSM-5 particles are detected, but it shows a sharp increase when these crystallites begin to grow (Table I, Fig. 2). The ordering of Si atoms into a ZSM-5 lattice is the only way to explain that increase. Under our experimental conditions, the intensities are not quantitatively related to the amount of Si present in a phase, probably because the ^{29}Si-NMR relaxation times are different when Si is ordered in a symmetric lattice or when it is located in a random gel-like phase. Figure 2 confirms that the ordering actually begins as soon as the XRD crystallinity is detected and that it is achieved very rapidly, even before the 100% crystalline ZSM-5 is formed.

Conclusions

^{13}C-NMR can be considered, along with DTA, as a very rapid and accurate technique to detect the presence of small ZSM-5 particles, which must contain less than 3 or 4 unit cells, corresponding to a size which is beyond the XRD detection limit. These techniques provide indirect proof of the presence of TPA ions incorporated within the zeolitic lattice during synthesis. The use of complementary techniques, more closely related to the structure of the ZSM-5 lattice itself, is also advisable.

For example, the measure of the IR absorbance of a typical ZSM-5 skeleton vibration at 550 cm^{-1} is also rapid and quite convenient [31, 33]. The use of certain Raman diffusion bands in the low frequency vibration region appears promising as well [34].

Intensities and widths of the ^{27}Al- and ^{29}-Si-NMR resonance lines are both sensitive to the Si/Al variation and to the progressive ordering of the Si—Al framework during the formation (and growth) of ZSM-5 in/from the corresponding amorphous hydrogel. In amorphous phases, both resonances can

be broadened beyond detection so that quantitative Al and Si determination from line intensities is only possible for crystalline (ordered) materials.

Together with ^{13}C-NMR, these techniques, however, provide valuable additional information on slight transformations and reorganizations that already occur during the early nucleation processes. However, neither ^{27}Al- and ^{29}Si-NMR line intensities, nor their widths, do allow to distinguish unambiguously XRD amorphous ZSM-5 particles from the true amorphous Si—Al gel wherein they are embedded. Nevertheless, the very sharp sensitivity of these parameters to a structural Si—Al reordering shall be advantageously used to detect accurately the moment when the actual growth of ZSM-5 starts.

REFERENCES

[1] Barrer, R. M.: Hydrothermal Chemistry of Zeolites, Academic Press, London 1982
[2] Derouane, E. G., Detremmerie, S., Gabelica, Z., Blom, N.: Appl. Catal., **1,** 101 (1981)
[3] Kulkarni, S. B., Shiralkar, V. P., Kotasthane, A. N., Borade, R. B., Ratnasamy, P.: Zeolites, **2,** 313 (1982)
[4] Gabelica, Z., Derouane, E. G., Blom, N.: Appl. Catal., **5,** 109 (1983)
[5] Gabelica, Z., Blom, N., Derouane, E. G.: Appl. Catal., **5,** 227 (1983)
[6] Lok, B. M., Cannan, T. R., Messina, C. A.: Zeolites, **3,** 282 (1983)
[7] Romannikov, V. N., Mastikhin, V. M., Hocevar, S., Drzaj, B.: Zeolites, **3,** 311 (1983)
[8] Gabelica, Z., Derouane, E. G., Blom, N.: in Catalytic Materials: Relationship between Structure and Reactivity, ACS Symp. Ser., **248,** 220 (1984)
[9] Rollmann, L. D.; in Zeolites: Science and Technology (Ed. F. R. Ribeiro et al.), pp. 109—126, Martinus Nijhoff, Den Haag (1984)
[10] Boxhoorn, G., Sudmeijer, O., Van Kasteren, P. H. G.: J. Chem. Soc. Chem. Commun. (submitted) (personal communication)
[11] Parker, L. M., Bibby, D. M., Patterson, J. E.: Zeolites, **4,** 168 (1984)
[12] Gabelica, Z., B. Nagy, J., Derouane, E. G., Gilson, J. P.: Clay Miner. (in press)
[13] Pelrine, B. P.: U.S. Patent 4,100,262 (1978)
[14] Chen, N. Y., Garwood, W. E.: J. Catal., **52,** 453 (1978)
[15] Gabelica, Z.: in Zeolites: Science and Technology (Ed. F. R. Ribeiro et al.), pp. 529—544, Martinus Nijhoff, Den Haag 1984
[16] Plank, C. J., Rosinski, E. J., Schwartz, A. R.: Brit. Pat. Specif. 1,402,981 (1975)
[17] Ball, W. J., Palmer, K. W., Stewart, D. G.: Eur. Pat. 9,976 (1982)
[18] Manton, R. S., Davidtz, J. C.: J. Catal., **60,** 156 (1979)
[19] Refs [6] to [9] cited in ref. [18]
[20] Paris, D.: Preparation of a high surface area, strongly acidic amorphous silica-alumina from tetrapropylammonium aluminate and silicate, CSIR Report CENG C-312 (1980)
[21] Howden, M. G.: Preparation and evaluation of an amorphous silica-alumina catalyst synthesized in the presence of tetrapropylammonium hydroxide, CSIR Report CENG 441 (1982)
[22] Espinoza, R. L., Stander, C. M., Mandersloot, W. G. B.: Appl. Catal., **6,** 11 (1983)
[23] Thomas, J. M., Bursill, C. A.: Angew. Chem. Int. Ed. Engl., **19,** 745 (1980)
[24] Gabelica, Z., B. Nagy, J., Debras, G., Derouane, E. G.: Proc. 6th Intern. Zeolite Conf., 1983 (in press)
[25] Gabelica, Z., B. Nagy, J., Debras, G., J. Catal., **84,** 256 (1983)
[26] Gabelica, Z., B. Nagy, J., Bodart, P., Debras, G., Derouane, E. G., Jacobs, P.: in Zeolites: Science and Technology (Ed. F. R. Ribeiro et al.) pp. 193—210, Martinus Nijhoff 1984
[27] B. Nagy, J., Gabelica, Z., Debras, G., Bodart, P., Derouane, E. G., Jacobs, P.: J. Molec. Catal., **20,** 327 (1983)
[28] Cavell, K. J., Masters, A. F., Wilshier, K. G.: Zeolites, **2,** 244 (1982)
[29] Kokotailo, G. T., Lawton, S. L., Olson, D. H., Meier, W. M.: Nature, **272,** 437 (1978)
[30] Derouane, E. G., B. Nagy, J., Gabelica, Z., Blom, N.: Zeolites, **2,** 299 (1982)
[31] Jacobs, P. A., Derouane, E. G., Weitkamp, J.: J. Chem. Soc., Chem. Commun., **1981,** 591

[32] Jacobs, P. A., Derouane, E. G., Gabelica, Z.: unpublished results
[33] Coudurier, G., Naccache, C., Vedrine, J. C.: J. Chem. Soc., Chem. Commun., **1982,** 1413
[34] Rulmont, A., Gabelica, Z.: unpublished results
[35] Derouane, E. G., Gilson, J. P., Gabelica, Z., Mousty-Desbuquoit, C., Verbist, J.: J. Catal., **71,** 447 (1981)
[36] Debras, G., Derouane, E. G., Gilson, J. P., Gabelica, Z., Demortier, G.: Zeolites, **3,** 37 (1983)
[37] B. Nagy, J., Gabelica, Z., Derouane, E. G.: Zeolites, **3,** 43 (1983)
[38] B. Nagy, J., Gabelica, Z., Debras, G., Derouane, E. G., Gilson, J. P., Jacobs, P. A.: Zeolites, **4,** 133 (1984)
[39] B. Nagy, J., Gabelica, Z., Debrouane, E. G., Jacobs, P. A.: Chem. Lett., **1982,** 2003
[40] Jacobs, P. A., Tielen, M., B. Nagy, J., Debras, G., Debrouane, E. G., Gabelica, Z.: Proc. 6th Intern. Zeolite Conf. 1983 (in press)

5th International Conference

CHEMISTRY FOR PROTECTION OF THE ENVIRONMENT

Place and date: Leuven (Belgium), 9—13 September 1985

Sessions:

- Opening session
- Key-note lectures sessions
- General problems
- Advances in environmental analytical chemistry. General applications
- Reductive and oxidative treatment of fossil fuels and other organic chemicals : treatment of waste streams
- Advances in environmental analytical chemistry instrumentation
- Reduction and oxidative treatment of fossil fuels and other organic chemicals : treatment of waste streams
- The fate of chemical pollutants and their environmental impact
- Reductive and oxidative treatment of fossil fuels and other organic chemicals : monitoring the environment
- Reductive and oxidative treatment of fossil fuels and other organic chemicals : fate and behaviour of hazardous organic chemicals in the environment
- Physico-chemical treatment : flocculation and flotation
- Physico-chemical treatment : ion exchange
- Physico-chemical treatment : filtration
- Physico-chemical treatment : adsorption
- Physico-chemical treatment : oxidation and disinfection
- Physico-chemical treatment : combined chemical-biological processes

The scientific programme will be completed by an important poster session and technical excursions. A very attractive social and cultural programme and a postcongress tour, will also be organised.

General information: 5th C.P.E. Conference,
c/o K.VIV
Jan van Rijswijcklaan 58
2018 Antwerp, Belgium

Ullmann's Encyclopedia of Industrial Chemistry

Fifth, completely revised edition
First international edition in English

Volume A1: Abrasives to Aluminum Oxide
1985. XIV, 594 pages with 188 figures and 180 tables.
Subscription price DM 340.–.
This price applies only when an order is placed for all 36 volumes.
ISBN 3-527-20101-7

Modern industrial chemistry is an enormously complex and multifarious part of our society. It is a multidimensional fabric of materials and markets, plants and products, work and waste, interwoven with everybody's life and prosperity, but at the same time dangerous when out of control.

Modern industrial chemistry in its entirety is the subject of

Ullmann's Encyclopedia of Industrial Chemistry.

Here, experts from the industrialized countries describe the state of the art. They do so in concise, amply illustrated articles, which are edited intensively so as to maintain lucidity and homogeneity throughout the series of, eventually, 36 volumes.

Ullmann's Encyclopedia has a long tradition. It was the very first compilation of its kind and as such appeared in 1914. Its fourth edition was completed in 1984. All these editions were written in German.

The new edition of Ullmann's Encyclopedia is a complete revision, written entirely in English. The Editorial Advisory Board is composed of members from the major industrialized countries. Accordingly, its articles benefit from international authorship, reflecting industrial practice, knowledge and skills from a worldwide perspective. In this respect Ullmann's Encyclopedia of Industrial Chemistry is once more unique, just as it was when it first appeared seventy years ago.

Ullmann's Encyclopedia serves readers in all branches of the chemical and allied industries around the world. It will be useful for institutions and authorities related to industry, and it will be an excellent teaching aid.

For a comprehensive information package please write to:

VCH Verlagsgesellschaft, P.O. Box 1260/1280,
D-6940 Weinheim, Federal Republic of Germany.
Telex 4 65 516 vchwh d.

Text

The text of the paper should be concise. The description of new compounds (in the Experimental) must include the complete analytical data. Special attention must be paid to structural formulas given within the text. Complicated (non-linear) formulas should be drawn on separate sheets of paper and their position in the text should be clearly marked. The numbering of formulas and equations (in parentheses on the right-hand side) is only needed if they are referred to in the text. Units should conform to the International System of Units (SI). In nomenclature the rules of the I.U.P.A.C. are accepted as standard. Symbols for physical quantities are printed in italic type and should, therefore, be underlined in the manuscript.

References

References should be numbered in order of appearance in the text (where the reference number appears in brackets) and listed at the end of the paper. The reference list, too, should by typed double-spaced. Journal titles are to be abbreviated as defined by the Chemical Abstracts Service Source Index.

Examples:

[1] Brossi, A., Lindlar, H., Walter, M., Schneider, O.: Helv. Chim. Acta, **41**, 119 (1958)
[2] Parr, R. G.: Quantum Theory of Molecular Electronic Structure, Benjamin, New York 1964
[3] Warshel, A.: in Modern Theoretical Chemistry, Vol. 7, Part A (Ed. G. A. Segal), Plenum Press, New York 1977

Tables

Each table should be given a Roman number and a brief informative title. Structural formulas should not be used in column headings or in the body of tables.

Figures

Figures should be numbered consecutively with Arabic numerals. Their approximate place should be indicated in the text on the margin. All figures must be identified on the back by the author's name and the figure number in pencil. Standard symbols (such as circles, triangles, squares) are to be used on line-drawings to denote the points determined experimentally. Line-drawings must not contain structural formulas and comments. Spectra or relevant segments thereof, chromatograms, and X-ray diffraction patterns will be reproduced only if concise numerical summaries are inadequate to replace them. Drawings and graphs should be prepared in black ink on good-quality white or tracing paper. Photographs should be submitted on glossy paper as high-contrast copies. Xerox or similar copies are not suitable for reproduction, but may be used for duplicate copies.

Redrawn illustrations will be sent to the authors for checking. No corrections of figures will, therefore, be accepted in the proofs.

Submission of manuscript

After having completed the corrections suggested by the referees and editors, the final manuscript should be submitted in duplicate, in a form ready for publication. If the corrected manuscript is not returned to the editors *within six weeks*, the intended publication of the paper will be regarded as withdrawn by the authors.

Page charge will not be assessed for the publication, however, authors from overseas countries must contribute to the postage of correspondence by sending, together with the manuscript, international postal coupons to the value of U.S. $ 10.—

Proofs and reprints

A set of proofs will be sent to the submitting author. The proofs must be returned within 48 hours of receipt. Late return may cause a delay in the publication of the paper. 100 reprints will be supplied to the authors free of charge.

Periodicals of the Hungarian Academy of Sciences are obtainable at the following addresses:

AUSTRALIA
C.B.D. LIBRARY AND SUBSCRIPTION SERVICE
Box 4886, G.P.O., *Sydney N.S.W. 2001*
COSMOS BOOKSHOP, 145 Ackland Street
St. Kilda (Melbourne), Victoria 3182

AUSTRIA
GLOBUS, Höchstädtplatz 3, *1206 Wien XX*

BELGIUM
OFFICE INTERNATIONAL DE LIBRAIRIE
30 Avenue Marnix, *1050 Bruxelles*
LIBRAIRIE DU MONDE ENTIER
162 rue du Midi, *1000 Bruxelles*

BULGARIA
HEMUS, Bulvar Ruszki 6, *Sofia*

CANADA
PANNONIA BOOKS, P.O. Box 1017
Postal Station "B", *Toronto, Ontario M5T 2T8*

CHINA
CNPICOR, Periodical Department, P.O. Box 50
Peking

CZECHOSLOVAKIA
MAD'ARSKÁ KULTURA, Národní třida 22
115 66 Praha
PNS DOVOZ TISKU, Vinohradská 46, *Praha 2*
PNS DOVOZ TLAČE, *Bratislava 2*

DENMARK
EJNAR MUNKSGAARD, Norregade 6
1165 Copenhagen K

FEDERAL REPUBLIC OF GERMANY
KUNST UND WISSEN ERICH BIEBER
Postfach 46, *7000 Stuttgart 1*

FINLAND
AKATEEMINEN KIRJAKAUPPA, P.O. Box 128
SF-00101 Helsinki 10

FRANCE
DAWSON-FRANCE S. A., B. P. 40, *91121 Palaiseau*
EUROPÉRIODIQUES S. A., 31 Avenue de Versailles, *78170 La Celle St. Cloud*
OFFICE INTERNATIONAL DE DOCUMENTATION ET LIBRAIRIE, 48 rue Gay-Lussac
75240 Paris Cedex 05

GERMAN DEMOCRATIC REPUBLIC
HAUS DER UNGARISCHEN KULTUR
Karl Liebknecht-Straße 9, *DDR-102 Berlin*
DEUTSCHE POST ZEITUNGSVERTRIEBSAMT
Sraße der Pariser Kommüne 3–4, *DDR-104 Berlin*

GREAT BRITAIN
BLACKWELL'S PERIODICALS DIVISION
Hythe Bridge Street, *Oxford OX1 2ET*
BUMPUS, HALDANE AND MAXWELL LTD.
Cowper Works, *Olney, Bucks MK46 4BN*
COLLET'S HOLDINGS LTD., Denington Estate
Wellingborough, Northants NN8 2QT
WM. DAWSON AND SONS LTD., Cannon House
Folkstone, Kent CT19 5EE
H. K. LEWIS AND CO., 136 Gower Street
London WC1E 6BS

GREECE
KOSTARAKIS BROTHERS INTERNATIONAL BOOKSELLERS, 2 Hippokratous Street, *Athens-143*

HOLLAND
MEULENHOFF-BRUNA B.V., Beulingstraat 2,
Amsterdam
MARTINUS NIJHOFF B.V.
Lange Voorhout 9–11, *Den Haag*
SWETS SUBSCRIPTION SERVICE
347b Heereweg, *Lisse*

INDIA
ALLIED PUBLISHING PRIVATE LTD., 13/14
Asaf Ali Road, *New Delhi 110001*
150 B-6 Mount Road, *Madras 600002*
INTERNATIONAL BOOK HOUSE PVT. LTD.
Madame Cama Road, *Bombay 400039*
THE STATE TRADING CORPORATION OF INDIA LTD., Books Import Division, Chandralok
36 Janpath, *New Delhi 110001*

ITALY
INTERSCIENTIA, Via Mazzé 28, *10149 Torino*
LIBRERIA COMMISSIONARIA SANSONI, Via Lamarmora 45, *50121 Firenze*
SANTO VANASIA, Via M. Macchi 58
20124 Milano
D. E. A., Via Lima 28, *00198 Roma*

JAPAN
KINOKUNIYA BOOK-STORE CO. LTD.
17-7 Shinjuku 3 chome, Shinjuku-ku, *Tokyo 160-91*
MARUZEN COMPANY LTD., Book Department,
P.O. Box 5050 Tokyo International, *Tokyo 100-31*
NAUKA LTD. IMPORT DEPARTMENT
2-30-19 Minami Ikebukuro, Toshima-ku, *Tokyo 171*

KOREA
CHULPANMUL, *Phenjan*

NORWAY
TANUM-TIDSKRIFT-SENTRALEN A.S., Karl Johansgatan 41–43, *1000 Oslo*

POLAND
WĘGIERSKI INSTYTUT KULTURY, Marszałkowska 80, *00-517 Warszawa*
CKP I W, ul. Towarowa 28, *00-958 Warszawa*

ROUMANIA
D. E. P., *Bucureşti*
ILEXIM, Calea Grivitei 64–66, *Bucureşti*

SOVIET UNION
SOJUZPECHAT — IMPORT, *Moscow*
and the post offices in each town
MEZHDUNARODNAYA KNIGA, *Moscow G-200*

SPAIN
DIAZ DE SANTOS, Lagasca 95, *Madrid 6*

SWEDEN
ALMQVIST AND WIKSELL, Gamla Brogatan 26
101 20 Stockholm
GUMPERTS UNIVERSITETSBOKHANDEL AB
Box 346, *401 25 Göteborg 1*

SWITZERLAND
KARGER LIBRI AG, Petersgraben 31, *4011 Basel*

USA
EBSCO SUBSCRIPTION SERVICES
P.O. Box 1943, *Birmingham, Alabama 35201*
F. W. FAXON COMPANY, INC.
15 Southwest Park, *Westwood Mass. 02090*
THE MOORE-COTTRELL SUBSCRIPTION AGENCIES, *North Cohocton, N. Y. 14868*
READ-MORE PUBLICATIONS, INC.
140 Cedar Street, *New York, N. Y. 10006*
STECHERT-MACMILLAN, INC.
7250 Westfield Avenue, *Pennsauken N. J. 08110*

YUGOSLAVIA
JUGOSLOVENSKA KNJIGA, Terazije 27, *Beograd*
FORUM, Vojvode Mišića 1, *21000 Novi Sad*

Index: 26.007

Acta Chimica Hungarica

VOLUME 119, NUMBER 4, AUGUST 1985

EDITOR-IN-CHIEF
F. MÁRTA

MANAGING EDITOR
GY. DEÁK

ASSISTANT EDITOR
L. HAZAI

EDITORIAL BOARD
M. T. BECK, R. BOGNÁR, GY. HARDY, K. LEMPERT, B. LENGYEL, K. POLINSZKY, E. PUNGOR, G. SCHAY, Z. G. SZABÓ, P. TÉTÉNYI

Akadémiai Kiadó, Budapest
ACTA CHIM. HUNG. ACHUDC 119 (4) 285–378 (1985) HU ISSN 0231–3146

ACTA CHIMICA HUNGARICA

A JOURNAL OF THE HUNGARIAN ACADEMY OF SCIENCES

Acta Chimica publishes original reports on all aspects of chemistry in English.

Acta Chimica is published in three volumes per year, each volume consisting of four issues, by

AKADÉMIAI KIADÓ

Publishing House of the Hungarian Academy of Sciences
H-1054 Budapest, Alkotmány u. 21.

Manuscripts and editorial correspondence should be addressed to

Acta Chimica
H-1450 Budapest P.O. Box 67

Subscription information

Orders should be addressed to

KULTURA Foreign Trading Company
H-1389 Budapest P.O. Box 149

or to its representatives abroad

Acta Chimica is indexed in Current Contents

NOTICE TO AUTHORS

Acta Chimica publishes original papers on all aspects of chemistry in English. Before preparing a manuscript for submission to this journal authors are advised to consult recent issues.

Form of manuscript

Manuscripts, tables and illustrations should be submitted in triplicate. Manuscripts should be typewritten double spaced (25 lines, 50 characters per line including spaces). The *title page* should include (1) the title of the paper, (2) the full names of the author(s) in the sequence to be published; apply an asterisk to designate the name of the author to whom correspondence should be addressed, (3) name and address of the institution where the work was done. If the paper is part of a series, reference to the previous communication must be given as a footnote.

Abstract

A summary is printed at the head of each paper. This should not exceed 200 words and should state briefly the principal results and major conclusions of the work. It should be suitable for use by abstracting services.

CONTENTS

PHYSICAL AND INORGANIC CHEMISTRY

Polarographic studies of some azo-triazol dyes (Short communication), **A. E. K. K. Abd El Kader, M. G. Abd El Wahed, G. El Sayed** 285
Separation of Hg(II), La(III) and Ce(III) on Dowex 50W-X8 columns in mixed NH_4NO_3—CH_3COOH media, **U. Srivastava, A. K. Ghose, L. C. T. Eusebius** 295
Ultraviolet and infrared study of 9-arylhydrazono- and 9-arylaminomethylene-6,7,8,9-tetrahydropyridopyrimidine derivatives, **G. Horváth, T. Breining, I. Hermecz, Á. Horváth, M. Pongor-Csákvári, B. Podányi, Á. I. Kiss, A. Martin** 305
Ionization properties of 6,7,8,9-tetrahydro-4*H*-pyrido[1,2-*a*]pyrimidin-4-one derivatives having a conjugated side chain in position 9, **A. Martin, Á. I. Kiss, G. Horváth, I. Hermecz** 321
Dioxouranium(VI) complexes of terdentate 16-membered macrocyclic ligands, **H. S. Yadav, S. K. Sengupta, S. C. Tripathi** 333
New metal complexes of 4-phenyl-1-diacetylmonoxime-3-thiosemicarbazone (BMPTS), **K. M. Ibrahim, A. A. El-Asmy, M. M. Bekheit, M. M. Mostafa** 355
Kinetic study on the hydrolysis of benzenesulfonyl chloride in water-dioxane solutions, **M. Mousa, A. Aly, A. Harfoush** 363

ORGANIC CHEMISTRY

By-products in the preparation of 1,1,1,5-tetrachloropent-3-ene from 1,3-butadiene and tetrachloromethane (Short communication), **Z. Vít, I. Kolb** 345
Preparation of derivatives of citronellal, **Gy. Körtvélyessy** 347
^{1}H-NMR study of restricted rotation in dithiophosphoromethyl acetanilides, **Zs. H-Kovács** 371

ANALYTICAL CHEMISTRY

Determination of some amino compounds with ammonium metavanadate, **S. Ahmad, Jamaluddin, I. C. Shukla** 339

BOOK REVIEWS 377

PRINTED IN HUNGARY

Akadémiai Kiadó és Nyomda, Budapest

Acta Chimica Hungarica 119 (4), pp. 285—294 (1985)

POLAROGRAPHIC STUDIES OF SOME AZO-TRIAZOL DYES

(SHORT COMMUNICATION)

Abd El Khany Kamel ABD EL KADER[1], Mohamed Gamal ABD EL WAHED[2]* and Galila EL SAYED[1]

([1]Faculty of Science, Al-Azhar University, [2]Faculty of Science, Zagazig University, Zagazig, Egypt)

Received July 11, 1983
Accepted for publication November 4, 1983**

The polarographic behaviour of the azo dyes, in different media and concentration, was always of interest. The studies of some azo compounds have been the subject of several investigations [1—5]. The electroreduction of these compounds occurs irreversibly and its half wave potentials are pH dependent. Holleck [6] indicated that the polarographic reduction of *p*-nitroazobenzene is completely reversible and contradicting to the unsubstituted azobenzene and the other substituted azo compounds. The polarographic reduction of nitrobenzene was studied by Zinate [7]. He found that the half wave potentials plotted against the pH of solutions give a *S*-shape representing the first step of nitrobenzene reduction. The polarographic behaviour of benzotriazol and its mono-and dimethyl derivatives at the dropping mercury electrode had been investigated by Henning [8]. He found that the reduction of benzotriazol in acid solution is a four-electron reduction to *o*-aminophenylhydrazine-2-methylbenzotriazol. In alkaline solution it is reduced to 1,3-dihydro-2-methylbenzotriazol which in acid solution is rearranged to 2-aminophenyl-2-methylimide.

The large organic molecules containing azo, nitro, and triazol centres have not been studied polarographically. Also the mechanism of the reduction of these centres are unknown. The present work illustrates the polarographic behaviour of some azo-triazol dyes which are not studied before to ascertain the mode of reduction and the effect of the medium used. The importance of this study comes from application of these compounds as dyestuffs and metal indicators.

Experimental

Preparation of the compounds

The compounds employed are listed in Table I. Compound I was prepared in the hydrogen form, where the amination was carried out by a reverse Buchrer reaction, then coupled to the appropriate naphthosulphonic acid. Compound II was provided by Mehalla El Kobra

* To whom correspondence should be addressed
** In final form received from Egypt December 4, 1984

Table I

	Compound	Structure	Mol. mass
I	C.I. Acid Red 13	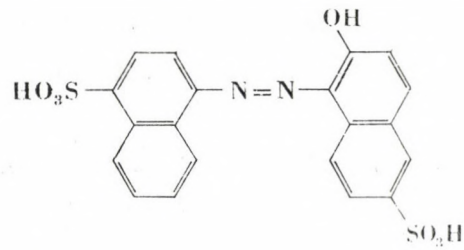	458.49
II	C.I. Acid Green 12	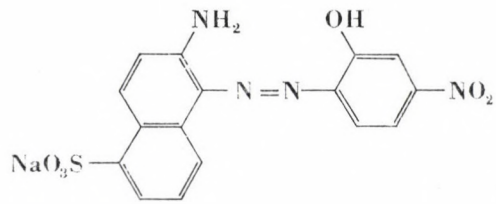	411.15
III	Dimethyl aniline azonitrobenzotriazol	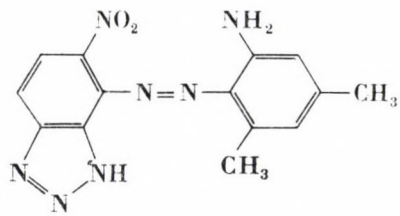	311.15
IV	H-Acid azonitro-benzotriazol	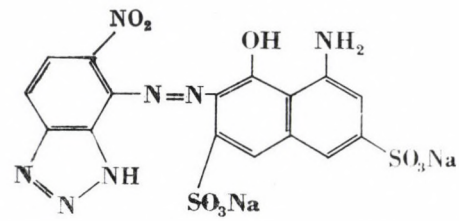	553.40

Spinning and Weaving Company. The commercial sample was dissolved in dimethylformamide, then precipitated with acetone. The precipitate was recrystallised from an alcohol/water mixture [9]. Compounds **III** and **IV** were provided in the pure form by Dr. Dorkham, National Research Centre, Cairo, Egypt.

Solutions and procedure

As supporting electrolytes Britton and Robinson buffers [10] were used. An appropriate volume of the compounds **I** and **II** was mixed with the buffer solution, but compounds **III** and **IV** were prepared by mixing the desired volume with the buffer solution containing 50% ethanol in a 25 mL measuring flask.

The polarograms were recorded on an ink recording polarograph of LP 7 type No. 1510 using a dropping mercury electrode with $m = 2.274$ mg s^{-1} and $t = 2.372$ s $drop^{-1}$ at a height of 35 mm. The pH values of the solutions were recorded on a pH-meter model GTC, Nr. 2431. The potential of the D.M.E. was registered relative to a saturated calomel electrode (SCE) of large surface area. Measurements were carried out at 20 °C.

Results and Discussion

All the dyes under investigation are reduced at the D.M.E. giving well developed irreversible polarographic waves. The reversibility of the waves are tested by plotting log $(i_d - i)$ vs. E and checked by the application of Tomes equation as rearranged by Meites [11]. The polarographic study of the compounds under investigation shows a different behaviour. Accordingly the reduction of each related compound is considered separately.

Electroreduction of C. I. Acid Red 13 and C. I. Acid Green 12

The polarographic behaviour of 10^{-4} M acid red 13 and 4.5×10^{-4} M acid green 12 as examined in buffer solutions of different pH are shown in Figs 1 and 2. Compound I is reduced in acid, neutral and alkaline media along a well developed wave. As the pH value increases the half wave potential $E_{1/2}$ shifts to more negative values indicating that $E_{1/2}$ is pH dependent and H^+ ions take part in the electrode reaction. Within the pH range 2.3—11.25, the half wave potential varies according to:

$$E_{1/2} = 0.012 - 0.054 \text{ pH V}$$

The limiting current remains approximately constant, i.e. pH independent. From the dependence of the limiting current on the effective mercury head ($i = Kh^*$), it is concluded that the wave is kinetically controlled ($x = 0.17$).

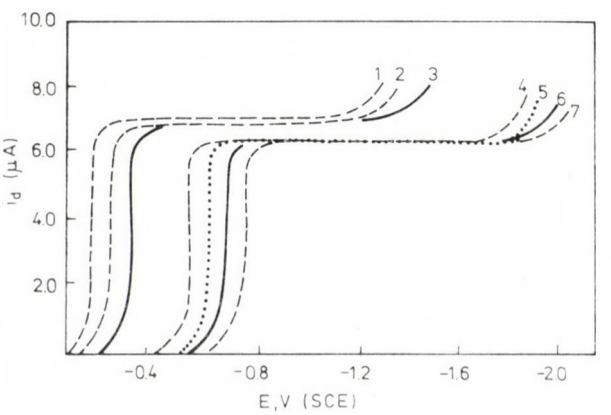

Fig. 1. Polarograms of compound I at different pH values: 1) 2.30, 2) 4.30, 3) 5.90, 4) 6.95, 5) 8.20, 6) 9.25, 7) 11.25

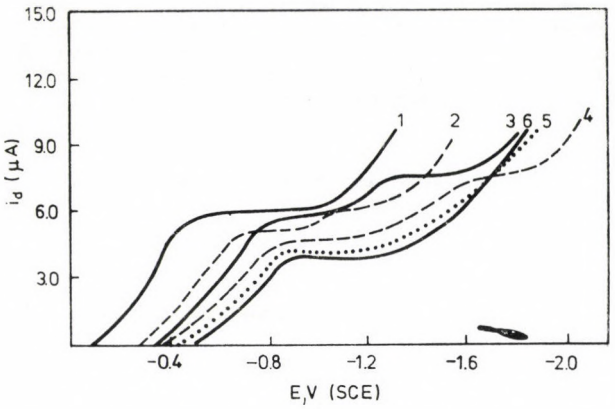

Fig. 2. Polarograms of compound **II** at different pH values: 1) 3.15, 2) 4.15, 3) 6.12, 4) 7.80, 6) 8.45, 6) 9.50

The increase in the pH value causes splitting of the single wave into two irreversible reduction waves in compound **II**. The half wave potentials of the reduction steps vary according to:

$$E_{1/2} = 0.018 - 0.07 \text{ pH V} \quad \text{first wave}$$

$$E_{1/2} = 0.490 - 0.14 \text{ pH V} \quad \text{second wave}$$

The effect of the pressure of mercury on the reduction current of compound **II** indicates that the reaction is diffusion-controlled ($x = 0.581$).

The number of electrons consumed in the rate-determining step has been determined according to Tomes [11], and from the diffusion coefficient D_0 of the compounds. The value of D_0 was determined from the molar volume applying the Stokes—Einstein relation:

$$D_0 = 3.31 \times 10^{-5} (d/M)^{1/3} \quad \text{cm}^2 \text{ s}^{-1}$$

The densities of the compounds were determined by the simple specific gravity bottle method, where the number of electrons n_a involved in the reduction process was then determined from the Ilkovic equation. These values are supported by the results of micro-coulometric analysis by Reynolds [12] for the determination of the number of electrons involved in the irreversible products. The obtained results of the different data concerning compounds **I** and **II** are given in Table II.

In order to understand the type of reduction, the structure of the molecule should be considered. From the molecular formula (Table I), it is apparent the compound **I** contains only one reducible centre, N=N, while compound

Table II

Comp.	pH	i_d μA	$E_{1/2}$ V	$\Delta E_{1/2}/\Delta$pH		αn_a analysis		αn_a Tomes		Z_{H^+}	
I	2.30	6.96		0.13		0.078		0.94	0.97	0.95	
	4.30	6.96		0.22		0.078		0.57	0.77	0.71	
	5.90	6.96		0.35		0.078		0.54	0.77	0.71	
	6.95	6.50		0.57		0.078		0.79	1.35	1.28	
	8.20	6.56		0.61		0.078		0.79	0.97	0.99	
	9.25	5.50		0.65		0.078		1.02	1.36	1.30	
	11.35	6.50		0.73		0.078		1.20	1.45	1.41	
II	3.15	6.15	—	0.22	—	0.25	—	1.02	—	1.20	—	1.80	—
	4.15	7.00	1.50	0.43	1.00	0.25	0.17	0.69	0.18	0.73	0.14	0.96	0.25
	6.12	7.00	1.50	0.75	1.34	0.25	0.17	0.65	0.22	0.57	0.27	0.85	0.41
	7.80	4.75	5.00	0.72	1.55	0.25	0.08	0.65	0.22	0.30	0.67	0.50	0.92
	8.45	4.50	6.50	0.72	1.58	0.25	0.08	0.09	0.28	0.32	0.37	0.48	0.55
	9.50	3.70	7.00	0.81	1.79	0.25	0.08	0.18	0.16	0.26	0.20	0.39	0.30

II contains two centres: N=N and NO_2. Knowing the n_a values, as mentioned for each compound, and the α values calculated using the relation:

$$E = E_{1/2} - \frac{0.059}{\alpha n_a} \log \frac{i}{i_d - i}$$

The most probable α values were obtained for different n_a values as determined. Substituting the most probable α values obtained in the relation:

$$\Delta E_{1/2}/\Delta \mathrm{pH} = \frac{0.059}{\alpha n_a} Z_{H^+}$$

shows that the rate determining step involve the same number of protons as electrons ($Z_{H^+}/\alpha n_a = 1$). The number of electrons consumed in the reduction process of compound **I** was found to be two, while the consumed electrons in the reduction of compound **II** is six in acidic and twelve in alkaline media. Thus the electrode reaction can be supposed as follows:

Compound **I**

$$R-N=N-R + 2e^- + 2H_3O^+ \longrightarrow R-\underset{H}{N}-\underset{H}{N}-R$$

Compound II in acidic media

in alkaline media

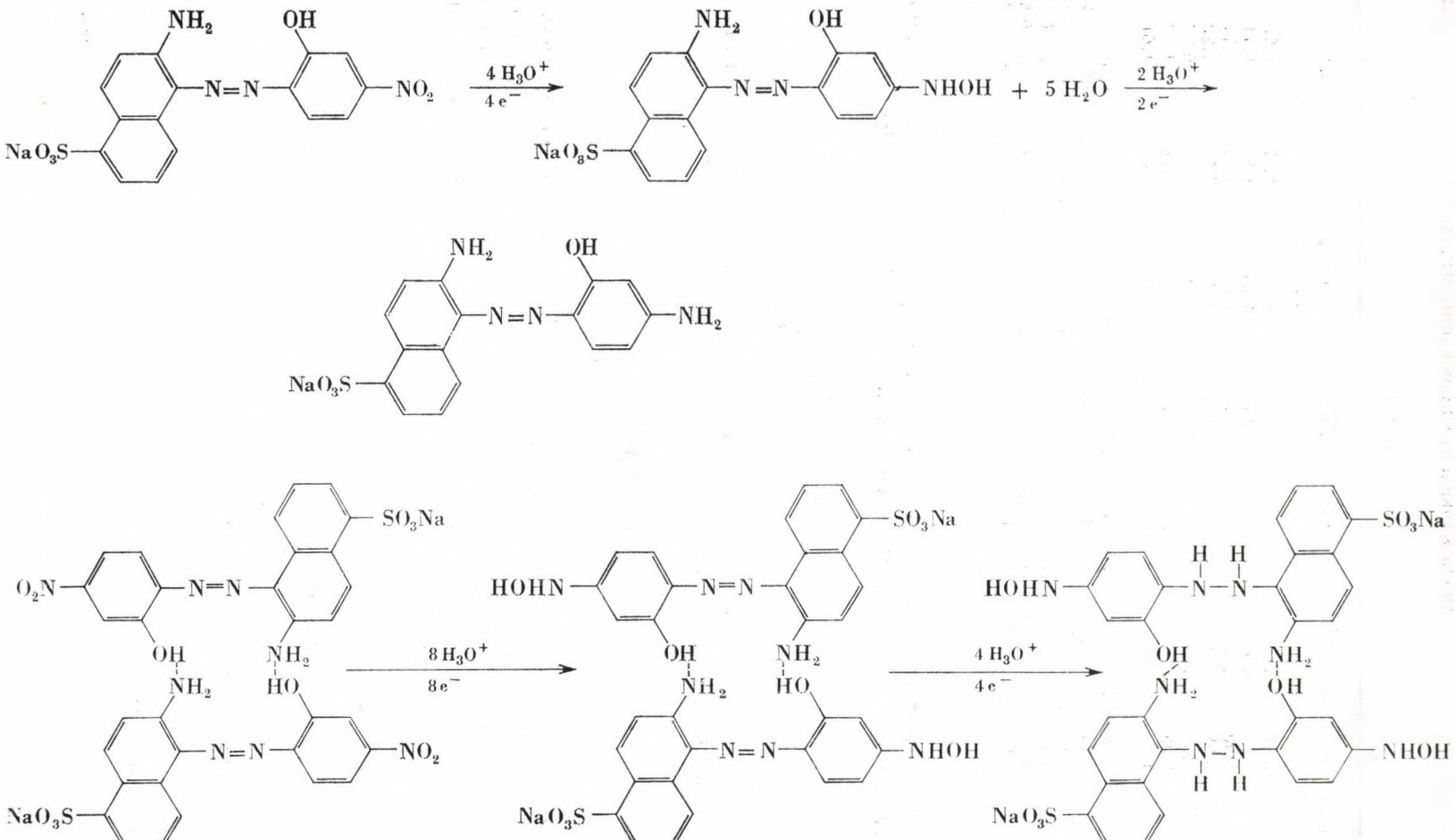
NH2
OH
N=N
NO2
NaO3S
4 H3O+
4 e−
NHOH
+ 5 H2O
2 H3O+
2 e−
SO3Na
O2N
HO
8 H3O+
8 e−
HOHN
4 H3O+
4 e−
H

Thus, the compound containing both reducible centres N=N and NO can be reduced to the amino-azo in acidic and hydroxylamine and hydrazo in alkaline media.

Electroreduction of azo-nitro-benzo-triazol derivatives

The electroreduction of 0.95×10^{-4} *M* of dimethylaniline azonitrobenzotriazol and of 1.8×10^{-3} *M* of H-acid azonitrobenzotriazol in universal buffer solutions of various pH values are shown in Figs 3 and 4. The polarograms of compound **III** at low pH values consist of three waves. The first and the third waves have higher limiting current than the second one. The second wave disappears by increasing the pH value. All the three waves are kinetically controlled, as revealed from the dependence of their limiting currents on the effective mercury head (x = 0.29, 0.296 and 0.312). Reduction occurs irrever-

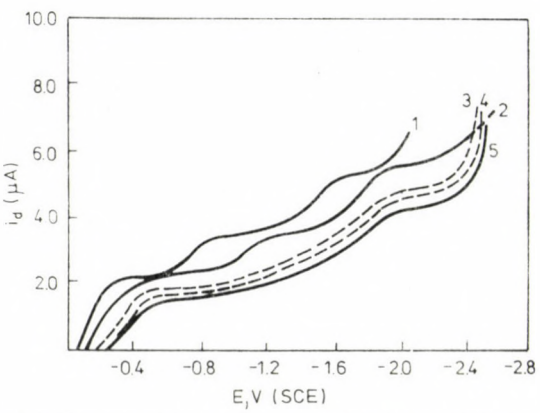

Fig. 3. Polarograms of compound **III** at different pH values: 1) 6.15, 2) 8.05, 3) 8.90, 4) 9.40, 5) 10.75

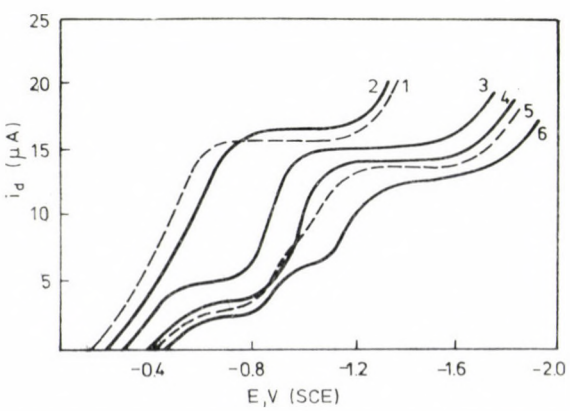

Fig. 4. Polarograms of compound **IV** at different pH values: 1) 3.65, 2) 4.35, 3) 7.85, 4) 8.90, 5) 9.90, 6) 12.10

sibly as ascertained from the fact that the logarithmic analysis of the waves give rise to straight lines for pH 6.12 and 10.95 with slopes of 8.50 and 7.14. The same conclusion is also reached from a consideration of the dependence of the reduction potentials of the three waves on the pH value of the solutions. Within the pH range 6.15 to 10.95 the half wave potentials are adequately given as:

$$E_{1/2} = 0.016 - 0.04 \text{ pH V} \qquad \text{first wave}$$

$$E_{1/2} = -0.045 - 0.13 \text{ pH V} \qquad \text{second wave}$$

$$E_{1/2} = 0.720 - 0.10 \text{ pH V} \qquad \text{third wave}$$

As will be shown later, each of the three steps involves the transfer of two electrons. This indicates that all three reducible centres in the molecule are susceptible to attack.

The polarographic behaviour of compound **IV** is different. A single wave appears at low pH values and by increasing the pH of the medium another wave emerges. In strongly alkaline medium, it splits into two waves of unequal height. The analysis of the waves demonstrates that the reduction takes place irreversibly and it is diffusion-controlled ($x = 0.53$ and 0.35). The reduction potential varies with the pH according to:

$$E_{1/2} = 0.31 - 0.03 \text{ pH V} \qquad \text{first wave}$$

$$E_{1/2} = 0.61 - 0.038 \text{ pH V} \qquad \text{second wave}$$

The number of electrons consumed in the reduction process is six. The obtained results are tabulated in Table III.

Table III

pH	i_d μA			$E_{1/2}$ V			αn_a analysis			αn_a Tomes			Z_{H+}		
	1st	2nd	3rd	1st	2nd	3rd	1st	2nd	3rd	1st	2nd	3rd	1st	2nd	3rd
6.15	2.40	1.20	2.2	0.25	0.73	1.31	0.51	0.83	0.44	0.37	0.52	0.30	0.44	0.88	0.37
8.05	2.40	0.80	2.4	0.28	0.90	1.44	0.33	0.40	0.25	0.23	0.32	0.19	0.28	0.54	0.40
8.90	2.25	3.20	—	0.42	1.38	—	0.48	0.46	—	0.34	0.16	—	0.41	0.27	—
9.40	2.20	3.00	—	0.42	1.30	—	0.46	0.44	—	0.29	0.29	—	0.36	0.43	—
10.7	2.20	3.00	—	0.42	1.36	—	0.42	0.44	—	0.30	0.23	—	0.35	0.39	—
3.65	15.5	—	—	0.43	—	—	0.27	—	—	0.26	—	—	0.27	—	—
4.85	5.00	10.0	—	0.41	0.73	—	1.30	0.65	—	1.26	0.61	—	1.28	0.62	—
7.85	5.05	10.0	—	0.48	0.82	—	0.13	0.70	—	0.34	0.75	—	0.30	0.71	—
8.90	3.75	11.0	—	0.51	0.86	—	0.62	0.60	—	0.54	0.65	—	0.52	0.63	—
9.90	3.75	11.0	—	0.51	0.88	—	0.58	0.61	—	0.54	0.65	—	0.53	0.63	—
12.1	3.75	3.00	8.0	0.50	0.79	1.30	0.71	0.48	—	0.68	0.49	—	0.65	0.48	—

From the structural point of view as well as the polarograms obtained (Figs 3 and 4), it seems that compounds **III** and **IV** posses the same reducible centres. The number of electrons consumed in the electrode reduction is six. The limiting current remains constant at all pH values studied. The half wave potential shifts to more negative values till pH 8.90, where it is independent on the pH of the media (no change of $E_{1/2}$). For the first wave $Z_{H^+}/\alpha n_a = 1$, while for the second $Z_{H^+}/\alpha n_a = 2/1$. Thus one can write the mechanism of the reduction process as follow:

in acidic media

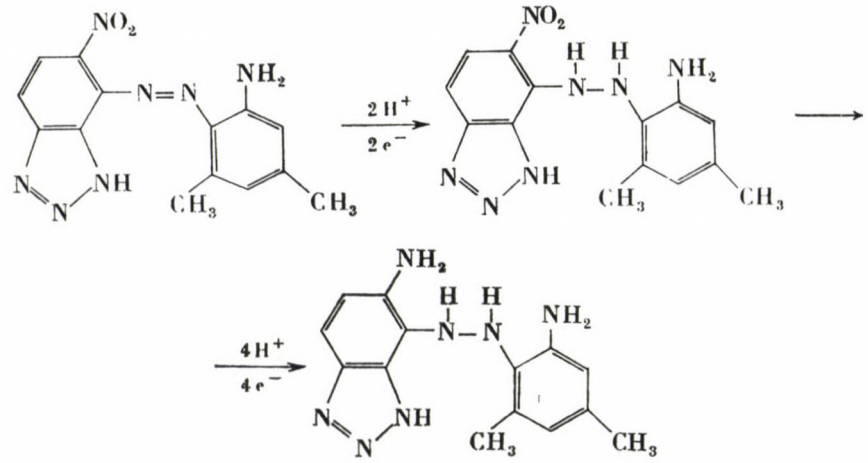

in alkaline media

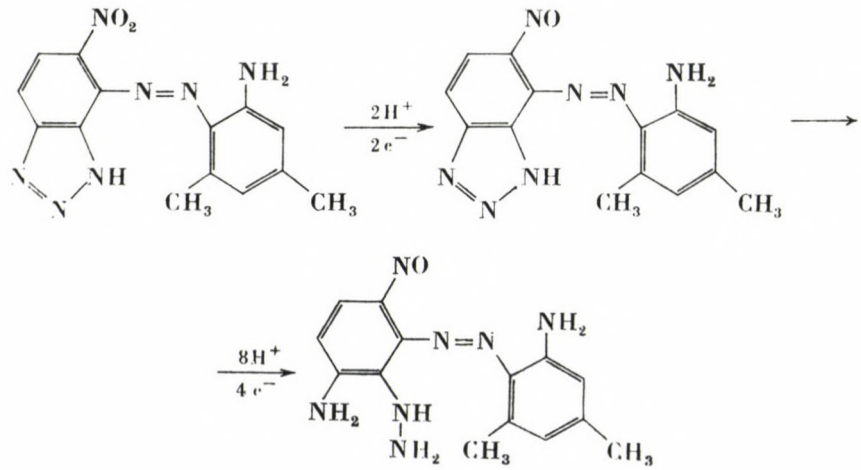

The electroreduction occurs on the nitro and azo centres only, since the triazol centre can not be reduced in the presence of these two centres.

REFERENCES

[1] Volpi, A.: Gazz. Chem. Ital., **77,** 473 (1947)
[2] Vladimirtsev, I. F., Postovski, Ya.: Dokl. Akad. Nauk. S.S.S.R., **83,** 855 (1952)
[3] Shams El-din, A. M. et al.: J. Electroanal. Chem., **21,** 377 (1969)
[4] Thomas, F. G., Boto, K. G.: Aust. J. Chem., **24,** 975 (1971)
[5] Florence, T. M.: J. Electroanal. Chem. Interfacial Electrochem., **52,** 115 (1974)
[6] Holleck, L., Holleck, G.: Monatsh, **95,** 990 (1964)
[7] Stradins, J., Kravis, I.: Lotv. PSR Zinate, Akod. Vestus Kim. Ser., **4,** 500 (1971)
[8] Henning, L., Saanitte, K.: Acta Chem. Scand., **22,** 2879 (1968)
[9] Chantrey, G.: Ph. D. Thesis, University of Leeds (1968)
[10] Britton, H. T.: "Hydrogen Items", 4th Edition, London Chapman and Hall Ltd. (1952)
[11] Meites, L. et al.: J. Am. Chem. Soc., **83,** 4903 (1961)
[12] Reynold, G. F., Shalgosky, H. I.: Anal. Chim. Acta, **10,** 386 (1954)

Acta Chimica Hungarica 119 (4), pp. 295—303 (1985)

SEPARATION OF Hg(II), La(III) AND Ce(III) ON DOWEX 50W-X8 COLUMNS IN MIXED NH_4NO_3—CH_3COOH MEDIA

Uma SRIVASTAVA[1], Animesh Kumar GHOSE[1] and Lalit Colvin Theodore EUSEBIUS[2]*

([1]Chemical Laboratories, University of Allahabad, Allahabad-211002, India, [2]Analytical Chemistry Laboratory, Department of Chemistry, Ewing Christian College, Allahabad 211003, India)

Received July 19, 1983
Accepted for publication August 15, 1984

Cation exchange characteristics of various metal ions in mixed ammonium nitrate—acetic acid media has been explored in order to find out the suitability of this media in achieving separations. The distribution coefficients (K) were determined by batch technique at fixed 1.0 mol/dm^3 CH_3COOH concentration and varying (0.1—1.5 mol/dm^3) amounts of NH_4NO_3, indicated the separation of Hg(III), La(III) and Ce(III) from other metal ions examined. The following separations were achieved in approximately 8.0 cm long column of Dowex 50W-X8 (H^+ form, 100—200 mesh size): Hg(II) from Al(III), Ca(II), Co(II), Ni(II), Cu(II), Zn(II), Sr(II), Cd(II), Ba(II), La(III), Pb(II) or Bi(III) in 0.10 mol/dm^3 NH_4NO_3—1.0 mol/dm^3 CH_3COOH; La(III)/Ce(III) from all other metal ions studied in 1.50 mol/dm^3 NH_4NO_3—1.0 mol/dm^3 CH_3COOH. The following ternary mixtures were also separated: Hg(II) from Al(III), Ca(II), Co(II), Ni(II), Cu(II), Zn(II), Sr(II), Cd(II), Ba(II), Pb(II) or Bi(III) from La(III) or Ce(III). In all the separations column kinetics was found to be quite favourable. The distribution coefficients, elution behaviour of metal ions, elution curves and the results of various artificial binary and ternary mixtures along with standard deviations are reported.

Introduction

Extensive ion-exchange studies in aqueous acid (inorganic as well as organic) media have been carried out and a number of procedures thus developed found application in the chemical analysis of rocks, minerals, soils, fission products, steel and alloys etc. Salts of many of these acids have also been reported to give equally good results or sometimes even more specific and selective separations. Mixtures of salts and acids provide a medium behaving as a buffer solution. Such medium are also proved to be of great importance in the inorganic analysis especially in affecting separations of metal ions of almost identical nature for e.g. cation exchange separation of alkaline earths and rare earths in citrate buffers [1].

Behaviour of number of elements in ammonium salts, malonate [2], formate [3], citrate [4, 5], lactate [6] and acetylacetonate [7], have been reported. A comparative study of distribution coefficients, from which the

* To whom correspondence should be addressed

most favourable eluant concentration can be estimated directly and which makes an evaluation and comparison of the various eluting agents possible, has been published by Strelow et al. [8]. Procedures have been developed for the separation of various metal ions especially alkaline earths, heavy metals, rare earths etc. in ammonium salts medium.

Ammonium nitrate has also been explored. Rare earths, actinides, alkaline earths, Ti, Al and Sc were separated by paper chromatography impregnated with Sn(IV) antimonate. The mobile phase was 0.1—4.0 mol/dm^3 HNO_3 or 0.1—1.0 mol/dm^3 NH_4NO_3 [9]. Alkali metals were separated in NH_4NO_3 medium on phosphoantimonic acid as a cation exchanger [10]. Separation of Na and K from other elements [11] and that of K, Pb and Cs from each other [12—15] were achieved in NH_4NO_3. Jenkins et al. [16], separated Th from U on a cation exchanger in HCl—NH_4NO_3 medium, while Abe Mitsuo [17] separated alkali metals in HNO_3—NH_4NO_3 medium. The dependence of distribution coefficients (K) of Rb, Cs and Tl on pH and on concentration of NH_4NO_3 and HNO_3 was examined by Malik and coworkers [18].

As salt—acid mixture provides a medium often suitable for chemical analysis, it thought to be of interest to explore the ion-exchange characterization of a number of metal ions in ammonium nitrate—acetic acid mixtures. No systematic study as regards the cation-exchange behaviour of metal ions in ammonium nitrate—acetic acid is available in the literature. The distribution coefficients of the following 14 metal ions were determined by the batch technique: Al(III), Ca(II), Co(II), Ni(II), Cu(II), Zn(II), Cd(II), Sr(II), Ba(II), Hg(II), Pb(II), Bi(III), La(III) and Ce(III). The cation exchanger used is Dowex 50W-X8, 100—200 mesh in H^+ — form. Distribution coefficients (K), elution characteristics of metal ions, elution curves, and results of resolution of binary and ternary mixtures along with standard deviations are presented. The separations were quantitative and column kinetics was found to be quite favourable.

Results and Discussion

The K values reported in Table I, indicate that the affinity of metal ions decrease with increasing the concentrations of NH_4NO_3 at 1.0 mol/dm^3 CH_3COOH. The K values of metal ions are either guided by the complexation reaction with acetate and ammonium ions or by the competition of NH_4^+ and H^+ counter ions. In general, the K values are lower in NH_4NO_3—CH_3COOH mixtures than in pure aqueous ammonium acetate probably firstly H^+ ions effectively compete for cation exchanger and secondly CH_3COOH lowers the dielectric constant of the medium favouring ion association or complexation thus further lowering the affinity of various metal ions towards cation exchang-

Table I

Distribution coefficients in varying concentration of NH_4NO_3 (0.1—1.5 mol/dm³) *at a fixed concentration* (1.0 mol/dm³) *of* CH_3COOH

Metal ion	Distribution coefficient (K)			
	Concentration of NH_4NO_3(mol/dm³)			
	0.1	0.5	1.0	1.5
Al(III)	300	30	29	7.5
Ca(II)	470	46	15	2.0
Co(II)	140	57	20	4.0
Ni(II)	222	98	20	5.0
Cu(II)	185	56	11	3.0
Zn(II)	200	52	22	4.0
Sr(II)	223	49	20	3.6
Cd(II)	800	60	22	6.3
Ba(II)	450	65	18	4.7
La(III)	787	178	110	6.5
Hg(II)	3.0	2.1	1.5	0.1
Pb(II)	173	54	16	4.3
Bi(III)	787	69	28	8.0
Ce(III)	h	1600	787	207

h = very high value

er except La(III) and Ce(III) which have slightly higher k values at high amounts of NH_4NO_3 perhaps due to higher charges. The sorption of trivalent metal ions is greater than that of a divalent metal ions.

Prediction of separation possibilities

The batch equilibration data (Table I) suggest that Hg(II) has very low affinity for cation exchanger at various concentrations of NH_4NO_3 at 1.0 mol/dm³ CH_3COOH. Other metal ions have high K values and therefore, Hg(II) can be separated from those metal ions. 0.10 mol/dm³ NH_4NO_3—1.0 mol/dm³ CH_3COOH is the most suitable for the separation of Hg(II) from other metal ions since at higher NH_4NO_3 concentrations (1.0—1.5 mol/dm³), also other metal ions have low values making the separations impossible.

From 1.5 mol/dm³ NH_4NO_3—1.0 mol/dm³ CH_3COOH mixture La(III) and Ce(III), due to the high K values, can be separated from elements of very low K value. La(III) and Ce(III) are strongly held on resin column whereas other metal ions can be easily stripped off with a 1.5 mol/dm³ NH_4NO_3—1.0 mol/dm³ CH_3COOH mixture. The separation of Hg(II) from other metal ions at lower NH_4NO_3 ($<$0.5 mol/dm³) concentrations and the separation of La(III) and Ce(III) from all other metal ions at higher (1.5 mol/dm³) concentration of NH_4NO_3, suggested the possibility of the following ternary separations: Hg(II)—Al(III), Ca(II), Co(II), Ni(II), Cu(II), Zn(II), Sr(II), Cd(II), Ba(II),

Pb(II) and Bi(III)—La(III) and Ce(III). The feed containing Hg(II) and La(III) or Ce(III) and one of the other metal ions may be prepared in 0.10 mol/dm^3 NH_4NO_3—1.0 mol/dm^3 CH_3COOH mixtures. The effluent is collected from the start of the sorption step since Hg(II) has a very low K value and some Hg(II) may pass through with the feed effluent. Hg(II) may be quantitatively eluted with a 0.10 mol/dm^3 NH_4NO_3—1.0 mol/dm^3 CH_3COOH mixture. Secondly not so strongly held metal ions may be stripped off with 1.5 mol/dm^3 NH_4NO_3—1.0 mol/dm^3 CH_3COOH mixture and finally the most strongly sorbed La(III) and Ce(III) can be desorbed with any other eluants for e.g. mineral acids, HCl or HNO_3.

Columnar separations

(A) *Binary separations*

(i) Hg(II) *from all other metal ions*

Metal ions to be separated are loaded onto the resin column from 0.1 mol/dm^3 NH_4NO_3—1.0 mol/dm^3 CH_3COOH mixture. Hg(II) followed the feed effluent and was quantitatively eluted with about 80 cm^3 (this also includes 25 cm^3 of feed effluent) of 0.10 mol/dm^3 NH_4NO_3—1.0 mol/dm^3 CH_3COOH mixture. Ca(II), Sr(II), Ba(II), Co(II), Ni(II), Cu(II), Zn(II), Cd(II), Pb(II), Al(III), Bi(III), La(III) and Ce(III) remained on the resin bed and were subsequently stripped off with 2.5 mol/dm^3 HNO_3. The elution behaviour of these metal ions are reported in Table II. The separation of Hg(II) from Cd(II) and Pb(II) are shown in Fig. 1. The results of these separations along with standard deviations are presented in Table III.

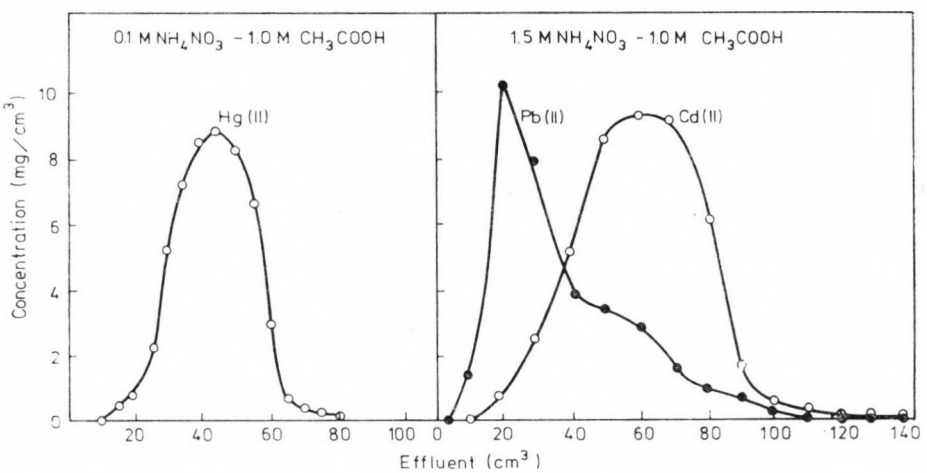

Fig. 1. Elution curves for Hg(II) — Cd(II)/Pb(II)

Tsble II

Elution characteristics of metal ions on Dowex 50W-X8 *columns*

Metal ion	BTV (cm^3)	VEP (cm^3)	TEV (cm^3)	Eluting agent
Al(III)	5	35	65	1.5 mol/dm^3 NH_4NO_3— 1.0 mol/dm^3 CH_3COOH
Ca(II)	2.5	25	70	1.5 mol/dm^3 NH_4NO_3— 1.0 mol/dm^3 CH_3COOH
Co(II)	5	20	90	1.5 mol/dm^3 NH_4NO_3— 1.0 mol/dm^3 CH_3COOH
Ni(II)	5	55	95	1.5 mol/dm^3 NH_4NO_3— 1.0 mol/dm_3 CH_3COOH
Cu(II)	5	30	100	1.5 mol/dm^3 NH_4NO_3— 1.0 mol/dm_3 CH_3COOH
Zn(II)	5	30	80	1.5 mol/dm^3 NH_4NO_3— 1.0 mol/dm^3 CH_3COOH
Sr(II)	5	25	95	1.5 mol/dm^3 NH_4NO_3— 1.0 mol/dm^3 CH_3COOH
Cd(II)	10	60	140	1.5 mol/dm^3 NH_4NO_3— 1.0 mol/dm^3 CH_3COOH
Ba(II)	10	40	110	1.5 mol/dm^3 NH_4NO_3— 1.0 mol/dm^3 CH_3COOH
La(III)	>150	—	—	1.5 mol/dm^3 NH_4NO_3— 1.0 mol/dm^3 CH_3COOH
Pb(II)	5	20	110	1.5 mol/dm^3 NH_4NO_3— 1.0 mol/dm^3 CH_3COOH
Bi(III)	10	30	100	1.5 mol/dm^3 NH_4NO_3— 1.0 mol/dm^3 CH_3COOH
Ce(III)	>200	—	—	1.5 mol/dm^3 NH_4NO_3— 1.0 mol/dm^3 CH_3COOH
Hg(II)	10	45	80	0.10 mol/dm^3 NH_4NO_3— 1.0 mol/dm^3 CH_3COOH

BTV = Break Through Volume
VEP = Volume Elution Peak
TEV = Terminal Elution Volume

Table III

Results of the separation of binary mixtures of Hg(II)

Metal ion	Mean amount taken/mg	n	Mean amount found/mg	Standard deviation/mg
Firts component ion:				
Hg(II)	102.75	30	103.50	0.40
Second component ion:				
Al(III)	11.65	4	11.68	0.05
Ca(II)	20.03	4	20.10	0.08
Co(II)	28.75	4	28.72	0.04
Ni(II)	31.90	4	31.95	0.05
Cu(II)	33.70	6	33.65	0.06
Zn(II)	37.05	6	37.22	0.12
Sr(II)	44.22	4	44.12	0.10
Cd(II)	47.60	6	47.50	0.12
Ba(II)	62.35	6	62.00	0.16
La(III)	59.59	4	59.65	0.04
Pb(II)	67.98	6	68.10	0.08
Bi(III)	75.00	6	74.50	0.25

n = Number of determinations

(ii) La(III) *and* Ce(III) *from other metal ions*

The feed was prepared in 1.5 mol/dm³ NH_4NO_3—1.0 mol/dm³ CH_3COOH by mixing La(III) or Ce(III) and one of the other cations to be separated and passed through the column. The weakly sorbed metal ions, Al(III), Co(II), Ni(II), Cu(II), Cd(II), Ca(II), Sr(II), Ba(II), Pb(II) and Bi(III) were collected quantitatively by using a 1.5 mol/dm³ NH_4NO_3—1.0 mol/dm³ CH_3COOH mixture as eluant (Table II). The strongly sorbed La(III) and Ce(III) were stripped off with about 80 cm³ and 120 cm³ of 2.5 mol/dm³ HNO_3, respectively. The results of these separations and the corresponding standard deviations are presented in Table IV.

Table IV

Results of the separation of binary mixtures of La(III)/Ce(III)

Metal ion	Mean amount taken/mg	*n*	Mean amount found/mg	Standard deviation/mg
First component ion:				
Al(III)	11.60	4	11.64	0.03
Co(II)	28.00	4	28.10	0.05
Ni(II)	32.00	4	31.90	0.08
Cu(II)	33.65	8	33.75	0.06
Zn(II)	37.00	6	36.90	0.07
Pb(II)	68.00	8	68.15	0.09
Bi(III)	75.00	6	75.70	0.30
Second component ion:				
La(III)	60.00	20	60.25	0.15
Ce(III)	65.75	20	65.20	0.24

n = Number of determinations

Table V

Results of the separation of various ternary mixtures

Metal ion	Mean amount taken/mg	*n*	Mean amount found/mg	Standard deviation/mg
First component ion:				
Hg(II)	102.00	18	101.00	0.30
Second component ion:				
Al(III)	11.00	4	10.95	0.02
Co(II)	20.00	4	20.10	0.04
Ni(II)	35.00	4	34.85	0.05
Cu(II)	33.70	6	33.80	0.04
Zn(II)	37.00	6	37.08	0.03
Pb(II)	67.50	6	67.70	0.15
Bi(III)	75.00	6	74.80	0.12
Third component ion:				
La(III)	50.05	14	50.25	0.14
Ce(III)	60.00	18	60.30	0.16

n = Number of determinations

(B) *Ternary separations*

Separation of Hg(II) from Al(III), Ca(II), Co(II), Ni(II), Cu(II), Zn(II), Sr(II), Cd(II), Ba(II), Pb(II) or Bi(III) from La(III) or Ce(III).

For the resolution of ternary mixtures the height of the resin bed was increased from approximately 8 cm to approximately 10 cm, and the flow of the feed and eluants through the column was decreased below 1.0 cm^3/minute. Three metal ions to be separated were loaded onto the pretreated resin bed from a 0.10 mol/dm^3 NH_4NO_3—1.0 mol/dm^3 CH_3COOH mixture. First, Hg(II) was recovered with about 80 cm^3 of a 0.10 mol/dm^3—1.0 mol/dm^3 CH_3COOH eluant, secondly Al(III), Ca(II), Co(II), Ni(II), Cu(II), Zn(II), Sr(II), Cd(II), Ba(II), Pb(II) or Bi(III) were desorbed quantitatively with a 1.5 mol/dm^3 NH_4NO_3—1.0 mol/dm^3 CH_3COOH eluant (Table II). This was followed by the elution of La(III) or Ce(III) with about 80 cm^3 and 120 cm^3 of 2.5 mol/dm^3 HNO_3, respectively. The separation of Hg(II)—Zn(II)—Ce(III) are shown in Fig. 2, and the results of the separations are presented in Table V.

Thus, the separation of alkaline earth metals are not possible in a 0.1—1.5 mol/dm^3 NH_4NO_3—1.0 mol/dm^3 CH_3COOH mixture whereas they can be easily separated in aqueous ammonium acetate medium [19]. The separations of La(III) and Ce(III) from other elements are not possible in aqueous as well as acidic NH_4OAc, while they can be separated from other metal ions in 0.10—1.5 mol/dm^3 NH_4NO_3—1.0 mol/dm^3 CH_3COOH media. Hg(II) can be separated from other metal ions in 0.10—1.5 mol/dm^3 NH_4NO_3—1.0 mol/dm^3 CH_3COOH media as well as in aqueous and also in acidic NH_4OAc media. All the separations achieved in NH_4NO_3—CH_3COOH media are quantitative and column kinetics too was observed to be favourable.

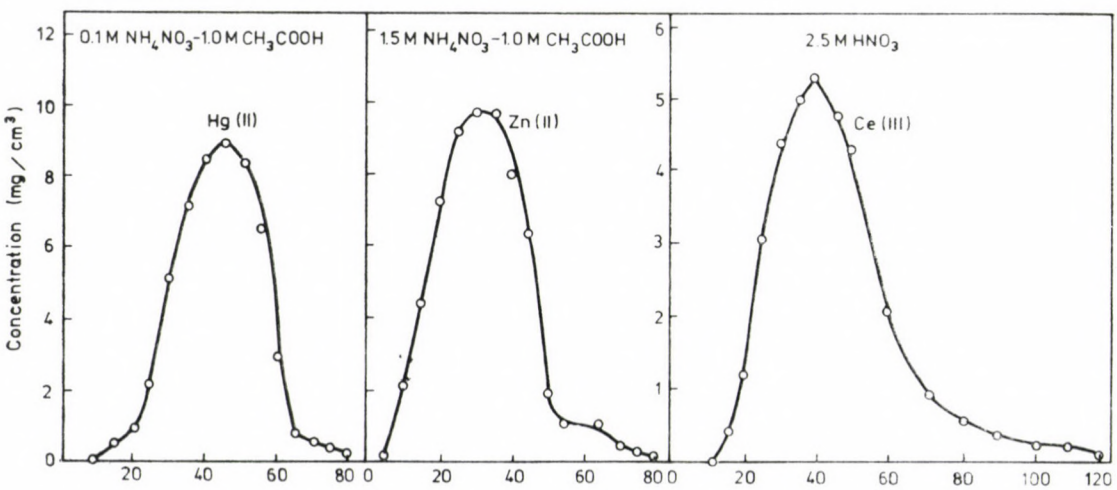

Fig. 2. Elution curves for Hg(II) — Zn(II) — Ce(III)

Experimental

Materials

Ion-exchange resin

Strongly acidic cation exchanger Dowex 50W-X8 (100—200 mesh size) in H^+-form was used. The capacity and water content were 3.22 meq/g and ~25%, respectively.

Metal ion solution

Standard 0.10 mol/dm^3 stock solutions of Ca(II), Sr(II), Ba(II), Co(II), Ni(II), Cu(II), Zn(II), Cd(II), Hg(II), Pb(II) and 0.06 mol/dm^3 stock solution of Al(III), La(III) and Ce(III) were prepared from their BDH (AnalaR) or E. Merck (GR) nitrate samples.

Ammonium nitrate

Aqueous 2.0 mol/dm^3 stock solution of NH_4NO_3 (E. Merck, G.R.) was used.

Acetic acid

5.0 mol/dm^3 stock solution of acetic acid was employed.

Wash solution

(a) 0.10 mol/dm^3 NH_4NO_3—1.0 mol/dm^3 CH_3COOH mixture.
(b) 1.5 mol/dm^3 NH_4NO_3—1.0 mol/dm^3 CH_3COOH mixture.

Eluting agent

(a) 0.10 mol/dm^3 NH_4NO_3—1.0 mol/dm^3 CH_3COOH mixture.
(b) 1.50 mol/dm^3 NH_3NO_3—1.0 mol/dm^3 CH_3COOH mixture.
(c) 2.5 mol/dm^3 HNO_3.

Procedure

Distribution studies

The batch equilibration method was employed for the determination of the distribution coefficients (K) of metal ions. 1 g of air dried resin was added to the solution containing metal ion, ammonium nitrate and acetic acid of desired amounts. All metal ions were examined separately at varying amounts, 0.1—1.5 mol/dm^3, of ammonium nitrate at fixed 1.0 mol/dm^3 concentration of acetic acid. In each case the overall volume was kept 25 cm^3 and ratio of total amount of metal ion to resin capacity ~0.30. The solutions were shaken for 1 h mechanically by a wrist motion microid shaker (Griffin and George). After shaking, the solutions were filtered and the metal content was determined in the solution phase complexometrically. The K values are reported in Table I. The experimental error is approximately ±5%.

Column chromatography

The following procedure was adopted for column chromatographic separations of metal ions.

Preparation and pretreatment of resin column

A slurry of approximately 5 g of fully water swollen cation exchanger Dowex 50W-X8 (H^+-form, 100—200 mesh) was transferred into a graduated ion-exchange column. The height of the resin bed was approximately 8 cm. It was rinsed several times with deionised water. Finally, the column was washed in small portions with about 50 cm^3 of 0.1/1.5 mol/dm^3 NH_4NO_3—1.0 mol/dm^3 CH_3COOH mixtures washing solutions.

Preparation of feed and sorption

The feed was prepared in duplicate by mixing known amounts of metal ions to be separated. The overall volume of the feed was kept 25 cm^3 and the concentration of NH_4NO_3 and CH_3COOH at 0.10 and 1.0 mol/dm^3, respectively. This feed was passed through the column at a flow rate of approximately 1.0 ± 0.3 cm^3/minute.

Chromatographic separations

The most weakly held metal ions were first recovered with 0.10 mol/dm^3 NH_4NO_3—1.0 mol/dm^3 CH_3COOH mixture eluant. The strongly sorbed metal ions were then stripped off with suitable concentration of NH_4NO_3—1.0 mol/dm^3 CH_3COOH mixtures eluants or with any other appropriate eluant as described in each separation.

REFERENCES

[1] Tomkins, E. R., Khym, J. X., Cohn, W. E.: J. Am. Chem. Soc., **69,** 2769 (1947)
[2] Strelow, F. W. E., Vanzyl, C. R., Nolte, C. R.: Anal. Chim. Acta, **40,** 145 (1968)
[3] Tsubota, H.: Bull. Chem. Soc. (Japan), **33,** 770 (1960)
[4] Hantabal, E., Fojtik, M., Rusek, V., Trnovec, T.: Chem. Zvesti, **18,** 203 (1964)
[5] Milton, G. M., Grammit, W. E.: Canad. J. Chem., **35,** 541 (1957)
[6] Lerner, M., Rieman, W.: Anal. Chem., **26,** 610 (1954)
[7] Carpenter, J. H.: Limnol. Oceanography, **2,** 271 (1957)
[8] Strelow, F. W. E., Weinert, C. H. S. W.: Talanta, **17,** 1 (1970)
[9] Qureshi, M., Zehra, N., Nabi, S. A.: Anal. Chem., **282,** 136 (1976)
[10] Abe, M.: J. Chromatogr., **134,** 507 (1977)
[11] Coetzee, C. J., Rohwer, E. F. C. H.: Anal. Chim. Acta, **44,** 293 (1969)
[12] Gangadharam, E. V., Reddy, G. R.: Radiochim. Acta, **11,** 90 (1969)
[13] George, D. R., Riley, J. M., Ross, J. R.: Chem. Eng. Progr., **54,** 96 (1968)
[14] Streckumaran, C., Pillai, K. C., Folsom, T. R.: Geochim. Cosmochim. Acta, **32,** 1229 (1968)
[15] Vol'khim, V. V., Kolesova, S. I., Koshcheeva, A., Zatonskaya, T. P.: Anal. Abstr., **17,** 49 (1969)
[16] Jenkins, I. L., Lidington, D. E., Wain, A. G.: J. Appl. Chem. (London), **19,** 213 (1969)
[17] Abe, M.: Bull. Chem. Soc. (Japan), **42,** 2683 (1969)
[18] Malik, W. V., Srivastava, S. K., Singh, R. P., Kumar, S.: J. Radioanal. Chem., **36,** 469 (1977)
[19] Honda, M.: Japan Analyst, **3,** 132 (1954)

Acta Chimica Hungarica 119 (4), pp. 305—320 (1985)

ULTRAVIOLET AND INFRARED STUDY OF 9-ARYLHYDRAZONO- AND 9-ARYLAMINO-METHYLENE-6,7,8,9-TETRAHYDROPYRIDO-PYRIMIDINE DERIVATIVES

Gábor HORVÁTH[1], Tibor BREINING[1], István HERMECZ[1], Ágnes HORVÁTH[1], Marianna PONGOR-CSÁKVÁRI[1], Benjámin PODÁNYI[1], Árpád István KISS[2]* and Antal MARTIN[2]

([1]CHINOIN Pharmaceutical and Chemical Works, Ltd., H-1325 Budapest, P.O.B. 110 and [2]Department of Physical Chemistry, Technical University, H-1521 Budapest, Budafoki út 8.)

Received May 10, 1984
Accepted for publication August 21, 1984

The structure of 9-arylhydrazono- and 9-arylaminomethylene-6,7,8,9-tetrahydro-4*H*-pyrido[1,2-*a*]pyrimidin-4-one derivatives was investigated by means of UV and IR spectra. The tautomerism and *Z*—*E* isomerism of the compounds, the effect of the solvents and substituents on the UV spectra, the skeletal stretching vibrations and the presence or absence of the frequency coupling of carbonyl groups were investigated.

Introduction

9-Substituted 6,7,8,9-tetrahydro-4*H*-pyrido[1,2-*a*]pyrimidin-4-ones are important compounds because of their pharmacological effects and therapeutical use [1—8]. This paper gives an account on the investigation of UV and IR spectroscopic features of some tetrahydropyridopyrimidin-4-ones having a side chain connected by double bond in position 9 (**11**—**21**, **26**—**28** and **33**—**56**) and some piperidine ring homologous derivatives (**22**—**25** and **29**—**32**). The compounds investigated are collected in Table I. In our previous papers [9—12] the structures of 9-aminomethylene- and 9-hydrazono-6,7,8,9-tetrahydropyridopyrimidin-4-ones were investigated in detail by means of NMR spectroscopy.

Compound **12** [9-(carboxymethylene)tetrahydropyridopyrimidine-3-carboxylate] is the intermediate of the product CHINOIN-123 [1, 2], which has antiaetherogenic effect. The enantiomer of compound **19** [9-(phenylhydrazono)-tetrahydropyridopyrimidine-3-carboxylic acid] having 6-*S* absolute configuration was investigated in more detail [5] because of its antiallergic-antiasthmatic effect [6]. Compounds **34** [9-(4-hydroxyphenylhydrazono)tetrahydropyridopyrimidine-3-carboxylic acid], also having pharmacological activity, is the main metabolite of **19** [6].

* To whom correspondence should be addressed

Table I

Compounds investigated

Structure	No.	R_3	R_6	R_9
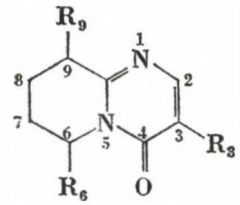 **1-15**	**1**	H	H	H
	2	Me	H	H
	3	H	Me	H
	4	Ph	H	H
	5	Ph	Me	H
	6	COOEt	H	H
	7	COOEt	Me	H
	8	COOEt	Me	Me
	9	COOH	H	H
	10	COOH	Me	H
	11	COOEt	H	=CH—COOH
	12	COOEt	Me	=CH—COOH
	13	COOEt	H	$=CH-N(CH_3)_2$
	14	COOEt	Me	$=CH-N(CH_3)_2$
	15	COOH	Me	$=CH-N(CH_3)_2$

Structure	No.	R_3	R_6	R_{12}	n
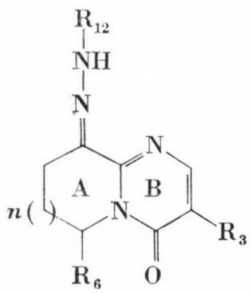 **16-25**	**16**	H	Me	Ph	1
	17	COOEt	H	Ph	1
	18	COOEt	Me	Ph	1
	19	COOH	Me	Ph	1
	20	COOH	Me	Me	1
	21	COOH	Me	COOEt	1
	22	COOEt	H	Ph	0
	23	COOEt	Me	Ph	0
	24	COOEt	H	Ph	2
	25	COOEt	H	Ph	3

Structure	No.	R_3	R_6	R_{12}	n
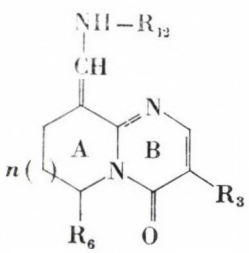 **26-32**	**26**	COOEt	H	Ph	1
	27	COOEt	Me	Ph	1
	28	COOH	Me	Ph	1
	29	COOEt	H	Ph	0
	30	COOEt	Me	Ph	0
	31	COOEt	H	Ph	2
	32	COOEt	H	Ph	3

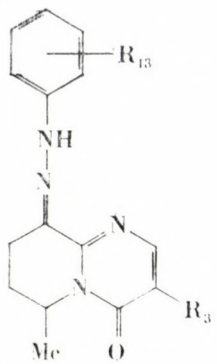

33-55

No.	R_3	R_{13}	No.	R_3	R_{13}
33	COOH	2-OH	**45**	COOH	4-NO_2
34	COOH	4-OH	**46**	COOH	2-CH_3
35	COOH	2-Cl	**47**	COOH	3-CH_3
36	COOH	3-Cl	**48**	COOH	4-CH_3
37	COOH	4-Cl	**49**	COOH	2-OEt
38	COOH	2-Br	**50**	COOH	3-OEt
39	COOH	3-Br	**51**	COOH	4-OEt
40	COOH	4-Br	**52**	COOH	2,6-diMe
41	COOH	2-COOH	**53**	COOH	2,6-diCl
42	COOH	4-COOH	**54**	COOEt	4-Cl
43	COOH	2-NO_2	**55**	COOEt	4-Br
44	COOH	3-NO_2			

Results and Discussion

Tautomerism

Four tautomeric forms of the 9-phenylhydrazono derivatives, characterized by structures *A*—*D* (Fig. 1), can be outlined. Further derivatives of compound **19** (**56**—**58**) were prepared [7, 8] in order to be able to choose the dominant tautomeric structure (Table II). The UV spectral data of the compounds, recorded in ethanol solution, are given in Table II. Based on the positions and intensities of the bands, the spectrum of compound **56** excludes the tautomer *C* to be the dominant form. The data of compound **57** exclude the tautomeric form *B*, and those of compound **58** exclude also the form *A*. On the basis of these facts the structure of the molecule seems to correspond to

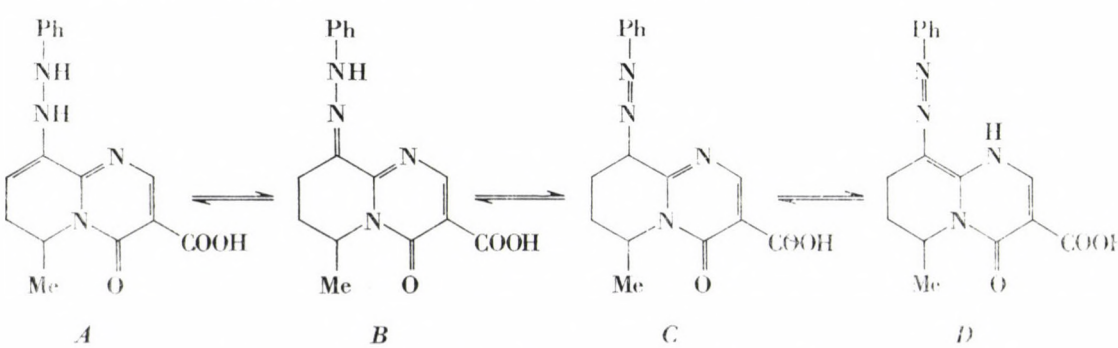

A *B* *C* *D*

Fig. 1. Tautomeric forms of 9-phenylhydrazono derivatives

Table II

UV spectral data of compounds **56**—**58** *and* **19** *in ethanol*

	Structure	λ_{max}	log ε	λ_{max}	log ε	λ_{max}	log ε	λ_{max}
56	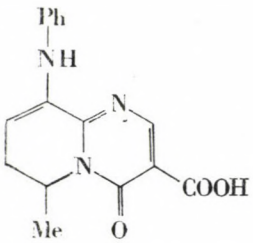	392	3.20	321	4.05	250	4.21	—
57	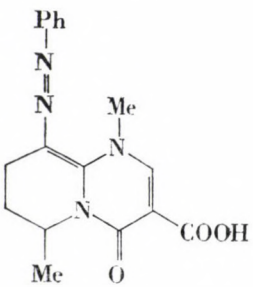	403	4.33	244	4.26	—		—
58	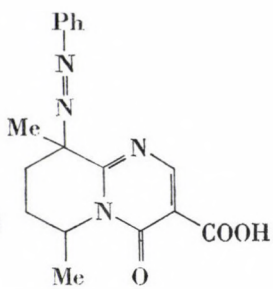	420	3.43	296 i		278	4.04	245 i 214 i
19	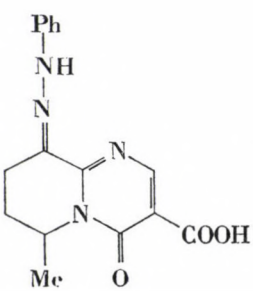	420	4.46	300	3.80	242	4.21	

i = inflexion

the tautomeric form *D*. This statement is in accordance with the results of X-ray diffraction [13], as well as with the ^{1}H, ^{13}C, ^{15}N-NMR spectra [9, 11, 12] measured in $CDCl_3$ and DMSO-d_6 solution and in the solid phase [10]. The tautomeric form *A* can be excluded because of the presence of the NH band appearing in the IR spectrum.

Isomerization

In protic and dipolar aprotic solvents the spectra of the compounds remain unchanged in time, but change does occur in aprotic solvents (Table II, Fig. 2) which can be explained by *Z*—*E* isomerization.

In the solid state the compounds are in the *E* form which was evidenced by IR, NMR [10] and X-ray diffraction [13] studies.

According to our investigations, also in protic and dipolar aprotic solvents, capable of forming hydrogen bonds, the sterically favourable *E* isomer occurs. In aprotic solvents the starting *E* form is transformed after dissolution to an equilibrium mixture of the *E* and *Z* forms. In the different derivatives the isomerization proceeds with different velocities and to different extents. In each case the *Z* isomer is predominating. This statement is in accordance with the results obtained by NMR investigations; namely, in chloroform the *Z* isomer, in dimethyl sulfoxide the *E* isomer is predominant [9, 12]. The *Z*—*E* equilibrium depends on the structure of the molecule and the substituents of the skeleton.

Table III

UV *spectra for the investigation of isomerization*

Comp. No.	λ_{max} (nm)			
	chloroform			DMSO
	a	b	*t* (min)	
16	391*	402	54	383
17	426*	436	2	405
18	430*	436	4	409
19	430*	454	15	418
22	390	398	5760	397
23	392	403	5700	400
24	374*	374	12	384
26	403*	417	60	414
27	408	417	240	414
28	410	424	240	422
29	390	400	345	402
30	388	399	210	404
31	393	399	200	409
32	392	422	90	410

a = measured instantly
b = measured after equilibrium
* = cannot be measured accurately
t(min) = time needed for equilibrium

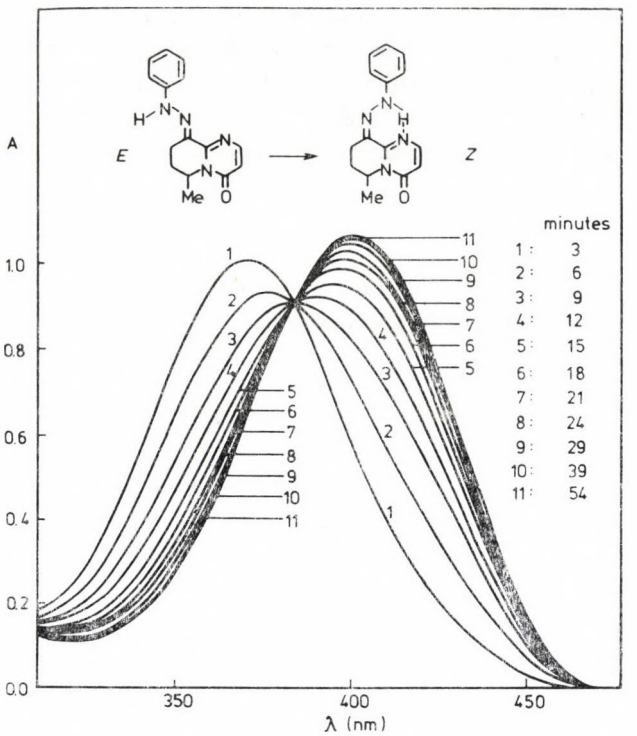

Fig 2. UV spectrum of compound **16** as a function of time

The formation of the *Z* isomer gives rise to further red shift of the π-electronic transition energies, in addition, to the negative solvent effect in aprotic solvents, because the intramolecular hydrogen bond loosens the π-electron system. The formation of the *Z* isomer can be detected in the IR spectrum, too. The narrow, medium intensity ν_{N-H} band of isomer *E* can be found between 3360 and 3240 cm^{-1}, measured in KBr disk. In chloroform the N—H band is shifted to lower frequencies and a broad band appears at about 3000 cm^{-1} which can be explained by the formation of intramolecular hydrogen bond and by the presence of the *Z* isomer.

Solvent effect

The π-electronic transitions in the spectra of tetrahydropyridopyrimidines dissolved in polar solvents are shifted to shorter wavelengths. For example, in the spectrum of compound **7** dissolved in water, this shift is 8 nm compared to the spectrum measured in cyclohexane solution (Table IV). This negative solvent effect can be interpreted by the strongly polarized ground state of these molecules.

Table IV

UV spectra for the investigation of solvent effect

Solvents	λ_{max} (nm)		
	7	**18**	**19**
Dist. water	300	406	388
Methanol	303	410	408
Ethanol	303	412	419
1-Propanol	305	—	414
2-Propanol	304	416	424
Acetonitrile	307	—	413
Nitromethane	307	410	416
Dimethylformamide	308	406	418
Dimethyl sulfoxide	308	409	418
Chloroform	307	436 430*	454 430*
Dioxane	308	424	447
Tetrachloroethane	308	—	454
Carbon tetrachloride	308	428	451
Cyclohexane	308	431	—

* Measured instantly after dissolution.

The solvent effect is substantially stronger in the spectra of the 9-substituted derivatives (Table IV). In aprotic solvents a $Z-E$ isomerism can occur and the red shift, due to this isomerism, strongly interferences with the investigation of the solvent effect. The shift caused purely by the solvent can be studied by means of the spectrum measured immediately after dissolution, because at this time mainly the E isomer is present in the solution. For example, the shift measured in chloroform is 11 nm for compound **19** and 18 nm for **18** compared with the spectra measured in ethanol. When the isomerization is completed, shifts of 35 nm and 23 nm can be observed.

Further information can be obtained for the solvent effect from the spectrum of the 9-phenylhydrazono-8-methyl derivative (**59**) because, in consequence of steric reasons, this compound exists only in the Z form (Fig. 3), which is also evidenced by NMR investigations [12]. The band shift is 15 nm in this case. Based on these observations, the band shift for the ethanol-chloroform solvent change is 10—15 nm in the spectrum of the 9-phenylhydrazono derivatives.

Band assignments in ultraviolet spectra

The spectra of compounds **1—10** were used for the assignment of the electronic transitions of the compounds investigated. Compounds **1—10** have absorption bands near 300, 230 and 200 nm, which can be assigned to $\pi-\pi^*$ transitions on the basis of their high intensity [14]. These transitions belong

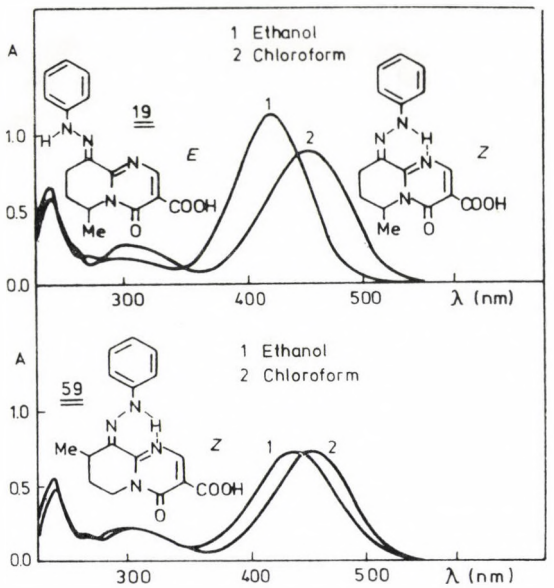

Fig. 3. **UV spectra of compounds 19 and 59**

Table V

UC *spectral data of the compounds investigated*

No.	λ_{max}	log ε	λ_{max}	log ε	λ_{max}	log ε	λ_{max}	log ε
1			278	3.67			229	3.76
2			276	3.75			229	3.71
3			278	3.68			226	3.78
4			301	4.00			244	3.74
5			302	4.01			244	3.75
6			301	3.96			230	3.80
7			303	3.92			230	3.81
8			304	3.90			230	3.67
10			300	3.90			230	3.80
11			341	4.03			251	4.14
12			339	4.00			253	4.11
13	397	4.70	299	3.41	275	3.52	231	4.10
14	397	4.71	300	3.45	276	3.55	232	4.14
15	398	4.69	303	3.38	274	3.50	233	4.07
16	383	4.40	290	3.64			238	4.25
17	412	4.49	290	3.69			240	4.27
18	412	4.43	290	3.49			240	4.19
19	420	4.46	300	3.80			242	4.21
20	384	4.51	300	3.61			227	4.04
21	340	4.22	280	3.96			210	4.10
26	413	4.71	295	3.75			243	4.22
27	412	4.67	300	3.69			243	4.18
28	414	4.72	300	3.70			244	4.22

to the conjugated part of the ring system. The band near 200 nm is not given in Table V, because of measuring difficulties. The bands near 300 nm in the spectra of compounds **16**—**25** and **26**—**32** can be found at nearly the same position as in case of compounds **1**—**10**, but a new band appears at about 410 nm which can be assigned to the conjugated system comprising the double bond substituent in position 9. The bands of the π-electron transitions belonging to the substituted benzene derivative attached to the side chain 9 are overlapped by the bands of the ring system.

Substituent effect

The effect of substituents on the tetrahydropyridopyrimidine ring are shown in Table V. The effect of the methyl groups in position 6 is insignificant (see, for example, compounds **1** and **3**). The spectrum hardly changes if the 3-substituent is a donor group (compound **2**) but a significant red shift, amounting to 23, 25 nm, respectively, occurs if the 3-substituent is an acceptor, as in compounds **6** and **7** [14].

The 9-methyl group (compound **8**) practically does not change the first band of the spectrum. In case of substituents, bound to position 9 by double bond, a red shift can be found in the spectrum (e.g. this red shift is 40 nm in the spectrum of compound **11**).

The positions of the lowest energy transitions of compounds **13**—**16**, **18**—**20**, **27** and **28** originate from the extensive conjugation, presuming that the two chromophore groups are situated nearly in the same plane. The 340 nm band of compound **21** can be interpreted by the effect of the amide group decreasing the conjugation.

The effect of the substituents bound to the phenyl group may be seen in Table VI. The long wavelength absorption maxima appear in the region 392—448 nm. It can be seen that strong donor and acceptor groups have nearly the same effect on the spectra, and generally the *ortho* substituents give rise to greater red shifts. From this irregular behaviour the conclusion can be drawn that the substituents influence the equilibrium of the $Z-E$ isomers, too.

This assumption is also supported by the NMR investigations because the equilibrium of the *ortho* substituted compounds is shifted towards the Z isomers. For example, the ratio of the $Z-E$ isomers is 76 : 24 in the case of the *ortho*-methyl derivative (**46**) and it is 11 : 89 for the *para* compound (**48**) [12].

The significant shifts of the bands associated with the substituents OH and COOH calls attention to various inter- and intramolecular H-bonded systems.

2,6-Disubstitution always causes a strong blue shift, which can be interpreted by turning the benzene ring out of the molecular plane.

Table VI

The effect of substituents in the phenyl ring of **19** *on the long wavelength bands*
Solvent: ethanol

R	Position of R substituent					
	ortho		*meta*		*para*	
	No.	λ_{max}	No.	λ_{max}	No.	λ_{max}
OH	**33**	392	—	—	**34**	440
Cl	**35**	414	**36**	412	**37**	420
Br	**38**	428	**39**	406	**40**	418
COOH	**41**	430	—	—	**42**	408
NO_2	**43**	432	**44**	400	**45**	414
CH_3	**46**	435	**47**	424	**48**	432
OEt	**49**	448	**50**	426	**51**	432
H	**19**			420		
2,6-diMe	**52**			392		
2,6-diCl	**53**			379		

The effect of change in the number of ring atoms

Table VII shows that in case of ring "A" homologues, conjugation is the most favourable in the six-membered rings. A change in the number of the members of ring "A" causes a 10 and 11 nm blue shift in the spectra of five-membered homologuous compounds (**22**, **29**), 22 and 5 nm in the spectra of seven-membered homologuous compounds (**24**, **31**) and only 5 nm in the spectrum of the eight-membered phenylaminomethylene homologue (**32**) but a very significant blue shift can be observed in the spectrum of the phenylhydrazono homologue (**25**). For the explanation of this conspicuous change we assumed that the plane of the exo double bond connected to C_9 in case of the most favourable *twisted* conformation of the eight-membered ring is turned out of the plane of the pyridone ring to such an extent that conjugation between the two chromophoric groups is completely hindered.

The spectrum of compound **25** can be assigned to two chromophoric groups. One of them is tetrahydropyridopyrimidine, the maxima of which are at 302 and 230 nm, in agreement with the spectrum of compound **6** Table V. The other chromophoric group, to which the maximum at 279 nm can be assigned, is the phenylhydrazone [15].

In the spectrum of the phenylaminomethylene derivative (**32**) this change does not occur; this can be explained by the fact that, according to experience, the C=N double bond is more localized than that of C=C [16]. Thus the 9—9a bond in the phenylaminomethylene derivative becomes shorter because of the delocalization, and the condition for conjugation is assured in consequence of the planarity.

Table VII

The effect of the change in number of ring atoms on the UV spectra

	λ_{max} (nm) log ε						
	$n = 0$ pyrrolo				$n = 1$ pyrido		
22	402 (4.56)	290 (3.70)	242 (4.28)	**17**	412 (4.49)	290 (3.69)	240 (4.27)
29	402 (4.68)	289 (3.72)	240 (4.14)	**26**	413 (4.71)	295 (3.75)	243 (4.22)
	$n = 2$ azepino				$n = 3$ azocino		
24	390 (4.32)	270 (3.93)	241 (4.12)	**25**	302 (2.24)	279 (4.31)	230i
31	408 (4.62)	280 (3.85)	250 (4.13)	**32**	408 (4.39)	272 (4.15)	255 (4.12)

This conclusion is in good accordance with the NMR experiments, namely, the large chemical shift of the NH proton observed in the deuterochloroform ^{1}H-NMR spectrum of the *Z* isomer of **32** indicates a H-bonded structure, but the similar signal of the *Z* isomer of **25** does not correspond to the planar H-bonded structure [10].

Infrared spectroscopic investigations

The group frequencies of the substituents appear at the expected wavenumbers. The stretching vibrations of carbonyl groups are exceptions; that will be discussed later.

Four stretching vibrations can be considered characteristic of the tetrahydropyridopyrimidinone skeleton. The wavenumbers of the unsubstituted skeleton (**1**) are 1600, 1580, 1522 and 1475 cm^{-1}. In the spectrum of compound **16** the first two frequencies are unchanged and the latter two are higher by 8 and 15 cm^{-1}, respectively, compared with the unsubstituted skeleton. The skeletal vibrations of the phenyl substituent (8a, 8b, 19a) overlap the former signals. Varying the number of carbon atoms in ring A and the substituents in the ring system, the frequencies of the four skeletal vibrations change as follows: the first band 1600 cm^{-1} can be found between 1595—1612 cm^{-1}, the second between 1564—1588 cm^{-1}, the third between 1505—1556 cm^{-1} and the fourth between 1450—1492 cm^{-1}. Accordingly, the change in the frequency of the first two bands is not significant, but the positions of the two other vibrations change considerably. However, these changes are not unambiguously connected either with the change of the number of carbon

atoms in ring A, or with the inductive and mesomeric effects of the substituents, though the change of the number of members in ring A greatly modifies the geometry (planarity) of the molecule, and thus a characteristic change of the skeletal vibrations would be expected.

In the following, the carbonyl stretching vibrations will be discussed in more detail.

The positions of the *carbonyl bands* depend on the substituents. The strong band of $C_4=O$ appears at 1670 cm^{-1} if there is no substituents in position 3. If there is an ethoxycarbonyl group having carbonyl bonds of *O,O-cis* conformation in position 3, a frequency coupling can occur between the carbonyl groups [17] (Fig. 4).

According to our investigations, frequency coupling can be observed in the spectra of some pyridopyrimidine derivatives [18] which produces the *symmetrical* vibration to appear as a strong band near 1750 cm^{-1} and the *asymmetrical* one as a medium intensity band at about 1670 cm^{-1}. The frequency coupling ceases under the influence of heating or solvation.

Among the derivatives substituted in position 9 only the compounds **18**α refers to the crystal structure and **54** have spectra showing frequency coupling (Table VIII). This is proved not only by the characteristic group of bands, but also by the changes which take place under the influence of heating or solvation, shown on the spectrum of compound **54** (Table IX): under the influence of heating or solvation the $C_3-C=O$ carbonyl group turns to *O,O-trans* orientation (Fig. 4) and the strong bands of the two carbonyl groups appear separately. At temperature 513 K the band of the ethoxycarbonyl group can be found at 1745 cm^{-1} and that of $C_4=O$ at 1710 cm^{-1}. The same is observed in chloroform at room temperature.

On the basis of the UV spectra [14] it can be stated that the π-electron system is strongly delocalized, and this demonstrates the planarity of the molecule as well as the strong interaction of the CO group. With a large number of compounds (for example **18**β, **24**, **25**, **27**, **31**, **32** and **55**) no frequency coupling can be observed in spite of the *O,O-cis* orientation of the two carbonyl groups. The proof of this fact can be demonstrated by the spectrum of compound **55** (Table IX). The *O,O-cis* orientation can be proved by the following

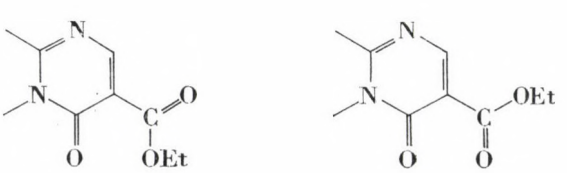

O,O-trans *O,O-cis*

Fig. 4. O,O-cis and *O,O-trans* conformations of the 3-ethoxycarbonyl group

Table VIII

Characteristic bands of IR *spectra measured in* KBr *disc*

No.	νC_3—C=O (cm^{-1})	νC_4=O (cm^{-1})		νC—C ** (cm^{-1})		
1	—	1670ie	1600gy	1580gy	1522e	1475k
3	—	1670ie	—	1588gy	1525ie	1470gy
9	1742ie	1640ie	—	1580k	1530ie	1465k
6	1748ie	1676k *	—	1582k	1522ie	1480k
7	1750ie	1680k	1615gy	1585k	1520ie	1450k
16	—	1670ie	1600gy	1580k	1530ke	1490e
18α	1745ie	1670k *	1595gy	1580k	1550ke	1465e
18β	1694ie		1600gy	1575k	1552gy	1463e
54	1745ie	1670k *	1596k	1576ke	1553ke	1485ie
55	1695ie		1595gy	1577ke	1556ke	1492ie
22	1695e	1672e	1605k	1575i	1515ie	1490i
24	1684e		1603gy	1567k	1510i	1485ie
25	1687e		1603gy	1568ke	1505ie	1475ie
19	1725ie	1622e	1612e	1570k	1532gy	1489e
27	1690e		1603gy	1575ke	1522i	1476ie
31	1688e		1603gy	1567k	1525i	1483ie
32	1686e		1603gy	1566ke	1520i	1475ie
28	1726e	1636e	1608k	1564e	1520i	1450ie

* = Frequency coupling
i = Inflexion gy = weak, k = medium, ke = medium-strong, e = strong, ie = very strong
** = 8a, 8b and 19a are vibrations of the phenyl group, as well as the skeletal stretching vibrations of the conjugated system including the B ring

observations: (1) The carbonyl band appears at 1695 cm^{-1}, and this can be interpreted by the conjugation of the ethoxycarbonyl group with the C_2=C_3 double bond. (2) Under the influence of heating and solvation the ethoxycarbonyl band shifts to 1745 and 1740 cm^{-1}, respectively, in consequence of turning to *O,O-trans* orientation accompanied by a decrease of conjugation *s-cis* orientation (3). The spectrum is similar to that of compound **54** measured in chloroform at 513 K. Compound **18**, having two polymorphic modifications, gives the explanation for the lack of frequency coupling. The polymorphic crystal structure can be proved by the following investigations: (1) The spectra of the two modifications measured in KBr disc are different (Table VIII), but they are fully identical in chloroform solution. (2) The **18**α modification is unstable, it changes into **18**β in a few days even at room temperature. (3) The X-ray diffraction powder diagrams of the two samples are different. There is a frequency coupling in the spectrum of the form α, but in case of

Table IX

The effect of heating and solvation on the IR *spectra of compounds* **54**—**55** *and* **19**

No.	Measuring conditions	K Temp.	cm^{-1} νC_3—C=O	cm^{-1} νC_4=O
	KBr	298	1745ie	1670k *
54	KBr	513	1745ie	1710e
	$CHCl_3$	298	1740ie	1705e
	KBr	298		1695ie
55	KBr	513	1745ie	1705e
	$CHCl_3$	298	1740ie	1710e
	KBr	298	1725ie	1622e
19	KBr	513		1680e
	DMSO	298		1680e

* Frequency coupling

β it is hindered by the different crystal lattice. The lack of frequency coupling in the spectra of compounds **27** and **55** can also be traced back to crystal structural reasons.

Intramolecular hydrogen bond is formed in derivatives having a carboxyl group in position 3 (**9**, **19**, **28**) (Fig. 5). This is evident from the fact that their frequencies are lower by 30—50 cm^{-1} (Table VIII) compared with the corresponding C_4=O frequencies of compounds having no substituents in position 3 [1, 3, 16]. The band of the C=O carboxyl group appears between 1742—1725 cm^{-1} because it is not involved in the hydrogen bond. Under the influence of heating or dissolving in dimethyl sulfoxide, the intramolecular hydrogen bond present in the solid state of **19** is cleaved, and intermolecular hydrogen

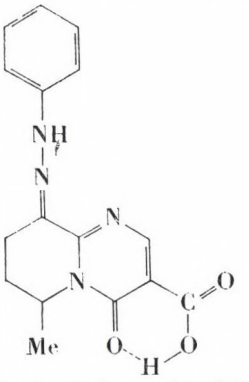

Fig. 5. Intramolecular hydrogen-bond in compound **19**

bonds are formed (Table IX). For this reason, the C=O band of the carboxyl group is shifted to 1680 cm^{-1} and the C_4=O band is also shifted to 1680 cm^{-1} due to the ceasing of the intramolecular hydrogen bond.

Experimental

The compounds investigated were prepared by methods published earlier [1, 2, 6, 7, 9, 12, 19—20]. Exceptions are compounds **1, 9** and **21** for which the way of preparation is shown in Scheme 1. The 9-carboxylic acid obtained by alkaline hydrolysis of ethyl-4-oxo-6,7,8,9-tetrahydro-4*H*-pyrido[1,2-*a*]pyrimidine-3-carboxylate [19] was decarboxylated with 85% phosphoric acid at 160 °C. The 9-ethoxycarbonylhydrazono-pyridopyrimidine **21** was obtained by the reaction of the 9-hydroxy-6,7-dihydropyrimidine derivative [8] and ethyl carbazate. The 9-aryl-tetrahydropyridopyrimidines (**19, 33—53**) were prepared from 6-methyl-4-oxo tetrahydropyridopyrimidine-3-carboxylic acid (**10**) [1] by azo-coupling with aryldiazonium chlorides in the presence of sodium acetate.

4-Oxo-6,7,8,9-tetrahydro-4*H*-pyrido[1,2-*a*]pyrimidine-3-carboxylic acid (9)

A solution of ethyl 4-oxo-6,7,8,9-tetrahydro-4*H*-pyrido[1,2-*a*]pyrimidine-3-carboxylate [1] 10 g; 40 mmol in 5% sodium hydroxide solution was stirred at ambient temperature for 2 h. After the filtration of the reaction mixture the pH of the filtrate was adjusted to 2 with 10% hydrochloric acid solution. The precipitated acid (6.2 g; 79.8%) was filtered off, washed with water and dried; m.p. 170—172 °C (decomp.) (from benzene).

Calcd. $C_9H_{10}N_2O_3$ (194.193). C 55.67; H 5.19; N 14.43. Found C 55.81; H 5.05; N 14.40%.

4-Oxo-6,7,8,9-tetrahydro-4*H*-pyrido[1,2-*a*]pyrimidine-4-one (1)

4-Oxo-6,7,8,9-tetrahydro-4*H*-pyrido[1,2-*a*]pyrimidine-3-carboxylic acid (10 g; 50 mmol) was heated in 85% phosphoric acid solution at 160—170 °C for 6 h. After the mixture had cooled it was poured onto crushed ice (50 g) and the pH of the aqueous reaction mixture was

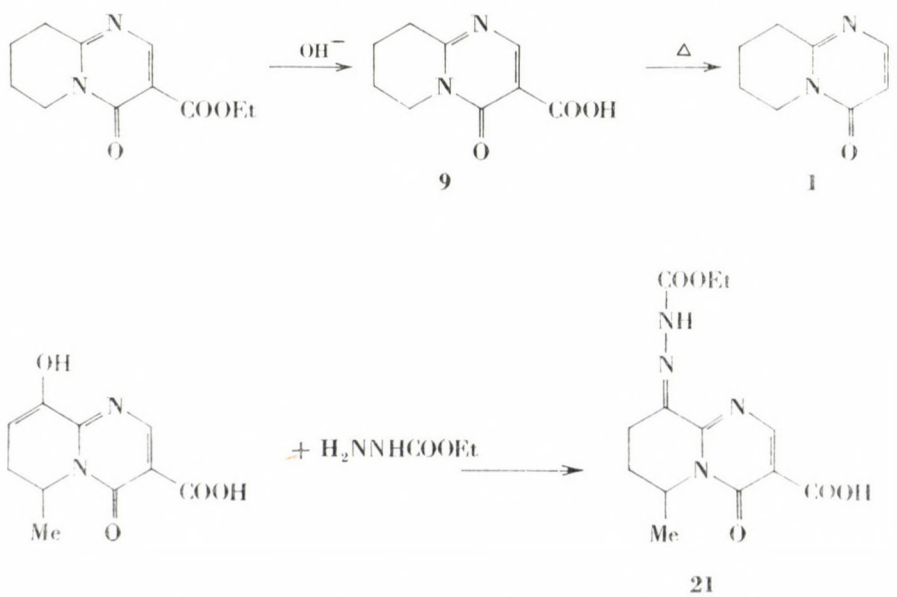

Scheme 1. Preparation of compounds **1, 9** and **21**

adjusted to 9 with 10% sodium hydroxide solution. The aqueous solution was extracted with chloroform (3×30 mL). The combined organic phase was dried (Na_2SO_4) and evaporated to dryness to obtain the pyridopyrimidine-4-one, 5.5 g, 73.2%, m.p. 85 °C (from diethyl ether).

Calcd. $C_8H_{10}N_2O$ (150.182). C 63.98; H 6.71; N 18.65. Found C 64.26; H 6.59; N 16.82%.

9-Ethoxycarbonylhydrazono-6-methyl-4-oxo-6,7,8,9-tetrahydro-4*H*-pyrido[1,2-*a*]pyrimidine-3-carboxylic acid (21)

9-Hydroxy-6-methyl-4-oxo-6,7-dihydro-4*H*-pyrido [1,2-*a*]pyrimidine-3-carboxylic acid [8] (1.0 g; 4.50 mmol) and ethyl carbazate (0.7 g; 6.75 mmol) were refluxed in ethanol (10 mL) for 1 h. The precipitate was then filtered off, and washed with ethanol. Yield: 1.2 g (86%), m.p. 246—248 °C.

Calcd. $C_{13}H_{16}N_4O_5$. C 50.65; H 5.23; N 18.17. Found C 50.41; H 5.62; N 18.17%.

The UV and IR spectra were recorded on UNICAM SP8-200 and ZEISS UR-20 spectrometers, respectively.

REFERENCES

[1] Mészáros, Z., Knoll, J., Szentmiklósi, P., Dávid, Á., Horváth, G., Hermecz, I.: Arzneim.-Forsch., **22,** 815 (1972)
[2] Hermecz, I., Mészáros, Z., Vasvári-Debreczy, L., Horváth, Á., Virág, S., Sipos, J.: Arzneim.-Forsch., **29,** 1833 (1979)
[3] Ecsedi, G. G., Virág, S., Hidvégi, E. J.: Atherosclerosis, **39,** 183 (1981)
[4] Bédi, J., Blaskó, G., Pálos, L. A.: Arzneim.-Forsch., **29,** 1405 (1979)
[5] De Vos, C., Dessy, F., Hermecz, I., Mészáros, Z., Breining, T.: Int. Arch. Allergy Appl. Immunol., **67,** 362 (1982)
[6] Hermecz, I., Breining, T., Mészáros, Z., Horváth, Á., Vasvári-Debreczy, L., Dessy, F., De Vos C., Rodrigues, L.: J. Med. Chem., **25,** 1140 (1982)
[7] Hermecz, I., Breining, T., Mészáros, Z., Kökösi, J., Mészáros, L., Dessy, F., De Vos, C.: J. Med. Chem., **26,** 1126 (1983)
[8] Hermecz, I., Breining, T., Vasvári-Debreczy, L., Horváth, Á., Mészáros, Z., Bitter, I., De Vos, C., Rodrigues, L.: J. Med. Chem. (In the press)
[9] Tóth, G., Szöllősy, Á., Podányi, B., Hermecz, I., Horváth, Á., Mészáros, Z., Bitter, I.: J. Chem. Soc., Perkin Trans. 2, **1983,** 165
[10] Tóth, G., Podányi, B., Hermecz, I., Horváth, Á., Horváth, G., Mészáros, Z.: J. Chem. Research (S), **1983,** 161; and (M), **1983,** 1721
[11] Tóth, G., Szöllősy, Á., Podányi, B., Hermecz, I., Horváth, Á., Mészáros, Z., Bitter, I.: J. Chem. Soc., Perkin Trans. 2 (In the press)
[12] Tóth, G., Szöllősy, Á., Almási, A., Podányi, B., Hermecz, I., Breining, T., Mészáros, Z.: Org. Magn. Reson., **21,** 687 (1983)
[13] Simon, K.: Private communication
[14] Horváth, G., Kiss, Á. I., Mészáros, Z., Hermecz, I.: Acta Chim. Acad. Sci. Hung., **83,** 15 (1974)
[15] Iffland, D. C., McAneny, M. P., Weber, D. J.: J. Chem. Soc., **1969,** 1703
[16] Simon, K., Mészáros, Z., Kálmán, A.: Cryst. Struct. Commun., **4,** 135 1975; Simon, K.: God. Jugosl. Cent. Kristalogr., **15,** 87 (1980)
[17] Bellamy, L. J., Conelly, B. R., Philpotts, A. R., Williams, R. L.: Z. Elektrochem., **64,** 563 (1960)
[18] Horváth, G., Pongor-Csákvári, M., Kiss, Á. I., Fogarasi, G., Pulay, P.: Tetrahedron, **33,** 2293 (1977)
[19] Náray-Szabó, G., Hermecz, I., Mészáros, Z.: J. Chem. Soc., Perkin Trans. 1, **1974,** 1753
[20] Horváth, Á., Hermecz, I., Vasvári-Debreczy, L., Simon, K., Pongor-Csákvári, M., Mészáros, Z.: J. Chem. Soc., Perkin Trans. 1, **1983,** 369

Acta Chimica Hungarica 119 (4), pp. 321—332 (1985)

IONIZATION PROPERTIES OF 6,7,8,9-TETRAHYDRO-4*H*-PYRIDO[1,2-*a*]PYRIMIDIN-4-ONE DERIVATIVES HAVING A CONJUGATED SIDE CHAIN IN POSITION 9

Antal MARTIN[1]*, Árpád István KISS[1], Gábor HORVÁTH[2] and István HERMECZ[2]

([1]Department of Physical Chemistry, Technical University, H-1521 Budapest, Budafoki út 8, and [2]CHINOIN Pharmaceutical and Chemical Works, Ltd., H-1325 Budapest, P.O.B. 110)

Received May 10, 1984
Accepted for publication August 6, 1984

The ionization of 6,7,8,9-tetrahydro-4*H*-pyrido[1,2-*a*]pyrimidin-4-one derivatives having a conjugated side chain in position 9 was investigated at different pH values by means of their ultraviolet spectra. PPP calculations were carried out for different ionized models and the correct structure was selected by comparing the calculated and experimental data.

Introduction

In our preceding paper [1] the structure of the derivatives, the tautomerism, the isomerization, as well as the solvent and substituent effects of 9-phenylhydrazono- and 9-phenylaminomethylene-6,7,8,9-tetrahydro-4*H*-pyrido[1,2-*a*]pyrimidin-4-one were investigated by means of their UV and IR spectra. This paper gives account on the results concerning the ionization properties of these compounds (**I**—**IV**).

The 3-ethoxycarbonyl-6-methyl derivative having a phenylhydrazono group in position 9 (**II**) has a characteristic ultraviolet spectrum which shows large pH dependence. The same feature can be observed in the spectra of derivatives having various electron-acceptor groups in position 3, as well as in case of derivatives variously substituted in the benzene ring of the 9-side chain. The π-electron system of the molecule is very sensitive to environmental effects and this is why the conjugation in acidic and basic solutions strongly differs from that existing in neutral media. This can be interpreted by assuming different ionic models but, making use of purely experimental spectroscopy, it was not possible to chose the correct one. If protonation occurs on the side chain in acid solution a strong red shift is expected on the basis of analogies, and this would explain the behaviour of the ultraviolet spectra observed

* To whom correspondence should be addressed

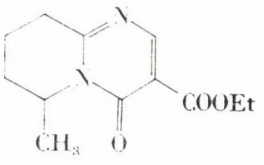

I

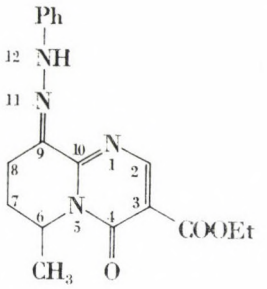

II

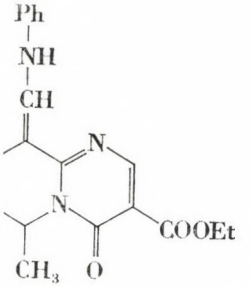

III

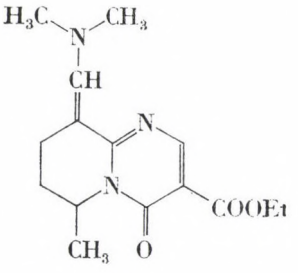

IV

in acidic solutions. At the same time the NMR spectra suggest the protonation of the nitrogen atom in position 1 [2]. Since this latter protonation also can cause a slight red shift and the UV spectrum does not preclude the possibility of this protonation either, selection of the correct model was tried via calculations. The calculations were carried out by means of a Pariser—Parr—Popole (PPP) type semiempirical quantumchemical method, thought to be one of the most successful treatments for calculating the spectra of conjugated π-electron systems. The ionization of the phenylamino-methylene and dimethylamino-methylene derivatives (**III**, IV) having similar conjugated chain in position 9 were investigated experimentally as well as theoretically to clarify the question.

Results

The compounds were dissolved in Britton—Robinson buffers of various pH. Aqueous solutions were used as reference. The pK_a values were calculated on the basis of the spectra measured as a function of pH.

The spectra were recorded on a Unicam-SP8-100 type visible-ultraviolet spectrometer under standard circumstances. The spectral data of compounds **I, II, III** and **IV** are given in Table I.

Table I

Spectroscopic data of compounds **I**, **II**, **III** *and* **IV**

Compound	Solvent	λ	log ε	λ	log ε	λ	log ε	λ	log ε	λ	log ε
	ethanol		—	303	3.92	—		230	3.81		
I	water		—	298	3.92	—		231	3.63		
$pK_a = 1.07$	1 *N* HCl		—	284	3.89	—		230	3.75		
	1 *N* NaOH		—	300	3.86	—		229	3.73		
	ethanol	412	4.43	290	3.49	—		240	4.19		
II	water	406	4.42	296	3.50	260i		241	4.20		
$pK_a = 3.0$	1 *N* HCl	425	4.40	299	3.58	261i		240	4.27		
	1 *N* NaOH	483	4.62	316i		268	4.07	242i			
	ethanol	412	4.67	300	3.69	—		243	4.18		
III	water	411	4.70	296	3.71	247i		238	4.20		
$pK_a = 3.1$	1 *N* HCl	399	4.68	282	3.54	—		238	4.22		
	1 *N* NaOH	411	4.68	296	3.67	—		238	4.18		
	ethanol	397	4.67	302i		276	3.48	235	4.06	208	3.95
IV	water	400	4.69	304i		270i		246	3.86	231	4.05
$pK_a = 4.0$	1 *N* HCl	375	4.60	—		262	3.28	228	4.27	—	
	1 *N* NaOH	394	4.64	—		268i		230	4.21	—	

λ values in nm, i = inflexion

The spectrum of compound **I** was used for the assignment of the electronic transitions of the compounds investigated. Compound **I** has absorption bands at about 300, 230 and 200 nm which can be assigned to $\pi-\pi^*$ transitions on the basis of their high intensity. These transitions can be related to the conjugated system of the molecule. The band near 200 nm is not given in Table I because of measuring difficulties.

In the spectrum of compound **II** the position of the band near 300 nm is similar to that found in compound **I**. A new band appears around 410 nm which can be assigned to the conjugated system including the double-bonded substituent in position 9. The bands of the local excitation of the substituent having a benzene ring are covered by the bands of the ring system of compound **I**. The spectrum of compound **II** is not affected essentially by the change of the substituents either in position 3 or in the benzene ring. The spectra of the substituted derivatives of the molecule have similar characteristics [3].

Compound **III** differs from compound **II** in the CH group in position 11. The spectrum of **III** consists of three strong $\pi-\pi^*$ bands (Table I) which, apart from a slight shift, correspond to those of **II**. This shift is due to the stronger conjugation of the C=C bond compared to that of the C=N bond.

In the spectrum of compound **IV** a blue shift can be observed (Table I) because of the less extended conjugation.

The spectral data of the neutral, basic and acidic forms of the compounds **I, II, III** and **IV** are given in Table I. As neutral reference the spectra of the ethanolic solutions were considered.

In alkaline solutions the first band of compound **II** shows a strong red shift and the intensity of the bands slightly increases. A simple explanation of these changes is the assumption of the cleavage of the carbonyl π-bond following the deprotonation and bond rearrangement of the molecule **II/1**. The negative charge formed on the carbonyl oxygen atom evokes a conjugated system with smaller excitation energy. This is well known in the case of the formation of phenolate ion. However, in compound **III** this rearrangement does not occur because its spectrum does not change essentially in alkaline solution compared to that in neutral media. The supposed molecular structure of compound **II** in alkaline solution mentioned above was justified by PPP calculation.

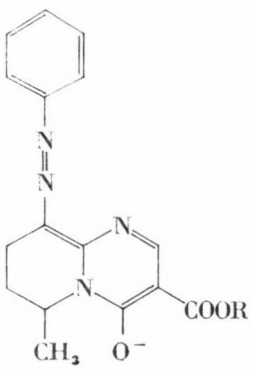

II/1

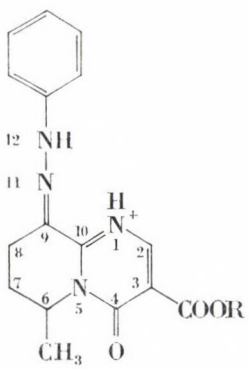

II/a

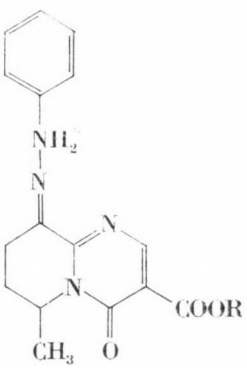

II/b

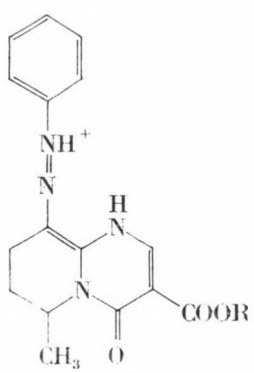

II/c

In acidic solution the bands of compound **II** are shifted to longer wavelengths, but this shift is smaller than that in alkaline media. On the other

hand, all bands of compound **III** show blue shifts compared to the neutral molecule. The intensities are practically unchanged in both cases. The change of the spectrum of compound **II** refers to the protonation of the molecule and the red shift means a more favourable conjugation. One of the probable sites of the protonation is the nitrogen atom in position 1 (*II*/**a**) or 12 (**II/b**). A further assumption may be a protonation of the nitrogen atom in position 11 which may be accompanied by sharing of the positive charge between the two nitrogen atoms 10 and 11. We have also considered the model protonated on nitrogen 1 and having a positive charge on nitrogen 12 (**II/c**). In acidie solution compound **III** is also protonated, but the blue shift refers to structural changes which differ from that of compound **II**. The cause of this difference may be the CH group instead of nitrogen 11. In this case the protonation can occur only on the nitrogen atom 1 or 12 and the right model was selected by PPP calculations. The transition energy of compound **IV** was also calculated for comparison.

Calculations

Only the π-electron part of the ring system was taken into consideration for the PPP calculations. The saturated pyridine ring was substituted by two methyl groups at the annelation points (Figs 1 and 2). The geometry of the molecule was based on the X-ray diffraction measurement of 3-ethoxycarbonyl-6-methyl-6,7,8,9-tetrahydro-4*H*-pyrido[1,2-*a*]pyrimidine-4-one [4]. The bond distances in the side chain 9 were taken from analogies (benzene, aniline, ethylene, hydrazine (r_{N-N}), dimethylglyoxime ($r_{C\equiv N}$) [5]); the bond angles were assumed 120° and the molecule was considered planar.

The atomic and bond parameters needed for the calculations were determined in the same manner as earlier [6]. Because of the numerous possibilities, the resonance integrals were not taken as variable parameters, but they were calculated using the formula given by Wolfsberg and Helmholz [7]. The overlap integrals were calculated according to Mulliken [8]. The resonance integrals of the C_9-CH_3 and N_5-CH_3 bonds were optimized for toluene and methylaniline, respectively. The one-centre repulsion integrals were calculated by the formula given by Pariser and Parr [9]; the method given by Mataga and Nishimoto [10] was applied for the calculation of the two-centre repulsion integrals.

The geometry of the molecule as well as the atomic and bond parameters are given in Fig. 1 (only the bond angles differing from 120° are included).

The geometry of the alkaline form of molecule **II** (**II/1**) was determined from the X-ray diffraction measurement [4] of 1-methyl-3-ethoxycarbonyl-6-methyl-6,7,8,9-tetrahydro-4*H*-pyrido[1,2-*a*]pyrimidine-4-one. As further data the N—C bond distances in side-chain 9 were taken 138 pm and the double

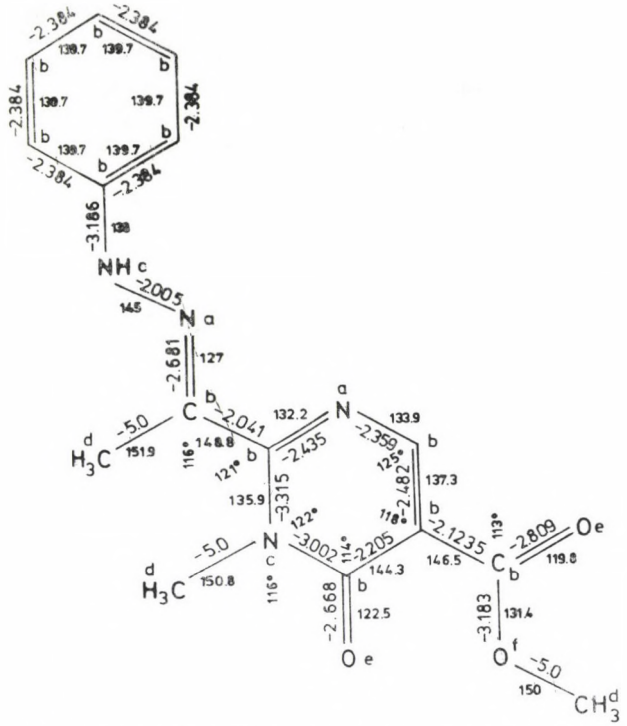

Fig. 1. Geometry and atomic- and bond parameters of molecule II

	I_v (eV)	A_v(eV)
a	14.12	1.78
b	11.16	0.03
c	25.73	8.97
d	29.0	19.0
e	17.70	2.47
f	30.07	10.83

bond distance was taken 124 pm. The C—O$^-$ bond distance is 125 pm on the basis of phenolate ion [13]. The C_3—C_4—N_5 bond angle was considered to be 117° and the C_2—C_3 bond distance to be 144.3 pm. Using these data, the lacking parameters can be calculated. The results are: the C_3—C_4 bond distance is 126.9 pm, the N_1—C_2—C_3 angle is 117.2° and the C_2—C_3—C_4 angle is 124.8°. In Fig. 2 are given the geometry, the resonance integrals determined by means of the overlap integrals calculated with this geometry, as well as the atomic parameters of the parts of the molecule which differ from those found in Fig. 1. The valence state ionization potential of the negatively charged oxygen atom is 24.28 eV and its electron affinity is 9.0 eV.

The structures of compound II assumed in acidic solution, except for model II/c, were calculated with the geometry identical with that of the neutral

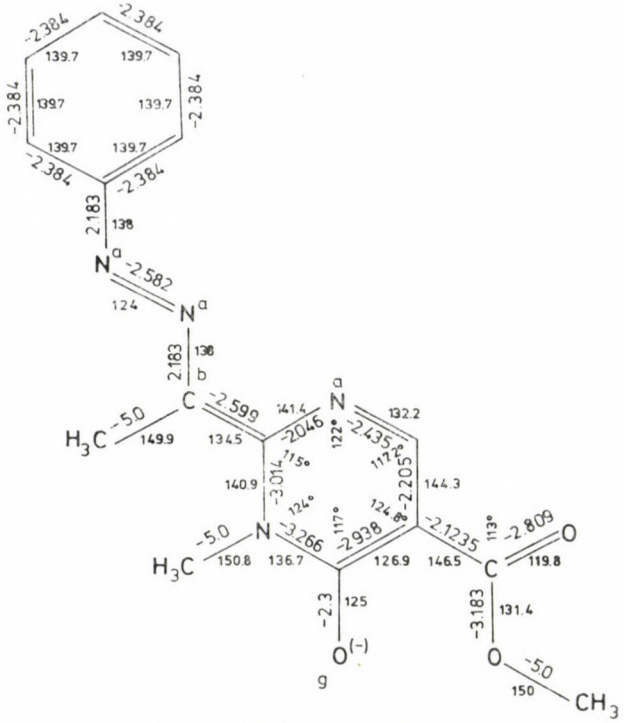

Fig. 2. Geometry and atomic- and bond parameters of the ionic form of molecule **II**

	I_v (eV)	A_v (eV)
a	14.12	1.78
b	11.16	0.03
c	24.28	9.0

form, and only the valence state ionization potential and electron affinity of the nitrogen atom at the assumed site of the protonation were modified. On the other hand, a bond rearrangement was assumed in case of the model **II/c**, and for this reason the corresponding parts of the geometry used for the calculation of the basic form were accepted. In this model the valence state ionization potentials and electron affinities were modified in positions 1 and 12. The bond parameters of these atoms also change because of the change of the ionization potential and orbital exponent. For the four supposed models the parameters differing from the neutral form are:

II/a: $I_{N_1} = 28.71$ eV, $A_{N_1} = 11.96$ eV, $q_1 = 1$ (q_1 being the number of π electrons), $\beta_{N_1-C_2} = -3.268$ eV, $\beta_{N_1-C_{10}} = -3.358$ eV.
II/b: $I_{N_{12}} = 33.304$ eV, $A_{N_{12}} = 14.139$ eV, $q_{12} = 0$, $\beta_{N_{11}-N_{12}} = -2.379$ eV, $\beta_{N_{12}-C_{13}} = -3.358$ eV.

II/c: $I_{N_1} = 25.73$ eV, $A_{N_1} = 8.97$ eV, $q_1 = 2$, $I_{N_{12}} = 28.71$ eV, $A_{N_{12}} = 11.96$ eV, $q_{12} = 1$, $\beta_{N_1-C_2} = -3.443$ eV, $\beta_{N_1-C_{10}} = -2.985$ eV, $\beta_{N_{11}-N_{12}} = -3.481$ eV, $\beta_{N_{12}-C_{13}} = -3.011$ eV.

II/d: In the delocalized charge model the charge of both nitrogen atoms were taken as $q = 0.5$. Using the method by Karlsson and Martensson [11], we established a quadratic formula by fitting a parabola through four points. The valence state ionization potentials and electron affinities were calculated using these following formulas:

For trigonal orientation: $I_v = 20.336 - 6.600\,q + 0.429\,q^2$

$$A_v = 5.638 - 4.354\,q + 0.475\,q^2$$

For tetragonal orientation: $I_v = 20.365 - 6.604\,q + 0.432\,q^2$

$$A_v = 8.372 - 4.711\,q + 0.474\,q^2$$

Assuming trigonal N_{11} atom, these quantities for $q = 0.5$ are: $I_v = 17.144$ eV and $A_v = 3.580$ eV and for tetragonal N_{12} atom they are: $I_v = 17.171$ eV and $A_v = 6.135$ eV. The nitrogen atoms 11 and 12 were thus distinguished according to their original orientation. Interpolated orbital exponents were used for the calculation of the corresponding resonance integrals and the obtained values are: $\beta_{C_9-N_{11}} = -2.825$ eV, $\beta_{N_{11}-N_{12}} = -1.721$ eV and $\beta_{N_{12}-C_{13}} = -2.288$ eV.

In the neutral molecule **III** the bond distances and bond parameters belonging to atom 11 (differing from that of molecule **II**) are as follows: $r_{C_9-C_{11}} = 134$ pm, $r_{C_{11}-N_{12}} = 138$ pm and $\beta_{C_9-C_{11}} = -2.621$ eV, $\beta_{C_{11}-N_{12}} = -3.186$ eV.

For the acidic form three assumed protonated models of molecule **III** were investigated. For these models the parameters differing from those of the neutral form, are:

(a) For the model protonated on nitrogen 1 the parameters of atom 1 are the same as those of the corresponding model of molecule **II** (**II/a**).

(b) For the model protonated on nitrogen 12 only the resonance integrals differ from that of the acidic form of molecule **II** (**II/b**): $\beta_{C_{11}-N_{12}} = \beta_{N_{12}-C_{13}} = -3.358$ eV.

(c) For the model protonated on nitrogen 1 and positively charged on nitrogen 12 the geometry of **II/c** was used and the further different parameter were taken by the analogy of this model, too: $I_{N_1} = 25.73$ eV, $A_{N_1} = 8.97$ eV, $q_1 = 2$, $I_{N_{12}} = 28.71$ eV, $A_{N_{12}} = 11.96$ eV, $q_{12} = 1$, $\beta_{C_9-C_{11}} = -2.453$ eV, $\beta_{C_{11}-N_{12}} = -2.831$ eV, $\beta_{N_{12}-C_{13}} = -3.011$ eV.

The calculation parameters for molecule **IV** were taken as for the former models.

Discussion

The calculated and experimental spectral data of the molecules investigated are collected in Table II. For the sake of comparability, the intensities of the experimental spectra were converted into oscillator strengths with the approximate formula $f = \varepsilon/k$ where $k = 41\ 700$ cm if ε is given in $dm^3 \cdot mol^{-1} \cdot cm^{-1}$ unit [12].

The calculated energies of the first two bands of the neutral compound **II** are in satisfactory agreement with the corresponding experimental values. On the basis of their intensities, the next two calculated bands can be considered forbidden, thus the calculated results seem to justify the applicability of the parameters used.

The energies calculated for the basic model of the molecule **II** correctly reproduce the experimental red shifts. The first two calculated bands can be assigned to the first experimental band, thus the agreement seems to be satisfactory. For this reason the ionic model assumed for the interpretation of the red shift observed in basic solution can be regarded as verified.

In order to interpret the observed behaviour of molecule **II** in acidic solution, we tried to select the right model from among the four supposed models by means of comparison of the calculated and experimental spectra. Only the first band of the spectrum calculated for the model (**a**) (protonation on nitrogen 1) has lower energy than the corresponding band calculated for the neutral molecule. The calculated second and thid bands can be assigned to the second calculated band of the neutral molecule, but the energies of these two bands are higher than the energy of the corresponding calculated band of the neutral molecule. For this reason this model can not be considered acceptable. Because the bands calculated for the model (**c**) have also higher energies, this model has to be rejected, too. In case of the model (**d**) the calculated energy of the first band is extremely low, thus this model was also rejected. The results obtained with model (**b**) (protonation on nitrogen 12) can be considered the most acceptable. If the calculated second and fourth transitions are regarded as forbidden, the corresponding transition energies are lower, in accordance with the experimental band shifts. By reason of these results we can conclude that in acidic solution the molecule **II** is protonated on nitrogen 12.

Contrary to the compound **II**, in the spectrum of the molecule **III** a blue shift is observed in acidic solutions. The spectra of the possible protonated forms of compound **III** were also calculated for the interpretation of this different feature; also, the similarly protonated forms of compound **IV** were calculated in order to obtain further informations.

The first band of the calculated spectrum of compound **III**, protonated in position 12 [(**b**) model] gives an extremely large red shift thus in this case

Table II

Experimental and calculated spectral data of ionized and non-ionized forms of compounds **II**, **III** *and* **IV**

Compound	Solution (model)	Calculated		Experimental	
		E (eV)	*f*	*E* (eV)	*f*
II	neutral (ethanolic)	3.203	0.845	3.009	0.645
		3.965	0.176	4.275	0.074
		4.222	0.065		
		4.679	0.007		
		4.801	0.116	5.166	0.371
		5.086	0.507		
	basic	2.598	0.606	2.567	1.000
		2.694	0.920		
	pH > 13	4.222	0.003	3.923	i
		4.329	0.239	4.626	0.282
		4.802	0.153	5.123	i
	acidic (**b**)	3.001	0.536	2.917	0.602
		3.189	0.041		
	pH = 0—2	3.470	0.267	4.146	0.091
		4.143	0.002		
		4.489	0.124	4.750	i
		4.621	0.003		
		4.932	0.211	5.166	0.447
	acidic (**a**)	3.039	0.877		
		4.206	0.186		
		4.247	0.083		
		4.415	0.008		
		4.846	0.204		
	acidic (**c**)	3.378	1.179		
		4.158	0.065		
		4.638	0.140		
		4.679	0.073		
		4.882	0.029		
		5.381	0.318		
	acidic (**d**)	2.359	0.230		
		3.260	0.001		
		4.118	0.335		
		4.277	0.029		
		4.421	0.063		
III	neutral (ethanolic)	3.297	1.204	3.009	1.122
		4.112	0.037	4.133	0.117
		4.126	0.134		
		4.666	0.165		
		4.887	0.407	5.102	0.363
	basic			3.017	1.148
				4.189	0.112
				5.209	0.363

Table II continued

Compound	Solution (model)	Calculated		Experimental	
		E (eV)	*f*	*E* (eV)	*f*
	acidic (**c**)	3.546	1.207	3.107	1.148
		4.228	0.007	4.396	0.083
	pH = 0—2	4.681	0.218	5.209	0.398
		4.744	0.073		
		5.231	0.045		
		5.442	0.291		
	acidic (**a**)	3.224	1.249		
		4.178	0.035		
		4.505	0.251		
		4.695	0.326		
		4.760	0.004		
		5.603	0.177		
	acidic (**b**)	2.709	0.078		
		3.085	1.023		
		4.345	0.021		
		4.519	0.136		
		4.651	0.128		
IV	neutral	3.257	1.112	3.123	1.122
	(ethanolic)	3.720	0.001	4.105	i
		4.459	0.121	4.492	0.072
		5.094	0.346	5.276	0.275
		5.382	0.149	5.961	0.214
	acidic (**a**)	3.300	1.000	3.306	0.955
		4.112	0.221		
		4.867	0.267	4.732	0.046
		5.240	0.007	5.438	0.447
	acidic (**b**)	2.518	0.056		
		3.033	1.082		
		4.383	0.134		
		4.631	0.092		
		5.379	0.394		

the protonation position 12 can be excluded. The calculation for the model (**a**) protonation on nitrogen 1 results in a blue shift for all but the first bands, if the calculated second and fifth bands are considered forbidden. The blue shift is in accordance with the experiment, however, this model cannot be considered satisfactory either because of the calculated red shift of the first band. At last, all band energies calculated for the model (c) protonated on nitrogen 1 and positively charged on nitrogen 12 show blue shifts. This is in complete accordance with the experiments. By reason of this results, we believe that the protonation of compound **III** takes place on nitrogen 1, as supposed in model (**c**).

Table III

Calculated atomic net π-charges

Numbering of atoms	Compound	
	II	III
1	−0.302	−0.337
11	−0.325	−0.085
12	+0.338	+0.378

The spectrum of compound **III** dissolved in alkaline solution differs from that of the neutral form only insignificantly. For this reason, the structure of the alkaline form is the same as that of the neutral one.

The (**b**) form of compound **IV** (protonated on nitrogen 12) can be rejected for the same reasons as in the case of **III**. Here the (**a**) form (protonated on nitrogen 1) is the most probable model according to the calculations.

Summing up it can be stated that the site of the protonation in acidic solutions for 9-phenyl-hydrazono type compounds (**II**) is the 12-nitrogen atom, whereas the 9-phenylamino type compounds (**III**) are protonated on nitrogen 1. This feature can be explained by the more positive character of the 11 carbon atom compared with that of the corresponding nitrogen atom of the hydrazono group. Table III proves this more positive character in which the net π charges calculated for models giving the best calculated spectral data are given. This positive character makes more difficult the protonation of nitrogen 12 and the protonation of nitrogen 1 having a more negative character is preferred. Accordingly, the calculations of the ground state charge distribution confirm our conclusions concerning the calculated spectra.

REFERENCES

[1] Horváth, G., Breining, T., Hermecz, I., Horváth, Á., Pongor-Csákvári, M., Podányi, B., Kiss, Á. I., Martin, A.: Acta Chim. Hung. (preceding paper)
[2] Tóth, G., Szöllősy, Á., Podányi, B., Hermetz, I., Horváth, Á., Mészáros, Z., Bitter, I.: J. Chem. Soc. Perkin Trans. 2, **1983**, 1409
[3] Pongor-Csákvári, M.: Ph. D. Thesis, Chinoin Pharmaceutical and Chemical Works Ltd. Budapest, Hungary 1981
[4] Sasvári, K., Csonka-Horvai, J., Simon, K.: Acta Crystallogr., **28B**, 2405 (1972)
[5] Sutton, L. E.: Tables of Interatomic Distances, Spec. Publ. No. 11, Chem. Soc., London 1958
[6] Kiss, Á. I., Szőke, J.: Acta Chim. (Budapest), **74**, 59 (1972)
[7] Wolfsberg, M., Helmholz, L.: J. Chem. Phys., **20**, 837 (1952)
[8] Mulliken, R. S., Rieke, C. A., Orloff, D., Orloff, H.: J. Chem. Phys., **17**, 1248 (1949)
[9] Pariser, R., Parr, R. G.: J. Chem. Phys., **21**, 568 (1953)
[10] Mataga, N., Nishimoto, K.: Z. Phys. Chem. N. F., **13**, 140 (1957)
[11] Karlsson, G., Martensson, O.: Theoret. Chim. Acta, **13**, 195 (1969)
[12] Allinger, N. L., Stuart, T. W., Tai, J. C.: J. Am. Chem. Soc., **90**, 2819 (1968)
[13] Kiss, Á. I., Martin, A., Horváth, G., Schawartz, J.: Tetrahedron, **39**, 3201 (1983)

Acta Chimica Hungarica 119 (4), pp. 333—338 (1985)

DIOXOURANIUM(VI) COMPLEXES OF TERDENTATE 16-MEMBERED MACROCYCLIC LIGANDS

Hardeo Singh YADAV, Soumitra Kumar SENGUPTA and Satish Chandra TRIPATHI*

(Department of Chemistry, University of Gorakhpur, Gorakhpur-273001, U.P., India)

Received February 3, 1984
In revised form June 4, 1984
Accepted for publication August 15, 1984

The reactions of dioxouranium(VI) complex of 2,6-diacetylpyridine bis-(semicarbazone) (DAPSC) with β-diketones, viz., acetylacetone, benzoylacetone, dibenzoyl methane and thenoyltrifluoroacetone have been studied. The reaction products, seven-coordinate dioxouranium(VI) complexes of the type $[UO_2(L)(NO_3)_2]$ (where L = macrocyclic ligand derived from 2,6-diacetylpyridine bis-(semicarbazone) (DAPSC) and a β-diketone) have been characterized on the basis of elemental analysis, electrical conductance and spectral (infrared and electronic) data. DAPSC acts as neutral, terdentate ligand having coordination sites at pyridine nitrogen and two azomethine nitrogens.

Introduction

2,6-Diacetylpyridine is a versatile chelating agent, having two reactive carbonyl groups capable of undergoing Schiff base condensation with a variety of di- and polyamines. The use of metals as templates in such reactions has led to the synthesis of a large number of metal complexes of macrocyclic ligands [1, 2]. Although a large number of Schiff base derivatives of uranyl cation are reported [3—6] but only two papers have appeared on the synthesis of its macrocyclic complexes [7, 8].

This paper reports the synthesis and characterization of dioxouranium (VI) complex of a high denticity ligand 2,6-diacetylpyridine bis(semicarbazone) (DAPSC) and its reactions with β-diketones which lead to the formation of macrocyclic systems.

Experimental

All the solvents and chemicals used were reagent grade B.D.H. products. The ligand 2,6-diacetylpyridine bis-(semicarbazone) (DAPSC) was prepared using the literature method [9] and recrystallised from a benzene-ethanol mixture.

The details of the analytical procedures and physical measurements are the same as described earlier [10]. Uranium was estimated by standard gravimetric procedure as its oxide [11].

* To whom correspondence should be addressed

Preparation of dioxouranium(VI) complex of DAPSC

Uranyl nitrate (0.02 mol) dissolved in a minimum quantity of ethanol was added to a refluxing solution of the ligand (0.02 mol) dissolved in a mixture of benzene and ethanol (1 : 1). The mixture was refluxed for 6 h when the colour of the solution became light green. The solvent was removed under vacuum at room temperature and the light brown coloured product was obtained. The complex was isolated by crystallising the product from tetrahydrofuran. Yield 52%.

Reactions of dioxouranium(VI) — DAPSC complex with β-diketones

A general procedure was adopted as follows. To uranyl nitrate (0.02 mol) in ethanol (20 mL), DAPSC (0.02 mol) dissolved in a mixture of benzene and ethanol (1 : 1, 20 mL) was added. To the yellow solution, an ethanolic solution of a β-diketone (0.02 mol in 10 mL) was added. The mixture was refluxed for 30 min when it became turbid. Then glacial acetic acid (5 mL) was added to the mixture which was refluxed for about 10 h; the colour of the solution intensified. The mixture was then cooled and allowed to stand for a few days. The dark crystals were separated out which were thoroughly washed with dichloromethane and crystallised from a mixture of tetrahydrofuran-hexane. Yield ~50—60%.

Results and Discussion

The uranyl(VI) complex of 2,6-diacetylpyridine bis-(semicarbazone) (DAPSC), has been synthesized by refluxing the equimolar solutions of uranyl nitrate with DAPSC dissolved in a mixture of benzene and ethanol.

$$UO_2(NO_3)_2 \cdot 6\,H_2O + \text{DAPSC} \xrightarrow[\text{ethanol}]{\text{benzene}} [UO_2(\text{DAPSC})\,(NO_3)_2]$$

The elemental analysis (Table I) of this complex shows 1 : 1 metal to ligand stoichiometry. The complex is soluble in all common organic solvents. The electrical conductance in methanol indicates non-electrolytic nature of the complex. The infrared and electronic spectral studies (discussed in the following section) suggest the following structure for the uranyl complex of DAPSC.

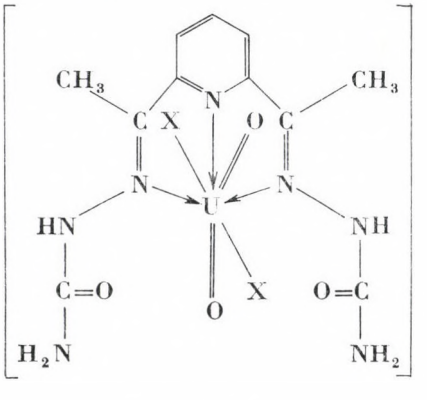

$X = NO_3^-$

It is obvious from the above structure that each terminal amino group contains a pair of unshared electrons. Accordingly, this complex may participate in nucleophilic condensation reactions with ketones. Therefore, the reactions of DAPSC complex of uranyl cation with β-diketones have been studied which causes the ring closure and formation of cyclic structures. Table I shows that the macrocyclic complexes can be formulated as $[UO_2(L)(NO_3)_2]$ where L = macrocyclic ligands derived from 2,6-diacetylpyridine bis-(semicarbazone) and different β-diketones. These complexes are soluble in dimethylformamide, dimethylsulfoxide and nitrobenzene. The complexes are non-electrolytes in dimethylformamide.

The following general structure is proposed for cyclic products on the basis of spectral studies:

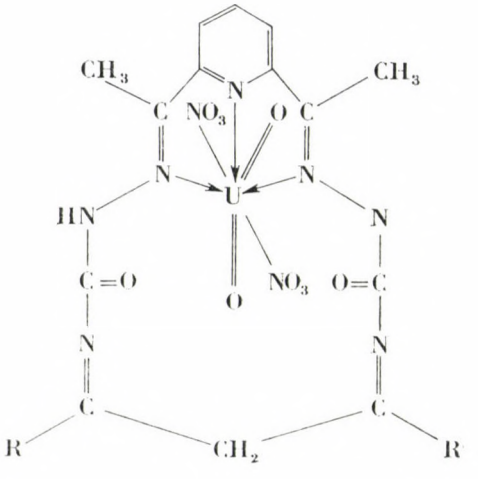

where

R	R'	β-diketone
CH_3	CH_3	acetylacetone
C_6H_5	CH_3	benzoylacetone
C_4H_3S	CF_3	thenoyltrifluoroacetone
C_6H_5	C_6H_5	dibenzoyl methane

Electronic spectra

The electronic spectra of all uranyl complexes in nitrobenzene show three bands at 21000—21500, 25000—25800 and 30000 cm^{-1}. The electronic spectra of the uranyl complexes resemble the spectra of other uranyl complexes involving entirely different types of ligands [6]. It has been found that the ligation has a minor influence on the spectrum, and the electronic structure

Table I

Physical and analytical data of the complexes

Complex	Colour	Decomp. temp. (°C)	Found (Calcd.) %		
			C	H	U
$[UO_2(DAPSC)(NO_3)_2]$	light brown	78	19.5 (19.6)	2.2 (2.2)	35.3 (35.4)
$[UO_2(mac^1)(NO_3)_2]$	yellowish brown	80	26.0 (26.1)	2.48 (2.58)	32.2 (32.3)
$[UO_2(mac^2)(NO_3)_2]$	light orange	82	31.6 (31.6)	2.6 (2.6)	29.8 (29.8)
$[UO_2(mac^3)(NO_3)_2]$	orange	85	36.1 (36.3)	2.4 (2.6)	27.4 (27.7)
$[UO_2(mac^4)(NO_3)_2]$	red	92	27.4 (27.6)	1.9 (1.9)	28.7 (28.8)

where mac^1 = macrocyclic ligand derived from acetylacetone
mac^2 = macrocyclic ligand derived from benzoylacetone
mac^3 = macrocyclic ligand derived from dibenzoylmethane
mac^4 = macrocyclic ligand derived from thenoyltrifluoroacetone

of the complexes is mainly dependent on the triatomic (O=U=O) entity [12]. The bands occurring in the 21000—21500 and 25000—25800 cm^{-1} regions are essentially vibration bands [13]. The higher energy band at 30000 cm^{-1} also appears in the ligand DAPSC and may be assigned to $n \rightarrow \pi^*$ or $\pi \rightarrow \pi^*$ transition in the azomethine (>C=N) group.

Infrared spectra

The i.r. spectrum of the ligand DAPSC has been reported earlier [9]. The ligand shows bands due to pyridine ring, amino groups, azomethine groups and ketonic groups. The infrared spectrum shows one strong band at 1680 cm^{-1} assignable to ν(C=O). In all uranyl complexes, this band persists at the same position indicating the non-coordination of the ketonic group.

The pyridine ring vibrations occurring [14, 15] at 1580 (8a, pyridine ring deformation), 610 (6a, in-plane ring deformation) and 400 cm^{-1} (16b, out-of-plane ring deformation) in DAPSC appear around 1600, 630 and 420 cm^{-1} in the uranyl complexes. The upward shifts in these frequencies indicate the coordination of pyridine nitrogen to the metal atom [16].

The ligand DAPSC also shows a weak band at ca. 1630 cm^{-1} which can be assigned to the ν(C=N) vibration of azomethine linkage [17]. The appearance of a weak ν(C=N) band is in accordance with the observations of several other workers [17, 18]. In the uranyl complexes, this band shifts to lower frequency (ca. 20—30 cm^{-1}) suggesting that the nitrogen atoms of the

Table II

Important infrared spectral bands (cm^{-1})

Complex	νNH	νC=N	Pyridine ring vibrations			ν(O=U=O)	ν(U=N)
$[UO_2(DAPSC)(NO_3)_2]$	3280sb, 3300sh, 3250sh	1610w	1600s	630s	420m	920s 880s	380m
$[UO_2(mac^1)(NO_3)_2]$	3200m	1640w 1610w	1590s	620s	420m	900s 880s	350w
$[UO_2(mac^2)(NO_3)_2]$	3200m	1640w 1600w	1590s	630s	400m	920s 860s	360w
$[UO_2(mac^3)(NO_3)_2]$	3180m	1640w 1610w	1600s	620s	420m	910s 875s	380w
$[UO_2(mac^4)(NO_3)_2]$	3200m	1640w 1600w	1590s	630s	420m	920s 870s	370w

where s = strong, m = medium, w = weak, b = broad, sh = shoulder

azomethines are coordinated to the metal atom [17]. The bands appearing in the region 350—380 cm^{-1} may be assigned to ν(U—N) vibrations. The ligand DAPSC shows a broad band at 3280 cm^{-1} along with two shoulders at 3300 and 3250 cm^{-1} which may be due to ν sym(NH) and ν asym(NH) vibrations [19]. In the parent complex, all these bands persist indicating the non-coordination of the terminal amino group to the metal.

The infrared spectra of the macrocyclic complexes do not show any significant changes as compared to parent complex. However, ν (NH_2) bands disappear. Only one band is observed in the ν (NH) region at 3200 cm^{-1} which may be due to a secondary amino group, establishing the condensation of the primary amino group with the carbonyl group. This is further supported by the appearance of a weak band at about 1640 cm^{-1} in the macrocyclic complexes, establishing the formation of azomethine linkage.

The UO_2 moiety shows three characteristic vibrations [20], viz., ν_1 (860 cm^{-1}), ν_2 (210 cm^{-1}) and ν_3 (930 cm^{-1}). The complexes under study show two strong bands ca. 880 (sym. O=U=O stretching) and 920 cm^{-1} (asym. O=U=O stretching). A weak band is also observed at ~230 cm^{-1} (O=U=O bending). The appearance of three bands indicates that the UO_2 group is linear [21].

In addition, the parent and all macrocyclic complexes show bands in the region 1450—1480, 1230—1250 and 750 cm^{-1} arising due to the vibrations of the nitrato groups. These bands fall in regions characteristic of monodentately coordinated nitrate group of C_{2v} symmetry [19].

*

The authors are thankful to the University Grants Commission for the financial help.

REFERENCES

[1] Melson, G. A.: "Coordination Chemistry of Macrocyclic Compounds", Plenum, New York 1979
[2] Nelson, S. M.: Pure and Appl. Chem., **52,** 2461 (1980)
[3] Syamal, A., Kumar, D.: J. Indian Chem. Soc., **59,** 96 (1982); Syamal, A., Kumar, D., Ahmad, S.: Indian J. Chem., **21A,** 634 (1982); Syamal, A., Singhal, O. P., Ahmad, S.: Indian J. Chem., **21A,** 193 (1982)
[4] Dia, G., Luparello, V., Maggio, F., Pizzino, T., Romano, V., Bocchi, G.: Inorg. Nucl. Chem. Lett., **16,** 109 (1980)
[5] Vidalli, M., Vigato, P. A., Casellato, U.: J. Inorg. Nucl. Chem., **37,** 955 (1975)
[6] Casellato, U., Vidali, M., Vigato, P. A.: Coord. Chem. Rev., **37,** 1 (1981)
[7] Casellato, U., Vidali, M., Vigato, P. A.: Inorg. Nucl. Chem. Lett., **10,** 437 (1974)
[8] Day, V. W., Marks, T. J., Wachter, W. A.: J. Am. Chem. Soc., **97,** 4519 (1975)
[9] Palenik, G. J., Wester, D. W., Rychlewska, U. A., Palenik, R. C.: Inorg. Chem., **15,** 1814 (1976)
[10] Pandey, O. P., Sengupta, S. K., Tripathi, S. C.: Transition Met. Chem., **8, 362** (1983)
[11] Vogel, A. I.: "A Text-book of Quantitative Inorganic Analysis" Longsman's Green Co. Ltd., London 1968
[12] Selbin, J.: J. Chem. Educ., **41,** 86 (1964)
[13] Wallrand, C. G., Vanquickenbarn, L. G.: J. Chem. Phys., **54,** 4178 (1971)
[14] Madden, D. P., daMota, M. M., Nelson, S. M.: J. Chem. Soc. A, **1970,** 890
[15] Madden, D. P., Nelson, S. M.: J. Chem. Soc., A, **1968,** 2342
[16] Sengupta, S. K., Sahni, S. K., Kapoor, R. N.: J. Coord. Chem., **12,** 113 (1982)
[17] Kher, S., Sahni, S. K., Kumari, V., Kapoor, R. N.: Inorg. Chim. Acta, **37,** 121 (1979)
[18] Sahni, S. K.: Transition Met. Chem., **4,** 73 (1979)
[19] Nakamoto, K.: "Infrared Spectra of Inorganic and Coordination Compounds". Wiley Interscience, New York 1970
[20] Syamal, A.: Coord. Chem. Rev., **16,** 309 (1975)
[21] Sacconi, L., Caroti, G., Paoletti, P.: J. Chem. Soc., **1958,** 4257; Conn, G. K. J., Wu, C. K.: Trans. Faraday Soc., **34,** 1483 (1938)

Acta Chimica Hungarica 119 (4), pp. 339—344 (1985)

DETERMINATION OF SOME AMINO COMPOUNDS WITH AMMONIUM METAVANADATE

Saeed AHMAD, JAMALUDDIN and Ishwar Chandra SHUKLA*

(Department of Chemistry, University of Allahabad, Allahabad-211002, India)

Received January 24, 1984
In revised form July 23, 1984
Accepted for publication August 21, 1984

A quick and convenient method has been developed for the micro determination of some hydrazines and aromatic amines. The sample (1—10 mg) is allowed to react with 2 mL of 0.3 *N* ammonium metavanadate reagent and 10 mL of 10 *N* H_2SO_4. The unconsumed reagent can be accurately titrated with 0.025 *N* Fe(II) solution using *N*-phenylanthranilic acid as indicator. The error does not exceed ±1%.

Hydrazines and aromatic amines have been quantitatively oxidized with various organic and inorganic oxidants. Hydrazines have been determined by using potassium metaperiodate as oxidant in HCl [1] and by thallium(III), potentiometrically [2]. Hydrazine hydrate and phenylhydrazines have been estimated with *N*-bromosuccinimide [3]. Isonicotinic acid hydrazide (Isoniazied) [4] has been determined by 0.05 *N* sodium pyrovanadate in 8 *N* H_2SO_4 using ammonium ferrous sulfate as standard solution. A number of other colorimetric [5], photometric [6] and polarographic [7] methods have also been used for the determination of hydrazines.

Aromatic amines are determined by using sodium hypobromate [8], sodium nitrate (9) and ceric sulfate [10]. *p*-Phenylenediamine has been determined with sodium orthovanadate (Na_3VO_4) [11]. Halogenating agents such as *N*-bromosuccinimide [12] and bromide bromate [13] have also been used for nuclear halogenation of aromatic compounds. Thermometric [14], chromatographic [15], amperometric [16], polarographic [17] and conductometric [18] methods have also been employed for the determination of aromatic amines and their derivatives. Taking advantage of the oxidizing capacity of ammonium metavandate [19, 20], we have developed a micro method for the analysis of some hydrazines and aromatic amines.

The present method is superior to the existing methods, such as oxidation with potassium periodate [21], potassium permanganate [22] and ceric sulfate [23, 24], as it utilizes a highly stable reagent [25], does not require a catalyst and sophisticated instrumentation.

* To whom correspondence should be addressed

Experimental

Reagents

Ammonium metavanadate (0.3 *N*) *solution*

Ammonium metavanadate (3.5 g; Reanal, Budapest, Hungary) was accurately weighed and dissolved in 10 mL of 10% sulfuric acid in a 100 mL measuring flask and made up to the mark with distilled water.

Ferrous ammonium sulfate (0.025 *N*) *solution*

The accurately weighed (2.4508 g; AnalaR, B.D.H.) compound was dissolved in distilled water in a 250 mL measuring flask and 10 mL of sulfuric acid was added to suppress hydrolysis. The solution was standardized by titration with standard potassium dichromate (0.02 *N*) solution, using diphenylaminesulfonic acid as indicator.

N-Phenylanthranilic acid

Solid *N*-phenylanthranilic acid (0.2 g; Nipa, Great Britain) was dissolved in 30 mL of 5% sodium carbonate and the solution was diluted up to 150 mL with distilled water.

Sample solution

A stock solution of the hydrazine derivatives (except hydrazine) was prepared by dissolving 50—100 mg of the sample in a minimum amount of glacial acetic acid, and amines in 10 mL of 2 *N* hydrochloric acid, in a 100 mL measuring flask and made up to the mark with distilled water. All the samples were either AnalaR, B.D.H. grade, or purified by crystallization.

Procedure

Aliquots containing 1—10 mg of the sample were placed in a 100 mL Erlenmeyer flask and 2 mL of a 0.3 *N* solution of ammonium metavanadate was added, followed by the addition of 10 mL of 10 *N* sulfuric acid. The reaction mixture was shaken gently and heated on a boiling water bath for the prescribed reaction time. After the reaction was over, the mixture was cooled to room temperature and titrated with 0.025 *N* Fe(II) solution using one drop of *N*-phenylanthranilic acid solution as indicator. A blank experiment was also run under identical conditions using all the reagents except the sample. The amount of the sample was calculated by the following expression:

$$\text{mg of the sample} = \frac{M(B - A)\,N}{n}$$

where

M = Molecular weight of the sample
N = Normality of ferrous ammonium sulfate
B = Volume of Fe(II) solution used to titrate the blank experiment
A = Volume of Fe(II) solution used to titrate the sample experiment
n = Number of moles of the V(V) reagent consumed per mole of the sample

Results and Discussion

The effect of variables such as the volume and concentration of the reagent and sulfuric acid, temperature and reaction time were studied. It was found that the recommended concentration of ammonium metavanadate reagent is suitable to achieve quantitative reaction. The addition of 10 mL of 10 *N* H_2SO_4 before the reaction helps in detecting the end-point. It was also observed that the reaction was incomplete at room temperature (27°) and direct heating

of the reaction mixture gave inconsistent results. Accurate and constant results were obtained when the reaction was carried out on a steam bath. Normally, the reaction is completed within 5 minutes, but in those cases where more than one groups are oxidized the reaction time is increased up to 25 minutes. Beyond the times listed in Table I there is no improvement in the results.

The number of moles of the V(V) reagent consumed for the sample depends upon the structure of the compound (Table I). Taking into consideration the moles of vanadium consumed for the sample and the isolation of the reaction products, a possible course of the reaction has been proposed for each compound.

While studying the oxidation of hydrazine derivatives it was noticed that hydrazine is completely oxidized to nitrogen and water. The evolution of nitrogen has qualitatively been established. In case of phenylhydrazine and *N*,*N*-diphenylhydrazine the final oxidation product was found to be *p*-benzoquinone.

The oxidation of 3-methyl-1-phenyl-5-pyrazolone gives *p*-quinone, nitrogen and carbon dioxide as the final oxidation products. The presence of *p*-quinone and nitrogen has qualitatively been established.

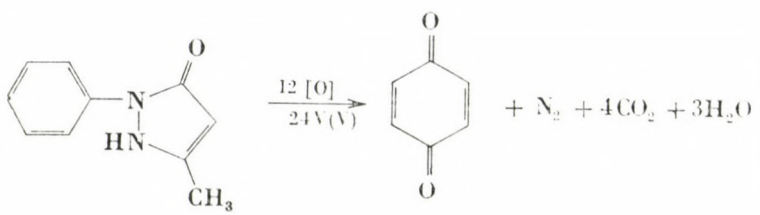

3-Methyl-1-phenyl-5-pyrazolon *p*-Quinone

In case of aromatic amines if the amino group is present along with a nitro group, like in *o*-, *m*- or *p*-nitroaniline, the amino group is oxidized to nitro group, giving rise to the corresponding dinitrobenzene as the final oxidation product; this has been confirmed by qualitative tests.

The oxidation of *p*-toluidine gives *p*-quinone, carbon dioxide and nitrogen.

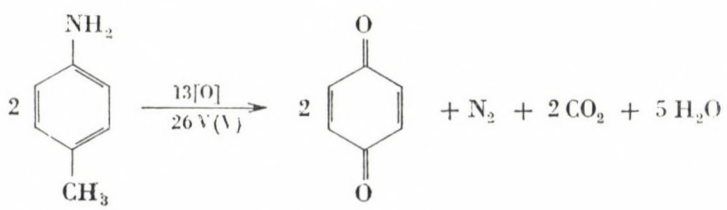

p-Toluidine *p*-Quinone

Table I

Determination of some hydrazines and aromatic amines with V(V) *reagent*

No. Compound	Amount* taken, mg	Reaction time, min	Amount recovered, mg	Moles of vanadium consumed	Error %	Standard deviation	Coefficient of variation
1. Hydrazine	1.0032		1.0062		+0.30	0.0039	0.3886
	5.0160	5	4.9908	4	−0.50	0.0215	0.4282
	10.0320		10.0727		+0.41	0.0264	0.2638
2. Phenylhydrazine	1.0041		0.9979		−0.62	0.0049	0.4893
	5.0205	10	5.0438	8	+0.46	0.0207	0.4123
	10.0410		10.0678		+0.27	0.0460	0.0458
3. 2,4-Dinitrophenyl-hydrazine	1.0018		1.0050		+0.32	0.0040	0.4002
	5.0200	15	5.0470	4	+0.54	0.0312	0.6209
	10.0410		10.0678		+0.27	0.0460	0.4581
4. Semicarbazide	1.0040		0.9980		−0.60	0.0042	0.4194
	5.0190	10	5.0425	4	+0.47	0.0012	0.0238
	10.0300		9.9721		−0.58	0.0420	0.4167
5. Phenylsemicarbi-zide	1.0033		1.0080		+0.48	0.0043	0.4281
	5.0090	25	4.9827	8	−0.53	0.0261	0.5799
	10.0400		10.0720		+0.32	0.0479	0.4788
6. *N,N*-Diphenyl-hydrazine	1.0035		1.0072		+0.37	0.0042	0.4184
	5.0205	20	5.0438	12	+0.46	0.0207	0.4123
	10.0380		10.0622		+0.24	0.0012	0.0119
7. 3-Methyl-1-phenyl-5-pyrazolone	1.0038		1.0060		+0.22	0.0039	0.3886
	5.0165	20	4.9920	24	−0.49	0.0263	0.5249
	10.0500		10.0800		+0.30	0.0469	0.4668
8. *p*-Nitroaniline	1.0021		0.9992		−0.29	0.0027	0.2696
	5.0250	5	5.0528	6	+0.45	0.0329	0.6542
	10.0180		10.0600		+0.42	0.0392	0.3907
9. *o*-Nitroaniline	1.0021		0.9992		−0.29	0.0027	0.2696
	5.0250	5	5.0528	6	+0.45	0.0329	0.6542
	10.0180		10.0600		+0.42	0.0392	0.3907
10. *m*-Nitroaniline	1.0018		0.9982		−0.36	0.0052	0.5998
	5.0160	5	5.0378	6	+0.38	0.0215	0.4282
	10.0330		10.0673		+0.34	0.0360	0.3585
11. *p*-Toluidine	1.0032		0.9982,		−0.50	0.0039	0.3886
	5.0090	20	5.0378	13	+0.57	0.0270	0.5379
	10.0350		10.0628		+0.28	0.0434	0.4326
12. *o*-Aminophenol	1.0050		0.9996		−0.54	0.0043	0.4289
	5.0105	10	5.0387	5	+0.54	0.0239	0.4759
	10.0210		10.0685		+0.47	0.0018	0.0179
13. *m*-Aminophenol	1.0029		0.9982		−0.47	0.0036	0.3598
	5.0150	10	5.0388	5	+0.47	0.0462	0.9207
	10.0320		9.9772		−0.55	0.0264	0.2638
14. *p*-Aminophenol	1.0042		0.9992		−0.50	0.0064	0.6369
	5.0150	10	5.0388	5	+0.47	0.0462	0.9207
	10.0420		10.0980		+0.56	0.0005	0.0050
15. *o*-Phenylene-diamine	1.0023		0.9998		−0.25	0.0041	0.4089
	5.0210	15	5.0492	8	+0.56	0.0007	0.0099
	10.0500		10.0800		+0.30	0.0006	0.0059
16. *m*-Phenylene-diamine	1.0044		1.0096		+0.52	0.0054	0.5369
	5.0115	15	5.0385	8	+054	0.0193	0.3891
	10.0230		10.0770		+0.54	0.0011	0.0109

Table I contd.)

No. Compound	Amount* taken, mg	Reaction time, min	Amount recovered, mg	Moles of vanadium consumed	Error %	Standard deviation	Coefficient of variation
17. *p*-Phenylene-diamine	1.0068		0.9990		−0.78	0.0062	0.6179
	5.0220	15	5.0520	8	+0.60	0.0267	0.5302
	10.0440		10.0985		+0.54	0.0503	0.4998
18. α-Naphthylamine	1.0031		1.0085		+0.54	0.0056	0.5573
	5.0200	25	5.0518	7	+0.63	0.0271	0.5386
	10.0310		10.0885		+0.57	0.0002	0.0019
19. *o*-Aminobenzoic acid	1.0040		1.0098		+0.58	0.0051	0.6071
	5.0250	25	5.0528	7	+0.55	0.0003	0.0059
	10.0400		10.0982		+0.58	0.0559	0.5357
20. *m*-Aminobenzoic acid	1.0050		0.9992		−0.58	0.0043	0.4290
	5.0225	20	4.9547	7	+0.64	0.0279	0.5541
	10.0450		10.0998		+0.54	0.0004	0.0039
21. *p*-Aminobenzoic acid	1.0045		0.9990		−0.55	0.0051	0.5087
	5.0155	20	5.0520	7	+0.72	0.0139	0.2751
	10.0680		10.1188		+0.50	0.0479	0.4700

* In each case three determinations were carried out

In aminophenols both the amino and phenolic groups are oxidized to give the corresponding quinone with the evolution of nitrogen. *m*-Aminophenol is supposed to give the corresponding quinone, but since it is unstable, it may be converted to *o*- or *p*-quinone as evidenced by the stoichiometry of the reaction.

In case of *ortho* and *para* phenylenediamines also the formation of the corresponding benzoquinones is noticed. However, *m*-phenylenediamine gives *o*- or *p*-benzoquinone.

The oxidation of *o*- and *p*-aminobenzoic acids furnish the corresponding quinone, nitrogen and CO_2, whereas *m*-aminobenzoic acid gives *o*- or *p*-benzoquinone, since the *m*-quinone is unstable.

REFERENCES

[1] Singh, B., Singh, A.: J. Ind. Chem. Soc., **29,** 34 (1952)
[2] Berka, A., Busev, A. K.: Anal. Chim. Acta **27,** 493 (1962)
[3] Barakat, M. Z., Wahab, M. F. A., Elsaov, M. M.: J. Am. Chem. Soc., **77,** 1670 (1955)
[4] Gowda, H. S., Rao, G. G.: Z. Anal. Chem., **36,** 165 (1959)
[5] Wood, P. R.: Anal. Chem., **25,** 1879 (1953)
[6] Preussman, R., Hengy, H., Lvebbe, D., Von Hondenberg, A.: Anal. Chim. Acta, **41,** 497 (1968)
[7] Banerjee, D. K., Reichmann, G. C., Budke, C. C.: Anal. Chem., **36,** 220 (1964)
[8] Reis, M. V., Nauchn, Tr.: Samarkandsk. Med. Inst., **11,** 117 (1956)
[9] Matrka, M.: Chemie Prague, **10,** 635 (1958)
[10] Sastri, T. P., Rao, G. G.: Anal. Chem., **163,** 263 (1958)
[11] Sastri, T. P.: Z. Anal. Chem., **196,** 349 (1963)

[12] Tiwari, R. D., Sharma, J. P., Shukla, I. C.: Talanta, **14**, 853 (1967)
[13] Day, A. R., Taggart, W. I.: Ind. Eng. Chem., **163**, 263 (1958)
[14] Spencer, G., Brimley, J. E.: J. Soc. Chem. Ind., **64**, 53 (1945)
[15] Lane, E. S.: Analyst, **80**, 675 (1955)
[16] Sarkanen, K., Shuerch, L.: Anal. Chem., **27**, 1245 (1955)
[17] Waters, M. A.: Zasshi, **79**, 1060 (1958)
[18] Pandaya, P. K., Halder, B. C.: J. Sci. Ind. Res., **218**, 503 (1962)
[19] West, D. M., Skoog, D. A.: Anal. Chem., **31**, 583 (1959)
[20] Rao, S. P., Rathi, H. B., Gaur, J. N.: Anal. Chim. Acta, **25**, 136 (1961)
[21] Hovorka, V.: Collect. Czech. Chem. Commun., **3**, 285 (1931)
[22] Issa, I. M., Issa, R. M.: Anal. Chim. Acta, **14**, 578 (1956)
[23] Singh, B., Singh, R.: Anal. Chim. Acta, **10**, 408 (1954)
[24] Gandikota, Krishna, M., Rao, G.: Anal. Chim. Acta, **67**, 469 (1973)
[25] Lang, R., Kurtenaeker, H.: Z. Anal. Chem., **81**, 123 (1942)

Acta Chimica Hungarica 119 (4), pp. 345—346 (1985)

BY-PRODUCTS IN THE PREPARATION OF 1,1,1,5-TETRACHLOROPENT-3-ENE FROM 1,3-BUTADIENE AND TETRACHLOROMETHANE

(SHORT COMMUNICATION)

Zdeněk Vít[1]* and Ivan Kolb[2]

([1]Institute of Chemical Process Fundamentals, Czechoslovak Academy of Sciences, 165 02 Prague 6 Czechoslovakia, and [2]Research Institute for Organic Synthesis, 532 18 Pardubice-Rybitví, Czechoslovakia)

Received July 9, 1984
Accepted for publication August 21, 1984

The addition of tetrachloromethane to 1,3-butadiene affords 1,1,1,5-tetrachloropent-3-ene (TCP) as the main product. Yields of 30—90% are obtained with copper, iron or ruthenium compounds as catalysts [1—4], whereas the use of organic peroxides leads mostly to polymerization of the diene [5]. 1,1,1,9-Tetrachlorononona-3,7-diene [1, 2, 5] and a $C_{13}H_{18}Cl_4$ telomer [1] are known as by-products of this reaction. The presence of a $C_5H_4Cl_2$ compound originating by dehydrochlorination of TCP was also observed [5].

In the present work, the addition of CCl_4 to 1,3-butadiene is catalyzed by a copper-piperidine system. By means of mass spectrometry, additional by-products have been detected in the reaction mixture. The formation of these compounds can be explained by the following equations[a]:

$$C_4H_6 + CCl_4 \longrightarrow \underset{\text{TCP. } 62\%}{CH_2Cl-CH=CH-CH_2-CCl_3} \xrightarrow{Cl_2} \underset{3\%}{C_5H_5Cl_5}$$

$$C_4H_6 + 2CCl_4 \longrightarrow [C_6H_6Cl_8] \begin{cases} \xrightarrow{-Cl_2} C_6H_6Cl_6 \ 1.3\% \xrightarrow{-HCl} C_6H_5Cl_5 \ 0.5\% \\ \xrightarrow{-HCl} C_6H_5Cl_7 \ 0.2\% \xrightarrow{-Cl_2} C_6H_5Cl_5 \ 0.5\% \end{cases}$$

$$2\,C_4H_6 + CCl_4 \longrightarrow \underset{7\%}{C_9H_{12}Cl_4} \quad (3 \text{ isomers})$$

* To whom correspondence should be addressed
[a] The numbers denote conversions of 1,3-butadiene to the corresponding compounds

It has been observed that the concentration of TCP goes through a mild maximum during the reaction indicating the consumption of TCP in a consecutive reaction. Owing to the presence of the $C_5H_6Cl_6$ compound it seems likely that chlorination of TCP occurs. On the other hand, the presence of the earlier observed $C_5H_4Cl_2$ compound [5] arising by elimination of two molecules of HCl has not been proved. The addition of two molecules of CCl_4 to one molecule of 1,3-butadiene occurs, as well as in the case of 1,5-hexadiene [6]. This is confirmed by the presence of $C_6H_6Cl_6$, $C_6H_5Cl_7$ and $C_6H_5Cl_5$, resulting from the decomposition of the primary 1 : 2 adduct. As regards 1,1,1,9-tetrachlorononа-3,7-diene [1, 2, 5] obtained earlier as a 2 : 1 addition product, three isomers with the formula $C_9H_{12}Cl_4$ have been found (molar ratios 70, 25 and 5%). In addition to the above mentioned compounds, small amounts of $C_7H_4Cl_8$ and $C_7H_6Cl_8$ have also been detected.

It follows from these results that the 1 : 1 addition of CCl_4 to 1,3-butadiene is accompanied by several undesirable processes decreasing the selectivity. Besides 1 : 2 and 2 : 1 additions, elimination of Cl_2 and HCl from the polychlorinated reaction products takes place. The consecutive chlorination of TCP or other unsaturated compounds may be favoured in the presence of iron, originating from the reactor material.

Experimenta

A mixture of CCl_4 (153 g), 1,3-butadiene (27 g), piperidine (1.7 g), copper powder (0.64 g) and acetonitrile (16 g) was heated at 100—110 °C in a stainless steel autoclave. The concentration of TCP was checked by GLC during the course of the reaction. After 1 h, the reactor was cooled and the acidic reaction mixture washed with water. 1,1,1,5-Tetrachloropent-3-ene (67 g; b.p. 95—100 °C at 2.67 kPa) and a high-boiling fraction (14 g; b.p. 105—135 °C at 0.7 kPa) were isolated by fractionation. The residue weighed 22 g.

1,1,1,5-Tetrachloropent-3-ene. $C_5H_6Cl_4$. Calcd. C 28.89; H 2.91. Found C 29.11; H 2.91%. ^{1}H-NMR(δ): 4.1 (d, 2H, $-CH_2Cl$), 5.9 (m, 2H, $-CH=CH-$), 3.4 (d, 2H, $-CH_2CCl_3$).

GLC analysis of the high-boiling fraction was performed on a JGC-20K instrument connected by means of a double jet separator with a mass spectrometer JMS 01-SG-2 (both Jeol, Japan). The glass column (2 m × 2 mm, 10% OV 101/Chromosorb W Silanized) was heated to 150—250 °C (gradient: 10 °C min^{-1}). The ionization chamber temperature was 270 °C, the electron energy 26 eV and the trap current 200 μA. The molecular formulas of the individual compounds were established on the basis of the detected molecular ions.

The ^{1}H-NMR spectrum of TCP was recorded on a BS 467 Tesla 60 spectrometer (ČSSR).

*

The authors thank V. Blechta for measuring the ^{1}H-NMR spectrum.

REFERENCES

[1] Asscher, M., Vofsi, D.: J. Chem. Soc., **1963,** 1887
[2] Asscher, M., Katchalsky, A., Vofsi, D.: Brit. Pat., 1 146 463 (1966); Chem. Abstr., **71,** 12514z (1969)
[3] Hájek, M., Šilhavý, P., Málek, J.: Collect. Czech. Chem. Commun., **45,** 3488 (1980)
[4] Matsumoto, H., Nakano, T., Nikaido, T., Nagay, Y.: Chem. Lett., **1978,** 115
[5] Arbuzov, B. A., Nikitina, V. I.: Izv. Akad. Nauk SSSR, Ser. Khim., **1960,** 1131
[6] Kharasch, M. S., Jensen, E. V., Urry, W. H.: J. Am. Chem. Soc., **69,** 1100 (1947)

Acta Chimica Hungarica 119 (4), pp. 347–354 (1985)

PREPARATION OF DERIVATIVES OF CITRONELLAL

Gyula KÖRTVÉLYESSY

(Development and Research Co. for Organic Chemical Industry, H-1085 Budapest, Stáhly u. 13.)

Received March 16, 1984
In revised form June 25, 1984
Accepted for publication September 6, 1984

The hydrogenation of citronellal and citral, if not separated from ethereal oils, leads regioselectively to dihydrocitronellal and citronellal, respectively. The reaction of citral with (+)-ephedrin or L-aspartic acid, followed by hydrogenation and deblocking the aldehyde function, yields optically active citronellal. Reacting the aldehyde function of citronellal with diethanoleamine, piperidine or morpholine, the alcohol addition to the 6,7-double bond results in 7-alkoxy substituted citronellals with acceptable yield. The formation of 7-hydroxy-6,7-dihydrocitronellal during this reaction has been proved and the effect of reaction parameters on the yield have been discussed.

Introduction

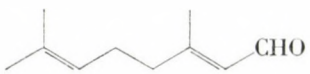

1

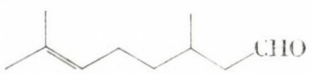

2

Citral (**1**) and citronellal (**2**) occurring in ethereal oile (Eucalyptus citriodora, Litsea cubeba) are very useful prime materials for the preparation of other terpene derivatives. Thus, the 6,7-dihydrocitronellal **3** and the 7-alkoxy 6,7-dihydrocitronellal **4** were transformed by Henrick and co-workers to 3,7,11-trimethyl-2,4-dodecadienoic acid esters and their 11-alkoxy analogs,

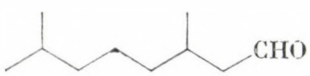

3

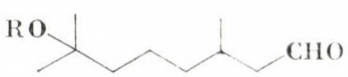

4

which are very useful and important insect-growth regulators [1]. Therefore, we studied the hydrogenation of citral **1** to citronellal **2** with special regard to regioselectivity and stereoselectivity of the hydrogenation and the alcohol addition at the 6,7-double bond in the citronellal molecule, as well.

The selective saturation of the 2,3-double bond in the citral has been studied by many authors [2, 3, 4, 5]. The descriptions, mostly that of patents, report rather contradictory results. Both the reduction of carbonyl group

and the simultaneous saturation of the 6,7-double bond should be taken into consideration: a yield of 80—95% can be achieved only with nickel or palladium catalysts treated with different additives. There are only few data about the enantioselective hydrogenation of citral: Rhône Poulenc's researchers [6] obtained nearly theoretical yield and 50—60% optical yield in the preparation of optically active citronellal using a catalyst system formed from rhodium and optically active phosphines.

The alcohol addition of citronellal was also claimed by Rhône Poulenc [7]: after blocking the aldehyde group with ammonia, butyl amine or dimethyl amine, the protected citronellal was reacted with methanol in the presence of sulphuric acid, the addition took place with a yield of 40—75%. After removal of the blocking group, the obtained 7-methoxy-6,7-dihydrocitronellal contained unreacted citronellal and dimethyl acetal of both compounds indicating the partial fission of the blocking group during the addition.

Henrick and co-workers [8] prepared 7-ethoxy-6,7-dihydrocitronellal from citronellol via ethanol addition followed by the oxydation of the product.

Results

Considering the technological and economic points of view, we tried to carry out direct hydrogenation using Litsea cubeba oil to obtain citronellal **2** from citral **1**. Surprisingly, it was found that the oil can be hydrogenated regioselectively to citronellal **2** without solvent in the presence of palladium catalyst at room temperature and atmospheric pressure in a rapid reaction. The quantity of 6,7-dihydrocitronellal (**3**) formed was as low as 5%. Under the same conditions, pure citral gave 20—30% of 6,7-dihydrocitronellal together with 70—80% of citronellal.

In solution or at elevated temperatures, the hydrogenation proceeds equally with poor selectivity. The same experiences were gained from the hydrogenation of citronellal **2** of Eucalyptus citriodora oil into 6,7-dihydrocitronellal: we achieved nearly theoretical yield without solvent using Pd/C catalyst at 30—40 °C. The accompanying impurities of the oils were also hydrogenated, but they did not interfere with the easy recovery of the products eventually by reaction, as they were not aldehydes.

The enantioselective hydrogenation of citral was aimed by a method different from those given in the literature: the aldehyde function was allowed to react with optically active amines, such as α-methylbenzylamine or ephedrine.

In the hydrogenation of compound **6**, both C—N and conjugated C—C double bonds reacted, thus this way proved to be unsuitable for the preparation of citronellal. In the case of aspartic acid **8**, however, only the C—C double bond was hydrogenated in alkaline methanol, and after acidifying the opti-

cally active citronellal could be separated. On the basis of the optical activity of the distilled product, the optical yield was 7%.

The oxazolidine (**7**) obtained by ephedrine formed oxazolidine of the formula **9** by the regioselective absorption of one equivalent of hydrogen. The formed compound hydrolysed rapidly to citronellal **2** in aqueous sulphuric acid. On the basis of optical activity of the distilled product, the optical yield was 28%.

During the reproduction of the method of methanol addition of citronellal **2** described in the literature [2], the formation of a by-product unknown in the reaction was observed: the GLC analysis showed that the reaction mixture contained also 7-hydroxy-6,7-dihydrocitronellal. The relative quantity of this by-product, strongly interfering in most chemical application because of its aldehyde group, depends on the sulphuric acid-methanol ratio. Using

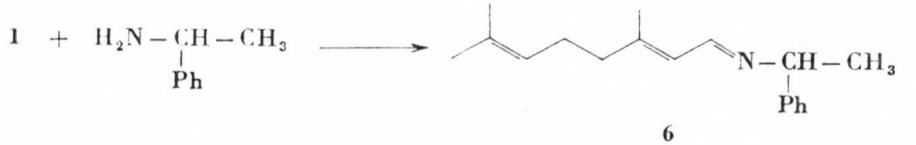

6

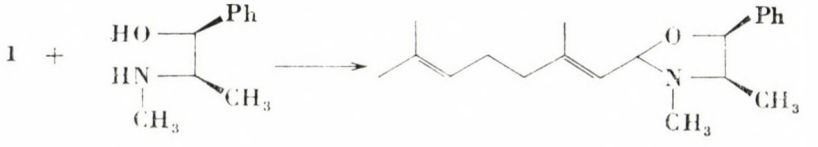

5 **7**

Scheme 1

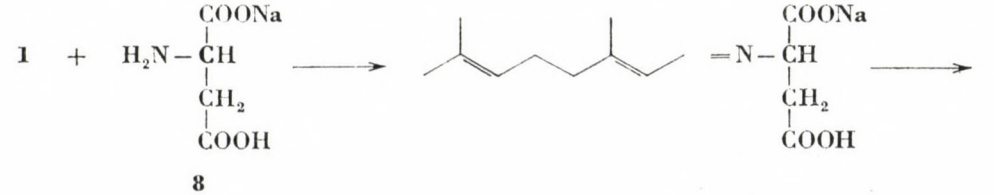

8

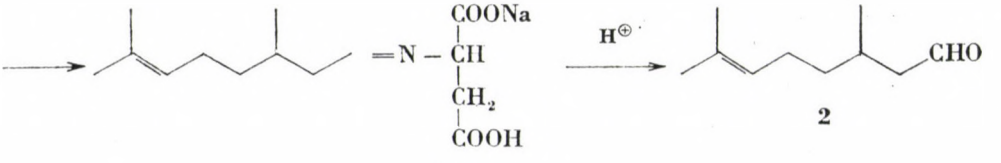

2

Scheme 2

the methanol in quantities less than given in the literature, the quantity of this by-product can reach even 50%. High concentrations of methanol, however, make the recovery more difficult and, in addition, cause an increasing ratio of the acetals in the product. Therefore, on the basis of analogies

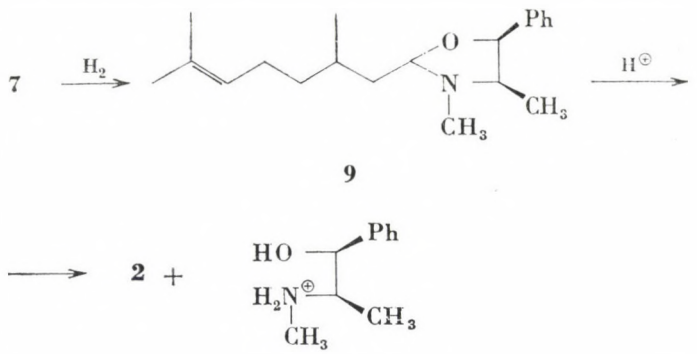

Scheme 3

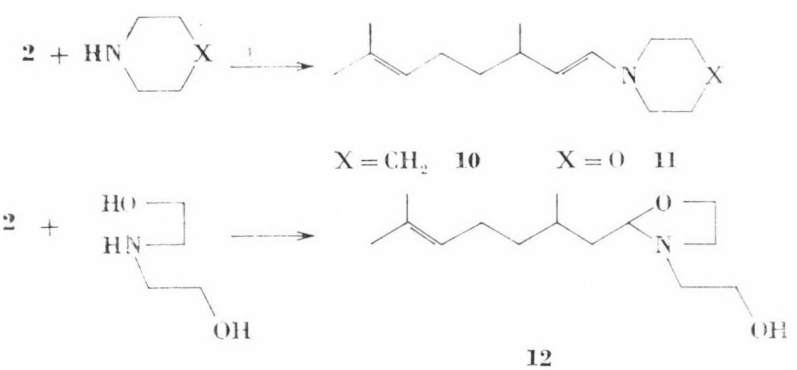

Scheme 4

[9], other aldehyde-blocking groups were tried, too. Enamines **10** and **11** obtained with piperidine and morpholine, respectively, and also oxazolidine **12** formed by diethanolamine gave 7-methoxy-6,7-dihydrocitronellal using methanol containing sulphuric acid, with a good yield. The effect of the reaction conditions on the yield is shown in Table I. where the distribution of products is given for 1 mole of oxazolidine **12** in the function of the ratio of methanol to sulphuric acid and that of temperature.

Reacting the protected citronellal derivatives **10**, **11** or **12** with other types of alcohols, we could prepare different, partly new 7-alkoxy-6,7-dihydrocitronellals.

Table I

Reaction of protected citronellal with methanol and sulphuric acid

Methanol mL	Sulphuric acid mL	Citronellal %	7-hydroxy-7-methoxy-6,7-dihydro-citronellal	
			%	%
185	92.5	25	5	68
185	185	4	37	59
370	185	4	8	87
370	185 (at 50 °C)	0	10	80
555	185	8	4	83

Reaction time 3 h at 25 °C

Experimental

The used materials and solvents were generally the products of Reanal. The Eucalyptus citriodora and Litsea cubeba oils were obtained from CAOLA. The ephedrine, α-methylbenzylamine and aspartic acid were Fluka products, and the treo-1-(4-nitrophenyl)-2-amino-1,3-propandiol origined from EGyT Pharmaceutical Works. IR spectra were taken on a Perkin Elmer 577, and ^{1}H-NMR and ^{13}C-NMR spectra on a Varian T 80 apparatus. The GLC analysis were performed on Chrom 4 and Chrom 5 chromatographs provided with FID. Column: 10% Carbowax 20 M on Chromosorb W. Temperature: 160 °C. Rt (min): dihydrocitronellal 1.4; citronellal 2.1; citronellal dimethylacetal 2.6; isopulegol 3.2; citronellol 5.7; 7-methoxy-6,7-dihydrocitronellal 5.8; 7-hydroxy-6,7-dihydrocitronellal 13.8.

Preparation of citronellal 2 from Litsea cubeba oil

To 20.1 g of Litsea cubeba oil (citral content 70%, the distribution of which 65% *E* isomer and 35% *Z* isomer) 1.1 g of 10% Pd/C catalyst (Engelhardt) was added and the mixture was hydrogenated at atmospheric pressure. The hydrogen absorption of the mixture was 2530 mL during 6 hours, then no more hydrogen absorption took place. The catalyst was filtered off. The 20.2 g product contained 5% of overhydrogenated (relative to the citronellal) material, i.e. 6,7-dihydrocitronellal, according to the GLC analysis. On addition of 10.5 g (0.1 mole) diethanolamine and 30 mL toluene to the product, warming and the separation of water were noticed. Water was removed using a Marcusson column. From the dehydrated solution, first the toluene at 3 kPa, then the impurities of the Litsea cubeba oil at 700 Pa were removed. At this pressure, the 2-(2,6-dimethyl-5-heptenyl)-3-oxazolidineethanol distils at 150 °C. Its quantity was 24 g.

IR (cm^{-1}): 3400 (OH), 2960 (CH), 1465, 1380 and 1365 (CH deformation), 1170 (CN) and 1050 (CO).

To the substance, 20 mL water and 20 mL cyclohexane and so much 20% sulphuric acid were added as to obtain pH 6—7 in the aqueous phase. The organic phase was washed with water, 50 mL of 20% sulphuric acid, then again with water and the solvent was distilled off at 10 kPa. Distilling the residue at 1.3 kPa, the boiling point of citronellal was 100 °C. Quantity obtained: 14.0 g. The product contained 5% of dihydrocitronellal according to GLC analysis.

IR (cm^{-1}): 2970, 2920 (CH), 2720 (aldehyde CH), 1730 (CO), 1610 (C=C), 1455, 1380 (CH deformation), 830 (CH deformation).

Preparation of dihydrocitronellal 3 from Litsea cubeba oil

In a stainless steel autoclave of 2.5 litres, 1500 g of Litsea cubeba oil (citral content 70%) was charged and 10% Engelhardt Pd/C catalyst added, then the mixture was hydrogenated at 30 °C and 0.4—0.5 MPa pressure. In two hours, the citral reacted and gave a 1 : 1

mixture of citronellal and dihydrocitronellal. On adding again 50 g catalyst and continuing the hydrogenation at 30—40 °C, the hydrogen absorption ceased after 5 hours. Filtering off the catalyst, the substance weighed 1500 g. This product contained, according to GLC analysis. 2% citronellal besides the dihydrocitronellal as the main reaction product. The purification of the reaction product could be done in the same way as described above, by reacting with diethanolamine and distilling the obtained 2-(2,6-dimethylheptyl)-3-oxazolidineethanol.

Anal. Cald. for $C_{14}H_{29}NO_2$: C, 69.1; H, 12.0; N, 5.76. Found: C, 69.0; H, 12.1; N, 5.80.

The ^{13}C-NMR absorption spectral data of purified oxazolidine were:

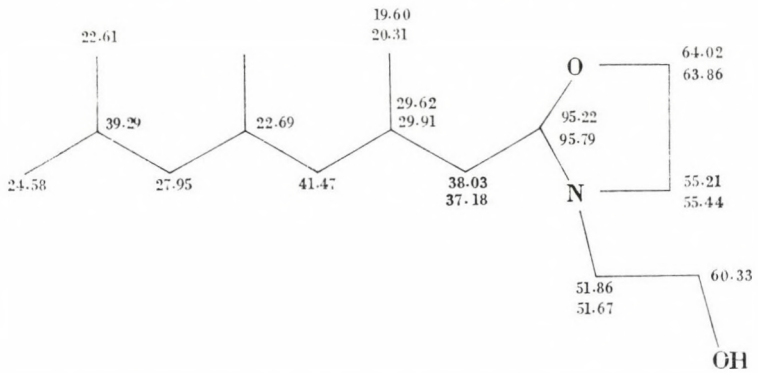

The C atoms beneath of the two centres of asymmetry gave two absorption peaks indicating that the substance was the mixture of two diastereomers. The highest difference in chemical shift appeared at the C atom lying between the two chiral centres.

Preparation of dihydrocitronellal 3 from Eucalyptus citriodora oil

In 13.4 kg Eucalyptus citriodora oil (containing 73% of citronellal, 20% of isopulegol and 7% of citronellol), 300 g 10% Engelhardt Pd/C catalyst was suspended and the mixture hydrogenated at 0.4—0.6 MPa pressure in a stainless steel autoclave of 20 litres. Initially, the autoclave was intensively cooled to maintain the temperature below 50 °C. The hydrogen absorption was terminated in 7 hours. After filtering off the catalyst, the reaction product obtained was 13.4 kg containing 70% of dihydrocitronellal. The recovery of dihydrocitronellal was carried out as described above.

Asymmetric hydrogenation using ephedrine

To 0.05 mole of (+)L-ephedrine base **5**, 30 mL ether, 3 g potassium carbonate and 7.6 g citral (mixture of *Z*—*E* isomers from Fluka) were added. After one hour mixing, the mixture was filtered off and the ether was stripped. The reaction was complete after 24-hour standing as it shown by IR analysis.

The IR absorption bands of the obtained 3,4-dimethyl-2-(2,6-dimethyl-1,5-heptadienyl)-5-phenyl-oxazolidine **7** (13.2 g) were (cm^{-1}); 3090, 3060, 3030 (aromatic CH), 2970, 2920, 2805, 2780 (aliphatic CH), 1630, 1610 (C=C), 1490, 1455, 1380 (CH deformation), 1330, 1220, 1200, 1050, 1040, 1030 (C—O and C—N), 755, 700 (aromatic deformation), 720 (CH double bond, deformation).

Anal. Calcd. for $C_{20}H_{29}NO$: C 80.22; H 9.76; N 4.68. Found: C 80.4; H 9.70; N 4.70.

The substance dissolved in 30 mL methanol was hydrogenated in the presence of 0.5 g Pd/C catalyst at atmospheric pressure and room temperature. In 70 minutes, 1085 mL of hydrogen was absorbed, then the reaction ceased. After filtering off the catalyst, the methanol was stripped at 10 kPa. To the residue of 1342 g **9** (on the IR spectrum of which the bands at 1630 and 720 cm^{-1} were missing compared to the initial oxazolidine), 20 mL water and 10 mL 20% sulphuric acid were added. The substance was dissolved, the clear solution became turbid and segregated into two phases after a few minutes. The substance was extracted three times with 20 mL of cyclohexane and the organic phase was washed with 20% sulphuric acid, then

with water. The residue free of solvent was distilled at 650 Pa yielding 2 g of product which, by IR spectrum and GLC analysis, proved to be pure citronellal with $\alpha_D^{25} = +0.373$ (neat). Optical yield: 28 percent.

Asymmetric hydrogenation using α-methylbenzylamine

To 3.8 g (0.025 mole) citral, 3 g α-methylbenzylamine was added. To the turbid and warmed up mixture, 1 g sodium sulphate was added and filtered off. The filtrate was a pure oil of α-methyl-*N*-(3,7-dimethyl-2,6-octadienilidene)-benzylamine **6**.

Anal. Calcd. for $C_{18}H_{25}N$: C 84.65; H 9.87; N 5.48. Found: C 84.4; H 9.80; N 5.40.

Specific IR bands (cm^{-1}): 3080, 3060, 3025 (aromatic CH), 2970, 2920, 2860 (aliphatic CH), 1650 (CN double bond), 1610 (C=C), 1480, 1450, 1360 (aliphatic CH), 760, 700 (aromatic CH).

The substance dissolved in 100 mL of methanol to which 0.3 g palladium was added, absorbed 0.05 mole of hydrogen on hydrogenation at 25 °C and atmospheric pressure. After filtration and evaporation, the obtained residue of 5.7 g was α-methyl-*N*-(3,7-dimethyl-6-octenyl)-benzylamine.

IR (cm^{-1}): 3080, 3060, 3025 (aromatic CH), 2970, 2920, 2860 (aliphatic CH), 1480, 1450, 1360 (aliphatic CH), 1130 (CN valence), 760, 700 (aromatic CH).

In diluted sulphuric acid, the reaction product forms a solution of honeylike consistency from the cyclohexane extract of which no citronellal was detectable by GLC.

Asymmetric hydrogenation using aspartic acid 8

3.75 g of L-aspartic acid, 3.8 g of citral, 10 mL methanol and 2 g of sodium hydroxide in 30 mL methanol were mixed. Aspartic acid was dissolved and citral reacted completely in half an hour as it was demonstrated by GLC analysis. Hydrogenating the solution in the presence of 0.5g palladium catalyst, the hydrogen absorption was 580 mL (0.025 mole) at room temperature and atmospheric pressure during 4 hours. The catalyst was filtered off and the reaction mixture was mixed with 10 mL of 20% sulphuric acid. The solution, which became turbid in a few minutes, was extracted with toluene and the toluene phase was washed with water and evaporated. The residue was distilled at 650 Pa yielding 1.5 g of citronellal.

$\alpha_D^{20} = 0.0850$ (neat). Optical yield: 7%.

N-(3,7-dimethyl-1,6-octadienyl)-morpholine 11 and -piperidine 10

To 211 g of Eucalyptus citriodora oil containing 73% of citronellal, 1.1 mole morpholine and, after turned to turbid and became warm, 300 mL of toluene were added. Using a Marcusson column, the formed water was stripped off. First, the toluene and the excess of amine was distilled off at 10 kPa, followed by the bulk of isopulegol and citronellol content of the Eucalyptus citriodora oil at 650 Pa and up to 100 °C still temperature. The residue of 220—230 g could be used directly for addition of alcohol to the double bond.

Specific IR (cm^{-1}): 3040 (unsaturated CH), 1690, 1650 (C—C double bond), 860, 830, 800 (unsaturated CH).

2-(2,6-dimethyl-5-heptenyl)-3-oxazolidineethanol 12

The procedure was the same as above, but 105 g (1 mole) of diethanolamine was used as an amine. 240—260 g of raw oxazolidine was obtained.

7-methoxy-6,7-dihydrocitronellal 4, $R = CH_3$

0.18 mole of 2-(2,6-dimethyl-5-heptenyl)-3-oxazolidineethanol (the one fifth quantity of the raw product obtained in the preceding example) was charged into the mixture of 37 mL sulphuric acid and 74 mL methanol below 37 °C. The mixture was allowed to react at 20—30 °C for 3 hours. Then, 100 mL of water and 20 mL of toluene were added under cooling, below 40 °C. The lower aqueous phase is the salt of 2-(2,6-dimethyl-6-methoxy-heptyl)-3-oxazolidineethanol formed with sulphuric acid and the upper toluene phase contains the by-products

transferred from the initial raw substance together with those formed during the reaction and containing no aldehyde group, thus forming no oxazolidine.

To the acidic aqueous phase, 100 g ice, 30 mL toluene and 87 g 40% sodium hydroxide were added and the pH was adjusted to 6—7. After one hour stirring, the phases were separated and twice extracted with each 30 mL of toluene. The toluene phases were washed using 30 mL of water, then stirred together with 30 mL of 20% sulphuric acid at least for four hours. During this, the citronellal contained underwent to esterification with the sulphuric acid and got into the aqueous phase. The organic phase was neutralized with water and condensed by evaporation. The obtained residue was 31 g containing 90% of 7-methoxy-6 7-dihydrocitronellal. The yield was 80%.

IR (cm^{-1}): 2970, 2940, 2820 (aliphatic CH), 2720 (aldehyde CH), 1730 (CO), 1465, 1380, 1365 (aligphatic CH), 1085 (7-methoxy).

7-ethoxy-6,7-dihydrocitronellal 4, R = C_2H_5

To the mixture of 160 mL ethanol and 37 mL concentrated sulphuric acid, 48 g of *N*-(3,7-dimethyl-1,6-octadienyl)-piperidine were added at 10 °C in five minutes. After allowing to react at room temperature for 20 hours, the reaction mixture was poured into ice and neutralized with 40% alkali. Having extracted three times with 30 ml of cyclohexane, the organic phase was washed twice with water, then mixed with 200 mL of 20% sulphuric acid at room temperature. The unreacted citronellal remained in the substance reacted with a half-life time of approximately one hour. After four hours, the organic phase was washed with water up to neutral and evaporated. The obtained raw product weighed 33 g and distilled over at 650 Pa and 80 °C. The distilled product was 26 g.

IR (cm^{-1}): 2980, 2940, 2880 (aliphatic CH), 2720 (aldehyde CH), 1735 (CO), 1465, 1385, 1370 (aliphatic CH), 1075 (ethoxy).

GLC, Rt: 6.5 min.

7-butoxy-6,7-dihydrocitronellal 4, R = C_4H_9

To 200 mL of *n*-butanol, 37 mL of concentrated sulphuric acid and thereafter 40 g of *N*-(3,7-dimethyl-1,6-octadienyl)-piperidine were added at a temperature lower than 10 °C. The reaction mixture was allowed to react for three days at room temperature, then poured into 300 mL of icy water and mixed with 300 mL of cyclohexane. Three phases were obtained, the upper of which — the butanol/cyclohexane phase — contained the by-products and the lower the aqueous sulphuric acid solution. The middle phase appeared to be the salt of *N*-(7-butoxy-3,7-dimethyl-1-heptenyl)-piperidine hydrogen sulphate, which dissolved in an ample excess of water. Adjusting the pH of the solution to 6—7 with sodium hydroxide solution, the segregating product was dissolved with cyclohexane, then washed with water, 20% sulphuric acid, then again with water. 13.8 g (41%) of 7-butoxy-6,7-dihydrocitronellal was obtained by distillation, the boiling point of which proved to be 95—105 °C at 650 Pa.

IR (cm^{-1}): 2960, 2935, 2870 (aliphatic CH), 2720 (aldehyde CH), 1725 (CO), 1475, 1385, 1365 (aliphatic CH) and 1090 (butoxy).

GLC, Rt: 7.0 min.

REFERENCES

[1] Henrick, C. A., Staal, G. B., Siddall, J. B.: J. Agric. Food Chem., **21,** 354 (1973)
[2] Szokolszkij, D. V., Pak, A. M., Ginzburg, M. A.: React. Kinet. Catal., Lett., **10,** 43 (1979)
[3] Pak, A. M., Konuszpajev, S. R., Szokolszkij, D. V.: React. Kinet. Catal. Lett., **18,** 311 (1981)
[4] Japan P. 76-113801; C. A., **86,** P190272m
[5] Ger. Offen. 2 832 699; C. A., **93,** P26198m
[6] Dang, T., Aviron-Violet, P., Colleuille, P., Varagnat, J.: J. Mol. Catal., **16,** 51 (1982)
[7] Ger. Offen. 2 262 740; C. A., **79,** P78997f
[8] Henrick, C. A., Anderson, R. J., Staal, G. B., Ludvik, G. F.: J. Agric. Food Chem., **26,** 542 (1978)
[9] Ishino, R., Kumanotani, J.: J. Org. Chem., **39,** 108 (1974)

Acta Chimica Hungarica 119 (4), pp. 355—361 (1985)

NEW METAL COMPLEXES OF 4-PHENYL-1-DIACETYLMONOXIME-3-THIOSEMICARBAZONE (BMPTS)

K. M. IBRAHIM, A. A. EL-ASMY, M. M. BEKHEIT and M. M. MOSTAFA*

(Chemistry Department, Faculty of Science, Mansoura University, A.R. Egypt.)

Received March 21, 1984
Accepted for publication September 6, 1984

The reaction of 4-phenyl-1-diacetylmonoxime-3-thiosemicarbazone (BMPTS) with cobalt(II) and nickel(II) salts results in diamagnetic complexes of the types $[Co(BMPTS\text{-}H)_3]$, $[Ni(BMPTS\text{-}H)Cl(H_2O)]$ and $[Ni(BMPTS\text{-}2H)(H_2O)]H_2O$. The reaction of copper(II) salts with BMPTS gave a pesudotetrahedral and/or distorted octahedral having the formulas $[Cu(BMPTS\text{-}H)X(H_2O)]$ (X = Cl or Br) and $[Cu(BMPTS\text{-}2H)(H_2O)_3]$. The nature of these complexes has been elucidated by spectral (u.v., visible, i.r., n.m.r.) and magnetic studies. Also, the zinc(II), cadmium(II) and mercury(II) complexes with the formulas $[M(BMPTS)X_2]$ [M = Zn(II), Cd(II) or Hg(II); X = Cl or Br] and $[M(BMPTS\text{-}2H)(H_2O)]H_2O$ [M = Zn(II) or Cd(II)] have been isolated and characterized.

Introduction

Recently, we have discussed the preparation and characterization of some hydrazone-oxime complexes with first row transition metals [1]. Also, the complexes of some ligands containing thiosemicarbazide moiety [2] have been synthesized and characterized. In this paper the substitution of the carbonyl group in the hydrazone-oxime ligands by a thioketo group is investigated. All the compounds obtained with nickel(II) and copper(II) are of 1 : 1 (M : L) stoichiometry displaying square planar, pseudotetrahedral and/or distorted octahedral structures depending on the metal salt used as well as on the condition of preparation. Cobalt(II) salts are readily oxidized in the presence of ligand (BMPTS), sodium acetate and in aqueous solution to cobalt(III) forming of low spin complex of octahedral geometry, and of 1 : 3 (M : L) stoichiometry.

Experimental

An ethanolic solution of 4-phenylthiosemicarbazide (1.7 g, 1 mmole) was treated with an EtOH solution of diacetylmonoxime (1 g, 1 mmole). The mixture was refluxed for ca. 3 h on a water bath. The solution was then concentrated to one half of its volume and cooled. Yellowish white needles separated which were recrystallized from absolute ethanol (m.p., 191—192 °C). The purity of the compound was checked by elemental analysis and spectral studies (i.r. and n.m.r.).

* To whom correspondence should be addressed

Synthesis of the complexes

[M(BMPTS)X_2] *and* [*M*(BMPTS-H)*X*(H_2O)]H_2O *complexes*

Equimolar amounts of BMPTS and the metal salt ($ZnCl_2$, $CdCl_2$, · $2^1/_2$ H_2O, $HgCl_2$, $NiCl_2$ · 6 H_2O, $CuCl_2$ · 2 H_2O, $CuBr_2$ or ZnBr) in ethanol were heated under reflux on a water bath for 1 h. The complexes with the composition [M(BMPTS)X_2] were isolated after the solution was concentrated to one-half of its volume and then cooled. On contrary to this, the complexes with the formula [M(BMPTS-H)X(H_2O)]H_2O were isolated on hot. The crystals were filtered off, washed several times with ethanol and with dry diethylether and finally dried in vacuum.

[M(MBPTS-2H)(H_2O)] *complexes*

An EtOH (50 cm^3) solution of BMPTS (1.3 g) and equivalent amount of the hydrated metal sulphate or acetate ($Zn(Ac)_2$ · $2H_2O$, $NiSO_4$ · 6 H_2O, $CuSO_4$ · 5 H_2O or $Cd(Ac)_2$ · 2 H_2O) in bidistilled water were heated under reflux on a water bath for 1 h. The erystals separated on hot were filtered, washed with ethanol and diethylether, and dried in vacuum.

[Co(BMPTS-H_3)] *complex*

An EtOH (25 cm^3) solution of BMPTS (1.3 g) and $CoSO_4$ · 7 H_2O (1.7 g) were mixed and heated under reflux on a water bath for 1 h. On adding anhydrous sodium acetate (0.5 g), the solution turned brown and heating was continued for 15 min. Water was added and the mixture shaken. Brown crystals separated out. The product was filtered off, washed successively with dry ethanol, diethylether and dried in vacuum. The same complex was obtained by using other cobalt salts, i.e. cobalt chloride, bromide or acetate.

The elemental analyses and physical measurements were carried out as described in our previous papers [1, 2].

Results and Discussion

Analytical results and some physical properties of the isolated metal complexes are listed in Table I. All the complexes are stable in air, (except for the Ni(II) complex, [Ni(BMPTS-2H)(H_2O)]H_2O, which changes gradually to brown), and insoluble in common organic solvents, but soluble in dimethyl formamide (DMF) and dimethyl sulphoxide (DMSO). The molar conductance values of the complexes in DMSO at room temperature (25 °C) are in the 2—22 ohm^{-1} cm^2 $mole^{-1}$ range indicating [3] their non-electrolytic nature. Molecular weight determinations of the complexes by Rast's method were found to be monomers (Table I).

The most important i.r. assignments in the spectrum of the free ligand as well as the bonding sites have been determined by a careful comparison of both the ligand and its metal complexes and by considering the work done by Maurya [4], Gupta [5], Butsko [6] and Campbell [7]. The i.r. spectrum of BMPTS, in nujol and/or KBr, shows three bands at 3460, 3290 and 3230 cm^{-1} attributed to ν(OH), ν($\bar{N}$H) and ν(NH) vibrations, respectively. The two medium bands at 1655 and 1555 cm^{-1} are assigned, respectively, to $\nu(C{=}\overset{1}{N})$ and $\nu(C{=}\overset{2}{N})$ vibrations. The strong band at 948 cm^{-1} which is absent in the spectrum of 4-phenylthiosemicarbazide [8] is mainly due to ν(NO) vibration. Also, the ν(CS) vibrations are observed at 1295 and 750 cm^{-1} with

contribution from other vibrations, in particular, ν(CN) [9]. Moreover, the n.m.r. spectrum of the ligand shows three signals in d_6-DMSO at 11.2, 10.0 9.2 ppm which are downfield from TMS and disappear upon adding D_2O. These signals are therefore assigned to (NOH), ($\overline{\text{N}}$H) and (NH) protons, respectively. All these observations indicate that the ligand exists mainly in thioketo form. Finally, the presence of broad and weak bands in the 2400—2200 and 2000—1900 cm^{-1} regions suggests the existence of intramolecular hydrogen bonding (O—H...N) [10] as shown below.

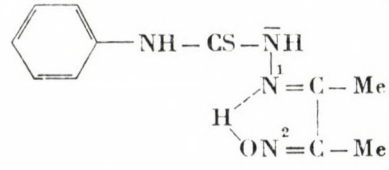

The i.r. spectral data of the complexes show that BMPTS behaves as a bidentate and/or tridentate ligand depending on the metal salt used, condition of preparation and the pH of the solution. The ligands is bidentate coordinating via the azomethine nitrogens of both the hydrazone ($\overset{1}{\text{CN}}$) and oxime ($\overset{2}{\text{CN}}$) groups, in the keto form, forming five membered ring around the metal ion. This behaviour was found for all metal complexes having the formula $[M(BMPTS)X_2]YH_2O$, where M=zinc(II), cadmium(II) or mercury(II); X=Cl or Br and Y=2 in case of cadmium(II) bromide only. The mode of chelation is suggested by the negative shift of the ($\overset{1}{\text{CN}}$) band to lower wavenumber as well as the positive shift of the band due to ($\overset{2}{\text{CN}}$). The bands due to ν(OH), ν(CS), and ν(NO) remain more or less at the same position. New band is observed at ca. 420 cm^{-1} is tentatively assigned to ν(M—N) [11]. Also, the observation of a three signals in the n.m.r. spectra of these complexes at the same regions observed for the free ligand can be taken as an evidence that the ligand coordinates to the metal ion in thioketo form.

A second mode of chelation is found for the complexes separated from copper(II) salts (chloride or bromide), cobalt(II) sulphate or chloride and nickel(II) chloride. The deprotonated ligand is bound to the metal ion, (cobalt(II), nickel(II) and copper(II), via the azomethine nitrogen, ($\overset{1}{\text{CN}}$), based on similar shifts as with the previous solid complexes. In addition, coordination occurs via the deprotonated NOH [disappearance of ν(OH); the negative shift of NO group to lower wavenumber ca. 25 cm^{-1} and the appearance of a new band at ca. 510 cm^{-1} assignable to ν(M—O)] [12]. Evidence for the presence of coordinated water molecules is the nickel(II) and copper(II) complexes is

Table I

Analytical, molecular weight, magnetic moment and some physical properties of the complexes

Compound	Colour	N.P., (°C)	Found (calcd.) %				M.Wt.	Λ_m[a]	μ_{eff} (B.M.)
			C	H	M	X[b]			
$[Cd(BMPTS)Cl_2]2H_2O$	Yellow	180	28.2 (28.1)	3.7 (3.9)	23.6 (23.9)	15.4 (15.1)	490 (497)	14	diam.
$[Zn(BMPTS)Cl_2]3H_2O$	Yellow	220	28.8 (29.9)	4.7 (4.6)	15.6 (14.8)	16.9 (16.1)	397 (441)	8	diam.
$[Cd(BMPTS)Br_2]H_2O$	Yellow	197	25.0 (24.4)	3.1 (3.0)	20.5 (20.8)	29.2 (29.6)	528 (541)	22	diam.
$[Zn(BMPTS)Br_2]$	Yellow	181	28.0 (27.8)	3.1 (3.0)	13.5 (13.7)	33.5 (33.6)	433 (475)	10	diam.
$[Hg(BMPTS)Cl_2]$	Yellow	214	— —	— —	38.0 (38.4)	13.5 (13.6)	510 (522)	12	diam.
$[Co(BMPTS\text{-}H)_3]$	Brown	200	49.3 (49.1)	4.4 (4.9)	7.0 (7.3)	— —	804 (807)	2	diam.
$[Ni(BMPTS\text{-}H)Cl.(H_2O)]$	Brick red	>300	38.0 (36.6)	4.3 (4.2)	16.5 (16.2)	9.9 (9.8)	351 361)	6	diam.
$[Cu(BMPTS\text{-}H)Cl.(H_2O)]$	Dull green	240	36.7 (36.1)	4.2 (4.1)	16.9 (17.3)	8.9 (9.7)	346 (366)	7	1.89
$[Cu(BMPTS\text{-}H)Br.(H_2O)]$	Yellowish-green	228	33.2 (32.2)	4.3 (3.7)	15.5 (15.5)	19.8 (19.4)	401 (411)	9	1.46
$[Zn(BMPTS\text{-}2H)(H_2O)]H_2O$	Pale orange	187	37.6 (37.8)	5.0 (4.6)	17.8 (18.7)	— —	336 (350)	7	diam.
$[Ni(BMPTS\text{-}2H)(H_2O)]H_2O$	Dark green	265	37.6 (38.5)	4.1 (4.7)	17.9 (17.1)	— —	350 (343)	4	diam.
$[Cu(BMPTS\text{-}2H)(H_2O)_3]$	Olive green	208	35.3 (36.1)	4.9 (5.0)	18.2 (17.4)	— —	324 (366)	3	1.65
$[Cd(BMPTS\text{-}2H)(H_2O)]H_2O$	Yellow	165	34.0 (33.3)	3.6 (4.1)	28.3 (28.3)	— —	398 (397)	2	diam.

[a] $ohm^{-1}\,cm^2\,mole^{-1}$
[b] Cl or Br

the same as those reported earlier [13]. The diamagnetic behaviour of the complex $[Co(BMPTS\text{-}H_3)]$ and $[Ni(BMPTS\text{-}H)Cl(H_2O)]$ suggests a low spin octahedral arrangement for the former and that of a square planar [14] for the latter. Both the electronic spectra in nujol and DMSO of the complexes are identical. The cobalt(III) complex, $[Co(BMPTS\text{-}H)_3]$, shows two bands at 30,300 and 20,600 cm^{-1} assignable to $^1A_{1g} \rightarrow {}^1T_{2g}$ and $^1A_{1g} \rightarrow {}^1T_{1g}$, respectively. Also, a weak shoulder is observed at 14,500 cm^{-1} which may be due to $^1A_{1g} \rightarrow {}^3T_{1g}$. Moreover, the values of 10 D_q, B and β are 21,000, 542 and 0.39 which are typical to those reported for low spin octahedral cobalt(III) [14]. The nickel(II) complex, $[Ni(BMPTS\text{-}H)Cl(H_2O)]$, shows two bands at 15,800 and 21,300 cm^{-1} assigned to $^1A_{1g} \rightarrow {}^1A_{2g}$, and $^1A_{1g} \rightarrow {}^1B_{1g}$, respectively. The

addition of pyridine to the brick red complex, [Ni(BMPTS-H)Cl(H_2O)] changes the colour the brown with the appearance of new bands at 18,200 and 25,600 cm^{-1} assigned to ν_2 and ν_3 transitions in octahedral structure [15]. This can be taken as an evidence for the square planar geometry around the nickel ion in the brick red complex which changes to octahedral geometry by addition of pyridine. Strong evidence for the square planar geometry around nickel ion as well as the participation of oxime group with replacement of hydrogen comes from the proton magnetic resonance in d_6-DMSO. The observation of two signals characterized for $\overline{\text{NH}}$ and NH protons together with the lack of the OH proton signal prove the participation of the oxime group with displacement of hydrogen (structure **I**).

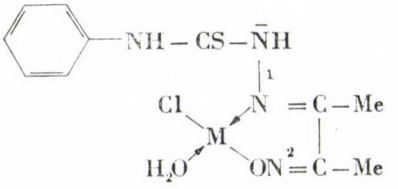

(I)

M = Cu or Ni; X = Cl or Br

The copper(II) complexes, [Cu(BMPTS-H)Cl(H_2O)] and [Cu(BMPTS-H)Br(H_2O)], have a pseudotetrahedral structure [16] in accordance with the results of electronic spectra and magnetic moments. The observation of three bands at ca. 12,000(sh), 13,900 and 18,900 cm^{-1} can be taken as an evidence for pseudotetrahedral geometry around the copper ion.

Finally, the ligand can be tridentate coordinating via the hydrazone N nitrogen and both the oxime and the thioketo groups in the enol form with displacement of two hydrogen atoms (structure **II**).

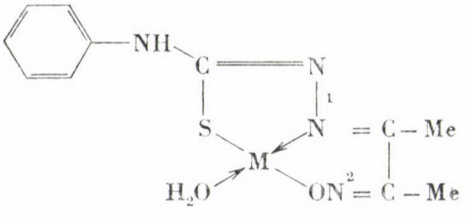

(II)

M = Ni, Cu, Zn or Cd

The disappearance of the bands attributed to both ν(CS) and ν(OH) vibrations, in the complexes having the formula [M(BMPTS-2H)(H_2O)]H_2O, suggests that the enolization occurred through both the deprotonated thioketo and NOH groups. Also, the lack of any signals characterized of the protons for the NOH and $\overline{N}H$ groups, in the n.m.r. spectra of the diamagnetic complexes, can be taken as an additional evidence for structure **II**. All the above mentioned results together with the existence of two bands in the spectrum of the nickel(II) complex, [Ni(BMPTS-2H)(H_2O)]H_2O at 16,600 and 23,900 cm^{-1} and attributable to $^1A_{1g} \rightarrow {}^1A_{2g}$ and $^1A_{1g} \rightarrow {}^1B_{1g}$, respectively, and the diamagnetic behaviour of the complex confirm a square planar geometry [14] around to nickel(II) ion. On adding pyridine to the deep green complex, [Ni(BMPTS-2H)H_2O] the colour changes to brown accompanied by the appearance of two bands at 17,800 and 25,900 cm^{-1} assignable to ν_2 and ν_3 transitions in octahedral structure [15]. Also, on leaving this complex outside the desiccator the colour changes gradually to brown confirming that the complex takes up two water molecules and thus becoming octahedral. On the other hand, the copper(II) complex, [Cu(BMPTS-2H)(H_2O)$_3$], shows a broad band centered at 16,400 cm^{-1} which may be due to $^2E_{2g} \rightarrow {}^2T_{2g}$ transition. Also, the value of magnetic moment (1.65 B.M.) is in a good agreement with those reported for distorted octahedral geometry [17].

In conclusion the following remarks may be of some interest. The substitution of the carbonyl group in the hydrazone-oxime by a thioketo group as in the case of BMPTS causes a large splitting of the d levels and hence the net effect is to increase Δ. All the complexes separated from metal sulphate and/or acetate always give complexes of the type [M(BMPTS-2H)(H_2O)]H_2O, while that prepared from metal halide in ethanolic solution produce complexes of the types [M(BMPTS-H)X(H_2O)] and [M(BMPTS)X_2]. This phenomenon could be explained on the basis that both the sulphate and acetate salts in complexation with BMPTS exert an increase of Δ due to the π bonding effect and at the same time weakened the bond between the metal and sulphate or acetate ions. As a result of that the anion (SO_4^{2-} or Ac^-) can be easily replaced on interaction with the deprotonated BMPTS. On the other hand, the metal halide behave in contrary to that discussed above as a result of the small splitting of the d levels, and the absence of π bonding.

REFERENCES

[1] Mostafa, M. M., Khattab, M. A., Ibrahim, K. M.: Trans. Met. Chem., **8**, 212 (1983)
[2] El-Asmy, A. A., Mostafa, M. M.: Polyhedron, **2**, 591 (1983)
[3] Geary, W. J.: Coord. Chem. Revs., **7**, 81 (1971)
[4] Maurya, P. L., Agarwala, B. V., Dey, A. K.: Rev. Chim. Miner., **15**, 501 (1978)
[5] Sen, A. B., Gupta, S. K.: J. Ind. Chem. Soc., **39**, 865 (1969)
[6] Ivashkovich, E. M., Butsko, S. S.: Zh. Obsh. Khim., **48**, 1156 (1978)

[7] Campbell, M. J., Grzeskowiak, R.: J. Chem. Soc., *A*, **1967**, 396
[8] Mostafa, M. M., Sliallaby, A. M., El-Asmy, A. A.: J. Inorg. Nucl. Chem., **43**, 2992 (1981)
[9] Mashima, M.: Bull. Chem. Soc. Japan, **37**, 974 (1964)
[10] Hall, D.: Acta Crystallogr., **18**, 955 (1965)
[11] Ferraro, J. R., Walker, W. R.: Inorg. Chem., **4**, 1382 (1965)
[12] Teotia, M. P., Rastogi, D. K., Malik, W. U.: Inorg. Chim. Acta, **7**, 339 (1973)
[13] Nakamoto, N.: Infrared Spectra of Inorganic and Coordination Compounds, p. 239 3rd Edit., Wiley, Interscience, N. Y. 1978
[14] Lever, A. B. P.: Inorganic Electronic Spectroscopy, 307, 343, Elsevier, Amsterdam 1968
[15] Sacconi, L.: Trans. Met. Chem., **4**, 119 (1969)
[16] Sacconi, L.: Coord. Chem. Rev., **1**, 126 (1966)
[17] Kato, M., Jonassen, H. B., Fanning, J. C.: Chem. Rev., **64**, 99 (1964)

Acta Chimica Hungarica 119 (4), pp. 363—369 (1985)

KINETIC STUDY ON THE HYDROLYSIS OF BENZENESULFONYL CHLORIDE IN WATER-DIOXANE SOLUTIONS

Mohmoud MOUSA[1]*, Aref ALY[2] and Aly HARFOUSH[3]

([1]Chemistry Department, Faculty of Science, Zagazig University, Zagazig, [2]Assiut University, Assiut, [3]Alexandria University, Alexandria, Egypt.)

Received April 26, 1984
In revised form August 6, 1984
Accepted for publication September 12, 1984

The pseudo-first order rate constants of the hydrolysis of benzenesulfonyl chloride in a series of a mixture of a dioxane and water have been measured over the temperature range of 25—55 °C, and the activation parameters ($\Delta H^{\ddagger}$ and $\Delta S^{\ddagger}$) were determined. The reaction was followed by conductance measurements. The reactivity was found to be enhanced first slowly, then it increased more rapidly with increasing concentration of water in the solvent mixture. The activation parameters for the reaction showed a regular increase in the solvent composition range 0.1 to 0.92 water mole fraction. The influence of solvent variation has been examined in terms of changes in the activation parameters.

Introduction

The knowledge of solvent effects on the reaction rate may assume a practical usefulness, both in research and in industry, because an appropriate choice of solvent allows many reactions to be probably accelerated or decelerated. To date, the more helpful treatments for rationalizing solvent effect are the correlation analysis of kinetic data by multiparameter empirical approaches [1—3], and the thermodynamic dissection of solvent energies on terms of initial state and transition state contribution [4—7]. The behaviour of the activation gives information about solvent reorganization in the activation process [8—11]. In some mixed solvent systems linear relations between $\Delta H^{\ddagger}$ and $\Delta S^{\ddagger}$ were observed [9—12], while other cases were reported where $\Delta H^{\ddagger}$—$\Delta S^{\ddagger}$ relationships tend to be complex [13—14]. We have undertaken a detailed study of the rate and mechanism of hydrolysis of benzenesulfonyl chloride in dioxane-water solutions, in order to test the various theories of solvent effects for the chemical reaction in solution.

* For correspondence: Faculty of Science, Zagazig University of Benha, Benha, Egypt.

Experimental

AnalaR benzenesulfonyl chloride was distilled before using for kinetic measurements. Doubly distilled water and 1,4-dioxane (A. R.) were purified according to the recommended procedures [15], and they were used for preparing the solutions (*v/v*).

The rate of hydrolysis in the mixed solvents was followed by conductance measurements. Conductance versus concentration calibration curves were constructed, using completely reacted solutions whose chloride ion contents were determined by a titrimetric method using Volhard's technique [16]. Successive dilutions of these solutions were made to cover the complete range of the conductance observed in the kinetic experiments. Large scale calibration curves were obtained at several experimental temperatures in the various solvent mixture, and they were used to convert the measured conductivity to molar concentration. The initial concentrations of benzenesulfonyl chloride (BSC) suitable for the kinetic studies were found to be in the range of $0.01-0.05$ mol dm^{-3}.

Results and Discussion

The observed pseudo-first order rate constants, $k(s^{-1})$, were calculated from the experimental data using Guggengeim's method [17]. Table I shows the results of the rate measurements in dioxane—water solutions at various temperatures and at different solvent compositions. Figure 1 shows the dependence of the observed rate constants on the solvent composition at different temperatures for hydrolysis. Table I and Fig. 1 show that the observed rate constant of hydrolysis is enhanced by increasing concentration of water in the solution in a non linear manner. The variation of the reaction rate with the change in the water concentration was tested by plotting logarithmic pseudo-first order rate constants against the logarithmic molar concentration of water. Non-linear relations were obtained, indicating that the order of the hydrolysis reaction of BSC was independent of the concentration of water. From these results it can be concluded that the reaction is unimolecular and first-order. This result is consistent with the ionization hypothesis, SN^1 mecha-

Table I

Effect of temperature and solvent composition on the rate constant of the hydrolysis of benzenesulfonyl chloride in water-dioxane mixtures

Water mole fraction	$k \times 10^4$ (s^{-1})						
	25 °C	30 °C	35 °C	40 °C	45 °C	50 °C	55 °C
0.10	0.30∓0.01	0.56∓0.02	1.03∓0.03	1.83∓0.03	3.23∓0.03	5.62∓0.05	9.44∓0.05
0.20	0.35∓0.02	0.65∓0.03	1.16∓0.03	2.00∓0.03	3.50∓0.03	5.89∓0.06	9.77∓0.06
0.29	0.45∓0.02	0.79∓0.02	1.46∓0.02	2.39∓0.02	4.15∓0.04	6.46∓0.06	10.29∓0.06
0.35	0.69∓0.02	1.14∓0.02	1.88∓0.02	3.02∓0.03	4.86∓0.04	7.56∓0.05	11.33∓0.05
0.45	1.09∓0.02	1.73∓0.03	2.71∓0.03	4.01∓0.03	6.37∓0.04	9.16∓0.05	13.31∓0.05
0.57	1.55∓0.03	2.37∓0.05	3.56∓0.04	5.22∓0.04	7.82∓0.05	11.28∓0.07	15.63∓0.06
0.75	2.26∓0.03	3.31∓0.04	4.80∓0.04	6.84∓0.05	9.72∓0.05	13.57∓0.07	18.65∓0.07
0.92	2.72∓0.04	3.80∓0.04	5.42∓0.05	7.51∓0.05	10.38∓0.06	14.09∓0.07	19.00∓0.07

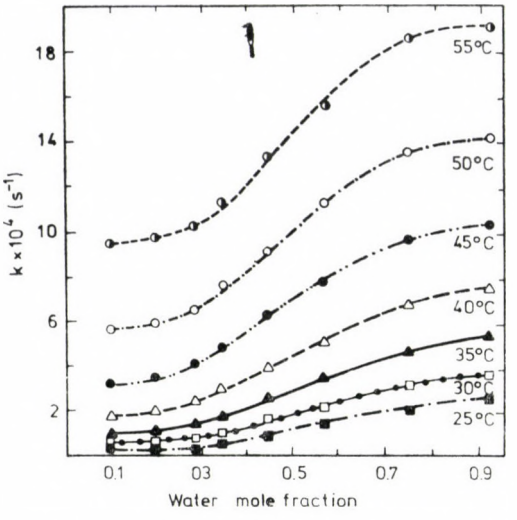

Fig. 1. Dependence of the first-order rate constant on solvent composition

nism, and can be represented by the following equation:

$$PhSO_2Cl \rightarrow [PhSO_2]^+ + Cl^- \xrightarrow{HOH} PhSO_3H + HCl$$

According to first order mechanism, the transition state is more polar than the ground state, therefore, it is expected that as the solvent polarity increases the reaction rate increases. Our data Table I show that this behaviour is observed in the range of the solvent mixture composition used.

According to the electrostatic theory of medium effects [17], a linear relation between $\log k$ and $(\varepsilon - 1)(\varepsilon + 1)^{-1}$ is to be expected. In the present study, the transition state was expected to have a larger dipole moment than that of the reactants (unimolecular, first order), and hence it was expected that the reaction should be accelerated in solvents of higher permittivity (ε). However, the plot of $\ln k$ versus $(\varepsilon - 1)(\varepsilon + 1)^{-1}$ shown in Fig. 2 gives a fairly linear relation for solvent mixtures with a composition range of 0.08—0.71 dioxane mole fraction, but it is strongly curved toward the pure dioxane end. The use of $(1/\varepsilon)$ values instead of $(\varepsilon - 1)(\varepsilon + 1)^{-1}$ values did not improve the linearity. Thus, it may be concluded that the simple electrostatic theory is not adequate to account for the results and, in general, the results here do not support any simple correlation between the reaction rate constants and the macroscopic permittivity of the medium.

The change in the activation parameters with the change in the solvent composition was used to examine the influence of the solvent on the reaction rate. The values of the activation energy (E_a) of the above reaction in different

mixed solvents was calculated from the temperature dependence of the reaction rate constant according to the Arrhenius equation, using the least squares method. The enthalpy and the entropy of activation were calculated from the

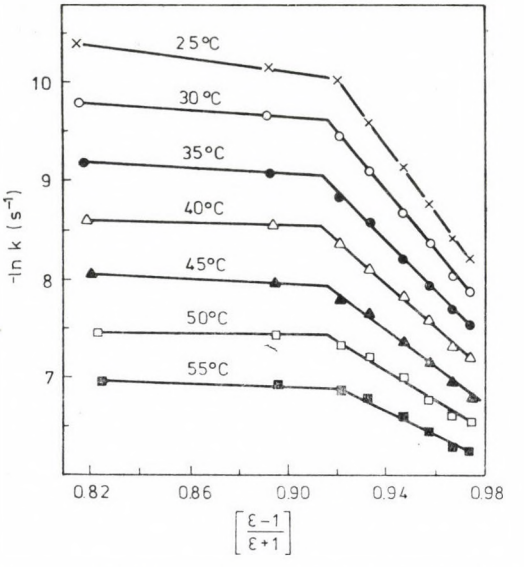

Fig. 2. Dependence of the first-order rate constant on the permittivity of the medium

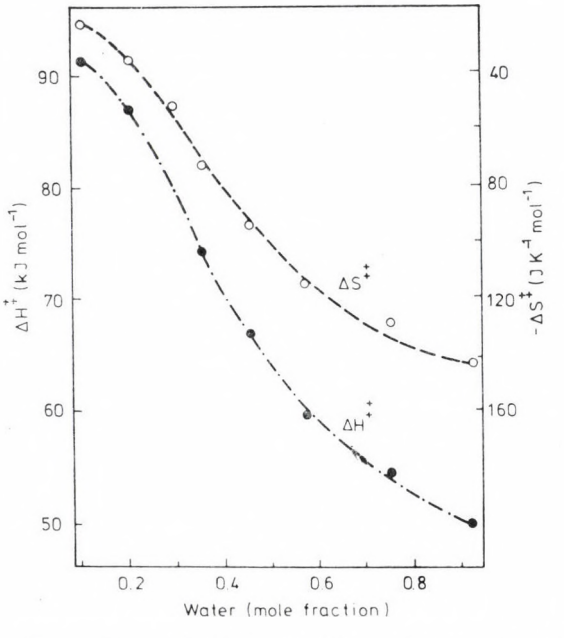

Fig. 3. Dependence of $\Delta H^{\ddagger}$ and $\Delta S^{\ddagger}$ on solvent composition

Table II

Thermodynamic activation parameters of benzenesulfonyl chloride hydrolysis in water-dioxane mixtures at 30 °C

Water (mole fraction)	ΔH^* (kJ mol^{-1})	ΔS^* (J mol^{-1} K^{-1})	ΔG^* (kJ mol^{-1})	E_a (kJ mol^{-1})
0.10	91.3∓1.9	23.8∓6.4	98.5∓4.4	93.8∓1.9
0.20	87.1∓1.9	36.4∓6.4	98.2∓4.4	89.7∓1.9
0.29	81.6∓1.7	53.0∓5.7	97.7∓4.0	84.1∓1.7
0.35	74.5∓1.5	73.6∓5.0	96.8∓3.5	77.0∓1.5
0.45	67.0∓1.4	94.9∓4.7	95.7∓3.3	69.5∓1.4
0.57	59.9∓1.1	115.6∓3.7	94.9∓2.5	62.4∓1.1
0.75	54.9∓0.9	129.5∓3.0	94.1∓2.1	57.4∓0.9
0.92	50.3∓0.9	143.2∓3.0	93.7∓2.1	52.7∓0.9

corresponding rate constants according to the absolute rate theory equation [18]. Table II shows the activation parameters calculated at 30 °C. Figure 3 shows that $\Delta H^{\ddagger}$ and $\Delta S^{\ddagger}$ values decrease regularly with increasing water concentration in the mixed solution without any inflection points. The change in the $\Delta H^{\ddagger}$ and $\Delta S^{\ddagger}$ values was found to be 41.0 kJ/mol and 117.9 J/K mol between 0.10 and 0.92 water mole fraction. The values of the entropy of activation were negative in all the investigated solvent mixtures. This indicates that, in all these mixtures, the structure of the activated complex is relatively more ordered than the structure of the separated reactants. The calculated $\Delta G^{\ddagger}$ values (Table II) do not change much with changing the solvent composition. This must be due to the linear compensation between $\Delta H^{\ddagger}$ and $\Delta S^{\ddagger}$ values. The linear relationship between $\Delta H^{\ddagger}$ and $\Delta S^{\ddagger}$, shown in Fig. 4, illustrates that the isokinetic temperature is at about 354 K.

The entropy of activation is connected with the activation volume $V^{\ddagger}$ and the volumes of the reacting species V^{R} and the activated complex $V^{\ddagger}$ in the organic solvent depends on the reacting species structure and on the ability of the solvent to compress this volume by electrostriction [19]. Then we expect that the volume of both the reacting molecules and the activated complex, in addition to the entropy of activation, are sensitive to changes in the solvent composition. The effect of the change in the solvent on the reaction rate (k) can be determined from the effect of both internal pressure and polarity on the volume of activation. The influence of the internal pressure on the chemical reactivity of BSC for hydrolysis may be discussed by considering the following equation:

$$RT \ln k = RT \ln k_0 + V^{R}(\sigma_R - \sigma_S)^2 - V^{\ddagger}(\sigma^{\ddagger} - \sigma_S)^2$$

where k_0 refers to the rate of the reaction in some standard state; V^{R} is the volume of the reactant molecule; $V^{\ddagger}$ is the volume of the activated complex

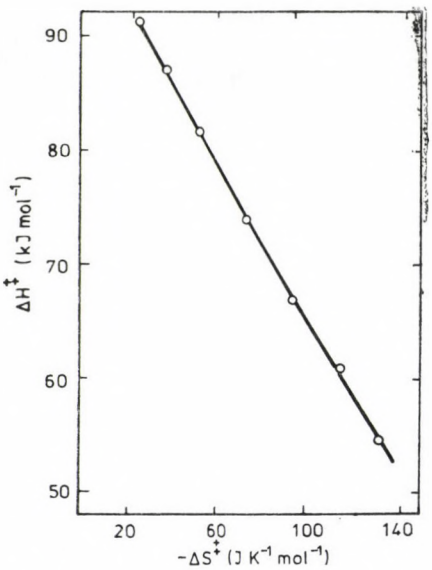

Fig. 4. A plot of $\Delta H^{\#}$ vs. $\Delta S^{\#}$ for the hydrolysis of benzenesulfonyl chloride in a series of water-dioxane mixture

and the σ's refer to the corresponding solubility parameters. In polar reactions, solvent electrostriction exerts a powerful effect on the volumes of the dissolved species and the internal pressure terms make a minor contribution to k values. For BSC the volumes of the reactant and the activated complex molecules are expected to be highly sensitive to changes in the solvent and the reaction involves a large change in the cohesion, with the product having a greater cohesion than the reactants. As the amount of water increases in the solvent mixture (i.e., polarity increases), $(V^{R}/V^{\#})$ increases (i.e., produces a greater decrease in the volume of activation) and the rate of the hydrolysis increases and the entropy decreases, as has been observed in our data.

REFERENCES

[1] Kamlet, M. J., Taft, R. W.: J. Am. Chem. Soc., **98,** 337 (1976); Taft, R. W., Kamlet, M. J.: Ibid.: **98,** 2886 (1976); Tokoyama, T., Taft, R. W., Kamlet, M. J.; **98,** 3233 (1976); Kamlet, M. J., Abboud, J. L., Taft, R. W.: **99,** 6027 (1977); Kamlet, M. J., Taft, R. W.: J. Chem. Soc. Perkin 2, **1979,** 337; Ibid.: **1979,** 349; Kamlet, M. J., Jones, M. E., Taft, R. W., Abboud, J. L.: J. Chem. Soc. Perkin 2, **1979,** 342

[2] Fowler, F. W., Kartitzky, A R., Rutherford, J. B.: J. Chem. Soc. (B), **1971,** 470; Krygowsky, T. M., Fawcett, W. R.: J. Am. Chem. Soc., **97,** 2143 (1975); Krygowsky, T. M., Milczarak, E., Wrona, P. K.: J. Chem. Soc, Perkin 2, **1980,** 1563

[3] Koppel, I. A., Palm, V. A.: in "Advances in Linear Free Energy Relationships" N. B. Chapman J. Shorter, Eds., p. 203—280, Plenum press, London 1972

[4] Arnett, E. M., Bentrude, W. C., Burke, J. J., Duggleby, P. M.: J. Am. Chem. Soc., **87,** 1541 (1965)

[5] Parker, A. J.: Chem. Rev., **69,** 1 (1969)

[6] Abraham, M. H.: J. Chem. Soc. (B), **1971,** 299
[7] Habberfield, P., Nudelman, A., Bloom, A., Room, R., Ginzberg, H., Steinhert, P.: Chem. Commun., **1968,** 194; Haberfield, P., Clayman, L., Cooper, J. S.: J. Am. Chem. Soc., **91,** 787 (1969)
[8] Diefallah, E. M., Gohnaim, S. A.: J. Chem. Soc. Perkin 2, **1977,** 1237; Diefallah, E. M., El-Nadi, A. M.: Can. J. Chem., **56,** 2053 (1978)
[9] Diefallah, E. M.: Can. J. Chem., **54,** 1687 (1976)
[10] Robertson, R. E., Sugamor, S. E.: Can. J. Chem., **50,** 1353 (1972)
[11] Robertson, R. E., Sugamor, S. E.: J. Am. Chem. Soc., **91,** 7254 (1969)
[12] Leffler, J. E.: J. Org. Chem., **20,** 1202 (1955)
[13] Winstein, S., Fainberg, A. H.: J. Am. Chem. Soc., **79,** 5937 (1957)
[14] Arnett, E. M., Bentrude, W. G., Duggleby, P. M.: J. Am. Chem. Soc., **87,** 2048 (1965)
[15] Vogel, A. E.: "A Text — Book of Practical Organic Chemistry", 3rd Ed. Longmans 1975
[16] Vogel, A. I.: "A Text — Book of Quantitative Inorganic Analysis", 2nd Ed. Longman's Green and Co. 1957
[17] Laidler, K. J.: Chemical Kinetics, 2nd. Ed. Mc Graw-Hill Book Co., New York 1965
[18] Frost, A. A., Pearson, R. G.: Kinetics and Mechanism, 2nd Ed., Chapter 7, John Wiley, New York 1961
[19] Dack, M. R.: J. Chem. Educ., **51,** 231 (1974)

Acta Chimica Hungarica 119 (4), pp. 371—375 (1985)

^{1}H-NMR STUDY OF RESTRICTED ROTATION IN DITHIOPHOSPHOROMETHYL ACETANILIDES

Zsuzsanna H-Kovács

(Research Institute for Heavy Chemical Industries, H-8201 Veszprém, P.O.B. 160)

Received May 25, 1984
In revised form August 8, 1984
Accepted for publication September 20, 1984

^{1}H-NMR spectra of a series of dithiophosphoromethyl acetanilide derivatives were investigated. The presence of an *ortho* substituted aryl group bonded to the nitrogen atom of the amide group allowed the observation of restricted internal rotation around the aryl-nitrogen bond. Coalescence temperature and the values of the free energy of activation were determined from the temperature-dependent NMR behaviour of these molecules. The possibility of *cis-trans* isomerism about the nitrogen carbonyl bond was also studied, and the assignment of the conformation of the existing isomer was also made using the aromatic solvent-induced shift.

Introduction

Recently numerous dithiophosphoromethyl acetanilides have been synthesized in our Institute. Some of these new compounds are biologically active, and a detailed analysis of the structures and conformational behaviour of these derivatives have become necessary.

In some cases nonequivalence was observed for the phosphomethoxy protons and for the methylene protons interconnecting the nitrogen and the sulfur atom. The aim of this paper is to give an account and an interpretation of these observations.

Results and Discussion

The investigated compounds can be described by the following general formula:

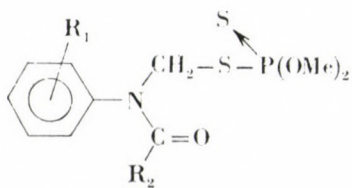

R_1: Cl, F, Me, Et, OMe,

R_2: Me, $(CH_2)_nMe$, $(CH_2)_nCl$, OMe, OEt and Ph,

n: 1-4

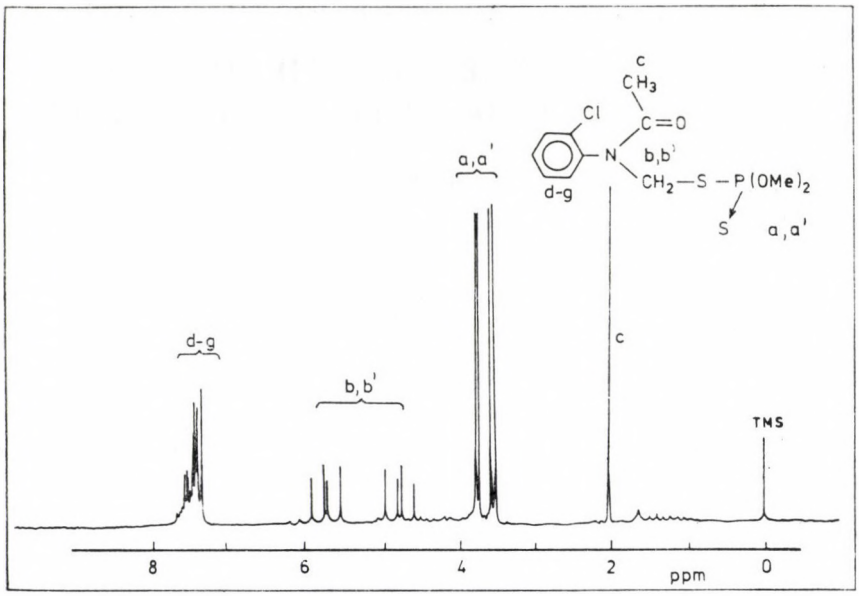

Fig. 1. ^{1}H spectrum and assignments

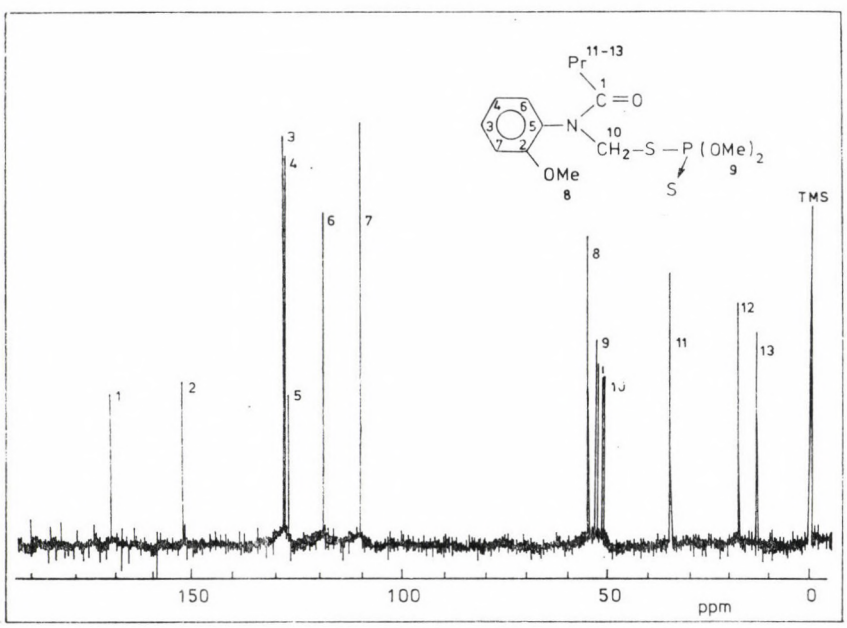

Fig. 2. ^{13}C spectrum and assignments

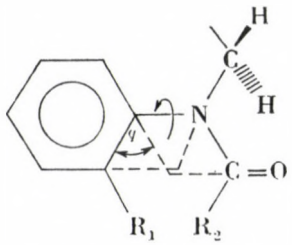

Fig. 3. Rotation around the aryl-nitrogen bond

Whenever an *ortho* substituent was attached to the *N*-aromatic ring — and only in that case — the *N*-methylene protons were chemically nonequivalent and gave rise to an AB quartet. In addition to the observed geminal coupling, each proton coupled with a ^{31}P nucleus leading to an ABX spin system (Fig. 1). The value of ^3J(P, H) was 14 ± 2.5 Hz, but J(A, X) and J(B, X) were different.

The anisochronism of the methylene protons can be interpreted by assuming hindered internal rotation. The energy barrier of this rotation, however, cannot be attributed to the well known restricted rotation around the amide bond, because the ^{13}C signals of the carbonyl carbon and those of the R_2 groups were singlets as can be seen on the ^{13}C spectrum in Fig. 2.

The source of this nonequivalence lies in the restricted rotation about the aryl-nitrogen bond. This phenomenon has long been known [1—7] and has been extensively studied. When an aromatic ring *ortho*-substituted and the rotation about the aryl nitrogen bond is slow, the *N*-methylene protons become diastereotopic and potentially anisochronous for the dihedral angles, φ, different from 0° and 180° (Fig. 3).

As the temperature is raised, the diastereomeric environments are exchanged by free rotation around the aryl-nitrogen bond, and the molecule has a plane of symmetry which bisects the methylene H—C—H bond angles, whereby these protons become isochronous.

Similarly, when the aromatic ring is *ortho*-substituted, the protons of the phosphomethoxy groups are also diastereotopic, giving a pair of doublets, because they are coupled with ^{31}P too (^3J(P, H) = 15.2 ± 0.2 Hz).

The chemical shift differences between the doublets of the diastereotopic methoxy groups changed from 1 to 6 Hz. The R_2 group attached to the carbonyl carbon affected the value of the chemical shift differences of the methylene protons and the phosphometoxy hydrogens as well. It is interesting to note that when R_2 was an aromatic ring, the chemical shift difference of the phosphomethoxy groups decreased and in some cases only a doublet was obtained; however, the nonequivalence of the methylene protons was still detectable.

This observation was strongly solvent- and temperature-dependent. At a lower temperature the doublet separated into a pair of doublets.

Choosing some model compounds — **1** (R_1 : *ortho*-Cl; R_2 : Pr), **2** (R_1 : *ortho*-Cl; R_2 : Me), **3** (R_1 : *ortho*-Cl; R_2 : Ph), **4** (R_1 : *ortho*-Et; R_2 : Et), **5** (R_1 : *ortho*-Et; R_2 : Ph) — the coalescence temperatures (T_c) and the values of free energy of activation ($\Delta G_c^{\ddagger}$) were determined and calculated.

Increasing the temperature, the ABX system of the *N*-methylene protons and the pairs of doublet of the phosphomethoxy groups coalesced into a doublet indicating coupling with the ^{31}P nucleus only. Rate constants at the coalescence temperatures were calculated in the usual way [8], and $\Delta G_c^{\ddagger}$ values were obtained from the Eyring equation [8, 9]. Data for calculations are reported in Table I. The $\Delta G_c^{\ddagger}$ values calculated, on one hand, from the coalescence temperatures and rate constants of the methylene protons and, on the other, from those of the phosphomethoxy groups, were nearly equal.

Several correlations can be observed in the rotational barrier data for these compounds. As expected, the $\Delta G_c^{\ddagger}$ values increased on changing the R_1 group from chlorine to ethyl. At the same time, R_2 did not seem to affect the values of free energy of activation, except for the case when R_2 was an aromatic ring, resulting in a decrease of the value of $\Delta G_c^{\ddagger}$.

It is well known that in *N*-substituted acetanilides two isomers *(cis* and *trans)* may exist due to hindered rotation around the amide bond [3, 4, 9,

Table I

Activation parameters for restricted rotation around the aryl-nitrogen bond

	Compound	$\Delta\nu_{AB}$ (Hz)	J(A, B) (Hz)	$\varkappa$ (s^{-1})	T_c (K)	$\Delta G_c^{\ddagger}$ KJ mol^{-1}	$\Delta\nu$ (Hz)	$\varkappa$ (s^{-1})	T_c (K)	$\Delta G_c^{\ddagger}$ KJ mol^{-1}
		for *N*-methylene protons					for phosphomethoxy protons			
1	R_1: *ortho*-Cl R_2: Pr	64	14.0	161.3	383	78.6	3.6	8.0	346	79.3
2	R_1: *ortho*-Cl R_2: Me	58	13.0	146.9	381	78.4	4.0	8.9	343	78.3
3	R_1: *ortho*-Cl R_2: Ph	42	13.5	118.8	347	71.7	2.5	5.5	313	72.4
4	R_1: *ortho*-Et R_2: Et	90	12.0	210.2	405	82.3	4.5	10.0	359	81.8
5	R_1: *ortho*-Et R_2: Ph	38	12.5	108.4	369	76.5	2.0	4.4	326	76.1

J — coupling constants
$\varkappa$ — rate constants at T_c
$\Delta\nu$ — chemical shift differences

15]. In this group of compounds, however, the presence of only one isomer was detected by the NMR sepctra recorded under normal circumstances. Changing solvents to avoid accidental equivalence of the signals, and lowering the temperature to 220 K, showed no indication of the presence of a second isomer.

The conformation of the existing isomer was elucidated by aromatic solvent-induced shift. From previous works [10—13] it can be expected that a change of solvent from chloroform to benzene would shift the signals of the molecules to different extents, depending on the position of the nuclei. In the case of all compounds studied in this series, the solvent shifts ($\Delta = \delta_{CDCl_3} - \delta_{C_6D_6}$) were downfield shifts from 3 to 12 Hz for the *N*-methylene porotons indicating that these protons are lying on the oxygen side of the carbonyl group.

At the same time large upfield shifts (18—20 Hz) were measured for the aromatic methyl protons and the methylene protons of the aromatic ethyl group as well.

These results clearly suggest the presence of the *trans* isomer, in which the carbonyl oxygen is *trans* to the aromatic ring, as already found in structurally similar systems [4, 5, 14].

Experimental

The identity and purity of the compounds were checked by elemental analysis, IR and NMR spectra. NMR spectra at ambient temperature were obtained on a VARIAN CFT 20 spectrometer operating at 80 MHz for ^{1}H and at 20 MHz for ^{13}C measurements. For the high and low temperature studies, spectra were recorded on a VARIAN EM 360 A (60 MHz) spectrometer equipped with a variable temperature unit calibrated with ethylene glycol and methanol.

The compounds were dissolved in chloroform-*d* for the low temperature measurements and in dioxane-d_8 and in dimethylformamide-d_7 for the high temperature measurements, with TMS added as internal standard.

REFERENCES

[1] Sidall III, T. H., Prohaska, C. A.: J. Am. Chem. Soc., **88,** 1172 (1966)
[2] Siddall III, T. H.: J. Org. Chem., **31,** 3719 (1966)
[3] Shvo, Y., Taylor, E. C., Mislow, K., Raban, M.: J. Am. Chem. Soc., **89,** 4910 (1967)
[4] Siddall III, T. H., Stewart, W. E.: Chem. Rev. **70,** 517 (1970)
[5] Siddall III, T. H.: J. Phys. Chem., **70,** 2249 (1966)
[6] Chupp, J., Olin, F., Landwehr, H.: J. Org. Chem., **34,** 1192 (1968)
[7] Julia, S., Ginebreda, A., Sala, P., Sancho, M., Annunziata, R., Cozzi, F.: Org. Magn. Reson., **21,** 575 (1983)
[8] Sohár, P.: Mágneses Magrezonancia Spektroszkópia, Akadémiai Kiadó, Budapest 1976
[9] Jackman, M., Cotton, F. A.: Dynamic Nuclear Magnetic Resonance Spectroscopy, Academic Press, New York 1975
[10] Bhacca, N. S., Williams, D. H.: Tetrahedron, **21,** 2021 (1965)
[11] Hatton, J. V., Richards, R. E.: Mol. Phys., **5,** 139 (1962)
[12] Emsley, J. W., Feeney, J., Sutchliffe, L. H.: Progress in NMR Spectroscopy, Vol. **3.** Pergamon Press, Oxford 1967
[13] Yonezawa, T., Morishima, I., Takeuchi, K.: Bull. Chem. Soc. Jpn., **40,** 1807 (1967)
[14] Ratts, K. W., Chupp, J.: J. Org. Chem., **39,** 3745 (1974)
[15] Walter, W.: The Chemistry of Amides, Interscience, London 1970

Acta Chimica Hungarica 119 (4), pp. 377—378 (1985)

BOOK REVIEWS

Theilheimer's Synthetic Methods of Organic Chemistry, Vol. **38**, *Yearbook 1984.*

Volume Editor A.F. Finch, London. S. Karger, Basel 1984. XXIV + 620 pages.

The reviewer thinks that Theilheimer's series of yearbooks must not be introduced to the reader. Indeed, since the publishing in 1945 of the first volume of the series, that now offers reference to 34,765 selected and coordinated key abstracts and even more supplementary references, became one of the most important standard reference works, indispensable for preparative organic chemists. The organization of the substance treated in the individual volumes is practically of unchanged form, the essence of which is contained in the introduction of the individual volumes. However, the extent of the volumes changed: while the first volume, covering literature between 1942 and 1944, contained 224 pages, the present volume discusses already on 620 pages literature published in 1982 and in the first half of 1983. The text also includes new references to material which appeared in the preceding volumes. According to the well proved practice of recent volumes, the present volume contained also a brief summary on "Trends in Synthetic Organic Chemistry in 1984", and at the end of the book indices (a subject index and a formula index of complex functional groups), for easier orientation. We are exactly of the same opinion as the reviewer of the J. Am. Chem. Soc., according to whom "the usefulness and importance of this nearly indispensable literature tool continue to grow with the increasing rate of appearance of new information. A new volume of 'Theilheimer' is as much aid to current awareness as a reference book".

Institute of Experimental Medicine
of the Hungarian Academy of Sciences,
Budapest

Gyula DEÁK

T. Shono: Electroorganic chemistry as a new Tool in Organic Synthesis.

(Reactivity and Structure Concepts in Organic chemistry. Volume 20)

Springer Verlag, Berlin, Heidelberg, New York, Tokyo, 1984; pp. 171, 7 Figures, 49 Tables

The preparation of organic compounds by means of electrolysis in aqueous or non-aqueous media has gained ever greater importance during the last 15 years; a number of such syntheses has been realized in commercial dimensions.

No doubt, a few books and many papers have been published, respectively, on the theoretical foundations or of experimental techniques of electroorganic syntheses or of results of syntheses carried out with several groups of compounds, but we have not yet been offered a comprehensive work of reference which would have helped orientation within this copious mass of literature.

This was the defect which Professor T. Shono, of the Chair of Synthetic Chemistry of Kyoto University, has successfully attempted partly to bring to an end. Our attention

is focused on the results achieved in the field of syntheses; results relevant to theoretical and analytical advances of electroorganic chemistry are not considered in this book.

Of it the first chapter, which has the length of round 120 pages, describes anodic oxidation processes which are utilizable in organic synthetic practice. Sub-chapters are arranged on the basis of the nature of the starting materials, accordingly, their subject matters are the reactions severally of aliphatic hydrocarbons, the anodic oxidation of the carbon-carbon double bond, the oxidation of alcohols, glycols, ethers, acetals, and of organic sulphur-, phosphorus- and boron-compounds, further the oxidative halogenation or dehalogenation of various molecules, and also the electro-oxidative synthesis of aliphatic or aromatic amines, carboxylate anions, finally several syntheses on aromatic substrates. This chapter about the electrolytic oxidation is completed by a part which describes the action mechanism of mediator substances that enable the electrooxidation, and the occasional subsequent chemical reactions, to proceed.

35 pages of this book describe the syntheses feasible by means of cathodic reductions of organic compounds. In contradistinction to the first chapter, this second one discusses the syntheses according to the various reaction types. Thus, how to realize addition, substitution, coupling, and some other reactions by means of cathodic reduction is the subject matter of this part.

A short introductory part to this book presents a theory of its author on the inversion of polarity by the substrate; a few examples describe stereochemical processes which occur on electrode surface.

In an Appendix, the schematic illustration of some apparatus suitable for praparative electrolyses to be carried out in them, proves that these are not sophisticated and easily accessible to any organic chemist.

This is a very valuable book for research staff that does work on an organic synthesis which cannot be achieved with traditional methods, or is tormentibly difficult so to achieve. The examples described in this book, and the more than 600 items of reference to pertinent literature, will help the readers of this book to devise, on the basis of analogy, new methods of synthesis.

The authors, and Japanese colleagues, have studied anodic oxidation mostly; this might be the cause why the part about these has become so much more voluminous, compared to the part about cathodic reduction. It would be well, in an amplified edition, to correct the disproportion by allotting more place to cathodic reductions ordered and described on the basis of the substrates in question.

Department of Applied Chemistry,
Technical University, Budapest

György KORÁNYI

Text

The text of the paper should be concise. The description of new compounds (in the Experimental) must include the complete analytical data. Special attention must be paid to structural formulas given within the text. Complicated (non-linear) formulas should be drawn on separate sheets of paper and their position in the text should be clearly marked. The numbering of formulas and equations (in parentheses on the right-hand side) is only needed if they are referred to in the text. Units should conform to the International System of Units (SI). In nomenclature the rules of the I.U.P.A.C. are accepted as standard. Symbols for physical quantities are printed in italic type and should, therefore, be underlined in the manuscript.

References

References should be numbered in order of appearance in the text (where the reference number appears in brackets) and listed at the end of the paper. The reference list, too, should by typed double-spaced. Journal titles are to be abbreviated as defined by the Chemical Abstracts Service Source Index.

Examples:

[1] Brossi, A., Lindlar, H., Walter, M., Schneider, O.: Helv. Chim. Acta, **41**, 119 (1958)
[2] Parr, R. G.: Quantum Theory of Molecular Electronic Structure, Benjamin, New York 1964
[3] Warshel, A.: in Modern Theoretical Chemistry, Vol. 7, Part A (Ed. G. A. Segal), Plenum Press, New York 1977

Tables

Each table should be given a Roman number and a brief informative title. Structural formulas should not be used in column headings or in the body of tables.

Figures

Figures should be numbered consecutively with Arabic numerals. Their approximate place should be indicated in the text on the margin. All figures must be identified on the back by the author's name and the figure number in pencil. Standard symbols (such as circles, triangles, squares) are to be used on line-drawings to denote the points determined experimentally. Line-drawings must not contain structural formulas and comments. Spectra or relevant segments thereof, chromatograms, and X-ray diffraction patterns will be reproduced only if concise numerical summaries are inadequate to replace them. Drawings and graphs should be prepared in black ink on good-quality white or tracing paper. Photographs should be submitted on glossy paper as high-contrast copies. Xerox or similar copies are not suitable for reproduction, but may be used for duplicate copies.

Redrawn illustrations will be sent to the authors for checking. No corrections of figures will, therefore, be accepted in the proofs.

Submission of manuscript

After having completed the corrections suggested by the referees and editors, the final manuscript should be submitted in duplicate, in a form ready for publication. If the corrected manuscript is not returned to the editors *within six weeks*, the intended publication of the paper will be regarded as withdrawn by the authors.

Page charge will not be assessed for the publication, however, authors from overseas countries must contribute to the postage of correspondence by sending, together with the manuscript, international postal coupons to the value of U.S. $ 10.—

Proofs and reprints

A set of proofs will be sent to the submitting author. The proofs must be returned within 48 hours of receipt. Late return may cause a delay in the publication of the paper. 100 reprints will be supplied to the authors free of charge.

Periodicals of the Hungarian Academy of Sciences are obtainable at the following addresses:

AUSTRALIA
C.B.D. LIBRARY AND SUBSCRIPTION SERVICE
Box 4886, G.P.O., *Sydney N.S.W. 2001*
COSMOS BOOKSHOP, 145 Ackland Street
St. Kilda (Melbourne), Victoria 3182

AUSTRIA
GLOBUS, Höchstädtplatz 3, *1206 Wien XX*

BELGIUM
OFFICE INTERNATIONAL DE LIBRAIRIE
30 Avenue Marnix, *1050 Bruxelles*
LIBRAIRIE DU MONDE ENTIER
162 rue du Midi, *1000 Bruxelles*

BULGARIA
HEMUS, Bulvar Ruszki 6, *Sofia*

CANADA
PANNONIA BOOKS, P.O. Box 1017
Postal Station "B", *Toronto, Ontario M5T 2T8*

CHINA
CNPICOR, Periodical Department, P.O. Box 50
Peking

CZECHOSLOVAKIA
MAD'ARSKÁ KULTURA, Národní třida 22
115 66 Praha
PNS DOVOZ TISKU, Vinohradská 46, *Praha 2*
PNS DOVOZ TLAČE, *Bratislava 2*

DENMARK
EJNAR MUNKSGAARD, Norregade 6
1165 Copenhagen K

FEDERAL REPUBLIC OF GERMANY
KUNST UND WISSEN ERICH BIEBER
Postfach 46, *7000 Stuttgart 1*

FINLAND
AKATEEMINEN KIRJAKAUPPA, P.O. Box 128
SF-00101 Helsinki 10

FRANCE
DAWSON-FRANCE S. A., B. P. 40, *91121 Palaiseau*
EUROPÉRIODIQUES S. A., 31 Avenue de Versailles, *78170 La Celle St. Cloud*
OFFICE INTERNATIONAL DE DOCUMENTATION ET LIBRAIRIE, 48 rue Gay-Lussac
75240 Paris Cedex 05

GERMAN DEMOCRATIC REPUBLIC
HAUS DER UNGARISCHEN KULTUR
Karl Liebknecht-Straße 9, *DDR-102 Berlin*
DEUTSCHE POST ZEITUNGSVERTRIEBSAMT
Sraße der Pariser Kommüne 3–4, *DDR-104 Berlin*

GREAT BRITAIN
BLACKWELL'S PERIODICALS DIVISION
Hythe Bridge Street, *Oxford OX1 2ET*
BUMPUS, HALDANE AND MAXWELL LTD.
Cowper Works, *Olney, Bucks MK46 4BN*
COLLET'S HOLDINGS LTD., Denington Estate
Wellingborough, Northants NN8 2QT
WM. DAWSON AND SONS LTD., Cannon House
Folkstone, Kent CT19 5EE
H. K. LEWIS AND CO., 136 Gower Street
London WC1E 6BS

GREECE
KOSTARAKIS BROTHERS INTERNATIONAL BOOKSELLERS, 2 Hippokratous Street, *Athens-143*

HOLLAND
MEULENHOFF-BRUNA B.V., Beulingstraat 2,
Amsterdam
MARTINUS NIJHOFF B.V.
Lange Voorhout 9–11, *Den Haag*

SWETS SUBSCRIPTION SERVICE
347b Heereweg, *Lisse*

INDIA
ALLIED PUBLISHING PRIVATE LTD., 13/14
Asaf Ali Road, *New Delhi 110001*
150 B-6 Mount Road, *Madras 600002*
INTERNATIONAL BOOK HOUSE PVT. LTD.
Madame Cama Road, *Bombay 400039*
THE STATE TRADING CORPORATION OF INDIA LTD., Books Import Division, Chandralok
36 Janpath, *New Delhi 110001*

ITALY
INTERSCIENTIA, Via Mazzé 28, *10149 Torino*
LIBRERIA COMMISSIONARIA SANSONI, Via Lamarmora 45, *50121 Firenze*
SANTO VANASIA, Via M. Macchi 58
20124 Milano
D. E. A., Via Lima 28, *00198 Roma*

JAPAN
KINOKUNIYA BOOK-STORE CO. LTD.
17-7 Shinjuku 3 chome, Shinjuku-ku, *Tokyo 160-91*
MARUZEN COMPANY LTD., Book Department, P.O. Box 5050 Tokyo International, *Tokyo 100-31*
NAUKA LTD. IMPORT DEPARTMENT
2-30-19 Minami Ikebukuro, Toshima-ku, *Tokyo 171*

KOREA
CHULPANMUL, *Phenjan*

NORWAY
TANUM-TIDSKRIFT-SENTRALEN A.S., Karl Johansgatan 41–43, *1000 Oslo*

POLAND
WĘGIERSKI INSTYTUT KULTURY, Marszałkowska 80, *00-517 Warszawa*
CKP I W, ul. Towarowa 28, *00-958 Warszawa*

ROUMANIA
D. E. P., *Bucureşti*
ILEXIM, Calea Grivitei 64–66, *Bucureşti*

SOVIET UNION
SOJUZPECHAT — IMPORT, *Moscow*
and the post offices in each town
MEZHDUNARODNAYA KNIGA, *Moscow G-200*

SPAIN
DIAZ DE SANTOS, Lagasca 95, *Madrid 6*

SWEDEN
ALMQVIST AND WIKSELL, Gamla Brogatan 26
101 20 Stockholm
GUMPERTS UNIVERSITETSBOKHANDEL AB
Box 346, *401 25 Göteborg 1*

SWITZERLAND
KARGER LIBRI AG, Petersgraben 31, *4011 Basel*

USA
EBSCO SUBSCRIPTION SERVICES
P.O. Box 1943, *Birmingham, Alabama 35201*
F. W. FAXON COMPANY, INC.
15 Southwest Park, *Westwood Mass. 02090*
THE MOORE-COTTRELL SUBSCRIPTION AGENCIES, *North Cohocton, N. Y. 14868*
READ-MORE PUBLICATIONS, INC.
140 Cedar Street, *New York, N. Y. 10006*
STECHERT-MACMILLAN, INC.
7250 Westfield Avenue, *Pennsauken N. J. 08110*

YUGOSLAVIA
JUGOSLOVENSKA KNJIGA, Terazije 27, *Beograd*
FORUM, Vojvode Mišića 1, *21000 Novi Sad*

Index: 26.007